Approche synthétique de produits naturels anticancéreux, les flavaglines

Qian Zhao

UNIVERSITÉ DE STRASBOURG

ÉCOLE DOCTORALE des SCIENCES CHIMIQUES – ED 222

Laboratoire d'Innovation Thérapeutique – UMR 7200

THÈSE

Présentée par :

Qian ZHAO

Soutenue le : **26 juin 2017**

pour obtenir le grade de : **Docteur de l'université de Strasbourg**

Discipline/ Spécialité : Chimie médicinale

Approche synthétique de produits naturels anticancéreux, les flavaglines

THÈSE dirigée par :

M. DESAUBRY Laurent	Directeur de recherche au CNRS, Université de Strasbourg

RAPPORTEURS :

Mme. PELLEGRINI-MOISE Nadia	Maître de conférences, Université de Lorraine
M. ZHANG Yongmin	Directeur de recherche au CNRS, Université Pierre et Marie Curie

---

AUTRES MEMBRES DU JURY :

Mme. MIESCH Laurence	Chargée de recherche au CNRS, Université de Strasbourg

In me the tiger sniffs the rose.

—— Siegfried Sassoon

修学好古，实事求是。*

——《汉书》

*Rechercher la vérité à partir des faits. – Livre de Han

Remerciement

*A*u terme de cette thèse, je tiens à remercier chaleureusement tous ceux qui ont contribué à sa réalisation.

En premier lieu, j'aimerais profondément exprimer ma reconnaissance à mon directeur de thèse, le Dr Laurent Désaubry. Grand merci de m'avoir encadrée et de m'avoir accordée une grande autonomie de travail. Je le remercie également pour tous les moments passés à discuter du projet. Sa confiance, ses conseils, son expérience et son accompagnement tout au long de ce cheminement ont permis à cette thèse de prendre forme.

Mes remerciements s'adressent au Professeur Marcel Hibert, directeur du laboratoire, pour m'avoir accueilli pendant ces trois années.

Ces travaux ont été financés par l'*Association Nationale de la Recherche et de la Technologie (ANRT)*, la *Fondation ARC pour la recherche sur le cancer*, et surtout par l'*AAREC Filia Research* représentée par le Dr Armant de Gramont. Je voudrais lui exprimer toute ma reconnaissance pour sa confiance à mon égard.

Mes remerciements s'adressent également au Dr Nadia Pellegrini-Moïse (Maître de conférences à l'Université de Lorraine) et au Dr Yongmin Zhang (Directeur de recherche au CNRS à l'Université Pierre et Marie Curie-Paris 6) pour d'avoir accepté d'être rapporteurs de ce travail.

Je voudrais exprimer toute ma gratitude envers le Dr Laurence Miesch (chargée de recherche au CNRS à l'Université de Strasbourg) pour d'avoir consacré du temps à l'examen de mes travaux.

Je tiens à remercier le Dr Christine Basmadjian pour l'aide qu'elle m'a apportée, sa disponibilité et ses conseils qui m'ont permis de mener à bien ces travaux. Merci aux stagiaires, Laura et Jordan, qui ont participé à ce travail.

Je remercie chaleureusement les stagiaires, thésards et post-doctorants côtoyés au cours de ces trois années : Fabrice, Fan, Amel, Jihu, Hussein, Hassan, Sabria, Rédouane. Ce fut un plaisir de travailler à vos côtés. Merci pour toutes ces discussions, plus ou moins chimiques selon les circonstances... Je tiens à remercier en particulier le Dr Wanyin Chen, pour m'avoir soutenue et accompagnée dans notre quotidien à des milliers de kilomètres de notre famille et de notre pays.

Merci aussi à tous les thésards et membres des autres laboratoires que j'ai eu l'occasion de rencontrer et avec qui j'ai eu le plaisir de passer ces trois années.

Mes remerciements s’adressent aussi au Professeur Sodeoka et aux membres de son équipe au RIKEN à Saitama au Japon. J’ai beaucoup apprécié de pouvoir faire un stage de six mois dans son laboratoire durant ma thèse.

Finalement, mes plus profonds remerciements vont à mes parents. Tout au long de mon cursus, ils m’ont toujours soutenue, encouragée et aidée. Cette thèse représente l’aboutissement de leurs efforts indéfectibles. Je remercie affectueusement toute ma famille pour m’avoir soutenue dans mes efforts pendant mes études.

Abbréviations

A	Å	Ångström
	Ac	Acétyle
	acac	Acétylacetonate
	AIF	*Apoptosis Inducing Factor*
	Akt	*Protein Kinase B*
	An	Anisyle
	Ar	Aryle
	ARN	Acide Ribonucléique
	ATM	*Ataxia telangiectasia mutated*
	ATR	*Ataxia telangiectasia and Rad3-related protein*
B	*Bcl-2*	*B-cell lymphoma 2*
	BMF	*Bcl-2 modifying factor*
	Bn	Benzyle
	Boc	*Di-tert-butyl dicarbonate*
	brsm	*Based on recovered starting material*
	Bu	Butyle
	BuLi	Butyllithium
C	*CamK*	*Calmodulin-dependent protein kinase*
	CAN	*Ceric ammonium nitrate*
	CDK	*Cyclin-dependent kinase*
D	DBDMH	1,3-Dibromo-5,5-diméthylhydantoin
	DBU	1,8-Diazabicyclo[5.4.0]-undec-7-ène
	DCC	*N*,*N'*-Dicyclohexyl-carbodiimide
	DCE	1,2-Dichloroéthane
	DDQ	2,3-Dichloro-5,6-dicyano-1,4-benzoquinone
	DIBAL-H	Hydrure de diisobutylaluminium
	DIPEA	*N*,*N*-Diisopropyléthylamine
	DMAP	4-Diméthylaminopyridine
	DMF	Diméthylformamide
	DMSO	Diméthyl sulfoxide
	DTBMP	2,6-Di-*tert*-butyl-4-méthylpyridine
E	*EGF*	*Endothelial growth factor*
	eIF4	*Eukaryotic initiation factors*
	éq	Equivalent
	ERK	*Extracellular-signal-regulated kinase*

	ESI	*Electrospray ionisation*
	Et	Ethyle
F	FL	Flavagline
G	Grp	*Gastrin-releasing peptide*
	GDP	Guanosine diphosphate
H	HMPA	Hexaméthylphosphoramide
	HR-MS	*High resolution-mass spectrometry*
	HSF	*Heat shock factor*
	Hsp	*Heat shock protein*
	HSQC	*Heteronuclear single-quantum correlation spectroscopy*
	HUVEC	*Human umbilical vein endothelial cells*
I	*IGF1*	*Insulin-like growth factor*
	IgM	*Immunoglobulin M*
J	*JNK*	*c-Jun N-terminal kinases*
K	KHMDS	Potassium bis(triméthyl-silyl)amide
L	LC-MS	*Liquid chromatography-mass spectrometry*
	LDA	Lithium Diisopropylamide
	L-selectride®	*Lithium tri-sec-butyl-borohydride*
M	Mcl-1	*Myeloid cell leukemia protein 1*
	MAP	*Mitogen activated proteins*
	m-CPBA	Acide *méta*-chloroperoxybenzoïque
	MCM	*Minichromosome maintenance protein complex*
	Me	Méthyle
	MEK	*Mitogen-activated protein kinase*
	MLK	*Mixed lineage kinases*
	m-TOR	*Mammalian target of rapamycin*
N	NAP	2-Naphthylméthyle
	NBS	*N*-bromosuccinimide
	NF-kB	*Nuclear factor-kappa B*
	NMO	N-méthylmorpholine N-oxide
	NMP	*N*-Méthylpyrrolidone
	NOESY	*Nuclear Overhauser effect spectroscopy*

P	Pd/C	Palladium sur charbon
	Ph	Phényle
	PHB	Prohibitine
	PhMe	Toluène
	PKC-δ	Protéine kinase C
	Pr	Propyle
	p-TsOH	Acide *para*-toluènesulfonique
R	*Raf*	*Rapidly accelerated fibrosarcoma*
	Red-Al®	*Sodium bis(2-methoxy-ethoxy) aluminum hydride*
S	*Shp*	*Src homology region 2 domain-containing phosphatase*
T	TADDOL	α,α,α,α-Tétraaryl-1,3-dioxolane-4,5-diméthanol
	TBAF	Fluorure de tétra-*n*-butylammonium
	TBDMS	Tert-butyldiméthylsilyl
	TES	Triéthylsilyle
	TEMPO	(2,2,6,6-Tétraméthylpipéridin-1-yl)oxyl
	Tf	Trifluorométhanesulfonyle
	TFA	Acide trifluoroacétique
	TGF-β	*Transforming growth factor*
	THF	Tétrahydrofurane
	TMS	Triméthylsilyle
	TMSOTf	Triméthylsilyl trifluorométhanesulfonate
	TRPM6	*Transient receptor potential ion channel 6*
	Ts	Tosyle
	TXNIP	*Thioredoxin-interacting protein*
V	VEGF	*Vascular endothelial growth factor*

SOMMAIRE

1. INTRODUCTION

1. Introduction

1.1. Les produits naturels : une source vitale d'agents anticancéreux

1.1.1. La place du produit naturel en oncologie

Les produits naturels sont les métabolites secondaires qui contribuent à la survie des organismes, notamment en tant qu'arme chimique ou en transmettant de l'information d'un organisme à l'autre. Comparé aux drogues synthétiques, les produits naturels ont une tendance à avoir plus de centres chiraux, plus d'atomes d'oxygène, moins d'atomes d'azote et des systèmes cycliques plus variés. Ils ciblent des protéines qui présentent statistiquement plus d'interactions protéine-protéine que celles qui sont ciblées par des drogues purement synthétiques.[1]

Les produits naturels ont une longue histoire dans le traitement du cancer. Hartwell, dans sa revue sur les plantes ayant une activité anticancéreuse, énumère plus de 3000 espèces de plantes qui auraient été utilisées dans le traitement du cancer.[2] Ces molécules isolées servent souvent de modèles pour la préparation d'analogues et de pro-drogues possédant une activité biologique plus efficace.

La synthèse de l'aspirine par Charles Gerhard à la faculté de pharmacie à Strasbourg en 1853, a pavé la route pour la chimie médicinale du produit naturel.[3] En 1964, l'actinomycine est devenue le premier produit naturel approuvé pour une indication oncologique. D'autres médicaments à base de produits naturels tel que les anthracyclines, les alcaloïdes de la pervenche, l'épipodophyllotoxine, les dérivés de la camptothécine et les taxoïdes sont toujours utilisés dans le traitement des cancers.

Avec l'émergence dans les années 90 des thérapies ciblées, qui reposent sur des

[1] Dancík, V., Seiler,K.P., Young,D.W., Schreiber,S.L., Clemons, P.A., *J. Am. Chem. Soc.*, **2010**, *132*, 9259–9261.

[2] Hartwell, J. L., *Plants Used Against Cancer: A SurVey*; Quarterman: Lawrence, MA, **1982**.

[3] Gerhardt, C., *Justus Liebigs Ann.Chem.,* **1853**, *87*, 149–179.

anticorps ou des petites molécules de synthèse, les groupes pharmaceutiques ont pour la plupart perdu leur intérêt dans les produits naturels. Si les thérapies ciblées ont un succès éclatant dans le traitement de la leucémie myéloïde chronique et de certaines formes de cancers du système gastro-intestinal, de la prostate ou du foie, dans la plupart des autres cas ces traitements prolongent rarement la vie des patients de plusieurs années. Il existe donc un besoin urgent de développer des médicaments originaux. Les effets limités des thérapies ciblées ont justifié un retour des produits naturels en oncologie. Ainsi, on observe depuis 2007 la mise sur le marché en moyenne d'un nouveau médicament anticancéreux dérivé de produit naturel chaque année (Figure 1).

Certains des nouveaux agents induisent une forte cytotoxicité en agissant sur des cibles classiques, comme l'ADN (pour la trabectédine) ou des microtubules (pour l'ixabépilone, la vinflunine et l'éribuline), tandis que d'autres ciblent des événements comme la biosynthèse de stéroïdes (pour l'acétate d'abiratérone), le remodelage des histones (pour le romidépsine), la synthèse des protéines (pour l'homoharringtonine) ou leur dégradation (pour le carfilzomib). Les dérivés de la rapamycine sont atypiques. Ces molécules ne sont pas cytotoxiques, mais peuvent être considérés comme des agents de thérapie ciblée grâce à leur inhibition de la signalisation mTOR.[4]

Au contraire des thérapies ciblées qui sont conçues pour un type spécifique de cancer, le développement de produits naturels s'appuie fortement sur la compétence des pharmacologues et cliniciens pour identifier leur mécanisme d'action et leur indication optimale en clinique.

Nous avons décrit dans une revue intitulée «Cancer wars: natural products strike back » (Publication n° 1) cette réhabilitations des produits naturels par les industries pharmaceutiques qui a lieu depuis quinze ans.[4]

[4] Basmadjian, C., Zhao, Q., Bentouhami, E., Djehal, A., Nebigil, C. G., Johnson, R. A., Serova, M., de Gramont, A., Faivre, S., Raymond, E., Désaubry, L. G., *Front. Chem.*, **2014**, *2* : 20.

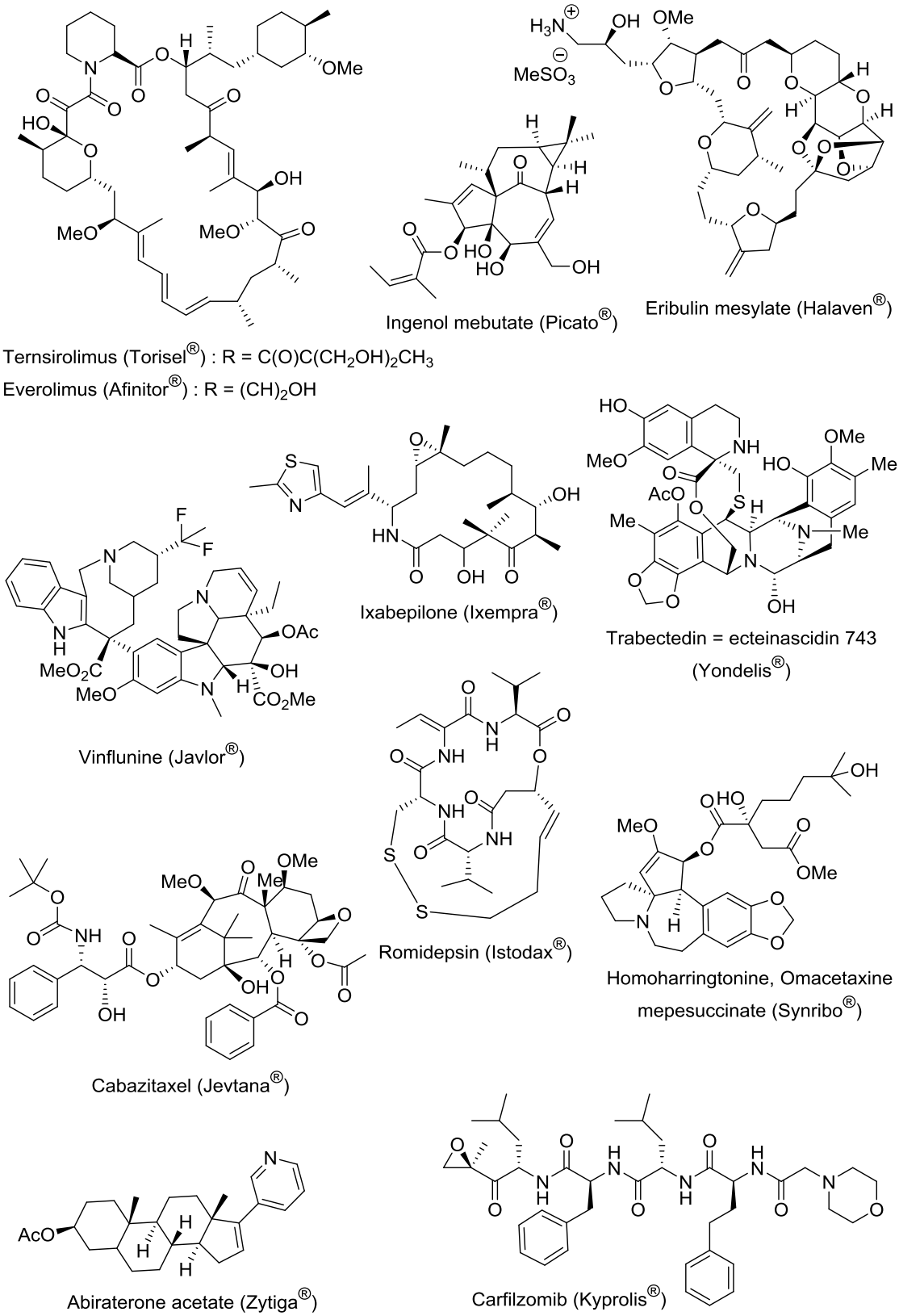

Figure 1. Structure des médicaments anticancéreux dérivés de produits naturels mis sur le marché depuis 2007.

1.1.2. Aglaia

La famille des Méliacées comprend environ 50 genres d'arbres et arbustes dicotylédones et 500 espèces d'origine tropicale, dont l'*Aglaia* est le genre le plus représenté (Figure 3). Les espèces d'*Aglaia* se trouvent principalement dans les forêts tropicales du sud-est de l'Asie, du Sri Lanka et l'Inde, traversant la Birmanie, la sud de Chine, le Viêt Nam, la Malaisie, l'Indonésie, l'Australie et les îles Fidji, à l'est jusqu'aux Samoa et au nord jusqu'aux îles Mariannes (Figure 2).

Figure 2. Distribution des espèces d'*Aglaia* (recopié de la référence 5).

Certaines espèces d'*Aglaia* sont utilisées en médecine traditionnelle pour l'insuffisance cardiaque, le traitement de la diarrhée, la toux, l'inflammation et des blessures.[5] Les extraits d'*Aglaia* sont aussi utilisés comme bactéricides, insecticides et en parfumerie.[6]

Après la première découverte d'un cyclopenta[*b*]benzofurane, le rocaglamide, par King et ses collègues en 1982,[7] une centaine de composés de la même famille,

[5] Proksch, P., Edrada, R., Ebel, R., Bohnenstengel, F.I., Nugroho, B.W., *Curr. Org. Chem.,* **2001**, *5*, 923-938.

[6] Janaki, S., Vijayasekaran, V., Viswanathan, S., Balakrishna, K., *J. Ethnopharmacol.,* **1999**, *67*(1), 45-51.

[7] Lu King, M., Chiang, C.-C., Ling, H.-C., Fujita, E., Ochiai, M., McPhail, A. T., *J. Chem. Soc., Chem. Commun.,* **1982,** *20*, 1150-1151.

les flavaglines, ont été isolées d'une trentaine d'espèces d'*Aglaia*.[8] Les autres types de composés issus de l'*Aglaia* comprennent des lignanes, des flavonoïdes, des bisamides, et terpénoïdes.[9]

Figure 3. Arbre, fruit et fleur d'*Aglaia* (recopié de la référence 10).

[8] Kim, S., Salim, A.A., Swanson, S.M., Kinghorn, A.D., *Anticancer Agents Med. Chem.*, **2006**, *6*(4), 319-345.

[9] (i) Brader, G., Vajrodaya, S., Greger, H., Bacher, M., Kalchhauser, H., Hofer, O., *J. Nat. Prod.*, **1998** *61*(12), 1482-90. (ii) Grege, H., Pache, T., Brem, B., Bacher, M., Hofer, O., *Phytochemistry*. **2001** *57*(1), 57-64. (iii) Greger, H., Pacher, T., Vajrodaya, S., Bacher, M., Hofer, O., *J. Nat. Prod.*, **2000**, 63(5), 616-20. (iv) Saifah, E., Puripattanavong, J., Likhitwitayawuid, K., Cordell, G.A., Chai, H, Pezzuto, J.M., J. Nat. Prod., **1993**, *56*(4), 473-7. (v) Puripattanavong, J., Weber, S., Brecht, V., Fram, A.W., *Planta Med*., **2000**, *66*(8):740-5. (vi) Ebada, S.S., Lajkiewicz, N., Porco, J.A. Jr, Li-Weber, M., Proksch, P. M., Proksch, P., *Fortschr Chem Org Naturst.*, **2011**, *94*, 1- 58.

[10] http://www.arkive.org/chinese-perfume-tree/aglaia-odorata/ et http://herbaria.plants.ox.ac.uk/bol/plants400/Profiles/AB/Aglaia

1.2. Flavaglines

1.2.1. Découverte

Les flavaglines sont caractérisées par un squelette cyclopenta[*b*]benzofurane, dont les représentants les plus connus sont le rocaglamide (**1**), le rocaglaol (**2**) et le silverstrol (**3**) (figure 4). Ce dernier est substitué par un pseudo-sucre.[11]

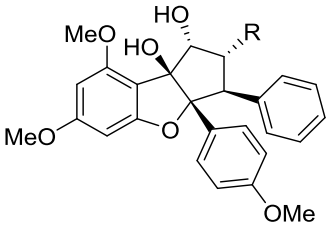

1 : R = $CONMe_2$
2 : R = H

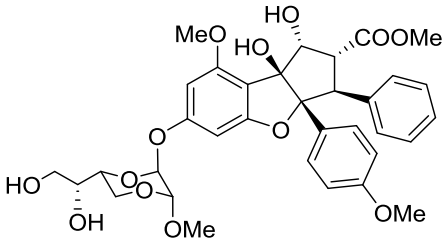

3

Figure 4. Exemples de flavaglines naturelles.

1.2.2. Propriétés pharmacologiques

Les flavaglines présentent un profil d'activité biologique unique qui a attiré l'attention de nombreux biologistes. En effet, elles présentent des activités insecticides, antifungiques, anti-inflammatoires, neuroprotectrices et surtout anticancéreuses. Ces dernières sont les plus étudiées jusqu'à présent.

A la concentration de l'ordre du nanomolaire, les flavaglines inhibent la prolifération des cellules tumorales et ne présentent pas de toxicité sur les cellules saines telles que les cellules HUVEC (cordons ombilicaux), les neurones, les cellules épithéliales intestinales et les lymphocytes.[12] A notre connaissances, Hausott et coll. sont les premiers à avoir montré que les cellules normales (dans ce cas-là les cellules épithéliales intestinale IEC18) sont 1,000 fois moins sensibles à la cytotoxicité

[11] Basmadjian, C., Thuaud, F., Ribeiro, N., Désaubry, L., *Fut. Med. Chem.,* **2013,** *5* (18), 2185-2197.

[12] Hausott, B., Greger, H., Marian, B., *Int. J. Cancer.*, **2004**, *109* (6), 933-940 ; Ribeiro, N., Thuaud, F., Bernard, Y., Gaiddon, C., Cresteil, T., Hild, A., Hirsch, E.C., Michel, P.P., Nebigil, C.G., Dé saubry, L., *J. Med. Chem.* **2012a***, 55*, 10064– 10073 ; Su, B.N., Chai, H., Mi, Q., Riswan, S., Kardono, L.B., Afriastini, J.J., Santarsiero, B.D., Mesecar, A.D., Farnsworth, N.R., Cordell, G.A., et al., *Bioorg. Med. Chem.*, **2006**, *14*, 960–972 ; Thuaud, F., Ribeiro, N., Gaiddon, C., Cresteil, T., Désaubry, L., *J. Med. Chem.*, **2011**, *54*, 411–415; Zhu, J.Y., Lavrik, I.N., Mahlknecht, U., Giaisi, M., Proksch, P., Krammer, P.H., Li-Weber, M., *Int. J. Cancer*, **2007**, *121*, 1839–1846.

des flavaglines (IC50 > 10 µM) par rapport aux cellules tumorales (SW480 et HT29/HI I) ou d'adénome prémalin (VACO235 et LT97).

Un autre effet intéressant des flavaglines est qu'elles potentialisent l'efficacité de médicaments anticancéreux dans divers modèles murins de cancer.[8]

Par ailleurs, les flavaglines présentent des activités anti-inflammatoires et cytoprotectrices. A une concentration nanomolaire, elles induisent une forte immunosuppression via l'inactivation du facteur nucléaire des lymphocytes T activées, suite à une activation des MAP kinases JNK et p38.[13] A une concentration plus élevée, les flavaglines peuvent aussi inhiber la voie de signalisation NF-kB, qui est impliquée dans l'inflammation.[14]

En 2005, des chercheurs de chez Bayer ont montré que la flavagline synthétique IMD-019064 inhibe la signalisation du NF-kB, et la libération des médiateurs pro-inflammatoires. De plus, ce composé protège les neurones dopaminergiques dans le modèle de Parkinson et aussi contre la neuro-inflammation consécutive à un traumatisme cérébral chez la souris.[15]

Nos collaborateurs, Christian Gaiddon et Canan Nebigil, tous à Strasbourg ont respectivement montré que des flavaglines synthétisées au laboratoire protègent les neurones contre l'apoptose induite par le cisplatine et les cardiomyocytes contre l'apoptose induite par un médicament anticancéreux, la doxorubicine.[16]

1.2.3. Cible moléculaire et mécanisme d'action

1.2.3.1. Les Prohibitines

En 2012, en utilisant un ligand de chromatographie d'affinité synthétisé au laboratoire, Li-Weber et ses collègues au DKFZ à Heidelberg ont identifié par spectrométrie de masse les prohibitines (PHBs) comme étant les cibles moléculaires

[13] Proksch, P., Giaisi, M., Treiber, M. K., *et al.*, *J. Immunol*, **2005**, *174*(11), 7075-7084.

[14] Baumann, B., Bohnenstengel, F., Siegmund, D., *et al.*, *J. Biol. Chem.*, **2002**, *277* (47), 44791-44800.

[15] Fahrig, T., Gerlach, I., Horva th, E., *Mol. Pharmacol.,* **2005**, *67*(5), 1544-1555.

[16] Bernard, Y., Ribeiro, N., Thuaud, F., Turkeri, G., Dirr, R., Boulberdaa, M., Nebigil, C.G., and Désaubry, L., *PLoS ONE,* **2011**, *6*, e25302.

des flavaglines.[17] Les prohibitines, PHB1 et PHB2, sont des protéines d'échafaudage qui s'associent entre elles pour former des oligomères, ou avec d'autres protéines pour contrôler leur activité. Les fonctions des PHBs sont régulées par des modifications post-traductionnelles induites par la signalisation d'Akt, la CamK IV, la PKC-δ et par les récepteurs d'insuline, de l'IGF1, de l'EGF, de l'TGF-β et de l'IgM. Ces modifications modulent l'affinité de PHBs pour des lipides spécifiques et contrôlent leur localisation intercellulaire.

Les PHBs sont essentielles pour maintenir l'intégrité structurelle et fonctionnelle des mitochondries, en particulier l'apoptose et la résistance au stress oxydatif. Dans le noyau, elles contrôlent la transcription et la synthèse de l'ADN en interagissant avec plusieurs facteurs de transcription, comme par exemple, les récepteurs aux androgènes et estrogènes ou encore p53. Elles interagissent aussi avec les histones désacétylases, l'histone méthyltransférases, les co-répresseurs transcriptionnels et les protéines d'entretien de minichromosomes (protéines MCM). Dans le cytoplasme, les PHBs régulent l'activité de nombreuse protéines de signalisation, par exemple, les kinases c-Raf, Akt et MLK2, la phosphatase Shp1/2, les protéines chaperonnes Hsp70 et mortaline/Grp75, la phospholipase Cγ2, et le canal au magnésium TRPM6.

K. Rajalingam *et al.* ont montré en particulier que l'activation de C-Raf par Ras requiert une interaction directe entre C-Raf et les PHBs.[18] G. Polier *et al.* ont montré qu'en se liant sur PHBs, les flavaglines inhibent cette intéraction et bloquent ainsi l'activation de la voie Ras-C-Raf-ERK qui est nécessaire à la survie cellulaire d'un grand nombre de tumeurs.[19]

1.2.3.2. eIF4A

eIF4A (les facteurs d'initiation eukaryotique de la traduction 4A) est une des trois

[17] Polier, G., Neumann, J., Thuaud, F., Ribeiro, N., Gelhaus, C., Schmidt, H., Giaisi, M., Köhler, R., Müller, Wolfgang W., Proksch, P., Leippe, M., Janssen, O., Désaubry, L., Krammer, Peter H., Li-Weber, M., *Chemistry & Biology,* **2012**, *19* (9), 1093-1104.

[18] Rajalingam, K., Rudel, T., *Chemistry&Biologiy,* **2012**, *19*, 1077–1078.

[19] Polier, G., Neumann, J., Thuaud, F., Ribeiro, N., Gelhaus, C., Schmidt, H., *et al., Chem. Biol.,* **2012**, *19*, 1093–1104.

sous-unités du complexe eIF4F impliqué dans le recrutement de l'ARNm aux ribosomes. Il est nécessaire à la traduction d'un petit nombre d'ARNm codant principalement les facteurs qui contrôlent l'oncogenèse, l'angiogenèse, et la chimiorésistance.[8]

Rizzacasa et ses collègues ont démontré en 2013 par chromatographie d'affinité que les flavaglines se fixent aussi directement à l'eIF4A.[20] Auparavant, Pelletier et collaborateur avaient montré que les flavaglines inhibent eIF4A en renforçant sa liaison avec l'ARNm et en empêchant ainsi son recyclage.[21]

De manière intéressante, les gènes domestiques n'ont pas besoin de l'eIF4A pour leur traduction, ce qui explique, au moins partiellement, pourquoi les flavaglines montrent une cytotoxicité sélective aux cellules cancéreuses.

1.2.3.3. Les mécanismes anticancéreux

Pour l'instant seuls les PHBs et eIF4A ont été découvertes comme étant les cibles des flavaglines (Figure 5). Laquelle de ces deux familles de cibles joue le rôle plus important reste une question soumise à débat. Cela peut d'ailleurs varier selon le type de tumeur. On ignore également si ce sont les PHBs ou eIF4A qui sont impliqués dans l'activation d'AIF (du facteur d'induction de l'apoptose), caspase 12, du p38, AFM, ATR et JNK. L'effet des flavaglines sur les voies de signalisation en aval des PHBs et d'eIF4a sont examinée par différentes équipes avec qui nous collaborons.

[20] Chambers, J. M., Lindqvist, L. M., Webb, A., Huang, D. C. S., Savage, G. P., Rizzacasa, M. A., *Org. Lett.,* **2013,** *15* (6), 1406-1409.

[21] Cencic, R., Carrier, M., Galicia-Vázquez, G., Bordeleau, M.-E., Sukarieh, R., Bourdeau, A., Brem, B., Teodoro, J. G., Greger, H., Tremblay, M. L., Porco, J. A., Jr., Pelletier, J., *PLoS ONE* **2009,** *4* (4), e5223.

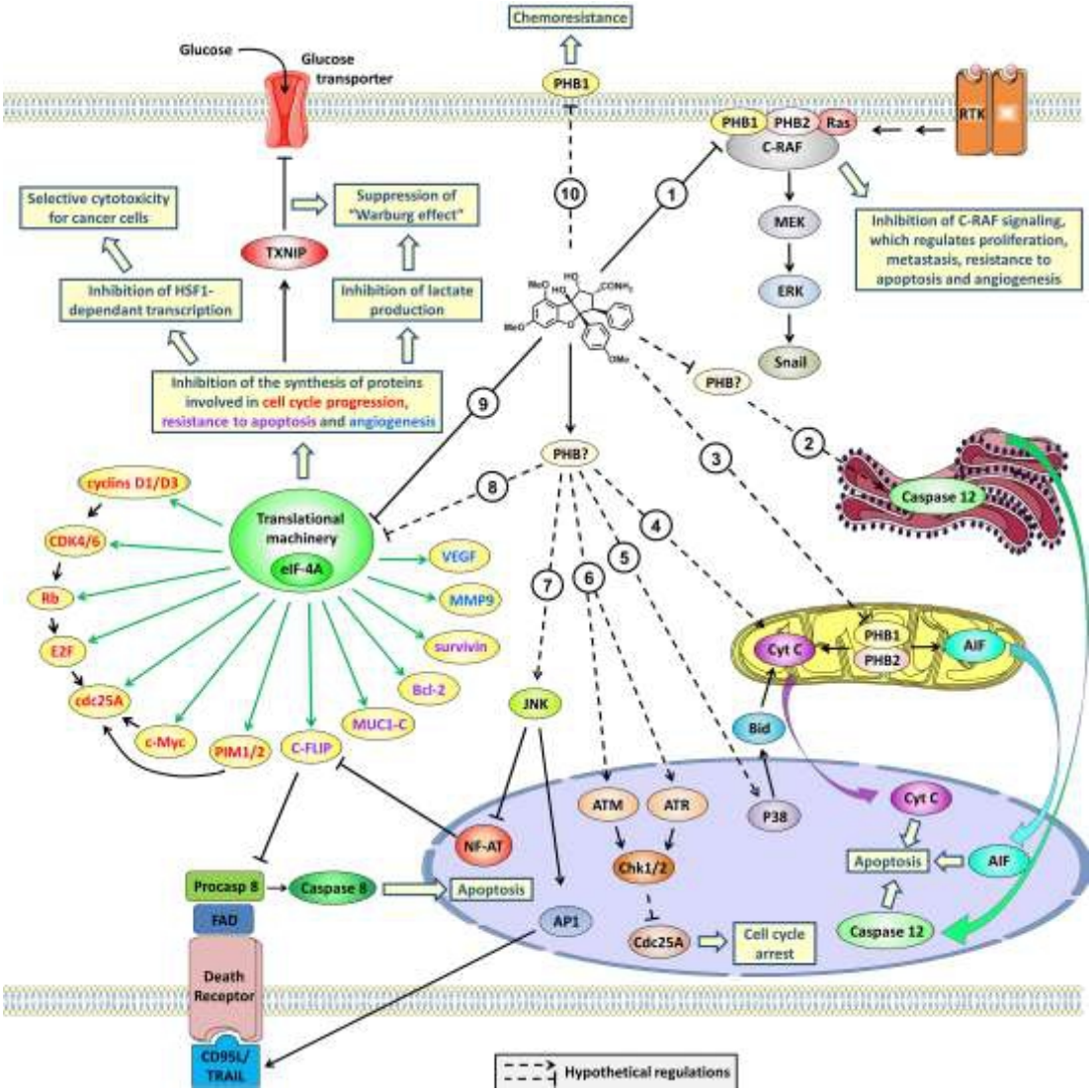

Figure 5. Mécanismes anticancéreux des flavaglines. **1.** Inhibition de l'activation du C-Raf Ras-dépendent. **2, 3.** Translocation du caspase-12 et de l'AIF au noyau pour induire l'apoptose. **4.** Translocation du cytochrome C au noyau pour induire la voie intrinsèque d'apoptose. **5.** Activation de la transcription médiée par p38 de la famille du Bcl-2 pro-apoptotique. **6.** Induction de la voie ATM/ATR-Chk1/2-Cdc25A menant à l'arrêt du cycle cellulaire. **7.** Activation de la transcription JNK-dépendante des protéines pro-apoptotiques c-FLIP et ligand de CD95. **8.** Inhibition hypothétique PHB-dépendante de machine de traduction. **9.** Inhibition de l'eIF4A mène à une baisse de l'expression des protéines impliquées dans la progression du cycle cellulaire, la résistance à l'apoptose et l'angiogenèse. Cette inhibition de la synthèse protéique s'accompagne d'une suppression de l'activité du facteur de transcription HSF1 et la surexpression du suppresseur de tumeur TXNIP. TXNIP bloque l'absorption du glucose et empêche "l'effet Warburg". **10.** Inhibition hypothétique de la chimiorésistance médiée par PHB1 à la surface cellulaire (recopié de la référence 11).

1.2.4. Relation structure-activité

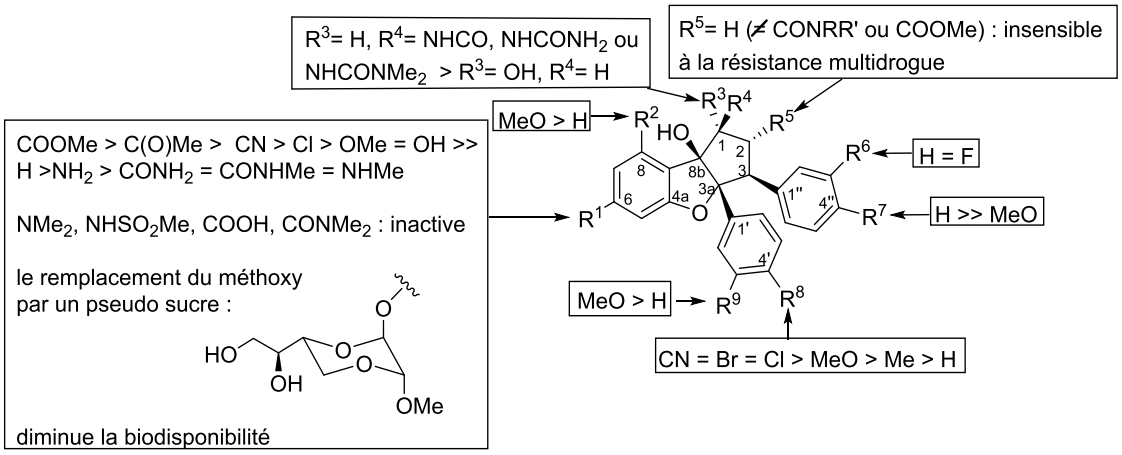

Figure 6. Relations structure-activité reliées à l'activité antiproliférative de flavaglines.[11]

Le remplacement du groupe méthoxy en position 4' de rocaglaol par un attracteur d'électron, par exemple le brome (R^8 = Br) renforce la cytotoxicité, lorsque sa suppression diminue la cytotoxicité de l'ordre de trois, suggérant que un groupe hydrophobe est nécessaire à cette position.[6] L'introduction d'un groupe méthoxy en position 4'' (R^7 = OMe) sur l'autre phényle est défavorable pour cette activité (Figure 6).

Le remplacement du groupe hydroxyle en position 1 par un groupe formamide ou un groupe sulfonamide ne change pas significativement l'activité antiproliférative. L'introduction d'un amide ou un ester méthylique en position 2 rend le composé sensible à la résistance multidrogue, ce qui a un effet délétère important quand à ses effets *in vitro* et *in vivo*.

L'introduction d'un méthoxy en position 8b rend le composé quasiment inactif, par contre la suppression du groupe méthoxy en position 8 diminue significativement l'activité du composé. Finalement, le remplacement du groupe méthoxy en position 6 par un groupe dioxanyle permet d'augmenter la cytotoxicité, mais altère sa biodisponibilité.

1.3. Synthèse de Flavaglines

Possédant un squelette compact, avec 2 centres chiraux quaternaires adjacents et 2 cycles aromatiques en position cis sur un cyclopentyle très fonctionnalisé, les flavaglines représentent un défi en synthèse organique qui a attiré l'attention de plusieurs laboratoires de synthèse organique depuis les années 90. Nous avons décrit ces travaux dans une revue publiée dans *Eur. J. Org. Chem.* (Publication N°2).

1.3.1. Première synthèse totale du Rocaglamide

En 1990, la première synthèse totale de Rocaglamide est réalisée par le groupe de Trost.[22] Cette approche est basée sur une cycloaddition [3+2] énantioselective du composé **4** avec l'oxazepinedinone **5** pour générer la cyclopentanone **6** (85%, Schéma 1). Ensuite, 7 étapes sont nécessaires pour former le squelette de flavagline, mais avec une mauvaise configuration par rapport au produit naturel. La stéréochimie est corrigée par 6 étapes supplémentaires pour donner le rocaglamide **1**. Bien que cette approche nécessite plusieurs étapes, elle demeure la seule synthèse énantiospécifique jusqu'à présent.

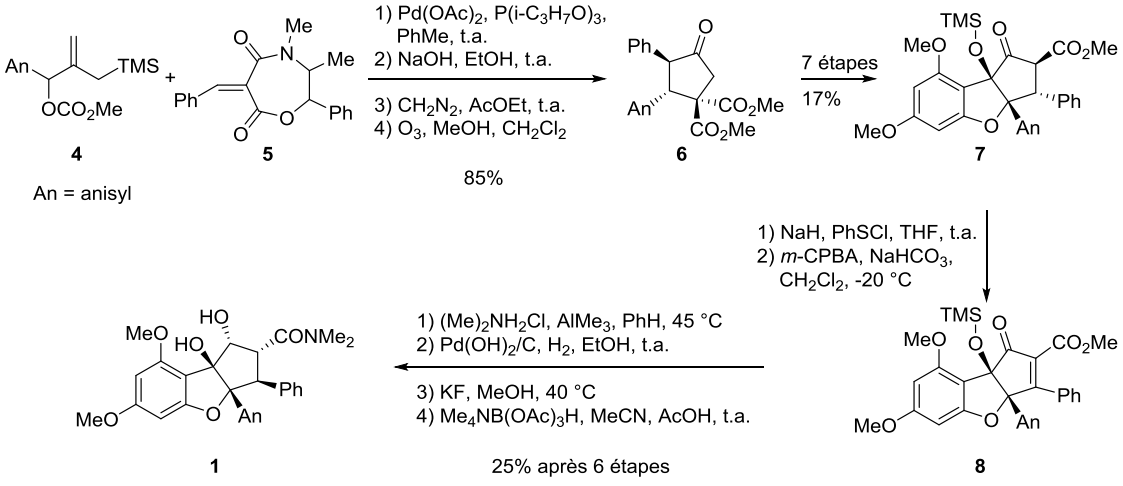

Schéma 1. Synthèse énantiospécifique de Trost.[22]

[22] Trost, B.M., Greenspan, P.D., Yang, B.V., Saulnier, M.G., *J. Am. Chem. Soc.* **1990**, *112*, 9022–9024.

1.3.2. Synthèse de rocaglamide avec une benzofuranone comme intermédiaire

Les stratégies développées par Taylor, Dobler, et Qin sont toutes basées sur un intermédiaire commun, la benzofuranone **9** qui est préparée par une addition de Michael intermoléculaire, puis transformée en squelette tricyclique par une cyclisation intramoléculaire (Schéma 2).

Cette approche a été originalement développée par Taylor et collaborateurs. Ils ont rapporté une synthèse basée sur une addition de Michael intermoléculaire associée à une cyclisation intramoléculaire induite par SmI_2, pour construire le squelette tricyclique de rocaglamide.[23] L'aldéhyde **10** a été préparé par addition de Michael du benzofurane **9** sur le cinnamaldéhyde trans, puis a été converti en cyclopentanone **13** via une cyclisation et une oxydation de Swern. Les trois étapes suivantes ont permis d'obtenir le β-cétoester **14** qui a été ensuite converti en

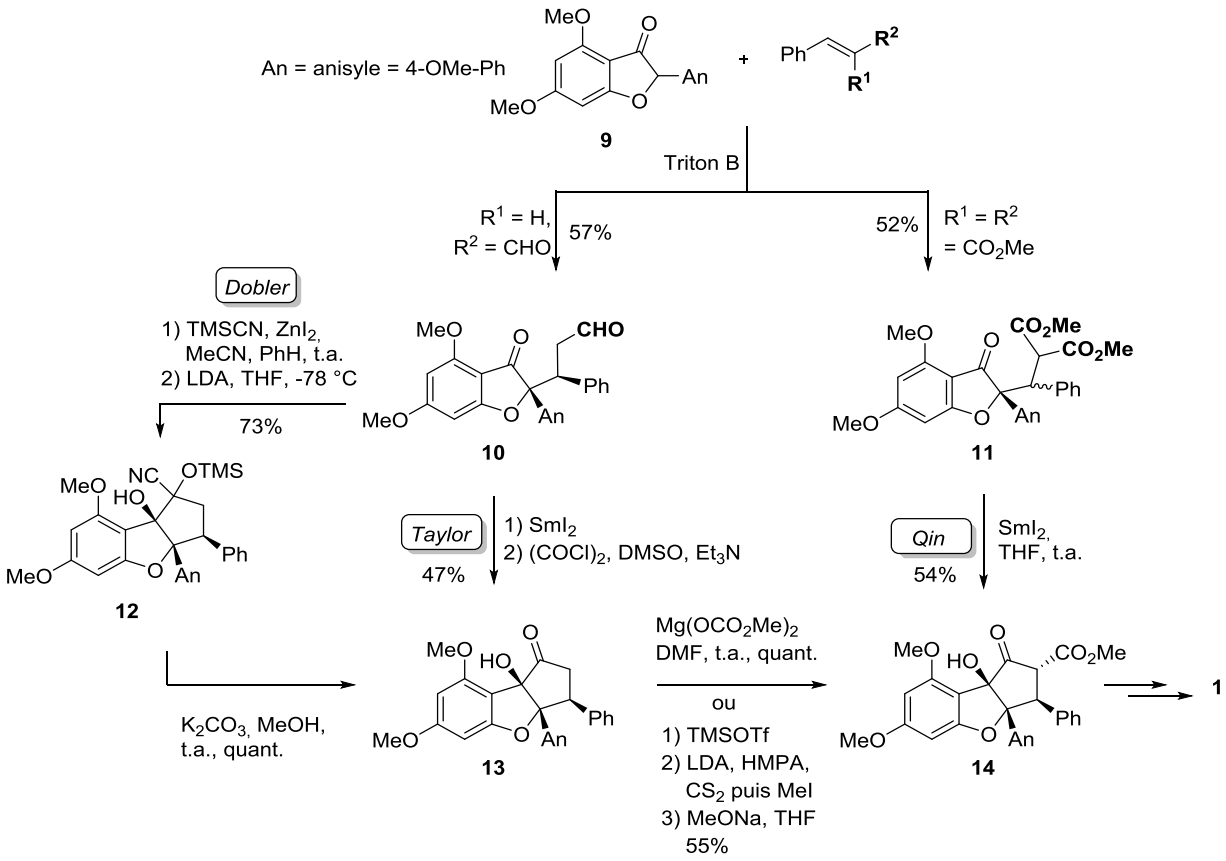

Schéma 2. Synthèse de rocaglamide de Taylor, Dobler et Qin.[24,25,26]

[23] Davey, A .E., Schaeffer, M. J., Taylor, R. J. K., *J. Chem. Soc., Chem. Commun.*, **1991**, 1137-1139 ; Davey, A. E., Schaeffer, M. J., Taylor, R. J. K., *J. Chem. Soc., Perkin Trans. 1,* **1992,** (20), 2657- 2666.

rocaglamide **1** en 2 étapes. Dobler et ses collègues ont ensuite amélioré cette synthèse. Ils ont utilisé le même type d'addition intermoléculaire pour former l'aldéhyde **10**, mais ont modifié l'étape de cyclisation. En effet, au lieu de la cyclisation catalysée par SmI_2, la cyanohydrine **12** a été utilisée dans une réaction umpolung pour générer la cyclopentanone **13** après déprotection. La carboxylation de la cétone a aussi été modifiée en utilisant le réactif de Stiles pour donner l'ester **14**. Ce dernier a ensuite été converti au rocaglamide **1** en 3 étapes.[24]

En 2008, Qin et ses collègues ont modifié l'approche de Taylor en introduisant d'un groupe méthoxycarbonyle sur l'accepteur de Michael. La carboxylation de Stiles n'est alors plus nécessaire. Une condensation de benzofuranone **9** avec le diméthyl 2-benxylidenemalonate a permis d'obtenir le composé **11**, qui a été ensuite engagé dans un couplage pinacolique initié par SmI_2 pour former le squelette du rocaglamide **14**.[25]

1.3.3. Synthèse du rocaglaol par le groupe de Ragot

En 2004, le groupe de Ragot a réalisé la synthèse de flavaglines basée sur une ouverture d'hydroxyépoxide (Schéma 3).[26] La cyclopentènone **17** a été obtenue en deux étapes à partir de la bromocétone **15** et l'ylure de triphénylphosphine **16**. Le β-cétoester a subit ensuite une décarbonylation, une α-bromination et une élimination de HBr pour donner l'énone α-bromé **18**. Ensuite une réaction de Suzuki avec l'acide boronique **19** a permis d'obtenir l'énone **20** qui a ensuite subit une réduction diastéréosélective par le *L*-sélectride, puis une époxydation et une ouverture d'époxyde pour former le didéméthoxyrocaglaol **22**.

[24] Dobler, M. R., Bruce, I., Cederbaum, F., Cooke, N. G., Diorazio, L. J., Hall, R. G., Irving, E., *Tetrahedron Lett.,* **2001,** *42* (47), 8281-8284.

[25] Li, H., Fu, B., Wang, M. A., Li, N., Liu, W. J., Xie, Z. Q., Ma, Y. Q., Qin, Z., *Eur. J. Org. Chem.,* **2008,** (10), 1753-1758.

[26] Diedrichs, N., Ragot, J. P., Thede, K., *Eur. J. Org. Chem.,* **2005,** (9), 1731-1735.

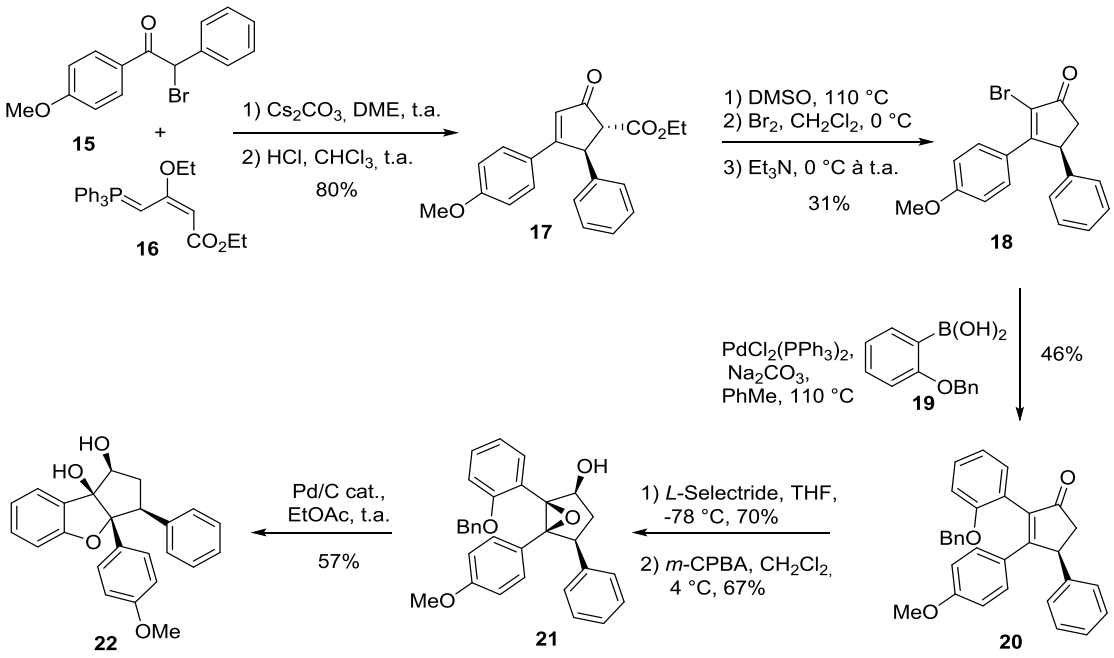

Schéma 3. Synthèse du rocaglaol de Ragot[26]

1.3.4. Synthèses des flavaglines par une réaction de Nazarov

Le groupe de Magnus est le premier à avoir synthétisé le squelette tricyclique des flavaglines en utilisant une cyclisation de Nazarov comme étape clée. Cette cyclisation est aussi connue comme la réaction d'Isler-Mukaiyama. Le composé **24** a été préparé à partir de l'alcyne **23**. Ensuite, une cyclisation de type Nazarov de **24** en présence de tétrachlorure d'étain a permis d'obtenir le composé **25**. Après hydrosilylation de ce dernier, l'ester méthylique a été introduit en présence de palladium et de monoxyde de carbone. Finalement, le composé **28** a été obtenu par formation d'un peroxyde de *tert*-butyle en présence de Darco G-60 qui est ensuite réduit par un amalgame d'aluminium et de mercure (Schéma 4).[27]

[27] Magnus, P., Stent, M. A. H., *Org. Lett.,* **2005,** *7* (18), 3853-3855.

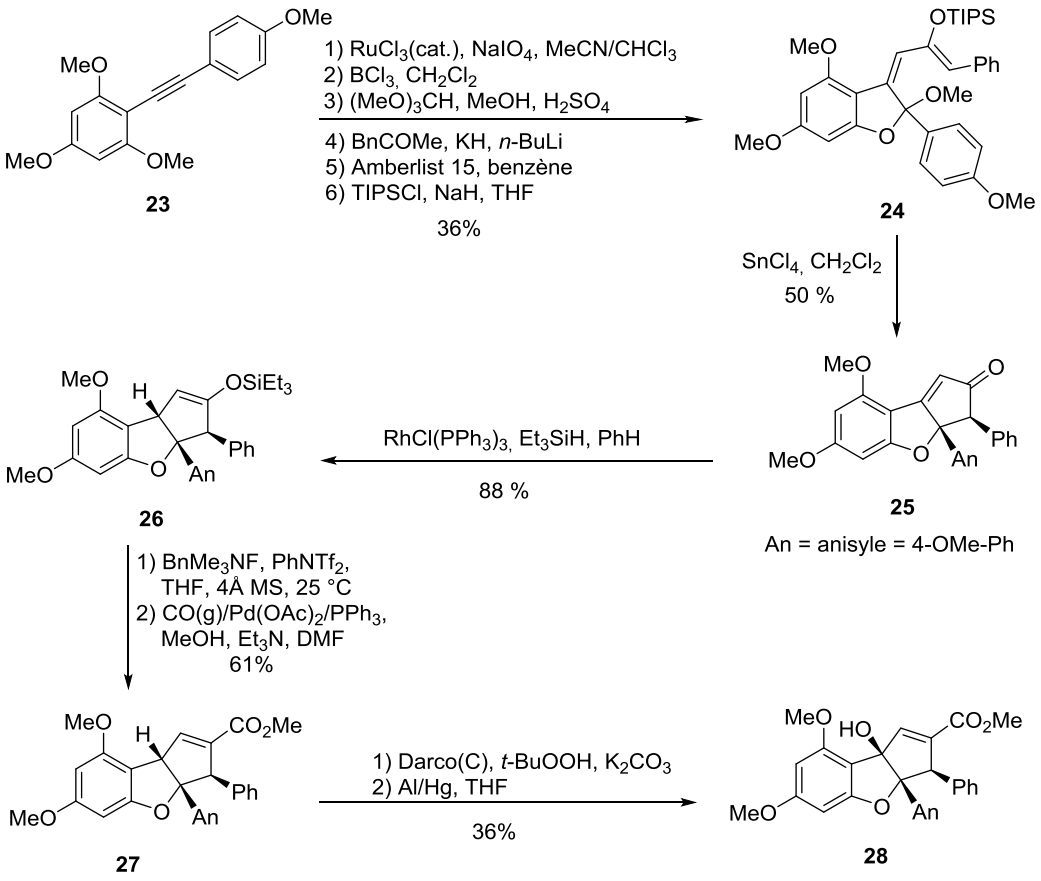

Schéma 4. Synthèse du (±)-1,2-anhydro-rocaglamide par Magnus.[27]

Cette approche n'a pas abouti au rocaglamide, mais de (±)-1,2-anhydro-rocaglamide **28**. En 2009, cette stratégie a été améliorée en utilisant une réaction de Nazarov induite par du bromure d'acétyle (Schéma 5).[28] Tout d'abord, l'iodophénol **29** a été engagé dans un couplage de Kumada/Sonogashira, suivi par une insertion de CO pour donner le composé **30**. L'ester a été d'abord converti en phosphonate pour réagir avec le benzaldéhyde dans les conditions de Masamune-Roush pour fournir le composé **31**. L'étape suivante est la réaction clé : la cyclisation de Nazarov. D'abord, le dièneone **31** est traité par divers acides de Lewis, y compris $SnCl_4$, $AlCl_3$, $TiCl_4$ and $Sc(OTf)_3$. Tous les essais ont donné le produit de réaction de rétro Friedel-Crafts. Ensuite, ils ont examiné des acides Bronsted. L'utilisation d'HCl concentré a donné la cyclopentènone désirée après 48h à 100°C mais avec un rendement faible (12%), et l'utilisation d'HBr n'a conduit qu'à une

[28]Magnus, P.,Freund, W. A., Moorhead, E. J., Rainey, T., *J.Am. Chem. Soc.,* **2012,** *134* (14), 6140-6142.

déméthylation de l'éther. Finalement, en présence du bromure d'acétyle, la cyclopentènone **34** a été obtenue avec un bon rendement (81%). Le remplacement de ce dernier par un chlorure d'acétyle n'a donné que le produit de départ inchangé même après chauffage à 150°C dans un tube scellé.

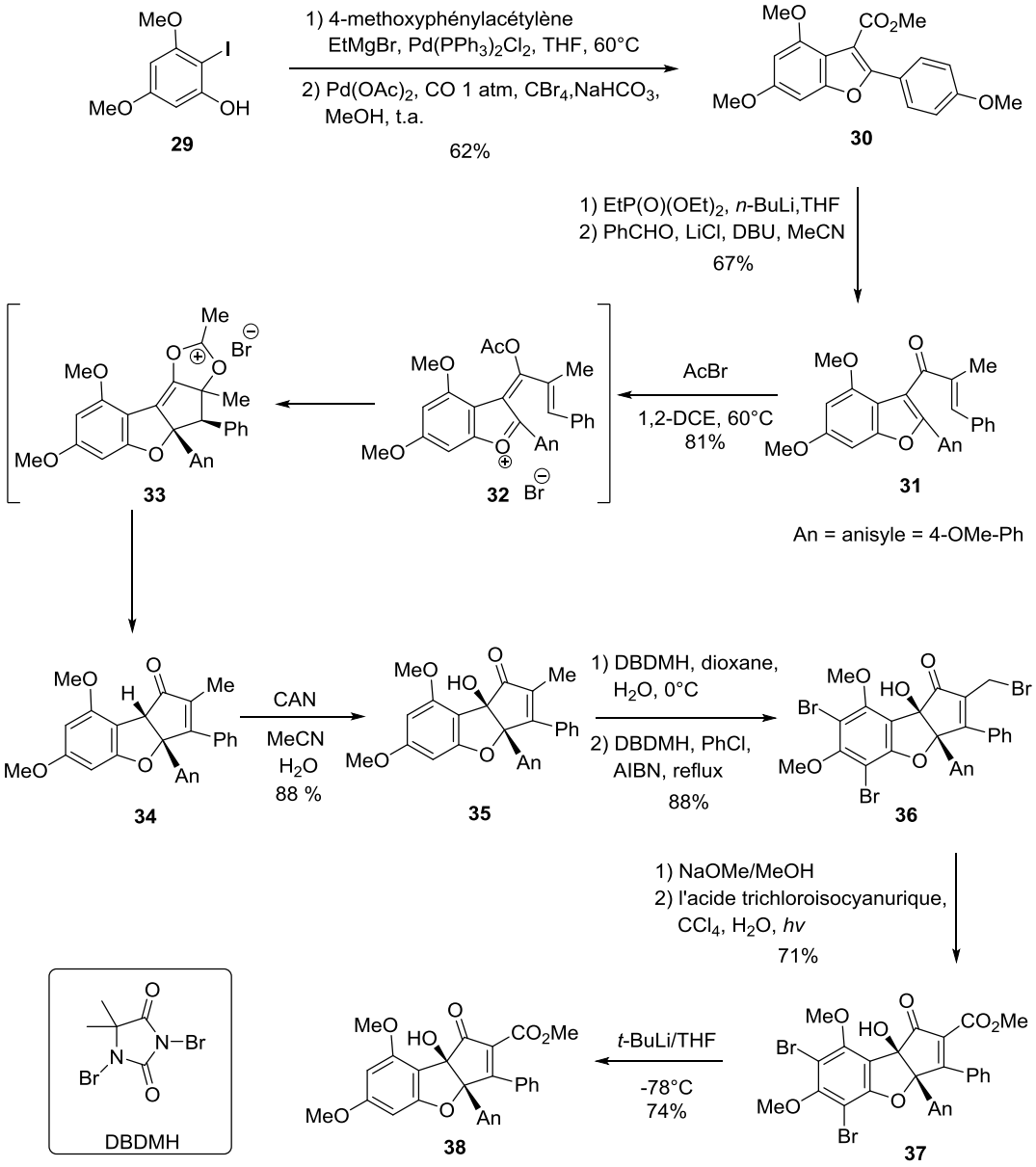

Schéma 5. Synthèse du rocaglate du méthyle de Magnus utilisant une réaction de Nazarov induite par du bromure d'acétyle.[28]

Ces auteurs ont proposé un mécanisme pour cette cyclisation : un oxonium **32** est obtenu après l'acétylation de la cétone **31**, celui-ci cyclise ensuite pour donner un acétoxonium **33** qui permet d'obtenir la cyclopentènone **34** après hydrolyse. Il est à

noter que le remplacement du groupe méthyle vinylique par un hydrogène diminue le rendement à 12%, et le produit cyclisé n'est pas observé lorsqu'il s'agit d'un nitrile. La cétone **34** a été ensuite transformée en déhydroflavagline **38** en 6 étapes avec un rendement de 41%. Seulement deux étapes supplémentaires sont nécessaires pour aboutir au rocaglate de méthyle.

En 2009, Frontier et coll. ont publié une synthèse de flavaglines qui utilise également une réaction de type Nazarov dans l'étape clé (Schéma 6).[29] Le produit de départ est la benzofuranone **9** qui a été convertie en aldéhyde **39** par alkylation en présence de bromure de vinylmagnésium, puis par clivage de l'alcool allylique ainsi obtenu. Après introduction du groupement phénylacétylène et protection de l'alcool propargylique, le composé **40** a été déprotoné par du *tert*-butyllithium et additionné à du chlorure de tributylétain pour donner l'intermédiaire **41**. Le squelette tricyclique des flavaglines a été ensuite obtenu par une cyclisation intramoléculaire de type Nazarov entre l'oxyde d'allène généré *in situ* par réaction avec du *m*-CPBA. Les étapes suivantes comprenant une carbonylation catalysée au paladium permettent d'aboutir au cétoester **14**, qui a été ensuite converti en rocaglamide **1**. Tout comme la stratégie initiale de Magnus, cette voie de synthèse utilise une réaction de Nazarov comme une approche directe et originale pour construire le squelette des flavaglines.

[29] Malona, J. A., Cariou, K., Frontier, A. J., *J. Am. Chem. Soc.,* **2009,** *131* (22), 7560-7561.

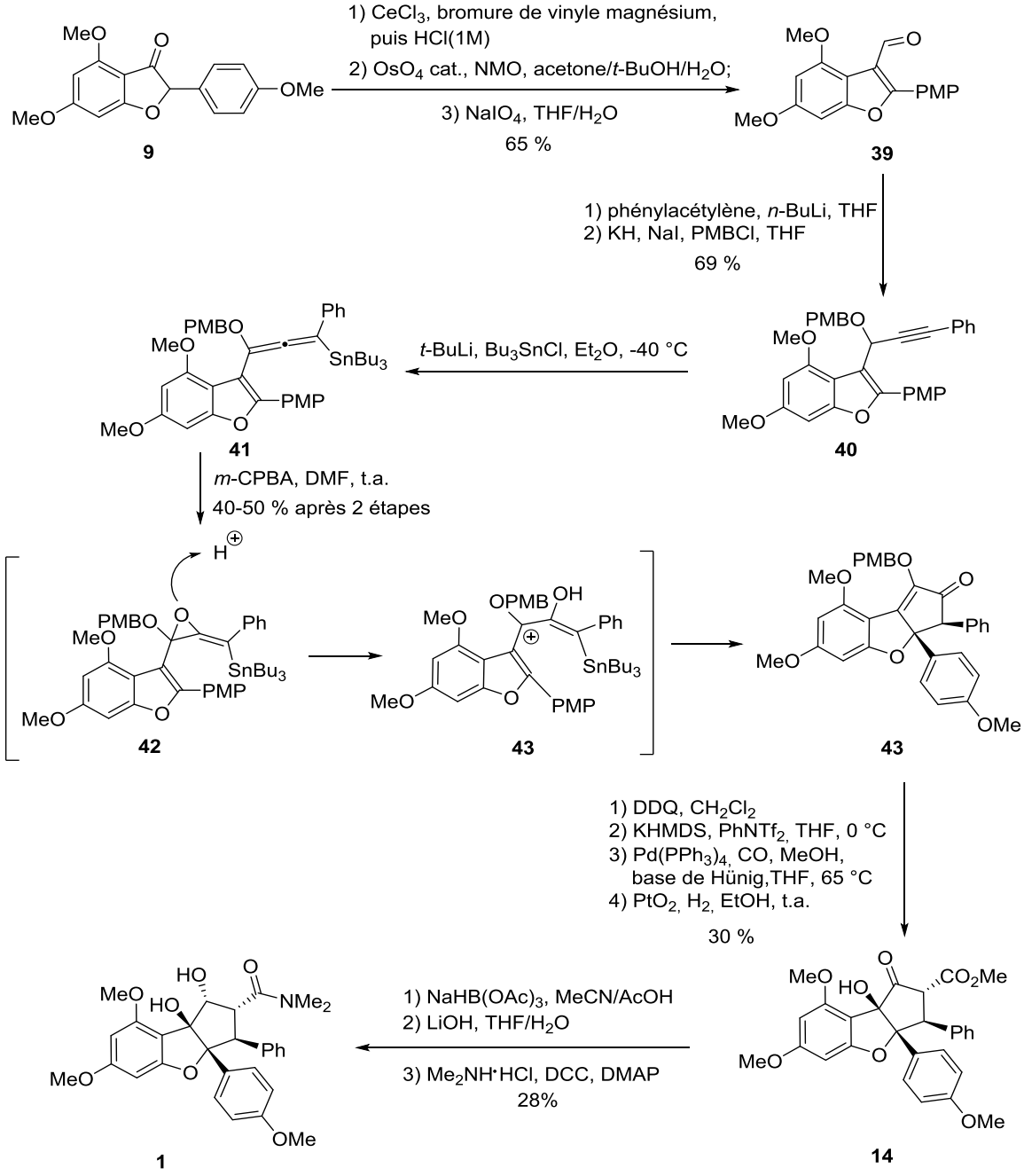

Schéma 6. Synthèse du rocaglamide de Frontier.[29]

2. OBJECTIFS

2. Objectifs

Notre objectif principal était de développer une nouvelle voie de synthèse de flavaglines, pour synthétiser des composés originaux ayant potentiellement de meilleures activités biologiques. Un deuxième objectif consistait à synthétiser deux isostères de flavaglines, FL47 et FL48 (Figure 7), pour lesquelles l'hydroxyle en position 8b a été remplacé par un formamide ou un sulfonamide, donneurs de liaison hydrogène.

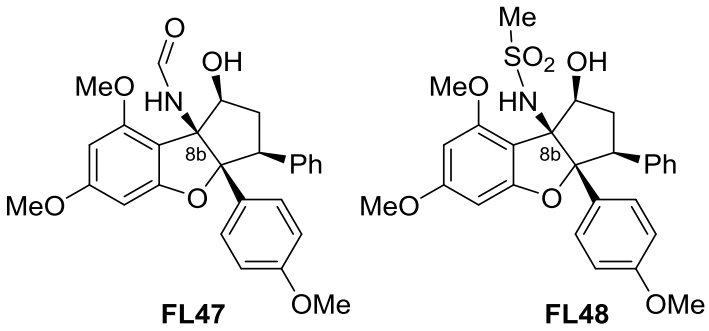

Figure 7. Isostères des flavaglines à synthétiser

3. RESULTATS

3. Résultats

Afin d'accéder au squelette cyclopenta[*b*]benzofurane des flavaglines, plusieurs approches ont été examinées.

3.1. Première approche pour la synthèse des flavaglines

3.1.1. Etude rétrosynthétique

Pour synthétiser les flavaglines, une nouvelle voie de synthèse est proposée basée sur la construction d'un intermédiaire clé **44**. Le rocaglaol **2** peut être synthétisé à partir de la cyclopentènone **44** en utilisant la méthode de Ragot qui a été décrite dans la partie 1.3.3. Cette cyclopentènone peut être synthétisée par un réarrangement allylique suivi par une cyclisation catalysée à l'or à partir de l'alcool propargylique **45**. Ce dernier peut être obtenu par une condensation avec du triméthoxybenzène lithié à partir du composé **46** qui peut être préparé par une acylation suivie par un couplage de Sonogashira à partir de l'acide **47**. Cet acide peut être formé par une réaction de Perkin à partir de l'acide carboxylique **48** et du benzaldéhyde. Cette partie des travaux a été effectuée conjointement avec Christine Basmadjian qui était aussi doctorante au laboratoire et a été décrite dans la publication N°3.[30]

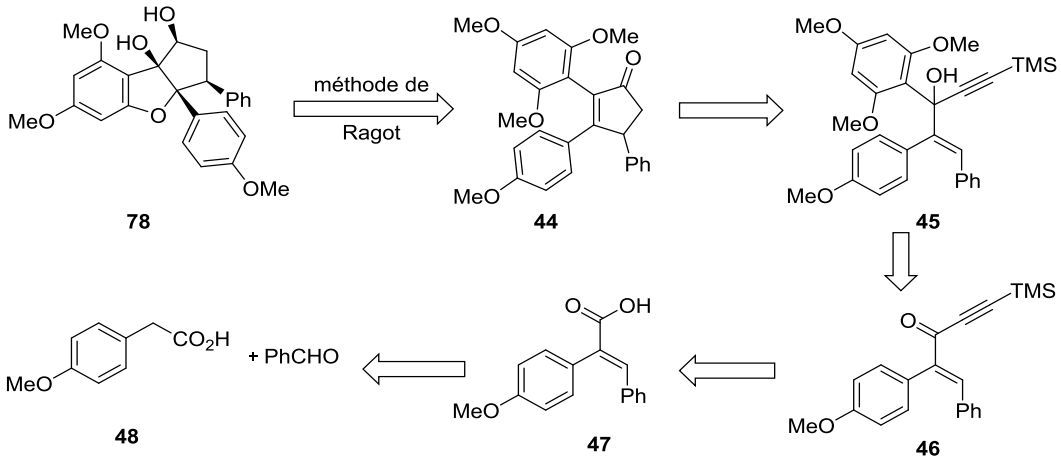

Schéma 7. Etude rétrosynthétique pour la préparation du rocaglaol **78.**

[30] Basmadjian C., Zhao Q., Désaubry L., *Tetrahedron lett,.* **2015**, 56, 727–730.

3.1.2. Synthèse de l'intermédiaire cyclopentènone 44

Tout d'abord, une réaction de Perkin a permis de former stéréosélectivement l'acide **47** qui a été ensuite transformé en chlorure d'acyle. Ce dernier a été engagé dans un couplage de Sonogashira pour obtenir le composé **46**. Enfin, l'alkylation avec du triméthoxybenzène lithié a conduit à l'alcool propargylique **45**.

Une étherification catalysée au molybdène (VI), en présence de NH_4PF_6 et d'EtOH, a permis de transformer le carbinol **45** en éther **49**.[31] Celui-ci a été ensuite engagé dans une désilylation pour donner le composé **50**.

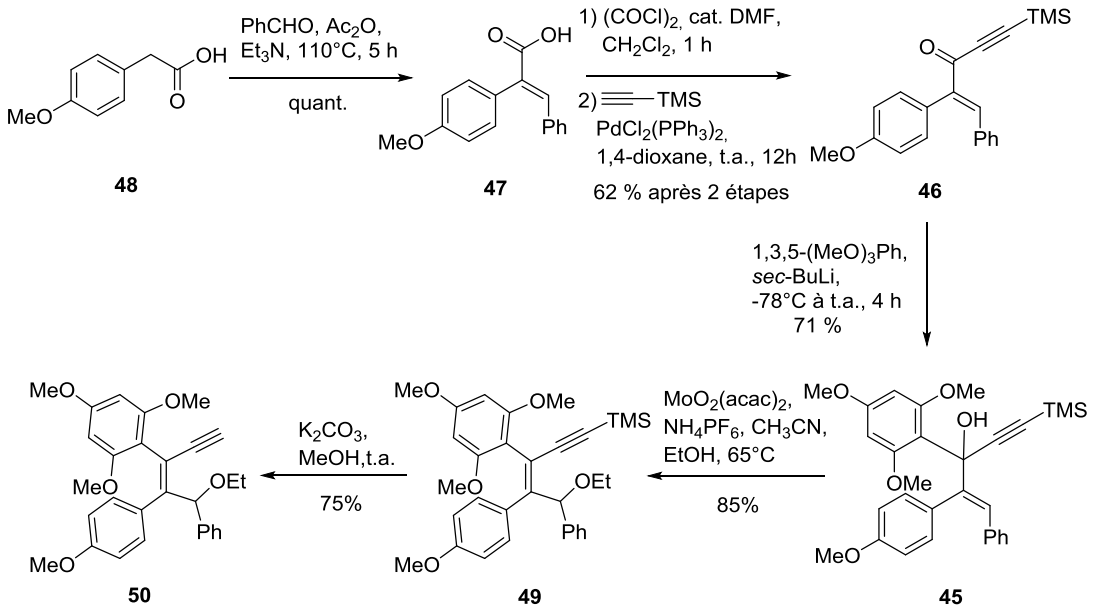

Schéma 8. Synthèse du précurseur de la cyclopenténone.[31]

3.1.3. Cyclisation catalysée à l'or (I)

Rhee et *al.* ont synthétisé la cyclopentènone **55** à partir du siloxypent-3-ène-1-ynes **51** en utilisant une cyclisation catalysée à l'or (I) (Schéma 9).[32] Ils ont proposé qu'en présence d'un complexe électrophile de l'or, une siloxycyclisation a conduit à l'intermédiaire **52**. Le carbocation **53** a été ensuite

[31] Yang, H., Fang, L., Zhang, M., Zhu, C., *Eur. J. Org. Chem.*, **2009**, 666-672.

[32] An, S. E., Jeong, J., Baskar, B., Lee, J., Seo, J., Rhee, Y. H., *Chem. Eur. J.*, **2009**, *15*, 11837-11841.

obtenu par une rupture de la liaison C-O. Une carbocyclisation intramoléculaire suivie par l'élimination de l'or (I) a donné l'intermédiaire **54** qui a été ensuite transformé en cyclopentènone **55** à l'aide de l'isopropanol.

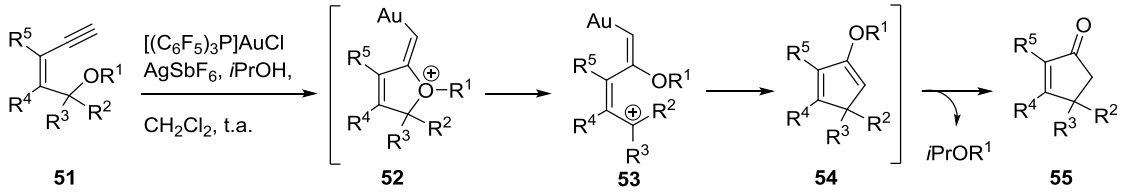

Travaux de Rhee *et al.*: R^1 = $SiEt_3$, R^2, R^3 ≠ H
Notre travail : R^1= Et, R^2= Ph, R^3 = H

Schéma 9. Méthode de cyclisation catalysé à l'or (I) développée par Rhee *et al.*[33]

Nous avons considéré que le groupe phényle et le groupe triméthoxyphényle du composé **50** peuvent suffisamment stabiliser le carbocation **53** pour permettre à cette réaction d'avoir lieu. Cette hypothèse a été supportée par le travail de Toste *et al.* sur la synthèse de l'éther d'indènyle à partir d'un éther benzylique en utilisant une carboalkoxylation catalysée à l'or.[33]

A partir du composé **50**, dans la condition décrite par Rhee *et al.*, la cyclopentènone **44** a été obtenue avec 63% de rendement (Schéma 3).

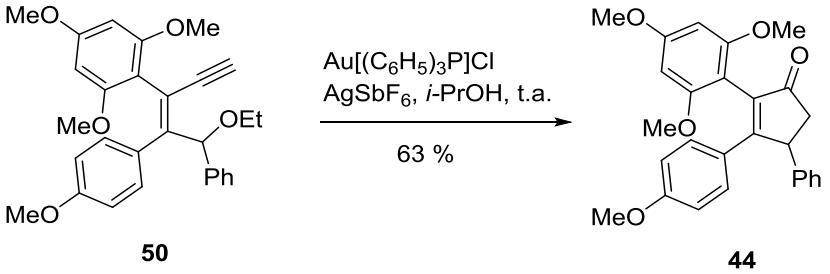

Schéma 10. Synthèse de la cyclopentènone **44**.

Nous avons ensuite essayé de synthétiser deux autres cyclopentènones (Schéma 11). Les substrats **58a** et **58b** ont été préparés à partir du chlorure d'acyle **56** qui a été engagé successivement dans un couplage de Suzuki, une éthynylation, une éthérification catalysée au molybdène (VI) et une désilylation. L'éther **58a**, substitué

[33] Dubé, P., Toste, D., *J. Am. Chem. Soc.,* **2006**, *128*, 12062–12063.

par un phényle (R = H), a été ensuite transformé en cyclopentènone **59a** avec 50% de rendement, dans les conditions de cyclisation précédentes. Nous avons noté de manière intéressante, que l'introduction d'un atome de chlore en position para du phényle améliore le rendement de 50% à 75%.

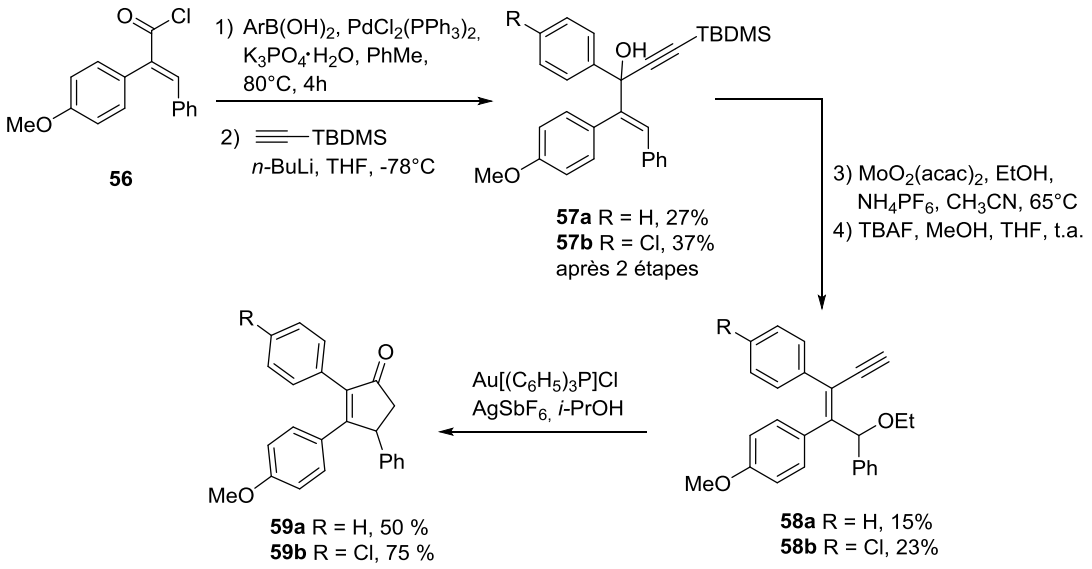

Schéma 11 : Synthèse des cyclopentènones **59a** et **59b**

3.1.4. Essais de transformation de la cyclopentènone aux flavaglines

A partir de la cyclopentènone **44**, une déprotection sélective du groupe méthoxy a permis d'obtenir l'ènone **60** qui a été ensuite réduite en l'alcool **61** (Schéma 12). Mais la synthèse du précurseur de flavagline **62** n'a pas abouti même si diverse méthodes ont été essayé pour activer cet alcool allylique, ces échecs sont probablement dus à la tension du cycle et à l'instabilité de l'intermédiaire carbocation.

Le groupe phénol du composé **60** a été ensuite protégé par un groupe 2-naphtylméthyle (NAP) pour donner une paire d'atropoisomères. Le NAP a été choisi parce que la déprotection peut être effectuée beaucoup plus facilement et rapidement que celle d'un benzyle par hydrogénation.[34] Une réduction en

[34] Gaunt, M. J., Yu, J., Spencer, J.B., *J. Org. Chem.*, **1998**, *63* (13), 4172–4173.

présence du *L*-sélectride a permis d'obtenir l'alcool **63**, mais l'époxydation de ce dernier n'a pas abouti bien qu'une quinzaine de conditions aient été essayées (*t*-BuOOH ; $Ti(OiPr)_4$; $VO(acac)_2$; *m*-CPBA ; H_2O_2 ; NaOH ; ...). Ce résultat suggère que la méthode de Ragot est limitée à la préparation des flavaglines ne possédant pas les substituants nécessaires pour l'activité pharmacologique.

Malheureusement aucune de ces méthodes n'a donné les produits désirés, nous conduisant ainsi à exploiter une nouvelle voie de synthèse des flavaglines.

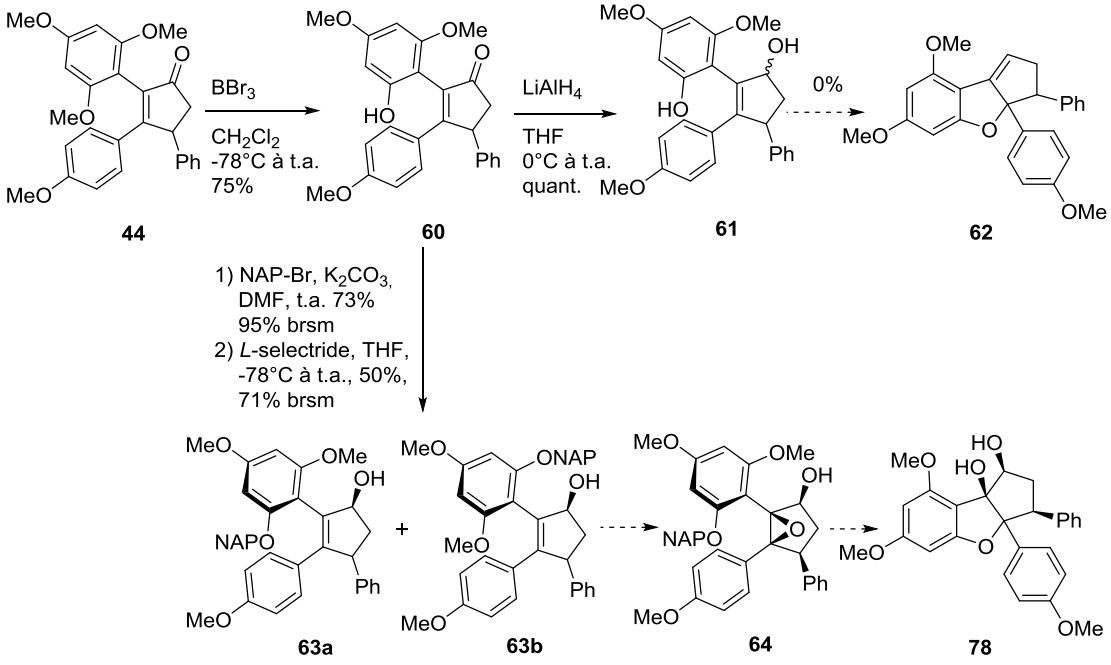

Schéma 12 : Essais pour synthétiser le rocaglaol **78** à partir de la cyclopentènone **44.**

3.2. Deuxième approche pour la synthèse des flavaglines basée sur une réaction de Nazarov

Nous nous sommes alors inspirés des travaux de Magnus dont l'étape clée repose sur une réaction de Nazarov.[35] Cette réaction met en jeu une électrocyclisation-4π conrotatoire du cation 1,4-pentadiènyle, lui-même formé à partir d'une ènone (Schéma 13).[36]

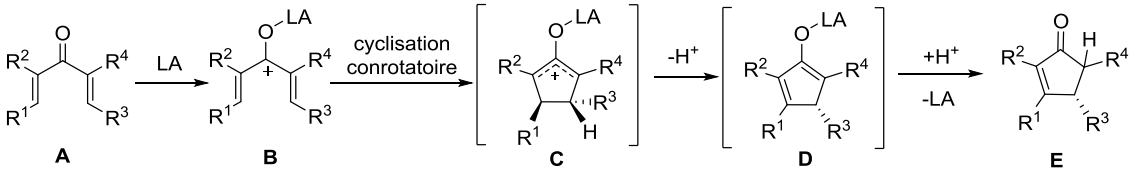

Schéma 13. Mécanisme de la réaction de Nazarov.

Dans les travaux de Magnus, le bromure d'acétyle a été utilisé pour activer la cétone (Schéma 14). Le mécanisme implique une acylation du carbonyle, suivi d'une cyclisation du cation allylique. Ce carbocation est stabilisé par les groupements voisins. L'énolate est formé après la perte d'un proton, qui est hydrolysé ensuite pour donner la cyclopentènone.

Les travaux de Cavalli[37] ont montré que l'introduction d'un groupement thioéther en position α du groupement carbonyle peut induire une meilleure réactivité et ainsi favoriser la cyclisation. En effet, le soufre stabilise davantage la charge positive du carbocation de l'état de transition. L'autre avantage du thioéther est qu'il peut être transformé en différents groupements fonctionnels.

[35] Magnus, P., Freund, W.A., Moorhead, E.J., Rainey, T., *J. Am. Chem. Soc*., **2012,** *134*, 6140−6142.

[36] Vaidya, T., Eisenberg, R., Frontier, A.J., *ChemCatChem*., **2011**, *3*, 1531-1548.

[37] Cavalli, A., Pacetti, A., Recanatini, M., Prandi, C., Sarpi, D., Occhiano, E.G., *Chem. Eur. J.,* **2008**, *14*, 9292–9304.

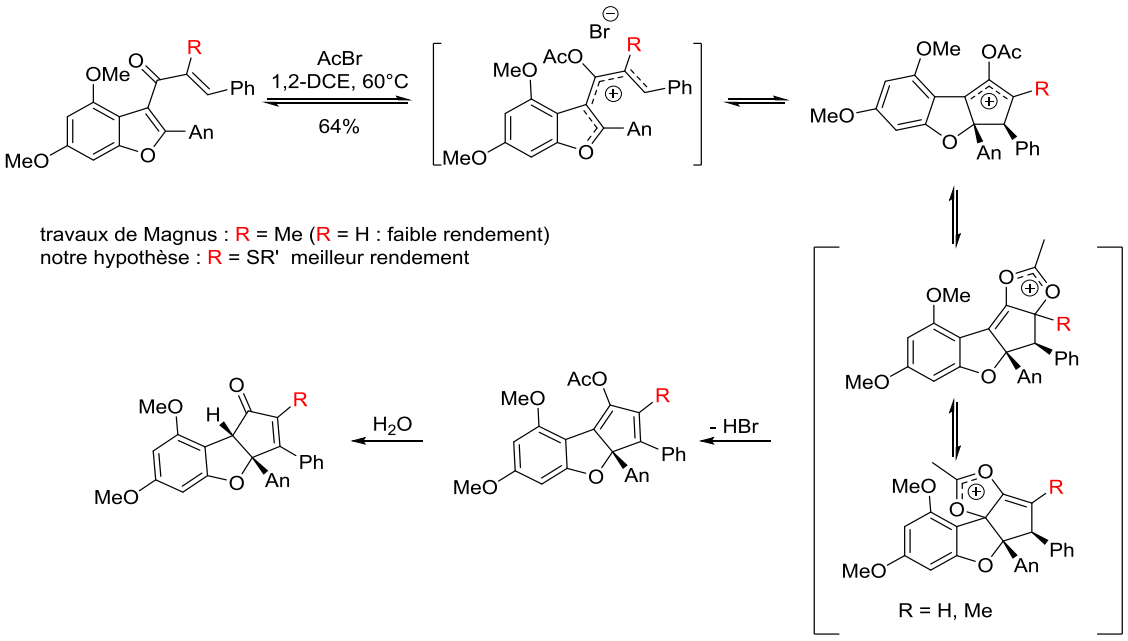

Schéma 14. Etape clé de la synthèse du rocaglate de méthyle et hypothèse de travail.[35]

Dans un premier temps, nous avons cherché à tester notre hypothèse en essayant de synthétiser la cyclopentènone **65**. Les précurseurs **66** puissent être préparée à partir de la benzofurane **67**, synthétisée à partir des produits commerciaux le **68** et le **69** (Schéma 15).

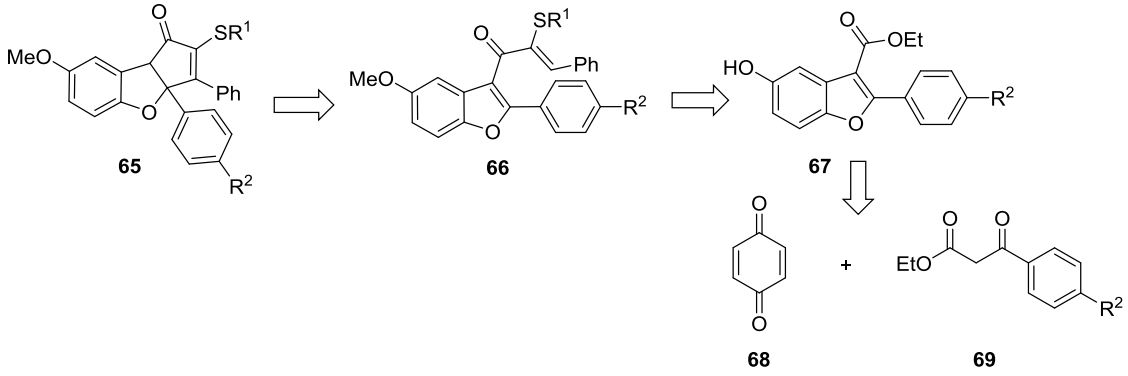

Schéma 15. Rétro-synthèse pour accéder à la cyclopentènone **65**.

Tout d'abord, une cycloaddition de l'oxopropionate **69** sur la benzoquinone **68** a permis d'obtenir les benzofuranes **67a** et **67b** selon la procédure décrite par Chan.[38] Après méthylation par l'iodométhane, une réduction de l'ester **70b** en aldéhyde **72b** par du DIBAL-H a été entreprise. Cette étape ne donnant qu'une dégradation, les esters **70a** et **70b** ont d'abord été réduits par $LiAlH_4$ en alcools **71a** et **71b**. Les essais d'oxydation par MnO_2 n'ayant que donné les produits de départ inchangés, les alcools ont été oxydés dans la condition de Swern pour obtenir les aldéhydes **72a** et **72b**.

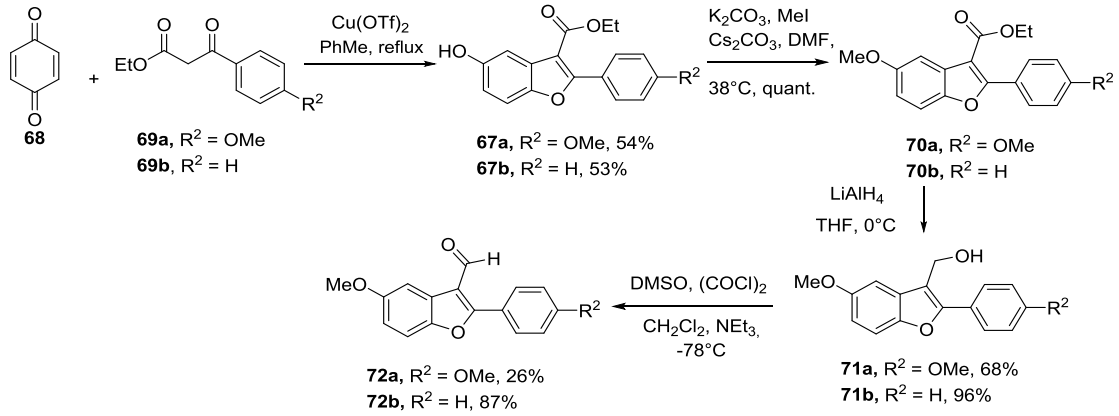

Schéma 16 : Synthèse des aldéhydes **72a** et **72b**.

Pour obtenir le précurseur de la cyclisation de Nazarov, nous avons préparé des thioéthers vinyliques comme décrit dans le schéma 17. A partir de phénylacétylène, le thioéther **73a** a été synthétisé par la méthode d'Oshima[39] en présence du TEMPO et de *n*-propanethiol. De même le thioéther **73b** a été préparé sélectivement à partir du 4-méthylthiophénol en présence d'éthylate de sodium.

[38] Mothe, S. R., Susanti, D., Chan, P. W. H., *Tetrahedron Lett.,* **2010**, *51* (16), 2136-2140.

[39] Kondoh, A., Takami , K., Yorimitsu, H., Oshima, K., *J. Org. Chem.,* **2005**, *70*, 6468–6473.

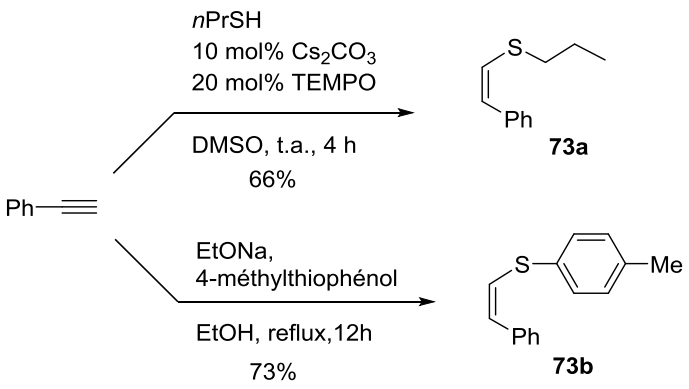

Schéma 17 : Synthèse des thioéthers **73a** et **73b**.

Les thioéthers ont été ensuite traités par du *n*-BuLi et additionné sur les aldéhydes **72a** et **72b** préalablement activé par du $BF_3{\cdot}Et_2O$ pour renforcer caractère électrophile (Scéma 18). Il est important de noter qu'un excès de thioéther est nécessaire à la réaction. Les substrats **74a**, **74b**, et **74c** ont ainsi été obtenus. L'oxydation des alcools divinyliques obtenus par MnO_2 a permis d'obtenir les précurseurs de la réaction de Nazarov **66a**, **66b** et **66c**.

Après obtention des ènones **66**, diverses conditions ont été testées pour la cyclisation de Nazarov. La cyclopentenone **65** a été seulement formée lorsque R^1 = *n*-Pr. Le meilleur rendement (31%) a été obtenu en présence de 1,5 équivalent de bromure d'acétyle. Cependant, la réaction est difficilement reproductible. Dans d'autres essais, les rendements n'étaient que de 14% et 13%.

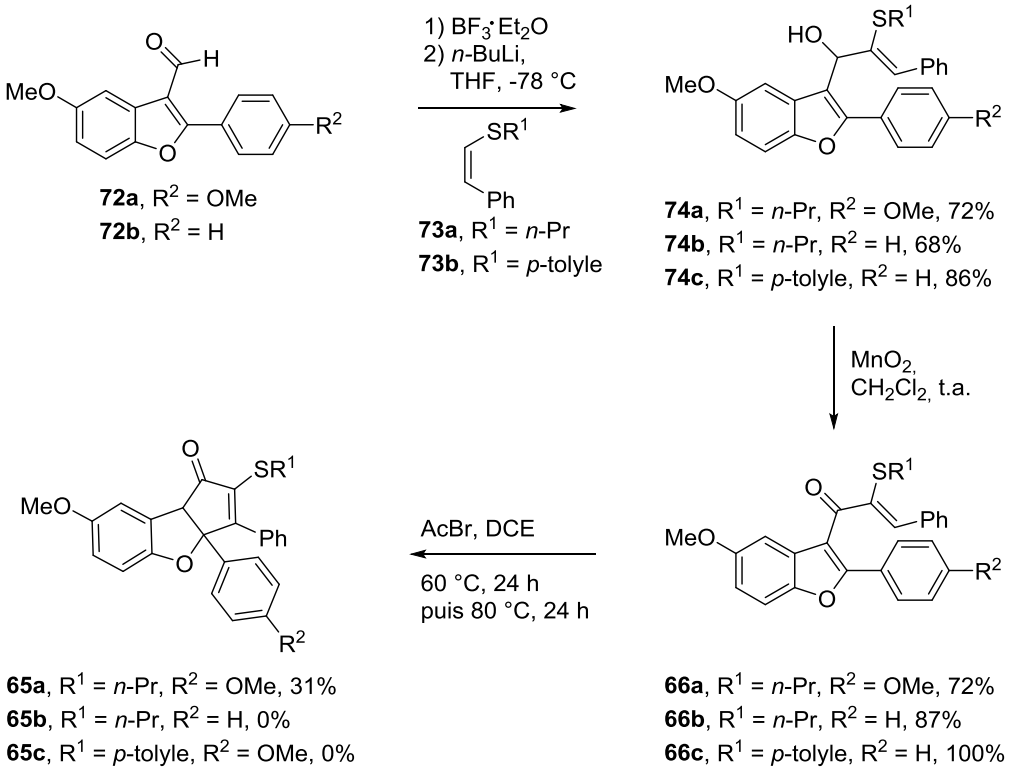

Schéma 18. Synthèse des cyclopentènones **65**.

Ne jugeant pas les substrats **66** suffisamment réactifs lors des essais de la réaction de Nazarov, nous avons décidé de synthétiser une autre ènone **75** qui devait présenter une meilleure réactivité (Figure 8). Pour obtenir ce composé, une voie de synthèse différente a été envisagée pour accéder au squelette benzofurane.

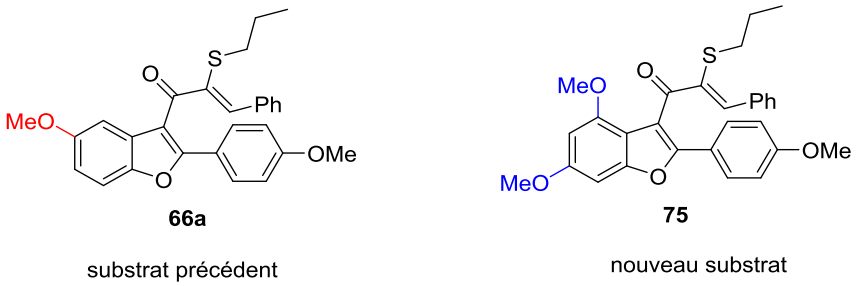

Figure 8. Nouveau substrat **75** pour la réaction de Nazarov.

En vue de l'obtention de ce composé, le benzofurane **30** a été préparé selon l'approche de Magnus et ses collaborateurs[7] (Schéma 19). La première étape a été

une iodation en position ortho du diméthoxyphénol. Le rendement de cette réaction est modéré (29%) en raison d'une compétition avec l'iodation en position para et la di-substitution. Le produit iodé a été ensuite engagé dans un couplage de Kumada/Sonogashira pour donner le composé **76** qui est alors cyclisé en présence du catalyseur au palladium sous atmosphère de CO. Le benzofurane **30** a été ainsi obtenu avec un rendement de 72%.

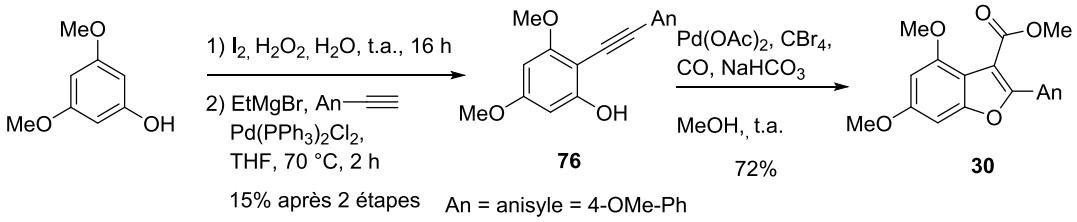

Schéma 19. Synthèse du benzofurane **30**.

Le rendement des premières étapes de la synthèse étant modéré, nous avons tenté de trouver une méthode plus efficace basée sur les travaux de Larock[40] (Schéma 10). Cette fois l'iodation de triméthoxybenzène a été effectuée avec un rendement de 94%. Cette amélioration repose sur la symétrie du produit de départ qui résout le problème de régiosélectivité. Le couplage de Sonogashira avec le 4-méthoxyphénylacétylène nous a donné l'alcyne **23** avec un rendement de 70%. La cyclisation catalysée au mercure n'a pas permis d'obtenir le produit désiré **30**, mais la cétone **77** qui résulte d'une hydratation de l'alcyne.

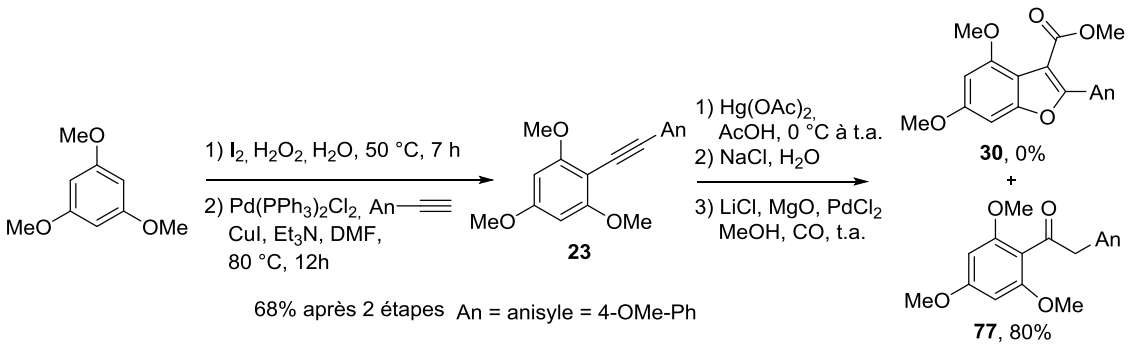

Schéma 20. Essais pour synthétiser le benzofurane **30**.

[40] Larock, R. C., Harrison, L. W., *J. Am. Chem. Soc.*, **1984**, *106* (15), 4218-4227.

A cause du problème de reproductibilité pour préparer la cyclopentènone **65** et l'inaccèssibilité du précurseur de la cyclopentènone **75**, il nous a semblé plus pertinent de chercher une nouvelle voie de synthèse des flavaglines.

3.3. Nouvelle approche pour la synthèse des flavaglines basée sur une sélénocyclisation *5-endo-trig*

3.3.1. Etude rétrosynthétique

Les réactions de sélénocyclisation représentent une approche performante pour la synthèse d'hétérocycles oxygénérés complexes.[41] Ce processus implique la formation d'un ion séléniranium qui sera capturé par le nucléophile pour former le produit cyclisé (Schéma 21).

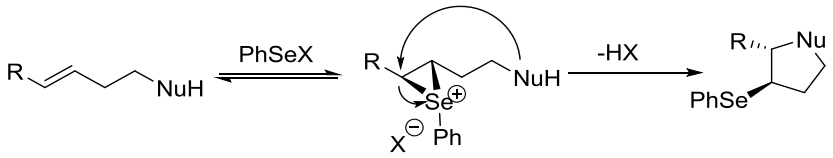

Schéma 21. Processus de sélénocyclisation.

Un des intérêts de cette reaction est qu'elle peut parfois s'effectuer en opposition aux règles de Baldwin.[42] En 2006, Denmark *et al.*[43] ont publié une sélénocyclisation de type *5-endo-trig* d'un acide β,γ-insaturé, en présence de chlorure de benzènesélénenyle et d'une base. Par ailleurs, He *et al.*[44] ont réalisé en 2014 une synthèse de furan-2(*5H*)-one par une cyclisation de type *5-endo-trig* en utilisant une résine de bromure de sélényle (Schéma 22).

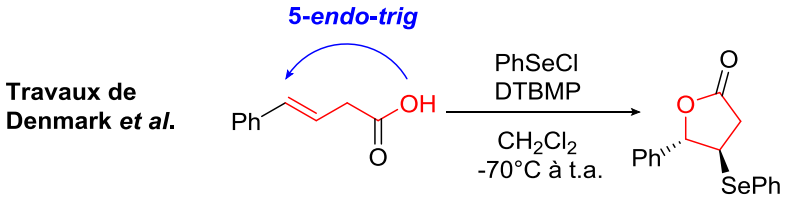

Schéma 22. Exemples de sélénocyclisations *5-endo-trig.*

En se basant sur leurs travaux, nous avons envisagé la synthèse des flavaglines

[41] Nicolaou, K.C., *Tetrahedron*, **1981**, *37*, 4097-4109.

[42] Johnson, C.D., *Acc. Chem. Res.*, **1993**, *26*, 476-482.

[43] Denmark, S.E., Edwards, M.G., *J. Org. Chem.,* **2006**, *71*, 7293-7306.

[44] He, R.J., Zhu, B.C., Wang, Y.G., *Appl. Organomet. Chem.,* **2014**, *28*, 523-528.

en utilisant une sélénocyclisation comme étape clée. L'analyse rétrosynthétique initiale est représentée dans le Schéma 23. La fonction diol de **78** peut être introduite par une dihydroxylation de la double liaison du composé **79**. Cette insaturation est formée par une élimination du sélénium du composé **80**, et ce dernier est obtenu par une sélénocyclisation de type *5-endo-trig* sur le composé **81** qui est formé par une condensation entre le diméthoxyphénol **83** et la cyclopentanone **82**.

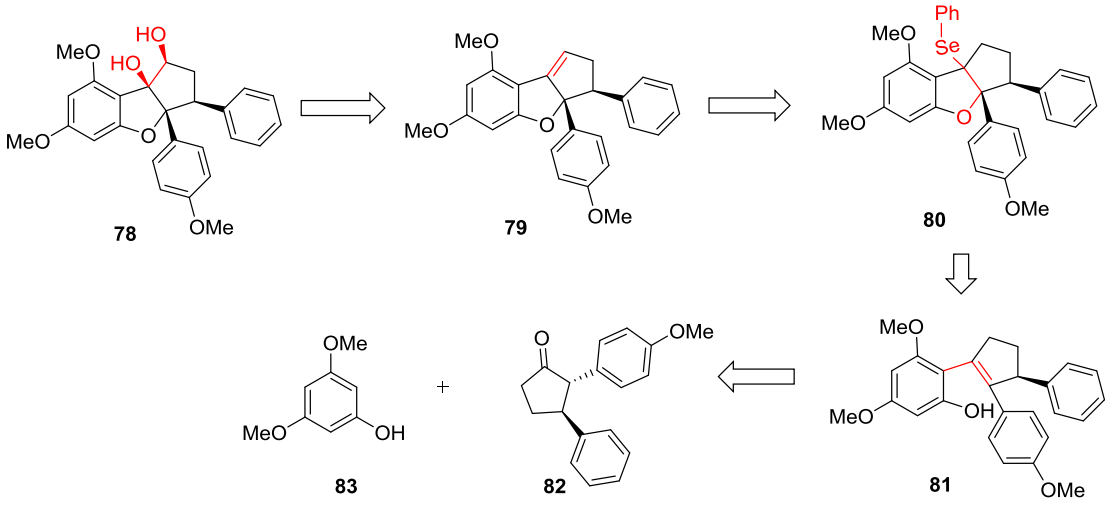

Schéma 23. Première analyse rétrosynthétique.

3.3.2. Modèle de réaction et découverte de la cyclisation spontanée

Pour tester la faisabilité de cette stratégie, nous avons d'abord examiné les condensations du 3,5-diméthoxyphénol sur la 2-phényl-cyclohexanone **84** commerciale, dans les conditions décrites par Trost dans la synthèse du rocaglamide.[45]

De manière intéressante, au lieu d'obtenir le produit de condensation, la réaction avec le composé **84** a nous donné un produit cyclisé **86** avec un rendement de 69%. Nous supposons que cette cyclisation spontanée fait intervenir la carbocation benzylique **85** (Schéma 24). La structure du composé **86** a été vérifiée par cristallographie RX (Figure 9).

[45] Trost, B.M., Greenspan, P.D., Yang, B.V., Saulnier, M.G., *J. Am. Chem. Soc.,* **1990**, *112*, 9022-9024.

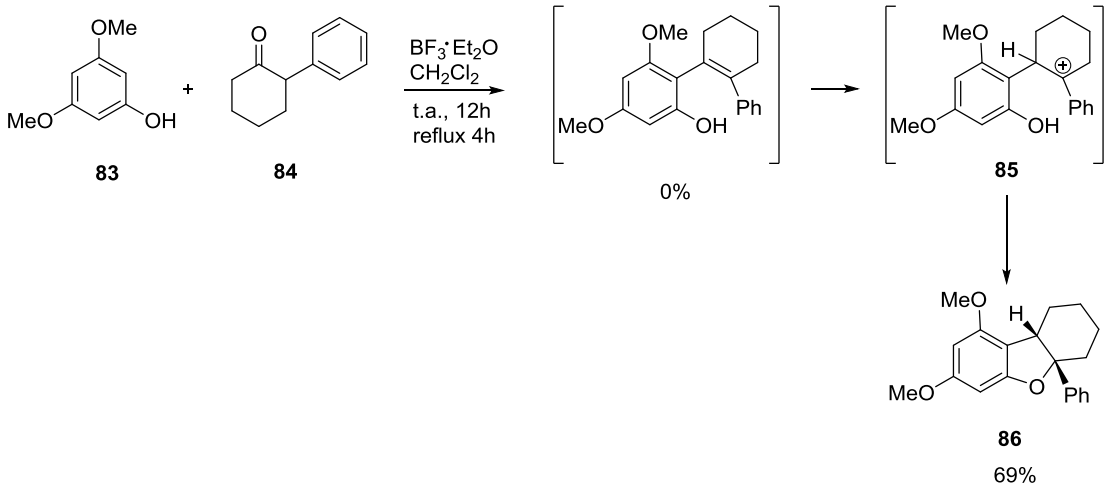

Schéma 24. Condensation du 3,5-diméthoxyphénol **83** avec la cyclohexanone **84**.

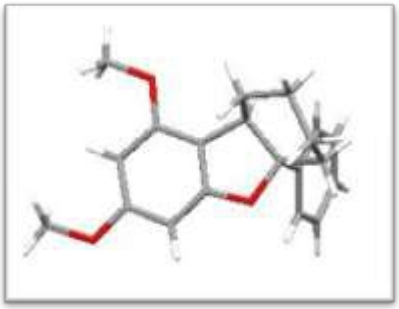

Figure 9. Structure cristallographique du composé **86**.

En nous basant sur ces résultats préliminaires, nous avons modifié notre rétrosynthèse (Schéma 25). Les dernières étapes sont restées inchangées, mais le système tricyclique sera construit par une addition du phénol **83** sur la cyclopentanone **82** suivie par une cyclisation spontanée.

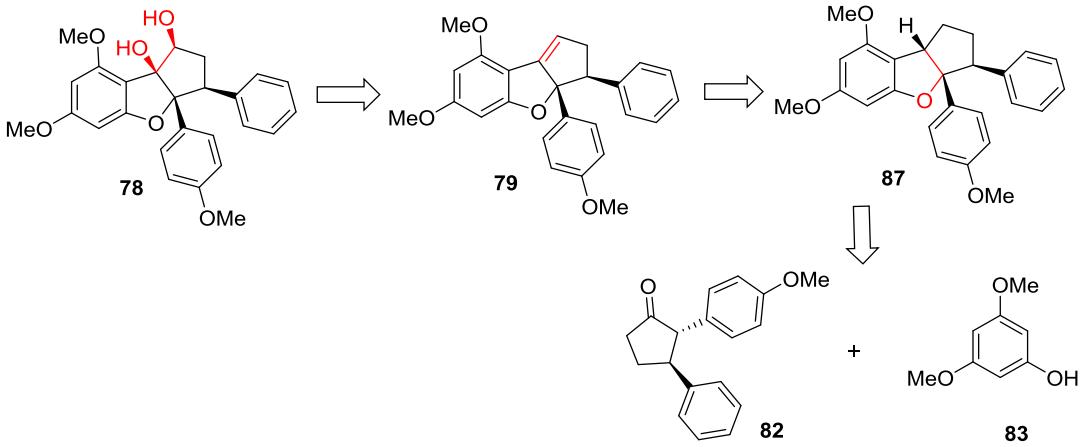

Schéma 25. Analyse rétrosynthétique modifiée.

3.3.3. Préparation des cyclopentènones et essais de cyclisation spontanée

Pour vérifier que l'étape de condensation peut s'effectuer entre le 3,5-diméthoxyphénol **83** et une cyclopentanone (ou bien une cyclohexanone comme précédemment), nous avons cherché, dans un premier temps, à synthétiser la cyclopentènone **88** (Schéma 26).

L'addition du réactif de Grignard préparé à partir de **89** sur la cyclopentanone[46] suivie d'une réaction de déshydratation[47] a permis de préparer la cyclopentène **91**. Malheureusement, ce dernier n'a pas pu être transformé en cyclopentanone **88** par oxydation.[48]

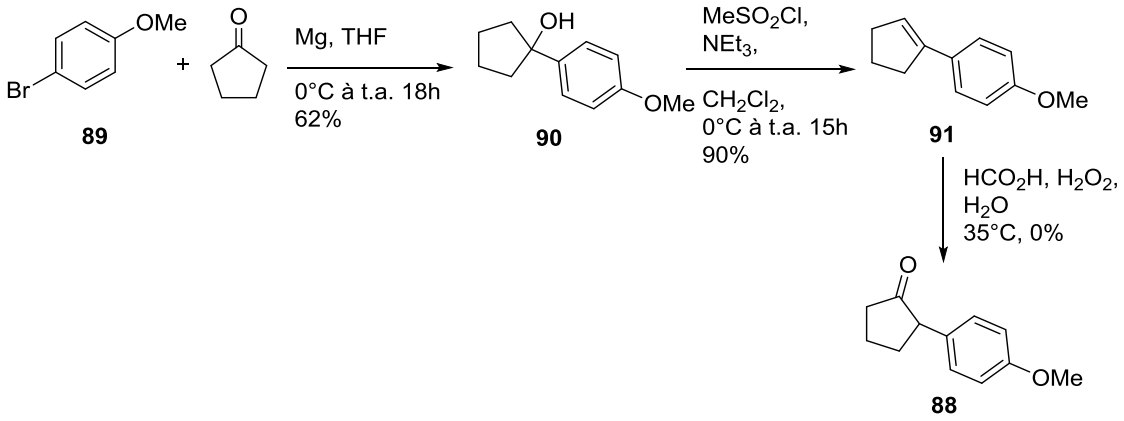

Schéma 26. Premier essai de synthèse de la cyclopentanone **88.**

Lors la recherche d'une nouvelle approche pour former le composé **88**, les travaux de Piancatelli *et al.* ont retenu notre attention.[49] Ces auteurs ont décrit la synthèse d'une hydroxycyclopentènone **93** par un réarrangement catalysé par un acide de Lewis, $ZnCl_2$ (Schéma 27). Dans le mécanisme proposé, ce réarrangement est initié par l'activation de carbinol **92** par du $ZnCl_2$, ensuite une cascade de transformations permet d'obtenir un cation pentadiènyle **94** qui subit une cyclisation conrotatoire pour former finalement le produit **93**. De plus, cette réaction est plus

[46] Zhou, L., Liu, X.H., Ji, J., Zhang, Y.H., Wu, W.B., Liu, Y.B., Lin, L.L., Feng. X.M., *Org. Lett.*, **2014**, *16* (15), 3938-3941.
[47] Hamon, D.P.G., Tuck, K.L., Christie, H.S., *Tetrahedron*, **2001**, *57*, 9499-9508.
[48] Thaher, B.A., Koch, P., Amo, V.D., Knochel, P., Laufer, S., *Synthesis*, **2008**, *2*, 225-228.
[49] Piancatelli, G., Scettri, A., David, G., D'Auria, M., *Tetrahedron*, **1978**, *34*, 2775-2778.

rapide et donne un meilleur rendement lorsque R est un groupe aromatique.

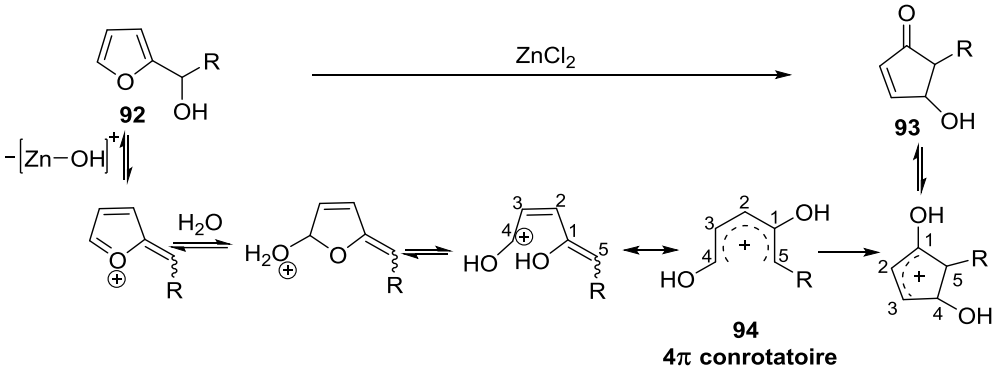

Schéma 27. Réaction de Piancatelli.[48]

Le carbinol **95** a été obtenu quantitativement à partir du furane et de l'anisaldéhyde. Ensuite, dans la condition de Piancatelli, cet alcool a été converti en composé **96** avec 64% de rendement (Schéma 28). L'hydrogénation de ce composé à 40 bars d'hydrogène a nous donné un mélange de produits : l'ènone **97** (34%) résultant de l'hydrogénation de la double liaison suivie d'une déshydratation, et l'alcool **98** (17%) issu d'une double hydrogénation du composé **97**. L'alcool **98** a été ensuite engagé dans une oxydation de Swern pour former le composé **88**.

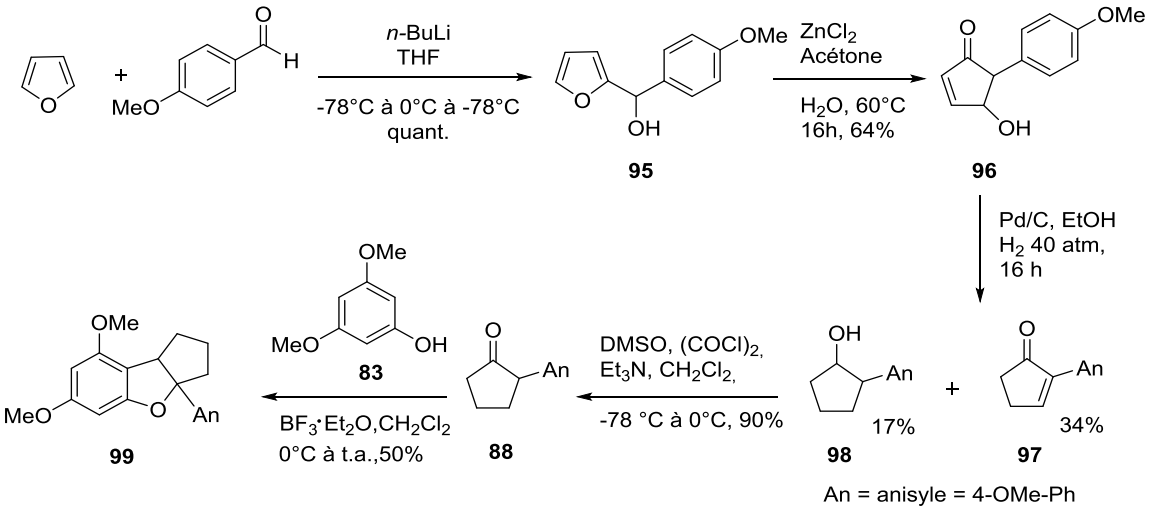

Schéma 28. Préparation du composé **88** et réaction modèle.

Ce composé **88** a été engagé dans une réaction modèle avec le 3,5-diméthoxyphénol **83** dans les conditions précédemment décrites, pour fournir le

produit cyclisé **99** avec 50% de rendement (Schéma 28).

Encouragé par ces résultats préliminaires, nous avons concentré ensuite nos efforts sur la préparation de la cyclopentanone **82** pour appliquer cette cyclisation à la formation du squelette de flavaglines. Pour cela, nous avons d'abord cherché à améliorer la préparation du composé **97**. L'hydrogénation du composé **96** sous pression atmosphérique a permis d'obtenir le composé **100** qui a été directement engagé sans purification dans une étape de déshydratation en présence de silice. La cyclopentènone **97** a été ainsi obtenue avec 70% de rendement (Schéma 29).

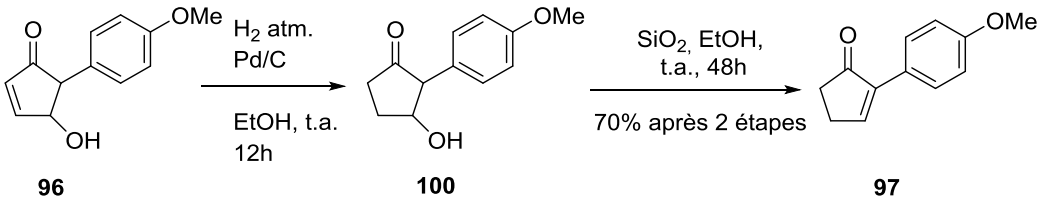

96 **100** **97**

Schéma 29. Conversion du composé **96** en cyclopentènone **97**.

Afin d'introduire un groupe phényle en position β de l'ènone **97**, plusieurs méthodes ont été testés. Dans un premier temps, l'addition 1,4 d'un phénylcuprate[50] n'a donné que le produit de départ et les produits oligomérisés qui n'ont pas été identifiés (Schéma 30).

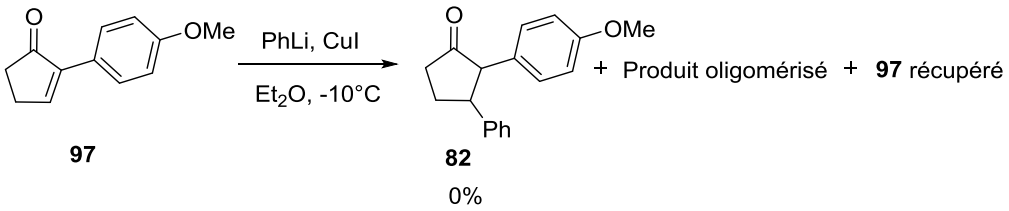

97 **82** 0%

Schéma 30. Essai de l'addition conjuguée du phényle.

Nous nous sommes ensuite inspirés des travaux du groupe de Csàkÿ qui a décrit l'addition d'acide phénylboronique sur une cyclopentènone catalysée au Rh(I).[51] Plusieurs essais ont été effectués dans les conditions de Csàkÿ avec différents additifs et systèmes de solvants (Schéma 31). Cependant, le composé **82** a été isolé une seule

[50] Becheanu, A., Baro, A. Laschat,S., Frey, W., *Eur. J. Org. Chem.*, **2006**, 2215-2225.

[51] De la Herrán, G., Mba, M., Murcia, M. C., Plumet, J., Csákÿ, A. G., *Org. Lett.*, **2005**, *7*, 1669-1671.

fois et avec un rendement faible (Entrée 4).

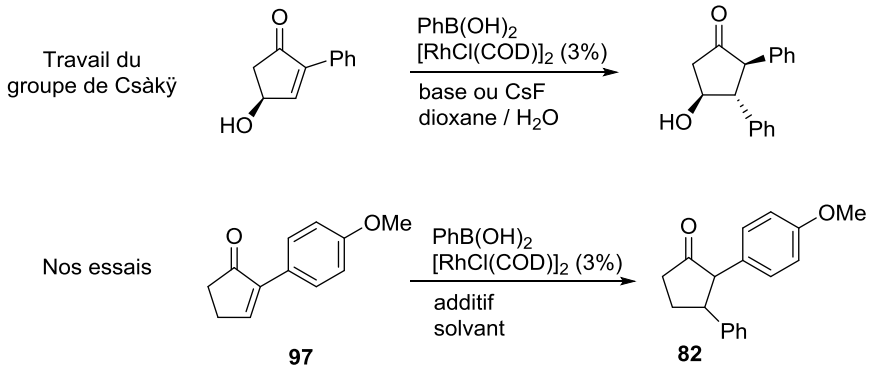

Schéma 31. Addition conjuguée catalysée au Rh(I).

Entrée	Additif	Solvant	Rdt du 82
1	LiOH (0,5 éq)	Dioxane / H_2O (4/1)	0%
2	LiOH (0,5 éq)	Dioxane / H_2O (10/1)	0%
3	Chlorure de guanidium / LiOH (1 éq)	Dioxane / H_2O (4/1)	0%
4	Chlorure de guanidium / LiOH (1 éq)	Dioxane / H_2O (10/1)	9%
5	CsF (3 éq)	Dioxane / H_2O (10/1)	trace en RMN

Tableau 1. Résultats de l'addition conjuguée catalysée au Rh(I).

La méthode qui a finalement été adoptée pour insérer un groupe phényle fait appel à l'addition de phényllithium sur le carbonyle pour former d'abord l'alcool **101**. Ce dernier a été engagé ensuite dans un réarrangement oxydatif en présence de pyridinium dichromate,[52] pour générer la cyclopentènone **102** (Schéma 32).

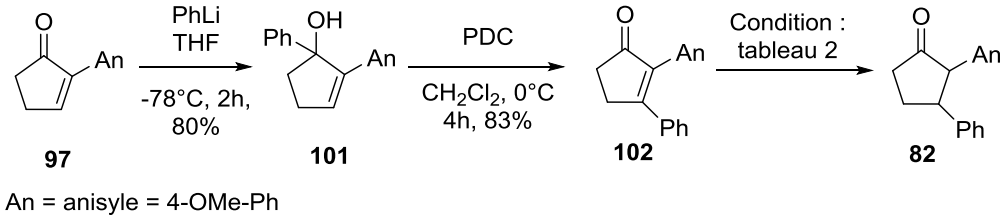

Schéma 32. Synthèse de la cyclopentanone **82**.

Pour réduire la cyclopentènone **102** en cyclopentanone **82**, divers essais ont

[52] Trost, B. M., Pinkerton, A. B., *J. Org. Chem.*, **2001**, *66*, 7714-7722.

été effectués (Schéma 32). Les résultats sont récapitulés dans le tableau 2.

Lorsque la réaction a été effectué dans l'éthanol, en présence de Pd/C et sous une pression atmosphérique d'hydrogène, la cyclopentanone **82** a été obtenue mais avec un rendement de 57%, avec l'alcool comme sous-produit et produit de dégradation (entrée 1). L'essai avec du catalyseur de Lindlar a permis de récupérer seul le produit de départ (entrée 2). Avec la 2-nosyle hydrazine comme agent de réduction, le produit de départ inchangé a été également récupéré (entrée 3). Le choix s'est finalement porté sur le $Pd(OH)_2$ qui a conduit à la formation de la cyclopentanone **82** accompagné uniquement de l'alcool correspondant comme produit secondaire (entrée 4). Lorsque l'éthanol a été remplacé par l'AcOEt, le rendement a été amélioré à 90% (entrée 5).

Entrée	Réactif-catalyseur	Durée	Solvant	Rendement
1	Pd/C, H_2	2 h	EtOH	57 %
2	Lindlar, H_2	24 h	EtOH	0 %
3	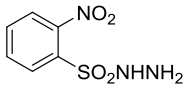	18 h	ACN	0 %
4	$Pd(OH)_2$/C, H_2	12h	EtOH	32%
5	$Pd(OH)_2$/C, H_2	4 h	AcOEt	90 %

Tableau 2. Résultats de l'hydrogénation de la cyclopentènone **102.**

Une fois obtenue, la cyclopentanone **82** a été engagée dans la condensation avec le 3,5-diméthoxyphénol selon la méthode précédemment développée (Schéma 33). Cependant, la réaction à température ambiante n'a pas permis d'obtenir le produit cyclisé et seuls les produits de départ ont été récupérés. La réaction chauffée à 50°C a donné les produits cyclisés **103a** et **103b** avec 22% de rendement dans un rapport 10/1.

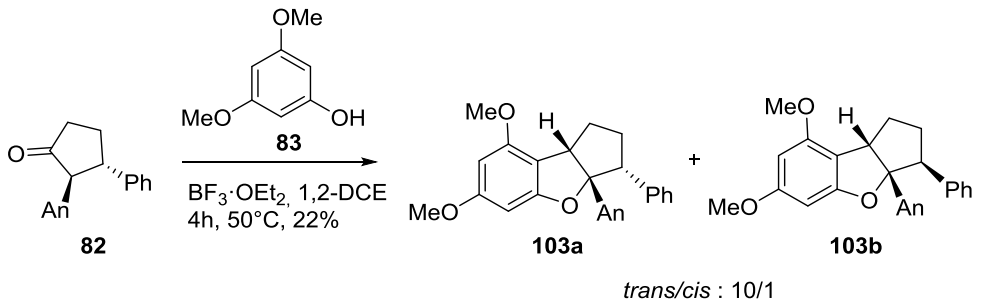

Schéma 33. Condensation et cyclisation spontanée.

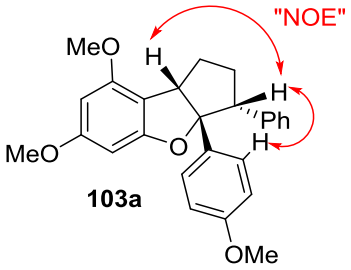

Figure 10. Résultat de Noesy du composé **103a.**

La stéréochimie relative de **103a** a été établie par analyse NOESY (figure 10). Cette cyclisation permet d'accéder au squelette tricyclique des flavaglines, mais avec une mauvaise stéréochimie de manière préférentielle.

3.3.4. Etude rétrosynthétique modifiée

Nous avons alors décidé de changer de stratégie en utilisant à nouveau une sélénocyclisation pour former le squelette tricyclique. (Schéma 34).

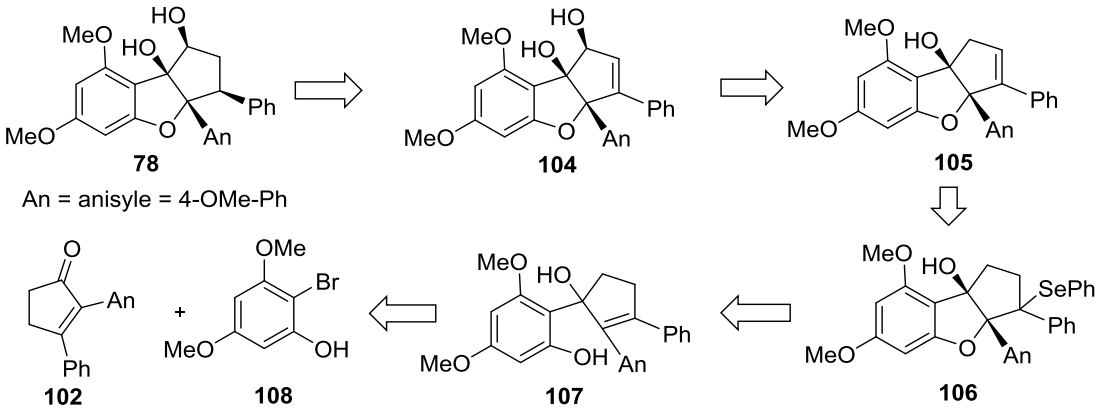

Schéma 34. Nouvelle analyse rétrosynthétique.

La configuration désirée peut être établie par une hydrogénation de la double liaison du composé **104** à la fin de synthèse, le groupe d'alcool allylique du **104** peut être installé à partir du composé **105** qui est obtenu par une oxidation/élimination à partir du composé **106**. Ce dernier est issu de la sélénocyclisation du composé **107** qui est le résultat de condensation entre la cyclopentènone **102** et le bromophénol **108**.

3.3.5. Essais de condensation de dérivés bromés du phloroglucinol sur cyclpentènone

Le bromophénol **108** a été préparé selon une méthode décrite dans la littérature (Schéma 35).[53] Une acylation du 3,5-diméthylephénol **83** suivie par une bromation en présence du NBS a permis d'obtenir le bromophénol acétylé **110**, qui a été ensuite saponifié pour former le bromophénol **108**.

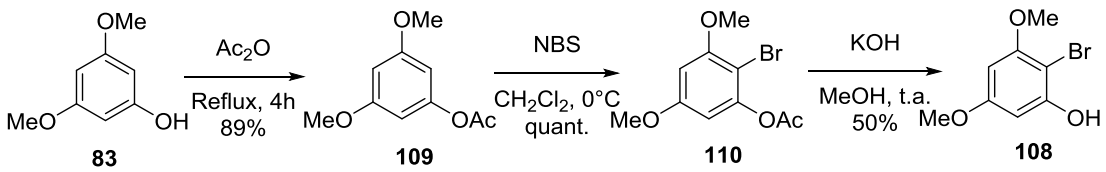

Schéma 35. Synthèse du bromophénol **108** selon la méthode de Haufe *et al.*[53]

Ensuite, la condensation entre le bromophénol **108** et la cyclopentènone **102** a été tentée avec plusieurs méthodes différentes, mais toujours en basant sur l'addition nucléophile du groupe carbonyle par un lithien. Pour étudier l'influence du groupe phénol, nous avons préparé également le bromophénol **111** protégé par un groupe benzyle.[54] Comme notre stock de cétone **102** était limité, nous avons examiné la réactivité du composé **108** ou **111** métallés sur du benzaldéhyde quand la réactivité de ces composés était incertaine (Schéma 36).

[53] Runge, M., Haufe, G., *J. Org. Chem.*, **2000**, *65* (25), 8737–8742.

[54] Murata, T., Shimada, M., Sakakibara, S., Yoshino, T., Masuda, T., Shintani, T., Sato, H., Koriyama, Y., Fukushima, K., Nunami, N., Yamaguchi, M., Fuchikami, K., Komura, H., Watanabe, A., Ziegelbauer, K.B., Bacon, K.B., Lowinger, T.B., *Bioorg. Med. Chem. Lett.*, **2004**, *14* (15), 4019-4022.

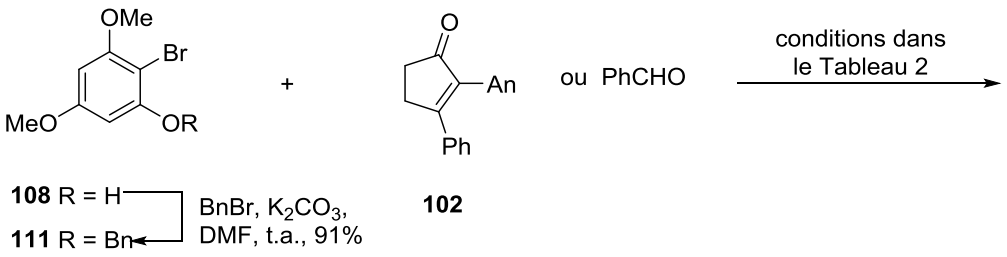

Schéma 36. Essais de condensation de dérivés bromés du phloroglucinol sur cyclpentènone **102** ou le benzaldéhyde

Entrée	Bromophénol	Condition[c]	Substrat	Résultat[a]
1	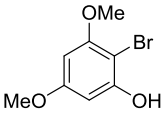 **108**	*n*-BuLi (2éq), THF -78°C à t.a.	PhCHO	PhCHO + 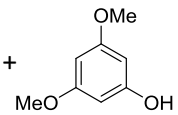 **83**
2	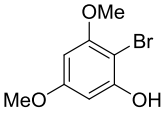 **108**	*n*-BuLi (2éq), THF -78°C à t.a.	**102**	**102** + 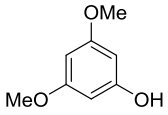 **83**
3	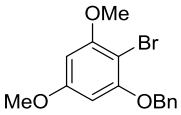 **111**	*n*-BuLi, THF -78°C à t.a.	PhCHO	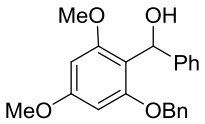 **112** (65%)[b]
4	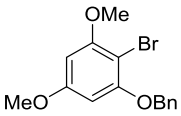 **111**	*n*-BuLi, THF -78°C à t.a.	**102**	**102** + 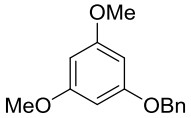 **113**
5	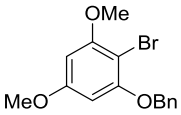 **111**	PhLi, THF -78°C à t.a.	PhCHO	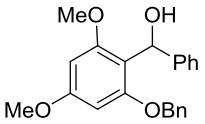 **112** (50%)[b]
6	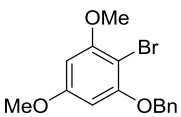 **111**	PhLi, THF -78°C à t.a.	**102**	**102** + 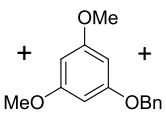 **113** + 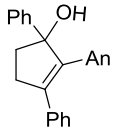 **114**

7	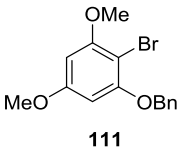 **111**	nBuLi, THF puis $LaCl_3 \cdot 2LiCl$ -78°C à t.a.	**102**	**102** + 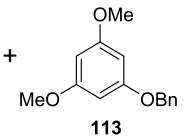 **113**
8	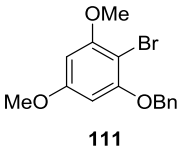 **111**	nBuLi, THF -78°C à t.a.	**102** + $CeCl_3$	**102** + 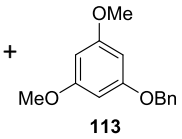 **113**
9	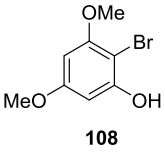 **108**	nBuLi (2éq), Et_2O 0°C à t.a.	**102** + $CeCl_3$	**102** + 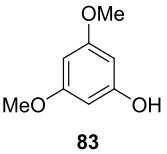 **83**

a : les résultats sont déterminés par analyse RMN ^{1}H du produit brut.

b : le rendement est calculé en basant sur produit **112** isolé après une chromatographie.

c : tous les solvants sont anhydres ou distillés avant l'utilisation.

Tableau 3. Essais de condensation de dérivées métallés du phloroglucinol protégé sur une cétone et du benzylaldéhyde.

Les résultats de la condensation ont été récapitulés dans le Tableau 3. D'abord, la méthode de Evans[55] basée sur la formation d'un lithien *o*-lithiophénoxide a été testée, mais elle n'a pas permis d'obtenir le produit désiré. L'analyse RMN ^{1}H du produit brut a montré que le phénol protoné **83** et les substrats inchangés ont été obtenus (entrées 1 et 2).

Dans un deuxième temps, les essais ont été effectués avec le bromophénol **111** protégé par un groupe benzyle. La réaction avec du benzaldéhyde a permis d'obtenir le produit désiré **112** avec 65% de rendement, en revanche, la réaction avec l'ènone **102** n'a donné que le produit protoné **113** et l'ènone inchangée **102** (entrées 4).

[55] Talley, J. J., Evans, I. A., *J. Org. Chem.*, **1984**, *49*, 5267-5269.

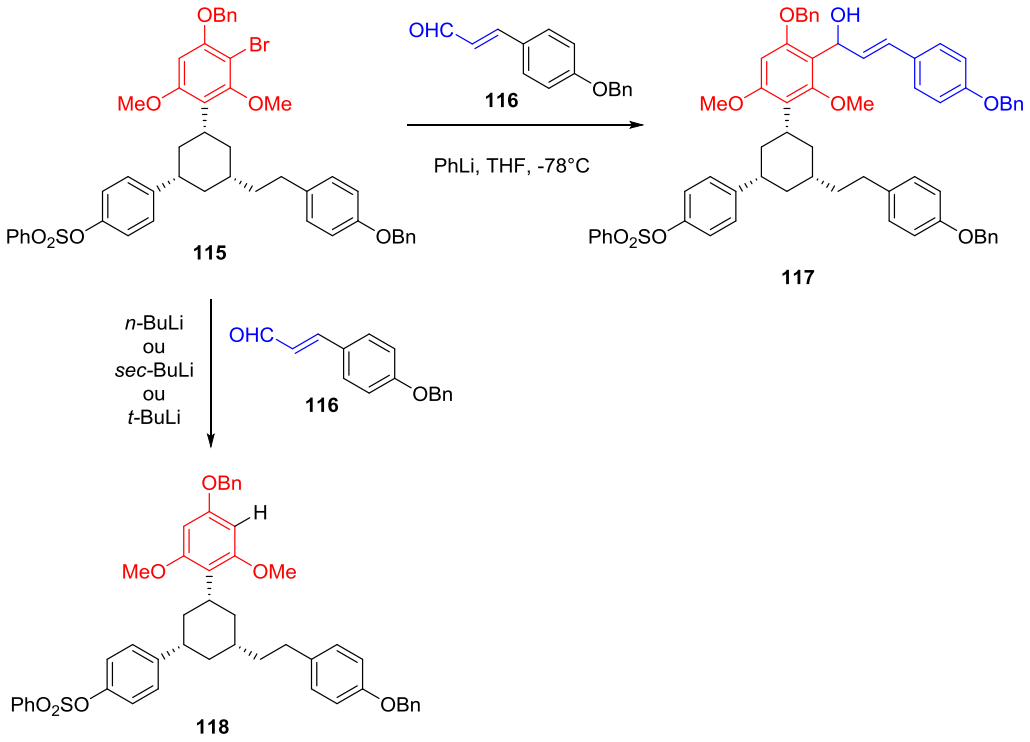

Schéma 37. Condensation décrite par Rychnovsky et coll.[56]

Nous nous sommes ensuite inspirés des travaux du groupe de Rychnovsky qui a réalisé une condensation entre un bromophénol protégé **115** et un aldéhyde α, β – insaturé **116** (Schéma 37).[56] Cette réaction ne peut marcher qu'avec du PhLi. Avec du *n*-BuLi, du *sec*-BuLi ou du *t*-BuLi, seul le produit protoné a été obtenu. En Basant sur ces travaux, nous avons effectué les condensations en remplaçant le *n*-BuLi par du PhLi. La réaction avec du benzaldéhyde a donné le produit **112** avec 50% de rendement (entrée 5), par contre, avec de l'ènone **102**, la réaction a donné toujours le produit protoné **113**, l'ènone inchangée et une faible quantité de composé **114** qui résulte d'une attaque de PhLi sur l'ènone (entrée 6).

Selon ces résultats, nous avons considéré que l'effet stérique des deux groupes aryle de l'ènone **102** a empêché l'attaque nucléophile du composé **108**. Pour compenser cet effet, nous avons pensé dans un premier temps à ajouter un halogénure de lanthanide, par exemple, du $LaCl_3 \cdot 2LiCl$ ou du $CeCl_3$, qui peut favoriser

[56] Tian, X., Jaber, J. J., and Rychnovsky, S. D., *J. Org. Chem.,* **2006**, *71*, 3176-3183.

l'attaque du lithien sur la cétone énolisable et encombrée.[57]

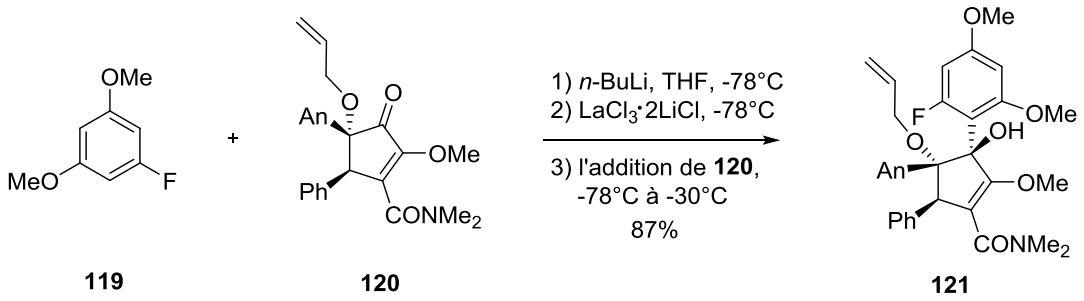

119 **120** **121**

Schéma 38. Condensation de Tius.[58]

Nous avons d'abord testé la méthode décrite par le groupe de Tius qui a condensé un aryle **119** et une ènone encombrée **120** en présence du $LaCl_3 \cdot 2LiCl$ (Schéma 38).[58] Malheureusement, cette méthode n'a pas abouti avec nos substrats (entrée 7).

La méthode de Dimitrov a été ensuite tentée en utilisant du $CeCl_3$ anhydre pour activer la cétone.[59] Les réactions n'ont donné toujours que les phénols protonés et l'ènone **102** inchangée (entrée 8 et 9).

3.3.6. Formation de l'oxime et essais de condensation

Nous avons pensé dans un deuxième temps à installer un groupe attracteur en position α de la fonction cétone, par exemple, une oxime, pour la rendre plus déficiente en électron et compenser la gêne stérique.

La céto-oxime **122** a été préparé à partir de l'ènone **102** en présence du butyle nitrite et du HCl concentré. Les oximes méthylées **123a** et **123b** ont été obtenus aussi par une conversion de l'oxime **122** en utilisant du diméthyle de sulfate comme agent de méthylation (Schéma 39).

[57] Krasovskiy, A., Kopp, F., Knochel, P., *Angew. Chem. Int. Ed.*, **2006**, *45*, 497-500.

[58] Zhou, Z., Tius, M. A., *Angew. Chem. Int. Ed.*, **2015**, *54*, 6037-6040.

[59] Dimitrov, V., Kostova, K., Genov, M., *Tetrahedron Lett.*, **1996**, *37*, 6787-6790.

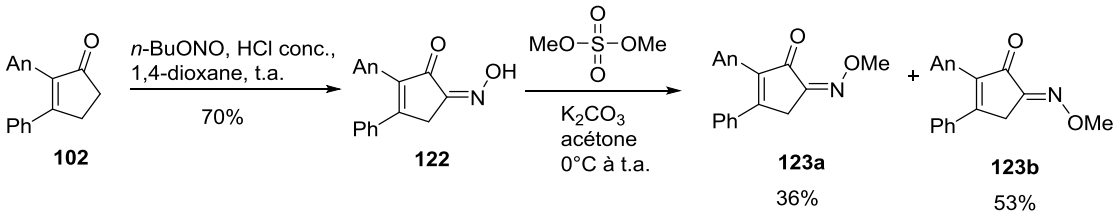

Schéma 39. Préparation des oximes méthylées **123a** et **123b**.

Ayant un proton acide en position α de l'oxime, le traitement de **123a** et **123b** par un composé lithié va conduire à un énolate non réactif vis-à-vis d'un nucléophile. Nous avons donc cherché à condenser ces composés avec un phénol dans des conditions acides (Schéma 40).

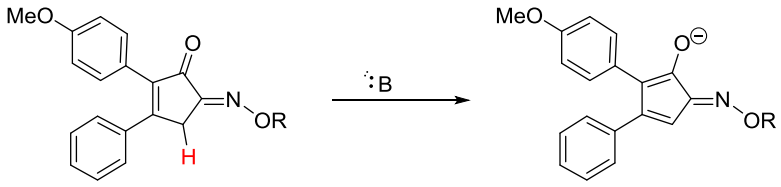

Schéma 40 : Déprotonation possible en condition basique.

De ce fait, la condensation en présence d'un acide de Lewis a été tentée entre l'oxime et le 3,5-diméthoxyphénol **83** (Schéma 42). La condensation entre l'oxime **122** et le 3,5-dimethoxyphénol a été effectuée en présence du $BF_3.Et_2O$, mais elle n'a donné que les produits de départ inchangés.

De manière intéressante, lorsque la condensation a été effectuée entre l'oxime méthylée **123a** ou **123b** avec du 3,5-diméthoxyphénol **83**, au lieu d'obtenir le composé désiré, les deux spiroxanthènones **124a** et **124b** ont été formées (Schéma 41). Nous avons considéré que ces deux composés spiro résultent d'une double addition du phénol sur l'oxime suivi par une déshydratation. La structure du composé **124a** a été vérifiée par cristallographie RX (Figure 11). La condensation de α-céto-oximes O-méthylées sur des phénols donnant lieu à des structures originales, l'étude de cette réaction sera poursuivie au laboratoire et les composés ainsi obtenus

seront testés pour leur cytotoxicité dans un panel de lignées cancéreuses et aussi pour leur activité dans des tests in vitro d'affections tropicales.

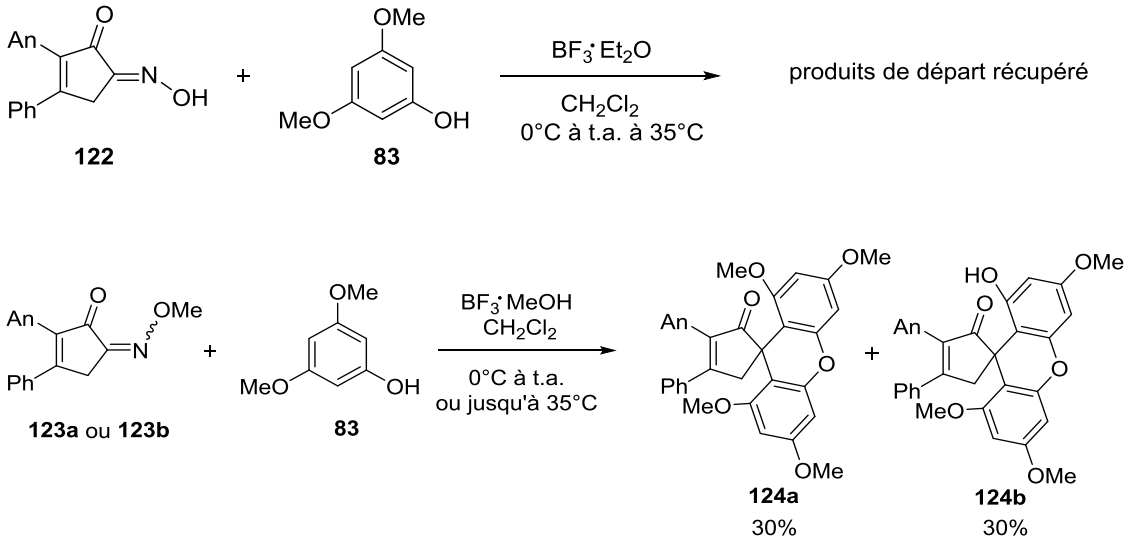

Schéma 41 : Essais de condensation avec l'oxime dans la condition acide.

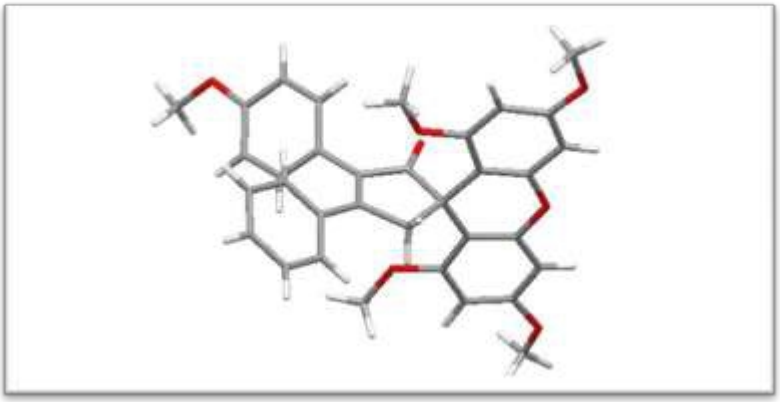

Figure 11 : Structure RX du composé **124a**.

3.4. Modification bioisostérique de flavaglines

Il a été décrit que la molécule **126** ayant un groupe méthoxy en position 8b n'est pas cytotoxique,[60] ce qui suggère qu'un groupe donneur d'hydrogène est nécessaire pour l'activité anticancéreuse (Figure 12). Par ailleurs, Il avait été déjà montré au laboratoire que le remplacement du groupe hydroxyle en position 1 par un groupe formamide (**127**) ou un groupe sulfonamide (**128**) ne change pas significativement leurs activités anticancéreuses et cardioprotectrices. Cette observation nous a incités à examiner si les remplacements en position 8b par les mêmes donneurs d'hydrogène sont aussi tolérés.

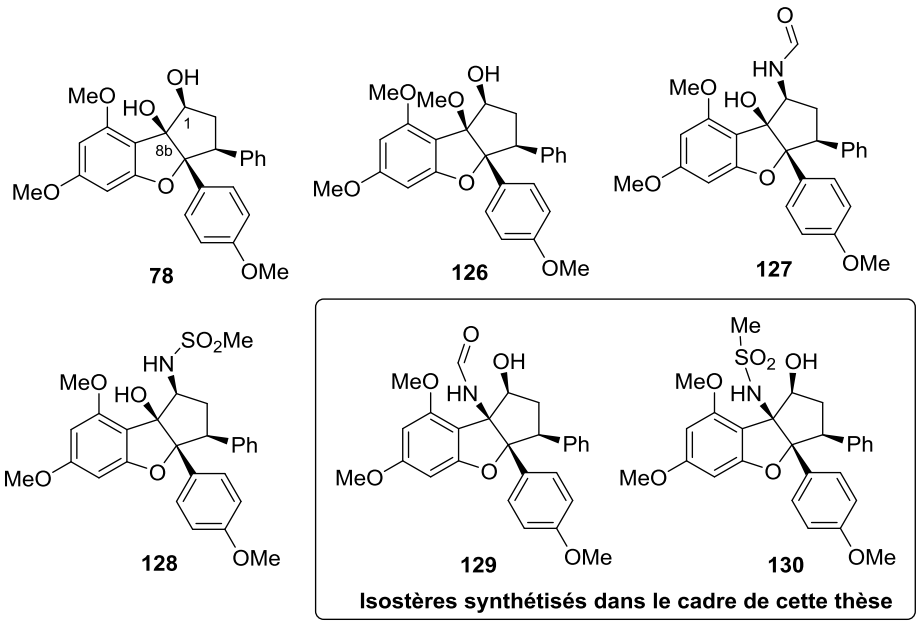

Figure 12 : Modification structurale des flavaglines en position C1 et C8b.

Deux conditions de substitution nucléophile par l'azoture ont été d'abord essayées,[61,62] mais aucune des deux n'a abouti, dans les deux cas, le produit de départ **78** reste inchangés (Schéma 42).

[60] Bohnenstengel, F. I., Steube, K. G., Meyer, C., Quentmeier, H., Nugroho, B. W., Proksch, P. *Z. Naturforsch., C., J. Biosci.,* **1999,** *54*, 1075-1083.

[61] Shiow-Jyi, W., O'Connor, K. J., Burrows, C. J., *Tetrahedron Lett.*, **1993**, *34*, 1905-1908.

[62] Bates, R.W., Khanizeman, R.N., Hirao, H., Tay, Y.S., Sae-Lao, P., *Org. Biomol. Chem*., **2014**, *12*, 4879-4884.

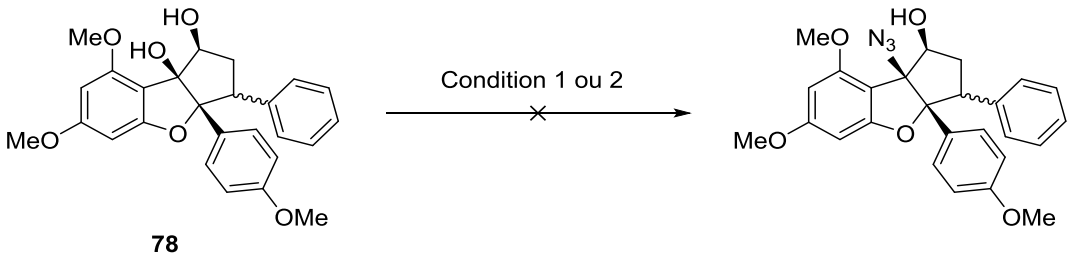

Condition 1 : NaN_3, NBu_4OH, CF_3COOH, $CHCl_3$, 0°C à t.a.
Condition 2 : $TMSN_3$, TMSOTf, CH_2Cl_2, -78°C à -20°C

Schéma 42 : Premiers essais de substitution nucléophile par un azoture.

Les premiers résultats indiquent que cet alcool tertiaire n'est pas assez activé dans la condition acide. Nous avons pensé, dans un deuxième temps, à transformer cet alcool tertiaire en groupe carbonate pour générer un carbocation benzylique (Schéma 43).

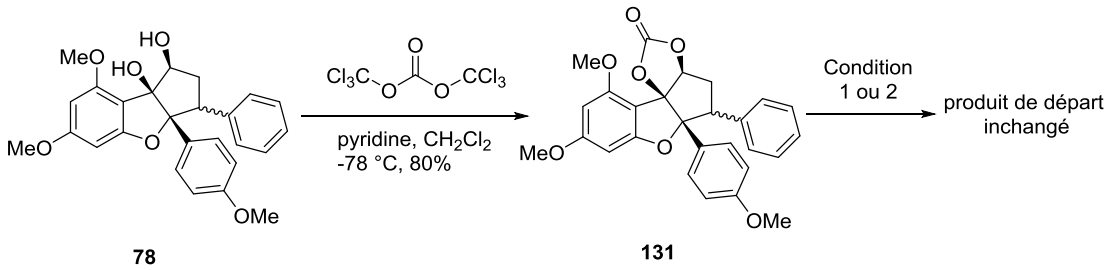

Condition 1 : NaN_3, NBu_4OH, CF_3COOH, $CHCl_3$, 0°C à t.a.
Condition 2 : $FeCl_3$ anhydre, AgOTf, $TMSN_3$, 1,2-DCE, t.a. puis en micro-onde 80°C à 140°C

Schéma 43 : Formation et réactivité du carbonate **2.**

L'épi-rocaglaol racémique **78** a été traité par le triphosgène en présence de la pyridine à basse température. Cette réaction a permis d'obtenir le carbonate **131** avec 80% de rendement. Ce dernier a ensuite été engagé dans les conditions de substitution nucléophile pour introduire le groupe azoture. Deux conditions ont été testées, mais aucune réaction n'a eu lieu. Même à 140°C au micro-onde (condition 3),[63] le produit de départ est resté inchangé.

Nous avons alors cherché à augmenter la réactivité de cet électrophile en passant par un sulfate cyclique (Schéma 44).

[63] Chan, L.Y., Kim, S., Chung, W.T., Long, C., Kim, S., *Synlett.*, ***2011***, 415-419

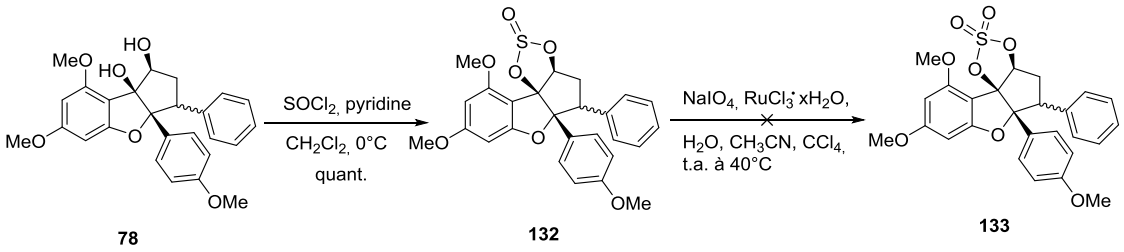

Schéma 44. Essai d'introduction d'un sulfate.

Le diol **78** a été d'abord traité par le chlorure de thionyle dans un milieu basique.[64] Le sulfite obtenu a été ensuite engagé dans une oxydation en présence du périodate de sodium et chlorure de ruthénium. Au lieu de former le sulfate désiré, une dégradation a été observée indiquant que le sulfate est instable.

Par rapport au groupe carbonate qui n'est pas assez réactif et au groupe sulfate qui l'est trop, nous avons considéré que le sulfite **132** peut être un meilleur choix pour introduire le groupe azoture. Nous avons été heureux d'observer la formation de l'azoture **134** avec un rendement de 63% (Schéma 45).

Pour réduire le groupe azoture en amine, une réaction de Staudinger en présence d'un triphénylphosphine a d'abord été tentée, mais n'a pas abouti. En revanche, l'espèce réductrice $Sn(SPh)_3$ formée in situ a permis d'obtenir l'amine désirée **135** avec un rendement de 85%.[65] Finalement, l'amine **135** a été transformée en formamide **129** et sulfonamide **130**.[66,67]

[64] Bonini, C., Chiummiento, L., De Bonis, M., Funicello, M., Lupattelli, P., Suanno, G., Berti, F., Campaner, P., *Tetrahedron*, **2005**, *61*, 6580-6589.

[65] Bartra, M., Romea, P., Urpí, F., Vilarrasa, J., *Tetrahedron*, **1990**, *46*, 587-594.

[66] Quasdorf, K.W., Huters, A.D., Lodewyk, M. W., Tantillo, D.J., Garg, N.K., *J. Am. Chem. Soc.*, **2012**, *134*, 1396–1399.

[67] Wu, K.-H., Gau, H. M., *Organometallics*, **2003**, *22*, 5193-5200.

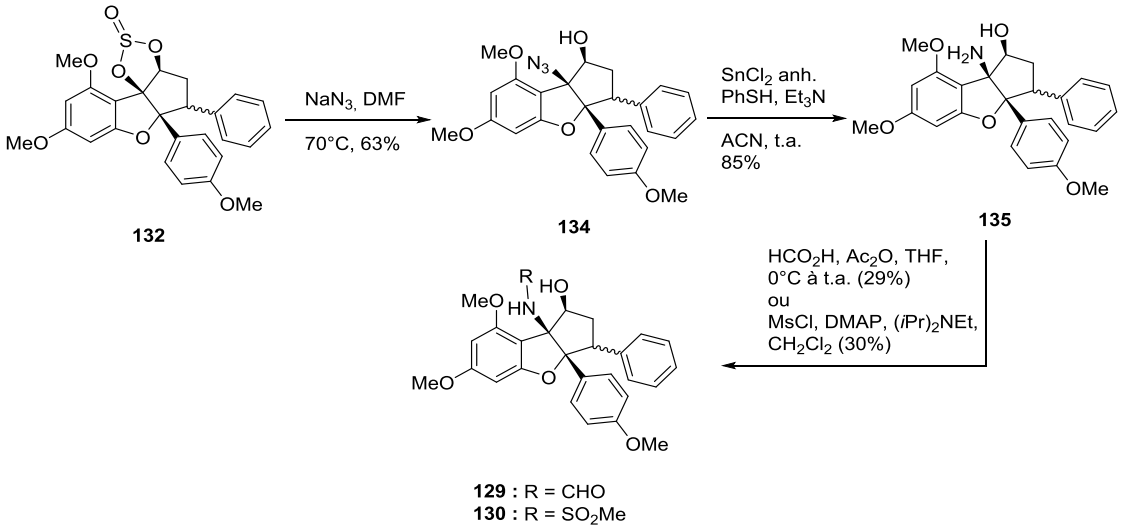

Schéma 45. Formation du formamide **129** et du sulfonamide **130**.

La cytotoxité des isostères **129** et **130** a été examinée dans des cellules cancéreuses humaines après 72h de traitement. Malheureusement, ces deux composés ne présentent pas de cytotoxicité significative dans les lignées de cellules cancéreuses Hep3B et HuH7. Ces travaux ont été publiés dans *Tetrahedron Letters.*[68]

[68] Zhao, Q., Tijeras-Raballand, A., de Gramont, A., Raymond, E., Désaubry, L., *Tetrahedron Lett.,* **2016**, *57*, 2943-2944.

3.5. Etude pharmacologique du FL3 et de la fluorizoline

Au cours de ma thèse, j'ai été amenée à synthétiser deux composés : le FL3 (selon une méthode développée au laboratoire, Schéma 46) et la fluorizoline, un ligand cytotoxique des prohibitines développé par Lavilla et ses collègues (Schéma 47).[69]

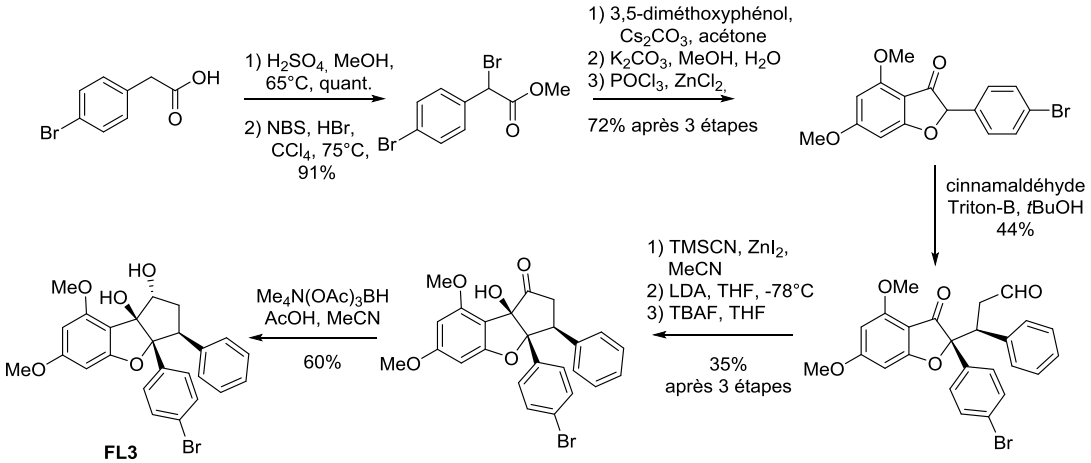

Schéma 46. Synthèse du FL3

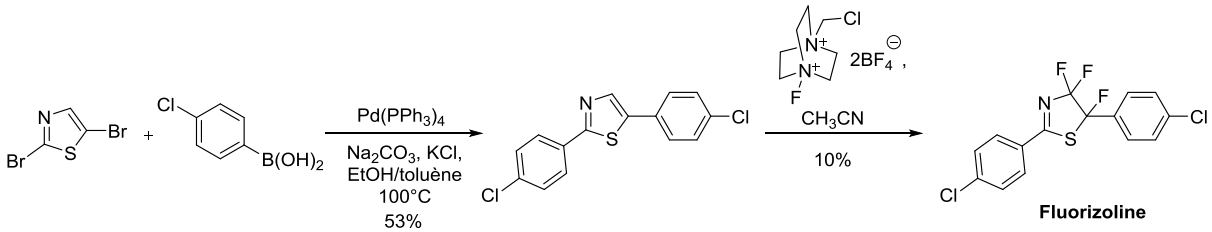

Schéma 47. Synthèse de la fluorizoline.

Ces composés ont été examinés dans les laboratoires de Canan Nebigil et Guy Fuhrmann à l'Université de Strasbourg, Stéphan Vagner à l'institut Curie à Orsay, Caroline Robert à Gustave Roussy à Villejuif, Arianne Theiss à l'Université Baylor à Dallas, Krishnaraj Rajalingam à l'Université du centre médical de Mayence et Joost

[69] Pérez-Perarnau, A., Preciado, S., Palmeri, C.M., Moncunill-Massaguer, C., Iglesias-Serret, D., González-Gironès, D.M., Miguel, M., Karasawa, S., Sakamoto, S., Cosialls, A.M., Rubio-Patiño, C., Saura-Esteller, J., Ramón, R., Caja, L., Fabregat, I., Pons, G., Handa, H., Albericio, F., Gil, J., Lavilla, R., *Angew. Chem. Int. Ed.*, **2014**, *53*(38), 10150-10154.

Hoenderop à l'Université Radboud à Nimèque.

3.5.1. Activation du canal au magnésium TRPM6 (publication n° 5).

L'homéostasie du magnésium est hautement régulée, notamment par le canal TRPM6 au niveau rénal et intestinal. L'équipe du Pr Joost G.J. Hoenderop à l'Université Radboud à Nimègue (Pays-Bas) concentre son activité sur les canaux au magnésium TRPM6 et TRPM7. Cette équipe avait précédemment montré que la PHB2 inhibe TRPM6.[70]

Dans la présente étude, cette équipe a démontré par patch clamp que les flavaglines lèvent cette inhibition.[71] Aucun autre composé testé dans ce laboratoire ne présente d'effet aussi prononcé. Des formes mutantes de TRPM6 insensibles à la régulation par l'insuline ne sont pas sensibles à cette activation par les flavaglines. La signalisation du récepteur à l'insuline active une GTPase, Rac1 (*Ras-related C3 botulinum toxin substrate 1*) pour induire la localisation de TRPM6 à la surface des cellules. La surexpression d'une forme mutante dominante négative de Rac1 bloque les effets des flavaglines sur TRPM6. Ces travaux suggèrent donc que les flavaglines agissent au niveau de Rac1 pour induire une translocation de TRPM6 dans les radeaux de la membrane plasmique à partir de réservoirs intracellulaires (Figure 13).

Des études préliminaires *in vivo* avec du FL3 (0.1 mg/kg i.p, 1 fois par jour durant 7 jours,) n'ont malheureusement pas montré de changement dans la concentration sérique et urinaire en Mg^{2+}.

[70] Cao, G., van der Wijst, J., van der Kemp, A., van Zeeland, F., Bindels, R. J., Hoenderop, J.G., *J. Biol. Chem.,* **2009**, *284*, 14788–14795.

[71] Blanchard, M. G., de Baaij, J. H. F., Verkaart, S. A. J., Lameris, A. L., Basmadjian, C., Zhao, Q., Désaubry, L., Bindels, R. J. M., Hoenderop, J. G., *Plos One*, **2015**, *10*: e0119028.

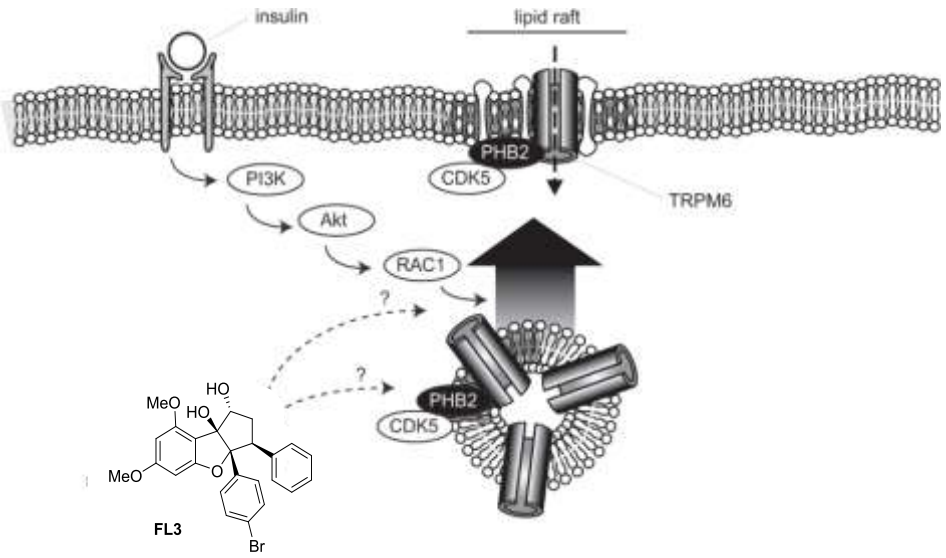

Figure 13. Modèle proposé d'induction de la translocation de TRPM6 à la surface des cellules par les flavaglines. Les flavaglines activent les effecteurs en aval du récepteur à l'insuline. La PHB2 et CDK5, qui régulent toutes deux TRPM6 sont localisées dans les radeaux lipidiques (Figure copiée de la référence 71).

3.5.2. Mécanisme d'action cardioprotectrice des flavaglines (publication n° 6).

La cardiotoxicité induite par les anthracyclines en général, et la doxorubicine en particulier, demeure un problème important en oncologie. Bien que plusieurs stratégies aient été explorées, la seule approche efficace est l'emploi du dexrazoxane (Cardioxane, Zineccard), un chélateur du fer. Cependant cette protection n'est pas totale et ce médicament peut induire la formation de tumeurs secondaires, ce qui a conduit à son limité de usage. La recherche de médicaments susceptibles de limiter la cardiotoxicité anthracyclines constitue donc un important domaine d'investigation au niveau international.[72]

L'équipe de Canan Nebigil à Strasbourg avait précédemment montré que les flavaglines protègent les cardiomyocytes *in vitro* et *in vivo* contre l'apoptose induite par la doxorubicine. La présente étude a montré que cette cardioprotection est

[72] Vejpongsa, P., Yeh, E.T., *J. Am. Coll. Cardiol.*, **2014**, *64*, 938-945.

médiée par la PHB1 et le facteur de transcription STAT3 (Figure 14).[73] La doxorubicine induit une translocation dans le noyau de la PHB1 et de STAT3 qui interagissent ensemble pour conduire à l'apoptose. En revanche, le FL3 induit une localisation de ces deux protéines dans les mitochondries où elles activent des voies de survie. Cette localisation de STAT3 est induite par une rapide phosphorylation de STAT3. Par ailleurs, le FL3 induit augmente considérablement l'expression de la PHB1 (Figure 15). Cette observation est importante, car comme beaucoup de types cellulaires, les cardiomyocytes surexpriment la PHB1 quand elles sont stressées pour activer des voies de survie.[74]

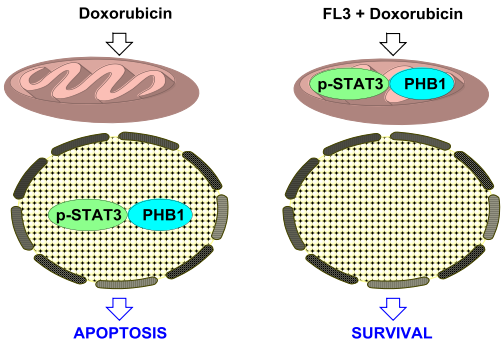

Figure 14. Mécanisme d'action cardioprotecteur des flavaglines (copié de la référence 72).

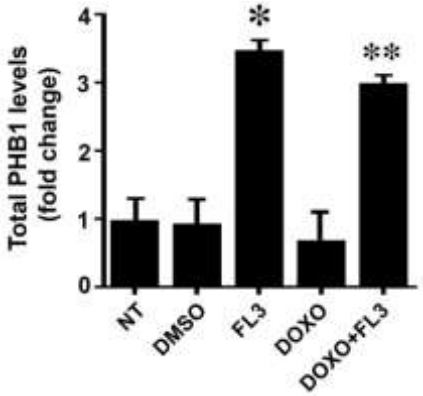

Figure 15. Expression de PHB1 après 10 h de traitement par le véhicule (DMSO), le FL3, la doxorubicine ou la doxorubicine + FL3 comparée aux cellules non traitées (NT) (n = 3) (copié de la référence 73).

[73] Qureshi, R., Yildirim, O., Gasser, A., Basmadjian, C., Zhao, Q., Wilmet, J-P., Désaubry, L., Nebigil, C.G., *Plos One.***2015***, 11*, e0141826.

[74] (i) Gratia, S., Kay, L., Michelland, S., Seve, M., Schlattner, U., Tokarska-Schlattner, M., *J. Proteomics*, **2012**, *75*, 4705-4716. (ii) Liu, X.H., Qian, L.J., Gong, J.B., Shen, J., Zhang, X.M., Qian, X.H., *Proteomics*, **2004**, *4*, 3167–3176. (iii) Liu, X., Ren, Z., Zhan, R., Wang, X., Wang, X., Zhang, Z., Leng, X., Yang, Z., Qian, L., *Cell Stress Chaperones,* **2009**, *14*, 311–319.

3.5.3. Effets cytotoxiques et pro-différenciateurs des flavaglines sur des cellules souches cancéreuses (publication n° 7).

Guy Fuhrmann, à la Faculté de pharmacie de Strasbourg, a montré que le FL3, bloque la prolifération des cellules de carcinome embryonnaire humain NT2/D1 ou induit leur différenciation selon la dose utilisée (Figure 16). Ces cellules représentent un modèle de cellules souches cancéreuses.[75] Il est important de noter que le FL3 n'affecte pas la survie des cellules souches non-cancéreuses, ce qui augmente son potentiel thérapeutique pour rendre les cellules souches cancéreuses sensibles aux thérapies conventionnelles.

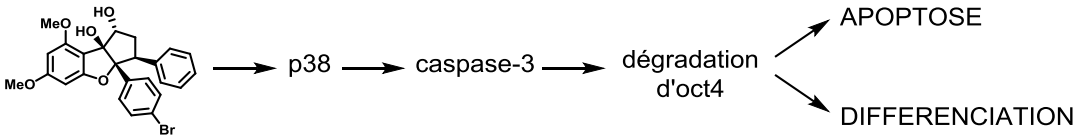

Figure 16. Induction de l'apoptose ou de la différenciation par les flavaglines de cellules de carcinome embryonnaire humain NT2/D1 (modèle de cellules souches cancéreuses).

3.5.4. Effet anti-inflammatoire et cytoprotecteur du FL3 dans un modèle murin de la maladie de Crohn (publication n° 8).

Le Pr Arianne Theiss à l'Université de Baylor à Dallas a démontré que le FL3 diminue l'inflammation dans un modèle d'inflammation chronique des intestins (maladie de Crohn) induite par du Dextran Sulfate de Sodium (DSS) chez la souris, et augmente aussi la résistance de l'épithélium intestinal face à l'apoptose induite par l'inflammation.[76] En effet, la structure de l'épithélium intestinal des souris traitées par du FL3 et du DSS est bien moins déstructurée que celui des souris ayant reçu du DSS seul (Figure 17A). Un calcul de score clinique et histologique met en évidence le caractère anti-inflammatoire et cytoprotecteur prometteur du FL3 dans ce modèle

[75] Emhemmed, F., Ali Azouaou, S., Zhao, Q., Appert-Collin, A., Bennasroune, A., Schini-Kerth, V. B., Muller, C. D., Désaubry, L., Fuhrmann, G., *Cell Biol Toxicol.,* **2017**, *33*, 295-306.

[76] Han, J., Zhao, Q., Basmadjian, C., Désaubry, L., Theiss, A.L., *Inflamm. Bowel Dis*., **2016**, *22*, 55-67.

d'affection (Figure 17B).

L'équipe du Pr Theiss a examiné le mode d'action du FL3 et a montré qu'il est dual. D'une part il diminue l'inflammation en bloquant la production de facteurs pro-inflammatoires comme le factor nucléaire kappa B (NF-kB) p65 ou la cyclooxygénase 2. D'autre part il augmente la survie de l'épithélium intestinal face au stress induit par des agents pro-inflammatoires comme le TNFα ou l'interféron γ. Au niveau moléculaire, le FL3 induit l'expression de la PHB1 de manière similaire à ce qui avait observé dans les cardiomyocytes. En résumé, ces travaux démontrent *in vitro* et *in vivo* que le FL3 présente de puissants effets anti-inflammatoires dans un modèle de la maladie de Crohn. L'étude du potentiel thérapeutique dans cette affection est actuellement poursuivie dans le laboratoire du Pr Theiss.

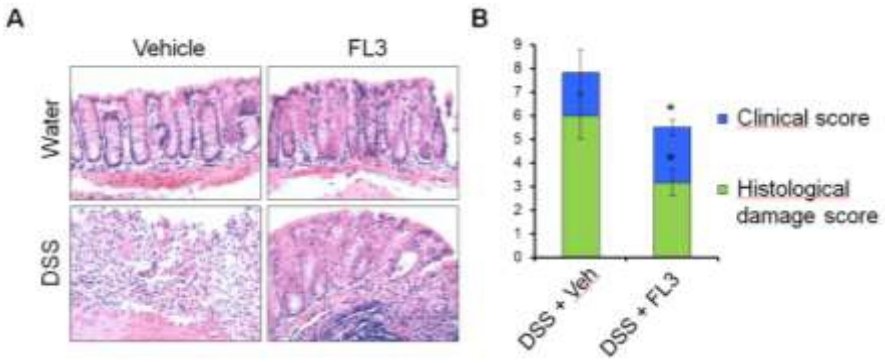

Figure 17. Effets anti-inflammatoires et cytoprotecteurs du FL3 dans un modèle d'inflammation du colon induit par du DSS. Les souris ont reçu du DSS pendant 6 jours et du FL3 (0.1 mg/kg i.p.) ou du véhicule (veh) une fois par jour de J0 à J4. Les souris témoins ont seulement eu de l'eau de boisson sans DSS. **A.** Photomicrographies représentatives de sections distales du colon colorées à l'hémotoxyline et à l'éosine. **B.** Scores de dommages cliniques et histologiques (copié de la référence 75).

3.5.5. Potentialisations des effets anticancéreux des inhibiteurs de MEK dans le mélanome métastatique N-RAS positif (publication n° 9).

Les protéines RAS sont des petites GTPases qui existent sous 4 formes : NRAS, HRAS, KRAS4A et KRAS4B, ces deux dernières résultant d'un épissage différentiel. Elles sont activées par des récepteurs tyrosine kinases pour réguler différentes voies de signalisation (Figure 18) impliquées notamment dans le contrôle du métabolisme,

de la prolifération et de la survie cellulaire. Un quart des patients présentent une mutation de ces gènes (*NRAS*, *HRAS* et *KRAS*), ce qui en fait une des familles d'oncogènes les plus fréquemment mutés dans les cancers humains. Ces 3 gènes ne sont pas mutés avec la même fréquence : KRAS est le plus fréquemment mutés (85%), suivi de NRAS (12%) et *HRAS* (3%).[77]

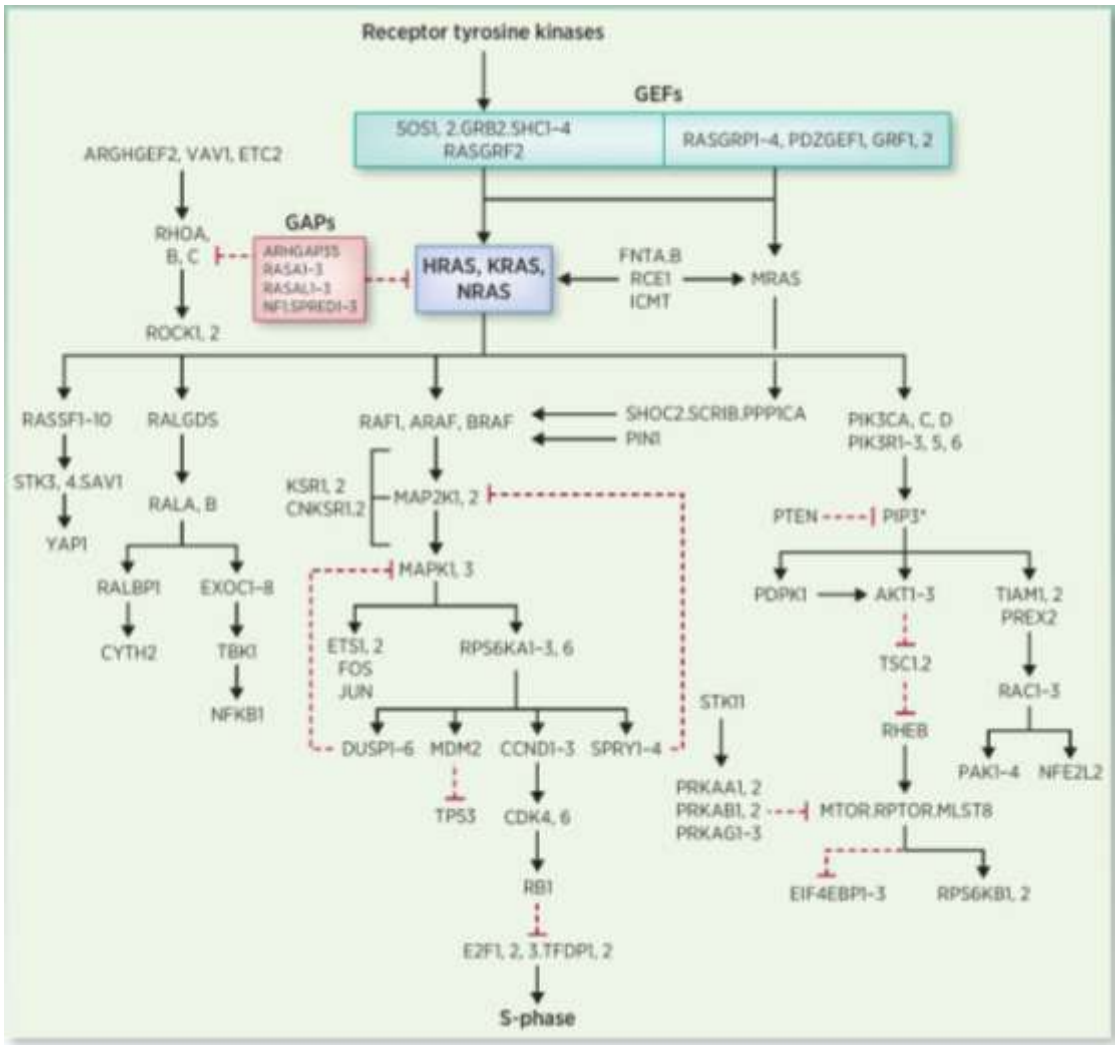

Figure 18. Signalisation de RAS. Ras est activée par des Facteurs d'Echange Guanyliques (GEFs, encadré vert) et désactivés par des protéines activatrices de GTPases (GAPs, encadré rouge). Les protéines RAS activent 4 types principaux d'effecteurs : les protéines RASSF (Ras association domain family), RalGDS (Ral Guanine nucleotide Dissociation Stimulator), les kinases RAF, et les phosphoinositide 3-kinases (PI3K) (copié de la référence 77).

Une mutation de NRAS conduisant à une activation constitutive des voies des

[77] McCormick, F., *Clin Cancer Res.*, **2015**, *21*, 1797-1801.

MAP kinases et PI3K/Akt/mTOR est retrouvée chez 10 à 15% des patients souffrant d'un mélanome, ainsi que dans une pléthore d'autres cancers, notamment des leucémies, et de cancers colorectaux ou pulmonaires. Malgré des efforts de recherche importants depuis plus de 30 ans, il n'y a pas encore d'inhibiteur de RAS qui soit actuellement utilisé comme médicament. En revanche, il existe des médicaments, comme le trametinib, cobimetinib ou le vemurafenib, qui ciblent les kinases MEK ou BRAF qui sont en aval de la signalisation de RAS. Cependant, comme pour beaucoup de thérapies ciblées, ces médicaments perdent leur efficacité après quelques mois de traitements.

Les équipes de Stéphan Vagner et Caroline Robert avaient montré que le FL3, permettait de lever la résistance aux inhibiteurs de BRAF dans un modèle murin de mélanome métastatique ayant développé une résistance au vémurafenib.[78]

Dans la présente étude, ces équipes ont montré qu'en inhibant eIF4F, le FL3 potentialise les effets cytotoxiques *in vitro* d'un inhibiteur de MEK, le rametinib, dans des lignées de mélanomes présentant une mutation de NRAS (Figure 19).[79]

[78] Boussemart, L., Malka-Mahieu, H., Girault, I., Hemmingsson, O., Allard, D., Tomasic, G., Thomas, M., Ribeiro, N., Thuaud, F., Basmadjian, C., Mateus, C., Routier, E., Kamsu-Kom, N., Agoussi, S., Eggermont, A., Désaubry, L., Robert, C., Vagner, S., *Nature,* **2014***, 513*, 105-109.

[79] Malka-Mahieu, H., Girault, I., Rubington, M., Leriche, M., Welsch, C., Kamsu-Kom, N., Zhao, Q., Désaubry, L., Vagner, S., Robert, C., *Cell Cycle*, **2016**, *15*, 2405-2409.

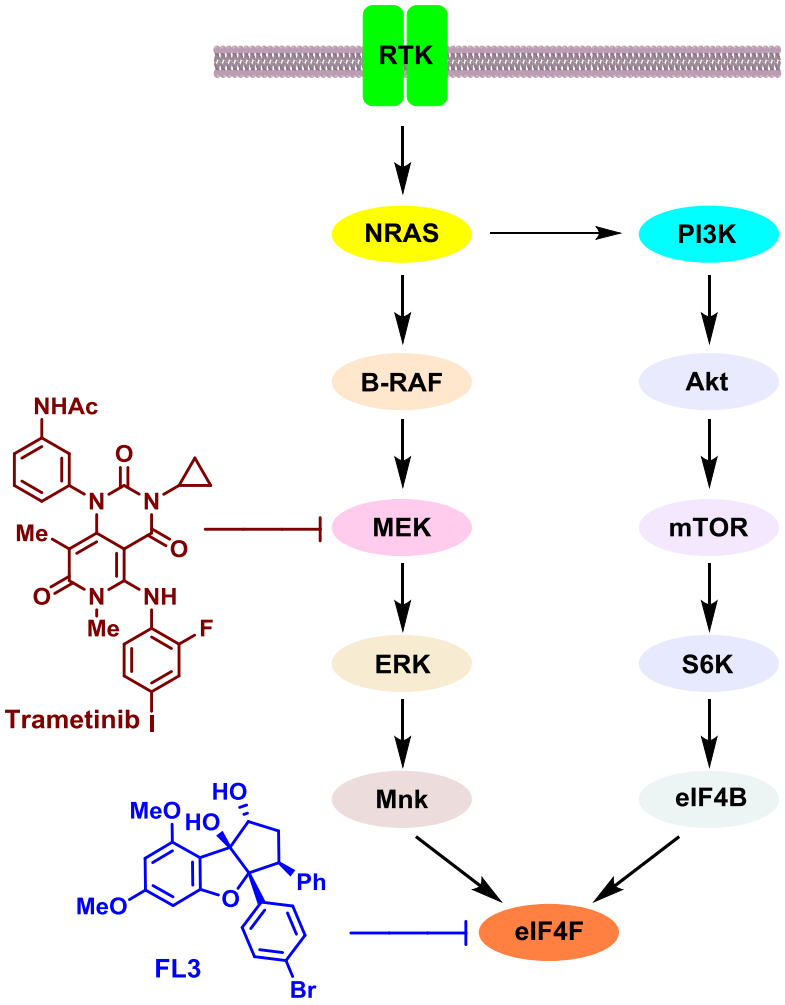

Figure 19. L'activation d'un récepteur tyrosine kinase (RTK) par un facteur de croissance active la voie PI3K/Akt/mTOR et celles des MAP kinases. Ces deux voies convergent vers l'activation du complexe eIF4F qui est inhibé par le FL3 (Figure copiée de la référence 78).

3.5.6. Inhibition de KRAS par les flavaglines et la fluorizoline (publication n° 10)

En 2014, les équipes de chimie organique des Pr Fernando Albericio et Rodolfo Lavilla de l'Université de Barcelone associés à leurs collaborateurs biologistes ont décrits une série de trifluorothiazolines diarylées qui présentent une cytotoxicité p53-dépendante sur un panel de lignées cancéreuses, le composé le plus cytotoxique

étant la fluorizoline.[80] Ces auteurs ont démontré par chromatographie d'affinité que ces composés se lient aux PHBs. Par la suite, l'équipe des Pr Daniel Iglesias-Serret et Joan Gil, au sein de la même université, ont montré qu'une déplétion partielle en PHBs confère une résistance aux effets cytotoxiques de la fluorizoline, démontrant ainsi l'implication des PHBs dans le mécanisme d'action cytotoxique de ce composé.[81]

Dans la présente étude, l'équipe du Pr Rajalingam a montré que la PHB1 est surexprimée dans les cancers du poumon non à petites cellules (NSCLCs), et que cette surexpression est corrélée à un pronostic défavorable.[82] De manière toute à fait inattendue, il a été trouvé que les flavaglines et la fluorizoline bloquent la liaison du GTP à KRAS muté ou activé par la signalisation de l'EGF. En effet l'activation d'un Récepteur Tyrosine Kinase, comme celui à l'EGF par exemple, induit le recrutement de Facteurs d'Echange de nucléotides Guanyliques (GEF, comme SOS par exemple) via les protéines adaptatrices SHC et Grb2 (Figure 20).[83] SOS induit le remplacement du GDP lié à RAS par du GTP, ce qui induit une dimérisation de cette protéine qui peut alors activer ses effecteurs, notamment les kinases RAF ou les phosphoinositide 3-kinases (PI3K).

Le Pr Rajalingam avait déjà démontré en 2005 que les PHBs doivent interagir avec B-RAF pour que celle-ci puisse être activée par RAS.[84] Cependant, une modulation de l'échange GTP-GDP lié à RAS par les PHBs n'avait jamais été examinée.

[80] Pérez-Perarnau, A., Preciado, S., Palmeri, C. M., Moncunill-Massaguer, C., Iglesias-Serret, D., González-Gironès, D. M., Miguel, M., Karasawa, S., Sakamoto, S., Cosialls, A.M., Rubio-Patiño, C., Saura-Esteller, J., Ramón, R., Caja, L., Fabregat, I., *Angew. Chemie. Int. Ed.*, **2014**, *53*, 10150–10154.

[81] Moncunill-Massaguer, C., Saura-Esteller, J., Pérez-Perarnau, A., Palmeri, C.M., Núñez-Vázquez, S., Cosialls, A. M., González-Gironès, D. M., Pomares, H., Korwitz, A., Preciado, S., Albericio, F., Lavilla, R., Pons, G., Langer, T., Iglesias-Serret, D., Gil, J., *Oncotarget*, **2015**, *6*, 41750-41765.

[82] Yurugi, H., Marini, F., Weber, C., David, K., Zhao, Q., Binder, H., Désaubry, L., Rajalingam, K., *Oncogene*, **2017**, *36*, 1-12.

[83] Lu, S., Jang, H., Muratcioglu, S., Gursoy, A., Keskin, O., Nussinov, R., Zhang, J., *Chem. Rev.,* **2016**, *116*, 6607−6665.

[84] Rajalingam, K., Wunder, C., Brinkmann, V., Churin, Y., Hekman, M., Sievers, C., Rapp, U. R., Rudel, T., *Nat. Cell Biol.*, **2005**, *7*(8), 837-843.

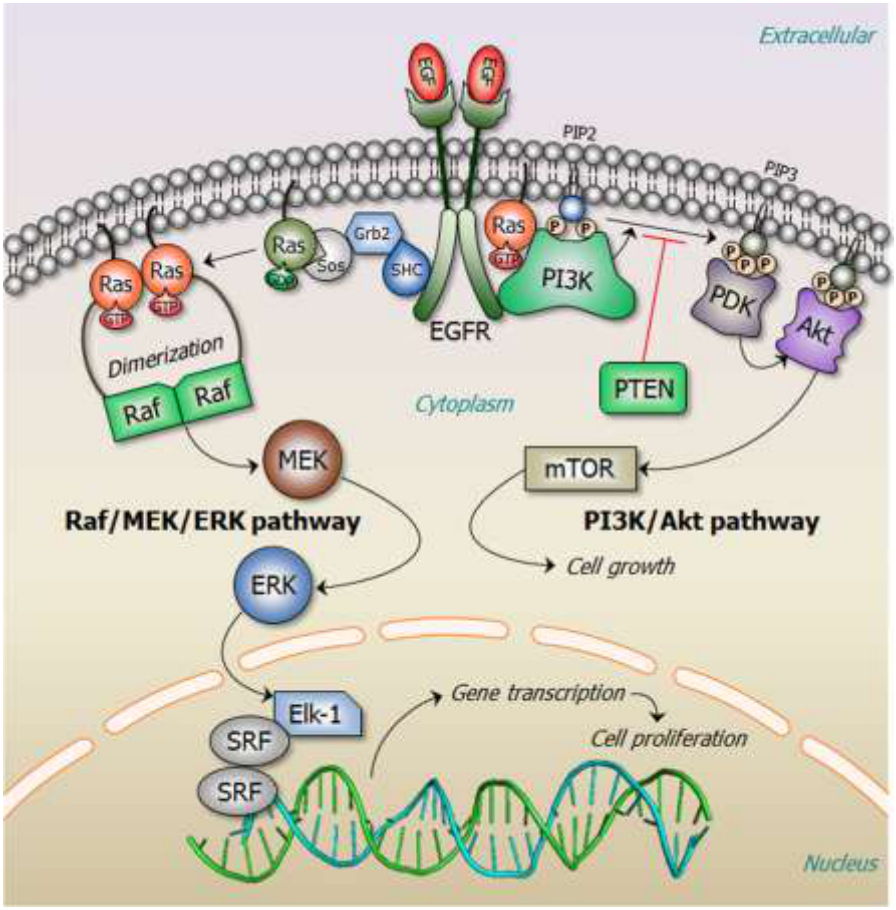

Figure 20. L'activation du récepteur à l'EGF induit une cascade d'événement conduisant à un échange du GDP lié à RAS par du GTP et à une activation des voies RAF/MEK/ERK et PI3K/Akt/ mTOR (Figure copiée de la référence 81).

Cette observation que les flavaglines et la fluorizoline bloquent KRAS est importante, car les mutations qui activent cette protéine sont retrouvées dans 75 à 95 % des cancers du pancréas, près de 50% des cancers colorectaux et dans de nombreux autres types de cancer. Après plus de trente ans de recherche intensive, aucun médicament ciblant KRAS n'est disponible. Plusieurs approches ont été envisagées, mais aucune ne combine efficacité thérapeutique et effets secondaires acceptables (Tableau 4).[85]

[85] Ostrem, J. M., Shokat, K. M., *Nat. Rev. Drug Discov.*, **2016**, *15*, 771-785.

Structure des inhibiteurs de KRAS	Mécanisme d'action
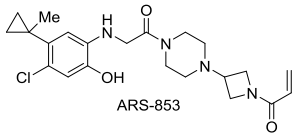 ARS-853	Inhibiteur spécifique du mutant oncogénique de KRAS-G12C.
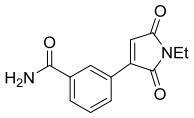	Inhibiteur irréversible qui alkyle le complexe RAS-SOS bloquant ainsi la liaison au GTP.
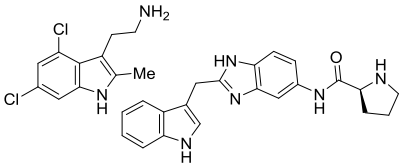	Inhibiteurs qui ralentissent l'échange GDP → GDP.
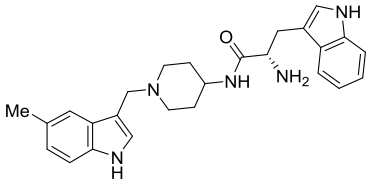	Activateur de l'échange GDP → GDP qui bloque l'activation des voies RAF/MEK/ERK et PI3K/Akt/mTOR.
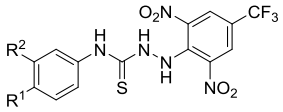 R^1= Me, R^2= Cl: Kobe 0065 R^1= F, R^2= H: Kobe 2602	Inhibiteurs qui se lient à GTP-RAS pour bloquer l'interaction avec RAF.
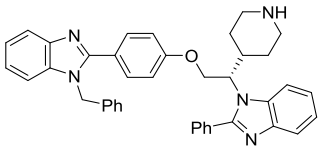 Deltarasine	Inhibiteur de la phosphodiestérase δ (PDEδ) qui bloque l'interaction entre cette protéine et KRAS, perturbant ainsi la localisation intracellulaire de ce dernier.

Tableau 4. Exemples représentatifs de composés inhibant KRAS.[83]

4. CONCLUSION

4. Conclusion

Nous avons développé trois accès synthétiques à des intermédiaires fonctionnalisés de flavaglines. Dans un premier temps, une cyclopentènone tri-substituée a été obtenue par une cyclisation catalysée à l'or (I). Les essais de transformation de cette cyclopentènone en flavaglines en utilisant une méthode déjà décrite n'ont pas abouti, ce qui suggère que cette approche est limitée à la préparation des flavaglines ne possédant pas les substituants nécessaires pour l'activité pharmacologique. Nous avons également montré les limites de la réaction de Nazarov pour synthétiser les flavaglines, en mettant notamment en évidence le manque de réactivité d'ènones substituées par un thioéther. Dans un troisième temps, une condensation/cyclisation spontanée a été découverte et a permis de transformer une cyclopentènone di-substituée en cyclopenta[*b*]benzofurane.

Nous avons aussi synthétisé deux isostères de flavaglines en introduisant un formamide ou un sulfonamide en position 8b, démontrant ainsi l'importance de l'hydroxyle dans cette position.

De plus, au cours de cette thèse, du FL3 et un autre ligand des prohibitines, la fluorizoline, ont été ré-synthétisés. Nos collaborateurs ont démontré leur efficacité thérapeutique dans des modèles de cancers, d'inflammation chronique des intestins (maladie de Crohn) ou encore dans la prévention des effets adverses des chimiothérapies au niveau cardiaque. Cette efficacité couplée à un mécanisme d'action originale nous incite à poursuivre ces travaux. Notre objectif ultime étant d'identifier des dérivés brevetables des flavaglines et de la fluorizoline susceptibles de rentrer dans des essais cliniques.

5. PARTIE EXPERIMENTALE

5. Partie expérimentale

Généralités :

Tous les réactifs commerciaux ont été utilisés sans purification sauf le benzaldéhyde qui a été distillé avant utilisation. Tous les solvants anhydres utilisés sont commerciaux ou conservés sur tamis moléculaire. Toutes les réactions sensibles à l'humidité ou l'oxygène ont été effectuées sous atmosphère d'argon et dans des ballons séchés à 110°C.

Les réactions ont été suivies par chromatographie sur couche mince (plaque CCM Merck DC Platten Kieselgel 60 F_{254}). La révélation des plaques a été effectuée par irradiation ultraviolette à 254 ou 365 nm, puis par immersion dans un révélateur ($KMnO_4$ ou vanilline) si nécessaire. Les colonnes chromatographiques ont été réalisées avec du gel de silice fine Merck 60 ; 0,040 - 0,065 mm (230 - 400 mesh).

Les spectres RMN ^{1}H et ^{13}C ont été enregistrés sur des spectromères Brüker (400 MHz/ 100 MHz) ou (500 MHz / 125 MHz). Les conditions sont spécifiées pour chaque spectre (température 25°C sauf indication contraire). Les multiplicités sont désignées comme suit : s, singulet ; d, doublet ; t, triplet ; q, quadruplet ; m, multiplet ; dd, doublet de doublet ; dt, doublet de triplet. Le déplacement chimique (δ) est donné en ppm. Le pic résiduel de solvant sert de référence, $CHCl_3$ (7.26 ppm, ^{1}H ; 77.16 ppm pour le pic central, ^{13}C), DMSO (2.50 ppm, ^{1}H ; 39.52 ppm pour le pic central, ^{13}C).

Les analyses par spectroscopie de masse basse et haute résolution ont été réalisées par le Service Commun d'Analyse (SCA) de la faculté de pharmacie d'Illkirch. Les spectres de masse basse résolution ont été réalisés avec un appareil Agilent 1200SL (LC-MS : simple quadripôle, source multimode ES/APCI). Les spectres de masse haute résolution ont été réalisés sur un appareil Brüker MicroTOF-Q (ESI Q-TOF).

5.1. Procédure pour le chapitre 3.1.

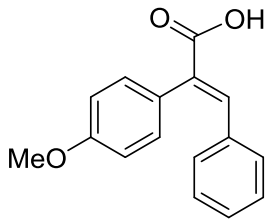

47

Acide (*E*)-2-(4-méthoxyphényl)-3-phénylacrylic (47)

De l'anhydride acétique (76 ml) a été ajouté aux gouttes à gouttes à 0°C à un mélange de l'acide acétique (33 g, 0.2 mol), du benzaldéhyde (22 ml, 0.22 mol) et de la triéthylamine (27.4 ml, 0.2 mol). Le milieu réactionnel a été sous agitation à 50°C pour 2h, à 100°C pour 5h. Le milieu réactionnel a été refroidi à température ambiante puis une solution de NaOH (1M) a été ajoutée jusqu'au pH = 8. Le milieu a été extrait avec de l'éther, et la phase aqueuse a été acidifié avec de l'HCl concentré à 0°C. Le précipité obtenu a été filtré et dissous dans de l'acétate d'éthyle, séché sur $MgSO_4$, filtré et évaporé à sec. Le composé **47** a été obtenu sous forme d'une poudre blanche quantitativement (50g).

RMN ^{1}H ($CDCl_3$, 400 MHz) δ 7.94 (s, 1H, CH), 7.47 - 7.11 (m, 5H, CH_{ar}), 7.18 (d, 2H, J = 8,9 Hz, CH_{ar}), 6.92 (d, 2H, J = 8,7 Hz, CH_{ar}), 3.85 (s, 3H, OCH_3) ppm ;

RMN ^{13}C ($CDCl_3$, 100MHz) δ 173.5, 159.5, 142.4, 131.2 (2C), 130.9 (2C), 129.5, 128.7, 128.5, 128.5 (2C), 128.2, 114.4 (2C), 55.4 ppm.

HR-MS masse calculée pour $C_{16}H_{14}O_3$: 254.0943, trouvée : 255.1013 $(M+H)^+$.

Point de fusion : 135.2 °C

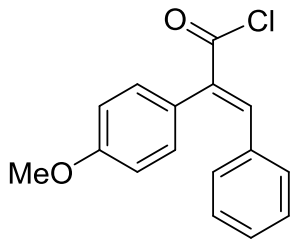

56

Chlorure de *(E)*-2-(4-Méthoxyphényl)-3-phénylacryloyle (56)

Une quantité catalytique de DMF (235µl, 3 mmol) a été ajoutée à une solution du composé **47** (30.75 g, 0.121 mol) dans du CH_2Cl_2 (160 ml). Le mélange a été refroidi à 0°C puis du chlorure d'oxalyle (11.76 ml, 0.139 mol) a été ajouté aux gouttes à gouttes. Le milieu réactionnel a été agité à température ambiante pour 12h puis concentré à sec. Il a été lavé 3 fois avec du toluène, puis évaporé à sec pour donner quantitativement le composé **56** (33g), sous forme d'une poudre beige.

RMN ^{1}H ($CDCl_3$, 400 MHz) δ 8.08 (s, 1H, CH), 7.30 - 7.12 (m, 7H, CH_{ar}), 6.75 (d, 2H, J = 8.9 Hz, CH_{ar}), 3.85 (s, 3H, OCH_3) ppm;

RMN ^{13}C ($CDCl_3$, 100 MHz) δ 169.8, 160.0, 147.6, 136.0, 131.5 (2C), 131.2 (2C), 130.6, 128.6 (2C), 128.4, 126.8, 114.7 (2C), 54.4 ppm.

HR-MS : masse calculée pour $C_{16}H_{13}ClO_2$: 272.0604, trouvée 272.0604 $[C_{16}H_{13}ClO_2^{\cdot}]^{+}$.

Point de fusion : 137.1 °C

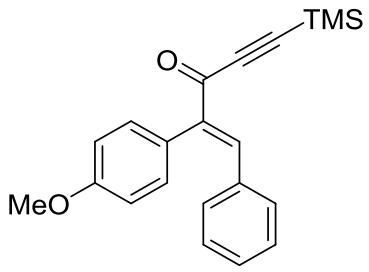

46

(*E*)-2-(4-Méthoxyphényl)-1-phényl -5- (trimethylsilyl)pent-1-èn-4-yn-3-one (46)

Le composé **56** (26 g, 0.095 mol), du $Pd(PPh_3)_2Cl_2$ (1.33 g, 1.9 mmol) et du CuI (720 mg, 3.8 mmol) ont été ajouté successivement sous argon à une solution du triméthylsilylacétylène (13.16 g, 0.134 mol) dans du 1,4-dioxane (500 ml). La triéthylamine (39.8 ml) a été ensuite ajouté à 0°C. Le milieu réactionnel a été agité à 80°C pour 12h, après refroidi à température ambiante, il a été filtré sur célite. Le filtrat a été concentré à sec. La chromatographie sur silice a donné le composé **46** sous forme d'une poudre jaune avec 64% de rendement.

RMN ^{1}H ($CDCl_3$, 400 MHz) δ 8.10 (s, 1H, CH), 7.27 - 7.20 (m, 3H, CH_{ar}), 7.15 (d, 2H, J = 7.1 Hz, CH_{ar}), 7.08 (d, 2H, J = 8.7 Hz, CH_{ar}), 6.93 (d, 2H, J = 8.7 Hz, CH_{ar}), 3.84 (s, 3H, OCH_3), 0.29 (s, 9H, CH_3) ppm;

RMN ^{13}C ($CDCl_3$, 100 MHz) δ 179.4, 159.7, 145.6, 141.2, 134.7, 131.2 (2C), 131.2 (2C), 129.9, 128.3 (2C), 126.6, 114.4 (2C), 101.1, 100.4, 55.3, -0.6 (3C) ppm.

HR-MS : masse calculée pour $C_{21}H_{22}O_2Si$: 334.1349, trouvée : 335.1469 $(M+H)^+$.

Point de fusion : 84.6 °C

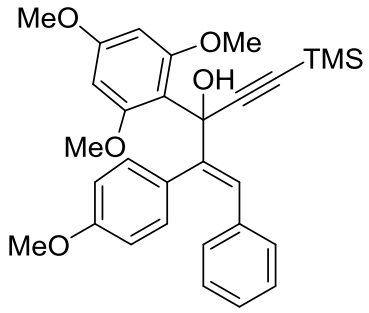

45

***(E)*-2-(4-Méthoxyphényl)-1-phényl-3-(2,4,6-triméthoxyphényl)-5-(tri-methylsilyl)pent-1-èn-4-yn-3-ol (45)**

Du *sec*-BuLi (1.4 M, 80.6 ml, 0.113 mol) a été ajouté au goutte à goutte à -78°C à une solution du 1,3,5-triméthoxybenzène (18.9 g, 0.113 mol) dans du THF anhydre (250 ml), puis le mélange a été agité à 0°C pour 1h. Le lithien a été ensuite ajouté au goutte à goutte à -78°C à une solution du composé **46** (25.2 g, 0.075 mol) dans du THF anhydre (250 ml). Le milieu réactionnel a été agité à 0°C pour 3h puis quenché avec une solution saturée de $KHSO_4$, extrait avec de l'éther. La phase organique a été séchée sur $MgSO_4$, filtrée et concentrée. La chromatographie sur silice a donné le composé **45** sous forme d'une poudre blanche avec 71% de rendement (26.6 g).

RMN ^{1}H ($CDCl_3$, 400 MHz) δ 7.21 (s, 1H, CH), 7.09 - 7.04 (m, 3H, CH_{ar}), 6.93 - 6.90 (m, 4H, CH_{ar}), 6.72 (d, 2H, J = 8.7 Hz, CH_{ar}), 6.50(s, 1H, OH), 6.07 (s, 2H), 3.78 (s, 3H, OCH_3), 3.77 (s, 3H, OCH_3), 3.63 (s, 6H, OCH_3), 0.21 (s, 9H, CH_3) ppm;

RMN ^{13}C ($CDCl_3$, 100 MHz) δ 160.4, 159.0 (2C), 158.7, 143.6, 137.4, 131.8 (2C), 130.2, 129.5, 127.9 (2C), 127.0, 126.5, 113.2 (2C), 111.4, 107.8, 92.8 (2C), 88.7, 76.9, 56.3 (2C), 55.4, 55.3, 0.3 (3C) ppm.

HR-MS : masse calculée pour $C_{30}H_{34}O_5Si$: 502.2176, trouvée : 525.2077 $(M+Na)^+$.

Point de fusion : 110.2 °C

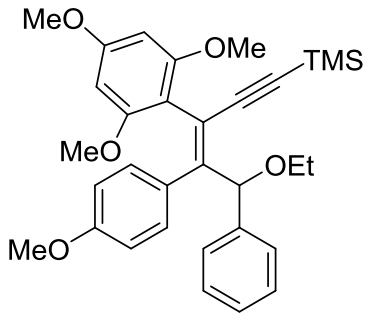

49

***(Z)*-(5-Ethoxy-4-(4-méthoxyphényl)-5-phényl-3-(2,4,6-triméthoxy-phényl) pent-3-èn-1-yn-1-yl) trimethylsilane (49)**

Un mélange de $MoO_2(acac)_2$ (26 mg, 0.08 mmol), NH_4PF_6 (13 mg, 0.08 mmol) et de l'éthanol (140 µl, 2.39 mmol) dans du CH_3CN (4 ml) a été agité à 65°C pour 10min, puis le composé **45** (400 mg, 0.8 mmol) a été ajouté. Le milieu réactionnel a été sous agitation à 65°C pour 3h, puis refroidi à température ambiante, filtré sur célite et concentré à sec. La chromatographie sur silice a donné le composé **49** sous forme d'un solide jaune avec 42% de rendement (296mg).

RMN ^{1}H ($CDCl_3$, 400 MHz) δ 7.48 (d, 2H, J = 7.6 Hz, CH_{ar}), 7.29 - 7.25 (m, 2H, CH_{ar}), 7.21 - 7.17 (m, 1H, CH_{ar}), 6.63 (dd, 2H, J = 8.9 et 2.0 Hz, CH_{ar}), 6.43 (dd, 2H, J = 8.8 et 2.0 Hz, CH_{ar}), 6.30 (s, 1H, CH), 5.92 (dd, 2H, J = 12.9 and 2.0 Hz, CH_{ar}), 3.97 - 3.89 (m, 1H, CH_2), 3.81 - 3.73 (m, 1H, CH_2), 3.72 (s, 3H, OCH_3), 3.69 (s, 3H, OCH_3), 3.63 (s, 3H, OCH_3), 3.61 (s, 3H, OCH_3), 1.30 (t, 3H, J = 7 Hz, CH_3), 0.17 (s, 9H, CH_3) ppm;

RMN ^{13}C ($CDCl_3$, 100 MHz) δ 160.8, 158.2, 158.2, 151.6, 141.4, 130.1, 130.0 (2C), 127.8 (2C), 126.6, 126.5 (2C), 117.0, 112.0 (2C), 110.3, 105.4, 97.0, 91.0, 91.0, 81.2, 64.0, 56.0, 55.8, 55.3, 55.3, 55.0, 15.4, 0.3 (3C) ppm.

HR-MS : masse calculée pour $C_{32}H_{38}O_5Si$: 530.2489, trouvée : 553.2394 $(M+Na)^+$.

Point de fusion : 119.9 °C

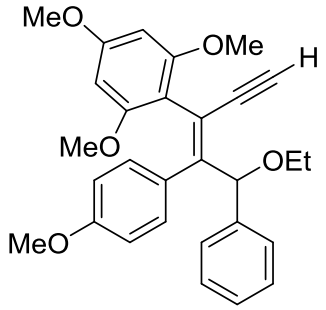

50

***(E)*-2-(5-Ethoxy-4-(4-méthoxyphényl)-5-phénylpent-3-èn-1-yn-3-yl)-1,3,5-triméthoxybenzène (50)**

Du K_2CO_3 (110 mg, 0.08 mmol) a été ajouté à une solution du composé **49** (210 mg, 0.396 mmol) dans du MeOH (500 µL). Le milieu a été agité à température ambiante pour 3h, puis lavé par de l'eau et extrait avec de l'éther. La phase organique a été séchée sur $MgSO_4$, filtrée et concentrée. La chromatographie sur silice a donné le composé **50** sous forme d'une huile jaune clair avec 75% de rendement (136 mg).

RMN ^{1}H ($CDCl_3$, 400 MHz) δ 7.54 (d, 2H, J = 8.0 Hz, CH_{ar}), 7.32 - 7.28 (m, 2H, CH_{ar}), 7.24 - 7.20 (m, 1H, CH_{ar}), 6.66 (dd, 2H, J = 9.0 et 2.1 Hz, CH_{ar}), 6.46 (dd, 2H, J = 8.9 et 2.1 Hz, CH_{ar}), 6.28 (s, 1H, CH), 5.94 (dd, 2 H, J = 19.3 et 2.1 Hz, CH_{ar}), 3.99 - 3.93 (m, 1H, CH_2), 3.82 - 3.77 (m, 1H, CH_2), 3.75 (s, 3H, OCH_3), 3.72 (s, 3H, OCH_3), 3.65 (s, 3H, OCH_3), 3.63 (s, 3H, OCH_3), 3.2 (s, 1H, CH), 1.31 (t, 3H, J = 6.9 Hz, CH_3) ppm;

RMN ^{13}C ($CDCl_3$, 100 MHz) δ 160.9, 158.2, 158.0, 157.9, 152.2, 141.0, 129.7, 129.7, 127.8, 126.7, 126.4, 115.9, 112.1, 109.7, 90.8, 90.7, 83.7, 81.3, 80.2, 64.1, 55.9, 55.76, 55.3, 54.9, 15.4 ppm.

HR-MS : masse calculée pour $C_{29}H_{30}O_5$: 458.2093, trouvée : 459.2171 $(M+H)^+$.

Procédure générale (N° 1) de la cyclisation catalysée à l'or :

Un mélange du $Au[(C_6H_5)_3P]Cl$ (5%) et du $AgSbF_6$ (5%) dans du CH_2Cl_2 a été agité à température ambiante pour 10 min. Une solution du composé **50**, **58a** ou **58b** (1 éq) dans du CH_2Cl_2 et de l'isopropanol (1.1 éq) ont été ajouté successivement. Le milieu réactionnel a été agité à température ambiante pour 12h, puis filtré sur célité et concentré à sec. La chromatographie sur silice a donné le composé cyclisé.

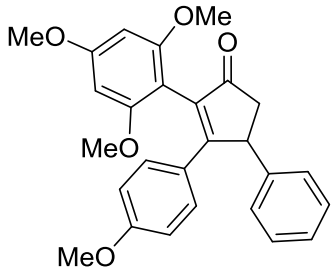

44

3-(4-Mméthoxyphényl)-4-phényl-2-(2 ,4, 6-triméthoxyphényl)cyclopent-2-èn-1-one (44)

Le composé **44** a été obtenu selon la procédure générale (N° 1) à partir du composé **50** (170 mg, 0.37 mmol), avec du $Au[(C_6H_5)_3P]Cl$ (9 mg, 0.019 mmol), du $AgSbF_6$ (6.5 mg, 0.019 mmol) et de l'isopropanol (31 µL, 0.4 mmol) dans du CH_2Cl_2 (4 ml). Le rendement est 63% (100 mg). Le composé est sous forme d'une huile marron.

RMN ^{1}H ($CDCl_3$, 400 MHz) δ 7.32 (d, 2H, J = 8.1 Hz, CH_{ar}), 7.27 - 7.24 (m, 4H, CH_{ar}), 7.16 (m, 1H, CH_{ar}), 6.62 (d, 2H, J = 9.0 Hz, CH_{ar}), 6.24 (d, 1H, J = 2.1 Hz, CH_{ar}), 6.17 (d, 1H, J = 2.1 Hz, CH_{ar}), 4.63 (dd, 1H, J = 7.4 et 1.9 Hz, CH_2), 3.85 (s, 3H, OCH_3), 3.76 (s, 3H, OCH_3), 3.70 (s, 3H, OCH_3), 3.57 (s, 3H, OCH_3), 3.17 (dd, 1H, J = 18.1 et 7.6 Hz, CH), 2.48 (dd, 1H, J = 18.3 et 1.9 Hz, CH_2) ppm;

RMN ^{13}C ($CDCl_3$, 100 MHz) δ 206.9, 168.6, 161.8, 160.3, 158.6, 156.9, 151.4, 144.3, 132.1, 129.9(2C), 129.4, 128.9(2C), 127.4(2C), 126.6, 113.4 (2C), 91.6, 91.4, 55.7,

55.9, 55.4, 55.1, 47.2, 45.9 ppm.

HR-MS : masse calculée pour $C_{27}H_{26}O_5$: 430.1780, trouvée: 431.2071 $(M+H)^+$.

Procédure générale (N° 2) pour synthétiser la propènone 56-1 :

Un mélange du chlorure d'acyle **56** (1 éq), de l'acide arylboronique (1.2 éq), du $PdCl_2(PPh_3)_2$ (2%), et du $K_3PO_4 \cdot H_2O$ (1.2 éq) dans du toluène a été agité à 80°C pour 4h sous argon. Le milieu a été refroidi à température ambiante, filtré sur célite et concentré. La chromatographie sur silice a donné la propènone **56-1**.

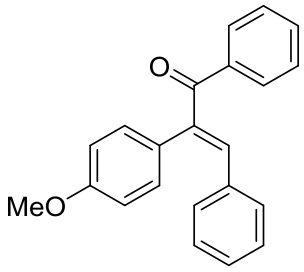

56a-1

***(E)*-2-(4-Méthoxyphényl)-1, 3-diphénylprop-2-èn-1-one (56a-1).**

Le composé **56a-1** a été obtenu selon la procédure générale (N° 2) à partir du chlorure d'acyle **56** (1 g, 3.7 mmol), de l'acide phénylboronique (540 mg, 4.4 mmol), du $PdCl_2(PPh_3)_2$ (49 mg, 0.07 mol), et du $K_3PO_4 \cdot H_2O$ (1.095 g, 4.41 mmol) dans du toluène (16 ml) selon la procédure générale. Le rendement est 54% (626 mg).

RMN ^{1}H ($CDCl_3$, 400 MHz) δ 7.86 (dd, 2H, J = 8.3 et 1.3 Hz, CH_{ar}), 7.56 - 7.52 (m, 1H, CH_{ar}), 7.46 - 7.42 (m, 2H, CH_{ar}), 7.23 - 7.18 (m, 6H, CH_{ar} et CH), 7.15 - 7.11 (m, 2H, CH_{ar}), 6.88 (d, 2H, J = 8.8 Hz, CH_{ar}), 3.82 (s, 3H, OCH_3) ppm;

RMN ^{13}C ($CDCl_3$, 100 MHz) δ 198.1, 159.5, 140.6, 139.5, 138.4, 135.2, 132.2, 131.1 (2C), 130.4, 129.9 (2C), 128.9, 128.8, 128.4 (4C), 114.4 (2C), 55.3 ppm.

HR-MS : masse calculée pour $C_{22}H_{18}O_2$: 314.1307, trouvée : 315.1385 $(M+H)^+$.

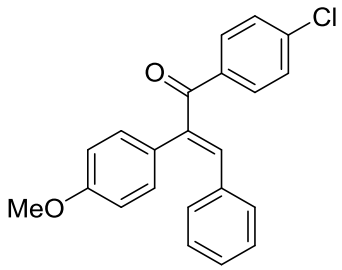

56b-1

***(E)*-1-(4-Chlorophényl)-2-(4-méthoxyphényl)-3-phénylprop-2-èn-1-one (56b-1)**

Le composé **56b-1** a été obtenu selon la procédure générale (N° 2) à partir du chlorure d'acyle **56** (1 g, 3.7 mmol), de l'acide 4-chlorophénylboronique (688 mg, 4.4 mmol), du $PdCl_2(PPh_3)_2$ (49 mg, 0.07 mol), et du $K_3PO_4 \cdot H_2O$ (1.095 g, 4.41 mmol) dans du toluene (16 ml). Le rendement est 54% (696 mg).

RMN ^{1}H ($CDCl_3$, 400 MHz) δ 7.78 (dd, 2H, J = 8.9 et 2.0 Hz, CH_{ar}), 7.40 (dd, 2H, J = 8.9 et 2.0 Hz, CH_{ar}), 7.24 - 7.20 (m, 3H, CH_{ar}), 7.19 - 7.13 (m, 5H, CH_{ar} et CH), 6.87 (dd, 2H, J = 8.9 et 2.0 Hz, CH_{ar}), 3.82 (s, 3H, OCH_3) ppm;

RMN ^{13}C ($CDCl_3$, 100 MHz) δ 196.8, 159.6, 140.3, 136.6, 138.6, 136.7, 135.1, 131.3 (2C), 131.0 (2C), 130.4 (2C), 129.1, 128.7 (2C), 128.5, 128.4 (2C), 114.5 (2C), 55.4 ppm.

HR-MS: masse calculée pour $C_{22}H_{17}ClO_2$: 348.0917, trouvée 349.0922 $(M+H)^+$.

Procédure générale (N° 3) pour synthétiser l'alcool propargylique :

Du *sec*-BuLi ou du *n*-BuLi (1.1 éq) a été ajouté sous argon au gouttes à goutte à -78°C à une solution du *tert*-Butyldiméthylsilylacétylène (1.05 éq) dans du THF anhydre, le mélange a été agité à 0°C pour 1h puis ajouté au goutte à goutte à une solution du composé **56-1** (1 éq) dans du THF anhydre. Le milieu réactionnel a été agité à -78°C pour 2h puis quenché avec une solution saturée de NH_4Cl, extrait avec de l'éther. La phase organique a été séchée sur $MgSO_4$, filtrée et concentrée. La chromatographie sur silice a donné l'alcool propargylique **57**.

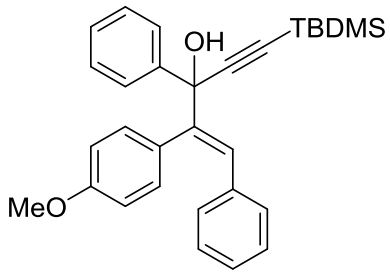

57a

(*E*)-5-(Tert-butyldimethylsilyl)-2-(4-méthoxyphényl)-1,3-diphénylpent-1-èn-4-yn-3-ol (57a)

Le composé **57a** a été obtenu selon la procédure générale (N° 3) à partir du composé **56a-1** (600 mg, 1.9 mmol), avec du *tert*-Butyldiméthylsilylacétylène (280 mg, 2 mmol) et du *sec*-BuLi (1.3M, 1.6 ml, 2.1 mmol) dans du THF anhydre (13 ml). Le rendement est 50% (430 mg). Le composé est sous forme d'une huile incolorée.

RMN ^{1}H ($CDCl_3$, 400 MHz) δ 7.58 - 7.56 (m, 2H, CH_{ar}), 7.34 - 7.26 (m, 3H, CH_{ar}), 7.23 (s, 1H, CH), 7.09 - 7.07 (m, 3H, CH_{ar}), 6.90 - 6.88 (m, 2H, CH_{ar}), 6.73 (dd, 4H, J = 16.4 et 9.0Hz, CH_{ar}), 3.77 (s, 3H, OCH_3), 2.64 (s, 1H, OH), 0.95 (s, 9H, CH_3), 0.15 (s, 3H, CH_3), 0.14 (s, 3H, CH_3) ppm;

RMN ^{13}C ($CDCl_3$, 100 MHz) δ 159.0, 143.7, 142.6, 136.5, 131.8, 129.6, 129.2, 128.0,

128.0, 127.9, 127.4, 127.1, 126.9, 113.6, 107.5, 91.8, 76.8, 55.2, 26.2, 16.8, -4.50, -4.54 ppm.

HR-MS: masse calculée pour $C_{30}H_{34}O_2Si$: 454.2328, trouvée : 454.2328 $[C_{30}H_{34}O_2Si^{\cdot}]^+$.

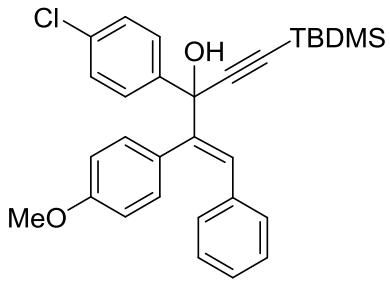

57b

***(E)*-5-(T*ert*-Butyldimethylsilyl)-3-(4-chlorophényl)-2-(4-méthoxy-phényl)-1-phénylpent-1-èn-4-yn-3-ol (57b)**

Le composé **57b** a été obtenu selon la procédure générale (N° 3) à partir du composé **56b-1** (68 mg, 0.49 mmol), avec du *tert*-Butyldiméthylsilylacétylène (170 mg, 0.49 mmol) et du *n*-BuLi (1.6M, 0.33 ml, 0.52 mmol) dans du THF anhydre (8 ml). Le rendement est 69% (162 mg). Le composé est sous forme d'une poudre blanche.

RMN ^{1}H ($CDCl_3$, 400 MHz) δ 7.49 (dd, 2H, J = 8.7 et 2.0 Hz, CH_{ar}), 7.27 (dd, 2H, J = 8.8 et 2.0 Hz, CH_{ar}), 7.24 (s, 1H, CH), 7.10 - 7.08 (m, 3H, CH_{ar}), 6.90 - 6.88 (m, 2H, CH_{ar}), 6.78 - 6.74 (m, 4H, CH_{ar}), 3.78 (s, 3H, OCH_3), 1.00 (s, 9H, CH_3), 0.15 (d, 6H, J = 6.5Hz, CH_3) ppm ;

RMN ^{13}C ($CDCl_3$, 100 MHz) δ 159.2, 143.3, 141.4, 136.3, 133.7, 131.8 (2C), 129.6 (2C), 128.8, 128.3 (2C), 128.2 (2C), 128.1(2C), 127.8, 127.3, 113.8 (2C), 107.1, 92.3, 76.4, 55.3, 26.3 (3C), 16.8, -4.5, -4.6 ppm.

HR-MS : masse calculée pour $C_{30}H_{33}ClO_2Si$: 488.1938, trouvée : 511.1840 $(M+Na)^+$.

Procédure générale (N° 4) pour synthétiser de l'éther 57-1:

Un mélange de $MoO_2(acac)_2$ (10%), du NH_4PF_6 (10%) et de l'éthanol (3 éq) dans du CH_3CN a été agité à 65°C pour 10min. Le composé **57** (1 éq) a été ajouté, puis le milieu a été agité à 65°C pour 2h. Il a été ensuite refroidi à température ambiante, filtré sur célite puis concentré. La chromatographie sur silice a donné de l'éther.

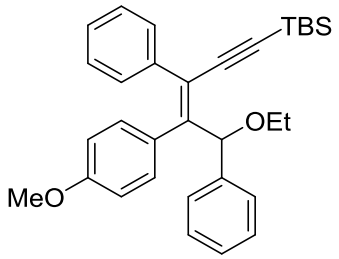

57a-1

***(Z)-Tert*-butyl(5-éthoxy-4-(4-méthoxyphényl)-3,5-diphénylpent-3-èn-1-yn-1-yl) dimethylsilane (57a-1)**

Le composé **57a-1** a été obtenu selon la procédure générale (N° 4) à partir du composé **57a** (400 mg, 0.88 mmol), avec du $MoO_2(acac)_2$ (29 mg, 0.088 mmol), du NH_4PF_6 (14 mg, 0.088 mmol) et de l'éthanol (150 µL, 2.64 mmol) dans du CH_3CN (4 ml). Le rendement est 16% (60 mg). Le composé est sous forme d'une poudre beige.

RMN ^{1}H ($CDCl_3$, 400 MHz) δ 7.41 (d, 2H, J = 7.2 Hz, CH_{ar}), 7.30 - 7.27 (m, 2H, CH_{ar}), 7.24 - 7.20 (m, 3H, CH_{ar}), 7.12 - 7.10 (m, 3H, CH_{ar}), 6.70 (d, 2H, J = 8.9 Hz, CH_{ar}), 6.57 (d, 2H, J = 8.9 Hz, CH_{ar}), 6.40 (s, 1H, CH), 3.88 - 3.81 (m, 1H, CH_2), 3.78 - 3.71 (m, 1H, CH_2), 3.70 (s, 3H, OCH_3), 1.32 (t, 3H, J = 7 Hz, CH_3), 1.03 (s, 9H, CH_3), 0.22 (d, 6H, J = 1.9 Hz, CH_3) ppm ;

RMN ^{13}C ($CDCl_3$, 100 MHz) δ 158.6, 149.7, 138.4, 131.6 (2C), 130.0 (2C), 129.0, 128.0 (2C), 127.7 (2C), 127.0, 126.1, 126.3 (2C), 124.3, 113.0 (2C), 106.1, 99.0, 82.3, 64.3, 55.0, 26.4 (3C), 17.0, 15.5, -4.4, -4.4 ppm.

HR-MS : masse calculée pour $C_{32}H_{38}O_2Si$: 482.2641, trouvée : 482.2641 pour $[C_{32}H_{38}O_2Si^{\cdot}]^+$.

Point de fusion : 105.9°C

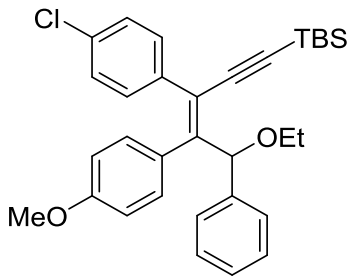

57b-1

***(Z)*-T*ert*-butyl(3-(4-chlorophényl)-5-éthoxy-4-(4-méthoxyphényl) -5-phénylpent-3-èn-1-yn-1-yl)diméthylsilane (57b-1)**

Le composé **57b-1** a été obtenu selon la procédure générale (N° 4) à partir du composé **57b** (100 mg, 0.2 mmol), avec du $MoO_2(acac)_2$ (7 mg, 0.02 mmol), du NH_4PF_6 (4 mg, 0.02 mmol) et de l'éthanol (40 µl, 0.6 mmol) dans du CH_3CN (1 ml). Le rendement est 30% (30 mg). Le composé est sous forme d'une huile incolorée.

RMN ^{1}H ($CDCl_3$, 400 MHz) δ 7.36 - 7.34 (m, 2H, CH_{ar}), 7.27 - 7.23 (m, 2H, CH_{ar}), 7.22 - 7.19 (m, 1H, CH_{ar}), 7.11 - 7.04 (m, 4H, CH_{ar}), 6.65 (dd, 2H, J = 8.9 et 2.1 Hz, CH_{ar}), 6.57 (dd, 2H, J = 9.0 et 2.3 Hz, CH_{ar}), 6.32 (s, 1H, CH), 3.70 (s, 3H, OCH_3), 3.81 - 3.79 (m, 1H, CH_2), 3.72 - 3.64 (m, 1H, CH_2), 1.28 (t, 3H, J = 7.0 Hz, CH_3), 1.00 (s, 9H, CH_3), 0.20 (d, 6H, J = 1.5 Hz, CH_3) ppm ;

RMN ^{13}C ($CDCl_3$, 100 MHz) δ 158.8, 150.3, 140.8, 136.9, 132.8, 131.5 (2C), 131.3 (2C), 128.6, 128.0 (2C), 128.0, 127.9(2C), 127.1, 126.3 (2C), 123.0, 113.1 (2C), 105.5, 99.5, 82.3, 64.4, 55.1, 26.4 (3C), 17.0, 15.5, -4.4, -4.4 ppm.

HR-MS : masse calculée pour $C_{32}H_{37}ClO_2Si$: 516.2251, trouvée : 516.2251 pour $[C_{32}H_{37}ClO_2Si^{\cdot}]^{+}$.

Procédure générale (N° 5) de désilylation des composés 58 :

Du méthanol (3 gouttes) et du TBAF (1.0 M, 2.4 éq) ont été ajouté à 0°C à une solution du composé **57-1** (1 éq) dans du THF. Le milieu a été agité à température ambiante pour 40 min, puis quenché avec une solution saturée de NH_4Cl et extrait à l'éther. La phase organique combinée a été lavée avec de la saumure, séchée sur $MgSO_4$, filtrée et concentrée. La chromatographie sur silice a donné le produit désilylé.

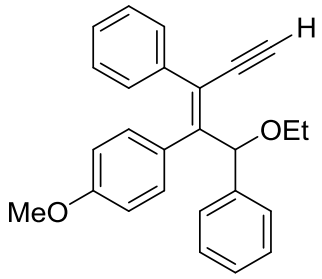

58a

***(E)*-(1-Éthoxy-2-(4-méthoxyphényl) pent-2-èn-4-yne-1,3-diyl) dibenzène (58a)**.

Le composé **58a** a été obtenu selon la procedure générale (N° 5) à partir du compose **57a-1** (50 mg, 0.14 mmol), avec du TBAF (1.0 M, 0.35 ml, 0.35 mmol) et 3 gouttes de méthanol dans du THF (18 ml). Le rendement est 93% (48 mg).

RMN ^{1}H ($CDCl_3$, 400 MHz) δ 7.39 (d, 2H, J = 8.0 Hz, CH_{ar}), 7.28 - 7.25 (m, 2H, CH_{ar}), 7.22 - 7.17 (m, 3H, CH_{ar}), 7.13 - 7.08 (m, 3H, CH_{ar}), 6.69 (d, 2H, J = 8.9 Hz, CH_{ar}), 6.54 (d, 2H, J = 8.9 Hz, CH_{ar}), 6.29 (s, 1H, CH), 3.84 - 3.78 (m, 1H, CH_2), 3.75 - 3.69 (m, 1H, CH_2), 3.68 (s, 3H, OCH_3), 3.42 (s, 1H, CH), 1.28 (t, 3H, J = 7.0 Hz, CH_3) ppm ;

RMN ^{13}C ($CDCl_3$, 100 MHz) δ 158.7, 150.5, 140.8, 138.4, 131.6 (2C), 129.9 (2C), 128.9, 128.0 (2C), 127.8 (2C), 127.1, 127.1, 126.3 (2C), 123.2, 112.9 (2C), 84.0, 83.3, 82.2, 64.3, 55.1, 15.4 ppm.

HR-MS : masse calculée pour $C_{26}H_{24}O_2$: 368.1776, trouvée : 391.1674 $(M+Na)^+$.

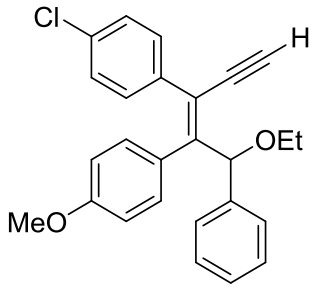

58b

(*E*)-1-Chloro-4-(5-éthoxy-4-(4-méthoxyphényl)-5-phénylpent-3-èn-1-yn-3-yl)benzène (58b)

Le composé **58b** a été obtenu selon la procédure générale (N° 5) à partir du composé **57b-1** (25 mg, 0.05 mmol), avec du TBAF (1.0 M, 0.12 ml, 0.12 mmol) et 3 gouttes de méthanol dans du THF (6 ml). Le rendement est 75% (15 mg).

RMN ^{1}H ($CDCl_3$, 400 MHz) δ 7.37 - 7.35 (m, 2H, CH_{ar}), 7.28 - 7.25 (m, 2H, CH_{ar}), 7.23 - 7.21 (m, 1H, CH_{ar}), 7.12 - 7.06 (m, 4H, CH_{ar}), 6.66 (dd, 2H, J = 8.9 et 2.1 Hz, CH_{ar}), 6.57 (dd, 2H, J = 8.9 et 2.1 Hz, CH_{ar}), 6.26 (s, 1H, CH), 3.83 - 3.75 (m, 1H, CH_2), 3.70 (s, 3H, OCH_3), 3.73 - 3.65 (m, 1H, CH_2), 3.43 (s, 1H, CH), 1.28 (t, 3H, J = 7.0 Hz, CH_3) ppm ;

RMN ^{13}C ($CDCl_3$, 100 MHz) δ 158.9, 151.1, 140.6, 136.8, 133.0, 131.5 (2C), 131.3 (2C), 128.4, 128.1 (2C), 128.0 (2C), 127.2, 126.3 (2C), 121.9, 113.1 (2C), 83.6, 83.5, 82.2, 64.4, 55.1, 15.5 ppm.

HR-MS : masse calculée pour $C_{26}H_{23}ClO_2$: 402.1387, trouvée : 402.1386 pour $[C_{26}H_{23}ClO_2^{\cdot}]^+$.

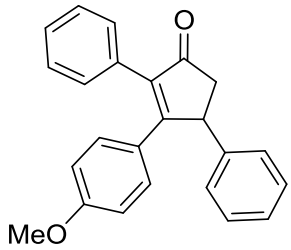

59a

3-(4-Méthoxyphényl)-2,4-diphénylcyclopent-2-èn-1-one (59a)

Le composé **11a** a été obtenu selon la procédure générale (N° 1) de la cyclisation catalysée à l'or, à partir du composé **58a** (48 mg, 0.13 mmol), avec du $Au[(C_6H_5)_3P]Cl$ (4 mg, 0.007 mmol), du $AgSbF_6$ (2 mg, 0.007mmol) et de l'isopropanol (11 µl, 0.148 mmol) dans du CH_2Cl_2 (0.8 ml). Le rendement est 50% (23 mg). Le composé est sous forme d'une huile jaune.

RMN ^{1}H ($CDCl_3$, 400 MHz) δ 7.46 - 7.40 (m, 3H, CH_{ar}), 7.39 - 7.31 (m, 5H, CH_{ar}), 7.25 - 7.23 (m, 2H, CH_{ar}), 7.19 (dd, 2H, J = 8.9 et 2.1 Hz, CH_{ar}), 6.70 (dd, 2H, J = 9.0 et 2.3 Hz, CH_{ar}), 4.64 (dd, 1H, J = 7.4 et 2.1 Hz, CH), 3.77 (s, 3H, OCH_3), 3.29 (dd, 1H, J = 18.7 et 7.4 Hz, CH_2), 2.65 (dd, 1H, J = 18.7 et 2.1 Hz, CH_2) ppm ;

RMN ^{13}C ($CDCl_3$, 100 MHz) δ 206.6, 169.6, 160.5, 143.0, 139.9, 132.7, 130.8 (2C), 129.8 (2C), 129.1 (2C), 128.6 (2C), 128.0, 127.5 (2C), 127.0, 127.0, 113.7 (2C), 55.3, 47.1, 46.2 ppm.

HR-MS : masse calculée pour $C_{24}H_{20}O_2$: 340.1463, trouvée : 340.1463 pour $[C_{24}H_{20}O_2^{\cdot}]^+$.

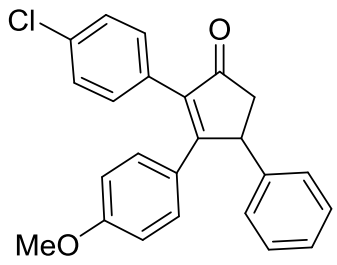

58b

2-(4-Chlorophényl) -3- (4-méthoxyphényl)-4- phénylcyclopent-2-èn-1-one (59b).

Le composé **59b** a été obtenu selon la procédure générale (N° 1) de la cyclisation catalysée à l'or, à partir du composé **58b** (48 mg, 0.119 mmol), avec du $Au[(C_6H_5)_3P]Cl$ (4 mg, 0.007 mmol), du $AgSbF_6$ (2 mg, 0.007mmol) et de l'isopropanol (11 µl, 0.148 mmol) dans du CH_2Cl_2 (0.8 ml). Le rendement est 75% (33 mg).

RMN ^{1}H ($CDCl_3$, 400 MHz) δ 7.33 (dd, 2H, J = 8.5 et 1.9 Hz, CH_{ar}), 7.27 -7.23 (m, 3H, CH_{ar}), 7.19 - 7.15 (m, 3H, CH_{ar}), 7.12 (dd, 2H, J = 9.0 et 2.1 Hz, CH_{ar}), 6.66 (dd, 2H, J = 8.9 et 2.0 Hz, CH_{ar}), 4.56 (dd, 1H, J = 7.4 et 2.1 Hz, CH), 3.72 (s, 3H, OCH_3), 3.22 (dd, 1H, J = 18.9 et 7.5 Hz, CH_2), 2.59 (dd, 1H, J = 18.8 et 2.1 Hz, CH_2) ;

RMN ^{13}C ($CDCl_3$, 100 MHz) δ 206.3, 170.2, 160.7, 142.7, 138.5, 134.0, 131.2(2C), 131.0, 130.8(2C), 129.1(2C), 128.9(2C), 127.5(2C), 127.1, 126.8, 113.9 (2C), 55.3, 47.2, 46.1 ppm.

HR-MS : masse calculée pour $C_{24}H_{19}ClO_2$: 374.1074, trouvée : 375.1155 $(M+H)^+$.

5.2. Procédure pour le chapitre 3.2.

Procédure générale (N° 6) pour l'addition des β-cétocarbonyles sur la benzoquinone :

Du $Cu(OTf)_2$ (0.05 éq) a été ajouté à une solution de l'oxopropionate (2éq) dans du toluène, puis une solution de benzoquinone (1éq) dans du toluène a été ajouté au goutte à goutte. Le milieu réactionnel a été chauffé à reflux pour 10h puis quenché avec une solution saturée de NH_4Cl. La phase aqueuse a été extraite avec de l'acétate d'éthyle. La phase organique combinée a été lavée avec de la saumure, puis séchée sur $MgSO_4$, filtrée et concentrée. La chromatographie sur silice et la cristallisation dans de l'éther a donné du benzofurane.

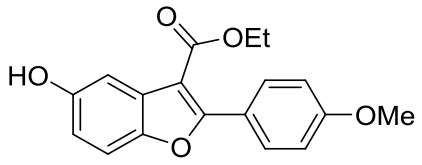

67a

5-Hydroxy-2-(4-méthoxyphényl)benzofuran-3-carboxylate d'éthyle (67a).

Le composé **67a** a été obtenu selon la procédure générale (N° 6) à partir de l'oxopropionate **69a** (82.2g, 370mmol) dans du toluène (500 ml) avec de la benzoquinone **68** (20 g, 185 mmol) et du $Cu(OTf)_2$ (3.05 g, 9.3 mmol). Le rendement est 54%. Le composé est sous forme d'une poudre blanche.

RMN ^{1}H ($CDCl_3$, 400 MHz) δ 7.93 (2H, d, J = 9.1 Hz, CH_{ar}), 7.41 (1H, d, J = 2.3Hz, CH_{ar}), 7.29 (1H, d, J = 8.8 Hz, CH_{ar}), 6.93 (2H, d, J = 9.1 Hz, CH_{ar}), 6.81 (1H, dd, J = 8.8 Hz et 2.5 Hz, CH_{ar}), 4.34 (2H, q, J = 7.1 Hz, CH_2), 3.83 (3H, s, OCH_3), 1.34 (3H, t, J = 7.2 Hz, CH_3) ppm ;

RMN ^{13}C ($CDCl_3$, 100 MHz) δ 164.5, 162.2, 161.4, 152.7, 148.8, 131.3, 128.5, 122.3, 113.7, 113.6, 111.7, 107.8, 107.7, 60.8, 55.5, 14.5 ppm.

Point de fusion : 157.5°C

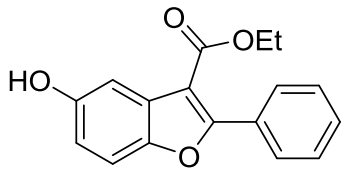

67b

5-Hydroxy-2-phénylbenzofuran-3-carboxylate d'éthyle (67b)

Le composé **67b** a été obtenu selon la procédure générale (N° 6) à partir de l'oxopropionate **69b** (32.4ml, 185mmol) dans du toluène (250 ml) avec de la benzoquinone **68** (10 g, 92 mmol) et du $Cu(OTf)_2$ (1.53 g, 4.6 mmol). Le rendement est 53% (13.8 g). Le composé est sous forme d'une poudre blanche.

RMN ^{1}H ($CDCl_3$, 400 MHz) δ 8.00 - 7.97 (m, 2H, CH_{ar}), 7.52 (dd, 1H, J = 0.4 et 2.6 Hz, CH_{ar}), 7.50 - 7.47 (m, 3H, CH_{ar}), 7.39 (d, 1H, J = 8.8 Hz, CH_{ar}), 6.89 (dd, 1H, J = 2.6 et 8.8 Hz, CH_{ar}), 4.99 (s, 1H, OH), 4.40 (q, 2H, J = 7.2 Hz, CH_2), 1.39 (t, 3H, J = 7.2 Hz, CH_3) ppm ;

RMN ^{13}C ($CDCl_3$, 100 MHz) δ 161.4, 161.8, 152.6, 148.9, 130.3, 129.7, 129.5 (2C), 128.2, 128.0 (2C), 113.9, 11.7, 108.8, 107.6, 60.7, 14.3 ppm.

BR-MS : masse calculée pour $C_{17}H_{14}O_4$: 282.1, trouvée : 283.0 $(M+H)^+$.

Procédure générale (N° 7) pour la méthylation des benzofuranes 70:

A une solution de benzofurane (1 éq) dans du DMF, du MeI (1.5 éq), du K_2CO_3 (2 éq), et du Cs_2CO_3 (0.1 éq) ont été ajoutés. Le milieu réactionnel a été agité pour 18h à 38°C, puis concentré à sec. Le mélange a été extrait avec de l'acétate d'éthyle. La phase organique a été lavée par de l'eau et de la saumure, séchée sur $MgSO_4$, filtrée et concentrée. La purification par chromatographie sur silice et la cristallisation dans l'éther a donné le produit méthylé.

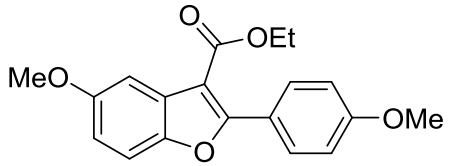

70a

5-Méthoxy-2-(4-méthoxyphényl)benzofuran-3-carboxylate d'éthyle (70a)

Le composé **70a** a été obtenu selon la procedure générale (N°7) à partir du benzofurane **67a** (30.92 g, 99 mmol) dans du DMF (370 ml) avec du MeI (9.25 ml, 149 mmol), du K_2CO_3 (27.39 g, 198 mmol) et du Cs_2CO_3 (3.23 g, 9.9 mmol). Le rendement est 77%. Le composé est sous forme d'un solide noir.

RMN ^{1}H ($CDCl_3$, 400 MHz) δ 7.93 (2H, d, J = 9.1 Hz, CH_{ar}), 7.41 (1H, d, J = 2.3 Hz, CH_{ar}), 7.29 (1H, d, J = 8.8 Hz, CH_{ar}), 6.93 (2H, d, J = 9.1 Hz, CH_{ar}), 6.81 (1H, dd, J = 8.8 et 2.5 Hz, CH_{ar}), 4.34 (2H, q, J = 7.1 Hz, CH_2), 3.89 (3H, s, OCH_3), 3.83 (3H, s, OCH_3), 1.34 (3H, t, J = 7.2 Hz, CH_3) ppm ;

RMN ^{13}C ($CDCl_3$, 100 MHz) δ 164.4, 161.8, 161.3, 156.9, 148.7, 131.3, 128.3, 122.4, 113.8, 113.7, 111.6, 108.0, 105.1, 77.2, 60.6, 56.0, 55.5, 14.5 ppm.

Point de fusion : 172.0°C

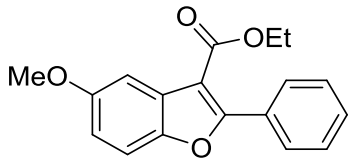

70b

5-Méthoxy-2-phénylbenzofuran-3-carboxylate d'éthyle (70b)

Le composé **70b** a été obtenu selon la procedure générale (N° 7) à partir du benzofurane **67b** (10 g, 35.2 mmol) dans du DMF (120 ml) avec du MeI (3.3 mL, 52.8 mmol), du K_2CO_3 (9.7 g, 70.4 mmol) et du Cs_2CO_3 (1.14 g, 3.5 mmol). La reaction est quantitative. Le composé est sous forme d'une poudre jaune.

RMN ^{1}H ($CDCl_3$, 400 MHz) δ 8.00 - 7.98 (m, 2H, CH_{ar}), 7.57 (d, 1H, J = 2.6 Hz, CH_{ar}), 7.50 - 7.47 (m, 3H, CH_{ar}), 7.42 (d, 1H, J = 8.9 Hz, CH_{ar}), 6.96 (dd, 1H, J = 9 et 2.8 Hz, CH_{ar}), 4.40 (q, 2H, J = 7.2 Hz, CH_2), 3.90 (s, 3H, OCH_3), 1.41 (t, 3H, J = 7.2 Hz, CH_3) ppm ;

RMN ^{13}C ($CDCl_3$, 100 MHz) δ 164.2, 161.5, 157.0, 149.0, 130.3, 129.9, 129.6(2C), 128.1(2C), 128.1, 114.3, 110.8, 109.1, 105.0, 60.7, 56.0, 14.4 ppm.

BR-MS : masse calculée pour $C_{18}H_{16}O_4$: 296,1, trouvée : 297.2 $(M+H)^+$.

Procédure générale (N° 8) pour la réduction des esters :

Une solution de l'ester (1éq) dans du THF anhydre a été ajouté sous argon au goutte à goutte à 0°C à une suspension du $LiAlH_4$ (5 éq) dans du THF anhydre. Le mélange a été agité à 0°C pour 2h puis quenché avec de l'eau. Une solution de NaOH (15%) a été ajoutée et le précipité a été filtré. Le filtrat a été concentré pour donner le produit de réduction.

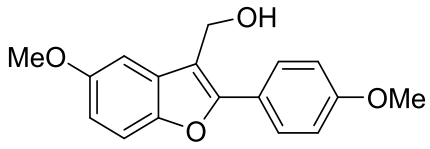

70a

(5-Méthoxy-2-(4-méthoxyphényl)-benzofuran-3-yl)méthanol (71a)

Le composé **71a** a été obtenu selon la procédure générale (N° 8) à partir de l'ester **70a** (24.9 g, 78 mmol) dans du THF anhydre (500 ml) avec du $LiAlH_4$ (14.7 g, 388 mmol). Le rendement est 88%.

RMN ^{1}H ($CDCl_3$, 400 MHz) δ 7.76 (d, 2H, J = 9.0 Hz, CH_{ar}), 7.37 (d, 1H, J = 8.9 Hz, CH_{ar}), 7.12 (d, 1H, J = 2.6 Hz, CH_{ar}), 7.01 (d, 2H, J = 9.0 Hz, CH_{ar}), 6.88 (dd, 1H, J = 8.9 et 2.6 Hz, CH_{ar}), 4.91 (d, 2H, J = 5.3 Hz, CH_2), 3.87 (s, 6H, OCH_3), 1.70 (t, 1H, J = 5.3 Hz, OH) ppm;

RMN ^{13}C ($CDCl_3$, 100 MHz) δ 160.3, 156.3, 154.7, 148.9, 130.1, 128.9(2C), 123.1, 114.4(2C), 113.7, 113.1, 111.7, 101.9, 56.1, 55.8, 55.5 ppm.

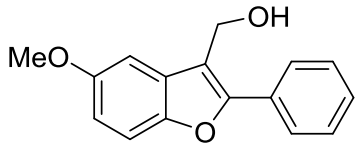

71b

(5-Méthoxy-2-phénylbenzofuran-3-yl)méthanol (71b)

Le composé **71b** a été obtenu selon la procédure générale (N° 8) à partir de l'ester **70b** (10.5 g, 35.2 mmol) dans du THF anhydre (175 ml) avec du $LiAlH_4$ (7.3 g, 193.6 mmol). Le rendement est 96%. Le composé est sous forme d'une poudre blanche.

RMN ^{1}H ($CDCl_3$, 400 MHz) δ 7.85 - 7.83 (m, 2H, CH_{ar}), 7.52 - 7.48 (m, 2H, CH_{ar}), 7.44 - 7.40 (m, 2H, CH_{ar}), 7.16 (d, 1H, J = 2.5 Hz, CH_{ar}), 6.93 (dd, 1H, J = 8.9 et 2.6 Hz, CH_{ar}),

4.98 (d, 2H, J = 5.4 Hz, CH_2), 3.89 (s, 3H, OCH_3) ppm ;

RMN ^{13}C ($CDCl_3$, 100 MHz) δ 156.2, 154.3, 149.0, 130.3, 129.8, 128.9, 128.8 (2C), 127.3 (2C), 115.0, 113.6, 111.8, 102.0, 56.0, 55.7 ppm.

BR-MS : masse calculée pour $C_{16}H_{14}O_3$: 254.0943, trouvée : 254.0949 $[C_{16}H_{14}O_3^{\cdot}]^+$.

Point de fusion : 102.7°C

Procédure générale (N° 9) pour l'oxydation de l'alcool primaire

A -78°C, une solution du DMSO (2 éq) dans du CH_2Cl_2 anhydre a été ajoutée sous argon au goutte à goutte à une solution de $(COCl)_2$ (1.2 éq) dans du CH_2Cl_2 anhydre. Une solution de l'alcool primaire (1 éq) dans du CH_2Cl_2 anhydre et de la triéthylamine (2.5 éq) ont été ensuite ajoutée successivement à la même température. Le milieu réactionnel a été agité pour 2h, et la température a été laissée remonter à -40°C. Le milieu réactionnel a été acidifié jusqu'à pH = 7 avec une solution saturée de NH_4Cl. La phase organique a été lavée avec de la saumure, séchée sur $MgSO_4$, filtrée et concentrée. La chromatographie sur silice a permis d'obtenir l'aldéhyde correspondant.

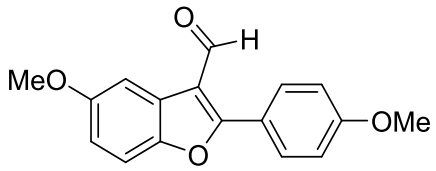

72a

5-Méthoxy-2-(4-méthoxyphényl)-benzofuran-3-carbaldehyde (72a)

Le composé 7**2a** a été obtenu selon la procédure général (N° 9) à partir de l'alcool **71a** (19.32 g, 68 mmol), dans du CH_2Cl_2 anhydre (450 ml), avec du $(COCl)_2$ (7 mL, 82

mmol), du DMSO (9.66 mL, 136 mmol) et de la triethylamine (23,5 mL, 170 mmol). Le rendement est 26%. Le composé est sous forme d'une poudre jaune.

RMN ^{1}H ($CDCl_3$, 400 MHz) δ 10.30 (s, 1H, CHO), 7.80 (d, 2H, J = 8.9 Hz, CH_{ar}), 7.74 (d, 1H, J = 2.6 Hz, CH_{ar}), 7.41 (d, 1H, J = 9.0 Hz, CH_{ar}), 7.07 (d, 2H, J = 8.9 Hz, CH_{ar}), 6.96 (dd, 1H, J = 9.0 et 2.6 Hz, CH_{ar}), 3.91 (s, 3H, OCH_3), 3.90 (s, 3H, CH_3) ppm ;

RMN ^{13}C ($CDCl_3$, 100 MHz) δ 186.8, 166.4, 162.1, 157.6, 148.8, 130.8, 126.4 (2C), 121.4, 117.0, 115.1, 114.8 (2C), 111.7, 104.4, 56.1, 55.7 ppm.

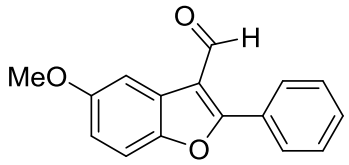

72b

5-Méthoxy-2-phénylbenzofuran-3-carbaldehyde (72b)

Le composé **72b** a été obtenu selon la procédure générale (N° 9) à partir de l'alcool **71b** (5 g, 19.7 mmol), dans du CH_2Cl_2 anhydre (130 ml), avec du $(COCl)_2$ (2 mL, 23.6 mmol), du DMSO (2.8 ml, 39.4 mmol) et de la triethylamine (7 mL, 49 mmol). Le rendement est 87%. Le composé est sous forme d'une poudre jaune claire.

RMN ^{1}H ($CDCl_3$, 400 MHz) δ 10.34 (s, 1H, CHO), 7.85 (m, 2H, CH_{ar}), 7.76 (d, 1H, J = 2.6 Hz, CH_{ar}), 7.57 (m, 3H, CH_{ar}), 7.45 (d, 1H, J = 8.9 Hz, CH_{ar}), 8.00 (dd, 1H, J = 9.0 et 2.8 Hz, CH_{ar}), 3.91 (s, 3H, OCH_3) ppm;

RMN ^{13}C ($CDCl_3$, 100 MHz,) δ 186.9, 166.1, 157.7, 149.1, 131.2, 129.3 (2C), 129.2 (2C), 128.9, 126.2, 117.9, 115.6, 111.9, 104.4, 56.2ppm.

Point de fusion : 112.0°C

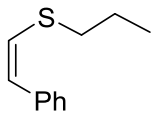

73a

(*Z*)-Propyl(styryl)sulfane (73a)

Du 1-propanethiol (10.63 ml, 117.6 mmol) a été ajouté à une suspension de Cs_2CO_3 (3.19 g, 9.8 mmol) dans du DMSO (600 ml), et le mélange a été agité pour 15 minutes. Du TEMPO (3.06 g, 19.5 mmol) a été ensuite ajouté, et après 15 minutes, du phénylacetylène (10.75 mL, 98.0 mmol) a été ajouté. Le milieu réactionnel a été agité à la température ambiante pour 3h puis quenché avec de l'eau et extrait avec de l'éther. La phase organique a été séchée sur $MgSO_4$, filtrée et concentrée. La chromatographie sur silice a donné l'éther thiovinylique **73a** avec un rendement de 66%.

RMN ^{1}H ($CDCl_3$, 400 MHz) δ 7.49 (d, 2H, J = 7.3 Hz, CH_{ar}), 7.35 (t, 2H, J = 7.5 Hz, CH_{ar}), 7.21 (t, 1H, J = 7.3 Hz, CH_{ar}), 6.33 (d, 1H, J = 10.9 Hz, CH), 6.25 (d, 1H, J = 10.9 Hz, CH), 2.77 (t, 2H, J = 7.2 Hz, CH_2), 1.73 (six., 2H, J = 7.3 Hz, CH_2), 1.03 (t, 3H, J = 7.4 Hz, CH_3) ppm ;

RMN ^{13}C ($CDCl_3$, 100 MHz) δ 137.2, 128.7, 128.3, 127.8, 126.7, 125.4, 77.2, 38.1, 23.7, 13.3 ppm.

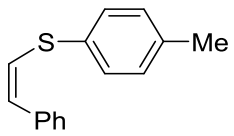

73b

(*Z*)-Styryl(*p*-tolyl)sulfane (73b)

A 0°C, du sodium (2.37 g, 0.103 mol) a été dissous dans de l'éthanol absolu (100 mL). Du 4-méthylbenzènethiol (12.75 g, 0.103 mol) et du phénylacétylène (10.8 mL, 0.098

mol) ont été ajouté successivement à la température ambiante. Le milieu réactionnel a été chauffé à reflux pour 12h puis refroidi à 0°C et versé dans de l'eau glacée. Le précipité obtenu a été filtré et séché sous vide pour donner le composé 73b avec un rendement de 73%.

RMN ^{1}H ($CDCl_3$, 400 MHz) δ 7.55 (d, 2H, J = 8.5 Hz, CH_{ar}), 7.42 - 7.36 (m, 4H, CH_{ar}), 7.29 - 7.25 (m, 1H, CH_{ar}), 7.17 (d, 2H, J = 7.9 Hz, CH_{ar}), 6.56 (d, 1H, J = 10.8 Hz, CH), 6.48 (d, 1H, J = 10.8 Hz, CH), 2.36 (s, 3H, CH_3) ppm;

RMN ^{13}C ($CDCl_3$, 100 MHz) δ 137.5, 136.7, 132.8, 130.6 (2C), 130.0 (2C), 128.8 (2C), 128.4 (2C), 127.1, 127.1, 126.6, 21.2 ppm.

Procédure générale (N°10) pour la formation de l'alcool divinylique

Du *n*-BuLi (1.6M, 1.6 éq) a été ajouté au goutte à goutte à -78°C sous argon à une solution de l'éther thiovinylique (1.5 éq) dans du THF anhydre. Le mélange a été agité pour 45 minutes à la même température. Parallèlement, du $BF_3.Et_2O$ (1.1 éq) a été ajouté à -78°C à une solution de l'aldéhyde (1 éq) dans du THF anhydre, et le mélange a été agité à la même température pour 45 minutes. Le milieu d'aldéhyde a été ajouté ensuite au goutte à goutte dans le milieu de l'éther thiovinylique lithié à -78°C. Après 2h de l'agitation à la même température, le milieu réactionnel a été quenché avec de l'eau et une solution saturée de bicarbonate. La phase aqueuse a été extraite avec de l'éther, la phase organique combinée a été lavée avec de l'eau et séchée sur $MgSO_4$, filtrée et concentrée. La chromatographie sur silice a donné l'alcool divinylique.

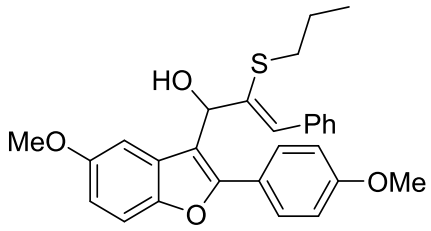

74a

(*Z*)-1-(5-Méthoxy-2-(4-méthoxyphényl)-benzofuran-3-yl)-3-phényl-2-(propylthio)prop-2-èn-1-ol (74a)

Le composé **74a** a été obtenu selon la procedure générale (N° 10) à partir de l'aldéhyde 7**2a** (1.50 g, 5.3 mmol) et du thiovinylether **73a** (1.42 g, 8.0 mmol) dans du THF anhydre (140 mL) avec du *n*-BuLi (5.3 mL, 8.5 mmol) et du $BF_3{\cdot}Et_2O$ (0.73 mL, 5.8 mmol). Le rendement est 72% (1.76 g). Le composé est sous forme d'une huile jaune.

RMN ^{1}H ($CDCl_3$, 400 MHz) δ 7.73 (d, 2H, J = 8.9 Hz, CH_{ar}), 7.62 (d, 2H, J = 7.3 Hz, CH_{ar}), 7.39 (d, 1H, J = 8.9 Hz, CH_{ar}), 7.33 (t, 2H, J = 7.3 Hz, CH_{ar}), 7.25 (t, 1H, J = 7.4 Hz, CH_{ar}), 7.24 (d, 1H, J = 2.6 Hz, CH_{ar}), 7.19 (s, 1H, CH), 6.90 (d, 2H, J = 8.9 Hz, CH_{ar}), 6.88 (dd, 1H, J = 8.9 et 2.6 Hz, CH_{ar}), 5.74 (s, 1H, CH), 3.97 (s, 3H, OCH_3), 3.76 (s, 3H, OCH_3), 2.84 (s, 1H, OH), 2.53 (m, 2H, CH_2), 1.50 (six., 2H, J = 7.4 Hz, CH_2), 0.80 (t, 3H, J = 7.4 Hz, CH_3) ppm;

RMN ^{13}C ($CDCl_3$, 100 MHz) δ 160.5, 155.9, 154.8, 149.4, 136.3, 132.0, 129.6, 129.5, 128.6, 128.2, 127.7, 123.1, 114.5, 114.3, 113.3, 111.7, 104.0, 77.2, 70.2, 66.0, 56.0, 55.5, 34.8, 23.2, 13.4 ppm.

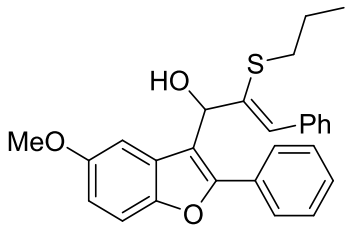

74b

(*Z*)-1-(5-Méthoxy-2-phénylbenzofuran-3-yl)-3-phényl-2-(propylthio) prop-2-èn-1-ol (74b)

Le composé **74b** a été obtenu selon la procedure générale (N°10) à partir de l'aldéhyde 7**2b** (200mg, 0.787 mmol) et du thiovinylether **73a** (200mg, 1.18 mmol) dans du THF anhydre (20 mL) avec du *n*-BuLi (788 µl, 8.5 mmol) et du $BF_3{\cdot}Et_2O$ (0.73 mL, 5.8 mmol). Le rendement est 23% (77 mg). Les produits de départ récupérés : l'éther thiovinylique **73a** (143mg, 68%) et l'aldéhyde **72b** (98mg, 50%).

RMN ^{1}H ($CDCl_3$, 400 MHz) δ 7.85 (d, 2H, J = 8.4 Hz, CH_{ar}), 7.62 (d, 2H, J = 7.3 Hz, CH_{ar}), 7.51 - 7.45 (m, 3H, CH_{ar}), 7.42 (d, 1H, J = 8.5 Hz, CH_{ar}), 7.34 (t, 2H, J = 7.3 Hz, CH_{ar}), 7.25 (m, 2H, CH_{ar}), 7.18 (s, 1H, CH), 6.91 (dd, 1H, J = 8.9 et 2.5 Hz, CH_{ar}), 5.78 (dd, 1H, J = 3.4 et 1.6 Hz, CH), 3.77 (s, 3H, OCH_3), 2.86 (d, 1H, J = 3.4Hz, OH), 2.62 - 2.48 (m, 2H, CH_2), 1.49 (sext., 2H, J = 7.3 Hz, CH_2), 0.80 (t, 3H, J = 7.3 Hz, CH_3) ppm;

RMN ^{13}C ($CDCl_3$, 100 MHz) δ 155.8, 154.4, 149.5, 136.1, 136.0, 132.1, 130.4, 129.5, 129.1, 128.7, 128.3, 128.1, 127.9, 127.6, 115.5, 113.6, 111.7, 104.0, 69.9, 55.9, 34.6, 23.1, 13.2 ppm.

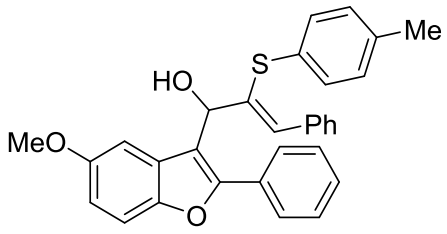

74c

(*Z*)-1-(5-Méthoxy-2-phénylbenzofuran-3-yl)-3-phényl-2-(p-tolylthio) prop-2-èn-1-ol (74c)

Le composé **74c** a été obtenu selon la procédure générale (N° 10) à partir de l'aldéhyde **72b** (3g, 0.012 mmol) et du thiovinylether **72b** (4g, 0.018 mmol) dans du THF anhydre (300 ml) avec du *n*-BuLi (11.8 ml, 0.019 mmol) et du $BF_3{\cdot}Et_2O$ (1.64 mL, 0.013 mmol). Le rendement est 86% (4.83 g).

RMN ^{1}H ($CDCl_3$, 400 MHz) δ 7.65 (d, 2H, J = 7.4 Hz, CH_{ar}), 7.58 - 7.55 (m, 2H, CH_{ar}), 7.45 (s, 1H, CH), 7.40 (d, 1H, J = 8.9 Hz, CH_{ar}), 7.37 - 7.26 (m, 7H, CH_{ar}), 7.13 (d, 2H, J = 8.0 Hz CH_{ar}), 6.90 (dd, 1H, J = 8.9 et 2.6 Hz, CH_{ar}), 6.92 (d, 2H, J = 7.8 Hz, CH_{ar}), 5.61 (dd, 1H, J = 3.5 et 1.4 Hz, CH), 3.76 (s, 3H, OCH_3), 2.60 (d, 1H, J = 3.5 Hz, OH), 2.24 (s, 3H, CH_3) ppm ;

RMN ^{13}C ($CDCl_3$, 100 MHz) δ 155.8, 154.5, 149.4, 137.3, 135.7, 135.2, 133.3, 131.2, 130.3, 129.7, 129.6, 129.1, 128.7, 128.5, 128.3, 128.1, 128.0, 127.6, 115.2, 113.6, 111.7, 103.8, 69.1, 55.9, 21.1 ppm.

Procédure générale(N° 11) pour l'oxidation de l'alcool secondaire

Du MnO_2 (6 éq) a été ajouté à une solution de l'alcool divinylique (6 éq) dans du CH_2Cl_2. Après l'agitation à la température ambiante pour 48h, le milieu réactionnel a été filtré sur célite et purifié sur silice pour donner la cétone divinylique correspondante.

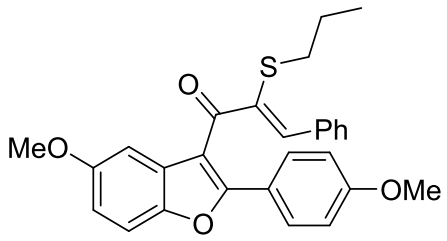

66a

(*Z*)-1-(5-Méthoxy-2-(4-méthoxyphényl)-benzofuran-3-yl)-3-phényl-2-(propylthio) prop-2-èn-1-one (66a)

Le composé **66a** a été obtenu selon la procédure générale (N° 11) à partir de l'alcool **74a** (1.5 g, 4.23 mmol) dans du CH_2Cl_2 (100 mL) avec du MnO_2 (2.21 g, 0.025 mol). Le rendement est 72% (1.4g). Le composé est sous forme d'un solide jaune.

RMN ^{1}H ($CDCl_3$, 400 MHz) δ 7.79 (d, 2H, J = 8.9 Hz, CH_{ar}), 7.49 (d, 2H, J = 7.3 Hz, CH_{ar}), 7.44 (d, 1H, J = 8.9 Hz, CH_{ar}), 7.43 (s, 1H, CH), 7.33 (t, 2H, J = 7.3 Hz, CH_{ar}), 7.31 (t, 1H, J = 7.3 Hz, CH_{ar}), 7.27 (d, 1H, J = 2.5 Hz, CH_{ar}), 6.94 (dd, 1H, J = 8.9 et 2.6 Hz, CH_{ar}), 6.92 (d, 2H, J = 8.9 Hz, CH_{ar}), 3.82 (s, 3H, OCH_3), 3.79 (s, 3H, OCH_3), 2.78 (t, 2H, J = 7.4 Hz, CH_2), 1.58 (six., 2H, J = 7.3 Hz, CH_2), 0.92 (t, 3H, J = 7.4 Hz, CH_3) ppm ;

RMN ^{13}C ($CDCl_3$, 100 MHz) δ 190.5, 161.3, 160.3, 157.0, 148.7, 141.3, 137.5, 135.1, 131.4, 130.5, 130.47, 129.2, 128.9, 128.3, 115.4, 114.3, 114.2, 113.4, 111.9, 103.7, 56.0, 55.5, 35.2, 23.5, 13.4 ppm.

BR-MS masse calculée pour $C_{28}H_{26}O_4S$: 458.2, trouvée : 459.1 $(M+H)^+$.

Point de fusion : 78.6°C

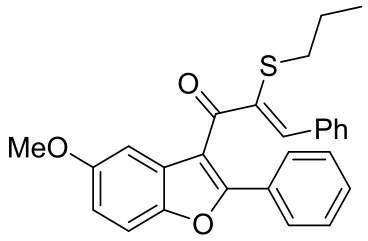

66b

(*Z*)-1-(5-méthoxy-2-phénylbenzofuran-3-yl)-3-phényl-2-(propylthio)prop-2-èn-1-one (66b)

Le composé **66b** a été obtenu selon la procédure générale (N° 11) à partir de l'alcool **74b** (75 mg, 0.174 mmol) dans du CH_2Cl_2 (3 mL) avec du MnO_2 (91 mg, 1.5 mmol). Le rendement est 87% (65 mg).

RMN ^{1}H ($CDCl_3$, 400 MHz) δ 7.82 - 7.79 (m, 2H, CH_{ar}), 7.48 - 7.45 (m, 4H, CH_{ar}), 7.41 - 7.39 (m, 3H, CH_{ar} et CH), 7.32 - 7.29 (m, 4H, CH_{ar}), 6.98 (dd, 1H, J = 9.0 et 2.6 Hz, CH_{ar}), 3.81 (s, 3H, OCH_3), 2.80 (t, 2H, J = 7.4 Hz, CH_2), 1.60 (six., 2H, J = 7.3 Hz, CH_2), 0.93 (t, 3H, J = 7.3 Hz, CH_3) ppm ;

RMN ^{13}C ($CDCl_3$, 100 MHz) δ 190.5, 159.7, 157.0, 149.0, 142.3, 137.0, 135.0, 130.5 (2C), 130.2, 130.0, 129.3, 128.9 (2C), 128.8, 128.7 (2C), 128.3 (2C), 116.5, 114.9, 112.1, 103.6, 56.0, 35.2, 23.5, 13.5 ppm.

BR-MS masse calculée pour $C_{27}H_{24}O_3S$: 428.1, trouvée : 429.1 $(M+H)^+$.

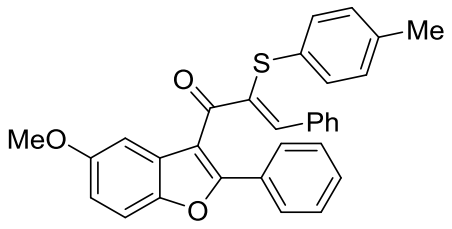

66c

(*Z*)-1-(5-Méthoxy-2-phénylbenzofuran-3-yl)-3-phényl-2-(*p*-tolylthio)prop-2-èn-1-on e (66c)

Le compose **66c** a été obtenu selon la procédure générale (N°11) à partir de l'alcool **74c** (2 g, 4.18 mmol) dans du CH_2Cl_2 (65 mL) avec du MnO_2 (2.18 g, 25.1 mmol). La réaction est quantitative (2 g). Le composé est sous forme d'une poudre jaune.

RMN ^{1}H ($CDCl_3$, 400 MHz) δ 7.67 - 7.65 (m, 3H, CH_{ar}), 7.56 - 7.54 (m, 2H, CH_{ar}), 7.38 - 7.33 (m, 7H, CH_{ar} et CH), 7.02 (d, 2H, J = 8.0 Hz, CH_{ar}), 6.97 (d, 1H, J = 2.5 Hz, CH_{ar}), 6.89 (dd, 1H, J = 8.9 et 2.5 Hz, CH_{ar}), 6.80 (d, 2H, J = 7.9 Hz, CH_{ar}), 3.78 (s, 3H, OCH_3), 2.11 (s, 3H, CH_3) ppm;

RMN ^{13}C ($CDCl_3$, 100 MHz) δ 156.3, 148.5, 141.4, 139.6, 137.8, 137.6, 134.8, 131.9 (2C), 130.6 (2C), 130.1, 130.0, 128.0, 123.9, 129.7 (2C), 129.6, 128.5 (2C), 128.5 (2C), 128.4 (2C), 116.8, 114.4, 111.6, 103.4, 56.0, 31.1, 21.0 ppm.

BR-MS masse calculée pour $C_{33}H_{24}O_3S$: 476.1, trouvée : 477.1 $(M+H)^+$.

Point de fusion : 122.5°C

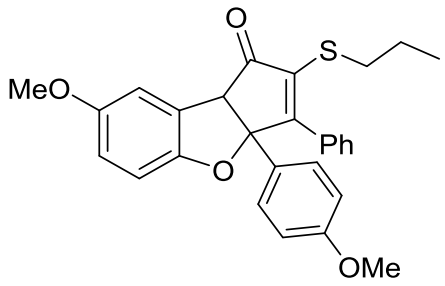

65a

7-Méthoxy-3a-(4-méthoxyphényl)-3-phényl-2-(propylthio)-3*a*,8*b*-dihydro-1H-cyclopenta[*b*]benzofuran-1-one (65a)

Du AcBr (24 µL, 0.33 mmol) a été ajouté à une solution de la cétone **66a** (100 mg, 0.22 mmol) dans du 1,2-DCE (3 mL). Le milieu réactionnel a été chauffé à 65°C pour 24h puis à 80°C pour 24h, après il a été quenché à température ambiante avec une solution saturée du bicarbonate, et la phase aquese a été extraite avec du CH_2Cl_2. La phase organique a été lavée avec de l'eau, séchée sur $MgSO_4$, filtrée et concentrée. La purification sur silice a donné la cyclopentènone **65a** avec 31% de rendement (31mg).

NMR ^{1}H ($CDCl_3$, 400 MHz) δ 7.53 (d, 2H, J = 7.3 Hz, CH_{ar}), 7.30 (t, 1H, J = 6.4 Hz, CH_{ar}), 7.33 (t, 2H, J = 7.3 Hz, CH_{ar}), 7.25 (d, 2H, J = 8.9 Hz, CH_{ar}), 6.97 (d, 1H, J = 2.5 Hz, CH_{ar}), 6.88 (d, 1H, J = 8.9 Hz, CH_{ar}), 6.80 (d, 2H, J = 8.9 Hz, CH_{ar}), 6.80 (dd, 1H, J = 2.6 et 8.9 Hz, CH_{ar}), 4.05 (s, 1H, CH), 3.77 (s, 3H, OCH_3), 3.76 (s, 3H, OCH_3), 2.91 (t, 2H, J = 7.4 Hz, CH_2), 1.40 (six., 2H, J = 7.4 Hz, CH_2), 0.80 (t, 3H, J = 7.4 Hz, CH_3) ppm ;

RMN ^{13}C ($CDCl_3$, 100 MHz) δ 165.2, 159.2, 155.0, 152.8, 137.7, 133.2, 132.5, 129.6 (2C), 128.0 (2C), 126.2 (2C), 124.1, 116.1, 114.2 (2C), 110.8, 109.8, 95.7, 62.8, 56.1, 55.3, 33.1, 23.4, 13.1 ppm.

BR-MS masse calculée pour $C_{28}H_{26}O_4S$: 458,2, trouvée : 459.8 $(M+H)^+$.

Procédure générale (N° 12) pour l'iodation des arènes

Du H_2O_2 (30% aq., 0.6-0.9 éq) et du I_2 (0.4-0.7 éq) ont été ajoutés à une solution d'arène(1 éq) dans de l'eau. La suspension a été agitée à température ambiante à 50°C pour 7 à 16 heures. Le milieu réactionnel a été dilué avec du CH_2Cl_2, lavé avec une solution saturée de $Na_2S_2O_3$ et de l'eau. La phase organique a été séchée sur $MgSO_4$, filtrée et concentrée. Une chromatographie sur silice a donné le produits iodé.

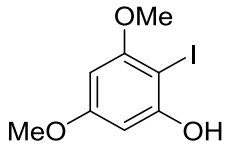

76-1

2-Iodo-3,5-diméthoxyphénol (76-1)

Le composé **76-1** a été obtenu selon la procédure générale (N° 12) à partir de 3,5-diméthoxyphénol (15 g, 97.4 mmol) dans de l'eau (180 mL) avec du H_2O_2 (30% aq., 7.17 g, 63.3 mmol) et du I_2 (12.4 g, 48.7 mmol). Le milieu a été agité pour 16 heures à temperature ambiante. Le rendement est de 29% (7.75 g). Le composé est sous forme d'une poudre beige.

RMN ^{1}H ($CDCl_3$, 400 MHz) δ 6.29 (d, 1H, J = 2.6 Hz, CH_{ar}), 6.06 (d, 1H, J = 2.6 Hz, CH_{ar}), 5.47 (s, 1H, OH), 3.84 (s, 3H, OCH_3), 3.79 (s, 3H, OCH_3) ppm;

RMN ^{13}C ($CDCl_3$, 100 MHz), δ 161.9, 158.7, 156.2, 92.7, 91.7, 66.8, 56.1, 55.2 ppm.

Point de fusion : 67.5°C

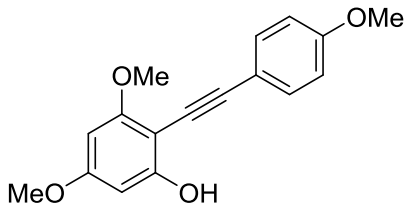

76

3,5-Diméthoxy-2-((4-méthoxyphényl)éthynyl)phénol (76)

L'iodophénol **76-1** (3.06 g, 10.92 mmol) et du 4-méthoxyphényl acéthylène (1.55 mL, 12.01 mmol) ont été dissous dans du THF anhydre (25 ml) sous argon. Du EtMgBr (22.93 mL, 22.93 mmol) a été ajouté au goutte à goutte à 0°C puis le mélange a été agité pour 5 minutes à la même température. Du $Pd(PPh_3)_2Cl_2$ (146 mg, 0.21 mmol) a été ensuite ajouté à température ambiante. Le milieu réactionnel a été chauffé à 70°C pour 2h puis quenché avec une solution de HCl (0.5 M), et la phase aqueuse a été extraite avec de l'acétate d'éthyle. La phase organique a été lavée avec de l'eau, séchée sur $MgSO_4$, filtrée et concentrée pour donner le tolane **76** avec 52% de rendement. Le composé est sous forme d'une poudre beige.

RMN ^{1}H ($CDCl_3$, 400 MHz) δ 7.48 (d, 2H, J = 8.9 Hz, CH_{ar}), 6.88 (d, 2H, J = 8.9 Hz, CH_{ar}), 6.19 (d, 1H, J = 2.3 Hz, CH_{ar}), 6.06 (d, 1H, J = 2.3 Hz, CH_{ar}), 5.98 (s, 1H, OH), 3.86 (s, 3H, OCH_3), 3.83 (s, 3H, OCH_3), 3.80 (s, 3H, OCH_3) ppm;

RMN ^{13}C ($CDCl_3$, 100 MHz) δ 161.8, 160.9, 159.7, 158.7, 133.1, 115.0, 113.9, 98.9, 92.4, 92.1, 91.4, 78.2, 56.0, 55.5, 55.3 ppm.

Point de fusion : 83.8°C

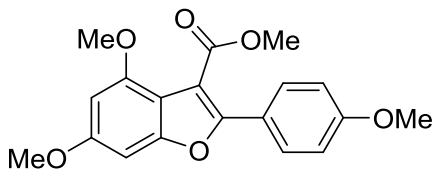

30

4, 6-diméthoxy-2-(4-méthoxyphényl)-benzofuran-3-carboxylate de méthyle (30)

Du CBr_4 (3.85 g, 11.6 mmol), du $Pd(OAc)_2$ (25 mg, 0.11 mmol) et du $NaHCO_3$ (0.970 g, 11.6 mmol) ont été ajoutés à une solution du tolane **76** (1.5 g, 5.29 mmol) dans du méthanol (30 ml). Le milieu réactionnel a été mis sous pression atmosphérique du CO et agité pour 12h à température ambiante. Il a été filtré sur célite, concentré et séché sous vide pour donner l'ester **30** avec 72% (1.3 g) de rendement. Le composé est sous forme d'une poudre marron.

RMN ^{1}H ($CDCl_3$, 400 MHz) δ 7.75 (d, 2H, J = 9.0 Hz, CH_{ar}), 6.96 (d, 2H, J = 8.9 Hz, CH_{ar}), 6.65 (d, 1H, J = 2.0 Hz, CH_{ar}), 6.35 (d, 1H, J = 1.9 Hz, CH_{ar}), 3.92 (s, 3H, OCH_3), 3.89 (s, 3H, OCH_3), 3.85 (s, 3H, OCH_3), 3.85 (s, 3H, OCH_3) ppm ;

RMN ^{13}C ($CDCl_3$, 100 MHz) δ 166.3, 160.4, 159.6, 155.5, 153.8, 153.6, 128.7(2C), 122.6, 114.1(2C), 111.0, 107.9, 95.3, 88.1, 56.0, 55.9, 55.5, 55.4 ppm.

Point de fusion : 64.2°C

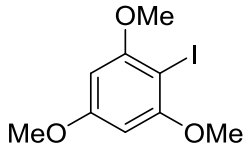

23-1

2-Iodo-1,3,5-triméthoxybenzène (23-1)

Le composé **23-1** a été obtenu selon la procédure générale (N° 12) à partir du 3,5-diméthoxyphénol (15 g, 97.4 mmol) dans de l'eau (180 mL) avec du H_2O_2 (30% aq.,

4.50 mL, 40,0 mmol) et du I_2 (5.08 g, 20.0 mmol). Le milieu a été agité à 50°C pour 7 heures. Le rendement est 94% (12.01 g).

RMN ^{1}H (DMSO-d_6, 400 MHz) δ 6.28 (s, 2H, CH_{ar}), 3.80 (s, 9H, OCH_3) ppm;

RMN ^{13}C ($CDCl_3$, 100 MHz) δ 161.9, 159.3, 91.6, 66.3, 56.4, 55.5 ppm.

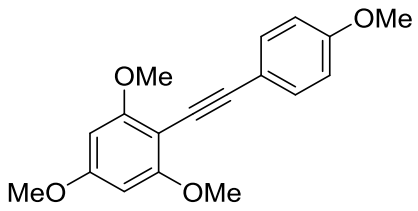

23

1,3,5-Triméthoxy-2-((4-méthoxyphényl)ethynyl)benzène (23)

Du 4-méthoxyphénylacétylène (3.5 g, 26.5 mmol), du $Pd(PPh_3)_2Cl_2$ (280 mg, 0.40 mmol) et du CuI (76 mg, 0.40 mmol) ont été ajouté à une suspension du 2-iodo-1,2,3-triméthoxybenzène **23-1** (3.91 g 13.3 mmol) dans du DMF (30 ml), de la triéthylamine (30 ml) a été ensuite ajouté au goutte à goutte sous argon. Le milieu réactionnel a été chauffé à 80°C pour 12h puis refroidi à température ambiante et filtré sur célite. Le filtrat a été concentré et purifié sur silice pour donner le tolane **23** avec 70% de rendement (2.73 g).

RMN ^{1}H ($CDCl_3$, 400 MHz) δ 7.49 (d, 2H, J = 8.9 Hz, CH_{ar}), 6.84 (d, 2H, J = 8.9 Hz, CH_{ar}), 6.12 (s, 2H, CH_{ar}), 3.88 (s, 6H, OCH_3), 3.83 (s, 3H, OCH_3), 3.81 (s, 3H, OCH_3) ppm ;

RMN ^{13}C ($CDCl_3$, 100 MHz) δ 162.2, 161.5, 159.3, 133.1 (2C), 116.6, 113.9 (2C), 96.3, 94.9 (2C), 90.7 (2C), 80.5, 56.2 (2C), 55.5, 55.4 ppm.

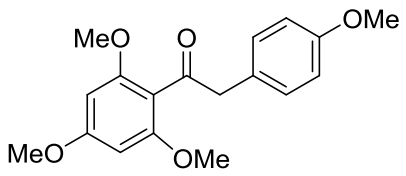

77

2-(4-Méthoxyphényl)-1-(2,4,6-triméthoxyphényl)ethan-1-one (77)

Du $Hg(OAc)_2$ (3.31 g, 10.4 mmol) a été ajouté à 0°C à une solution du tolane **23** (2.40 g, 8.4 mmol) dans de l'acide acétique glacial (150 ml). Le milieu réactionnel a été agité à 0°C pour 1h et sous sonication pour 1h. Il a été versé à une solution de saumure (150 ml) à 0°C, et le mélange a été agité à température ambiante pour 10 min. Il a été ensuite filtré, lavé par de l'eau et du pentane puis séché sous vide. La recristallisation dans du $CHCl_3$ a donné 2.11 g de produit brut qui a été engagé directement à l'étape suivante.

Du LiCl anhydre (379 mg, 8.9 mmol), du $PdCl_2$ (721 mg, 4.1 mmol), et du MgO (327 mg, 8.2 mml) ont été mélangé dans du méthanol (50 mL). Le milieu a été agité à -78°C pour 20 minutes. L'intermédiare synthétisé (2.11 g, 4.1 mmol) a été ajouté puis le milieu réactionnel a été mis sous pression atmosphérique du CO et agité à température ambiante pour 16h. Du charbon activé et de l'éther ont été ajouté puis le milieu a été filtré sur célité, lavé avec une solution saturée de NH_4Cl. La phase organique a été séchée sur $MgSO_4$, filtrée et concentrée pour donner la cétone **77** avec 80% de rendement (1.04 g).

RMN ^{1}H ($CDCl_3$, 400 MHz) δ 7.12 (d, 2H, J = 8.7 Hz, CH_{ar}), 6.81 (d, 2H, J = 8.7 Hz, CH_{ar}), 6.01 (s, 2H, CH_{ar}), 3.97 (s, 2H, CH_2), 3.81 (s, 3H, OCH_3), 3.78 (s, 3H, OCH_3), 3.74 (s, 6H, OCH_3) ppm ;

RMN ^{13}C ($CDCl_3$, 100 MHz) δ 201.9, 162.4 (2C), 158.4, 158.2, 130.9 (2C), 127.1, 113.7 (2C), 90.7 (2C), 55.9, 55.5, 55.3 (2C), 50.7 ppm.

BR-MS : masse calculée pour $C_{18}H_{20}O_5$: 316,1, trouvée : 317.2 $(M+H)^+$.

5.3. Procédure pour le chapitre 3.3

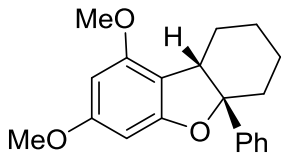

86

(4a*S*,9b*S*)-7,9-dimethoxy-4a-phenyl-1,2,3,4,4a,9b-hexahydrodibenzo[b,d]furan (86)

A 0°C, du $BF_3{\cdot}OEt_2$ (180 µl, 2.96 mmol) et le composé **83** (200 mg, 1.3 mmol) qui est dissous préallablement dans du dichlorométhane anhydre (2 ml) ont été ajouté successivement dans une solution du composé **84** (227 mg, 1.3 mmol) dans du dichlorométhane (3 ml). Le milieu réactionnel a été agité à température ambiante pour 12h puis a été chauffé à 50°C pour 4h. Il a été ensuite neutralisé par une solution saturée de sodium bicarbonate, puis extrait par de l'éther, séché sur $MgSO_4$, filtré et concentré. Le produit brut obtenu a été purifié par une chromatographie sur la silice, et le produit **86** a été obtenu sous forme d'une poudre blanche, avec un rendement de 69% (278 mg).

RMN ^{1}H ($CDCl_3$, 400 MHz) δ 7.46 (d, 2H, J = 7.5 Hz, CH_{ar}), 7.29 (t, 2H, J = 7.6 Hz, CH_{ar}), 7.20 (t, 1H, J = 7.6 Hz, CH_{ar}), 6.18 (s, 1H, CH_{ar}), 5.97 (s, 1H, CH_{ar}), 3.77 (s, 3H, OCH_3), 3.72 (s, 3H, OCH_3), 3.56 (t, 1H, J = 6.1 Hz, CH), 2.17 - 2.11 (m, 1H, CH_2), 2.08 - 2.03 (m, 1H, CH_2), 2.01 - 1.94 (m, 1H, CH_2), 1.75 - 1.68 (m, 1H, CH_2), 1.68 - 1.61 (m, 2H, CH_2), 1.52 - 1.46 (m, 2H, CH_2) ppm ;

RMN ^{13}C ($CDCl_3$, 100 MHz) δ 161.5, 160.7, 156.9, 147.6, 128.2, 126.9, 125.0, 111.1, 91.6, 91.4, 88.9, 55.6, 55.3, 45.5, 35.1, 27.1, 20.0, 19.9 ppm.

Point de fusion : 100.8°C

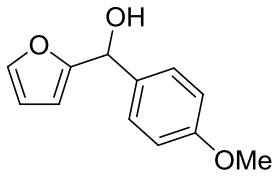

95

Furan-2-yl(4-méthoxyphényl)méthanol (95)

A -78°C, du *n*-BuLi dans de l'hexane (1.6M, 20.6 ml, 33.0 mmol) a été ajouté sous argon à une solution de furane (3.2 ml, 44.1 mmol) dans du THF anhydre (35 ml). Le mélange a ensuite été agité à 0°C pendant 30 minutes. Du *p*-anisaldéhyde (2.7 ml, 22.05 mmol) dilué dans du THF (20 ml) a été ajouté au goutte à goutte à -78°C. Le mélange a été agité à la même température pour 30 minutes puis quenché par l'ajout de 5 ml de solution aqueuse saturée de NH_4Cl. Les deux phases ont été séparées et la phase aqueuse a été extraite avec de l'éther. Les phases organiques recombinées ont été lavées à la saumure, séchées sur MgSO, filtrées et concentrée. Le produit **95** a été obtenu quantitativement sous forme d'huile jaune (9g).

RMN ^{1}H ($CDCl_3$, 400 MHz) δ 7.39 (s, 1H, OH), 7.35 (d, 2H, J = 8.7 Hz, CH_{ar}), 6.90 (d, 2H, J = 8.7 Hz, CH_{ar}), 6.32 (dd, 1H, J = 3.1 et 1.8 Hz, CH), 6.11 (d, 1H, J = 3.3 Hz, CH), 5.77 (d, 1H, J = 4.3 Hz, CH), 3.81 (s, 3H, OCH_3), 2.46 (d, 1H, J = 4.4 Hz, CH) ppm ;

RMN ^{13}C ($CDCl_3$, 100 MHz) δ 159.5, 156.5, 142.5, 133.4, 128.1 (2C), 114.0 (2C), 110.3, 107.3, 69.9, 55.4 ppm.

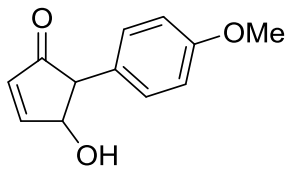

96

4-hydroxy-5-(4-méthoxyphényl)cyclopent-2-èn-1-one (96)

Du composé **95** (4.7 g, 23 mmol) a été dissous dans un mélange acétone/eau (160 ml/6.5 ml), puis du $ZnCl_2$ (3.13 g, 23 mmol) a été ajouté. Le mélange a été agité pour 24h en reflux. La solution obtenue refroidie à température ambiante a été acidifiée jusqu'à pH = 3 par une solution de HCl (1N). Le mélange a été extrait avec de l'éther puis séché sur $MgSO_4$, filtré et concentré. La chromatographie sur silice a donné le produit **96** sous forme d'un solide brun avec 66% de rendement (3.1g).

RMN ^{1}H ($CDCl_3$, 400 MHz) δ 7.61 (dd, 1H, J = 5.7 et 2.0 Hz, CH), 7.05 (d, 2H, J = 8.7 Hz, CH_{ar}), 6.88 (d, 2H, J = 8.7 Hz, CH_{ar}), 6.35 (d, 1H, J = 5.8 Hz, CH), 4.97 (s, 1H, OH), 3.80 (s, 3H, OCH_3), 3.41 (d, 1H, J = 2.8 Hz, CH), 2.24 (d, 1H, J = 6.1 Hz, CH) ppm ;

RMN ^{13}C ($CDCl_3$, 100 MHz) δ 205.8, 161.8, 159.1, 134.5, 129.6, 128.9 (2C), 114.6 (2C), 79.2, 61.6, 55.5 ppm.

Point de fusion : 75.4°C

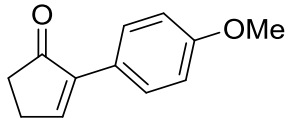

97

2-(4-méthoxyphényl)cyclopent-2-èn-1-one (97)

Du Pd/C (10 wt. %, 267 mg, 0.25 mmol) a été ajouté à une solution du composé **96** (1 g, 4.89 mmol) dans de l'éthanol (125 ml), et le milieu réactionnel a été agité sous H_2

(1 atm) pour 4h. Le mélange réactionnel a été filtré sur célite, puis de la silice (15 g) a été ajoutée au filtrat. La suspension obtenue a été agitée pour 48h à température ambiante, filtré et concentré. La chromatographie sur silice a donné le produit **97** sous forme d'un solide jaune avec 70% de rendement (643 mg).

RMN ^{1}H ($CDCl_3$, 400 MHz) δ 7.74 (t, 1H, J = 3.0 Hz, CH), 7.67 (d, 2H, J = 8.7 Hz, CH_{ar}), 6.92 (d, 2H, J = 8.7 Hz, CH_{ar}), 3.82 (s, 3H, OCH_3), 2.71 - 2.67 (m, 2H, CH_2), 2.60 - 2.57 (m, 2H, CH_2) ppm.

RMN ^{13}C ($CDCl_3$, 100 MHz) δ 208.0, 159.9, 143.0, 128.5 (2C), 124.5, 114.1 (2C), 55.5, 36.0, 26.3 ppm.

Point de fusion : 108.8 °C

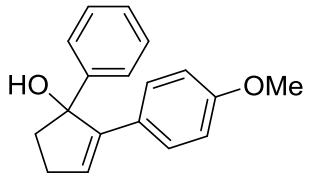

101

2-(4-méthoxyphényl)-1-phénylcyclopent-2-èn-1-ol (101)

A -78°C, une solution de phényllithium dans de l'éther (1.8 M, 7.11 ml, 12.8 mmol) a été ajoutée au goutte à goutte à une solution du composé **97** (1.5 g, 8.0 mmol) dans du THF anhydre (75 ml). Le mélange a été agité à la même température pour 1h, puis quenché par l'ajout d'une solution aqueuse saturée de NH_4Cl. Les deux phases ont été séparées, et la phase aqueuse a été extraite avec de l'éther. Les phases organiques recombinées ont été séchées sur $MgSO_4$, filtrées et concentrées. La chromatographie sur silice a donné le produit **15** sous forme d'une huile jaune avec 80% de rendement (1.7 g).

RMN ^{1}H ($CDCl_3$, 400 MHz) δ 7.48 (d, 2H, J = 8.7 Hz, CH_{ar}), 7.34 (m, 2H, CH_{ar}), 7.28 - 7.23 (m, 3H, CH_{ar}), 6.74 (d, 2H, J = 8.7 Hz, CH_{ar}), 6.99 (t, 1H, J = 2.5 Hz, CH), 3.75 (s, 3H, OCH_3), 2.67 - 2.61 (m, 1H, CH_2), 2.55 - 2.48 (m, 1H, CH_2), 2.40 (t, 2H, J = 6.5 Hz, CH_2), 2.21 (s, 1H, OH) ppm ;

RMN ^{13}C ($CDCl_3$, 100 MHz) δ 158.7, 146.3, 129.3 (2C), 128.3 (2C), 128.1, 126.8 (2C), 126.5, 124.7, 113.6 (2C), 87.7, 55.1, 45.5, 29.2 ppm.

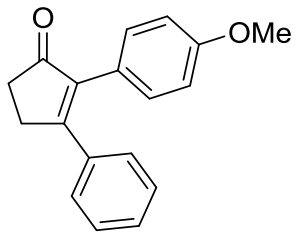

102

Synthèse du 2-(4-méthoxyphényl)-3-phénylcyclopent-2-èn-1-one (102)

A 0°C, du pyridinium dichromate (4.60 g, 12.24 mmol) a été ajouté à une solution du composé **101** (1.63 g, 6.12 mmol) dans du CH_2Cl_2 (40 ml). Le mélange a été agité à la même température pour 4h. Le milieu réactionnel a été dilué dans de l'éther, filtré sur célite, puis lavé à l'éther, et le filtrat a été concentré à sec. La chromatographie sur silice a donné le produit **102** sous forme d'un solide blanc avec 76% de rendement (1.23 g).

RMN ^{1}H ($CDCl_3$, 400 MHz) δ 7.37 - 7.28 (m, 5H, CH_{ar}), 7.15 (d, 2H, J = 8.7 Hz, CH_{ar}), 6.86 (d, 2H, J = 8.7 Hz, CH_{ar}), 3.81 (s, 3H, OCH_3), 3.05 - 3.03 (m, 2H, CH_2), 2.71 - 2.69 (m, 2H, CH_2) ppm ;

RMN ^{13}C ($CDCl_3$, 100 MHz) δ 208.0, 167.1, 159.2, 139.3, 136.0, 130.7, 129.7 (2C), 128.4 (2C), 128.0 (2C), 124.4, 114.0 (2C), 55.2, 34.8, 29.5 ppm.

Point de fusion : 94.0°C

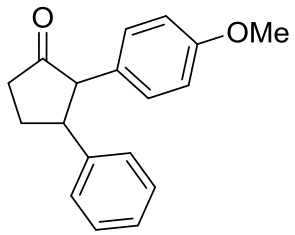

82

2-(4-méthoxyphényl)-3-phénylcyclopentan-1-one (82)

Du $Pd(OH)_2/C$ (20 wt. %, 400 mg, 0.57 mmol) a été ajouté à une solution du composé **102** (1.15 g, 4.34 mmol) dans de l'acétate d'éthyle (40 ml). Le mélange a été agité sous H_2 (1 atm) pour 4h à température ambiante, puis filtré sur célite. Le filtrat a été concentré, puis séché sous pression réduite pour obtenir le composé **82** sous forme d'un solide jaune avec 90% de rendement (1.04 g).

RMN ^{1}H ($CDCl_3$, 400 MHz) δ 7.30 - 7.26 (m, 2H, CH_{ar}), 7.22 - 7.18 (m, 3H, CH_{ar}), 6.97 (d, 2H, J = 8.7 Hz, CH_{ar}), 6.81 (d, 2H, J = 8.7 Hz, CH_{ar}), 3.75 (s, 3H, OCH_3), 3.48 - 3.40 (m, 2H, CH_2), 2.73-2.66 (m, 1H, CH), 2.50 - 2.44 (m, 2H, CH_2), 2.14 - 2.07 (m, 1H, CH) ppm ;

RMN ^{13}C ($CDCl_3$, 100 MHz) δ 217.1, 158.8, 141.9, 129.8 (2C), 129.3 (2C), 128.8 (2C), 127.3, 127.0, 114.3 (2C), 62.3, 55.4, 50.7, 38.8, 29.6 ppm.

Point de fusion : 78.1°C

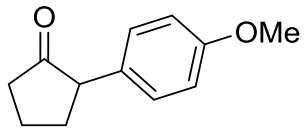

2-(4-méthoxyphényl)cyclopentan-1-one (88)

A -78°C, une solution de DMSO (0.15 ml, 2.07 mmol) dans du CH_2Cl_2 (2 ml) a été ajoutée doucement à une solution de chlorure d'oxalyle (0.09 ml, 1.05 mmol) dans du CH_2Cl_2 (3 ml). Après 5 minutes d'agitation, une solution de cyclopentanol **98** (180 mg, 0.94 mmol) dans du CH_2Cl_2 (1 ml) a été ajoutée pendant 10 minutes. Après 15 minutes d'agitation, de la triéthylamine (0.63 ml, 4.7 mmol) a été ajoutée pendant 15 minutes. La température a ensuite été laissée remonter à température ambiante. Le mélange a été dilué avec 4 ml d'eau, et les phases obtenues ont été séparées. La phase aqueuse a été extraite avec du CH_2Cl_2, et les phases organiques recombinées ont été lavées successivement avec d'une solution aqueuse de HCl (1%), de Na_2SO_4 (5%) et de l'eau, puis séchées sur $MgSO_4$, filtrées et concentrées. La chromatographie sur silice a donné le produit **88** avec 90% de rendement (159 mg).

RMN ^{1}H ($CDCl_3$, 400 MHz) δ 7.12 (d, 2H, J = 8.7 Hz, CH_{ar}), 6.88 (d, 2H, J = 8.7 Hz, CH_{ar}), 3.79 (s, 3H, OCH_3), 3.30 - 3.25 (m, 1H, CH), 2.50 - 2.43 (m, 2H, CH_2), 2.30 - 2.25 (m, 1H, CH_2), 2.17 - 2.05 (m, 2H, CH_2), 1.98 - 1.89 (m, 1H, CH_2) ppm ;

RMN ^{13}C ($CDCl_3$, 100 MHz) δ 218.5, 158.7, 130.6, 129.2(2C), 114.3 (2C), 55.5, 54.7, 38.5, 32.0, 21.0 ppm.

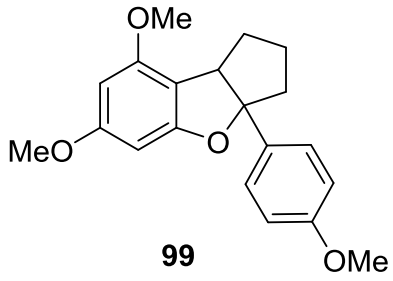

99

6,8-diméthoxy-3a-phényl-2,3,3a,8b-tétrahydro-1H-cyclopenta[b]benzofurane (99)

A 0°C, du $BF_3{\cdot}Et_2O$ (0.07 ml, 0.54 mmol) et du 3,5-diméthoxyphénol (69 mg, 0.48 mmol) ont été ajouté sous argon à une solution du composé **88** (90 mg, 0.48 mmol) dans du CH_2Cl_2 anhydre (2,5 ml). Le mélange a été agité pour 4h à 0°C puis 12h à température ambiante. La réaction a ensuite été quenchée par l'ajout de 2 ml de solution aqueuse saturée du $NaHCO_3$, les phases obtenues ont été séparées et la phase aqueuse a été extraite avec de l'éther. La phase organique a été séchée sur $MgSO_4$, filtrée et concentrée. La chromatographie sur silice a donné le produit **99** sous forme d'une huile incolore avec 54% de rendement (85 mg).

RMN ^{1}H ($CDCl_3$, 400 MHz) δ 7.34 (d, 2H, J = 8.7 Hz, CH_{ar}), 6.90 (d, 2H, J = 8.7 Hz, CH_{ar}), 6.08 (d, 1H, J = 1.8 Hz, CH_{ar}), 6,05 (d, 1H, J = 1.9 Hz, CH_{ar}) 3.72 (s, 6H, OCH_3), 3.70 (s, 3H, OCH_3), 3.61 (d, 1H, J = 8.4 Hz, CH), 2.25 (dd, 1H, J = 13.3 et 5.4 Hz, CH_2), 2.08 - 1.96 (m, 2H, CH_2), 1.79 (m, 2H, CH_2), 1.58 - 1.47 (m, 1H, CH_2) ppm ;

RMN ^{13}C ($CDCl_3$, 100 MHz) δ 161.9, 161.7, 158.9, 156.7, 137.5, 126.1 (2C), 113.9 (2C), 110.1, 101.4, 91.3, 87.8, 52.8, 42.7, 34.5, 25.4 ppm.

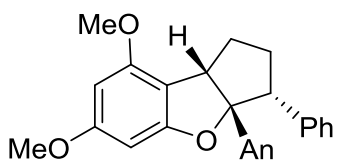

103a

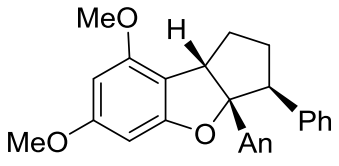

103b

(3*R*,3a*S*,8b*S*)-6,8-diméthoxy-3a-(4-méthoxyphényl)-3-phényl-2,3,3a,8b-tétrahydro-1*H*-cyclopenta[*b*]benzofuran (103a)
(3*S*,3a*S*,8b*S*)-6,8-diméthoxy-3a-(4-méthoxyphényl)-3-phényl-2,3,3a,8b-tétrahydro-1*H*-cyclopenta[*b*]benzofuran (103b)

Du $BF_3{\cdot}Et_2O$ (0.03 ml, 0.17 mmol) et du 3,5-diméthoxyphénol (22 mg, 0.15 mmol) ont été ajouté sous argon à une solution du composé **82** (40 mg, 0.15 mmol) dans du CH_2Cl_2 anhydre (1,2 ml). Le mélange a été agité pour 4h à 50°C, puis neutralisé par l'ajout de 1 ml de solution aqueuse saturée de $NaHCO_3$, les phases obtenues ont été séparées et la phase aqueuse a été extraite avec de l'éther. La phase organique a été séchée sur $MgSO_4$, filtrée et concentrée. La chromatographie sur silice a donné un mélange du produit **103a** et **103b** avec 22% de rendement (13 mg).

Composé 103a

RMN ^{1}H ($CDCl_3$, 400 MHz) δ 7.27 (d, 2H, J = 8.7 Hz, CH_{ar}), 7.20 - 7.19 (m, 3H, CH_{ar}), 7.02 - 7.00 (m, 2H, CH_{ar}), 6.82 (d, 2H, J = 8.7 Hz, CH_{ar}), 6.11 (s, 1H, CH_{ar}), 6.00 (s, 1H, CH_{ar}), 6.92 (d, 1H, J = 7.3 Hz, CH), 3.78 (s, 6H, OCH_3), 3.77 (s, 3H, OCH_3), 3.41 (dd, 1H, J = 11.7 et 5.5 Hz, CH_2), 2.17 - 2.23(m, 2H, CH_2), 2.11 - 2.04 (m, 2H, CH_2) ppm ;

RMN ^{13}C ($CDCl_3$, 100 MHz) δ 161.8, 161.7, 158.6, 156.6, 138.4, 136.8, 129.3(2C), 127.7(2C), 126.6, 126.2(2C), 113.6(2C), 109.8, 100.8, 91.4, 87.9, 59.6, 55.7, 55.4, 55.3, 54.0, 32.4, 30.5 ppm.

Composé 103b

RMN ^{1}H ($CDCl_3$, 400 MHz) δ 7.11 - 7.07 (m, 3H, CH_{ar}), 6.93 - 6.90 (m, 2H, CH_{ar}), 6.63 (d, 2H, J = 8.7 Hz, CH_{ar}), 6.18 (s, 1H, CH_{ar}), 6.05 (s, 1H, CH_{ar}), 4.12 - 4.08 (m, 1H, CH), 3.82 (s, 3H, OCH_3), 3.79 (s, 3H, OCH_3), 3.70 (s, 3H, OCH_3), 3.58 (d, 1H, J = 5.4 Hz, CH),

1.98 - 2.23 (m, 2H, CH_2) ppm.

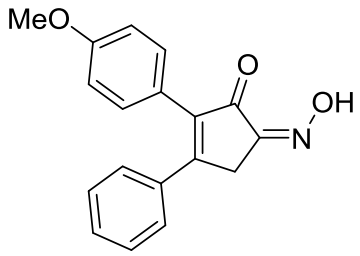

122

(*Z*)-5-(Hydroxyimino)-2-(4-méthoxyphényl)-3-phénylcyclopent-2-èn-1-one (122)

A 0°C, du nitrite de *n*-butyle (53µl, 0.46 mmol) et de l'HCl concentré (46µl, 1.5mmol) ont été ajouté sous argon à une solution du composé **102** (100mg, 0.38mmol) dans du 1,4-dioxane (2ml). Le milieu réactionnel a été agité pour 30 min à température ambiante, puis versée dans de l'eau glacée. Les phases obtenues ont été séparées et la phase aqueuse a été extraite avec de l'acétate d'éthyle. Les phases organiques recombinées ont été séchées sur $MgSO_4$, filtré et concentré. La chromatographie sur silice a donné le produit **122** sous forme d'une poudre jaune avec 70% de rendement (78 mg).

RMN ^{1}H ($CDCl_3$, 400 MHz) δ 8.57 (bs, 1H, OH), 7.42 (m, 2H, CH_{ar}), 7.38 - 7.37 (d, 1H, J=6.9 Hz, CH_{ar}), 7.34 - 7.31 (m, 2H, CH_{ar}), 7.24 - 7.22 (d, 2H, J=8.7 Hz, CH_{ar}), 6.91 - 6.89 (d, 2H, J=8.5 Hz, CH_{ar}), 3.83 (s, 3H, OCH_3), 3.76 (s, 2H, CH_2) ppm ;

RMN ^{13}C ($CDCl_3$, 100 MHz) δ 159.7, 158.9, 153.5, 141.4, 134.6, 130.7(2C), 130.6, 128.6(2C), 128.5(2C), 123.5, 114.2(2C), 55.3, 30.9 ppm.

HR-MS masse calculée pour $C_{18}H_{15}NO_3$: 293.1052, trouvée : 294.1122 ($M+H^+$).

Point de fusion : 224.7°C

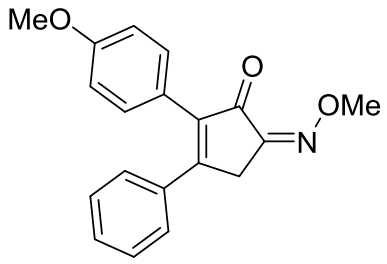

123a

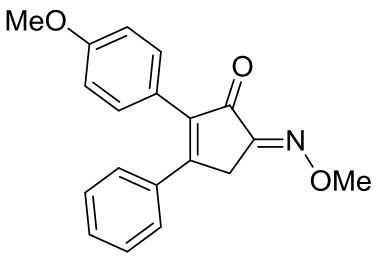

123b

(*Z*)-5-(Méthoxyimino)-2-(4-méthoxyphényl)-3-phénylcyclopent-2-èn-1-one (123a)
(*E*)-5-(Méthoxyimino)-2-(4-méthoxyphényl)-3-phénylcyclopent-2-èn-1-one (123b)

A 0°C, du sulfate de diméthyle (50µl, 0.51mmol) a été ajouté à une solution du composé **122** (100mg, 0.34mmol) dans l'acétone, puis du K_2CO_3 (70mg, 0.51mmol) a été ajouté en 3 portions. Le milieu réactionnel a été agité pour 1h à température ambiante, puis filtré et concentré. La chromatographie sur silice a donné le produit **123a** sous forme d'un solide jaune clair avec 36% de rendement (38 mg) et le produit **123b** sous forme d'une huile jaune avec 53% de rendement (55 mg).

Composé **123a** (f1 36%)

RMN ^{1}H ($CDCl_3$, 400 MHz) δ 7.40 - 7.33 (m, 5H, CH_{ar}), 7.21 (d, 2H, J=8.7Hz, CH_{ar}), 6.89 (d, 2H, J=8.7 Hz, CH_{ar}), 4.16 (s, 3H, OCH_3), 3.82 (s, 3H, OCH_3), 3.67 (s, 2H, CH_2) ppm ;

RMN ^{13}C ($CDCl_3$, 100 MHz) δ 190.4, 159.8, 158.7, 152.2, 141.5, 134.8, 130.9, 130.6, 128.7, 128.6, 123.8, 114.3, 63.7, 55.4, 31.5 ppm.

HR-MS : masse calculée pour $C_{19}H_{17}NO_3$: 307.1208, trouvée : 308.1268 ($M+H^+$).

Point de fusion : 116.7°C

Composé **123b** (f2 53%)

RMN ^{1}H ($CDCl_3$, 400 MHz) δ 7.42 - 7.29 (m, 5H, CH_{ar}), 7.21 (d, 2H, J=8.7 Hz, CH_{ar}), 6.91 (d, 2H, J = 8.7 Hz, CH_{ar}), 4.28 (s, 3H, OCH_3), 3.89 (s, 2H, CH_2), 3.84 (s, 3H, OCH_3) ppm ;

RMN ^{13}C ($CDCl_3$, 100 MHz) δ 190.4, 159.8, 158.7, 152.2, 141.5, 134.8, 130.9 (2C), 130.6, 128.7(2C), 128.6 (2C), 123.8, 114.3 (2C), 63.7, 55.4, 31.5 ppm.

HR-MS : masse calculée pour $C_{19}H_{17}NO_3$: 307.1208, trouvée : 330.1093 ($M+Na^+$).

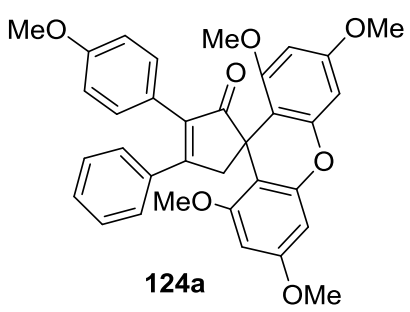

124a

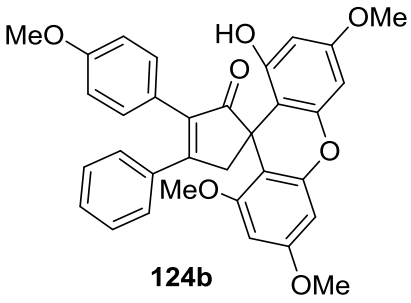

124b

1',3',6',8'-Tétraméthoxy-3-(4-méthoxyphényl)-4-phénylspiro[cyclopentane-1,9'-xanthen]-3-èn-2-one (124a)
1'-hydroxy-3',6',8'-trimethoxy-3-(4-methoxyphenyl)-4-phenylspiro[cyclopentane-1,9'-xanthen]-3-en-2-one (124b)

A 0°C, une solution de BF_3 méthanolate (50% w/w, 50µl, 0.6mmol) a été ajouté sous argon à une solution du composé **123a** ou **123b** (80mg, 0.26mmol) dans du 1,2-dichloroéthane (2 ml). Le milieu a été agité pour 30min à 0°C. Une solution de 3,5-diméthoxyphénol (60mg, 0.39mmol) dans du 1,2-dichloroéthane (1 ml) a été ajouté doucement à 0°C, puis le milieu réactionnel a été agité à la même température pour 2h, et à température ambiante pour 12h. Le milieu réactionnel a été neutralisé par l'ajout d'une solution saturée de bicarbonate, et la phase aqueuse a été extraite avec de l'éther. Les phases organiques recombinées ont été séchées sur $MgSO_4$, filtrées et concentrée. La chromatographie sur silice a donné le produit **124a** sous forme d'un solide jaune avec 30% de rendement (43 mg) et le produit **124b** sous forme d'un solide jaune avec 30% de rendement (41mg).

<u>Composé 124a</u>

RMN ^{1}H ($CDCl_3$, 400 MHz) δ 7.32 - 7.22 (m, 5H, CH_{ar}), 7.29 (d, 2H, J = 8.0 Hz, CH_{ar}), 6.84 (d, 2H, J = 8.7 Hz, CH_{ar}), 6.21 (d, 2H, J = 1.5Hz, CH_{ar}), 6.07 (d, 2H, J = 1.5Hz, CH_{ar}),

3.78 (s, 3H, OCH_3), 3.75 (s, 6H, OCH_3), 3.58 (s, 6H, OCH_3), 3.23 (s, 2H, CH_2) ppm.

RMN ^{13}C ($CDCl_3$, 100 MHz) δ 210.2, 160.7, 160.1(2C), 159.3, 158.7(2C), 152.3(2C), 137.3, 137.3, 137.3, 131.0 (2C), 129.0, 128.7 (2C), 128.1 (2C), 126.1, 114.2 (2C), 107.1, 94.5 (2C), 93.4 (2C), 55.8 (2C), 55.7 (2C), 55.5, 51.7, 46.7 ppm

HR-MS : calculé pour $C_{34}H_{30}O_7$: 550.1992, trouvé : 573.1879 ($M+Na^+$).

Point de fusion : 248.6°C

Composé 124b

RMN ^{1}H ($CDCl_3$, 400 MHz) δ 7.31 (d, 2H, J = 7.1 Hz, CH_{ar}), 7.26 - 7.24 (m, 3H, CH_{ar}), 6.76 (d, 2H, J = 8.5 Hz, CH_{ar}), 6.23 (s, 1H, CH_{ar}), 6.16 (s, 1H, CH_{ar}), 6.09 (s, 1H, CH_{ar}), 5.93 (s, 1H, OH), 5.86 (s, 1H, CH_{ar}), 3.75 (s, 3H, OCH_3), 3.72 (s, 3H, OCH_3), 3.65 (s, 3H, OCH_3), 3.59 (s, 3H, OCH_3), 3.31(d, 2H, J = 11 Hz, CH_2) ppm ;

RMN ^{13}C ($CDCl_3$, 100 MHz) δ 211.0, 162.0, 160.0, 159.5, 159.0, 158.5, 155.1, 152.3, 137.3, 136.9, 130.9 (2H), 129.0, 128.5 (2H), 128.1 (2H), 125.7, 114.0 (2H), 106.6, 105.3, 97.8, 94.3, 93.7, 93.2, 55.7, 55.6, 55.4, 55.3, 51.3, 46.6, 30.5 ppm.

HR-MS : calculé pour $C_{33}H_{28}O_7$: 536.1835, trouvé : 537.1907 ($M+H^+$)

Point de fusion : 242.8°C

5.4. Procédure pour le chapitre 3.4

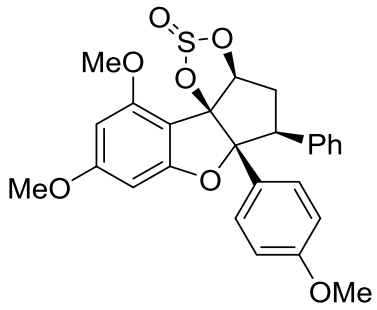

132

8,10-Diméthoxy-5a-(4-méthoxyphényl)-5-phényl-3a,4,5,5a-tétrahydro-[1,3,2]dioxathiolo[4',5':2,3] cyclopenta[1,2-*b*] benzofuran 2-oxide (132).

A 0°C, de la pyridine (0.23 ml, 2.87 mmol) et du chlorure de thionyle (0.17 ml, 2.3 mmol) ont été ajouté doucement sous argon à une solution d'*épi*-rocaglaol (500 mg, 1.15 mmol) dans du CH_2Cl_2 anhydre (5ml). Le milieu réactionnel a été agité pour 3h à 0°C, puis lavé par une solution saturée de bicarbonate et une solution saturée de $KHSO_4$ successivement. La phase organique a été séchée sur $MgSO_4$ et évaporée à sec. Le sulfite **132** a été obtenu quantitativement (552 mg).

RMN ^{1}H ($CDCl_3$, 400 MHz) δ 7.23 (d, 2H, J = 8.9 Hz, CH_{ar}), 7.20 - 7.18 (m, 2H, CH_{ar}), 7.16 - 7.12 (m, 3H, CH_{ar}), 6.68 (d, 2H, J = 9.0 Hz, CH_{ar}), 6.26 (d, 1H, J = 1.9 Hz, CH_{ar}), 6.12 (d, 1H, J = 1.9 Hz, CH_{ar}), 5.35 (dd, 1H, J = 8.8 and 7.5 Hz, CH), 3.85 (s, 3H, OCH_3), 3.84 (s, 3H, OCH_3), 3.71 (m, 1H, CH), 3.70 (s, 3H, OCH_3), 3.08 - 2.92 (m, 2H, CH_2) ppm.

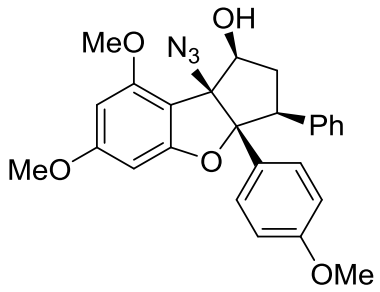

134

8b-Azido-6,8-diméthoxy-3a-(4-méthoxyphényl)-3-phényl-2,3,3a,8b-tétrahydro-1H-cyclopenta[*b*]benzofuran-1-ol (134).

De l'azoture de sodium (434 mg, 6.66 mmol) a été ajouté sous argon à une solution du sulfite **132** (535mg, 1.11 mmol) dans du DMF anhydre (10ml). Le milieu a été agité pour 24h à 75°C puis a été refroidi à température ambiante et quenché par une solution de l'acide sulfurique (20%, 3.3ml). La phase aqueuse a été extraite avec de l'éther, puis la phase organique combinée a été lavée par de l'eau et une solution saturée de bicarbonate, séchée sur $MgSO_4$, filtrée et concentrée. La trituration avec du *tert*-butyl methyl ether a donné le produit **134** sous forme d'un précipité blanc qui a été filtrée et séchée sous vide, avec 63% de rendement (320 mg).

RMN ^{1}H ($CDCl_3$, 400 MHz) δ 7.22 (d, 2H, J = 8.9 Hz, CH_{ar}), 7.10 – 7.07 (m, 3H, CH_{ar}), 6.92 -6.90 (m, 2H, CH_{ar}), 6.70 (d, 2H, J = 8.9 Hz, CH_{ar}), 6.35 (d, 1H, J = 1.9 Hz, CH_{ar}), 6.16 (d, 1H, J = 1.9 Hz, CH_{ar}), 4.86 (td, 1H, J = 7,7 and 2.5 Hz, CH), 3.90 (s, 3H, OCH_3), 3.86 (s, 3H, OCH_3), 3.73 (s, 3H, OCH_3), 3.51 (dd, 1H, J = 14.4 and 6.3 Hz, CH), 2.87 (d, 1H, J = 2.5 Hz, OH), 2.57 - 2.51 (m, 1H, CH_2), 2.38 - 2.29 (m, 1H, CH_2) ppm ;

RMN ^{13}C ($CDCl_3$, 100 MHz) δ 164.4, 160.2, 158.8, 157.8, 137.8, 128.9 (2C), 128.3 (2C), 127.8 (2C), 127.1, 126.7, 112.8 (2C), 106.9, 103.7, 92.5, 89.4, 81.4, 73.4, 55.9, 55.8, 55.2, 51.4, 36.7 ppm.

HR-MS masse calculée pour $C_{26}H_{25}N_3O_5$: 459.1794, trouvée : 482.1678 $(M + Na)^+$.

Point de fusion : 168.0°C

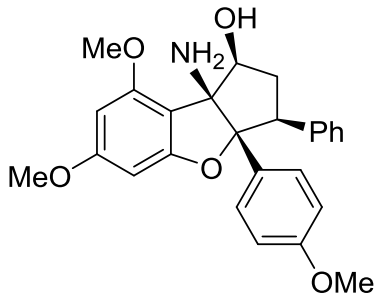

135

8b-Amino-6,8-diméthoxy-3a-(4-méthoxyphényl)-3-phényl-2,3,3a,8b-tétrahydro-1H-cyclopenta[*b*]benzofuran-1-ol (135).

Sous argon, un mélange du $SnCl_2$ anhydre (87 mg, 0.457 mmol), du thiophénol (0.19 ml, 1.829 mmol) et de la triéthylamine (0.19 ml, 1.372 mmol) a été agité à temperature ambiante pour 2 minutes. Une solution du composé **134** (140 mg, 0.305 mmol) dans du THF anhydre (6 ml) a été ajoutée. Le milieu réactionnel a été agité à température ambiante pour 3h, puis neutralisé jusqu'à pH = 7 avec une solution saturée de bicarbonate. La phase aqueuse a été extraite avec de l'éther et la phase organique combinée a été séchée sur $MgSO_4$ et évaporée à sec. La trituation avec l'éther a donné le produit **135** sous une forme d'un précipité blanc, avec 85% de rendement (112mg,).

RMN ^{1}H ($CDCl_3$, 400 MHz) δ 7.20 (d, 2H, J = 8.9 Hz, CH_{ar}), 7.10 -6.07 (m, 5H, CH_{ar}), 6.71 (d, 2H, J = 8.9 Hz, CH_{ar}), 6.27 (d, 1H, J = 1.9 Hz, CH_{ar}), 6.11 (d, 1H, J = 2.0 Hz, CH_{ar}), 4.67 (t, 1H, J = 7.5 Hz, CH), 3.86 (s, 3H, OCH_3), 3.84 (s, 3H, OCH_3), 3.72 (s, 3H, OCH_3), 3.57 (dd, 1H, J = 14.4 et 7 Hz, CH), 2.68 -2.61 (m, 1H, CH_2), 2.33 – 2.24 (m, 1H, CH_2) ppm ;

RMN ^{13}C ($CDCl_3$, 400 MHz) δ 163.2, 159.1, 158.7, 157.3, 138.8, 128.5 (2C), 128.2 (2C), 127.8, 127.7 (2C), 126.4, 113.8, 113.3 (2C), 104.2, 92.3, 89.4, 72.3, 71.1, 55.8, 55.7, 55.2, 50.3, 37.4 ppm.

HR-MS masse calculée pour $C_{26}H_{27}NO_5$: 433.1889, trouvée : 434.1959 $(M + H)^+$.

Point de fusion : 207.8°C

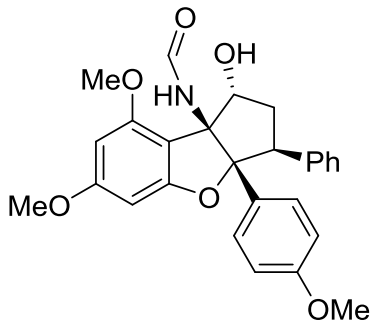

129

***N*-1-Hydroxy-6,8-diméthoxy-3a-(4-méthoxyphényl)-3-phényl-1,2,3,3a-tétrahydro-8 bH-cyclopenta[*b*]benzofuran-8b-yl)formamide (129).**

Un mélange de l'acide formique (1ml) et l'anhydride acétique (1 ml) a été agité à 60°C pour 1h puis refroidi à 0°C. Une solution du composé **135** (50 mg, 0.12 mmol) dans du THF (2ml) a été ajouté et le milieu réactionnel a été ensuite agité à 0°C pour 15min puis à température ambiante pour 12h. Le milieu a été quenché avec une solution saturée du bicarbonate, et la phase aqueuse a été extraite avec de l'éther. La phase organique a été séchée sur $MgSO_4$ et concentrée à sec. Le produit brut obtenu a été traité ensuite par une solution du méthanol ammoniaque et agité à température ambiante pour 12h, puis évaporé à sec. Le résidu obtenu a été lavé par de l'eau puis séché sous vide. La chromatographie de phase inverse semi-préparative a donné le composé **129** avec 30% de rendement (16mg).

RMN ^{1}H ($CDCl_3$, 400 MHz) δ 7.45 (d, 1H, J = 11.9 Hz, CHO), 7.10 - 7.07 (m, 3H, CH_{ar}), 7.08 (d, 2H, J = 9.3 Hz, CH_{ar}), 6.97 - 6.95 (m, 2H, CH_{ar}), 6.70 (d, 2H, J = 8.8 Hz, CH_{ar}), 6.30 (d, 1H, J = 1.4 Hz, CH_{ar}), 6.13 (d, 1H, J = 1.4 Hz, CH_{ar}), 6.08 (t, 1H, J = 7.4 Hz, CH), 3.86(s, 3H, OCH_3), 3.83(s, 3H, OCH_3), 3.71(s, 3H, OCH_3), 3.65 (dd, 1H, J = 14.3 et 7.5 Hz, CH), 2.88 - 2.81 (m, 1H, CH_2), 2.44 - 2.35 (m, 1H, CH_2) ppm;

RMN ^{13}C ($CDCl_3$, 400 MHz) δ 164.7, 164.2, 159.1, 159.0, 157.3, 137.3, 128.5 (2C), 128.0 (2C), 126.9, 126.7, 113.7 (2C), 108.0, 103.5, 92.9, 89.8, 73.4, 71.4, 55.9, 55.8, 55.2, 50.4, 35.5 ppm.

HR-MS masse calculée pour $C_{27}H_{27}NO_6$: 461.1834, trouvée 484.1727 $(M + Na)^+$.

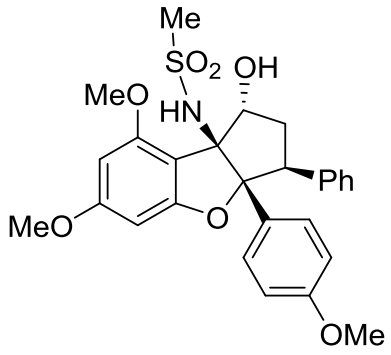

130

***N*-1-Hydroxy-6,8-diméthoxy-3a-(4-méthoxyphényl)-3-phényl-1,2,3,3a-tétrahydro-8 bH-cyclopenta[*b*]benzofuran-8b-yl)methanesulfonamide (130)**

A 0°C, du chlorure de mésyle (10 µl, 0.12 mmol), du *N*,*N*-diisopropyléthylamine (30 µl, 0.24 mmol) et de la DMAP (2 mg, 0.012 mmol) ont été ajoutée successivement à une solution du composé **12** dans du CH_2Cl_2 (1ml). Le milieu réactionnel a été agité à 0°C pour 15min puis à température ambiante pour 48h. La reaction a été quenchée avec une solution saturée de NH_4Cl et la phase aqueuse a été extraite avec de l'éther. La phase organique a été séchée sur $MgSO_4$ et concentrée à sec. La trituation avec de l'éther a donné le produit **6** sous forme d'un précipité blanc qui a été filtré puis séché sous vide, avec 29% de rendement (18mg).

RMN ^{1}H ($CDCl_3$, 400 MHz) δ 7.24 (d, 2H, J = 8.9 Hz, CH_{ar}), 7.12 -7.07 (m, 3H, CH_{ar}), 7.02 - 7.00 (m, 2H, CH_{ar}), 6.74 (d, 2H, J = 8.9 Hz, CH_{ar}), 6.26 (d, 1H, J = 2.0 Hz, CH_{ar}), 6.09 (d, 1H, J = 1.9 Hz, CH_{ar}), 5.63 (t, 1H, J = 7.5 Hz, CH), 3.82 (s, 3H, OCH_3), 3.76 (s, 3H, OCH_3), 3.70 (s, 3H, OCH_3), 3.67 (m, 1H, CH), 3.38 (s, 3H, OCH_3), 2.89 (m, 2H, CH_2) ppm ;

RMN ^{13}C ($CDCl_3$, 400 MHz) δ 165.6, 160.0, 159.6, 157.7, 136.1, 128.7, 128.6, 128.1(2C), 128.0 (2C), 127.1, 124.1, 114.4, 114.3 (2C), 101.7, 93.1, 89.6, 78.6, 72.2, 55.9, 55.8, 55.3, 50.7, 39.4, 36.5 ppm.

HR-MS : masse calculée pour $C_{27}H_{29}NO_7S$: 511.1675, trouvée : 512.1747 $(M + H)^+$.

5.5. Procédure pour le chapître 3.5

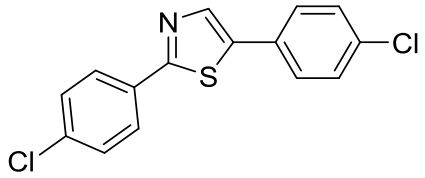

2,5-Bis(4-chlorophényl)-4,5-dihydrothiazole

Une solution aqueuse du Na_2CO_3 (2 M, 4 ml) a été ajouté à une solution de 2,5-dibromo-4,5-dihydrothiazole (0.25 g, 1.03 mmol) dans un mélange de solvant (EtOH/PhMe = 4/1, 10ml), suivi par l'addition de KCl (0.223 g, 3 mmol) et du 4-chloro-phénylboronic acide (0.362 g, 2.31 mmol). De l'argon a été barboté dans le milieu pour 3 min. Du $Pd(PPh_3)_4$ (0.116 mg, 10mol%) a été ajouté et le milieu réactionnel a été chauffé à 100 °C pour 4h. Après refroidi à température ambiante, il a été filtré sur célite, rincé par du CH_2Cl_2, et le filtrat a été évaporé à sec. La chromatographie sur silice a donné le produit avec 53% de rendement (166 mg).

RMN ^{1}H ($CDCl_3$, 400 MHz) δ 7.99 (s, 1H, CH), 7.90 (d, 2H, J = 8.0 Hz, CH_{ar}), 7.53 (d, 2H, J = 8.1 Hz, CH_{ar}), 7.41 (m, 4H, CH_{ar}) ppm ;

RMN ^{13}C ($CDCl_3$, 400 MHz) δ 166.1, 139.6, 138.4, 136.1, 134.3, 132.0, 129.7, 129.4, 129.3, 127.8, 127.6 ppm.

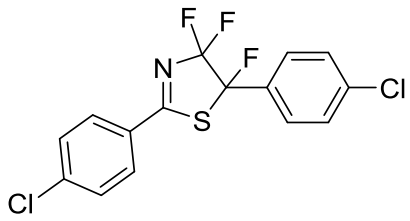

2,5-Bis(4-chlorophényl)-4,4,5-trifluoro-4,5-dihydrothiazole (fluorizoline)

Le Selectfluor (0.465 g, 0.52 mmol) a été ajouté sous argon à une solution du 2,5-Bis(4-chlorophényl)-4,5-dihydrothiazole (0.16 g, 0.52 mmol) dans de l'acétonitrile (18 ml). Le milieu réactionnel a été chauffé à reflux pour 6h puis quenché avec une solution saturée de bicarbonate, extrait à de l'éther. La phase organique a été séchée sur $MgSO_4$, filtrée et concentrée. La chromatographie sur silice a donné le fluorizoline avec 10% de rendement (18 mg).

RMN ^{1}H ($CDCl_3$, 400 MHz) δ 7.93 (d, 2H, J = 8.5 Hz, CH_{ar}), 7.64 (d, 2H, J = 8.0 Hz, CH_{ar}), 7.55 (d, 2H, J = 8.1 Hz, CH_{ar}), 7.45 (d, 2H, J = 8.5 Hz, CH_{ar}) ppm ;

RMN ^{19}F ($CDCl_3$, 400 MHz) δ -79.3 (dd, J = 218 Hz et 10.3 Hz), - 103.3 (dd, J = 218.6 Hz et 8.0 Hz), - 130.9 (dd, J = 9.7 Hz et 8.6 Hz) ppm.

BR- MS : masse calculée pour $C_{15}H_8Cl_2F_3NS$: 360.9, trouvée : 361.9 $(M+H)^+$.

6. PUBLICATIONS

Publication N°*1*

Cancer wars: Natural products strike back.

Basmadjian, C., Zhao, Q., Bentouhami, E., Djehal, A., Nebigil, C. G., Johnson, R. A., Serova, M., de Gramont, A., Faivre, S., Raymond, E., Désaubry, L. G., *Front. Chem.*, **2014**, *2* : 20.

frontiers in CHEMISTRY

REVIEW ARTICLE
published: 01 May 2014
doi: 10.3389/fchem.2014.00020

Cancer wars: natural products strike back

Christine Basmadjian[1,2], Qian Zhao[1,2], Embarek Bentouhami[3], Amel Djehal[1,3], Canan G. Nebigil[4], Roger A. Johnson[5], Maria Serova[2], Armand de Gramont[2], Sandrine Faivre[2,6], Eric Raymond[2,6] and Laurent G. Désaubry[1]*

[1] Therapeutic Innovation Laboratory, UMR7200, CNRS/University of Strasbourg, Illkirch, France
[2] AAREC Filia Research, Clichy, France
[3] L.C.I.M.N Laboratory, Department of Process Engineering, Faculty of Technology, University Ferhat Abbas, Sétif, Algeria
[4] Biotechnology and Cell Signaling Laboratory, UMR 7242, CNRS/ University of Strasbourg, Illkirch, France
[5] Department of Physiology and Biophysics, State University of New York, Stony Brook, NY, USA
[6] Department of Medical Oncology, Beaujon University Hospital, INSERM U728/AP-HP, Clichy, France

Edited by:
Asier Unciti-Broceta, The University of Edinburgh, UK

Reviewed by:
Luis Álvarez De Cienfuegos Rodríguez, University of Granada, Spain
Francisco Franco-Montalbán, University of Granada, Spain

***Correspondence:**
Laurent G. Désaubry, Therapeutic Innovation Laboratory (UMR 7200), Faculté de Pharmacie, 74 Route du Rhin, 67401 Illkirch, France
e-mail: desaubry@unistra.fr

Natural products have historically been a mainstay source of anticancer drugs, but in the 90's they fell out of favor in pharmaceutical companies with the emergence of targeted therapies, which rely on antibodies or small synthetic molecules identified by high throughput screening. Although targeted therapies greatly improved the treatment of a few cancers, the benefit has remained disappointing for many solid tumors, which revitalized the interest in natural products. With the approval of rapamycin in 2007, 12 novel natural product derivatives have been brought to market. The present review describes the discovery and development of these new anticancer drugs and highlights the peculiarities of natural product and new trends in this exciting field of drug discovery.

Keywords: natural products, cancer, drug discovery, pharmacognosy, molecular targets, privileged structures

INTRODUCTION

Recent analyses of tooth plaques showed that ∼50,000 years ago Neanderthals already used medicinal plants to treat their ailments (Hardy et al., 2012). Currently, more than half of humanity does not have access to modern medicine and relies on traditional treatments (Cordell and Colvard, 2012). A recent analysis of the strategies used in the discovery of new medicines showed that 36% of the first-in-class small-molecules approved by U.S. Food and Drug Administration (FDA) between 1999 and 2008 were natural products or natural products derivatives (Swinney and Anthony, 2011).

Natural products are small-molecule secondary metabolites that contribute to organism survival. These substances display considerable structural diversity and "privileged scaffolds," i.e., molecular architectures that are tailored to protein binding, as first coined by Evans in the late 1980s (Evans et al., 1988). Indeed natural products have evolved to bind biological targets and elicit biological effects as chemical weapons or to convey information from one organism to another. Steroid derivatives are often not considered as natural products because their design is not based on a research in pharmacognosy, however we subjectively decided to include them here due to their importance in drug discovery.

The synthesis of aspirin by Charles Gerhard at Strasbourg faculty of pharmacy in 1853 paved the road for the medicinal chemistry of natural products (Gerhardt, 1853). In 1964, actinomycin became the first natural product approved for an indication in oncology. Other natural products based medicines such as anthracyclines, *vinca* alkaloids, epipodophyllotoxin lignans, camptothecin derivatives, and taxoids that were launched before 1997, are still an essential part of the armament for treating cancers.

From 1997 to 2007 no new natural product was approved for the treatment of cancer (Bailly, 2009). With the imminent achievement of the genome project, the head of a pharmaceutical company declared that natural products were outdated. Their development was greatly reduced and many big pharmaceutical companies closed their departments of natural product chemistry (Bailly, 2009). The future was targeted therapies, which uses fully synthetic molecules or antibodies to target specific proteins in tumor growth and progression. In some forms of leukemia, gastrointestinal, prostate or breast cancers, targeted therapies greatly delayed tumor progression, and/or improved the life expectancy of the patients. Some tumors with specific oncogenic addictions (for example fusion proteins leading to ALK expression in lung cancer or Bcr-Abl in chronic myeloid leukemia, KIT expression or mutations in GIST or EGFR mutation in lung cancer, HER2 amplification in breast cancer or MET overexpression in liver tumors) greatly benefited from targeted agents. However, the vast majority of common tumors were found to be not dependent of a single "targetable" oncogenic activation. For instance altogether ALK activations and EGFR mutations account for less than 10% of lung adenocarcinoma and while those targeted agents are more efficient than chemotherapy in oncogenic tumors, antitumor effects are limited to few months. Importantly, most tumors were shown to activate multiple signaling pathway redundancies and adaptive mechanisms that either render tumors primarily resistant to targeted drugs or facilitate acquired resistance to cell signaling inhibition after only few months of treatments. As a result, the expected progression-free survival benefit from targeted therapy is often less than 6-months. For those later forming complex but rather frequent tumors, chemotherapy alone remains the cornerstone of treatment with

some limited add-on benefits by use of monoclonal antibodies in a limited proportion of patients. Combinations of several targeted agents have also been proposed to counteract potential adaptive mechanisms although one should notice that combining targeted agent together was more often associated with unacceptable toxicity than great clinical synergy. Then there is the additional influence of cost-to-benefit concerns. The financial cost of such targeted therapies, to patients or health insurance entities, can be considered enormous, e.g., thousands to tens of thousands of euros per day of extended life. However, the net financial benefit to pharmaceutical companies of those agents that are given only for few months (or years) in only a small proportion of patients in niche indications may lead to restricted investment by pharmaceutical industries; blockbuster indications usually provide higher revenues.

These drawbacks are at the origin of the re-emergence of natural products in oncology. Since 2007, with the approval of rapamycin and derivatives of it, 12 natural product derivatives have been approved for the treatment of cancers (**Table 1**).

Recently Stuart Schreiber, Paul Clemons and coworkers at the Broad Institute in Boston performed a bioinformatics analysis of natural product targets and demonstrated that natural products statically tend to target proteins with a high number of protein–protein interactions that are particularly essential to an organism (Dančík et al., 2010). This observation is consistent with the common role played by natural products as chemical weapons against predators or competitors.

Henkel et al. at Bayer AG in Germany offered a statistical analysis of the structural differences between natural products and fully synthetic drugs (Henkel et al., 1999). Compared with fully synthetic drugs, natural product tend to have more chiral centers, more oxygen atoms, less nitrogen atoms, and more varied ring systems. Complementary analyses of structural features of natural products have been reviewed (Lee and Schneider, 2001; Ortholand and Ganesan, 2004; Ganesan, 2008; Grabowski et al., 2008). A consequence of this structural complexity is that natural products tend to be more selective toward their targets than fully synthetic drugs, and consequently rarely display off-target—induced iatrogenicity.

Moreover, complex natural products tend to act through only one class of molecular target, even though there are some exceptions. Indeed, taxanes are known to target β-tubulin and interfere with microtubule dynamics; however they also bind to Bcl-2 to block its anti-apoptotic activity. Both β-tubulin and Bcl-2 interact with the orphan nuclear receptor Nur77 (NGFI-B, TR3, NR4A1). Ferlini et al. showed that in fact taxanes mimic the domain of Nur77 involved in the interaction with β-tubulin and Bcl-2 (Ferlini et al., 2009). Another example concerns flavaglines, an emerging family of natural compounds found in medicinal plants of South-East Asia, which display potent anticancer effects through their direct effects on the scaffold proteins prohibitins and the initiation factor of translation eIF4a (Basmadjian et al., 2013; Thuaud et al., 2013).

Modifying the structure of a drug may change the nature of its molecular target. A striking example concerns the not so rational development of the anticancer medicines etoposide and teniposide (**Figure 1**). Considering that cardiac glycosides display enhanced pharmacological properties compared to the cognate aglycone, Sandoz scientists hypothesized that conjugating podophyllotoxin to a glucose moiety could improve the activity of this cytotoxic agent that binds tubulin and inhibits assembly of the mitotic spindle. Fortunately, this glycoconjugate named etoposide displayed a promising anticancer activity with reduced adverse effects compared with podophyllotoxin. Surprisingly, etoposide did not affect tubulin polymerization but inhibited another very important target in oncology: DNA topoisomerase II. This story illustrates well the importance in drug discovery of serendipity, which was likened to "looking for a needle in a haystack and discovering the farmer's daughter" by Professor Pierre Potier, inventor of the anticancer drug taxotere (Zard, 2012).

Another non-rational issue regarding the SAR of derivatives of natural compounds concerns the relationship between the chemical structure of a drug and its therapeutic indication. Indeed, transforming the structure of a drug may modify the nature of the targeted cancer. This is well established for *vinca* alkaloids for instance (**Table 2**). If we could understand the influence of the molecular structure of a drug with its optimal therapeutic indication, then we might be able to adapt known medicines to treat cancers that are reluctant to current therapies.

In spite of the major achievements in systems biology and translational medicine over the last decade, there is still, at best, a presumptive relationship between the efficacy of a drug in preclinical assays and the likelihood of its value in clinic.

RAPALOGUES: TEMSIROLIMUS® AND EVEROLIMUS®

In 1975, researchers at Ayerst Laboratories (Canada) reported the isolation of rapamycin as a secondary metabolite from a strain of *Streptomyces hygroscopicus* based on its antifungal activity (Sehgal et al., 1975; Vezina et al., 1975). Its name comes from Rapa Nui (Easter Island) where its producer strain had been collected from a soil sample. Its richly adorned macrocyclic structure was fully elucidated a few years later (Swindells et al., 1978; Findlay and Radics, 1980; McAlpine et al., 1991). Rapamycin did not attract so much attention until the discovery in 1987 of the structurally related immunosuppressant FK506 (Kino et al., 1987a,b). Rapamycin was eventually developed without further structural modifications as the oral immunosuppressant drug sirolimus. It was approved for prevention of rejection in organ transplantation in 1999 (Calne et al., 1989; Kahan et al., 1991; Watson et al., 1999; Calne, 2003).

Determining the mode of action of rapamycin unraveled one of the most important signaling pathways in cell biology, which illustrates another important aspect of the pharmacology of natural products. Indeed a common caveat of developing an original natural product toward clinical application is the requirement to identify its molecular target and understand its mode of action (Krysiak and Breinbauer, 2012). However, when the target is identified, it may lead to major breakthroughs in cell biology (Pucheault, 2008). Gratefully, current technologies render this task increasingly easier (Ares et al., 2013).

In 1991, Michael Hall et al. identified the molecular target of rapamycin in a gene complementation assay in yeast and named it TOR for "Target Of Rapamycin" (Hietman et al., 1991).

Table 1 | Novel anticancer medicines based on natural products.

Name (trade name), structure	Year of approval, company	Therapeutic indication, mode of action
Temsirolimus (Torisel®): R=R^1 Everolimus (Afinitor®), R=R^2 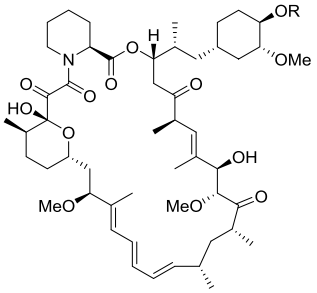 $R^1 = C(O)C(CH_2OH)_2CH_3$ $R^2 = (CH_2)_2OH$	2007, Wyeth	Treatment of renal cell carcinoma (RCC), inhibition of mTOR
	2009, Novartis	Treatment of advanced kidney cancer, inhibition of mTOR
Ixabepilone (Ixempra®) 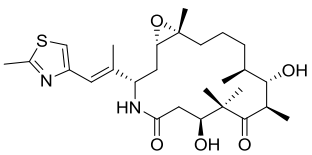	2007, Bristol-Myers Squibb	Treatment of aggressive metastatic or locally advanced breast cancer no longer responding to currently available chemotherapies, stabilization of microtubules
Vinflunine (Javlor®) 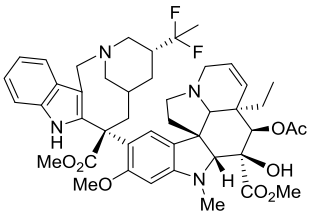	2009, Pierre Fabre	Treatment of bladder cancer, inhibition of tubulin polymerization
Romidepsin (Istodax®) 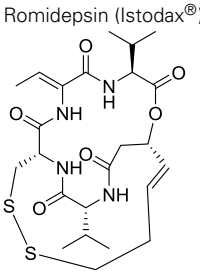	2009, Celgene	Treatment of cutaneous T-cell lymphoma (CTCL), inhibition of the isoforms 1 and 2 of histone deacetylases
Trabectedin = ecteinascidin 743 (Yondelis®) 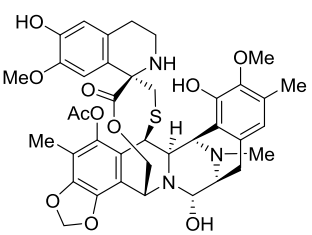	2009, Zeltia and Johnson and Johnson	Treatment of advanced soft tissue sarcoma and ovarian cancer, induction of DNA damage

(Continued)

Table 1 | Continued

Name (trade name), structure	Year of approval, company	Therapeutic indication, mode of action
Cabazitaxel (Jevtana®) 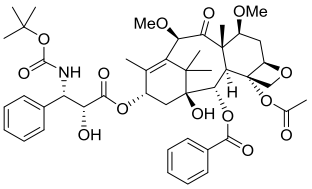	2010, Sanofi-Aventis	Treatment of hormone-refractory metastatic prostate cancer, microtubule stabilization
Abiraterone acetate (Zytiga®) 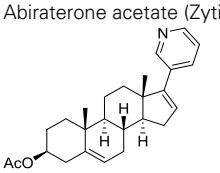	2011, Janssen	Treatment of castration-resistant prostate cancer, inhibition of 17 α-hydroxylase/C17, 20 lyase (CYP17A1)
Eribulin mesylate (Halaven®) 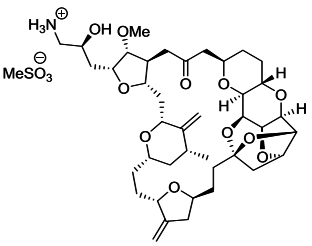	2011, Eisai Co.	Treatment of metastatic breast cancer, inhibition of microtubule dynamics
Homoharringtonine, Omacetaxine mepesuccinate (Synribo®) 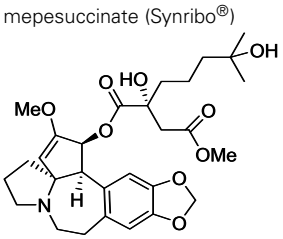	2012, Teva	Chronic myelogenous leukemia (CML), inhibition of protein synthesis
Carfilzomib (Kyprolis®) 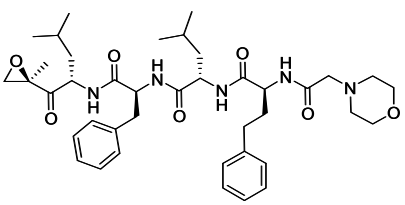	2012, Onyx	Treatment of multiple myeloma, inhibition of proteasome
Ingenol mebutate (Picato®) 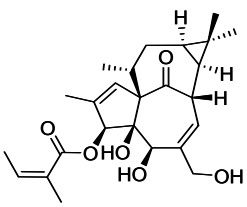	2012, LEO Pharma	Actinic keratosis, activation of PKCδ

Three years later, Stuart Shreiber et al. identified its mammalian homolog referred to today as the kinase mTOR (mammalian TOR) (Brown et al., 1994). The mode of action of rapamycin is unique: it binds to two proteins at the same time, mTOR and the immunophilin FKBP-12, to form a ternary complex devoid of any kinase activity. mTOR plays a central role integrating signals from growth factors, nutrients, stress, and hormones to regulate metabolism, proliferation, cell growth, and apoptosis. However, the exact mechanisms of action of rapamycin derivatives, called rapalogues, remain only moderately understood. Some recent evidence indicates that rapalogues may primarily display their anticancer effects through an inhibition of angiogenesis in patients (Faivre and Raymond, 2008). This hypothesis would explain why rapologues are particularly effective in hypervascularized tumors.

Currently, two rapalogues, temsirolimus, and everolimus, have been developed for the treatment of renal, breast, and pancreas cancers, astrocytoma, and mantle cell lymphoma. These drugs differ in their formulation, application, and dosing schemes, thereby yielding varying bioavailabilities. They are all prepared by semi-synthesis.

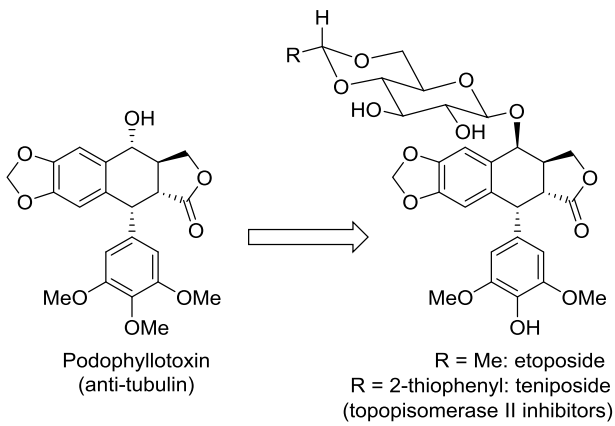

FIGURE 1 | Structures of podophyllotoxin, etoposide, and teniposide.

IXABEPILONE (IXEMPRA®)

Drugs that target microtubules, such as taxoids and *vinca* alkaloids, continue to represent an important class of chemotherapeutic agents (Jordan and Wilson, 2004). Over the last two decades other classes of naturally occurring nontaxoid compounds, the epothilones (Gerth et al., 1996; Höfle et al., 1996), discodermolides (Gunasekera et al., 1990), eleutherobins (Lindel et al., 1997), and laulimalides (Mooberry et al., 1999) that stabilize microtubule assemblies similarly to taxol, have been identified (**Figure 2**). Based upon extensive structure-activity data, a common pharmacophore for these different classes of compounds has been proposed (Ojima et al., 1999).

Not only is epothilone B more cytotoxic than taxol, but it is also much less sensitive toward the development of multidrug-resistance, a major concern in the clinic (Horwitz, 1994; Bollag et al., 1995; Kirikae et al., 1996). This impressive pharmacological profile coupled with the challenge of its total synthesis has attracted the attention of some of the most well-known organic chemists in the world, including Samuel Danishefsky (Balog et al., 1996; Su et al., 1997), followed by Nicolaou (Nicolaou et al., 1997; Yang et al., 1997), Schinzer (Schinzer et al., 1997), Mulzer (Mulzer et al., 2000) and Carreira (Bode and Carreira, 2001).

Early investigations indicated that natural epothilones display poor metabolic stability and unfavorable pharmacokinetic properties (Lee et al., 2000). Several synthetic and semi-synthetic analogs were then examined and evaluated in preclinical studies. Eventually, isosteric replacement of the lactone by a lactam afforded ixabepilone (also known as azaepothilone B) (Lee et al., 2008). Not only is this drug not susceptible to hydrolysis by esterases, conferring metabolic stability, but it also displays improved water solubility, which greatly alleviate galenic problems associated with hypersensitivity reaction in patients.

Table 2 | Structures and therapeutic indications of *vinca* alkaloids.

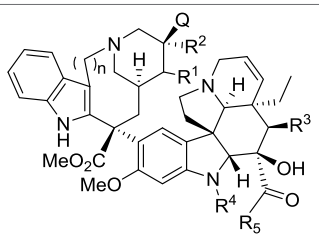

Name	*n*	Q	R^1	R^2	R^3	R^4	R^5	Therapeutic indication
Vinblastine	2	OH	H	Et	OAc	Me	OMe	Lymphomas, germ cell tumors, breast, head and neck cancer and testicular cancers
Vinorelbine	1	Q=R^1=Ø (alkene)		Et	OAc	Me	OMe	Osteosarcoma, breast, and non-small cell lung cancers
Vincristine	2	OH	H	Et	OAc	CHO	OMe	Acute lymphoblastic leukemia, rhabdomyosarcoma, neuroblastoma, lymphomas, and nephroblastoma
Vindesine	2	OH	H	Et	OH	Me	NH_2	Melanoma, lung, breast and uterine cancers, leukemia and lymphoma
Vinflunine	1	H	H	CF_2Me	OAc	Me	OMe	Bladder cancer

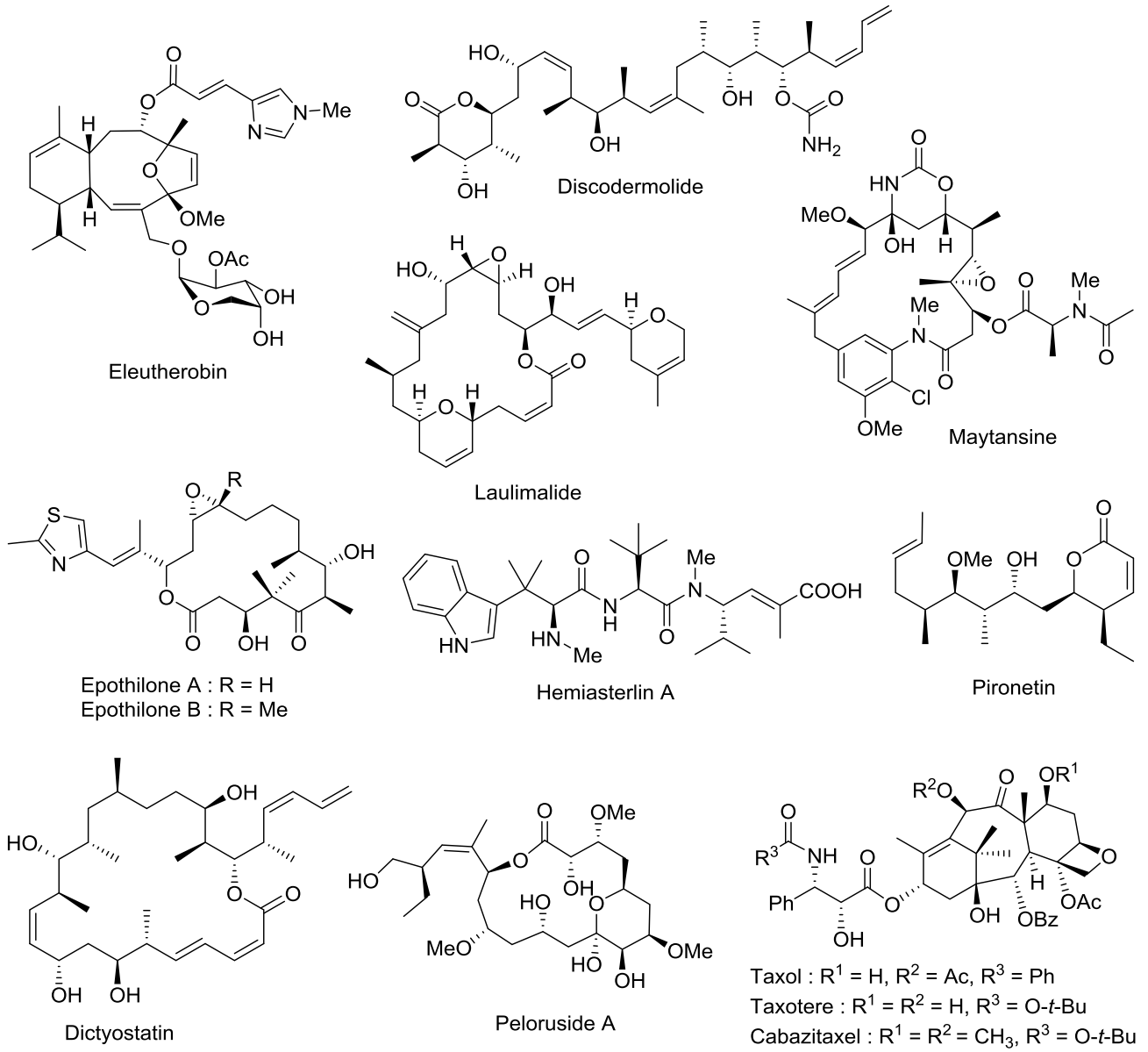

FIGURE 2 | Chemical structures of representative natural compounds that stabilize microtubule assemblies.

In 2007, the FDA (but not its European equivalent, European Medicines Agency or EMA) approved ixabepilone for the treatment of aggressive metastatic or locally advanced breast cancer no longer responding to currently available chemotherapies.

VINFLUNINE (JAVLOR®)

Vinca alkaloids were the first chemotherapeutic agents that target microtubules. The first member of this class, vinblastine, was isolated in 1958 (Noble et al., 1959). Latter, some derivatives, vincristine, vinorelbine, and finally avelbine, were developed to treat hematological and solid malignancies in both adult and pediatric patients (**Table 1**). *Vinca* alkaloids block the polymerization of tubulin molecules into microtubules to prevent the formation of the mitotic spindle.

In the course of their study on the reactivity of functionalized molecules in superacid media, Jacquesy and collaborators found that the treatment of vinorelbine with a combination of HF and SbF_5 gave a difluoro analog, later called vinflunine (**Scheme 1**) (Fahy et al., 1997). Importantly, this new compound displayed an enhanced bioavailability compared to other *vinca* alkaloids. Indeed, its terminal half-life was calculated to be about 40 h and the terminal half-life for its active metabolite (4-*O*-deacetylvinflunine) was reported to be 4–6 days in several phase I trials (Bennouna et al., 2003, 2005; Johnson et al., 2006).

Resistance to vinflunine develops more slowly than with other *vinca* alkaloids. In addition, vinflunine *in vitro* neurotoxicity is lower than that of vincristine or vinorelbine (Etiévant et al., 1998, 2001; Estève et al., 2006). Further development by Pierre Fabre

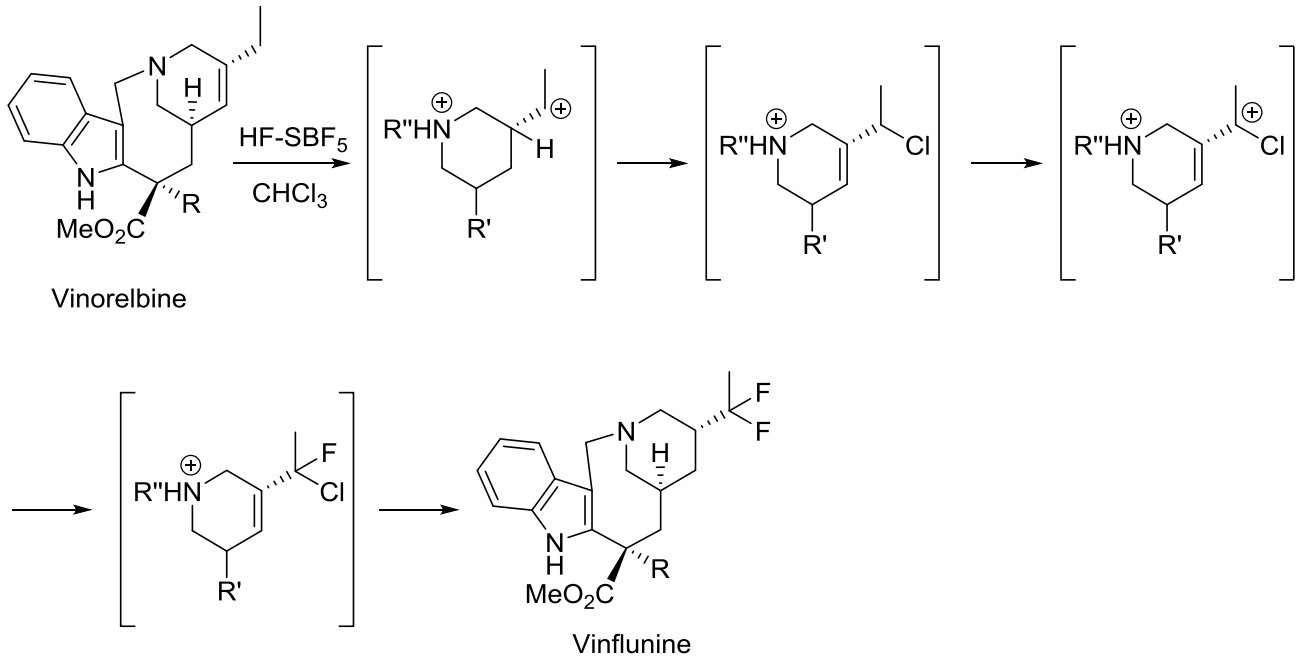

SCHEME 1 | Synthesis of vinflunine from vinorelbine (Fahy et al., 1997).

and Bristol Myers Squibb laboratories ended with the approval of vinflunine for the treatment of bladder cancer by the European Medicines Agency (EMA) in 2009.

ROMIDEPSIN (ISTODAX®)

The cyclic depsi-pentapeptide romidepsin, also called FR901228, FK228, or NSC 630176, was isolated and identified by Ueda and colleagues at Fujisawa Pharmaceutical in Japan through a screening program of fermentation products able to revert the transformed morphology of a Ha-ras NIH3T3 cells to normal (Ueda et al., 1994). Indeed Ha-ras is an oncogene involved in tumorigenesis and consequently represents an important target in oncology. Importantly, romidespsin displayed potent antitumor activities against A549 and MCF-7 tumors in xenografted mice. These results attracted the attention of NCI scientists who continued to explore its anticancer properties under a Cooperative Research and Development Agreement with Fujisawa Corporation (now Astellas).

When romidepsin was discovered, histone deacetylases (HDAC) were emerging as important targets for the treatment of cancer (Thaler and Mercurio, 2014). Screening of microbial metabolites for their effects on transcription showed that romidepsin behaves similarly to trichostatin A, a known HDAC inhibitor (Nakajima et al., 1998). Romidepsin acts as a prodrug, which is reduced in cells to its active form by glutathione, yielding a monocyclic dithiol that preferentially inhibits the isoforms HDAC1 and HDAC2 (Furumai et al., 2002).

In 2002, when it became established that romidepsin holds a promising therapeutic potential, Fujisawa Corporation began clinical trials. Romidepsin was licensed to Gloucester Pharmaceuticals in 2004 (latter acquired by Celgene Co) and was approved by the FDA in 2009 for the treatment of cutaneous T-cell lymphoma. The preclinical and clinical development has been described in an excellent review (Vandermolen et al., 2011).

ECTEINASCIDIN 743 = TRABECTEDIN (YONDELIS®)

In 1969, unidentified alkaloids from the Caribbean tunicate *Ecteinascidia turbinate* were shown to display some anticancer activities, but the structure of these complex alkaloids could not be determined because of their natural scarcity and the limitation of analytical chemistry at that time (Sigel et al., 1970). In 1990, Rinehart et al. from the University of Illinois at Urbana-Champaign elucidated the structure and reported the cytotoxicity of these tetrahydroisoquinoline alkaloids, the ecteinascidins (Rinehart et al., 1990). These compounds displayed greater *in vitro* and *in vivo* antitumor activity than those reported for the structurally related microbial metabolites saframycins and safracins.

Ecteinascidin 743, also called trabectedin and ET-743, was then selected for preclinical development based on its exceptional *in vitro* cytotoxicity. Pommier et al. at NCI demonstrated that this drug binds in the minor groove of DNA and alkylates the exocyclic amino group at position 2 of guanine in GC-rich regions (**Scheme 2**) (Pommier et al., 1996).

Ecteinascidin 743 was shown to block the DNA excision repair system (Takebayashi et al., 2001; Zewail-Foote et al., 2001), to cross-link DNA with topoisomerase I (Martinez et al., 1999; Takebayashi et al., 1999; Zewail-Foote and Hurley, 1999), and also to inhibit the binding of DNA to some transcription factors (Bonfanti et al., 1999; Jin et al., 2000; Minuzzo et al., 2000). However, the cascade of events that links DNA damage

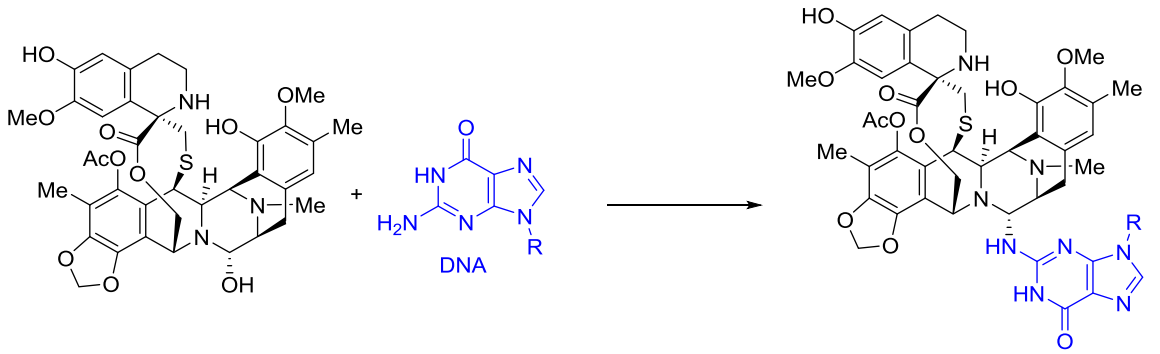

SCHEME 2 | DNA Alkylation by ecteinascidin 743.

to the resulting antitumor activity is far from being understood (D'Incalci and Galmarini, 2010).

When ecteinascidin 743 was licensed to PharmaMar; this company launched a very challenging program of aquaculture to produce sufficient quantities of tunicate biomass to feed clinical trials program. After several years of intensive development, the cumulative total biomass reached some 250 metric tons. However, isolation of ecteinascidin 743 required complex and costly steps of purification with final yields less than 1 g/ton (Cuevas and Francesch, 2009). Several total syntheses have been reported, but they cannot be translated into industrial production (Corey et al., 1996; Endo et al., 2002; Chen et al., 2006; Zheng et al., 2006; Fishlock and Williams, 2008; Imai et al., 2012; Kawagishi et al., 2013). Eventually, this supply problem was solved by use of a complex semi-synthesis from cyanosafracin B, which is available in kilogram quantities by fermentation (Cuevas et al., 2000; Menchaca et al., 2003).

Preclinical studies did not reveal that soft tissue sarcoma is more sensitive to ecteinascidin 743 than other solid tumors. This response was unveiled first during phase I clinical trials and confirmed in phase II (Taamma et al., 2001; Villalona-Calero et al., 2002; D'Incalci and Jimeno, 2003). This drug was approved under the name of Yondelis in 2007 in the European Union for the treatment of patients with advanced soft tissue sarcoma. This compound was the first anticancer medicine of marine origin to be approved. It was followed by eribulin (vide infra), validating the concept that marine natural products should be considered important contenders in drug discovery.

CABAZITAXEL (JEVTANA®)

The taxane anticancer drug cabazitaxel is a semi-synthetic derivative of the natural taxoid 10-deacetylbaccatin III. It was approved in 2010 by the FDA, in combination with prednisone, for the treatment of patients with hormone-refractory metastatic prostate cancer who had already been administered a treatment containing the taxane docetaxel (Galsky et al., 2010). In 2013, Vrignaud et al. showed that *in vitro*, cabazitaxel stabilized microtubules as effectively as docetaxel but was also 10 times more potent than docetaxel in chemotherapy-resistant tumor cells. They also noted that cabazitaxel was active in docetaxal-resistant tumors (Vrignaud et al., 2013). In addition, cabazitaxel penetrates the blood-brain barrier. Cabazitaxel was approved 20 years after taxol, illustrating that there is still room to improve well established anticancer medicines.

ABIRATERONE ACETATE (ZYTIGA®)

Abiraterone acetate is an oral inhibitor of androgen synthesis used since 2011 for the treatment of castration-resistant prostate cancer. Previous treatments of prostatic cancers prevented androgen production by the testes, but not by the adrenals. Abiraterone acetate is rapidly hydrolyzed *in vivo* to abiraterone, which is a selective, irreversible inhibitor of cytochrome P450 17α (CYP17), an enzyme that catalyzes the conversion of pregnenolone and progesterone into DHEA or androstenedione, two precursors of testosterone. This drug was originally designed and synthesized by Jarman et al. at the Institute of Cancer Research in Sutton (UK) based on the hypothesis that the nitrogen lone pair of a pyridyl moiety linked to the steroid skeleton would coordinate with the iron atom of the heme cofactor in the active site of CYP17 (Potter et al., 1995; Jarman et al., 1998).

The inhibition of CYP17 by abiraterone acetate blocks androgen biosynthesis and significantly improves the therapy of castration-resistant prostate cancer, which remains a challenge to treat (Rehman and Rosenberg, 2012). Unfortunately, this CYP17 inhibition also decreases glucocorticoid and increases mineralocorticoid production, which results in the main source of adverse effects.

Since the invention of abiraterone, different steroids bearing a heteroaromatic substituent on the D ring continued to be developed as CYP17 inhibitors. Among those, galeterone (TOK-001 or VN/124-1) recently entered clinical trials for the treatment of chemotherapy-naive, castration-resistant prostate cancer (**Figure 3**) (Vasaitis and Njar, 2010). Interestingly, this drug not only inhibits CYP17, but is also an androgen receptor antagonist (Handratta et al., 2005).

ERIBULIN MESYLATE (HALAVEN®)

In 1985, Uemura et al. isolated and identified norhalichondrin A from the marine sponge *Halichondria okadai* based on its potent *in vitro* toxicity (Uemura et al., 1985). Related polyether macrolides, including halichondrin B (Hirata and

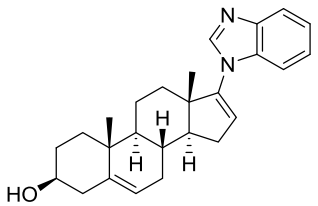

FIGURE 3 | Structure of galeterone.

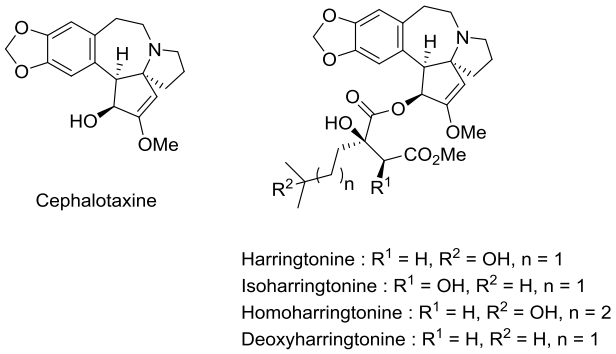

FIGURE 4 | Structures of cytotoxic *Cephalotaxus* alkaloids.

Uemura, 1986) were identified in the following years (Qi and Ma, 2011). Tests with NCI's 60-cell line screen suggested that halichondrin B affects tubulin polymerization. Further studies showed that this drug displays subtle differences in mechanism of action from those of other known antimitotics targeting tubulin. Although halichondrin B displayed promising activity, its preclinical investigation has been hampered by its scarcity from natural sources.

Due to its complexity, the total synthesis of halichondrin B was considered as an attractive objective by Kishi et al. at Harvard University. This team achieved this formidable challenge in 1992 (Aicher et al., 1992). Further collaborative studies from this group and Eisai Co. ultimately led to the development of the simplified and pharmaceutically improved analog eribulin (Jackson et al., 2009). Although it is less complex than natural halichondrins, eribulin contains 19 stereogenic centers, two exocyclic olefins, seven polyoxygenated pyrans and tetrahydrofurans, a 22-membered macrolactone ring, and a 36 carbon backbone. With its 35 steps, eribulin synthesis extended the limit of feasibility for industrial production. Indeed, eribulin is the single most complex molecule synthesized at an industrial scale and represents an awe-inspiring testimony to the current power of organic synthesis. Eribulin was approved by FDA in 2010 to treat patients with metastatic breast cancer who have received at least two prior chemotherapy regimens for late-stage disease.

HOMOHARRINGTONINE = OMACETAXINE MEPESUCCINATE (CEFLATONIN®)

Toxic seeds of the conifer *Cephalotaxus harringtonia K. Koch* var*harringtonia* belong to the traditional Chinese pharmacopeia. In observance with Mao Tse-tung's judgment that Chinese medicine and pharmacology represent a national treasure that needs to be valorized, Chinese investigators established that the total alkaloids from *Cephalotaxus fortunei Hook.f* possesses antitumor activity in preliminary clinical trials (Group, 1976). In the same period, National Cancer Institute (NCI) scientists found that *Cephalotaxus harringtonia* seed extracts displayed significant *in vivo* activity against L-1210 and P-388 leukemia tumors in mice. Powell et al. from the U.S. Department of Agriculture isolated and identified the structure of cytotoxic *Cephalotaxus* alkaloids: harringtonine, isoharringtonine, homoharringtonine, and deoxyharringtonine (Powell et al., 1970) (**Figure 4**). These compounds are esters of cephalotaxine, an inactive alkaloid first isolated by Paudler et al. in 1963 at Ohio University (Paudler et al., 1963). Homoharringtonine was found to be the most effective in prolonging survival of P388 leukemic mice (Powell et al., 1972). Clinical trials performed in China demonstrated the efficacy of this agent against acute myeloid leukemia (AML), myelodysplastic syndrome (MDS), acute promyelocytic leukemia (APL), polycythemia vera, and central nervous system (CNS) leukemia (Kantarjian et al., 2013).

Homoharringtonine inhibits protein synthesis (Huang, 1975). More specifically, it blocks the aminoacyl-tRNA binding to free ribosomes and monosomes, but not to polyribosomes (Fresno et al., 1977). Tang et al. demonstrated that decreased expression of the antiapoptotic factor myeloid cell leukemia-1 (Mcl-1) is a key event in this antileukemic mechanism of action (Tang et al., 2006).

In 1998, a Texan biotech company developed the semisynthetic form of homoharringtonine, designated "omacetaxine mepesuccinate" (Synribo®), and provided a reliable source supply for clinical investigations by ChemGenex and the M.D. Anderson Cancer Center (Robin et al., 1999).

This preparation of homoharringtonine [Omacetaxine mepesuccinate (Synribo®)] has been granted orphan drug status in Europe and the U.S. to treat chronic myelogenous leukemia (CML). It was approved by the US FDA in October 2012 for the treatment of adult patients with CML after failure of two or more tyrosine kinase inhibitors (for a review on its clinical development, see Kantarjian et al., 2013). It is interesting to note that these approvals occurred more than 40 years after the initial discovery of this compound. Even though omacetaxine has a narrow indication in the U.S. and Europe, it has been part of standard acute myeloid leukemia (AML) therapy in China, which begs for extending its use for additional indications.

CARFILZOMIB (KYPROLIS®)

In 1992, Bristol-Myers Squibb scientists from Tokyo reported the structure of epoxomicin, a microbial tetrapeptide appended with an electrophilic epoxy ketone group. This compound displayed potent *in vivo* antitumor activity against murine B16 melanoma tumors. However, because the mechanism of action could not be established, its investigation was abandoned, thereby leading to the publication of the initial discovery. Eventually, BMS closed the research center in Tokyo. It was a common practice

during that period for big pharmaceutical companies to close their departments of natural product chemistry.

In 1999, the potent anticancer activity of epoxomicin attracted the attention of Craig Crews at Yale University, who designed the first synthesis of epoxomicin. In the course of this endeavor, he established the absolute configuration of the epoxide stereocenter and synthesized also a biotinylated probe, which was used to identify the proteasome as the molecular target of epoxomicin. The proteasome is a multiprotein complex that degrades unneeded or damaged proteins by proteolysis. Importantly, epoxomicin does not display any cross-inhibition with proteases, which is a major problem encountered with other anticancer proteasome inhibitors, such as bortezomib (Velcade®). The source of this selectivity was elucidated by a crystallographic approach (Groll et al., 2000). The crystal structure of the proteasome bound to epoxomicin revealed the formation of a morpholino ring between the amino terminal threonine of the proteasome and the electrophilic moiety of epoxomicin, probably through the mechanism displayed in **Scheme 3**.

The specificity of epoxomicin toward proteasome prompted Crews to associate with Caltech professor Raymond Deshaies to establish a start-up company, Proteolix, dedicated to the development of a clinical candidate. During this process, they identified YU-101, which had better inhibitory activity than bortezomib (**Figure 5**). Addition of a morpholine moiety to YU-101 improved its solubility, thereby creating carfilzomib, which rapidly entered Phase I and II clinical trials. Importantly, the peripheral neuropathy that was observed with bortezomib did not occur with carfilzomib. In 2009, Onyx Pharmaceuticals acquired Proteolix and this compound was approved for the treatment of multiple myeloma in 2012.

INGENOL MEBUTATE (PICATO®)

Phorbol diesters, such as 12-*O*-tetradecanoylphorbol-13-acetate (TPA), rank among the most potent tumor promoters identified so far (**Figure 6**) (Nishizuka, 1984). These compounds induce tumor formation by activating protein kinase C (PKC). Interestingly, a natural compound extracted from *Euphorbia peplus* plants, Ingenol mebutate, also activates PKC but with a different pharmacological profile. Indeed, this compound induces the death of precancerous skin lesions induced by sunlight, called actinic keratosis.

The sap of *Euphorbia peplus* (known commonly as petty spurge) is commonly used as an alternative therapy for skin diseases in Australia (Weedon and Chick, 1976). In 1998, its efficacy was established for the self-treatment of skin cancers and actinic keratosis (Green and Beardmore, 1988).

Ingenol mebutate was first identified in 1980 by Evans et al. from the National Research Center in Cairo (Egypt) (Sayed et al., 1980). These authors demonstrated also that this compound is cytotoxic to cancer cells. For more than 20 years, ingenol mebutate remained poorly investigated, until 2004, when the lab of Peter Blumberg at NCI showed that it activates PKC isoforms, but with a different pharmacological profile than that of TPA. Importantly, the activation of protein kinase C delta (PKCδ) was shown to promote the production and release of inflammatory cytokines contributing to the elimination of actinic keratosis.

At the same time, Eric Raymond in Clichy (France) showed that ingenol mebutate-induced activation of PKCδ and reduced expression of PKCα lead to an activation of Ras/Raf/MAPK, an inhibition of the phosphatidylinositol 3-kinase/AKT signaling pathways, and ultimately to apoptosis of cancer cells (Benhadji et al., 2008; Serova et al., 2008; Ghoul et al., 2009).

After few years of preclinical investigations, ingenol mebutate entered clinical trials (Siller et al., 2009) and was eventually approved by FDA and EMA in 2012 for the topical treatment of actinic keratosis. This compound is produced by extraction from the petty spurge plant in low yield (1 g of pure compound/800 kg of plant). To improve the production of this molecule, Jakob Felding of LEO pharma associated with Phil Baran from Scripps Institute to develop an elegant synthesis of ingenol in only 14 steps from inexpensive (+)-3-carene (Jørgensen et al., 2013). This synthesis has been rapidly scaled-up to kilogram levels (Ritter, 2013).

CONJUGATION OF NATURAL PRODUCTS TO ANTIBODIES OR FOLIC ACID TO TARGET TUMORS

At the end of 19th century, Paul Ehrlich already considered the conjugation of a toxin to a compound that selectively targets a disease-causing organism to generate a "magic bullet" ("*magische kugel*") that would destroy the origin of the disease without toxicity to healthy tissues in the body (Ehrlich, 1897). About 60 years later, Mathé et al. conjugated anti-tumor antibodies to the folic acid antagonist, methotrexate (Loc et al., 1958). Although the experiments in mice were encouraging, this approach did not attract interest in the scientific community and returned to limbo for two decades, until 1975, when Ghose et al. demonstrated the efficacy of an anticancer alkylating

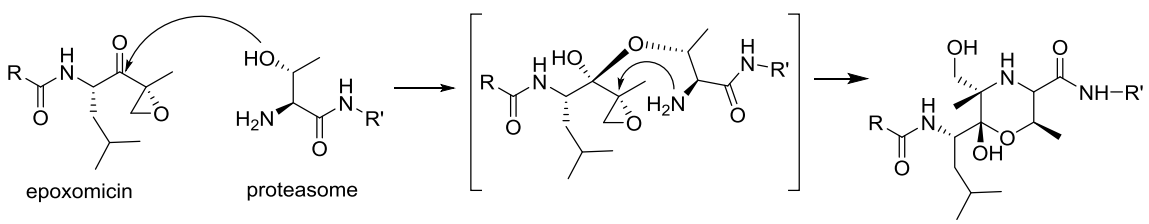

SCHEME 3 | Proposed mechanism of alkylation of the proteasome by epoxomicin.

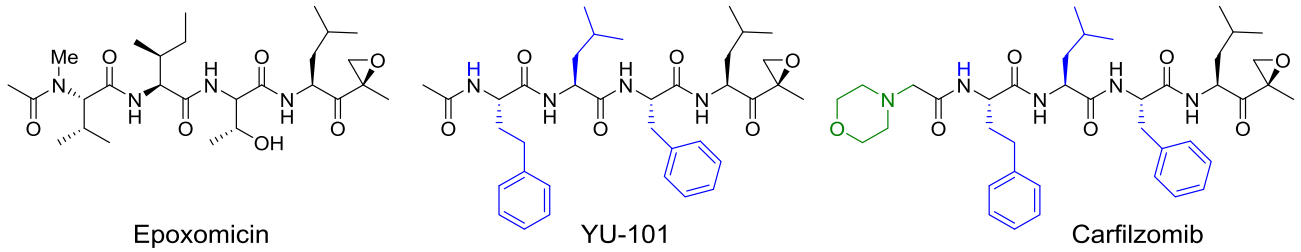

FIGURE 5 | Structures of epoxomicin, YU-101, carfilzomib.

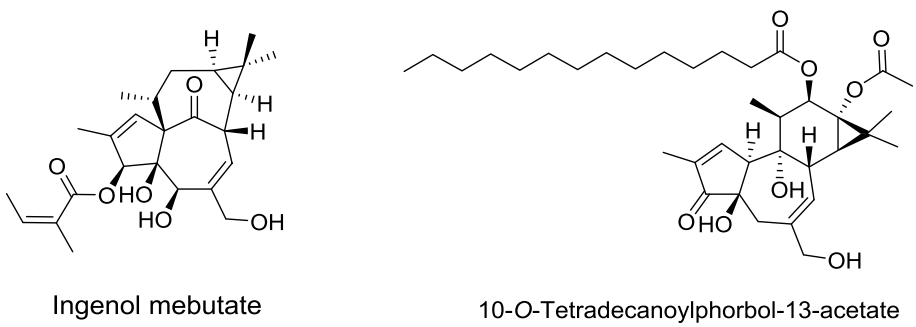

FIGURE 6 | Structures of 12-*O*-tetradecanoylphorbol-13-acetate and ingenol mebutate.

agent, chloranbucil, conjugated to an antibody against a mouse lymphoma (Ghose et al., 1975). The advent of monoclonal antibodies the same year definitely boosted this field of research (Kohler and Milstein, 1975). Since then, almost every cytotoxic agent has been conjugated to antibodies following various strategies.

After two decades of endeavor, low cytotoxicity, and lack of specificity of antibodies for their targeted antigens, conjugate instability, immunogenicity, and heterogeneous product characteristics were identified as important sources of failure in the clinic (Scott et al., 2012; Ho and Chien, 2014). However, a significant step forward was made with the use of extremely highly toxic agents such as calicheamicin, maytansine, or auristatin (**Figure 7**). These drugs are so toxic that they cannot be used by themselves without a targeting agent.

In 2000, four decades after Mathé's pioneering work and one century after Ehrlich's dream, Wyeth received approval to commercialize Gemtuzumab ozogamicin (Mylotarg®) which results from the conjugation of a monoclonal antibody targeting CD33 with a calicheamicin derivative. This drug was used for 10 years against acute myelogenous leukemia, before being withdrawn in 2010, when it was demonstrated that it does not provide any significant benefit over conventional cancer therapies. In 2011 and 2013, two other immunoconjugates were marketed: brentuximab vedotin (Adcetris®) and trastuzumab emtansine (Kadcyla®). The first one targets the protein CD30, which is expressed in classical Hodgkin lymphoma and systemic anaplastic large cell lymphoma. This antibody is conjugated to a fully synthetic analog of the antimitotic agent dolastatin (**Figure 7**).

Trastuzumab emtansine results of the conjugation of a monoclonal antibody targeting the receptor HER2 (a receptor tyrosine-kinase erbB-2), which is overexpressed mainly in some forms of breast and gastric cancers to the highly cytotoxic natural product maytansine. The development of this class of agents requires a careful optimization of the monoclonal antibody, the cytotoxic payload, and the chemical linker (Ducry, 2012). The successful introduction of immunoconjugates has validated this approach to treat cancers, and currently as many as 415 antibody–drug conjugates are under clinical evaluation.

In addition to antibodies, alternative tumor-selective ligands have been conjugated to anticancer drugs. Based on observations that cells internalize vitamins, such as folate, by receptor-mediated endocytosis, Leamon, and Low from Purdue University demonstrated in 1991, that macromolecules conjugated to folic acid could be delivered into living cells (Leamon and Low, 1991). Following this seminal observation, hundreds of publications have improved upon this approach, which is currently being examined in clinical trials. The efficacy of this technology lies on the overexpression of the folate receptor in tumors, while it is quasi-absent in normal tissues. Very importantly also, folic acid retains a high affinity to its receptor when it is conjugated via its γ-carboxyl (Vlahov and Leamon, 2012).

Early attempts were limited by the release properties of the conjugates. After two decades of intensive research, some guiding rules were identified to lead compounds toward clinics:

1. anticancer agents must display a high cytotoxicity (similar to immunoconjugates);

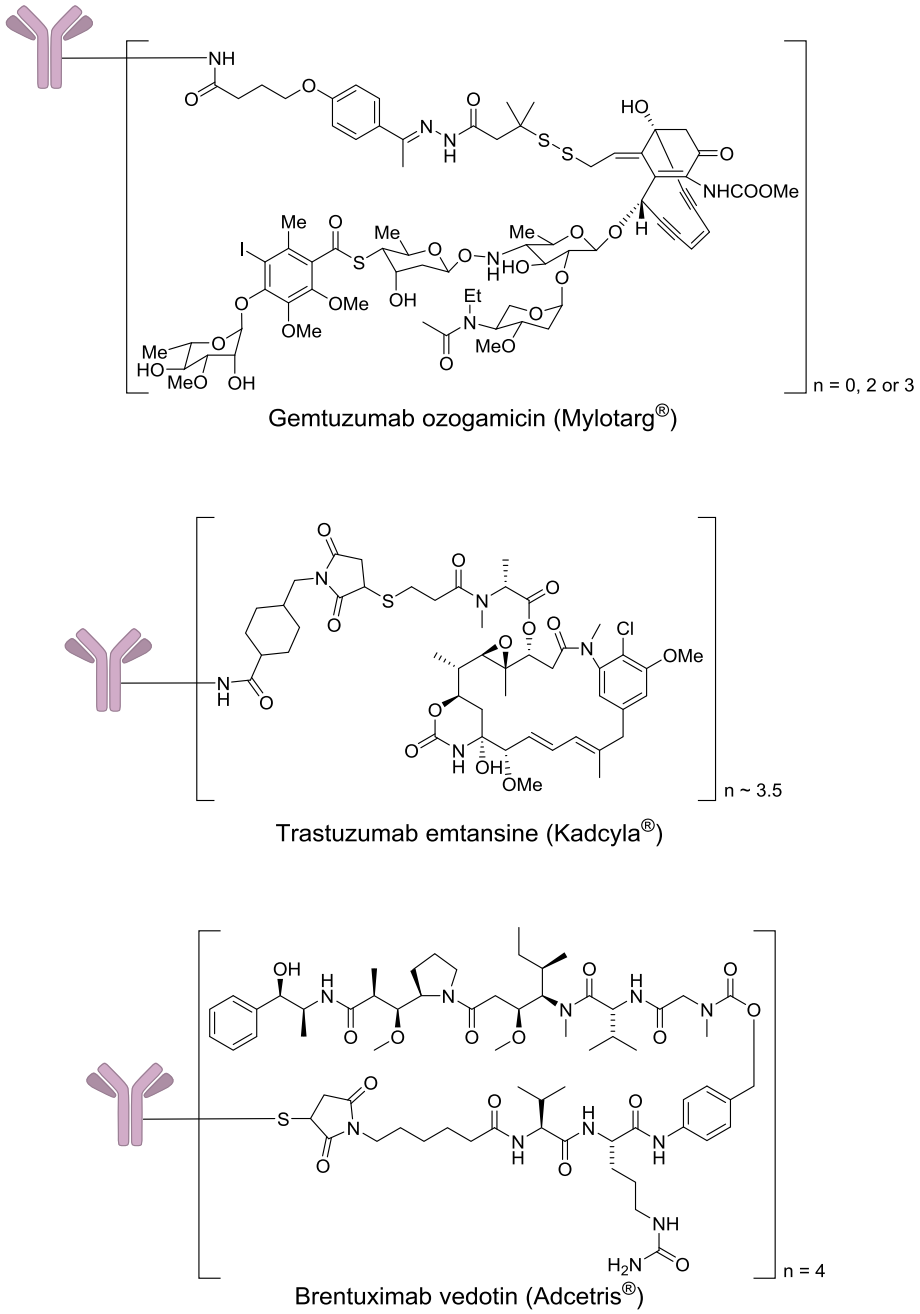

FIGURE 7 | Structures of marketed immunoconjugates.

2. enhanced hydrophilicity, to prevent passive diffusion into normal tissue;
3. an efficient cleavable linker system that releases the anticancer drug at a reliable rate once inside the targeted cell;
4. a low molecular weight, to optimize the penetration into solid tumor tissue with concomitant rapid systemic clearance.

Following these guidelines, five folic acid conjugates have reached clinical trials, including the most advanced one, vintafolide (EC145), which is currently in a phase 3 trial in women with cisplatin -resistant ovarian cancer.

In vintafolide, the highly cytotoxic vinblastine is connected to the folate moiety trough a self-immolative linker and a peptidic spacer (**Figure 8**). To provide the desired hydrophilicity to the final drug-conjugate and prevent unspecific internalization, acidic, and basic amino acids such as aspartic acid and arginine were introduced in the peptide-based unit.

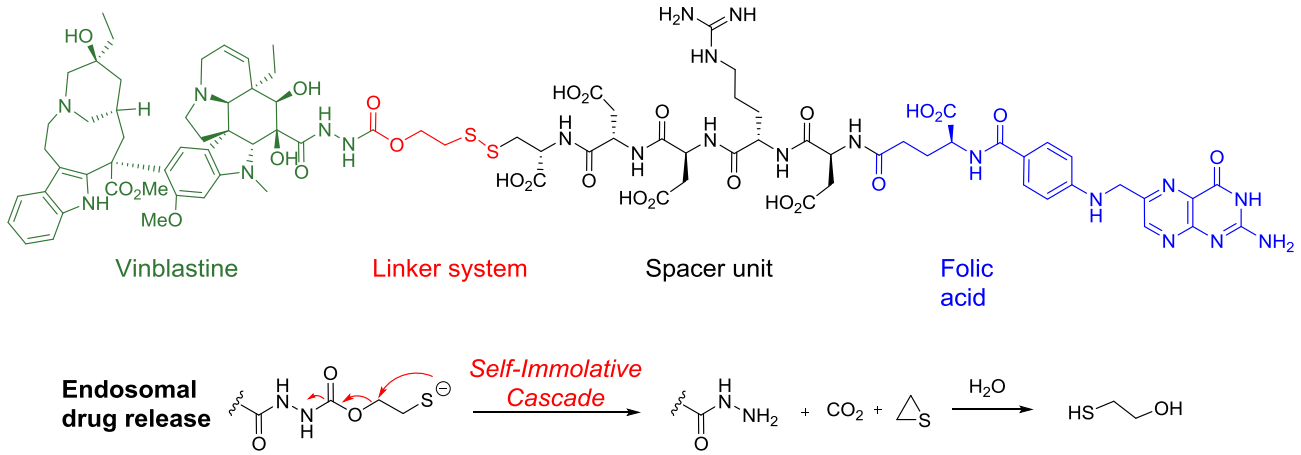

FIGURE 8 | Structure of vintafolide and mechanism of release of the payload in the endosome.

The self-destructive linker system is based on a 1,2-elimination mechanism by reduction of the disulfide bond between the cysteine of the spacer and the linker, which occurs in the endosome through a not fully understood mechanism (**Figure 8**) (Yang et al., 2006).

TRADITIONAL HERBAL REMEDIES

In addition to purified molecules, traditional herbal remedies are slowly emerging in modern Western medicine (Basu, 2004). An injectible form of an extract of the Chinese medicinal plant *Semen coicis* called Kanglaite® (Kang-Lai-Te) has been used in China as a lipid emulsion since the end of the 90's for the treatment of non-small cell lung, liver, stomach, and breast cancers. It has been marketed also in the Russian Federation since 2003 and is the first traditional Chinese herbal remedy to enter into clinical trials in the US. As with many other traditional Chinese medicines, Kanglaite activity probably results from the combined actions of multiple pharmacologically active ingredients that have not been yet identified (Xu, 2011). Over the last decade, other botanical drugs have entered clinical trials in the West to treat cancers or other ailments.

NANOPARTICLE DELIVERY OF ANTICANCER DRUGS

Tumor growth requires angiogenesis, i.e., the formation of new blood vessels. In contrast to normal angiogenesis, newly formed vessels in tumors display many structural and functional defects, which permit the leakage of macromolecules. This feature is referred to as the "enhanced permeability and retention (EPR) effect." Recent advances in the application of nanotechnology to medicine enabled the approval of five nanoparticle chemotherapeutics for cancer (Wang et al., 2012). Four liposomal formulations have been approved for clinical use in oncology: pegylated liposomal doxorubicin (DOXIL®, Caelyx®), nonpegylated liposomal doxorubicin (Myocet®), and liposomal cytarabine (DepoCyte®) (Hofheinz et al., 2005). Nab-paclitaxel (Abraxane®) is an albumin bound approved for the treatment of breast cancer and is undergoing clinical trials for other clinical indications. And finally, Genexol-PM is a polymeric micelle formulation of paclitaxel composed of block copolymers of PEG and poly-(D,L-lactic acid) (Kim et al., 2004).

Although nanomedicine is a new discipline, its translation into clinics has been rapid. A novel generation of nanoparticle chemotherapeutics is under development and expected to greatly improve cancer treatments. These new formulations may also offer novel opportunities for established anticancer drugs (Wang et al., 2012).

MISSED OPPORTUNITIES AND HOW TO RESCUE THEM

In 2010, Bristol-Myers Squibb stopped the phase III clinical trial of Tanespimycin, an inhibitor of heat shock protein 90, for the treatment of multiple myeloma, probably because of the expiration of the patent in 2014. In addition to drug developments that were terminated because of the shortness of patent life, there are many interesting drugs that did not reach clinical trial or that failed in clinical trial because the conceptual tools to correctly perform these assays were not available at that time. Indeed, "there are no bad anticancer agents, only bad clinical trial designs" as stated by Von Hoff (1998).

Flavaglines, such as rocaglamide, represent a striking example of natural products that are enjoying reinvigorated investigation after their original discovery by King et al. from the National Defense Medical Center of Taiwan (King et al., 1985). The recent identification of their molecular targets, the scaffold proteins prohibitins and the initiation factor of translation eIF4A, coupled with a description in *Science* about the origin of their selective cytotoxicity in cancer cells should promote further investigations to unveil their therapeutic usefulness (Basmadjian et al., 2013; Santagata et al., 2013). However, clinical trials with these compounds are unlikely unless some structurally original and patentable analogs are identified. Indeed, clinical trials of non-patentable compounds are still scarce (Roin, 2009; Cvek, 2012). For instance, a non-profit company, the Institute for OneWorld Health, developed in 2007 paromomycin, which is not patentable, as an effective treatment for visceral leishmaniasis. This was accomplished with financial support from the Bill and Melinda Gates Foundation, the Special Program for Research and Training

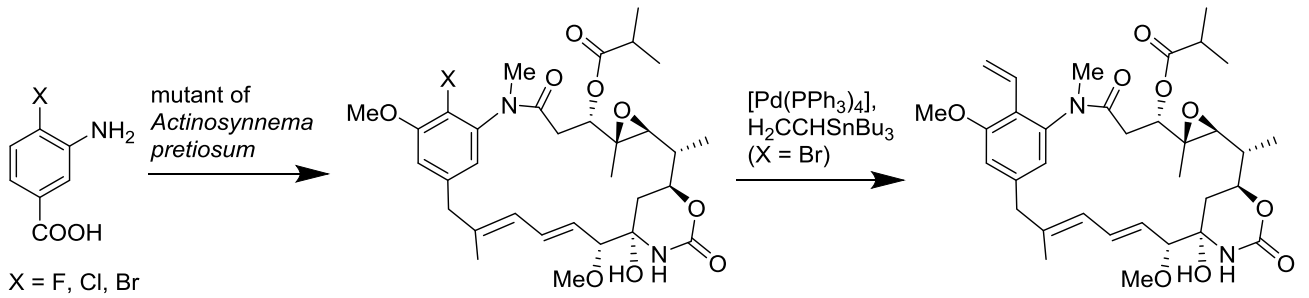

SCHEME 4 | Combination of biotechnology and organic synthesis for the synthesis of ansamitocin derivatives (Taft et al., 2008).

in Tropical Diseases of the United Nations Development Program, the World Bank, and the World Health Organization (Sundar et al., 2007). GlobalCures is another example of a non-profit medical research organization, which aims to develop novel and cost-effective treatments for cancers (Cvek, 2012). State agencies, such as the National Center for Advancing Translational Sciences are also deeply involved in the development of non-profitable drugs. Only a radical change in public or international policy could support the further development of clinically useful compounds that are currently fated to be traded as generics.

BIOTECHNOLOGY-BASED GENERATION OF NOVEL NATURAL PRODUCTS

Since the seminal synthesis of aspirin by Gerhardt (1853), all the natural product derivatives were prepared by total synthesis or semi-synthesis. Alternate approaches are currently emerging based on the progress in the deciphering of biosynthetic pathways and advances in biotechnologies. Currently, only a tiny fraction of microbes can be cultured with conventional approaches, yet uncultivated microorganisms represent an attractive source of novel natural products. It is now possible to isolate large fragments of microbial DNA directly from environmental samples and to express them in an easily cultured microorganism. This approach provides access to secondary metabolites that were originally produced by inaccessible microorganisms. Additionally, the manipulation of these biosynthetic pathways can lead to novel natural product derivatives. Metabolic engineering and synthetic biology are poised to revolutionize conventional chemical and pharmaceutical manufacturing in the coming decade (Yadav et al., 2012). Recently, methods and concepts of organic synthesis have begun to be integrated to synthetic biology to generate novel natural product derivatives. Such approaches that merge biotechnology with organic synthesis are rapidly blooming and are expected to efficiently generate novel natural product analogs in the near future (Goss et al., 2012; Kirschning and Hahn, 2012). A representative example of such an approach has been the use of an *Actinosynnema pretiosum* mutant that accepts 3-amino-4-bromobenzoic acid as a substrate to prepare pharmacologically active ansamitocin derivatives, which can then be transformed by classical organic reactions (**Scheme 4**; Taft et al., 2008).

CONCLUSION

The success of glivec and herceptin in the 90's announced the obsolescence of natural products in therapeutics. A decade later, many cancer patients continue to die and pharmaceutical companies have reconsidered their position on the potential of natural products in oncology. Indeed, for too many solid tumors of advanced grades, the only therapeutic options remain exclusively palliative. There is therefore an urgent need to develop original medicines.

Some of newly developed agents induce a strong cytotoxicity targeting conventional targets, DNA (for trabectedin) or microtubules (for ixabepilone, vinflunine, or eribulin), while other target specific biochemical events such as steroid biosynthesis (abiraterone acetate), histone remodeling (for romidepsin), protein translation (homoharringtonine), or degradation (carfilzomib). The case of rapamycin derivatives is atypical. These drugs are not cytotoxic, but can be considered as targeted therapy agents due to their inhibition of mTOR signaling.

In contrast with targeted therapeutics, which are designed for a specific type of cancer, the development of natural products is often more erratic and heavily relies on the skill of pharmacologists to unravel their mechanism of action and clinicians to identify the optimal indication in the clinic.

Over the last 15 years, natural products have been rehabilitated by pharmaceutical companies, even though some complementary approaches, such as molecular modeling based drug design are gaining in momentum. This latter methodology, which was pioneered by 2013 Nobel laureates, has successfully led to innovative medicines. When it is possible to predict the 3D structure of proteins, then it will probably overshadow other methods for identifying drug candidates. Until then, natural products should continue to play a major role in drug discovery, especially in the treatment of cancers and infectious diseases.

ACKNOWLEDGMENTS

We are grateful to the "Association pour la Recherche sur le Cancer" (ARC, grant numbers 3940 and SFI20111204054) for generous financial support. We also thank AAREC Filia Research for fellowships to Christine Basmadjian and Qian Zhao.

REFERENCES

Aicher, T. D., Buszek, K. R., Fang, F. G., Forsyth, C. J., Jung, S. H., Kishi, Y., et al. (1992). Total synthesis of halichondrin B and norhalichondrin B. *J. Am. Chem. Soc.* 114, 3162–3164. doi: 10.1021/ja00034a086

Ares, J., Durán-Peña, M. J., Hernández-Galán, R., and Collado, I. (2013). Chemical genetics strategies for identification of molecular targets. *Phytochem. Rev.* 12, 895–914. doi: 10.1007/s11101-013-9312-6

Bailly, C. (2009). Ready for a comeback of natural products in oncology. *Biochem. Pharmacol.* 77, 1447–1457. doi: 10.1016/j.bcp.2008.12.013

Balog, A., Meng, D., Kamenecka, T., Bertinato, P., Su, D.-S., Sorensen, E. J., et al. (1996). Totalsynthese von (-)-Epothilon A. *Angew. Chem.* 108, 2976–2978. doi: 10.1002/ange.19961082318

Basmadjian, C., Thuaud, F., Ribeiro, N., and Désaubry, L. (2013). Flavaglines: potent anticancer drugs that target prohibitins and the helicase eIF4A. *Future Med. Chem.* 5, 2185–2197. doi: 10.4155/fmc.13.177

Basu, P. (2004). Trading on traditional medicines. *Nat. Biotechnol.* 22, 263–265. doi: 10.1038/nbt0304-263

Benhadji, K. A., Serova, M., Ghoul, A., Cvitkovic, E., Le Tourneau, C., Ogbourne, S. M., et al. (2008). Antiproliferative activity of PEP005, a novel ingenol angelate that modulates PKC functions, alone and in combination with cytotoxic agents in human colon cancer cells. *Br. J. Cancer* 99, 1808–1815. doi: 10.1038/sj.bjc.6604642

Bennouna, J., Campone, M., Delord, J. P., and Pinel, M.-C. (2005). Vinflunine: a novel antitubulin agent in solid malignancies. *Expert Opin. Investig. Drugs* 14, 1259–1267. doi: 10.1517/13543784.14.10.1259

Bennouna, J., Fumoleau, P., Armand, J.-P., Raymond, E., Campone, M., Delgado, F.-M., et al. (2003). Phase I and pharmacokinetic study of the new vinca alkaloid vinflunine administered as a 10-min infusion every 3 weeks in patients with advanced solid tumours. *Ann. Oncol.* 14, 630–637. doi: 10.1093/annonc/mdg174

Bode, J. W., and Carreira, E. M. (2001). Stereoselective syntheses of epothilones A and B via directed nitrile oxide cycloaddition1. *J. Am. Chem. Soc.* 123, 3611–3612. doi: 10.1021/ja0155635

Bollag, D. M., McQueney, P. A., Zhu, J., Hensens, O., Koupal, L., Liesch, J., et al. (1995). Epothilones, a new class of microtubule-stabilizing agents with a taxol-like mechanism of action. *Cancer Res.* 55, 2325–2333.

Bonfanti, M., La Valle, E., Fernandez Sousa Faro, J. M., Faircloth, G., Caretti, G., Mantovani, R., et al. (1999). Effect of ecteinascidin-743 on the interaction between DNA binding proteins and DNA. *Anticancer Drug Des.* 14, 179–186.

Brown, E. J., Albers, M. W., Tae Bum, S., Ichikawa, K., Keith, C. T., Lane, W. S., et al. (1994). A mammalian protein targeted by G1-arresting rapamycin-receptor complex. *Nature* 369, 756–758. doi: 10.1038/369756a0

Calne, R. Y. (2003). The development of immunosuppression: the rapamycin milestone. *Transplant. Proc.* 35, S15–S17. doi: 10.1016/S0041-1345(03)00209-4

Calne, R. Y., Lim, S., Samaan, A., Collier, D. S. J., Pollard, S. G., White, D. J. G., et al. (1989). Rapamycin for immunosuppression in organ allografting. *The Lancet* 334, 227. doi: 10.1016/S0140-6736(89)90417-0

Chen, J., Chen, X., Bois-Choussy, M. L., and Zhu, J. (2006). Total synthesis of ecteinascidin 743. *J. Am. Chem. Soc.* 128, 87–89. doi: 10.1021/ja0571794

Cordell, G. A., and Colvard, M. D. (2012). Natural products and traditional medicine: turning on a paradigm. *J. Nat. Prod.* 75, 514–525. doi: 10.1021/np200803m

Corey, E. J., Gin, D. Y., and Kania, R. S. (1996). Enantioselective total synthesis of ecteinascidin 743. *J. Am. Chem. Soc.* 118, 9202–9203. doi: 10.1021/ja962480t

Cuevas, C., and Francesch, A. (2009). Development of Yondelis[registered sign] (trabectedin, ET-743). A semisynthetic process solves the supply problem. *Nat. Prod. Rep.* 26, 322–337. doi: 10.1039/b808331m

Cuevas, C., Pérez, M., Martin, M. J., Chicharro, J. L., Fernandez-Rivas, C., Flores, M., et al. (2000). Synthesis of ecteinascidin ET-743 and phthalascidin Pt-650 from cyanosafracin B. *Org. Lett.* 2, 2545–2548. doi: 10.1021/ol0062502

Cvek, B. (2012). Nonprofit drugs as the salvation of the world's healthcare systems: the case of antabuse (disulfiram). *Drug Discov. Today* 17, 409–412. doi: 10.1016/j.drudis.2011.12.010

D'Incalci, M., and Jimeno, J. (2003). Preclinical and clinical results with the natural marine product ET-743. *Expert Opin. Investig. Drugs* 12, 1843–1853. doi: 10.1517/13543784.12.11.1843

D'Incalci, M., and Galmarini, C. M. (2010). A review of trabectedin (ET-743): a unique mechanism of action. *Mol. Cancer Ther.* 9, 2157–2163. doi: 10.1158/1535-7163.mct-10-0263

Dančík, V., Seiler, K. P., Young, D. W., Schreiber, S. L., and Clemons, P. A. (2010). Distinct biological network properties between the targets of natural products and disease genes. *J. Am. Chem. Soc.* 132, 9259–9261. doi: 10.1021/ja102798t

Ducry, L. (2012). Challenges in the development and manufacturing of antibody-drug conjugates. *Methods Mol. Biol.* 899, 489–497. doi: 10.1007/978-1-61779-921-1_29

Ehrlich, P. (1897). Zur kenntnis der antitoxinwirkung. *Fortschr. Med.* 15, 41–43.

Endo, A., Yanagisawa, A., Abe, M., Tohma, S., Kan, T., and Fukuyama, T. (2002). Total synthesis of ecteinascidin 743. *J. Am. Chem. Soc.* 124, 6552–6554. doi: 10.1021/ja026216d

Estève, M.-A., Carré, M., Bourgarel-Rey, V., Kruczynski, A., Raspaglio, G., Ferlini, C., et al. (2006). Bcl-2 down-regulation and tubulin subtype composition are involved in resistance of ovarian cancer cells to vinflunine. *Mol. Cancer Ther.* 5, 2824–2833. doi: 10.1158/1535-7163.mct-06-0277

Etiévant, C., Barret, J.-M., Kruczynski, A., Perrin, D., and Hill, B. (1998). Vinflunine (20′,20′-difluoro- 3′,4′-dihydrovinorelbine), a novel Vinca alkaloid, which participates in P-glycoprotein (Pgp)-mediated multidrug resistance *in vivo* and *in vitro*. *Invest. New Drugs* 16, 3–17. doi: 10.1023/A:1006022811895

Etiévant, C., Kruczynski, A., Barret, J.-M., Tait, A., Kavallaris, M., and Hill, B. (2001). Markedly diminished drug resistance-inducing properties of vinflunine (20′,20′-difluoro-3′,4′-dihydrovinorelbine) relative to vinorelbine, identified in murine and human tumour cells *in vivo* and *in vitro*. *Cancer Chemother. Pharmacol.* 48, 62–70. doi: 10.1007/s002800100275

Evans, B. E., Rittle, K. E., Bock, M. G., Dipardo, R. M., Freidinger, R. M., Whitter, W. L., et al. (1988). Methods for drug discovery: development of potent, selective, orally effective cholecystokinin antagonists. *J. Med. Chem.* 31, 2235–2246. doi: 10.1021/jm00120a002

Fahy, J., Duflos, A., Ribet, J.-P., Jacquesy, J.-C., Berrier, C., Jouannetaud, M.-P., et al. (1997). Vinca alkaloids in superacidic media: a method for creating a new family of antitumor derivatives. *J. Am. Chem. Soc.* 119, 8576–8577. doi: 10.1021/ja971864w

Faivre, S., and Raymond, E. (2008). Mechanism of action of rapalogues: the antiangiogenic hypothesis. *Expert Opin. Investig. Drugs* 17, 1619–1621. doi: 10.1517/13543784.17.11.1619

Ferlini, C., Cicchillitti, L., Raspaglio, G., Bartollino, S., Cimitan, S., Bertucci, C., et al. (2009). Paclitaxel directly binds to Bcl-2 and functionally mimics activity of Nur77. *Cancer Res.* 69, 6906–6914. doi: 10.1158/0008-5472

Findlay, J. A., and Radics, L. (1980). On the chemistry and high field nuclear magnetic resonance spectroscopy of rapamycin. *Can. J. Chem.* 58, 579–590. doi: 10.1139/v80-090

Fishlock, D., and Williams, R. M. (2008). Synthetic studies on Et-743. Assembly of the pentacyclic core and a formal total synthesis. *J. Org. Chem.* 73, 9594–9600. doi: 10.1021/jo801159k

Fresno, M., Jiménez, A., and Vázquez, D. (1977). Inhibition of translation in eukaryotic systems by harringtonine. *Eur. J. Biochem.* 72, 323–330. doi: 10.1111/j.1432-1033.1977.tb11256.x

Furumai, R., Matsuyama, A., Kobashi, N., Lee, K. H., Nishiyama, M., Nakajima, H., et al. (2002). FK228 (depsipeptide) as a natural prodrug that inhibits class I histone deacetylases. *Cancer Res.* 62, 4916–4921

Galsky, M. D., Dritselis, A., Kirkpatrick, P., and Oh, W. K. (2010). Cabazitaxel. *Nat. Rev. Drug Discov.* 9, 677–678. doi: 10.1038/nrd3254

Ganesan, A. (2008). The impact of natural products upon modern drug discovery. *Curr. Opin. Chem. Biol.* 12, 306–317. doi: 10.1016/j.cbpa.2008.03.016

Gerhardt, C. (1853). Untersuchungen über die wasserfreien organischen Säuren. *Justus Liebigs Ann. Chem.* 87, 57–84. doi: 10.1002/jlac.18530870107

Gerth, K., Bedorf, N., Hofle, G., Irschik, H., and Reichenbach, H. (1996). Epothilons A and B: antifungal and cytotoxic compounds from *Sorangium cellulosum* (Myxobacteria). Production, physico-chemical and biological properties. *J. Antibiot. (Tokyo)* 49, 560–563. doi: 10.7164/antibiotics.49.560

Ghose, T., Guclu, A., and Tai, J. (1975). Suppression of an AKR Lymphoma by antibody and chlorambucil. *J. Natl. Cancer Inst.* 55, 1353–1357. doi: 10.1093/jnci/55.6.1353

Ghoul, A. D., Serova, M., Astorgues-Xerri, L., Bieche, I., Bousquet, G., Varna, M., et al. (2009). Epithelial-to-mesenchymal transition and resistance to ingenol 3-angelate, a novel protein kinase C modulator, in colon cancer cells. *Cancer Res.* 69, 4260–4269. doi: 10.1158/0008-5472.can-08-2837

Goss, R. J. M., Shankar, S., and Fayad, A. A. (2012). The generation of "unNatural" products: synthetic biology meets synthetic chemistry. *Nat. Prod. Rep.* 29, 870–889. doi: 10.1039/C2NP00001F

Grabowski, K., Baringhaus, K.-H., and Schneider, G. (2008). Scaffold diversity of natural products: inspiration for combinatorial library design. *Nat. Prod. Rep.* 25, 892–904. doi: 10.1039/B715668P

Green, A. C., and Beardmore, G. L. (1988). Home treatment of skin cancer and solar keratoses. *Australas. J. Dermatol.* 29, 127–130. doi: 10.1111/j.1440-0960.1988.tb00383.x

Groll, M., Kim, K. B., Kairies, N., Huber, R., and Crews, C. M. (2000). Crystal structure of the 20 s proteasome:TMC-95A complex: a non-covalent proteasome inhibitor. *J. Am. Chem. Soc.* 122, 1237–1238. doi: 10.1021/ja993588m

Group, C. R. C. (1976). Cephalotaxine esters in the treatment of acute leukemia. A preliminary clinical assessment. *Chin. Med. J. (Engl).* 2, 263–272.

Gunasekera, S. P., Gunasekera, M., Longley, R. E., and Schulte, G. K. (1990). Discodermolide: a new bioactive polyhydroxylated lactone from the marine sponge *Discodermia dissoluta*. *J. Org. Chem.* 55, 4912–4915. doi: 10.1021/jo00303a029

Handratta, V. D., Vasaitis, T. S., Njar, V. C. O., Gediya, L. K., Kataria, R., Chopra, P., et al. (2005). Novel C-17-heteroaryl steroidal CYP17 inhibitors/antiandrogens: synthesis, *in vitro* biological activity, pharmacokinetics, and antitumor activity in the LAPC4 human prostate cancer xenograft model. *J. Med. Chem.* 48, 2972–2984. doi: 10.1021/jm040202w

Hardy, K., Buckley, S., Collins, M. J., Estalrrich, A., Brothwell, D., Copeland, L., et al. (2012). Neanderthal medics? Evidence for food, cooking, and medicinal plants entrapped in dental calculus. *Naturwissenschaften* 99, 617–626. doi: 10.1007/s00114-012-0942-0

Henkel, T., Brunne, R. M., Müller, H., and Reichel, F. (1999). Statistical investigation into the structural complementarity of natural products and synthetic compounds. *Angew. Chem. Int. Ed. Engl.* 38, 643–647. doi: 10.1002/(SICI)1521-3773(19990301)38:5<643::AID-ANIE643>3.0.CO;2-G

Hietman, J., Movva, N. R., and Hall, M. N. (1991). Targets for cell cycle arrest by the immunosuppressant rapamycin in yeast. *Science* 253, 905–909. doi: 10.1126/science.1715094

Hirata, Y., and Uemura, D. (1986). Halichondrins - antitumor polyether macrolides from a marine sponge. *Pure Appl. Chem.* 58, 701–710. doi: 10.1351/pac198658050701

Ho, R. J. Y., and Chien, J. (2014). Trends in translational medicine and drug targeting and delivery: new insights on an old concept—targeted drug delivery with antibody–drug conjugates for cancers. *J. Pharm. Sci.* 103, 71–77. doi: 10.1002/jps.23761

Hofheinz, R. D., Gnad-Vogt, S. U., Beyer, U., and Hochhaus, A. (2005). Liposomal encapsulated anti-cancer drugs. *Anticancer Drugs* 16, 691–707. doi: 10.1097/01.cad.0000167902.53039.5a

Höfle, G., Bedorf, N., Steinmetz, H., Schomburg, D., Gerth, K., and Reichenbach, H. (1996). Epothilone A and B - novel 16-membered macrolides with cytotoxic activity: isolation, crystal structure, and conformation in solution. *Angew. Chem. Int. Ed. Engl.* 35, 1567–1569. doi: 10.1002/anie.199615671

Horwitz, S. B. (1994). Taxol (paclitaxel): mechanisms of action. *Ann. Oncol.* 5(Suppl. 6), S3–S6.

Huang, M. T. (1975). Harringtonine, an inhibitor of initiation of protein biosynthesis. *Mol. Pharmacol.* 11, 511–519.

Imai, T., Nakata, H., Yokoshima, S., and Fukuyama, T. (2012). Synthetic studies toward ecteinascidin 743 (Trabectedin). *Synthesis* 44, 2743–2753. doi: 10.1055/s-0032-1316579

Jackson, K. L., Henderson, J. A., and Phillips, A. J. (2009). The halichondrins and E7389. *Chem. Rev.* 109, 3044–3079. doi: 10.1021/cr900016w

Jarman, M., Barrie, S. E., and Llera, J. M. (1998). The 16,17-double bond is needed for irreversible inhibition of human cytochrome P45017α by abiraterone (17-(3-Pyridyl)androsta-5,16-dien-3β-ol) and related steroidal inhibitors. *J. Med. Chem.* 41, 5375–5381. doi: 10.1021/jm981017j

Jin, S., Gorfajn, B., Faircloth, G., and Scotto, K. W. (2000). Ecteinascidin 743, a transcription-targeted chemotherapeutic that inhibits MDR1 activation. *Proc. Natl. Acad. Sci. U.S.A.* 97, 6775–6779. doi: 10.1073/pnas.97.12.6775

Johnson, P., Geldart, T., Fumoleau, P., Pinel, M.-C., Nguyen, L., and Judson, I. (2006). Phase I study of Vinflunine administered as a 10-minute infusion on days 1 and 8 every 3 weeks. *Invest. New Drugs* 24, 223–231. doi: 10.1007/s10637-005-3902-0

Jordan, M. A., and Wilson, L. (2004). Microtubules as a target for anticancer drugs. *Nat. Rev. Cancer* 4, 253–265. doi: 10.1038/nrc1317

Jørgensen, L., McKerrall, S. J., Kuttruff, C. A., Ungeheuer, F., Felding, J., and Baran, P. S. (2013). 14-step synthesis of (+)-ingenol from (+)-3-carene. *Science* 341, 878–882. doi: 10.1126/science.1241606

Kahan, B. D., Chang, J. Y., and Sehgal, S. N. (1991). Preclinical evaluation of a new potent immunosuppressive agent, rapamycin. *Transplantation* 52, 185–191. doi: 10.1097/00007890-199108000-00001

Kantarjian, H. M., O'Brien, S., and Cortes, J. (2013). Homoharringtonine/Omacetaxine mepesuccinate: the long and winding road to food and drug administration approval. *Clin. Lymphoma Myeloma Leuk.* 13, 530–533. doi: 10.1016/j.clml.2013.03.017

Kawagishi, F., Toma, T., Inui, T., Yokoshima, S., and Fukuyama, T. (2013). Total synthesis of ecteinascidin 743. *J. Am. Chem. Soc.* 135, 13684–13687. doi: 10.1021/ja408034x

Kim, T. Y., Kim, D. W., Chung, J. Y., Shin, S. G., Kim, S. C., Heo, D. S., et al. (2004). Phase I and pharmacokinetic study of Genexol-PM, a Cremophor-free, polymeric micelle-formulated paclitaxel, in patients with advanced malignancies. *Clin. Cancer Res.* 10, 3708–3716. doi: 10.1158/1078-0432.CCR-03-0655

King, M. L., Chiang, C. C., Ling, H. C., Ochiai, M., Fujita, E., and Mcphail, A. T. (1985). X-Ray crystal structure of rocaglamide, a novel antileulemic 1H-cyclopenta[b]benzofuran from Aglaia elliptifolia. *J. Chem. Soc. Chem. Commun.* 1982, 1150–1151. doi: 10.1039/C39820001150

Kino, T., Hatanaka, H., Hashimoto, M., Nishiyama, M., Goto, T., Okuhara, M., et al. (1987a). FK-506, a novel immunosuppressant isolated from a Streptomyces. I. Fermentation, isolation, and physico-chemical and biological characteristics. *J. Antibiot. (Tokyo)* 40, 1249–1255.

Kino, T., Hatanaka, H., Miyata, S., Inamura, N., Nishiyama, M., Yajima, T., et al. (1987b). FK-506, a novel immunosuppressant isolated from a Streptomyces. II. Immunosuppressive effect of FK-506 *in vitro*. *J. Antibiot. (Tokyo)* 40, 1256–1265.

Kirikae, T., Ojima, I., Kirikae, F., Ma, Z., Kuduk, S. D., Slater, J. C., et al. (1996). Structural requirements of taxoids for nitric oxide and tumor necrosis factor production by murine macrophages. *Biochem. Biophys. Res. Commun.* 227, 227–235. doi: 10.1006/bbrc.1996.1494

Kirschning, A., and Hahn, F. (2012). Merging chemical synthesis and biosynthesis: a new chapter in the total synthesis of natural products and natural product libraries. *Angew. Chem. Int. Ed. Engl.* 51, 4012–4022. doi: 10.1002/anie.201107386

Kohler, G., and Milstein, C. (1975). Continuous cultures of fused cells secreting antibody of predefined specificity. *Nature* 256, 495–497. doi: 10.1038/256495a0

Krysiak, J., and Breinbauer, R. (2012). Activity-based protein profiling for natural product target discovery. *Top. Curr. Chem.* 324, 43–84. doi: 10.1007/128_2011_289

Leamon, C. P., and Low, P. S. (1991). Delivery of macromolecules into living cells: a method that exploits folate receptor endocytosis. *Proc. Natl. Acad. Sci. U.S.A.* 88, 5572–5576. doi: 10.1073/pnas.88.13.5572

Lee, F. F., Borzilleri, R., Fairchild, C., Kamath, A., Smykla, R., Kramer, R., et al. (2008). Preclinical discovery of ixabepilone, a highly active antineoplastic agent. *Cancer Chemother. Pharmacol.* 63, 157–166. doi: 10.1007/s00280-008-0724-8

Lee, F. Y. F., Vite, G., Borzilleri, R. M., Arico, M. A., Clark, J. L., Fager, K. L., et al. (2000). Preclinical pharmacology of the epothilone B analog BMS-247550—an epothilone analog possessing potent activity against paclitaxel sensitive and resistant human tumors. *Clin. Cancer Res.* 6:4580s.

Lee, M.-L., and Schneider, G. (2001). Scaffold architecture and pharmacophoric properties of natural products and trade drugs:? application in the design of natural product-based combinatorial libraries. *J. Comb. Chem.* 3, 284–289. doi: 10.1021/cc000097l

Lindel, T., Jensen, P. R., Fenical, W., Long, B. H., Casazza, A. M., Carboni, J., et al. (1997). Eleutherobin, a new cytotoxin that mimics paclitaxel (Taxol) by stabilizing microtubules. *J. Am. Chem. Soc.* 119, 8744–8745. doi: 10.1021/ja9717828

Loc, T. B., Mathé, G., and Bernard, J. (1958). Effet sur la leucémie 1210 de la souris d'une combinaison par diazotation d'A-méthopterine ct de γ-globulins de hamsters porteurs de cette leucémic par hétérogreffe. *C. R. Acad. Sci. Paris* 246, 1626–1628.

Martinez, E. J., Owa, T., Schreiber, S. L., and Corey, E. J. (1999). Phthalascidin, a synthetic antitumor agent with potency and mode of action comparable to ecteinascidin 743. *Proc. Natl. Acad. Sci. U.S.A.* 96, 3496–3501. doi: 10.1073/pnas.96.7.3496

McAlpine, J. B., Swanson, S. J., Jackson, M., and Whittern, D. N. (1991). Revised NMR assignments for rapamycin. *J. Antibiot. (Tokyo)* 44, 688–690. doi: 10.7164/antibiotics.44.688

Menchaca, R., Martinez, V., Rodriguez, A., Rodriguez, N., Flores, M., Gallego, P., et al. (2003). Synthesis of natural ecteinascidins (ET-729, ET-745, ET-759B, ET-736, ET-637, ET-594) from cyanosafracin B. *J. Org. Chem.* 68, 8859–8866. doi: 10.1021/jo034547i

Minuzzo, M., Marchini, S., Broggini, M., Faircloth, G., D'Incalci, M., and Mantovani, R. (2000). Interference of transcriptional activation by the

antineoplastic drug ecteinascidin-743. *Proc. Natl. Acad. Sci. U.S.A.* 97, 6780–6784. doi: 10.1073/pnas.97.12.6780

Mooberry, S. L., Tien, G., Hernandez, A. H., Plubrukarn, A., and Davidson, B. S. (1999). Laulimalide and isolaulimalide, new paclitaxel-like microtubule-stabilizing agents. *Cancer Res.* 59, 653–660.

Mulzer, J., Mantoulidis, A., and Öhler, E. (2000). Total syntheses of epothilones B and D. *J. Org. Chem.* 65, 7456–7467. doi: 10.1021/jo0007480

Nakajima, H., Kim, Y. B., Terano, H., Yoshida, M., and Horinouchi, S. (1998). FR901228, a potent antitumor antibiotic, is a novel histone deacetylase inhibitor. *Exp. Cell Res.* 241, 126–133. doi: 10.1006/excr.1998.4027

Nicolaou, K. C., Ninkovic, S., Sarabia, F., Vourloumis, D., He, Y., Vallberg, H., et al. (1997). Total syntheses of epothilones A and B via a macrolactonization-based strategy. *J. Am. Chem. Soc.* 119, 7974–7991. doi: 10.1021/ja971110h

Nishizuka, Y. (1984). The role of protein kinase C in cell surface signal transduction and tumour promotion. *Nature* 308, 693–698. doi: 10.1038/308693a0

Noble, R. L., Beer, C. T., and Cutts, J. H. (1959). Further biological activities of vincaleukoblastine - an alkaloid isolated from *Vinca rosea* (L.). *Biochem. Pharmacol.* 1, 347–348. doi: 10.1016/0006-2952(59)90123-6

Ojima, I., Chakravarty, S., Inoue, T., Lin, S., He, L., Horwitz, S. B., et al. (1999). A common pharmacophore for cytotoxic natural products that stabilize microtubules. *Proc. Natl. Acad. Sci. U.S.A.* 96, 4256–4261. doi: 10.1073/pnas.96.8.4256

Ortholand, J.-Y., and Ganesan, A. (2004). Natural products and combinatorial chemistry: back to the future. *Curr. Opin. Chem. Biol.* 8, 271–280. doi: 10.1016/j.cbpa.2004.04.011

Paudler, W. W., Kerley, G. I., and McKay, J. (1963). The alkaloids of *Cephalotaxus drupacea* and *Cephalotaxus fortunei*. *J. Org. Chem.* 28, 2194–2197. doi: 10.1021/jo01044a010

Pommier, Y., Kohlhagen, G., Bailly, C., Waring, M., Mazumder, A., and Kohn, K. W. (1996). DNA sequence- and structure-selective alkylation of guanine N2 in the DNA minor groove by ecteinascidin 743, a potent antitumor compound from the caribbean tunicate *Ecteinascidia turbinata*. *Biochemistry* 35, 13303–13309. doi: 10.1021/bi960306b

Potter, G. A., Barrie, S. E., Jarman, M., and Rowlands, M. G. (1995). Novel steroidal inhibitors of human cytochrome P45017.alpha.-hydroxylase-C17,20-lyase): potential agents for the treatment of prostatic cancer. *J. Med. Chem.* 38, 2463–2471. doi: 10.1021/jm00013a022

Powell, R. G., Weisleder, D., and Smith, C. R. (1972). Antitumor alkaloids from *Cephalotaxus harringtonia*: structure and activity. *J. Pharm. Sci.* 61, 1227–1230. doi: 10.1002/jps.2600610812

Powell, R. G., Weisleder, D., Smith C. R. Jr., and Rohwedder, W. K. (1970). Structures of harringtonine, isoharringtonine, and homoharringtonine. *Tetrahedron Lett.* 11, 815–818. doi: 10.1016/S0040-4039(01)97839-6

Pucheault, M. (2008). Natural products: chemical instruments to apprehend biological symphony. *Org. Biomol. Chem.* 6, 424–432. doi: 10.1039/b713022h

Qi, Y., and Ma, S. (2011). The medicinal potential of promising marine macrolides with anticancer activity. *ChemMedChem* 6, 399–409. doi: 10.1002/cmdc.201000534

Rehman, Y., and Rosenberg, J. E. (2012). Abiraterone acetate: oral androgen biosynthesis inhibitor for treatment of castration-resistant prostate cancer. *Drug Des. Devel. Ther.* 6, 13–18. doi: 10.2147/DDDT.S15850

Rinehart, K. L., Holt, T. G., Fregeau, N. L., Stroh, J. G., Keifer, P. A., Sun, F., et al. (1990). Ecteinascidins 729, 743, 745, 759A, 759B, and 770: potent antitumor agents from the Caribbean tunicate *Ecteinascidia turbinata*. *J. Org. Chem.* 55, 4512–4515. doi: 10.1021/jo00302a007

Ritter, S. K. (2013). 2013's notable advances. *Chem. Eng. News* 91, 16–19.

Robin, J.-P., Dhal, R., Dujardin, G., Girodier, L., Mevellec, L., and Poutot, S. (1999). The first semi-synthesis of enantiopure homoharringtonine via anhydrohomoharringtonine from a preformed chiral acyl moiety. *Tetrahedron Lett.* 40, 2931–2934. doi: 10.1016/S0040-4039(99)00327-5

Roin, B. N. (2009). Unpatentable drugs and the standards of patentability. *Tex. Law Rev.* 87, 503–570.

Santagata, S., Mendillo, M. L., Tang, Y.-C., Subramanian, A., Perley, C. C., Roche, S. P., et al. (2013). Tight coordination of protein translation and HSF1 activation supports the anabolic malignant state. *Science* 341, 1238303-1–1238303-10. doi: 10.1126/science.1238303

Sayed, M. D., Riszk, A., Hammouda, F. M., El-Missiry, M. M., Williamson, E. M., and Evans, F. J. (1980). Constituents of Egyptian Euphorbiaceae. IX. Irritant and cytotoxic ingenane esters from *Euphorbia paralias* L. *Experientia* 36, 1206–1207. doi: 10.1007/BF01976131

Schinzer, D., Limberg, A., Bauer, A., Böhm, O. M., and Cordes, M. (1997). Total synthesis of (-)-epothilone A. *Angew. Chem. Int. Ed. Engl.* 36, 523–524. doi: 10.1002/anie.199705231

Scott, A. M., Wolchok, J. D., and Old, L. J. (2012). Antibody therapy of cancer. *Nat. Rev. Cancer* 12, 278–287. doi: 10.1038/nrc3236

Sehgal, S. N., Baker, H., and Vezina, C. (1975). Rapamycin (AY 22,989), a new antifungal antibiotic. II. Fermentation, isolation and characterization. *J. Antibiot. (Tokyo)* 28, 727–732.

Serova, M., Ghoul, A. D., Benhadji, K. A., Faivre, S., Le Tourneau, C., Cvitkovic, E., et al. (2008). Effects of protein kinase C modulation by PEP005, a novel ingenol angelate, on mitogen-activated protein kinase and phosphatidylinositol 3-kinase signaling in cancer cells. *Mol. Cancer Ther.* 7, 915–922. doi: 10.1158/1535-7163.mct-07-2060

Sigel, M. M., Wellham, L. L., Lichter, W., Dudeck, L. E., Gargus, J. L., and Lucas, A. H. (1970). "Anticellular and antitumor activity of extracts from tropical marine invertebrates," in *Food-Drugs from the Sea Proceedings 1969*, ed H. W. Youngken Jr. (Washington, DC: Marine Technology Society), 281–294.

Siller, G., Gebauer, K., Welburn, P., Katsamas, J., and Ogbourne, S. M. (2009). PEP005 (ingenol mebutate) gel, a novel agent for the treatment of actinic keratosis: results of a randomized, double-blind, vehicle-controlled, multicentre, phase IIa study. *Australas. J. Dermatol.* 50, 16–22. doi: 10.1111/j.1440-0960.2008.00497.x

Su, D.-S., Meng, D., Bertinato, P., Balog, A., Sorensen, E. J., Danishefsky, S. J., et al. (1997). Total synthesis of (–)-epothilone B: an extension of the suzuki coupling method and insights into structure–activity relationships of the epothilones. *Angew. Chem. Int. Ed. Engl.* 36, 757–759. doi: 10.1002/anie.199707571

Sundar, S., Jha, T. K., Thakur, C. P., Sinha, P. K., and Bhattacharya, S. K. (2007). Injectable paromomycin for visceral leishmaniasis in India. *N. Engl. J. Med.* 356, 2571–2581. doi: 10.1056/NEJMoa066536

Swindells, D. C. N., White, P. S., and Findlay, J. A. (1978). The X-ray crystal structure of rapamycin, C51H79NO13. *Can. J. Chem.* 56, 2491–2492. doi: 10.1139/v78-407

Swinney, D. C., and Anthony, J. (2011). How were new medicines discovered? *Nat. Rev. Drug Discov.* 10, 507–519. doi: 10.1038/nrd3480

Taamma, A., Misset, J. L., Riofrio, M., Guzman, C., Brain, E., Lopez Lazaro, L., et al. (2001). Phase I and pharmacokinetic study of ecteinascidin-743, a new marine compound, administered as a 24-hour continuous infusion in patients with solid tumors. *J. Clin. Oncol.* 19, 1256–1265.

Taft, F., Brünjes, M., Floss, H. G., Czempinski, N., Grond, S., Sasse, F., et al. (2008). Highly active ansamitocin derivatives: mutasynthesis using an AHBA-blocked mutant. *Chembiochem* 9, 1057–1060. doi: 10.1002/cbic.200700742

Takebayashi, Y., Pourquier, P., Yoshida, A., Kohlhagen, G., and Pommier, Y. (1999). Poisoning of human DNA topoisomerase I by ecteinascidin 743, an anticancer drug that selectively alkylates DNA in the minor groove. *Proc. Natl. Acad. Sci. U.S.A.* 96, 7196–7201. doi: 10.1073/pnas.96.13.7196

Takebayashi, Y., Pourquier, P., Zimonjic, D. B., Nakayama, K., Emmert, S., Ueda, T., et al. (2001). Antiproliferative activity of ecteinascidin 743 is dependent upon transcription-coupled nucleotide-excision repair. *Nat. Med.* 7, 961–966. doi: 10.1038/91008

Tang, R., Faussat, A.-M., Majdak, P., Marzac, C., Dubrulle, S., Marjanovic, Z., et al. (2006). Semisynthetic homoharringtonine induces apoptosis via inhibition of protein synthesis and triggers rapid myeloid cell leukemia-1 down-regulation in myeloid leukemia cells. *Mol. Cancer Ther.* 5, 723–731. doi: 10.1158/1535-7163.mct-05-0164

Thaler, F., and Mercurio, C. (2014). Towards selective inhibition of histone deacetylase isoforms: what has been achieved, where we are and what will be next. *ChemMedChem* 9, 523–536. doi: 10.1002/cmdc.201300413

Thuaud, F., Ribeiro, N., Nebigil, C. G., and Désaubry, L. (2013). Prohibitin ligands in cell death and survival: mode of action and therapeutic potential. *Chem. Biol.* 20, 316–331. doi: 10.1016/j.chembiol.2013.02.006

Ueda, H., Nakajima, H., Hori, Y., Goto, T., and Okuhara, M. (1994). Action of FR901228, a novel antitumor bicyclic depsipeptide produced by *Chromobacterium violaceum* no. 968, on Ha-ras transformed NIH3T3 cells. *Biosci. Biotechnol. Biochem.* 58, 1579–1583.

Uemura, D., Takahashi, K., Yamamoto, T., Katayama, C., Tanaka, J., Okumura, Y., et al. (1985). Norhalichondrin A: an antitumor polyether macrolide from a marine sponge. *J. Am. Chem. Soc.* 107, 4796–4798. doi: 10.1021/ja00302a042

Vandermolen, K. M., McCulloch, W., Pearce, C. J., and Oberlies, N. H. (2011). Romidepsin (Istodax, NSC 630176, FR901228, FK228, depsipeptide): a natural product recently approved for cutaneous T-cell lymphoma. *J. Antibiot. (Tokyo)* 64, 525–531. doi: 10.1038/ja.2011.35

Vasaitis, T. S., and Njar, V. C. O. (2010). Novel, potent anti-androgens of therapeutic potential: recent advances and promising developments. *Future Med. Chem.* 2, 667–680. doi: 10.4155/fmc.10.14

Vezina, C., Kudelski, A., and Sehgal, S. N. (1975). Rapamycin (AY 22,989), a new antifungal antibiotic. I. Taxonomy of the producing streptomycete and isolation of the active principle. *J. Antibiot. (Tokyo)* 28, 721–726.

Villalona-Calero, M. A., Eckhardt, S. G., Weiss, G., Hidalgo, M., Beijnen, J. H., Van Kesteren, C., et al. (2002). A phase I and pharmacokinetic study of ecteinascidin-743 on a daily x 5 schedule in patients with solid malignancies. *Clin. Cancer Res.* 8, 75–85.

Vlahov, I. R., and Leamon, C. P. (2012). Engineering folate-drug conjugates to target cancer: from chemistry to clinic. *Bioconjug. Chem.* 23, 1357–1369. doi: 10.1021/bc2005522

Von Hoff, D. D. (1998). There are no bad anticancer agents, only bad clinical trial designs–twenty-first Richard and Hinda Rosenthal Foundation Award Lecture. *Clin. Cancer Res.* 4, 1079–1086.

Vrignaud, P., Sémiond, D., Lejeune, P., Bouchard, H., Calvet, L., Combeau, C., et al. (2013). Preclinical antitumor activity of cabazitaxel, a semisynthetic taxane active in taxane-resistant tumors. *Clin. Cancer Res.* 19, 2973–2983. doi: 10.1158/1078-0432.ccr-12-3146

Wang, A. Z., Langer, R., and Farokhzad, O. C. (2012). Nanoparticle delivery of cancer drugs. *Annu. Rev. Med.* 63, 185–198. doi: 10.1146/annurev-med-040210-162544

Watson, C. J. E., Friend, P. J., Jamieson, N. V., Frick, T. W., Alexander, G., Gimson, A. E., et al. (1999). Sirolimus: a potent new immunosuppressant for liver transplantation. *Transplantation* 67, 505–509. doi: 10.1097/00007890-199902270-00002

Weedon, D., and Chick, J. (1976). Home treatment of basal cell carcinoma. *Med. J. Aust.* 1, 928.

Xu, Z. (2011). Modernization: one step at a time. *Nature* 480, S90–S92. doi: 10.1038/480S90a

Yadav, V. G., De Mey, M., Giaw Lim, C., Kumaran Ajikumar, P., and Stephanopoulos, G. (2012). The future of metabolic engineering and synthetic biology: towards a systematic practice. *Metab. Eng.* 14, 233–241. doi: 10.1016/j.ymben.2012.02.001

Yang, J., Chen, H., Vlahov, I. R., Cheng, J.-X., and Low, P. S. (2006). Evaluation of disulfide reduction during receptor-mediated endocytosis by using FRET imaging. *Proc. Natl. Acad. Sci. U.S.A.* 103, 13872–13877. doi: 10.1073/pnas.0601455103

Yang, Z., He, Y., Vourloumis, D., Vallberg, H., and Nicolaou, K. C. (1997). Total synthesis of epothilone A: the olefin metathesis approach. *Angew. Chem. Int. Ed. Engl.* 36, 166–168. doi: 10.1002/anie.199701661

Zard, S. Z. (2012). Some aspects of the chemistry of nitro compounds. *Helv. Chim. Acta* 95, 1730–1757. doi: 10.1002/hlca.201200324

Zewail-Foote, M., and Hurley, L. H. (1999). Ecteinascidin 743: a minor groove alkylator that bends DNA toward the major groove. *J. Med. Chem.* 42, 2493–2497. doi: 10.1021/jm9902411

Zewail-Foote, M., Li, V.-S., Kohn, H., Bearss, D., Guzman, M., and Hurley, L. H. (2001). The inefficiency of incisions of ecteinascidin 743–DNA adducts by the UvrABC nuclease and the unique structural feature of the DNA adducts can be used to explain the repair-dependent toxicities of this antitumor agent. *Chem. Biol.* 8, 1033–1049. doi: 10.1016/S1074-5521(01)00071-0

Zheng, S., Chan, C., Furuuchi, T., Wright, B. J. D., Zhou, B., Guo, J., et al. (2006). Stereospecific formal total synthesis of ecteinascidin 743. *Angew. Chem. Int. Ed. Engl.* 45, 1754–1759. doi: 10.1002/anie.200503983

Conflict of Interest Statement: The authors declare that the research was conducted in the absence of any commercial or financial relationships that could be construed as a potential conflict of interest.

Received: 06 March 2014; accepted: 04 April 2014; published online: 01 May 2014.
Citation: Basmadjian C, Zhao Q, Bentouhami E, Djehal A, Nebigil CG, Johnson RA, Serova M, de Gramont A, Faivre S, Raymond E and Désaubry LG (2014) Cancer wars: natural products strike back. Front. Chem. ***2****:20. doi: 10.3389/fchem.2014.00020*
This article was submitted to Medicinal and Pharmaceutical Chemistry, a section of the journal Frontiers in Chemistry.

Publication N°*2*

Recent advances in the synthesis of flavaglines, a family of potent bioactive natural compounds coming from traditional Chinese medicine.

Zhao, Q., Abou-Hamdan, H., Désaubry, L., *Eur. J. Org. Chem.*, **2016**, *36*, 5908-5916.

ChemPubSoc Europe

DOI: 10.1002/ejoc.201600437

EurJOC European Journal of Organic Chemistry

Microreview

Total Synthesis

Recent Advances in the Synthesis of Flavaglines, a Family of Potent Bioactive Natural Compounds Originating from Traditional Chinese Medicine

Qian Zhao,[a] Hussein Abou-Hamdan,[a] and Laurent Désaubry*[a,b]

Abstract: Flavaglines constitute a distinctive family of plant metabolites isolated from medicinal plants of the genus *Aglaia*. These compounds exhibit a broad spectrum of distinctive pharmacological properties, including anti-inflammatory, neuroprotective, cardioprotective, and anticancer activities. These natural cyclopenta[*b*]benzofurans are characterized by densely functionalized tricyclic frameworks, as exemplified by the structures of rocaglamide or silvestrol, which makes them extremely attractive targets for total synthesis, in addition to their therapeutic potential. In this review we describe the various synthetic approaches to the total synthesis of flavaglines, culminating in a new generation of diastereo- and enantioselective total syntheses.

1. Introduction

In the post-genomics era, natural products continue to be a major source of inspiration for the development of new medicines, especially in oncology. Indeed, fourteen natural product derivatives were approved for treatment of cancer between 2007 and 2013.[1] This context, coupled with major discoveries in cell biology, explains the renewed interest in the pharmacological potential of flavaglines to treat cancer.[2] Flavaglines are a unique class of natural compounds characterized by a cyclopenta[*b*]benzofuran scaffold. In nature they have so far exclusively been found in plants of the genus *Aglaia*. These compounds were first identified by King and colleagues in 1982.[3] This Taiwanese group determined the structure of rocaglamide (**1**, Figure 1) and demonstrated its antileukemic activity. It took 20 years to identify the molecular target. We now know that flavaglines display their pharmacological effects due to their binding to prohibitins-1 and 2 (PHB1/2) and the translation initiation factor eIF4A.[4] These discoveries greatly accelerated the

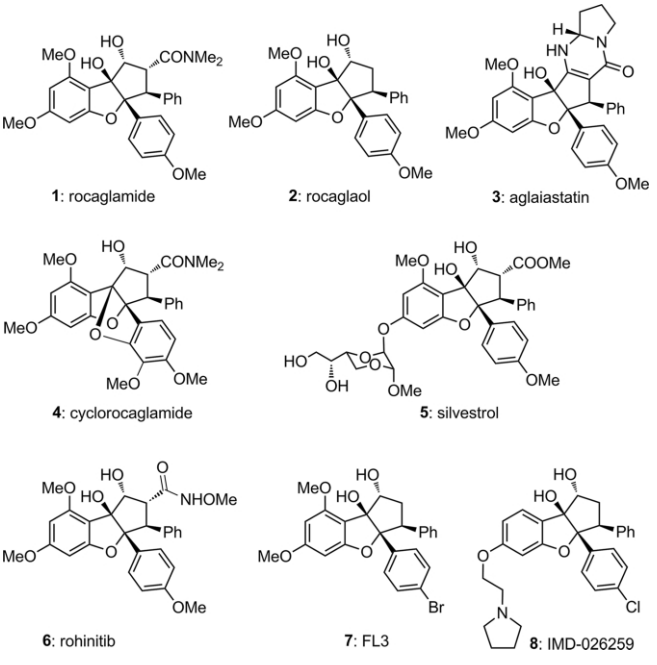

Figure 1. Selected examples of natural (**1–5**) and synthetic (**6–8**) flavaglines.

[a] *Laboratory of Therapeutic Innovation (UMR 7200), Faculty of Pharmacy, University of Strasbourg-CNRS, Illkirch, France*
E-mail: desaubry@unistra.fr
http://desaubry.u-strasbg.fr
[b] *Sino-French Joint Lab of Food Nutrition/Safety and Medicinal Chemistry, College of Biotechnology, Tianjin University of Science and Technology, Tianjin 300457, P. R. China*

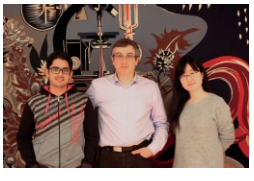

Laurent Désaubry (center) obtained a Ph.D. degree in medicinal chemistry in 1992 from the University Louis Pasteur in Strasbourg. From 1993 to 1996 he was a postdoctoral fellow at SUNY at Stony Brook under the mentorship of Prof. Roger A. Johnson. In 2007 he returned to France as a postdoctoral fellow in the laboratory of Prof. Pierre Chambon at the University of Strasbourg, before obtaining the position of CNRS Research Senior Scientist at the same university. He was promoted to the position of CNRS research director in 2014, and also became an adjunct professor in 2015 at the Tianjin University of Science and Technology (TUST) in China. Qian Zhao (right) received a B.S. degree in 2009 from Dalian Medical University, China, and a M.S. degree in 2012 from the University of Rennes, France. She is currently preparing her Ph.D. under the guidance of Laurent Désaubry. Hussein Abou-Hamdan (left) received a B.S. degree in 2013 from the Lebanese University in Beirut and a M.S. degree in 2015 from Paris-Sud University. He is currently preparing his Ph.D. under the guidance of Laurent Désaubry.

pharmacological investigation of these drugs, principally for the treatment of cancer, but also in the context of other ailments including neurological, cardiac, and inflammatory diseases. Their most striking feature is that they induce the death of cancer cells and promote the survival of non-cancer cells against many stresses at nanomolar and subnanomolar concentrations.[2] The reasons for this unusual pharmacological profile remain enigmatic, but these compounds are attracting the attention of a growing number of scientists.

Since the discovery of rocaglamide, more than one hundred other natural flavaglines, such as rocaglaol (**2**), aglaiastatin (**3**), cyclorocaglamide (**4**), and silvestrol (**5**), have been found (Figure 1). In addition, several synthetic, pharmacologically active analogues have been developed. The most intensively studied of these are rohinitib (**6**), FL3 (**7**), and IMD-026259 (**8**). Rohinitib displays anticancer[5] and antiviral effects.[6] It also prevents hair loss (alopecia) induced by chemotherapies.[7] FL3 exhibits potent anticancer,[4b,8] cardioprotective,[9] anti-Parkinsonian,[10] anti-inflammatory,[11] and antiviral properties.[12] It also protects the heart[9] and neurons[10] against the adverse effects of cancer chemotherapies. IMD-026259 (**8**, Figure 1) is a promising preclinical candidate developed by the German biotech company IMD Natural Solutions to treat Parkinson's disease.[13]

A histogram of publications on flavaglines reflects the growing interest in these compounds (Figure 2). The identification of their molecular targets (the scaffold proteins "prohibitins" and the protein synthesis initiation factor eIF4A), coupled with several recent articles in *Science*[5b] and *Nature*[5a,8d] on their extraordinary anticancer effects, have provided supporting evidence of their therapeutic potential and stimulated an intense effort to develop additional synthetic flavaglines.

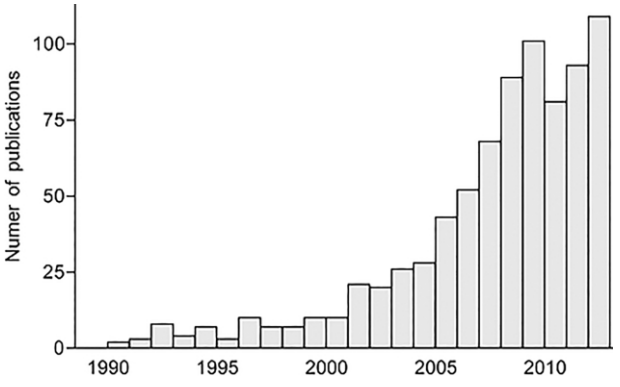

Figure 2. Histogram of publications on flavaglines (Scifinder, CAPLUS database).

With their high density of functionality, which includes the two contiguous quaternary chiral centers C-3a and C-8b, the total synthesis of flavaglines represents a challenge that has attracted the attention of some of the most prominent chemists. Over the last years, several reviews have described the identification, synthesis, and pharmacological activities of flavaglines.[2,14] The purpose of this article is to provide an updated presentation of their total syntheses. Much effort has also been spent on preparing analogues for medicinal chemistry studies, but that is beyond the scope of this review. This report

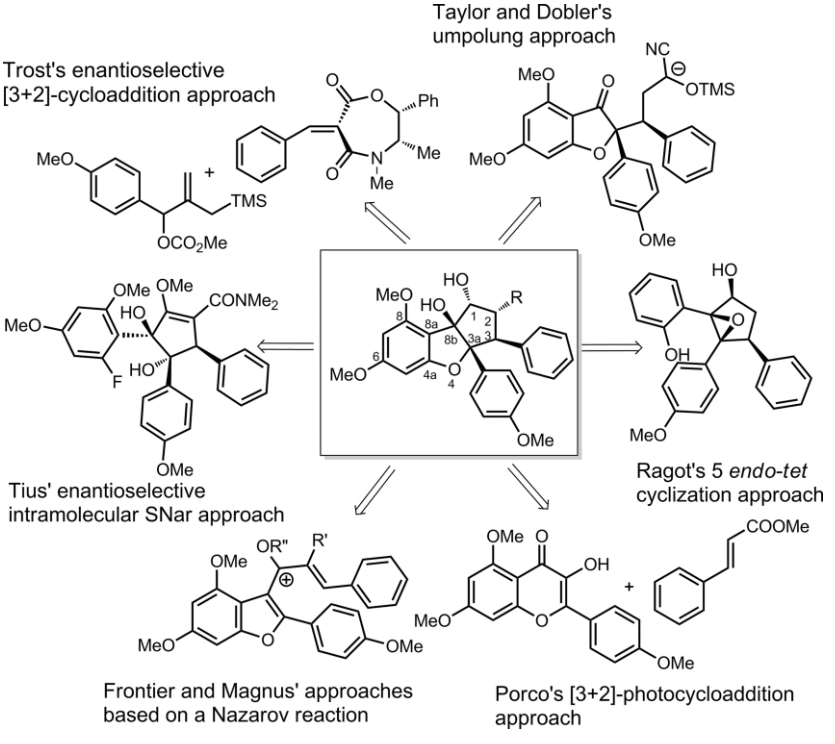

Figure 3. Approaches to the total synthesis of flavaglines.

is organized according to synthetic strategies to create the flavagline skeleton, as illustrated in Figure 3.

2. Trost's Enantioselective [3+2] Cycloaddition Approach

With the synthesis of rocaglamide (**1**) in 1990, Trost et al. disclosed the first total synthesis of a flavagline.[15] Their strategy was based on the enantioselective [3+2] cycloaddition between **10** and the chiral oxazepinedione **9** to give the cyclopentene **11** (Scheme 1). Cleavage of the chiral auxiliary and ozonolysis gave the cyclopentanone **12**, which was condensed with 3,5-dimethoxyphenol to provide cyclopentene **13**.

Monotransesterification with benzyl alcohol, followed by oxidative ring-closure mediated by DDQ, gave rise to the intermediate **14**, which has the basic skeleton of the flavaglines, but with the wrong relative configuration at C-3a and C-3. After catalytic hydroxylation, Moffatt–Doering oxidation, silylation, and decarbobenzyloxylation, the stereochemistry of protected intermediate **16** was adjusted by its oxidation into enone **17**, followed by a catalytic hydrogenation. Subsequent deprotection and amidation under Weinreb's conditions efficiently completed the total synthesis of rocaglamide. This accomplishment also established the absolute stereochemistry of this natural compound.

3. Taylor and Dobler's Umpolung Approaches

One year after Trost's accomplishment, Taylor and co-workers developed a shorter racemic synthesis of rocaglamide,[16] which was later improved by the groups of Dobler and Qin.[17]

Taylor's synthesis commenced with a Hoesch reaction between cyanohydrin **19** and phloroglucinol **18** to prepare benzofuranone **20** (Scheme 2).[16a] A Michael addition with *trans*-cinnamaldehyde gave rise to the adduct **21**. A straightforward SmI_2-mediated pinacolic coupling of this keto aldehyde generated, with good diastereoselectivity (6:1), *epi*-rocaglaol **22a** and its epimer **22b**, which could be separated. Completion of the synthesis was accomplished in six steps, including a Swern oxidation, the generation of a ketene dithioacetal, its transformation into an amide via an ester, and a diastereoselective $NMe_4BH(OAc)_3$-mediated reduction.

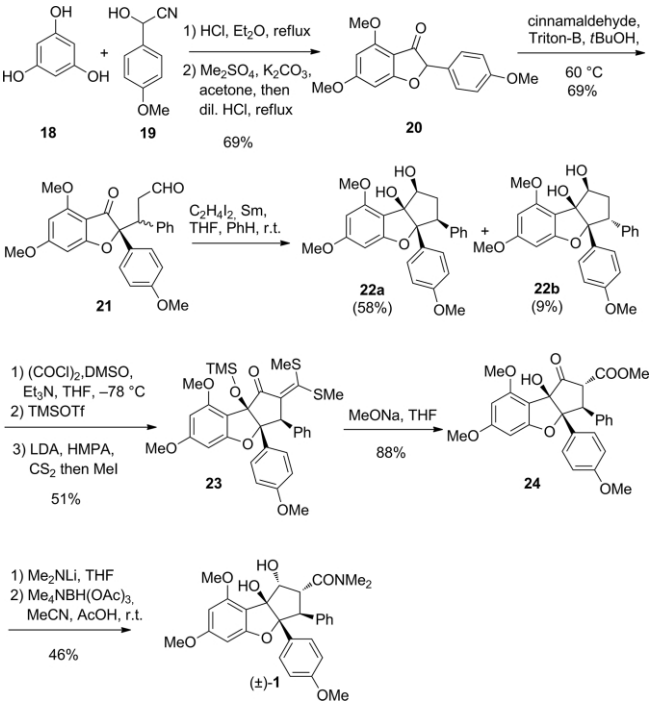

Scheme 2. Taylor's synthesis of racemic rocaglamide (**1**).[16]

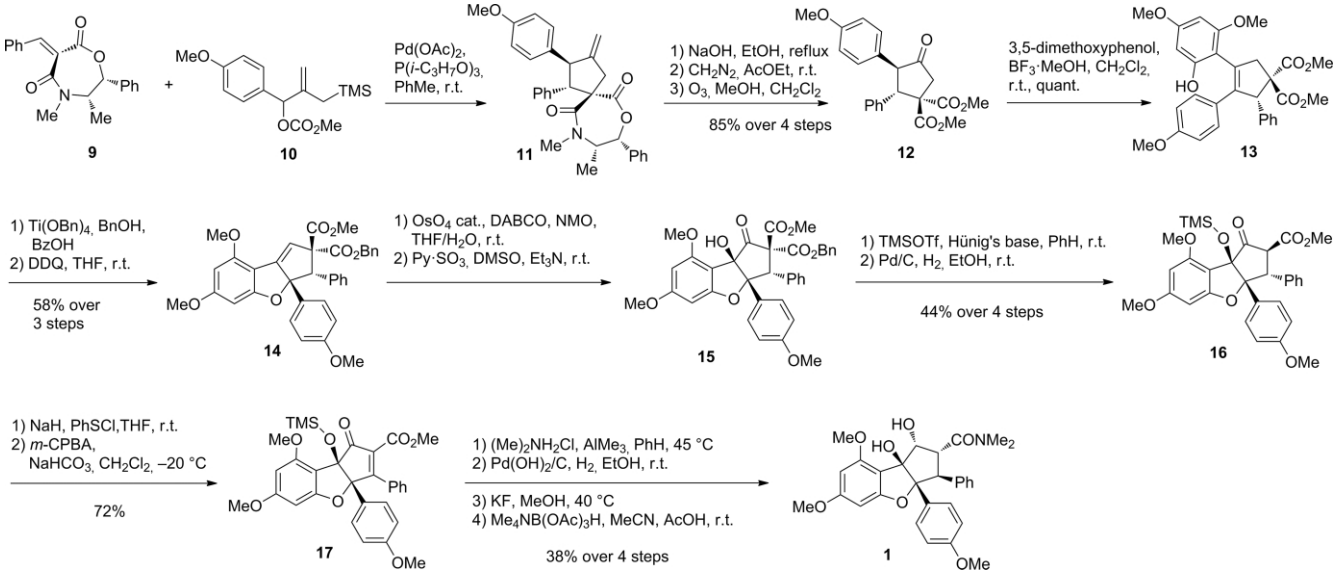

Scheme 1. First (and enantioselective) total synthesis of a flavagline (rocaglamide), by Trost et al.[15]

This elegant and efficient strategy was later improved by Dobler and colleagues, who replaced SmI_2-induced cyclization by an umpolung reaction with cyanohydrin **25** to generate the cyclopentanone **26** (Scheme 3). The carboxyl moiety was then straightforwardly introduced by use of the Stiles reagent, which circumvented the ketene dithioacetal intermediate.

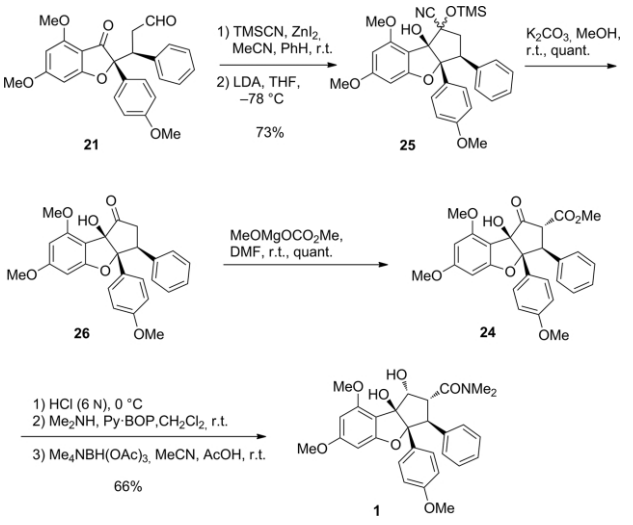

Scheme 3. Dobler's synthesis of racemic rocaglamide.[17a]

In 2008, Qin and his group further shortened the number of steps by using the benzylidenemalonate **27** as a Michael acceptor to generate keto-diester **28**, which was then able to undergo an SmI_2-induced cyclization (Scheme 4).[17b] Amidation and reduction of the β-ketoamide furnished a diastereomeric mixture of cyclopenta[*b*]benzofurans in only four steps from benzofuranone **20**.

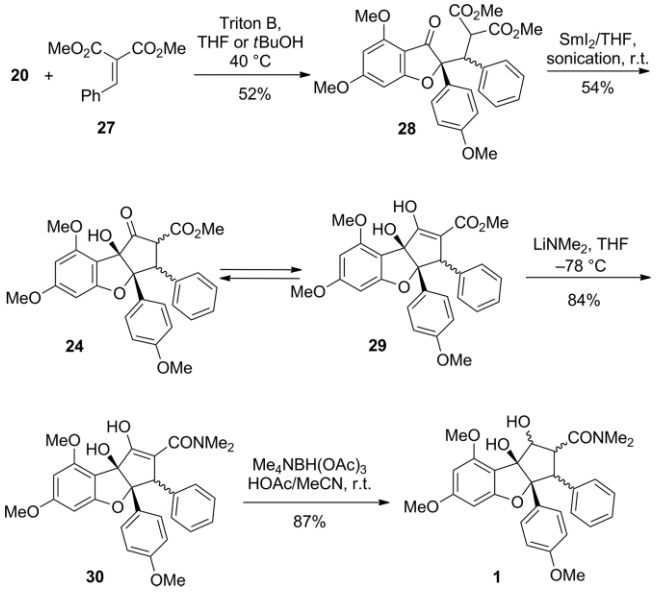

Scheme 4. Qin's synthesis of racemic rocaglamide.[17b]

4. Ragot's 5 *endo-tet* Cyclization Approach

In 2004, Ragot's group developed a strategy based on the intramolecular 5 *endo-tet* cyclization of a phenolic epoxide to generate the flavagline skeleton (Scheme 5).[18] Their synthesis began with the condensation of bromoketone **31** and triphenylphosphorane **32** to provide cyclopentenone **33**. After decarboxylation and bromination, α-bromoenone **34** was engaged in a Suzuki reaction with boronate **35** to give rise to enone **36**. Diastereoselective reduction and epoxidation of **36** yielded key intermediate **37**, which underwent spontaneous cyclization into didemethoxyrocaglaol **38** triggered by phenol deprotection.

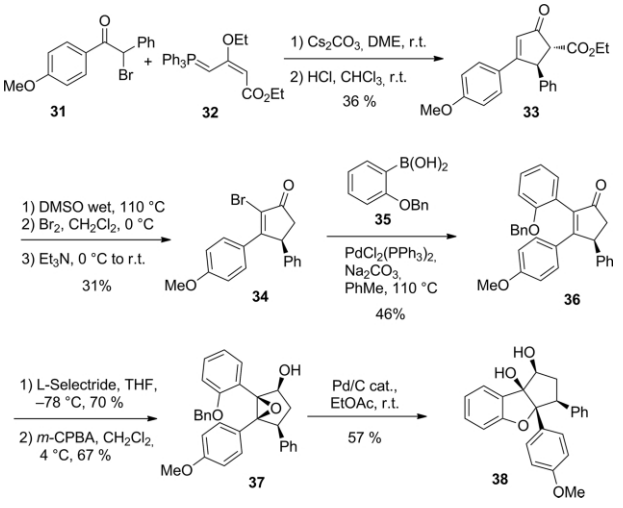

Scheme 5. Ragot's synthesis of the flavagline skeleton.[18]

We tried to use this approach to synthesize rocaglaol (**2**), which bears the methoxy groups necessary for pharmacological activity (Scheme 6).[19] Our synthesis of the cyclopentenone core commenced with a Perkin reaction between carboxylic acid **39** and benzaldehyde, followed by a Sonogashira coupling to deliver ketone **40** solely as the *E* isomer. This was treated

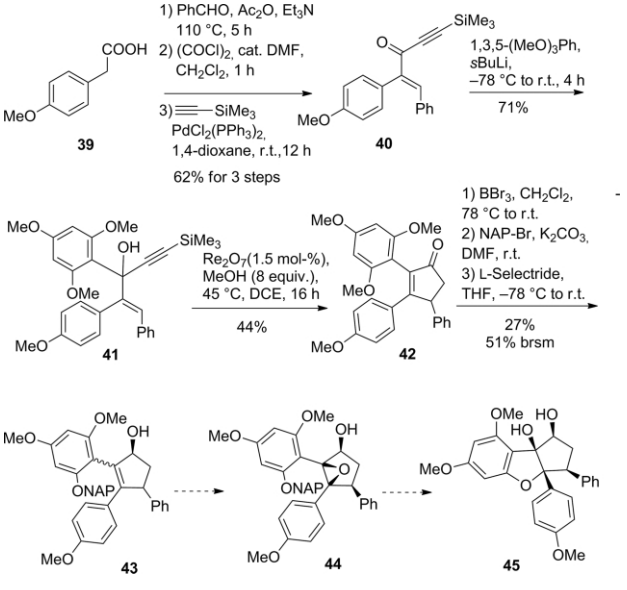

Scheme 6. Désaubry's attempt to synthesize rocaglaol.[19]

with lithiated trimethoxybenzene to provide carbinol **41**, which easily underwent an unprecedented annulation reaction in acidic medium to give, in only one step, the adduct cyclopentanone **42** with a 44 % yield.[20] Finally, selective demethylation, protection with a 2-naphthylmethyl (NAP) group (which can be easily removed by hydrogenolysis), and ketone reduction afforded the intermediates **43** as a pair of atropoisomers. Extensive trials directed towards transforming these compounds into epirocaglaol **45** via epoxide **44** were unfruitful, suggesting that the scope of Ragot's method is narrow. Indeed, their later article and patent only report the use of SmI_2-mediated pinacol coupling to synthesize pharmacologically active flavaglines.[21]

5. Porco's [3+2] Photocycloaddition Approach

In 2004, Porco and co-workers disclosed a brilliant synthesis of flavaglines inspired by the biosynthesis previously published by Proksch (Scheme 7).[14f] The key step of this approach was an original photochemical [3+2] cycloaddition between 3-hydroxyflavone **46** and cinnamic ester **47**, involving photoexcited triplet biradical **48**, to furnish aglain **49**.[22] This was treated with sodium methoxide to provide flavagline **24** (Scheme 2) through a β-acyloin rearrangement.

These authors later applied this elegant [3+2] photocycloaddition to a variety of dipolarophiles,[23] and made this trans-

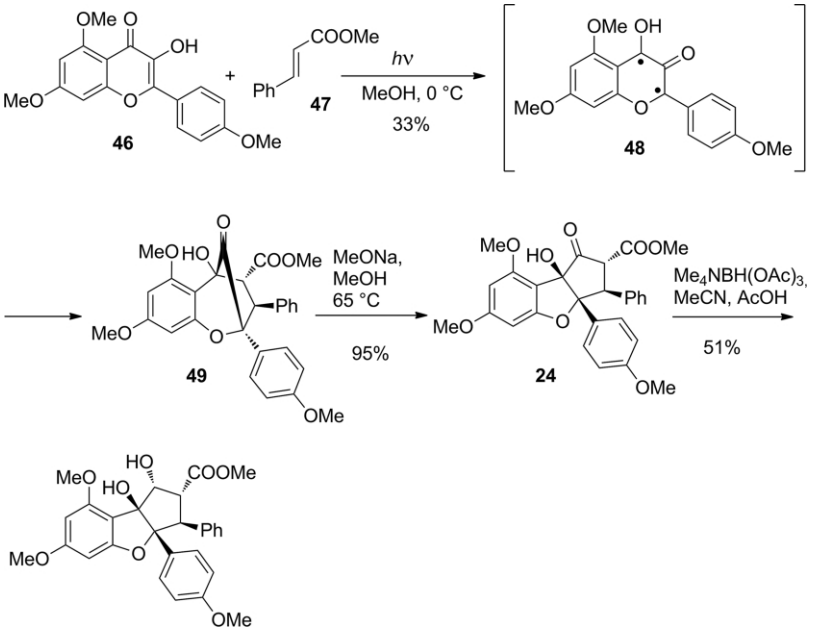

Scheme 7. Porco's biomimetic synthesis of flavaglines.[22]

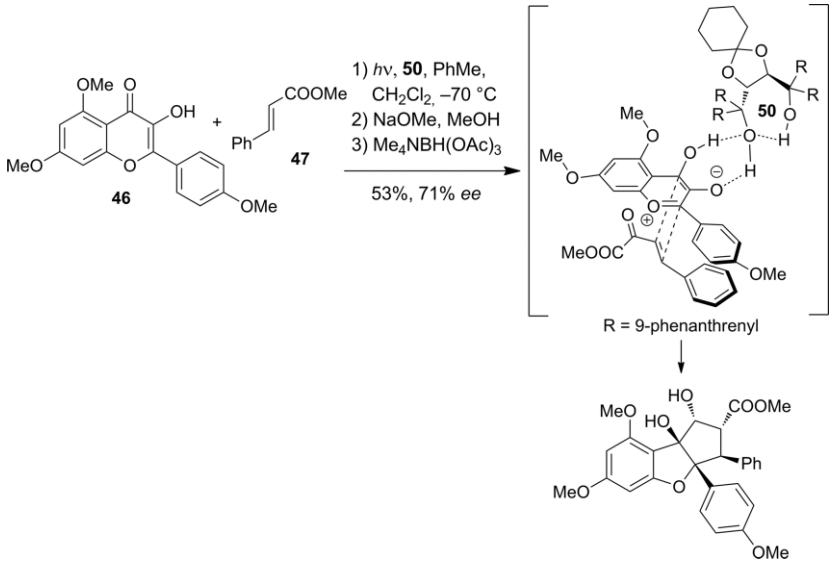

Scheme 8. Porco's enantioselective synthesis of flavaglines.[24a]

formation enantioselective by using TADDOL derivative **50** (Scheme 8).[24a] Another improvement to this reaction was disclosed by Tremblay and colleagues, who used flow chemistry to produce ten grams of racemic photoadducts in only a few hours.[25]

More recently, Porco and co-workers developed a kinetic resolution of the bridged ketone **49** utilizing an enantioselective transfer hydrogenation catalyzed by the Rh^{III} complex **51** (Scheme 9).[24b] This approach was efficiently applied to the asymmetric synthesis of (+)-aglaiastatin and (–)-aglaroxin C.

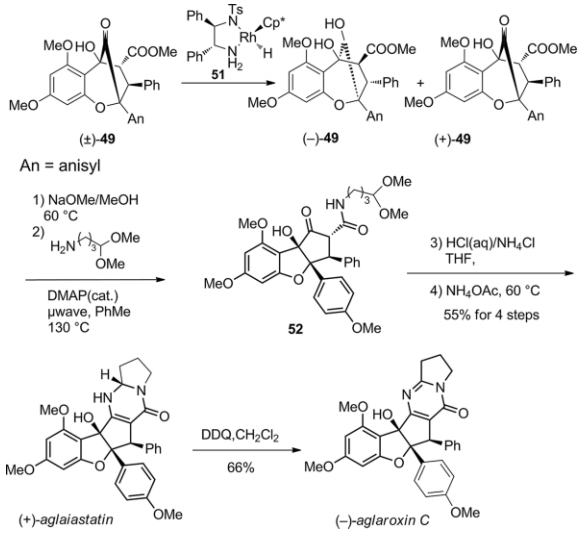

Scheme 9. Porco's kinetic-resolution-based asymmetric synthesis of (+)-aglaiatatin and (–)-aglaroxin C.[24b]

6. Frontier's and Magnus' Approaches Based on a Nazarov Reaction

The approach of Frontier and co-workers to fashioning the flavagline skeleton elegantly exploited an original Nazarov-type reaction designed for this purpose (Scheme 10).[26] Their synthesis began with the homologation of benzofuranone **20** to provide aldehyde **54** in three steps. Alkylation with phenylacetylene and protection of the alcohol gave propargyl ether **55**, which was then deprotonated and quenched with nBu$_3$SnCl to give stannyl alkoxyallene **56**. Epoxidation of this with *m*-CPBA generated a transient epoxide that underwent further transformation to establish the flavagline skeleton through an atypical Nazarov reaction. Deprotection, conversion into a triflate, and Pd-mediated carbonylation yielded dehydroflavagline **61**. The strategy was completed in two more steps by Trost's approach.

Two other strategies based on a Nazarov reaction were developed by Magnus and co-workers.[27] In their first approach, Magnus and co-workers developed a unique Nazarov cyclization that provides a straightforward means to generate the flavagline skeleton (Scheme 11).[27a] This route began with the Sonogashira cross-coupling of iodoarene **63** with 4-methoxyphenylacetylene. A palladium-catalyzed carbonylative annulation of the obtained alkyne **64** provided benzofuran **65**, which was then converted into enone **66**. Although treatment with many Lewis acids resulted in the fragmentation of this compound, Magnus and co-workers found that acetyl bromide efficiently promotes the Nazarov cyclization with an 81 % yield, probably through intermediates **67** and **68**. Oxidation with ceric ammonium nitrate (CAN) efficiently installed the tertiary hydroxy group. Further redox manipulations provided dehydroflavagline **72**, which was treated under the condition described by Trost to afford methyl rocaglate **62** in two steps.

The second approach began with the conversion of alkyne **64** into benzofuranone **74** in three steps (Scheme 12).[27b] Condensation of the latter with benzyl methyl ketone, then *O*-silylation, provided **75**, which was subjected to the Nazarov reaction in the presence of $SnCl_4$ to yield the cyclopentenone **76**. Hydrosilylation, palladium-mediated carboxymethylation, and hydroxylation gave rise to the dehydrated flavagline **79**.

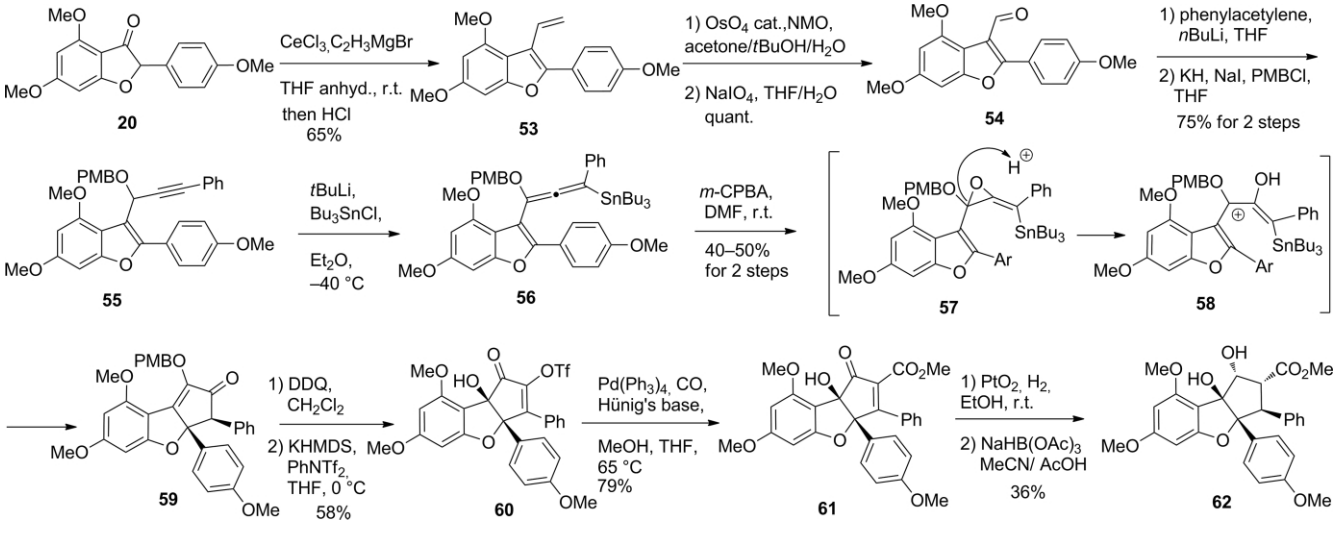

Scheme 10. Frontier's synthesis of racemic rocaglamide based on a Nazarov reaction.[26]

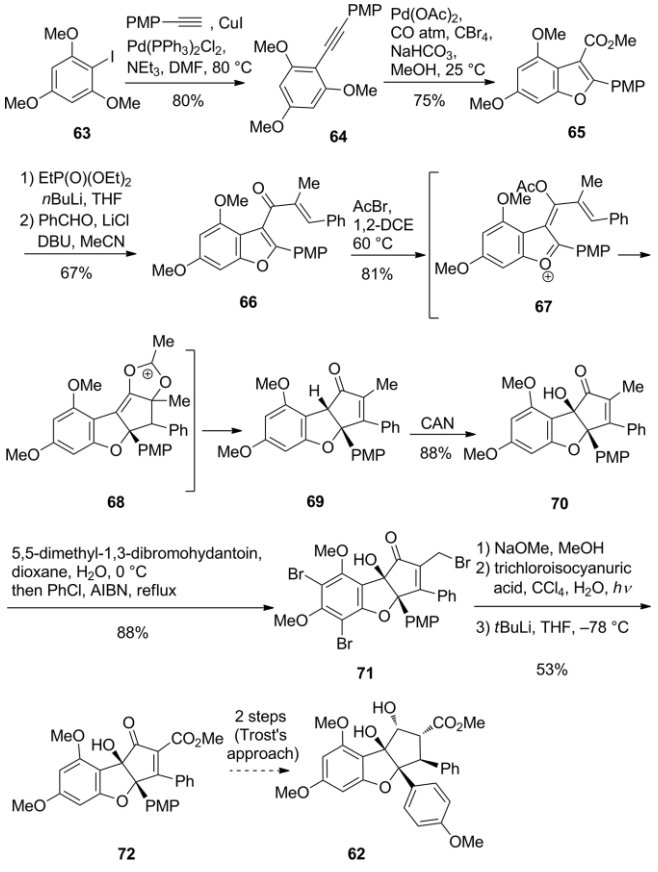

Scheme 11. Magnus' first synthesis of racemic flavaglines.[27a]

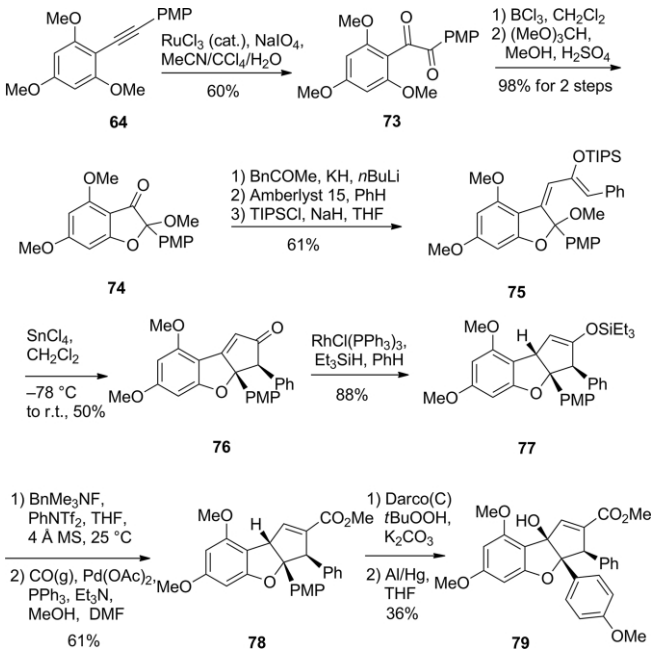

Scheme 12. Magnus' racemic synthesis of methyl rocaglate.[27b]

7. Tius' Enantioselective Intramolecular S_NAr Approach

In 2015, Tius and co-workers reported a new synthesis of flavaglines. It was also based on a Nazarov reaction, but their strategy used a different disconnection from that used by Frontier and Magnus.[28] The preparation of dienone **82** employed a selective deprotonation of **80** with TMPMgCl·LiCl (TMP = 2,2,6,6-tetramethylpiperidyl) and its condensation with acid chloride **81**. Subsequent removal of the 3,4-dimethoxybenzyl (DMB) protecting group, followed by an enantioselective Pd^0-catalyzed Nazarov-type cyclization, afforded the cyclic product **85** in 70 % yield and 89:11 *er*. Then, an allyloxy group was stereoselectively introduced under oxidative (PIFA) conditions to provide enol ether **86** after an *O*-methylation step with Meerwein's salt. Conversion of the ester into a dimethyl amide and alkylation with lithiated 1-fluoro-3,5-dimethoxybenzene in the presence of $LaCl_3$•2 LiCl efficiently gave rise to tertiary alcohol **89** as a single isomer. SeO_2-mediated oxidative cleavage of the allyl protecting group and a subsequent intramolecular S_NAr efficiently generated the flavagline scaffold, which was further advanced to rocaglamide in two steps (Scheme 13).

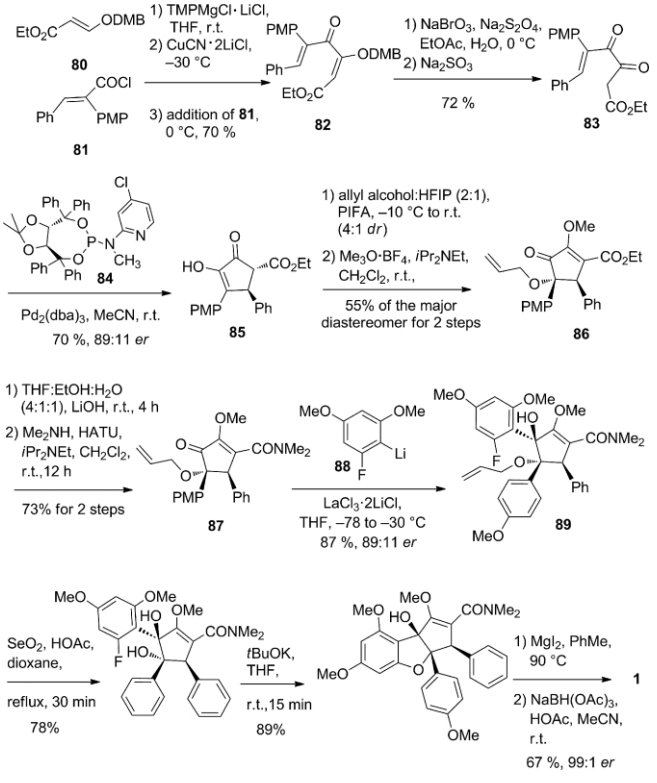

Scheme 13. Tius' enantioselective synthesis of rocaglamide.[28]

8. Porco's and Rizzacasa's Syntheses of Silvestrol (5)

The enantioselective synthesis of silvestrol (**5**) was independently disclosed in the same issue of *Angewandte Chemie* by Porco's and Rizzacasa's groups in 2007 (Scheme 14).[29] Both teams relied on Porco's [3+2] photocycloaddition to prepare the cyclopenta[*b*]benzofuran core. The main difference between Porco's and Rizzacasa's strategies is in the preparation of the pseudosugar moiety. Porco and co-workers started from D-dimethyl tartrate to prepare the lactol **94** via the known diol **93**,[30] whereas Rizzacasa and co-workers prepared a similar syn-

thon through periodic cleavage of D-glucose derivative **96** (Scheme 14). These approaches were used to prepare several pharmacologically active silvestrol analogues.[5c,26,29a,31]

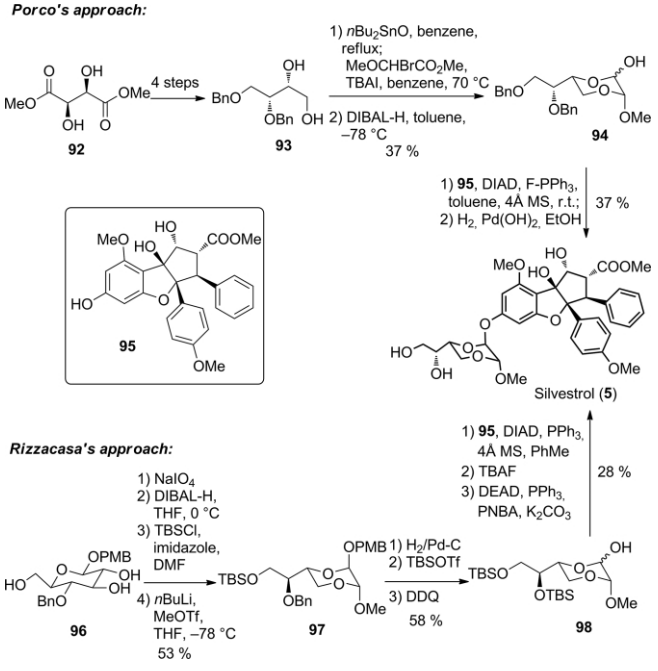

Scheme 14. Porco's and Rizzacasa's syntheses of silvestrol (**5**).[29]

9. Concluding Remarks

In summary, the synthetic studies directed towards the creation of flavaglines have been rich in intellectual excitement and have not only stimulated the discovery of new reactions but have also paved the way for SAR studies and subsequent promising preclinical investigations for the treatment of cancers and of neurological, cardiac, and inflammatory diseases. In addition, the recent demonstration that eIF4a and prohibitins are valid targets for treatment of cancer is expected to foster this field of research.

Acknowledgments

This work was supported by the Association pour la Recherche sur le Cancer (ARC) (grant numbers 3940, SFI20111204054, and PJA 20141201909). The authors also thank the AAREC Filia Research, the Association Nationale de la Recherche et de la Technologie (ANRT) and the Ministère de l'Education Nationale, de l'Enseignement Supérieur et de la Recherche (MENSR) for fellowships to Q. Z. and H. A.-H.

Keywords: Natural products · Total synthesis · Synthesis design · Medicinal chemistry · Antitumor agents

[1] C. Basmadjian, Q. Zhao, E. Bentouhami, A. Djehal, C. G. Nebigil, R. A. Johnson, M. Serova, A. de Gramont, S. Faivre, E. Raymond, L. G. Désaubry, *Front. Chem.* **2014**, *2*, 20.
[2] C. Basmadjian, F. Thuaud, N. Ribeiro, L. Désaubry, *Future Med. Chem.* **2013**, *5*, 2185–2197.
[3] M. L. King, C. C. Chiang, H. C. Ling, E. Fujita, M. Ochiai, A. T. McPhail, *J. Chem. Soc., Chem. Commun.* **1982**, 1150–1151.
[4] a) J. M. Chambers, L. M. Lindqvist, A. Webb, D. C. Huang, G. P. Savage, M. A. Rizzacasa, *Org. Lett.* **2013**, *15*, 1406–1409; b) G. Polier, J. Neumann, F. Thuaud, N. Ribeiro, C. Gelhaus, H. Schmidt, M. Giaisi, R. Kohler, W. W. Muller, P. Proksch, M. Leippe, O. Janssen, L. Désaubry, P. H. Krammer, M. Li-Weber, *Chem. Biol.* **2012**, *19*, 1093–1104; c) H. Sadlish, G. Galicia-Vazquez, C. G. Paris, T. Aust, B. Bhullar, L. Chang, S. B. Helliwell, D. Hoepfner, B. Knapp, R. Riedl, S. Roggo, S. Schuierer, C. Studer, J. A. Porco, J. Pelletier, N. R. Movva, *ACS Chem. Biol.* **2013**, *8*, 1519–1527.
[5] a) A. L. Wolfe, K. Singh, Y. Zhong, P. Drewe, V. K. Rajasekhar, V. R. Sanghvi, K. J. Mavrakis, M. Jiang, J. E. Roderick, J. Van der Meulen, J. H. Schatz, C. M. Rodrigo, C. Zhao, P. Rondou, E. de Stanchina, J. Teruya-Feldstein, M. A. Kelliher, F. Speleman, J. A. Porco, J. Pelletier, G. Ratsch, H.-G. Wendel, *Nature* **2014**, *513*, 65–70; b) S. Santagata, M. L. Mendillo, Y.-c. Tang, A. Subramanian, C. C. Perley, S. P. Roche, B. Wong, R. Narayan, H. Kwon, M. Koeva, A. Amon, T. R. Golub, J. A. Porco Jr., L. Whitesell, S. Lindquist, *Science* **2013**, *341*, 1238303; c) C. M. Rodrigo, R. Cencic, S. P. Roche, J. Pelletier, J. A. Porco, *J. Med. Chem.* **2012**, *55*, 558–562.
[6] D. K. Rozelle, C. M. Filone, N. Kedersha, J. H. Connor, *Mol. Cell Biol.* **2014**, *34*, 2003–2016.
[7] Z. Nasr, L. E. Dow, M. Paquet, J. Chu, K. Ravindar, R. Somaiah, P. Deslongchamps, J. A. Porco, S. W. Lowe, J. Pelletier, *BMC Pharmacol. Toxicol.* **2013**, *14*, 58/51–58/12.
[8] a) F. Thuaud, N. Ribeiro, C. Gaiddon, T. Cresteil, L. Désaubry, *J. Med. Chem.* **2011**, *54*, 411–415; b) F. Thuaud, Y. Bernard, G. Turkeri, R. Dirr, G. Aubert, T. Cresteil, A. Baguet, C. Tomasetto, Y. Svitkin, N. Sonenberg, C. G. Nebigil, L. Désaubry, *J. Med. Chem.* **2009**, *52*, 5176–5187; c) F. Emhemmed, S. Ali Azouaou, F. Thuaud, V. Schini-Kerth, L. Désaubry, C. D. Muller, G. Fuhrmann, *Biochem. Pharmacol.* **2014**, *89*, 185–196; d) L. Boussemart, H. Malka-Mahieu, I. Girault, D. Allard, O. Hemmingsson, G. Tomasic, M. Thomas, C. Basmadjian, N. Ribeiro, F. Thuaud, C. Mateus, E. Routier, N. Kamsu-Kom, S. Agoussi, A. M. Eggermont, L. Désaubry, C. Robert, S. Vagner, *Nature* **2014**, *513*, 105–109.
[9] Y. Bernard, N. Ribeiro, F. Thuaud, G. Turkeri, R. Dirr, M. Boulberdaa, C. G. Nebigil, L. Désaubry, *PLoS One* **2011**, *6*, e25302.
[10] N. Ribeiro, F. Thuaud, Y. Bernard, C. Gaiddon, T. Cresteil, A. Hild, E. C. Hirsch, P. P. Michel, C. G. Nebigil, L. Désaubry, *J. Med. Chem.* **2012**, *55*, 10064–10073.
[11] J. Han, Q. Zhao, C. Basmadjian, L. Désaubry, A. L. Theiss, *Inflamm. Bowel. Dis.* **2016**, *22*, 55–67.
[12] P. Wintachai, F. Thuaud, C. Basmadjian, S. Roytrakul, S. Ubol, L. Désaubry, D. R. Smith, *Microbiol. Immunol.* **2015**, *59*, 129–141.
[13] IMD-026259: an innovative drug for disease modifying treatment of Parkinson's diseases www.michaeljfox.org/foundation/grantdetail.php?grant_id = 1020.
[14] a) S. S. Ebada, N. Lajkiewicz, J. A. Porco Jr., M. Li-Weber, P. Proksch, *Prog. Chem. Org. Nat. Prod.* **2011**, *94*, 1–58; b) S. Kim, A. A. Salim, S. M. Swanson, A. D. Kinghorn, *Anti-Cancer Agents Med. Chem.* **2006**, *6*, 319–345; c) L. Pan, J. L. Woodard, D. M. Lucas, J. R. Fuchs, A. D. Kinghorn, *Nat. Prod. Rep.* **2014**, *31*, 924–939; d) P. Proksch, R. Edrada, R. Ebel, F. I. Bohnenstengel, B. W. Nugroho, *Curr. Org. Chem.* **2001**, *5*, 923–938; e) N. Ribeiro, F. Thuaud, C. Nebigil, L. Désaubry, *Bioorg. Med. Chem.* **2012**, *20*, 1857–1864; f) P. Proksch, R. Edrada, R. Ebel, F. Bohnenstengel, B. Nugroho, *Curr. Org. Chem.* **2001**, *5*, 923–938.
[15] B. M. Trost, P. D. Greenspan, B. V. Yang, M. G. Saulnier, *J. Am. Chem. Soc.* **1990**, *112*, 9022–9024.
[16] a) A. E. Davey, M. J. Schaeffer, R. J. K. Taylor, *J. Chem. Soc., Chem. Commun.* **1991**, 1137–1139; b) A. E. Davey, R. J. K. Taylor, *J. Chem. Soc., Chem. Commun.* **1987**, 25–27.
[17] a) M. R. Dobler, I. Bruce, F. Cederbaum, N. G. Cooke, L. J. Diorazio, R. G. Hall, E. Irving, *Tetrahedron Lett.* **2001**, *42*, 8281–8284; b) H. Li, B. Fu, M. A. Wang, N. Li, W. J. Liu, Z. Q. Xie, Y. Q. Ma, Z. Qin, *Eur. J. Org. Chem.* **2008**, 1753–1758.
[18] K. Thede, N. Diedrichs, J. P. Ragot, *Org. Lett.* **2004**, *6*, 4595–4597.
[19] C. Basmadjian, Q. Zhao, L. Désaubry, *Tetrahedron Lett.* **2015**, *56*, 727–730.
[20] C. Basmadjian, F. Zhang, L. Désaubry, *Beilstein J. Org. Chem.* **2015**, *11*, 1017–1022.

[21] a) N. Diedrichs, T. Fahrig, I. Gerlach, J. Ragot, J. Schuhmacher, K. Thede, E. Horvath, in: *Preparation of cyclopenta[b]benzofuran derivatives as inhibitors of interleukin-8*, Bayer Healthcare AG, Germany, **2005**, p. 202; b) N. Diedrichs, J. P. Ragot, K. Thede, *Eur. J. Org. Chem.* **2005**, 1731–1735.
[22] B. Gerard, G. Jones II, J. A. Porco Jr., *J. Am. Chem. Soc.* **2004**, *126*, 13620–13621.
[23] S. P. Roche, R. Cencic, J. Pelletier, J. A. Porco Jr., *Angew. Chem. Int. Ed.* **2010**, *49*, 6533–6538; *Angew. Chem.* **2010**, *122*, 6683.
[24] a) B. Gerard, S. Sangji, D. J. O'Leary, J. A. Porco Jr., *J. Am. Chem. Soc.* **2006**, *128*, 7754–7755; b) S. D. Stone, N. J. Lajkiewicz, L. Whitesell, A. Hilmy, J. A. Porco Jr., *J. Am. Chem. Soc.* **2015**, *137*, 525–530.
[25] T. Liu, S. J. Nair, A. Lescarbeau, J. Belani, S. Peluso, J. Conley, B. Tillotson, P. O'Hearn, S. Smith, K. Slocum, K. West, J. Helble, M. Douglas, A. Bahadoor, J. Ali, K. McGovern, C. Fritz, V. J. Palombella, A. Wylie, A. C. Castro, M. R. Tremblay, *J. Med. Chem.* **2012**, *55*, 8859–8878.
[26] a) J. A. Malona, K. Cariou, W. T. Spencer III, A. J. Frontier, *J. Org. Chem.* **2012**, *77*, 1891–1908; b) J. A. Malona, K. Cariou, A. J. Frontier, *J. Am. Chem. Soc.* **2009**, *131*, 7560–7561.
[27] a) P. Magnus, M. A. H. Stent, *Org. Lett.* **2005**, *7*, 3853–3855; b) P. Magnus, W. A. Freund, E. J. Moorhead, T. Rainey, *J. Am. Chem. Soc.* **2012**, *134*, 6140–6142.
[28] Z. Zhou, M. A. Tius, *Angew. Chem. Int. Ed.* **2015**, *54*, 6037–6040; *Angew. Chem.* **2015**, *127*, 6135.
[29] a) M. El Sous, M. L. Khoo, G. Holloway, D. Owen, P. J. Scammells, M. A. Rizzacasa, *Angew. Chem. Int. Ed.* **2007**, *46*, 7835–7838; *Angew. Chem.* **2007**, *119*, 7981; b) B. Gerard, R. Cencic, J. Pelletier, J. A. Porco, *Angew. Chem. Int. Ed.* **2007**, *46*, 7831–7834; *Angew. Chem.* **2007**, *119*, 7977.
[30] S. Takano, A. Kurotaki, Y. Sekiguchi, S. Satoh, M. Hirama, K. Ogasawara, *Synthesis* **1986**, 811–817.
[31] a) T. E. Adams, M. El Sous, B. C. Hawkins, S. Hirner, G. Holloway, M. L. Khoo, D. J. Owen, G. P. Savage, P. J. Scammells, M. A. Rizzacasa, *J. Am. Chem. Soc.* **2009**, *131*, 1607–1616; b) J. M. Chambers, D. C. Huang, L. M. Lindqvist, G. P. Savage, J. M. White, M. A. Rizzacasa, *J. Nat. Prod.* **2012**, *75*, 1500–1504; c) B. C. Hawkins, L. M. Lindqvist, D. Nhu, P. P. Sharp, D. Segal, A. K. Powell, M. Campbell, E. Ryan, J. M. Chambers, J. M. White, M. A. Rizzacasa, G. Lessene, D. C. S. Huang, C. J. Burns, *ChemMedChem* **2014**, *9*, 1556–1566.

Received: April 7, 2016
Published Online: July 26, 2016

Publication N°*3*

Exploratory studies toward a synthesis of flavaglines. A novel access to a highly substituted cyclopentenone intermediate.

Basmadjian, C., Zhao, Q., Désaubry, L., *Tetrahedron lett.* **2015**, *56*, 727–730.

Tetrahedron Letters 56 (2015) 727–730

Contents lists available at ScienceDirect

Tetrahedron Letters

journal homepage: www.elsevier.com/locate/tetlet

Exploratory studies toward a synthesis of flavaglines. A novel access to a highly substituted cyclopentenone intermediate

Christine Basmadjian, Qian Zhao, Laurent Désaubry *

Laboratory of Therapeutic Innovation (UMR 7200), University of Strasbourg-CNRS, Faculty of Pharmacy, 67401 Illkirch, France

ARTICLE INFO

Article history:
Received 13 September 2014
Revised 14 December 2014
Accepted 16 December 2014
Available online 23 December 2014

Keywords:
Cyclopentenones
Carbocationic rearrangement
Propargyl alcohols
Flavaglines

ABSTRACT

The gold(I)-catalyzed intramolecular siloxycyclization developed by Rhee and collaborators was shown to operate also on alkyl ethers to generate a highly substituted 2-cyclopentenone **8**, extending the application of this reaction. Conversion of **8** to known anticancer natural products following a reported strategy was examined.

Isolated from medicinal plants of the genus *Aglaia*, flavaglines have attracted considerable attention due to their remarkable structural complexity and unique biological activities, which include a strong cytotoxicity that is specific to cancer cells.[1–5] In the course of our medicinal program aiming at developing flavaglines with enhanced pharmacological properties,[5,6] we considered to prepare novel flavaglines using a strategy developed by Ragot and coll. at Bayer (Scheme 1).[7] These authors achieved the synthesis of the flavagline core **3** in three steps from cyclopentenone **1a**, using an intramolecular hydroxy epoxide opening in the key step.

Although the disclosed preparation of unsubstituted cyclopentenone **1a** could be achieved in 4 steps with an overall yield of 14%, the introduction of substituents necessary for the anticancer activity (e.g., R = OMe) was not reported. In order to synthesize pharmacologically active flavaglines, we considered to prepare **1b** by another approach. While symmetrical 3,4-diaryl-cyclopent-2-enones can easily be obtained from α,β-diketones, the synthesis of cyclopentenones substituted by different aryl moieties is more tedious.

At the heart of our approach to prepare **1b** is the Rautenstrauch rearrangement, which is particularly efficient to prepare variously substituted cyclopentenones.[8] To test the viability of this strategy, we first examined the reactivity of the Rautenstrauch's substrate **7**.

Our attempt of synthesis of ester **7** is depicted in Scheme 2. Perkin condensation of acid **4** and benzaldehyde followed by the conversion to an acyl chloride and a Sonogashira coupling conveniently afforded ketone **5** as a sole *E* isomer. Condensation with lithiated trimethoxybenzene gave adduct **6** in 71% yield.

With carbinol **6** in hand, we tested many esterification protocols.[9] However, all our attempts were unsuccessful due to lack of reactivity or high instability of expected ester **7**.

This failure led us to explore another strategy based on the recently described gold(I)-catalyzed synthesis of highly substituted cyclopentenones by an intramolecular siloxycyclization process developed by Rhee and coll. (Scheme 3).[10] The utility of this approach was validated with the total synthesis of herbertene natural products.[11] Although this reaction was described exclusively with tertiary silyl ethers (R^1 = $SiEt_3$, R^2 and $R^3 \neq H$), we considered that the phenyl and the trimethoxyphenyl groups of substrate **11** should sufficiently stabilize the carbocationic intermediate to allow the reaction to proceed (Scheme 4). This hypothesis was supported by Toste's report of a related Au(I)-catalyzed carboxyalkoxylation using benzylic ethers as substrates to synthesize indenyl ethers.[12] Thus, the silyl ether was replaced by an ethoxy group due to its easier preparation.

Indeed, the direct molybdenum(VI)-catalyzed transposition and etherification of allylic alcohol **6** at 50 °C afforded a 1:1 mixture of ethers **9** and **10** in a 55% yield.[13] Gratifyingly, increasing the temperature to 65 °C improved the ratio to 1:3 in favor of the desired ether **10** in a 85% yield. Increasing the temperature further promoted the decomposition of this product. Desilylation provided alkyne **11**, which gratifyingly proved to be a good substrate for the Rhee's annulation reaction. The attempt to perform this reaction on silylated alkyne **10** also afforded **8** (58%).

* Corresponding author. Tel.: +33 036 885 4141; fax: +33 036 885 4320.
E-mail address: desaubry@unistra.fr (L. Désaubry).

http://dx.doi.org/10.1016/j.tetlet.2014.12.093
0040-4039/

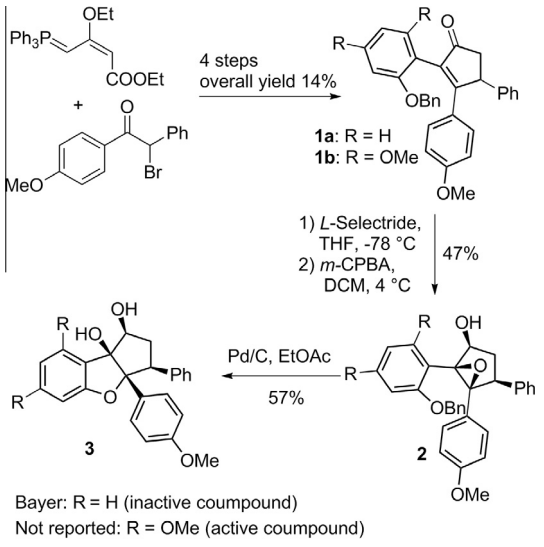

Scheme 1. Bayer synthesis of the flavagline core (the synthesis of pharmacologically active compounds (R = OMe) was not reported with this approach).[7]

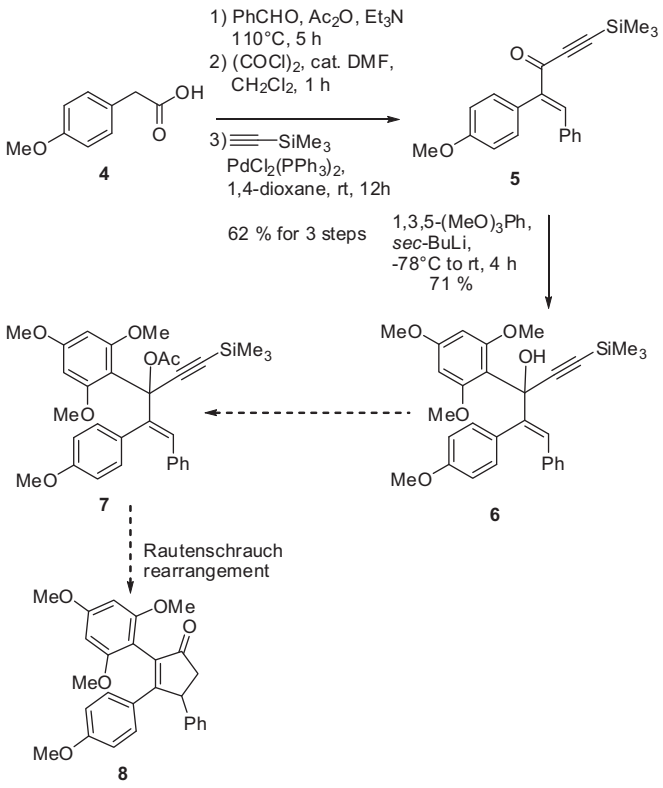

Scheme 2. Attempt synthesis of an advanced precursor of flavaglines.

The synthesis of two other cyclopentenones was next examined (Scheme 5). The substrates of the Au-catalyzed cyclization were prepared from acyl chloride **12** through Suzuki coupling, ethynylation, rearrangement and desilylation of the alkyne. Enyne **13** harboring an unsubstituted phenyl afforded the desired cyclopentenone **15** in a satisfactory yield of 50%. Interestingly, introduction of a chlorine atom in the *para* position increased the yield to 75%, probably due to a higher stabilization of the carbocationic intermediate.

Thanks to the assistance of ketone, **8** was selectively monodemethylated upon treatment with BBr_3 in a 75% yield (Scheme 6).

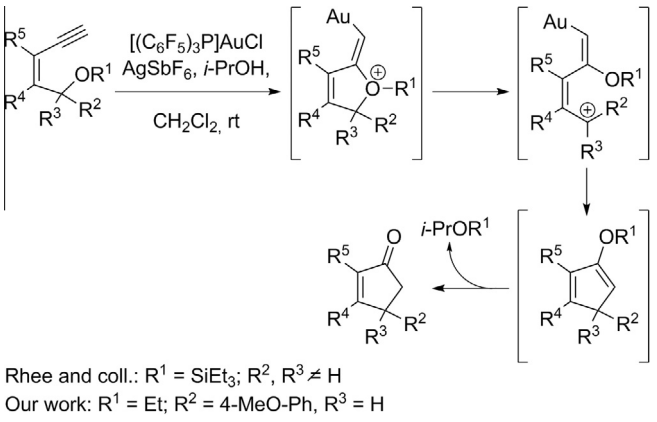

Scheme 3. Proposed mechanism for the gold(I)-catalyzed cyclopentanone formation developed by Rhee and coll.[10]

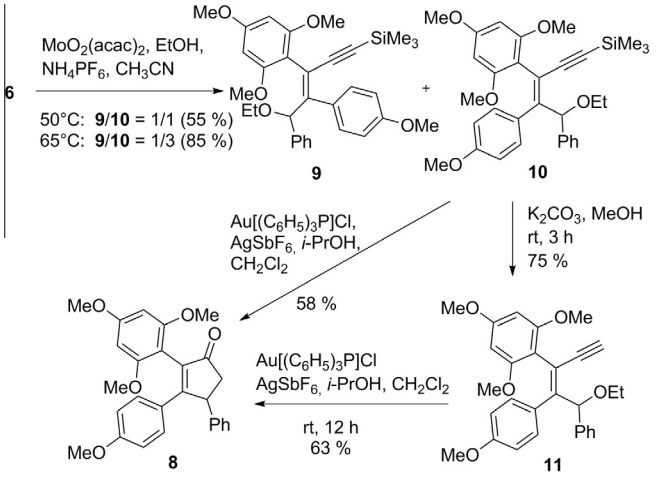

Scheme 4. Synthesis of cyclopentenone **8**.

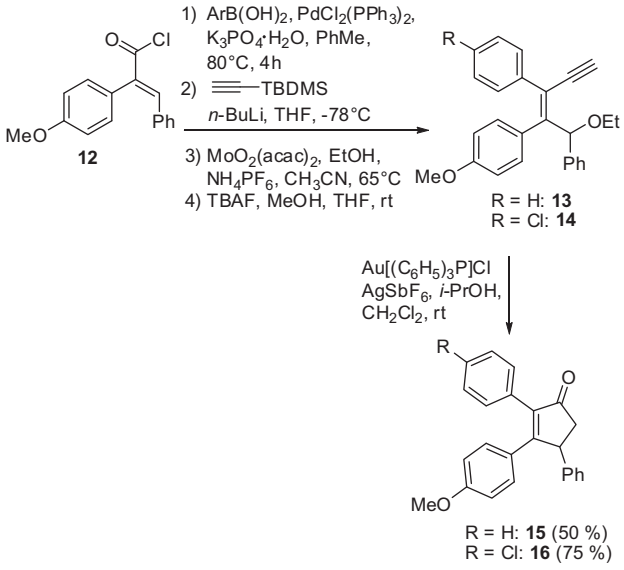

Scheme 5. Synthesis of cyclopentenones **15** and **16**.

Reduction of ketone **17** was not diastereoselective under various conditions (L-selectride; Red-Al; $NaBH_4$; $NaBH_4$, $CeCl_3{\cdot}7H_2O$). In addition, the mixture of **18** and **19** significantly degraded during

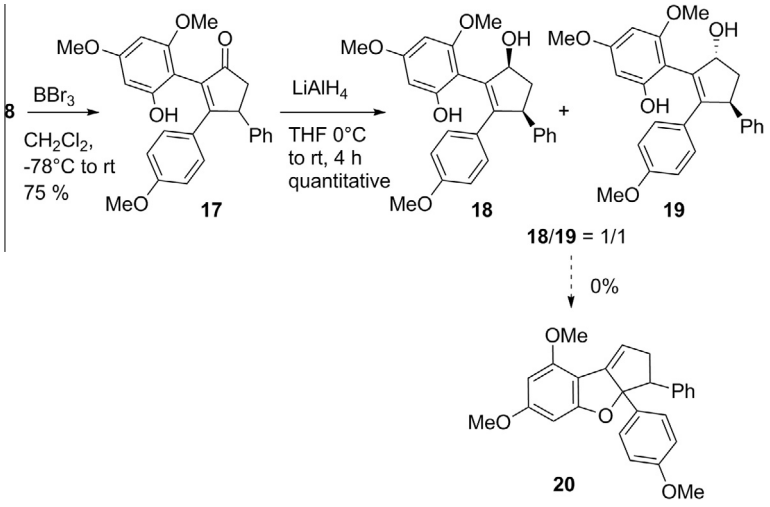

Scheme 6. Synthesis of the allylic alcohols **18/19** and attempts to generate the flavagline scaffold.

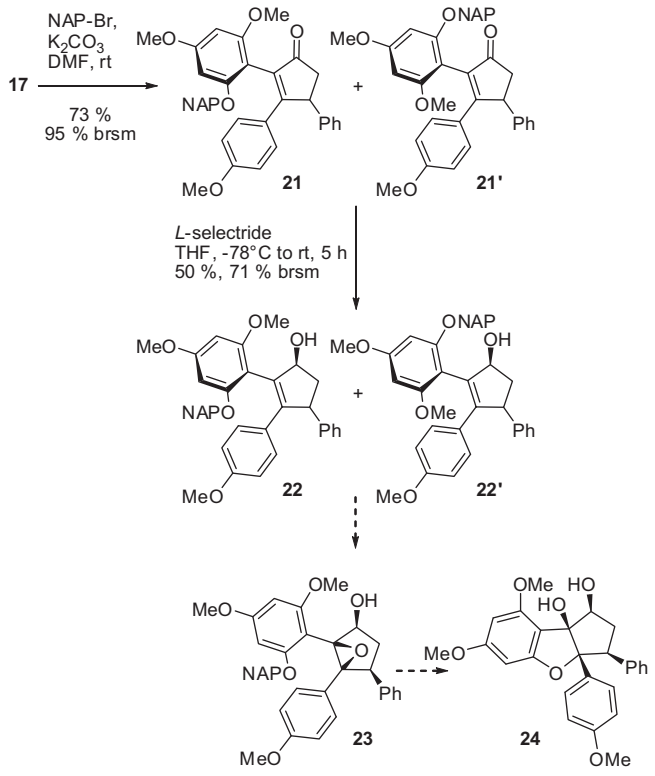

Scheme 7. Synthesis of the atropoisomeric allylic alcohols **22**/**22′** and epoxidation attempts to synthesize flavagline **24**.

purification steps. After extensive work, we eventually were able to quantitatively prepare a mixture of **18**/**19** in a 1/1 ratio using 4 equivalents of $LiAlH_4$.

With **18** and **19** in hand, we tried to convert these reactive allylic alcohols into the flavagline precursor **20** using many methods of activation of allylic alcohols ($Pd[P(OC_6H_5)_3]_4$, Na_2SO_4; PPh_3-AuCl, AgOTf, 4 Å MS; $Bi(OTf)_3$, KPF_6, $CaSO_4$; Ar-$B(OH)_2$; $FeCl_3$; $MoO_2(acac)_2$, NH_4PF_6; Re_2O_7).[14–18] Unfortunately, all of these assays only generated degradation products. Even though compounds similar to **20** have been described,[19–23] it is probable that the inherent ring strain of this product and the kinetic lability of the carbocationic intermediate prevent such a cyclization.

At this point, attempts at following Ragot's strategy using a protected phenol were examined (Scheme 7). 2-Naphthylmethyl (NAP) group was selected as the protecting group due to extremely mild conditions involved in its removal by catalytic hydrogenolysis.[24] The adduct was obtained as a pair of atropoisomers **21** and **21′**. As far as we know atropoisomerism for 1,2-diaryl cyclopentenes has not been reported hitherto.

Diastereoselective reduction with L-selectride afforded alcohols **22** and **22′** with 71% of conversion. Epoxidation of cyclopentenols **21/22′** under various conditions (*m*-CPBA, $NaHCO_3$; $VO(acac)_2$, *t*-BuO_2H; H_2O_2, NaOH; 4-nitroperbenzoic acid, $NaHCO_3$) provided none of the desired product probably due to the low reactivity of the sterically hindered alkene and instability of the product. Under Sharpless type conditions (*t*-BuO_2H, $Ti(Oi\text{-}Pr)_4$, 4 Å MS), formation of the ketone was predominant, probably due to ring strain release.

The inability to obtain substrate **23** suggests that the method reported by Bayer scientist is restricted to the synthesis of flavaglines that are not substituted by the functional groups necessary for the pharmacological activity. Indeed, none of the required decorations proposed in this Letter were described in Bayer patents.

Acknowledgments

L.D. was supported by the 'Association pour la Recherche sur le Cancer' (ARC). We are also grateful to AAREC Filia Research and ANRT for fellowships to C.B. and Q.Z. and also Julie Schmitt for technical help.

Supplementary data

Supplementary data (experimental procedures for the synthesis of compounds **5**, **6**, **8**, **10**–**16**) associated with this article can be found, in the online version, at http://dx.doi.org/10.1016/j.tetlet.2014.12.093.

References and notes

1. Santagata, S.; Mendillo, M. L.; Tang, Y.; Subramanian, A.; Perley, C. C.; Roche, S. P.; Wong, B.; Narayan, R.; Kwon, H.; Koeva, M.; Amon, A.; Golub, T. R.; Porco, J. A., Jr.; Whitesell, L.; Lindquist, S. *Science* **2013**, *341*, 1238303.
2. Wolfe, A. L.; Singh, K.; Zhong, Y.; Drewe, P.; Rajasekhar, V. K.; Sanghvi, V. R.; Mavrakis, K. J.; Jiang, M.; Roderick, J. E.; Van der Meulen, J.; Schatz, J. H.; Rodrigo, C. M.; Zhao, C.; Rondou, P.; de Stanchina, E.; Teruya-Feldstein, J.; Kelliher, M. A.; Speleman, F.; Porco, J. A., Jr.; Pelletier, J.; Rätsch, G.; Wendel, H. G. *Nature* **2014**, *513*, 65–70.

3. Boussemart, L.; Malka-Mahieu, H.; Girault, I.; Hemmingsson, O.; Allard, D.; Tomasic, G.; Thomas, M.; Ribeiro, N.; Thuaud, F.; Basmadjian, C.; Mateus, C.; Routier, E.; Kamsu-Kom, N.; Agoussi, S.; Eggermont, A. M.; Désaubry, L.; Robert, C.; Vagner, S. *Nature* **2014**, *513*, 105–109.
4. Pan, L.; Woodard, J. L.; Lucas, D. M.; Fuchs, J. R.; Douglas Kinghorn, A. *Nat. Prod. Rep.* **2014**, *31*, 924–939.
5. Basmadjian, C.; Thuaud, F.; Ribeiro, N.; Désaubry, L. *Future Med. Chem.* **2013**, *5*, 2185–2197.
6. Ribeiro, N.; Thuaud, F.; Bernard, Y.; Gaiddon, C.; Cresteil, T.; Hild, A.; Hirsch, E. C.; Michel, P. P.; Nebigil, C. G.; Désaubry, L. *J. Med. Chem.* **2012**, *55*, 10064–10073.
7. Thede, K.; Diedrichs, N.; Ragot, J. P. *Org. Lett.* **2004**, *6*, 4595–4597.
8. Shiroodi, R. K.; Gevorgyan, V. *Chem. Soc. Rev.* **2013**, *42*, 4991–5001.
9. Attempted esterification methods: Ac_2O, Et_3N/DMAP or DIPEA/$P(Bu)_3$; AcCl, *n*-BuLi or Et_3N/DMAP; BzCl, *n*-BuLi or NaH; TsNCO, *n*-BuLi; (4-NO_2-Ph)OCHO, *n*-BuLi.
10. An, S. E.; Jeong, J.; Baskar, B.; Lee, J.; Seo, J.; Rhee, Y. H. *Chem. Eur. J.* **2009**, *15*, 11837–11841.
11. Jeong, J.; Lee, J.; Seo, J.; Rhee, Y. H. *Bull. Korean Chem. Soc.* **2013**, *34*, 303–305.
12. Dubé, P.; Toste, D. *J. Am. Chem. Soc.* **2006**, *128*, 12062–12063.
13. Yang, H.; Fang, L.; Zhang, M.; Zhu, C. *Eur. J. Org. Chem.* **2009**, *5*, 666–672.
14. Kayaki, Y.; Koda, T.; Ikariya, T. *J. Org. Chem.* **2004**, *69*, 2595–2597.
15. Aponick, A.; Biannic, B. *Synthesis* **2008**, *20*, 3356–3359.
16. Qin, H.; Yamagiwa, N.; Matsunaga, S.; Shibasaki, M. *Angew. Chem., Int. Ed.* **2007**, *46*, 409–413.
17. Zheng, H.; Ghanbari, S.; Nakamura, S.; Hall, D. G. *Angew. Chem., Int. Ed.* **2012**, *51*, 6187–6190.
18. Guérinot, A.; Serra-Muns, A.; Gnamm, C.; Bensoussan, C.; Reymond, S.; Cossy, J. *Org. Lett.* **2010**, *12*, 1808–1811.
19. Giese, M. W.; Moser, W. H. *Org. Lett.* **2008**, *10*, 4215–4218.
20. Magnus, P.; Stent, M. A. H. *Org. Lett.* **2005**, *7*, 3853–3855.
21. Malona, J. A.; Cariou, K.; Frontier, A. J. *J. Am. Chem. Soc.* **2009**, *131*, 7560–7561.
22. Malona, J. A.; Cariou, K.; Spencer, W. T. I. I. I.; Frontier, A. J. *J. Org. Chem.* **2012**, *77*, 1891–1908.
23. Trost, B. M.; Greenspan, P. D.; Yang, B. V.; Saulnier, M. G. *J. Am. Chem. Soc.* **1990**, *112*, 9022–9024.
24. Gaunt, M. J.; Yu, J.; Spencer, J. B. *J. Org. Chem.* **1998**, *63*, 4172–4173.

Publication N°*4*

Bioisosteric modification of flavaglines.

Zhao, Q., Tijeras-Raballand, A., de Gramont, A., Raymond, E., Désaubry, L., *Tetrahedron Lett*. **2016**, *57*, 2943-2944.

Tetrahedron Letters 57 (2016) 2943–2944

Contents lists available at ScienceDirect

Tetrahedron Letters

journal homepage: www.elsevier.com/locate/tetlet

Bioisosteric modification of flavaglines

Qian Zhao [a], Annemilaï Tijeras-Raballand [b], Armand de Gramont [b], Eric Raymond [b,c], Laurent Désaubry [a,*]

[a] Therapeutic Innovation Laboratory, UMR7200, CNRS/Université de Strasbourg, 67401 Illkirch, France
[b] AAREC Filia Research, Translational Department, Boulogne-Billancourt, France
[c] Department of Oncology, Bichat-Beaujon University Hospital, Paris, France

ARTICLE INFO

Article history:
Received 7 May 2016
Revised 20 May 2016
Accepted 23 May 2016
Available online 24 May 2016

Keywords:
Natural product
Cancer
Total synthesis
Structure–activity relationships

ABSTRACT

Flavaglines represent a class of potent anticancer agents. Herein, we demonstrated that a classical strategy in pharmacomodulation, i.e. the isosteric replacement of an alcohol by an acylamino or a mesylamino moiety leads to inactive compounds. In addition, the development of a convenient method to introduce an azide on the cyclopenta[*b*]benzofuran skeleton of these compounds was achieved using a cyclic sulfite intermediate.

The resistance to treatments and the adverse effects, in particular cardiac ones, remain the two major obstacles to anticancer treatments. Flavaglines, a class of natural compounds coming from plants of the genus *Aglaia* used in traditional Chinese medicine, may tackle both of these issues. Indeed, these cyclopenta[*b*]benzofurans induce apoptosis selectively in cancer cells at nanomolar concentrations.[1–6] In vivo, these compounds display spectacular anticancer effects. As an example they are able to relieve the resistance to B-Raf inhibitors in a mouse model of chemoresistant metastatic melanoma.[3] In addition, flavaglines may prevent the adverse effects of cancer treatments. In particular, we demonstrated that they may alleviate the cardiotoxicity of doxorubicin,[6–8] a widely used chemotherapeutic agent that induces severe cardiac dysfunction. This remarkable profile of pharmacological activities comes from their unique mode of action:—they directly modulate the activity of the scaffold proteins prohibitins-1 and 2 and the translation initiation factor eIF4a. We previously clarified the structural requirements for both their anticancer and cardioprotective activities.[4,6] We demonstrated in particular that the 1-hydroxy can be replaced by a formylamino or a mesylamino moiety without modifying significantly the anticancer and cardioprotective activities (Fig. 1).[6] This observation prompted us to examine whether the replacement of the 8b-hydroxy by the same H bond donors was also tolerated.

Our approach to synthesize was based on Burns and Rizzacasa's observation that the hydrogenolysis of protected flavagline **7** gen-

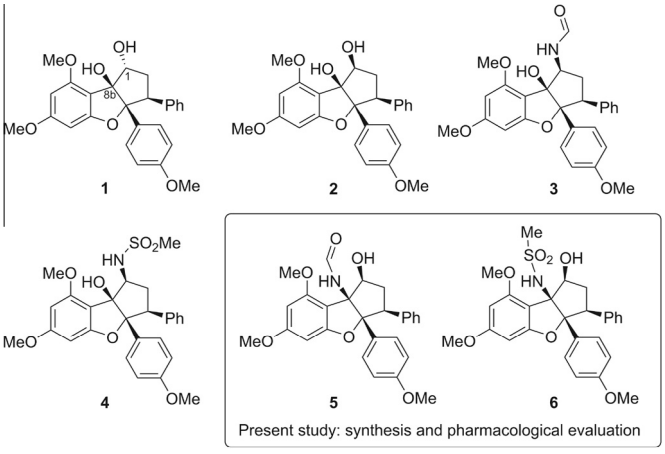

Figure 1. Representative examples of pharmacologically active flavaglines and their isosteres **5** and **6**.

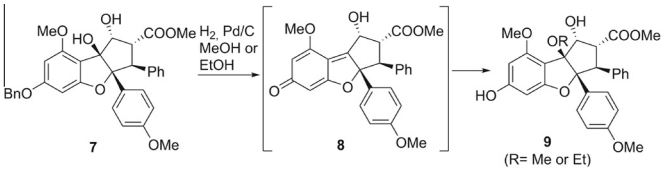

Scheme 1. Serendipitous addition of alcohol to flavaglines reported by Burns and Rizzacasa.[5]

* Corresponding author. Tel.: +33 368 854 141; fax: +33 368 854 310.
E-mail address: desaubry@unistra.fr (L. Désaubry).

http://dx.doi.org/10.1016/j.tetlet.2016.05.089
0040-4039/

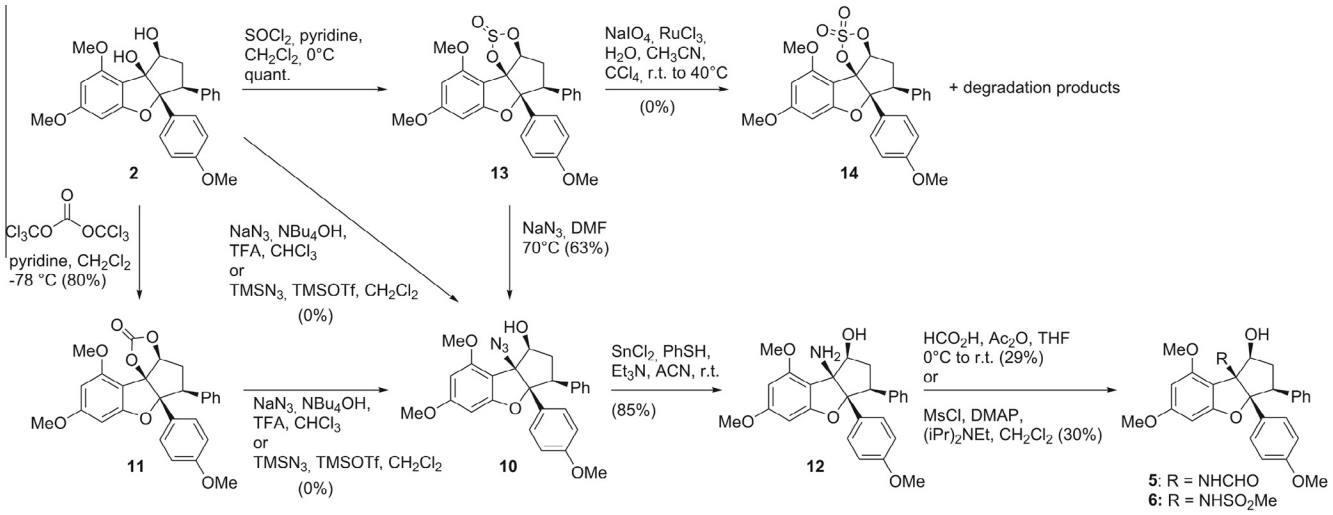

Scheme 2. Synthesis of isosteres **5** and **6**.

erates methyl or ethyl ethers **9** via solvolysis of the intermediate quinone methide **8** (Scheme 1).[5] In addition, similar methyl and ethyl ethers have been isolated from purification of *Aglaia* extracts, suggesting that these compounds may have been generated during the HPLC purification in the presence of an acid via a benzylic carbocationic intermediate.[9,10] Thus, we envisioned synthesizing **5** and **7** from azide **10** prepared from the known carbinol **2**[4] (Scheme 2).

Initial attempt to introduce the azide on diol **2** or carbonate **11** were unsuccessful. These substrates were unreactive. To increase the reactivity of the substrate, we considered using the cyclic sulfate **14**. Unfortunately, oxidation of the intermediate sulfite **13** afforded exclusively degradation products, due to the high reactivity of **14**. This observation suggested that the introduction of the azide could be achieved through the use of sulfite **13**, which is expected to have a reactivity intermediate between those of carbonate **11** and sulfate **14**. This proved to be a key to success.

The azide **10** was remarkably unreactive toward triphenylphosphine, but the use of thiophenol and $SnCl_2$ according to Fuch's method[11] allowed us to prepare amine **12** (85%), which was readily converted to formamide **5** and mesylamide **6**.

The cytotoxicity of **5** and **6** was determined on human cancer cell lines by the MTS assay after a 72 h treatment. Unfortunately, both compounds did not display any significant cytotoxicity in Hep3B and HuH7 cancer cell lines (Fig. S1).

Because of their promising anticancer properties, flavaglines continue to attract much attention from medicinal chemists. Herein, we demonstrated that a classical strategy in pharmacomodulation, i.e. the isosteric replacement of an alcohol by an acylamino or a mesylamino moiety leads to inactive compounds.

Acknowledgments

Generous financial support for this work was provided by the 'Association pour la Recherche sur le Cancer'. We are also grateful to AAREC Filia Research and ANRT for fellowships to Q.Z.

Supplementary data

Supplementary data (cytotoxicity in cancer cells and experimental procedures for the synthesis of **5** and **6**) associated with this article can be found, in the online version, at http://dx.doi.org/10.1016/j.tetlet.2016.05.089.

References and notes

1. Pan, L.; Woodard, J. L.; Lucas, D. M.; Fuchs, J. R.; Douglas Kinghorn, A. *Nat. Prod. Rep.* **2014**, *31*, 924–939.
2. Basmadjian, C.; Thuaud, F.; Ribeiro, N.; Désaubry, L. *Future Med. Chem.* **2013**, *5*, 2185–2197.
3. Boussemart, L.; Malka-Mahieu, H.; Girault, I.; Hemmingsson, O.; Allard, D.; Tomasic, G.; Thomas, M.; Ribeiro, N.; Thuaud, F.; Basmadjian, C.; Mateus, C.; Routier, E.; Kamsu-Kom, N.; Agoussi, S.; Eggermont, A. M.; Désaubry, L.; Robert, C.; Vagner, S. *Nature* **2014**, *513*, 105–109.
4. Thuaud, F.; Bernard, Y.; Turkeri, G.; Dirr, R.; Aubert, G.; Cresteil, T.; Baguet, A.; Tomasetto, C.; Svitkin, Y.; Sonenberg, N.; Nebigil, C. G.; Désaubry, L. *J. Med. Chem.* **2009**, *52*, 5176–5187.
5. Hawkins, B. C.; Lindqvist, L. M.; Nhu, D.; Sharp, P. P.; Segal, D.; Powell, A. K.; Campbell, M.; Ryan, E.; Chambers, J. M.; White, J. M.; Rizzacasa, M. A.; Lessene, G.; Huang, D. C. S.; Burns, C. J. *ChemMedChem* **2014**, *9*, 1556–1566.
6. Ribeiro, N.; Thuaud, F.; Bernard, Y.; Gaiddon, C.; Cresteil, T.; Hild, A.; Hirsch, E. C.; Michel, P. P.; Nebigil, C. G.; Désaubry, L. *J. Med. Chem.* **2012**, *55*, 10064–10073.
7. Bernard, Y.; Ribeiro, N.; Thuaud, F.; Turkeri, G.; Dirr, R.; Boulberdaa, M.; Nebigil, C. G. *PLoS ONE* **2011**, *6*, e25302.
8. Qureshi, R.; Yildirim, O.; Gasser, A.; Basmadjian, C.; Zhao, Q.; Wilmet, J. P.; Désaubry, L.; Nebigil, C. G. *PLoS ONE* **2015**, *10*, e0141826.
9. Dumontet, V.; Thoison, O.; Omobuwajo, O. R.; Martin, M.-T.; Perromat, G.; Chiaroni, A.; Riche, C.; Pais, M.; Sevenet, T.; Hadi, A. H. *Tetrahedron* **1996**, *52*, 6931–6942.
10. Hiort, J.; Chaidir, I.; Bohnenstengel, F. I.; Nugroho, B. W.; Schneider, C.; Wray, V.; Witte, L.; Hung, P. D.; Kiet, L. C.; Proksch, P. *J. Nat. Prod.* **1999**, *62*, 1632–1635.
11. Lee, J. W.; Fuchs, P. L. *Org. Lett.* **1999**, *1*, 179–181.

Publication N°*5*

Flavaglines stimulate transient receptor potential melastatin type 6 (TRPM6) channel activity.

Blanchard, M. G., de Baaij, J. H. F., Verkaart, S. A. J., Lameris, A. L., Basmadjian, C., Zhao, Q., Désaubry, L., Bindels, R. J. M., Hoenderop, J. G., *Plos One*, **2015**, *10*: e0119028.

PLOS | ONE

RESEARCH ARTICLE

Flavaglines Stimulate Transient Receptor Potential Melastatin Type 6 (TRPM6) Channel Activity

Maxime G. Blanchard[1☯], Jeroen H. F. de Baaij[1☯], Sjoerd A. J. Verkaart[1], Anke L. Lameris[1], Christine Basmadjian[2], Qian Zhao[2], Laurent Désaubry[2], René J. M. Bindels[1], Joost G. J. Hoenderop[1*]

1 Department of Physiology, Radboud Institute for Molecular Life Sciences, Radboud University Medical Center, Nijmegen, The Netherlands, **2** Laboratory of Therapeutic Innovation (UMR7200), CNRS-University of Strasbourg, Faculty of Pharmacy, Illkirch, France

☯ These authors contributed equally to this work.
* joost.hoenderop@radboudumc.nl

Citation: Blanchard MG, de Baaij JHF, Verkaart SAJ, Lameris AL, Basmadjian C, Zhao Q, et al. (2015) Flavaglines Stimulate Transient Receptor Potential Melastatin Type 6 (TRPM6) Channel Activity. PLoS ONE 10(3): e0119028. doi:10.1371/journal.pone.0119028

Academic Editor: Stuart E Dryer, University of Houston, UNITED STATES

Received: October 10, 2014

Accepted: January 1, 2015

Published: March 16, 2015

Data Availability Statement: All relevant data are within the paper.

Funding: This work was supported by grants from the Netherlands Organization for Scientific Research (ZonMW 9120.8026, NWO Vici 016.130.668) and the EURenOmics project from the European Union seventh framework programme (FP7/2007-2013, agreement no. 305608). The authors also thank the Association Nationale Recherche Technologie (ANRT) and the Association d'Aide à la Recherche et à l'Enseignement en Cancérologie (AAREC Filia Research) for fellowships to C. Basmadjian and Q.

Abstract

Magnesium (Mg^{2+}) is essential for enzymatic activity, brain function and muscle contraction. Blood Mg^{2+} concentrations are tightly regulated between 0.7 and 1.1 mM by Mg^{2+} (re)absorption in kidney and intestine. The apical entry of Mg^{2+} in (re)absorbing epithelial cells is mediated by the *transient receptor potential melastatin type 6* (TRPM6) ion channel. Here, flavaglines are described as a novel class of stimulatory compounds for TRPM6 activity. Flavaglines are a group of natural and synthetic compounds that target the ubiquitously expressed prohibitins and thereby affect cellular signaling. By whole-cell patch clamp analyses, it was demonstrated that nanomolar concentrations of flavaglines increases TRPM6 activity by ~2 fold. The stimulatory effects were dependent on the presence of the alpha-kinase domain of TRPM6, but did not require its phosphotransferase activity. Interestingly, it was observed that two natural occurring TRPM6 mutants with impaired insulin-sensitivity, TRPM6-p.Val1393Ile and TRPM6-p.Lys1584Glu, are not sensitive to flavagline stimulation. In conclusion, we have identified flavaglines as potent activators of TRPM6 activity. Our results suggest that flavaglines stimulate TRPM6 via the insulin receptor signaling pathway.

Introduction

Magnesium (Mg^{2+}) is an essential electrolyte for cell growth, protein synthesis and enzymatic activity. Therefore, physiological mechanisms maintain blood Mg^{2+} concentrations within a tightly regulated range (0.7–1.1 mM) [1,2]. The apically expressed *Transient Receptor Potential Melastatin type 6* (TRPM6) channels are the gatekeepers of epithelial Mg^{2+} transport in colon and in the distal convoluted tubule segment (DCT) of the kidney nephron [3]. Loss-of-function mutations of TRPM6 cause intestinal Mg^{2+} malabsorption and renal Mg^{2+} wasting, as evidenced in patients suffering from hypomagnesemia with secondary hypocalcemia (HSH, OMIM #602014) [4,5].

Zhao. The funders had no role in study design, data collection and analysis, decision to publish, or preparation of the manuscript.

Competing Interests: The authors have declared that no competing interests exist.

TRPM6 channels are thought to form tetramers of subunits comprising six transmembrane segments, with a central divalent-selective pore (Ba^{2+}>Ni^{2+}>Mg^{2+}>Ca^{2+}) [3]. Functional channels are inhibited by intracellular Mg^{2+} [3,6] and consequently display a time-dependent increase in currents upon dialysis of cells with a pipette solution containing a strong Mg^{2+} chelator such as ethylenediaminetetraacetic acid (EDTA). Like its close homolog TRPM7, TRPM6 channels comprise an intrinsic intracellular Ser/Thr kinase domain, which has similarities to proteins of the alpha-kinase family [7]. TRPM6 channels undergo autophosphorylation, but the role of the alpha-kinase on channel function and cell physiology is still incompletely understood [6,8–11].

Over the last decade, the epidermal growth factor (EGF) and insulin were shown to stimulate the activity and membrane expression of TRPM6 [12,13]. Two TRPM6 single nucleotide polymorphisms (SNPs: p.Val1393Ile and p.Lys1584Glu) were recently associated with an increased risk of diabetes development in humans [13,14]. Subsequently, it was shown that these mutations prevent a rapid insulin-evoked increase in channel plasma membrane expression [13].

By combined pull down and mass spectrometry studies of the TRPM6 alpha-kinase domain, three interacting proteins have been identified: I) *Methionine sulfoxide reductase B1* (MSRB1) which reduces the sensitivity of TRPM6 to oxidative stress [15], II) *Guanine nucleotide-binding protein subunit beta-2-like 1* (GNB2L1/RACK1) which inhibits TRPM6 activity in a alpha-kinase-dependent manner [16]. III) *Prohibitin 2* or *Repressor protein of Estrogen receptor Activity* (PHB2/REA) which inhibits TRPM6, an effect that is relieved by estrogens [17].

Prohibitins (PHB1 and PHB2) are ubiquitously expressed members of the family of stomatin/prohibitin/flotillin and HflK/C (SPFH) domain containing proteins [18–20]. PHBs are found in the nucleus, cytoplasm and plasma membrane, where they play an important role in cellular differentiation, anti-proliferation and mitochondrial morphogenesis. PHBs modulate the cell cycle progression, regulate transcription and facilitate cell surface signaling [18,19]. Recently, a family of natural compounds named flavaglines was established as high affinity ligand of PHBs [21].

Flavaglines are a family of natural compounds characterized by a cyclopenta*[b]*benzofuran structure [22]. Natural flavaglines and synthetic analogs have been intensively studied, owing to their pleiotropic favorable properties (anti-inflammatory, anticancer, cardioprotective and neuroprotective) [23]. Flavaglines bind PHB1 and PHB2 (with nM affinity) and prevent the CRaf-mediated activation of oncogenic MAPK signaling [21]. Additionally and independently from PHBs, flavaglines inhibit *eukaryotic initiation factor-4A* (eIF4A)-dependent oncogenic protein synthesis [23]. In addition, the binding properties of flavaglines to PHB and/or eIF4A lead to the induction of apoptosis in *apoptosis inducing factor* (AIF) and caspase-12-dependent manners [23,24]. The mechanism of flavaglines neuro- and cardioprotection are likely mediated by their PHB-interacting properties, thereby reducing oxidative stress, deleterious growth factor signaling and release of inflammatory mediators [23].

Given the previously described inhibitory interaction of PHB2 on TRPM6 and the high affinity binding of flavaglines to PHB1 and PHB2, this study aims to identify and characterize the effect of flavaglines on TRPM6 activity.

Materials and Methods

Cell culture

Human embryonic kidney cells (HEK293) were grown at 37°C in DMEM (Biowhittaker Europe, Vervier, Belgium) supplemented with 10% (v/v) fetal calf serum (PAA Laboratories, Linz, Austria), non-essential amino acids and 2 mM L-glutamine in a humidified 5% (v/v) CO_2 atmosphere. Cells were seeded in 12-well plates and subsequently transfected with 1 μg of human NH_2-terminal HA-tagged TRPM6 or empty pCINeo IRES GFP vectors (mock) cDNA using Lipofectamine 2000 (Invitrogen) at 1:3 DNA:Lipofectamine ratio. For patch clamp

experiments, cells were seeded two days after transfection on glass coverslips coated with 50 μl/cm^2 of 50 μg/ml fibronectin (Roche, Mannheim, Germany). Two hours later, cells were placed in the recording chamber and selected based on the intensity of the fluorescent reporter.

Electrophysiology

All experiments were undertaken and analyzed using an EPC-9 amplifier and the Patchmaster software (HEKA electronics, Lambrecht, Germany). The sampling interval was set to 200 ms and data was low-pass filtered at 2.9 kHz. Patch clamp pipettes were pulled from thin-walled borosilicate glass (Harvard Apparatus, March-Hugstetten, Germany) and had resistance between 1 and 3 MΩ when filled with the pipette solution. Series resistance compensation was set to 75–95% in all experiments. Current densities were obtained by normalizing the current amplitude to the cell capacitance.

Compound synthesis and purity

FL2, FL3 and FL23 were synthesized as previously described [24,25]. Purity of the compounds was >95%, as assessed by reversed-phase high performance liquid chromatography (HPLC) analyses (Hypersil Gold column 30×1 mm, C18, Thermo Scientific) under the following conditions: flow rate: 0.3 mL/min; buffer A: CH_3CN, buffer B: 0.01% aqueous Trifluoroacetic Acid (TFA); gradient: 98–10% (v/v) buffer B over 8 min (detection: λ = 220/254 nm).

Solutions and compound application

The extracellular solution contained (in mM): 150 NaCl, 1 $CaCl_2$, 10 HEPES/NaOH pH 7.4. The pipette solution was made of (in mM): 150 NaCl, 10 Na_2EDTA, 10 HEPES/NaOH pH 7.2 [3]. Cells were pre-incubated 15 minutes at 37°C in bath solution containing the compound of interest diluted from a 1000x stock solution or vehicle (0.1% v/v dimethyl sulfoxide (DMSO)).

Immunoblotting

HEK293 cells were lysed for 1 hour at 4° C in TNE lysis buffer containing (in mM): 50 Tris/HCl (pH 8.0), 150 NaCl, 5 EDTA, 1% (v/v) Triton X-100 and protease inhibitors (pepstatin 1 μg/ml, PMSF 1 mM, leupeptin 5 μg/ml and aproptin 5 μg/ml). Protein lysates were denatured in Laemmli containing 100 mM dithiothreitol (DTT, 30 minutes, 37°C) and subsequently subjected to SDS-PAGE. Immunoblots were incubated with mouse anti-HA (Roche, high affinity 3F10, 1:5,000), rabbit anti-Akt (Cell signaling, 1:1000) and rabbit anti-ERK1/2 (Cell signaling, 1:1,000) primary antibodies and peroxidase conjugated sheep anti-mouse secondary antibodies (Jackson Immunoresearch, 1:10,000).

Statistical analysis

All results are depicted as mean ± standard error of the mean (SEM). Statistical analysis was conducted by one-way Student's t-test when comparing two treatment groups or experimental conditions. Difference in means with P values <0.05 were considered statistically significant and indicated by a star (*).

Curve fitting

Current time-development curves were fitted with a logistic equation: $I = I_0+((I_{max}-I_0)/(1+(t/t_{1/2})^{-h})^s)$, with I the current density, I_0 the baseline current density, t the time, $t_{1/2}$ the time of half-maximal current density, h the slope and s a parameter. Half-maximal stimulatory

concentration (EC_{50}) was obtained by fitting a Hill equation to the data points: $I = I_0+(I_{max}—I_0) * (([FL23]^n)/(IC_{50}^n+[FL23]^n))$, with I the current density, I_0 the baseline current density obtained in control conditions, I_{max} the maximal current value and n the Hill equation.

Results

Synthetic flavaglines stimulate TRPM6 activity

HEK293 cells were transfected with the previously described pCINeo-TRPM6-HA-IRES-GFP vector [3]. This construct allows the visual identification of cells expressing TRPM6. Cells were then subjected to whole-cell patch clamp analysis, as previously described [3]. Briefly, currents were elicited by a series of voltage ramps applied at 0.5 Hz from a holding voltage of 0 mV. Due to the dialysis of the cytoplasm with a pipette solution containing EDTA, time-dependent outwardly rectifying currents were observed in response to this ramp protocol (Fig. 1A). In order to assess the effect of flavaglines on TRPM6, cells were first exposed to FL23 (50 nM) [25], a potent analog of the established PHB2 ligand FL3 [21]. This protocol yielded a

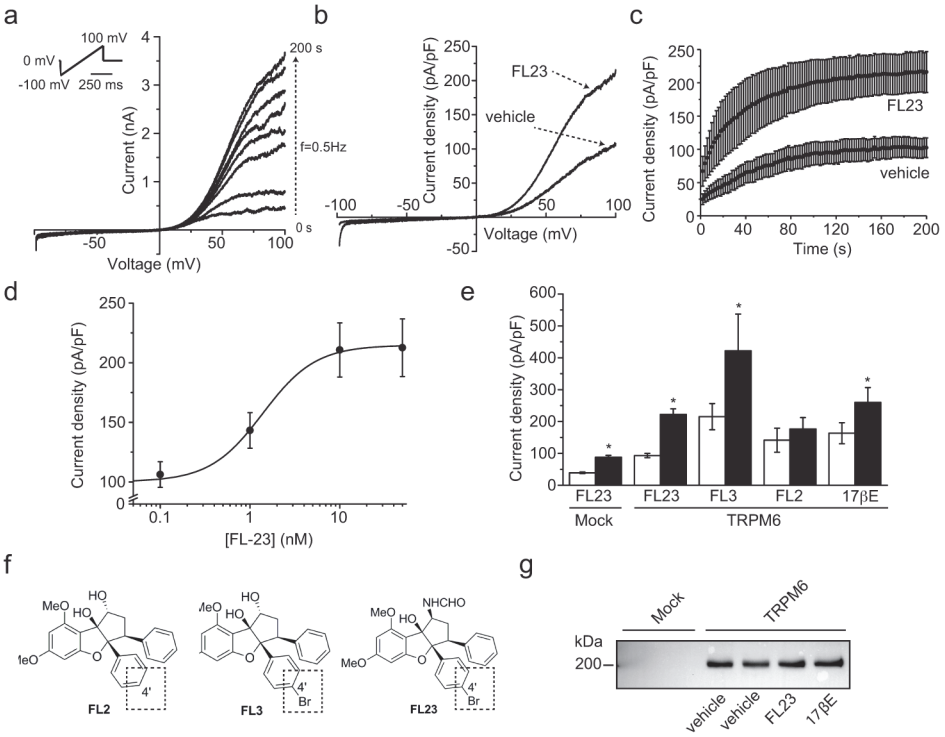

Fig 1. Flavaglines stimulate TRPM6 at nanomolar concentration. a. TRPM6 currents were evoked by a series of 500 ms voltage ramp from -100 to +100 mV applied every 2 s (0.5 Hz) from a holding potential of 0 mV (top left inset). A typical set of current-voltage curves obtained from a single cell is shown. **b.** Typical current-voltage curves obtained 200 s after break-in from cells pre-incubated 15 minutes with vehicle or FL23 (50 nM). **c.** The average time-course of TRPM6 current development with (n = 19) or without (n = 19) FL23 pre-treatment are shown for current values measured at +80 mV. **d.** FL23 increases TRPM6 current density in a concentration-dependent manner (n≥3 per data points). Line represents the fit of data points with a Hill equation (see Material and Methods). **e.** Incubation of TRPM6 expressing cells with FL3 (50 nM, n≥10), FL23 (50 nM, n≥22) or 17βE (50 nM, n≥9) significantly increased the average current densities measured at +80 mV 200 s after break-in. Mock-transfected cells showed a similar increase in current density (n≥8). TRPM6 currents were not sensitive to FL2 (n≥10). Stars indicate statistically significant difference ($P<0.05$) between vehicle- (white bar) and compound-treated cells (black bar). **f.** The chemical structures of FL2, FL3 and FL23 are shown. **g**. Cells were pre-incubated with vehicle, FL23 (50 nM) or 17βE (50 nM). Total lysate were subjected to Western blot analysis using an anti-HA primary antibody. FL23 and estradiol (17βE) did not significantly affect the expression of TRPM6. A representative blot of three separate experiments is shown.

doi:10.1371/journal.pone.0119028.g001

significant increase in the current density without affecting the characteristic shape of the current-voltage (IV) curve (Fig. 1B) or the current time-development characteristics (Fig. 1C). The average time-development curves were fitted with a logistic equation (see Material and Methods). This analysis revealed that the time of half-maximal activation ($t_{1/2}$) was not changed between control and FL23-treated cells (control: 48 ± 2 s, FL23: 43 ± 3 s). The rate of current development (the slope *h*) was increased with FL23 treatment (control: 1.8 ± 0.1 $pApF^{-1}s^{-1}$, FL23: 3.0 ± 0.2 $pApF^{-1}s^{-1}$). Pre-incubation of the cells with concentrations of FL23 ranging from 0.01 to 50 nM revealed a concentration-dependent stimulation of TRPM6 activity with an EC_{50} = 1.4 ± 0.2 nM and Hill equation n = 1.5 ± 0.3 (see Material and Methods, Fig. 1D). A similar increase in TRPM6 activity was observed with FL3 (50 nM, Fig. 2A-B). Next, cells were pre-incubated with FL2 (50 nM, Fig. 1F), a flavagline that does not display significant cytotoxicity in cancer cells [24] nor cytoprotection in cardiomyocytes [26]. In contrast to FL3 and FL23, this treatment did not significantly alter the current density of TRPM6-expressing cells (Fig. 2C-D). As previously reported, estradiol (17βE) significantly stimulated TRPM6 currents (Fig. 1E) [17]. On average, 17βE, FL3 and FL23 stimulated TRPM6 activity by 1.5 to 2-fold (Fig. 1E). Interestingly, mock-transfected cells demonstrated a similar ~2-fold increase in current density upon FL23 treatment, indicating that TRPM7 is also a likely target of flavaglines action (Fig. 1E). As expected from the short pre-incubation period, the expression of TRPM6 was not influenced by FL23 or 17βE (Fig. 1G).

The stimulating effects of flavaglines require the intrinsic kinase domain of TRPM6

To assess the involvement of the intrinsic alpha-kinase domain in the flavagline-mediated potentiation of TRPM6 currents, cells were transfected with the previously described kinase-truncated

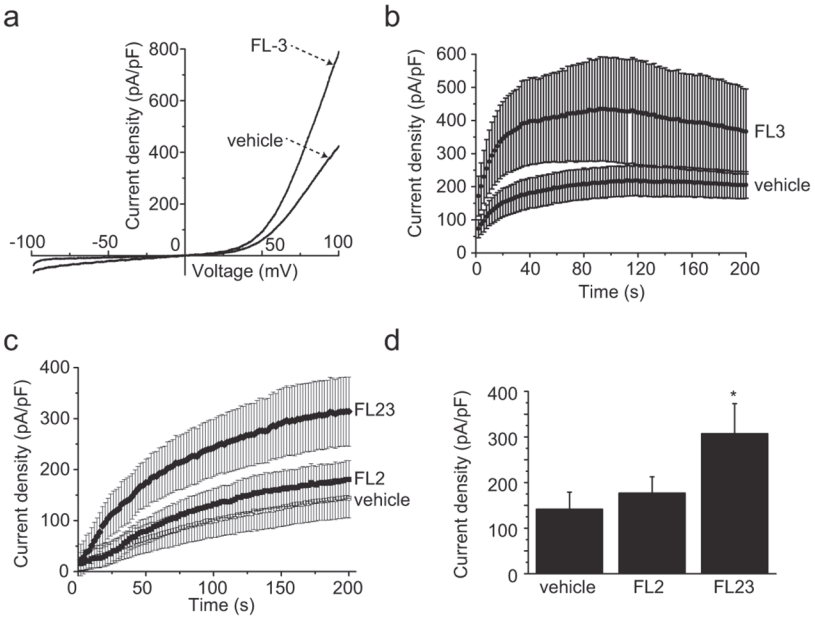

Fig 2. Analogs of FL23 show distinct effects on TRPM6 currents. a. Typical current-voltage curves obtained 200 s after break-in are shown for vehicle and FL23 (50 nM) pre-incubated cells. **b.** The average time-course of TRPM6 current development with (n = 8) or without (n = 11) FL23 (50 nM) is shown for current values measured at +80 mV. **c.** The average time-course of TRPM6 current development with FL2 (50 nM, n = 12), vehicle (n = 10) or FL23 (50 nM, n = 10) pre-treatment is shown for current values measured at +80 mV. **d.** FL2 incubation did not significantly stimulate TRPM6 activity (n≥10). Stars indicate statistically significant difference (P<0.05) between vehicle and compound-treated cells.

doi:10.1371/journal.pone.0119028.g002

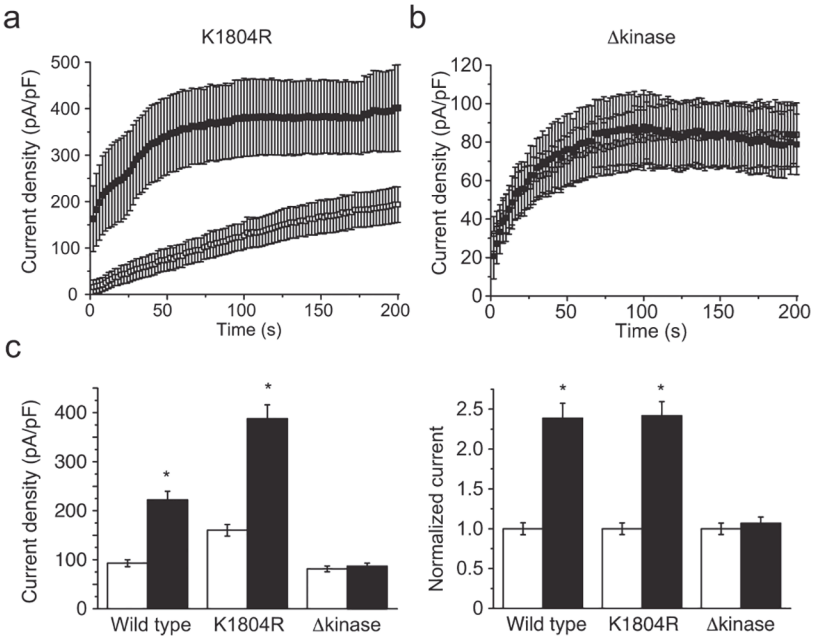

Fig 3. The presence of the intrinsic alpha-kinase domain of the channel but not its activity is required for flavagline-mediated stimulation of TRPM6. a. The average time-course of current development of the kinase-inactive channels ($TRPM6^{K1804R}$) with (n = 7, full symbols) or without (n = 9, empty symbols) FL23 (50 nM) pre-incubation is shown for current values measured at +80 mV. **b.** The average time-course of current development of $TRPM6^{L1749X}$ (Δkinase) with (n = 8, full symbols) or without (n = 9, empty symbols) FL23 (50 nM) pre-incubation is shown for current values measured at +80 mV. **c.** Pre-incubation of cells with FL23 (50 nM) stimulated wild type ($n \geq 22$), K1804R ($n \geq 9$), but not Δkinase ($n \geq 8$, $p > 0.05$) channel activity. Right panel shows current values normalized to each control condition. Stars indicate statistically significant difference ($P < 0.05$) between vehicle- (white bar) and compound-treated cells (black bar).

doi:10.1371/journal.pone.0119028.g003

(p.Leu1749*, Δkinase) or kinase-inactive (p.Lys1804Arg, KI) TRPM6 constructs [9]. While the first construct produces mutant channels lacking the complete kinase domain, the KI construct form channels without intrinsic alpha-kinase phosphotransferase activity. Both constructs produce functional proteins with apparently normal channel function in the absence of intracellular Mg^{2+}. Using an identical pre-incubation protocol, cells expressing the KI mutant demonstrated a FL23-mediated increase in current densities similar to wild type (Fig. 3A and C). In contrast, the Δkinase mutant failed to respond to this treatment (Fig. 3B-C).

Flavaglines act along a shared pathway with insulin

The intracellular amino acid residues p.Val1393 and p.Lys1584 have been shown to independently confer sensitivity of TRPM6 channels to insulin stimulation, probably by altering the phosphorylation of the neighboring p.Thr1391 and p.Ser1583 residues, respectively [13]. Phosphomimicking mutations of either p.Thr1391Asp or p.Ser1583Asp were shown to be permissive in the insulin-mediated potentiation of TRPM6 [13]. To address whether flavaglines act on TRPM6 in a similar way as insulin, cells expressing either of two naturally occurring insulin-insensitive TRPM6 SNPs (p.Val1393Ile or p.Lys1584Glu) were pre-incubated with FL23 (50 nM). These mutants failed to respond to FL23 (Fig. 4A-B and E).

Following the activation of the insulin receptor, a complex multi-branched signaling cascade is activated. One of these branches involves the activation of *Phosphoinositide 3-kinase* (PI3K), Akt and *Ras-related C3 botulinum toxin substrate 1* (Rac1) [27]. Co-expression of TRPM6 together with the constitutively active (p.Gly12Val) or dominant-negative (p.Thr17Asn)

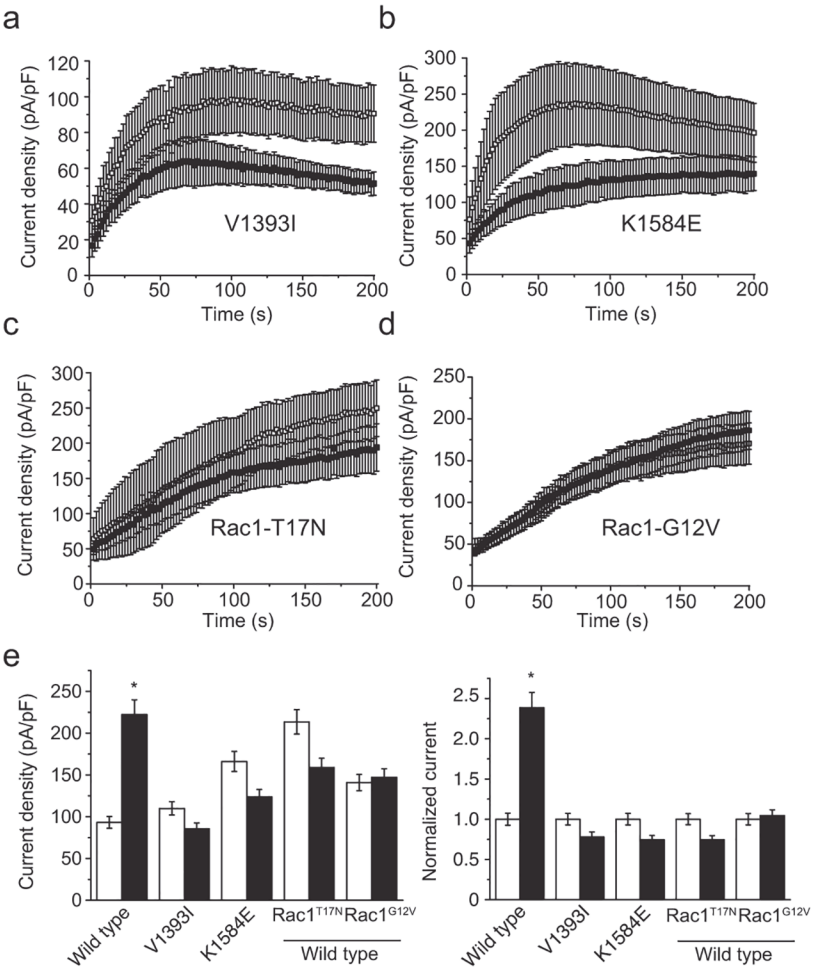

Fig 4. Flavaglines act upon a common pathway with insulin receptor signaling. a-d. The average time-course of current development of cells pre-incubated with (full symbols) or without (empty symbols) FL23 (50 nM) for: (**a**) TRPM6^{V1393I} (n≥8), (**b**) TRPM6^{K1584E} (n≥7), (**c**) wild type TRPM6 together with Rac1^{T17N} (n≥6) and (**d**) wild type TRPM6 together with Rac1^{G12V} (n≥11). **e.** FL23 pre-incubation failed to alter currents in cells expressing TRPM6^{V1393I} (n = 11), TRPM6^{K1584E} (n≥8) and cells co-expressing wild type TRPM6 together with Rac1^{T17N} (n = 8) and TRPM6 together with Rac1^{G12V} (n≥14). Right panel shows current values normalized to each control condition. Stars indicate statistically significant difference ($P<0.05$) between vehicle- (white bar) and compound-treated cells (black bar).

doi:10.1371/journal.pone.0119028.g004

mutants of Rac1 have been shown to respectively allow and prevent the increase of TRPM6 membrane expression by insulin [13]. Here, cells were co-transfected with TRPM6 and either the p.Thr17Asn or p.Gly12Val Rac1 mutants. Both mutants prevented the stimulation of TRPM6 by FL23 (Fig. 4C-D and F).

Flavaglines do not affect Akt phosphorylation

Given the previously described modulation of Akt by PHBs [28], the effects of flavaglines on Akt phosphorylation were examined using the same experimental conditions as were used in the patch clamp experiments. Following 15 minutes of incubation, phosphorylation of Akt was not induced by FL2, FL3 and FL23 (50 nM, Fig. 5). It has been previously demonstrated that flavaglines prevent ERK1/2 phosphorylation in a manner that depends on CRaf [21]. Here,

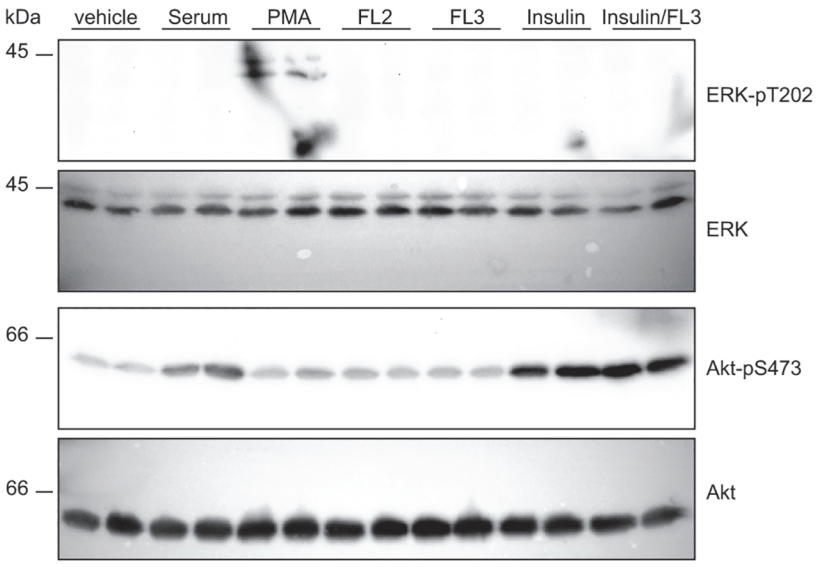

Fig 5. Cellular Akt and ERK signaling is unaffected by FL3. HEK293 cells were incubated with FL2 (50 nM), FL3 (50 nM), PMA (100 nM), insulin (10 nM) or 17βE (50 nM) for 15 minutes. Protein lysates were immediately obtained and immunoblots were performed to detect pERK1/2 and pAkt. PMA and insulin served as positive controls for ERK and Akt phosphorylation, respectively.

doi:10.1371/journal.pone.0119028.g005

basal ERK1/2 phosphorylation was not apparent in control condition and no additional phosphorylation was detected upon flavaglines stimulation (Fig. 5).

Discussion

The present study demonstrates that the activity of the Mg^{2+}-permeant TRPM6 channel is stimulated ~2-fold by the flavaglines compounds FL3 and FL23. This is the first report of an exogenous natural compound that stimulates TRPM6 activity.

The activity of TRPM6 and its plasma membrane expression have been shown to be increased upon stimulation with insulin. This effect relied on the PI3K, Akt and Rac1 signaling cascade (Fig. 6). Detailed electrophysiological and total internal reflection fluorescence (TIRF)

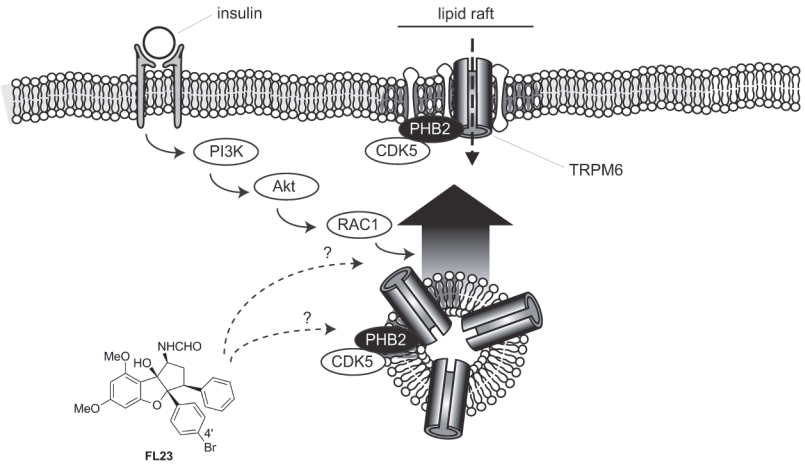

Fig 6. Proposed model of flavaglines action. Flavaglines stimulate TRPM6 activity by acting on downstream effector(s) of the insulin receptor. PHB2 and CDK5, proteins which are known to regulate TRPM6 are localized in lipid rafts.

doi:10.1371/journal.pone.0119028.g006

microscopy analyses have revealed a permissive role for TRPM6-p.Val1393 and TRPM6-p.Lys1584 sites in insulin-evoked insertion of channels in the plasma membrane [13]. Here, it is proposed that flavaglines stimulate TRPM6 by acting along the same pathway (Fig. 6). This hypothesis is based on the following observations: (I) flavaglines increased TRPM6 activity ~1.5–2 fold, which is quantitatively similar to the previously described action of insulin on TRPM6 activity [13]; (II) the insulin-insensitive (TRPM6-p.Val1393Ile and TRPM6-Lys1584-Glu) TRPM6 mutants were not potentiated by flavaglines; (III) flavaglines-induced TRPM6 stimulation was absent when overexpressing TRPM6 together with Rac1 mutants; (IV) in concordance with the mechanism of insulin action on TRPM6, flavaglines stimulated the kinase-inactive (TRPM6-p.Lys1804Arg) mutant. Taken together, it is hypothesized that flavaglines act by triggering or relieving a tonic inhibition on one (or more) of the molecular player(s) involved in insulin signaling, effectively promoting the plasma membrane insertion of wild type TRPM6 channels but not of TRPM6 channels containing insulin-insensitive SNP mutants. Our data suggest that the effects of flavagline-stimulation take place downstream of Akt, since no additional Akt phosphorylation was evident upon treatment with FL3. Further experiments investigating the detailed molecular action of flavaglines on the localization and phosphorylation of the known kinases involved in growth-factor stimulation of TRPM6 (PI3K/Akt/Rac1/Cdk5) will be necessary to elucidate the exact molecular targets.

Flavaglines have recently been identified as potent interactors of PHBs [18,19]. Interestingly, PHB1 and PHB2 are enriched in detergent resistant (lipid rafts) fractions of the plasma membrane [18]. Given the previously described action of PHBs as chaperone of Ras-dependent CRaf activation in the plasma membrane [21], a general function of PHBs is to provide spatial constraints necessary for the proper regulation of proteins in specialized regions (*eg* the lipid rafts) of the plasma membrane. It can be hypothesized that TRPM6 channels transiently or permanently localize together with PHB in the lipid raft fractions of the plasma/vesicular membrane, where channels undergo regulatory phosphorylation. The following facts support this hypothesis: (I) TRPM6 has been shown to establish a inhibitory interaction with PHB2 [17]; (II) TRPM6 requires CDK5 phosphorylation for proper insulin-mediated regulation, CDK5 localizing and being activated in the lipid raft fraction of plasma membrane [29]; (III) the close homolog TRPM7 has been reported to localize in lipid rafts [30], (IV) TRPM6 requires PIP2 for proper function [31], a lipid that is enriched in lipid rafts. Therefore, it is tempting to speculate that PHBs binding to TRPM6 promotes the formation of a macromolecular regulatory complex in the lipid rafts of the plasma membrane. In this perspective, it is interesting to note that the insulin-induced signaling pathway becomes more active when the insulin receptor is expressed in lipid rafts [32–34]. In addition to the inhibitory PHB2-TRPM6 interaction, other TRP channels are modulated by members of the SPFH protein family [20]. Podocin, an SPFH protein similar to prohibitin, regulates the insulin sensitive *transient receptor potential canonical type 6* (TRPC6) ion channel in the kidney [35]. In line with the current hypothesis, it has been proposed that podocin organize TRPC6-lipid complexes in the plasma membrane, thereby modulating channel activity [36]. Altogether, these findings point towards a compartmentalized insulin signaling cascade on/near the lipid rafts in the vesicular/plasma membrane. In this model, expression of TRPM6 and the insulin receptor in the lipid rafts allows for the rapid local regulation of TRPM6 by insulin.

Comparison of structure-function activity between active (FL3, FL23) and inactive (FL2) flavaglines analogs revealed a positive correlation between cytostatic/cytotoxic properties of flavaglines in cancer cell lines and their action on TRPM6 [21,24,25]. While the effects of flavaglines on cellular proliferation and growth factor signaling were evident starting from 2 hours after compound application, the stimulatory effect shown here occurs within 15 minutes. These results suggest that the short-term effects of flavaglines on TRPM6 take place

independently from any translational effect (*eg* eIF4A-dependent). However, the concurrent structure-function relationship of flavaglines in their TRPM6-stimulatory effects and in their cytotoxic properties suggests that both mechanisms are PHB-dependent. It has previously been shown that PHB2 interacts with TRPM6 and that 17βE reduces this inhibitory interaction [17]. However, the current results suggest that 17βE and FL23 only share a partially overlapping mechanism of action. Exogenous PHB2 inhibits TRPM6 in an alpha-kinase phosphotransferase-dependent manner [17]. In contrast, flavaglines stimulated the kinase-inactive TRPM6-p.Lys1804Arg mutant. Moreover, flavaglines induce an increase in endogenous TRPM7 currents, while TRPM7 currents were insensitive to PHB2-mediated inhibition [17]. Further work identifying the major players that are part of the TRPM6-PHB macromolecular complex and its regulation by flavaglines and 17βE are necessary to further understand the stimulatory but slightly distinct effects of these compounds on the activity of TRPM6.

Evidences suggest that the stimulatory action of flavaglines is not restricted to TRPM6. Here, a stimulatory effect of FL23 was also observed in mock-transfected cells. Given the experimental conditions used in this study, a substantial part of the current in mock-transfected HEK293 cells is carried by endogenous TRPM7 channels [3]. Further experiments investigating the action of flavaglines on other members of the SPFH protein and TRP channel (*eg* TRPC6) families will be needed to understand the complex mechanism of action of flavaglines.

Reduced TRPM6 channel activity results in a clinically relevant hypomagnesemia due to renal Mg^{2+} wasting. Because insulin and EGF stimulate TRPM6 function, patients with diabetes mellitus type 2 or users of EGFR inhibitors are at risk to develop hypomagnesemia [12,13]. Given that FL3 and FL23 stimulate TRPM6 activity, flavaglines may provide an important therapeutic potential for these patient groups. A preliminary experiment with FL3 (daily i.p. injection 0.1 mg/kg, 7 days,) did not reveal changes in serum or urinary Mg^{2+} concentration in mice (data not shown). In addition to the optimization of treatment duration, the actual dose of FL3 reaching the DCT cells in the kidney where TRPM6 is located may be much lower and challenging to assess. Future experiments assessing the bioavailability of flavaglines should be performed to assess putative magnesiotropic effects *in vivo*. Additionally, given the physiological mechanism of intestinal and/or renal compensation of Mg^{2+} transport, the effects of flavaglines should be assessed in a murine model of hypomagnesemia.

In conclusion, the natural compounds flavaglines stimulate the activity of TRPM6 Mg^{2+} channels at nanomolar concentrations. The effect is rapid (within 15 minutes) and probably relies on a near-plasma membrane mechanism that likely involves PHBs.

Author Contributions

Conceived and designed the experiments: MB JDB SV RB JH. Performed the experiments: MB JDB SV AL. Analyzed the data: MB JDB RB JH. Contributed reagents/materials/analysis tools: CB QZ LD. Wrote the paper: MB JDB LD JH RB.

References

1. de Baaij JH, Groot Koerkamp MJ, Lavrijsen M, van Zeeland F, Meijer H, Holstege FC, et al. Elucidation of the distal convoluted tubule transcriptome identifies new candidate genes involved in renal Mg(2+) handling. Am J Physiol Renal Physiol. 2013; 305: F1563–1573. doi: 10.1152/ajprenal.00322.2013 PMID: 24089412
2. de Baaij JHF, Hoenderop JGJ, Bindels RJM. Regulation of magnesium balance: lessons learned from human genetic disease. Clinical kidney journal. 2012; 5: i15–i24.
3. Voets T, Nilius B, Hoefs S, van der Kemp AW, Droogmans G, Bindels RJ, et al. TRPM6 forms the Mg2+ influx channel involved in intestinal and renal Mg2+ absorption. J Biol Chem. 2004; 279: 19–25. PMID: 14576148

4. Walder RY, Landau D, Meyer P, Shalev H, Tsolia M, Borochowitz Z, et al. Mutation of TRPM6 causes familial hypomagnesemia with secondary hypocalcemia. Nat Genet. 2002; 31: 171–174. PMID: 12032570
5. Schlingmann KP, Weber S, Peters M, Niemann Nejsum L, Vitzthum H, Klingel K, et al. Hypomagnesemia with secondary hypocalcemia is caused by mutations in TRPM6, a new member of the TRPM gene family. Nat Genet. 2002; 31: 166–170. PMID: 12032568
6. Zhang Z, Yu H, Huang J, Faouzi M, Schmitz C, Penner R, et al. The TRPM6 kinase domain determines the Mg ATP-sensitivity of TRPM7/M6 heteromeric ion channels. J Biol Chem. 2014; doi: 10.1074/jbc.M113.512285.
7. Ryazanova LV, Dorovkov MV, Ansari A, Ryazanov AG. Characterization of the protein kinase activity of TRPM7/ChaK1, a protein kinase fused to the transient receptor potential ion channel. J Biol Chem. 2004; 279: 3708–3716. PMID: 14594813
8. van der Wijst J, Blanchard MG, Woodroof HI, Macartney TJ, Gourlay R, Hoenderop JG, et al. Kinase and channel activity of TRPM6 are co-ordinated by a dimerization motif and pocket interaction. Biochem J. 2014; 460: 165–175. doi: 10.1042/BJ20131639 PMID: 24650431
9. Thebault S, Cao G, Venselaar H, Xi Q, Bindels RJ, Hoenderop JG. Role of the alpha-kinase domain in transient receptor potential melastatin 6 channel and regulation by intracellular ATP. J Biol Chem. 2008; 283: 19999–20007. doi: 10.1074/jbc.M800167200 PMID: 18490453
10. Schmitz C, Dorovkov MV, Zhao X, Davenport BJ, Ryazanov AG, Perraud AL. The channel kinases TRPM6 and TRPM7 are functionally nonredundant. J Biol Chem. 2005; 280: 37763–37771. PMID: 16150690
11. Brandao K, Deason-Towne F, Zhao X, Perraud AL, Schmitz C. TRPM6 kinase activity regulates TRPM7 trafficking and inhibits cellular growth under hypomagnesic conditions. Cell Mol Life Sci. 2014; doi: 10.1007/s00018-014-1647-7.
12. Thebault S, Alexander RT, Tiel Groenestege WM, Hoenderop JG, Bindels RJ. EGF increases TRPM6 activity and surface expression. J Am Soc Nephrol. 2009; 20: 78–85. doi: 10.1681/ASN.2008030327 PMID: 19073827
13. Nair AV, Hocher B, Verkaart S, van Zeeland F, Pfab T, Slowinski T, et al. Loss of insulin-induced activation of TRPM6 magnesium channels results in impaired glucose tolerance during pregnancy. Proc Natl Acad Sci U S A. 2012; 109: 11324–11329. doi: 10.1073/pnas.1113811109 PMID: 22733750
14. Song Y, Hsu YH, Niu T, Manson JE, Buring JE, Liu S. Common genetic variants of the ion channel transient receptor potential membrane melastatin 6 and 7 (TRPM6 and TRPM7), magnesium intake, and risk of type 2 diabetes in women. BMC Med Genet. 2009; 10: 4. doi: 10.1186/1471-2350-10-4 PMID: 19149903
15. Cao G, Lee KP, van der Wijst J, de Graaf M, van der Kemp A, Bindels RJ, et al. Methionine sulfoxide reductase B1 (MsrB1) recovers TRPM6 channel activity during oxidative stress. J Biol Chem. 2010; 285: 26081–26087. doi: 10.1074/jbc.M110.103655 PMID: 20584906
16. Cao G, Thebault S, van der Wijst J, van der Kemp A, Lasonder E, Bindels RJ, et al. RACK1 inhibits TRPM6 activity via phosphorylation of the fused alpha-kinase domain. Curr Biol. 2008; 18: 168–176. doi: 10.1016/j.cub.2007.12.058 PMID: 18258429
17. Cao G, van der Wijst J, van der Kemp A, van Zeeland F, Bindels RJ, Hoenderop JG. Regulation of the epithelial Mg2+ channel TRPM6 by estrogen and the associated repressor protein of estrogen receptor activity (REA). J Biol Chem. 2009; 284: 14788–14795. doi: 10.1074/jbc.M808752200 PMID: 19329436
18. Chowdhury I, Thompson WE, Thomas K. Prohibitins role in cellular survival through Ras-Raf-MEK-ERK pathway. J Cell Physiol. 2014; 229: 998–1004. doi: 10.1002/jcp.24531 PMID: 24347342
19. Thuaud F, Ribeiro N, Nebigil CG, Desaubry L. Prohibitin ligands in cell death and survival: mode of action and therapeutic potential. Chem Biol. 2013; 20: 316–331. doi: 10.1016/j.chembiol.2013.02.006 PMID: 23521790
20. Browman DT, Hoegg MB, Robbins SM. The SPFH domain-containing proteins: more than lipid raft markers. Trends Cell Biol. 2007; 17: 394–402. PMID: 17766116
21. Polier G, Neumann J, Thuaud F, Ribeiro N, Gelhaus C, Schmidt H, et al. The natural anticancer compounds rocaglamides inhibit the Raf-MEK-ERK pathway by targeting prohibitin 1 and 2. Chem Biol. 2012; 19: 1093–1104. doi: 10.1016/j.chembiol.2012.07.012 PMID: 22999878
22. Pan L, Woodard JL, Lucas DM, Fuchs JR, Kinghorn AD. Rocaglamide, silvestrol and structurally related bioactive compounds from Aglaia species. Nat Prod Rep. 2014; 31: 924–939. doi: 10.1039/c4np00006d PMID: 24788392
23. Basmadjian C, Thuaud F, Ribeiro N, Desaubry L. Flavaglines: potent anticancer drugs that target prohibitins and the helicase eIF4A. Future Med Chem. 2013; 5: 2185–2197. doi: 10.4155/fmc.13.177 PMID: 24261894

24. Thuaud F, Bernard Y, Türkeri G, Dirr R, Aubert G, Cresteil T, et al. Synthetic analogue of rocaglaol displays a potent and selective cytotoxicity in cancer cells: involvement of apoptosis inducing factor and caspase-12. Journal of medicinal chemistry. 2009; 52: 5176–5187. doi: 10.1021/jm900365v PMID: 19655762

25. Thuaud F, Ribeiro N, Gaiddon C, Cresteil T, Desaubry L. Novel flavaglines displaying improved cytotoxicity. J Med Chem. 2011; 54: 411–415. doi: 10.1021/jm101318b PMID: 21142180

26. Bernard Y, Ribeiro N, Thuaud F, Turkeri G, Dirr R, Boulberdaa M, et al. Flavaglines alleviate doxorubicin cardiotoxicity: implication of Hsp27. PLoS One. 2011; 6: e25302. doi: 10.1371/journal.pone.0025302 PMID: 22065986

27. Bezzerides VJ, Ramsey IS, Kotecha S, Greka A, Clapham DE. Rapid vesicular translocation and insertion of TRP channels. Nat Cell Biol. 2004; 6: 709–720. PMID: 15258588

28. Ande SR, Mishra S. Prohibitin interacts with phosphatidylinositol 3,4,5-triphosphate (PIP3) and modulates insulin signaling. Biochem Biophys Res Commun. 2009; 390: 1023–1028. doi: 10.1016/j.bbrc.2009.10.101 PMID: 19854158

29. Okada S, Yamada E, Saito T, Ohshima K, Hashimoto K, Yamada M, et al. CDK5-dependent phosphorylation of the Rho family GTPase TC10(alpha) regulates insulin-stimulated GLUT4 translocation. J Biol Chem. 2008; 283: 35455–35463. doi: 10.1074/jbc.M806531200 PMID: 18948252

30. Yogi A, Callera GE, Tostes R, Touyz RM. Bradykinin regulates calpain and proinflammatory signaling through TRPM7-sensitive pathways in vascular smooth muscle cells. Am J Physiol Regul Integr Comp Physiol. 2009; 296: R201–207. doi: 10.1152/ajpregu.90602.2008 PMID: 18799634

31. Xie J, Sun B, Du J, Yang W, Chen HC, Overton JD, et al. Phosphatidylinositol 4,5-bisphosphate (PIP(2)) controls magnesium gatekeeper TRPM6 activity. Sci Rep. 2011; 1: 146. doi: 10.1038/srep00146 PMID: 22180838

32. Cohen AW, Razani B, Wang XB, Combs TP, Williams TM, Scherer PE, et al. Caveolin-1-deficient mice show insulin resistance and defective insulin receptor protein expression in adipose tissue. Am J Physiol Cell Physiol. 2003; 285: C222–235. PMID: 12660144

33. Morino-Koga S, Yano S, Kondo T, Shimauchi Y, Matsuyama S, Okamoto Y, et al. Insulin receptor activation through its accumulation in lipid rafts by mild electrical stress. J Cell Physiol. 2013; 228: 439–446. doi: 10.1002/jcp.24149 PMID: 22740366

34. Vainio S, Heino S, Mansson JE, Fredman P, Kuismanen E, Vaarala O, et al. Dynamic association of human insulin receptor with lipid rafts in cells lacking caveolae. EMBO Rep. 2002; 3: 95–100. PMID: 11751579

35. Anderson M, Kim EY, Hagmann H, Benzing T, Dryer SE. Opposing effects of podocin on the gating of podocyte TRPC6 channels evoked by membrane stretch or diacylglycerol. Am J Physiol Cell Physiol. 2013; 305: C276–289. doi: 10.1152/ajpcell.00095.2013 PMID: 23657570

36. Huber TB, Schermer B, Benzing T. Podocin organizes ion channel-lipid supercomplexes: implications for mechanosensation at the slit diaphragm. Nephron Exp Nephrol. 2007; 106: e27–31. PMID: 17570936

Publication N°*6*

FL3, a synthetic flavagline and ligand of prohibitins, protects cardiomyocytes via STAT3 from doxorubicin toxicity.

Qureshi, R., Yildirim, O., Gasser, A., Basmadjian, C., Zhao, Q., Wilmet, J-P., Désaubry, L., Nebigil, C.G., *Plos One.,* **2015**, *11*, e0141826.

PLOS ONE

RESEARCH ARTICLE

FL3, a Synthetic Flavagline and Ligand of Prohibitins, Protects Cardiomyocytes via STAT3 from Doxorubicin Toxicity

Rehana Qureshi[1☯], Onur Yildirim[1☯], Adeline Gasser[1], Christine Basmadjian[2], Qian Zhao[2], Jean-Philippe Wilmet[1], Laurent Désaubry[2,3]*, Canan G. Nebigil[1]*

1 GPCRs in cardiobiology and Metabolism team, UMR 7242, CNRS–University of Strasbourg, LabEx Medalis, Strasbourg School of Biotechnology, Illkirch, France, **2** Laboratory of Therapeutic Innovation (UMR 7200), Faculty of Pharmacy, University of Strasbourg–CNRS, Illkirch, France, **3** Sino-French Joint Lab of Food Nutrition/Safety and Medicinal Chemistry, College of Biotechnology, Tianjin University of Science and Technology, Tianjin, 300457, China

☯ These authors contributed equally to this work.
* desaubry@unistra.fr (LD); nebigil@unistra.fr (CGN)

Citation: Qureshi R, Yildirim O, Gasser A, Basmadjian C, Zhao Q, Wilmet J-P, et al. (2015) FL3, a Synthetic Flavagline and Ligand of Prohibitins, Protects Cardiomyocytes via STAT3 from Doxorubicin Toxicity. PLoS ONE 10(11): e0141826. doi:10.1371/journal.pone.0141826

Editor: Partha Mukhopadhyay, National Institutes of Health, UNITED STATES

Received: March 31, 2015

Accepted: October 13, 2015

Published: November 4, 2015

Data Availability Statement: All relevant data are within the paper.

Funding: This work was supported by the "Association pour la Recherche sur le Cancer" (ARC, grant numbers 3940, SFI20111204054 and PJA 20141201909) and the "Agence National la Recherche" (ANR, grant number ANR-11-EMMA-021). This work has also been published within the LABEX ANR-10-LABX-0034_Medalis and received a financial support from the French government managed by Agence Nationale de la recherche under Programme d'investissement d'avenir. Christine

Abstract

Aims

The clinical use of doxorubicin for the treatment of cancer is limited by its cardiotoxicity. Flavaglines are natural products that have both potent anticancer and cardioprotective properties. A synthetic analog of flavaglines, FL3, efficiently protects mice from the cardiotoxicity of doxorubicin. The mechanism underlying this cardioprotective effect has yet to be elucidated.

Methods and Results

Here, we show that FL3 binds to the scaffold proteins prohibitins (PHBs) and thus promotes their translocation to mitochondria in the H9c2 cardiomyocytes. FL3 induces heterodimerization of PHB1 with STAT3, thereby ensuring cardioprotection from doxorubicin toxicity. This interaction is associated with phosphorylation of STAT3. A JAK2 inhibitor, WP1066, suppresses both the phosphorylation of STAT3 and the protective effect of FL3 in cardiomyocytes. The involvement of PHBs in the FL3-mediated cardioprotection was confirmed by means of small interfering RNAs (siRNAs) targeting PHB1 and PHB2. The siRNA knockdown of PHBs inhibits both phosphorylation of STAT3 and the cardioprotective effect of FL3.

Conclusion

Activation of mitochondrial STAT3/PHB1 complex by PHB ligands may be a new strategy against doxorubicin-induced cardiotoxicity and possibly other cardiac problems.

Introduction

Anthracyclines (*e.g.*, doxorubicin) remain a mainstay therapy for cancers such as leukemias, lymphomas, and breast and gastric cancers, even though these compounds cause substantial cardiotoxicity that can ultimately lead to congestive heart failure [1]. Therefore, approaches to

Basmadjian and Qian Zhao were supported by AAREC Filia Research and the Association Nationale de la Recherche et de la Technologie. Onur Yildirim received an Erasmus fellowship. This work was supported by grants from Centre National de la Recherche Scientifique, and Université de Strasbourg. The funders had no role in study design, data collection and analysis, decision to publish, or preparation of the manuscript.

Competing Interests: The authors have declared that no competing interests exist.

alleviation of the cardiotoxic effects of doxorubicin are urgently needed in oncology. Dexrazoxane, which is the only clinically approved cardioprotectant against anthracycline cardiotoxicity, had been shown to induce secondary tumors and was consequently removed from the European market [2]. Thus, there is a need for efficacious and safe drugs that can protect cancer patients from the cardiotoxicity of anthracyclines.

Flavaglines are natural products isolated from Chinese medicinal plants that have potent anticancer effects without toxicity to healthy tissues [3]. Not only are flavaglines specifically toxic to cancer cells, but they also promote the survival of neurons, T lymphocytes, and cardiomyocytes under conditions of adverse effects of chemotherapeutic agents: cisplatin, etoposide, and doxorubicin respectively [4–6]. In particular, in a previous study, we found that a synthetic flavagline, FL3, almost doubles the survival rate of mice (56% treated versus 31% untreated) in an in vivo model of doxorubicin-induced acute cardiotoxicity [4]. Recently, we also showed that flavaglines directly bind to prohibitins (PHBs) in cancer cells [7]. PHBs are scaffold proteins that exist in two isoforms: PHB1 and PHB2 [8]. PHBs seem to perform a function in cancer cells that is different from that in healthy cells: PHBs may be located in several compartments, but they are mainly concentrated in mitochondria in healthy cells and in the nucleus in cancer cells [8]. This divergence of cellular localization (and possibly function) may explain why flavaglines promote apoptosis in cancer cells and survival in healthy cells.

PHB1 has been shown to prevent mitochondrial dysfunction via activating STAT3 in intestinal epithelium (as reviewed elsewhere [9]), but whether this event occurs in cardiomyocytes remains unreported. STAT3 phosphorylation [10] and overexpression [11] have been shown to protect the heart from doxorubicin-induced cardiotoxicity. Moreover, cardiac-restricted deletion of STAT3 increases the susceptibility to doxorubicin-induced heart failure [12, 13].

In this study our aim was to determine whether flavaglines exert their cardioprotective effect by modulating PHB1 localization and activating STA3 signaling.

Methods

Cell culture

The H9c2 cardioblast cell line that was derived from an embryonic rat heart was obtained from American Type Culture Collection (Manassas, VA, USA). The cells were grown in Dulbecco's modified Eagle's medium (DMEM) supplemented with 10% fetal calf serum at 37°C in a humidified atmosphere containing 5% CO_2. The medium was changed every 2–3 days.

The *in vitro* cardiotoxicity assay

H9c2 cells were plated and grown for 24 h in 100-mm culture dishes at $7 \times 10^3/cm^2$. Next, the cells were washed and cultured for 12 h in a glucose-free medium (Gibco; DMEM with L-glutamine, without D-glucose and sodium pyruvate) supplemented with only 1% fetal calf serum. The cells were pretreated with FL3 (100 nM) under serum-free conditions for 10 h, and then either doxorubicin (1 μM) or vehicle alone (DMSO) was added to the medium for additional incubation for 14 h. The doxorubicin concentration and incubation time were chosen in accordance with a known model of acute cardiotoxicity [14]. The H9c2 cardiomyocytes were preincubated with WB1066 (1 μM) for 1 h before FL3 treatment. The cells were then washed, and either terminal deoxynucleotidyl transferase dUTP nick end labeling (TUNEL) or fluorescence-activated cell sorting (FACS) analysis was performed.

Detection and quantification of apoptosis

Terminal deoxynucleotidyl transferase dUTP nick end labeling (TUNEL) assays of fragmented DNA was performed according to according to the manufacturer's instructions (Millipore) [4]. Cells were fixed in 4% formaldehyde, permeabilized. The cells were incubated with TdT terminal transferase and fluorescein-dUTP. Then, the cells were counterstained with 4',6-diamidino-2-phenylindole (DAPI). The TUNEL labeling index was calculated as the percentage of DAPI-stained TUNEL-positive cells among total DAPI-labeled cells by viewing each visual field at 40× magnification. Generally, 10 different visual fields containing around 20 cells were analyzed in each sample, and each experiment was repeated at least three times.

Apoptosis was also analyzed by FACS analysis (FACSCalibur, Becton-Dickinson Biosciences, Le Pont De Claix, France). We harvested 7×10^3 cells and washed them with "annexin binding buffer" (0.01 M HEPES, 0.14 M NaCl, 2.5 mM $CaCl_2$) and labeled the cells with annexin V (dilution 1:50) and Topo (6.7 μg/mL). All assays were performed at least in triplicate, and the results were analyzed in the BD Cell Quest Pro software (Becton-Dickinson Biosciences).

Pull-down assay

This assay was performed by means of FL3-Affigel as described previously [7]. One hundred million H9c2 cells were washed in PBS and lysed in 2 mL of a lysis buffer consisting of 50 mM Tris-HCl pH 8.0, 120 mM NaCl, 1% NP-40, 5 mM dithiothreitol (DTT), 200 μM Na_3VO_4, 25 mM NaF, and a protease inhibitor cocktail (Roche Diagnostics, Switzerland). Cellular debris were removed by centrifugation at 10 000 × *g* for 30 min. Five hundred micrograms of total protein extract was incubated for 12 h at 4°C with 40 μL of FL3-Affigel, negative control (NC)-coupled beads, or uncoupled Affi-Gel beads. The beads were extensively washed with the lysis buffer, and the bound proteins were eluted and reduced in a sample buffer consisting of 63 mM Tris-HCl pH 6.8, 2% SDS, 10% glycerol, a trace of bromophenol blue (0.05%), and 200 mM DTT for 30 min at 65°C. After cooling on ice, each sample was alkylated with a final concentration of 150 mM iodoacetamide for additional 30 min. The proteins were separated by SDS-PAGE (10% gel; Bio-Rad Laboratories, USA) and western blot analyses were performed using anti-PHB1 and anti-PHB2 antibodies.

Immunohistochemical analysis

H9c2 cells were plated and grown for 24 h in Labtek-8 dishes at the density 2×10^4/well in an incubator with 5% CO_2 at 37°C. The medium was changed to DMEM containing 2% fetal calf serum for starvation of the cells for 24 h. After the starvation procedure, the cells were pretreated with MitoTracker Red CMXRos (Life Technologies) for 1 h, then treated with 0.1% dimethyl sulfoxide (DMSO) as a vehicle or FL3 (100 nM) for 0, 5, 10, 15, 30, 45, or 60 min. After that, the cells were fixed with 3.7% (v/v) formaldehyde for 15 min at room temperature and incubated with a blocking solution consisting of 5% BSA (bovine serum albumin) and 1% Triton X-100 in PBS at room temperature for 1 h. The cells were incubated with the anti-PHB1 antibody at 4°C overnight and then incubated for 1 h with an Alexa Fluor 488-conjugated anti-rabbit IgG antibody (Life Technologies/Molecular Probes) [15]. The cells were mounted on slides with the Vectashield Mounting Medium (Vector Labs) and DAPI for counterstaining of the nucleus. The cell images were acquired using a Leica TCS SP5 Confocal Microscopy System (Leica M, Germany) equipped with a 63×/1.40 NA oil-immersion objective lens. The images were captured at the scanning speed of 400 Hz and image resolution 512 × 512 pixels and were then analyzed using the Leica Application Suite, Advanced Fluorescence (LAS AF) software.

Plasmid transfection

The PE935 (PHB1-Flag) and PE936 (PHB2-Flag) plasmids were transfected into H9c2 cells using Jet Prime (POL114-07, PolyPlus Transfection). The cells at 60–80% confluence in a 60-cm^2 culture plate were incubated with an antibiotic-free medium. Twelve micrograms of plasmid DNA was used for the transfection. Forty-eight hours after the transfection, the FLAG-PHB1 and FLAG-PHB2 proteins were purified from the transfectant H9c2 cells by immunoprecipitation using an anti-FLAG antibody and FLAG-peptide elution.

Protein purification by immunoprecipitation

Immunoprecipitation of PHBs with the anti-FLAG antibody from the transfectant H9c2 cells was performed as described previously [7]. The H9c2 cells were incubated for 0, 15, or 30 min with FL3 (Enzo Life Sciences). Subsequently, the cells were washed in ice-cold PBS, lysed in the IP buffer (20 mM Tris-HCl, 5 M NaCl, 2 mM EDTA, 1% Triton X-100, and protease inhibitors) and centrifuged (10 000 × *g*, 20 min) to clear the lysates. Aliquots were taken for input control, and the lysates were incubated with protein G Plus/A-agarose beads (#IP10, Calbiochem) for 30 min at 4°C, then overnight with an anti-FLAG antibody (anti-FLAG M2, Sigma-Aldrich, St. Louis, MO, USA; cat. # F1804). After that, the immunoprecipitates were washed with a lysis buffer (1% NP-40, 300 mM NaCl, 10% glycerin, 10 mM Tris-HCl pH 7.5), then a buffer without salt (1% NP-40, 10% glycerin, 10 mM Tris pH 7.5), and centrifuged for 10 min at 20 000 rpm and 4°C. Next, the samples were boiled in a denaturing sample buffer at 95°C for 5 min. The binding of STAT3 to the PHB1 proteins was detected by western blot analyses using anti-STAT3 or anti-phospho-STAT3 antibodies (Cell Signaling).

Subcellular fraction of H9c2 cells and the STAT3 phosphorylation assay via western blotting

H9c2 cells were plated and grown for 24 h. Next, the cells were washed and cultured for 12 h in the above-mentioned glucose-free medium, supplemented with only 1% fetal calf serum. The cells were then incubated with either FL3 or vehicle alone (0.1% DMSO) for 0, 5, 10, 15, or 30 min and harvested with a lysis buffer (50 mM Tris-HCl pH 7.0, 1 mM EDTA, 100mM NaCl, 0.1% SDS, 1% NP-40, 1 mM Na_3VO_4, 1 mg/mL aprotinin, 1 mg/mL pepstatin, and 1 mg/mL leupeptin). The whole-cell lysates were centrifuged at 12 000 × g for 15 min at 4°C. The cell debris was removed.

Cytoplasmic and mitochondrial fractions from cultured cells were prepared using Subcellular Protein Fractionation Kit for Cultured Cells (Thermo Scientific) and nuclear isolation kit, employing the nuclear protein extraction buffer (20 mM Tris–HCl, pH 7.6, 50 mM KCl, 400 mM NaCl, 1 mM EDTA, 0.2 mM PMSF, 5 mM β-mercaptoethanol, aprotinin (1000 U/ml), 1% Triton X-100, and 20% glycerol as described [16]. 30μg of total protein, 5μg or 10μg of cytosolic, mitochondrial proteins or nuclear protein were used for Western blot analyses. The proteins were separated under denaturing conditions using SDS-PAGE (10% gel) and transferred to a polyvinylidene difluoride (PVDF) membrane. The blots were incubated with a blocking solution consisting of a 5% solution of a fat-free milk powder in PBS-T (PBS plus Tween 20, 0.1%) at room temperature for 1 h. After three washes with PBS-T for 10 min, the blots were incubated overnight at 4°C with gentle shaking with a primary antibody anti-phospho-STAT3 antibody Ser (727) (Cell Signaling), (1:500 dilution in PBS-T containing 0.5% of the fat-free milk powder) or PHB1 (Cell Signaling).

After three washes with PBS-T, the membrane was incubated for 1 h at room temperature with gentle shaking with a horseradish peroxidase-conjugated goat anti-IgG antibody (1:1000

dilution) in PBS-T containing 0.5% of the fat-free milk powder. The expected bands were visualized after 5-min incubation to induce enzyme-linked chemiluminescence (GE HealthCare), and then the blots were washed, stripped, and reprobed with a Total -STAT3 antibody (Cell Signaling) or vinculin (Cell Signaling) or actin (Santa Cruz) as internal control, followed by incubation with a suitable secondary antibody. The phospho-STAT3 or PHB1 signals were quantified by scanning laser densitometry and normalize to total amounts of the corresponding STAT3 or vinculine protein, respectively.

Transfection with small interfering RNA (siRNA)

A 50-nM solution of siRNA against rat PHB2 (Ambion; siRNA #258474) or a mixture (10 nM each) of siRNAs against rat PHB2 and PHB1 (Ambion, USA; siRNA #199561) were used for transfection of 90%- to 95%-confluent cells in a serum-free medium. Nonspecific siRNA (Ambion) served as a negative control. The transfection was based on Lipofectamine 2000 (Invitrogen, USA), according to the manufacturer's instructions. Forty-eight hours after the transfection, the PHB1 levels were measured by quantitative PCR and western blot analysis.

Statistical analysis

All samples were prepared (and used in experiments) at least in triplicate. The results of the quantitative experiments were expressed as mean ± SEM. Multigroup comparisons were performed using one-way analysis of variance (ANOVA) with *post hoc* Bonferroni's correction. Comparisons between two groups were conducted using unpaired Student's *t* test. In all analyses, $p < 0.05$ was assumed to denote statistical significance. All calculations were performed in the Prism software.

Results

FL3 binds to PHB1 and PHB2 in cardiomyocytes

To test whether FL3 binds to PHBs in cardiomyocytes, we performed a pull-down assay with protein extracts of the H9c2 cardiomyocytes using a biologically active flavagline (FL3) conjugated to Affi-Gel beads [7,17]. Whole-cell extracts from H9c2 cells (input), the bound and eluted proteins (Affi-Gel-FL3), and output proteins (output Affi-Gel-FL3) were subjected to western blot analysis using antibodies against PHB1 and PHB2. Both PHB1 and PHB2 (Fig 1A) were retained by the affinity matrix. The blank beads did not pull down any PHB proteins (lane 4 in Fig 1A). These data showed that PHB1 and PHB2 were the cellular targets of FL3 in the H9c2 cardiomyocytes. Next, we examined whether doxorubicin and/or FL3 modify the content of PHB1 in these cells (Fig 1B and 1C). FL3 treatment of the H9c2 cells for 10h (with or without doxorubicin) greatly augmented PHB1 protein levels. Doxorubicin has no significant effect on PHB1 levels (Fig 1B and 1C), but it induced its accumulation in the nucleus (Fig 1D, 1E and 1F). This translocation of PHB1 from cytoplasm to the nucleus was blocked by FL3 (Fig 1D, 1E and 1F). This data indicate that PHB1 levels and localization can be greatly modified by FL3 treatment.

FL3 promotes the localization of PHB1 to mitochondria

A large body of evidence suggests that the subcellular location of PHBs determines whether a PHB protein promotes apoptosis or cytoprotection [8,18]. Accordingly, we examined the intracellular localization of PHB1 after treatment with FL3 to gain some insight into FL3's mechanism of action. H9c2 cells were double-labeled with an anti-PHB1 antibody and the mitochondrial dye Mitotracker Red. PHB1 was detected throughout the cytoplasm of the H9c2

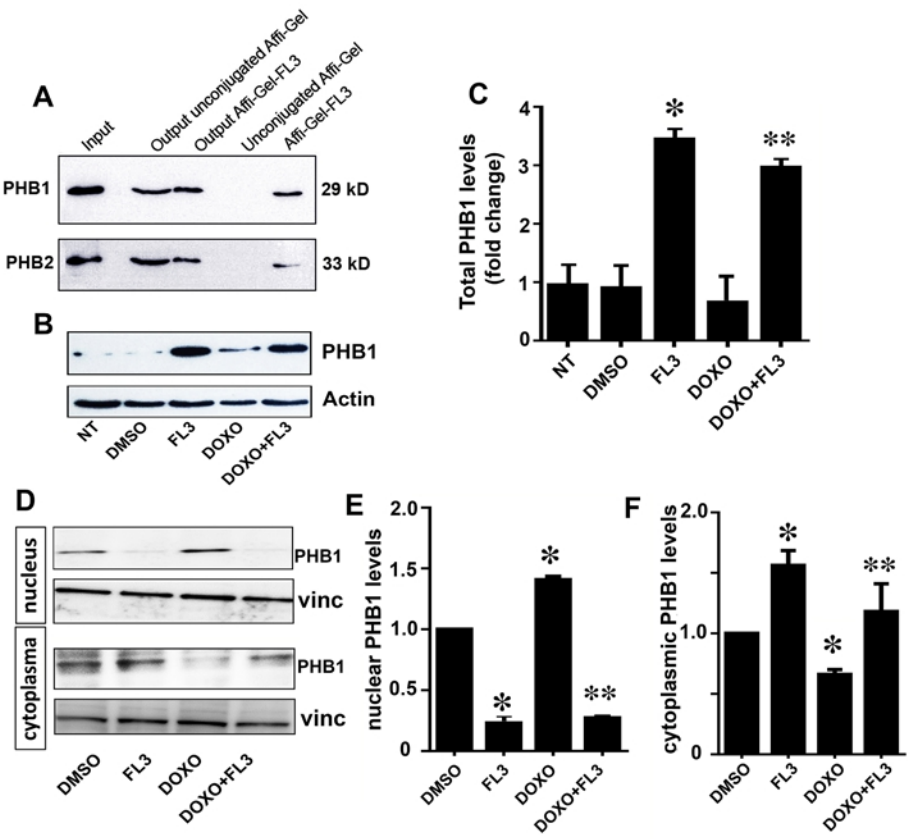

Fig 1. Synthetic flavagline (FL3) binds PHB1 and PHB2 and increases PHB1 leves in H9c2 cells. A. Whole-cell extracts of the H9c2 line (input) were either incubated with the beads Affi-Gel 10 conjugated with FL3 or blocked with ethanolamine (unconjugated Affi-Gel) [7,17]. The bound and eluted proteins (Affi-Gel-FL3) and output proteins (output Affi-Gel-FL3) were analyzed by western blotting using antibodies against PHB1 and PHB2 ($n = 3$). **B and C.** Representative western blot analyses and histogram based quantification of total PHB1 levels in the cell lysates by. FL3 alone increased PHB1 protein levels within 10h as compare to non-treated cells (NT). However PHB1 level was lower in the present of both FL3 and doxorubicin (n = 3). **D and E.** Representative western blot analyses and histogram based quantification of nuclear PHB1 levels by. Doxorubicin accumulates PHB1 in the nucleus but lowers in the cytoplasm that was reduced by preconditioning with FL3. * Indicates $p<0.05$ as compare to control, ** indicates $p<0.05$ as compare to the doxorubicin alone group.

doi:10.1371/journal.pone.0141826.g001

cardiomyocytes in the basal condition (Fig 2A). The staining pattern for PHB1 maximally matched that of Mitotracker Red after 15-min incubation of the cells with FL3, indicating that FL3 promoted PHB1 accumulation predominantly in mitochondria (Fig 2B). Mitochondrial fraction of the FL3 treated H9c2 cells confirmed an amplification of PHB1 levels in mitochondria after 15 min (Fig 2C and 2D). PHB1 accumulation in nucleus was elevated within 10 min and was consequently reduced within 20 min upon FL3 treatment (Fig 2C and 2E). This data clearly showed that FL3 promotes nuclear translocation of PHB1 to mitochondria.

FL3 promotes activation of STAT3 by PHB1

FL3 enhanced phosphorylation of STAT3 in mitochondria in time dependent manner (Fig 3A and 3B) and correlated with PHB1 accumulation in the mitochondria and nucleus (Fig 3C and 3D), indicating that FL3 promotes nuclear translocation of PHB1 to mitochondria and consequently STAT3 phosphorylation. Next we investigated whether PHB1 accumulation and

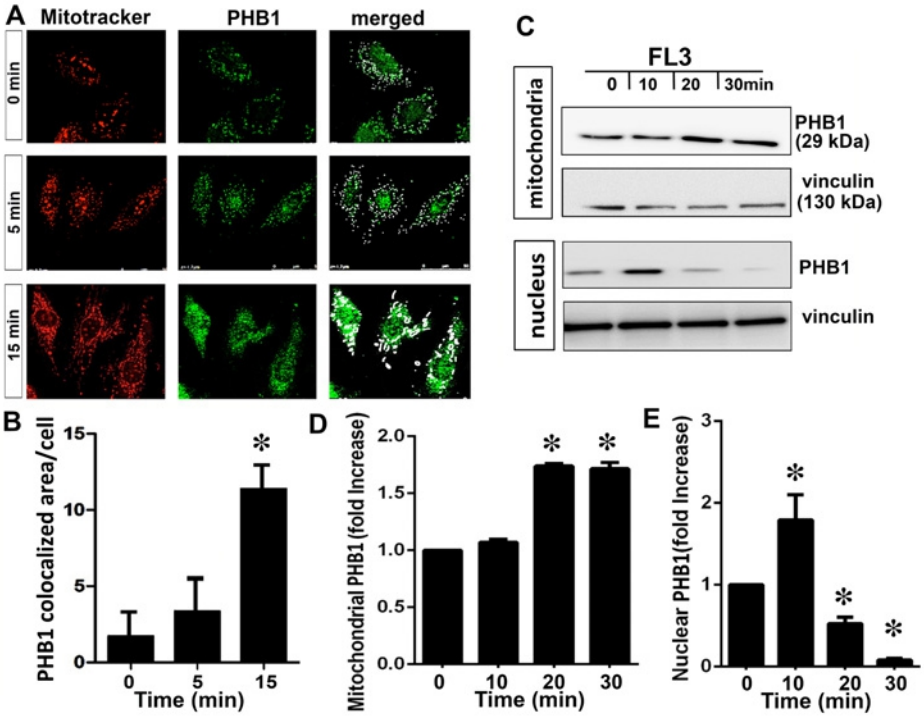

Fig 2. The flavagline FL3 induces translocation of PHB1 to mitochondria in cardiomyocytes. A. H9c2 cells were incubated with FL3 (100 nM) and analyzed by confocal microscopy. The cells were co-labeled with the anti-PHB1 antibody (green staining), mitotracker (red staining), and (DAPI; blue staining). The latter two dyes stained mitochondria and the nucleus, respectively. Merged confocal images show that FL3 induced the translocation of PHB1 to mitochondria (white arrows show PHB1 and mitotracker co-localization). **B.** The histogram shows quantitative analyses of co-localization of PHB1 and Mito Tracker in each cell by confocal analyses (n = 6). **C.** Representative illustration of PHB1 levels in mitochondrial and nuclear fractions upon FL3 treatment. In the mitochondrial fraction PHB1 accumulation by FL3 occurred within 20 min. PHB1 was initially increased in nucleus and rapidly reduced within 20 min. **D and E.** The histogram shows quantitative analyses of mitochondrial and nuclear PHB1 levels upon treatment of H9c2 cells with FL3 (100 nM).
* Indicates $p<0.05$ as compare to vehicle (n = 3).

doi:10.1371/journal.pone.0141826.g002

STAT3 phosphorylation are also correlated upon doxorubicin treatment of the H9c2 cells. Accordingly, phosphorylation of nuclear STAT3 is elevated by doxorubicin that was blocked by FL3 preconditioning (Fig 3E and 3F).

Next, we addressed whether FL3 promotes interaction of PHB1 with STAT3 in H9c2 cells, since PHB1 accumulation and STAT3 phosphorylation are correlated in mitochondria and nucleus. Moreover, PHB1 has been shown to heterodimerize with STAT3 [8]. H9c2 cells that were cotransfected with plasmids encoding FLAG-tagged PHB1 and PHB2 were incubated with FL3 (100 nM) for immunoprecipitation of PHBs with an anti-FLAG antibody. The immunoprecipitated cell lysates (input) from the H9c2 cells that were transfected with PHB1 or PHB2 (IP-α-Flag) were subjected to western blot analyses with anti-flag antibodies. Significant coimmunoprecipitation of PHB1 with STAT3 was observed at the data point 15 min after FL3 treatment (Fig 4A, left panels), whereas interactions of PHBs with either AKT or ERK were not detected. These results showed that FL3 induced heterodimerization of STAT3 with PHBs. When the immunoprecipitated PHB1 proteins were visualized with an antibody recognizing the phosphorylated form of STAT3, the phospho-STAT3 was significantly upregulated 15 min after FL3 treatment (Fig 4A, right panels). Taken together, these data suggested that PHBs

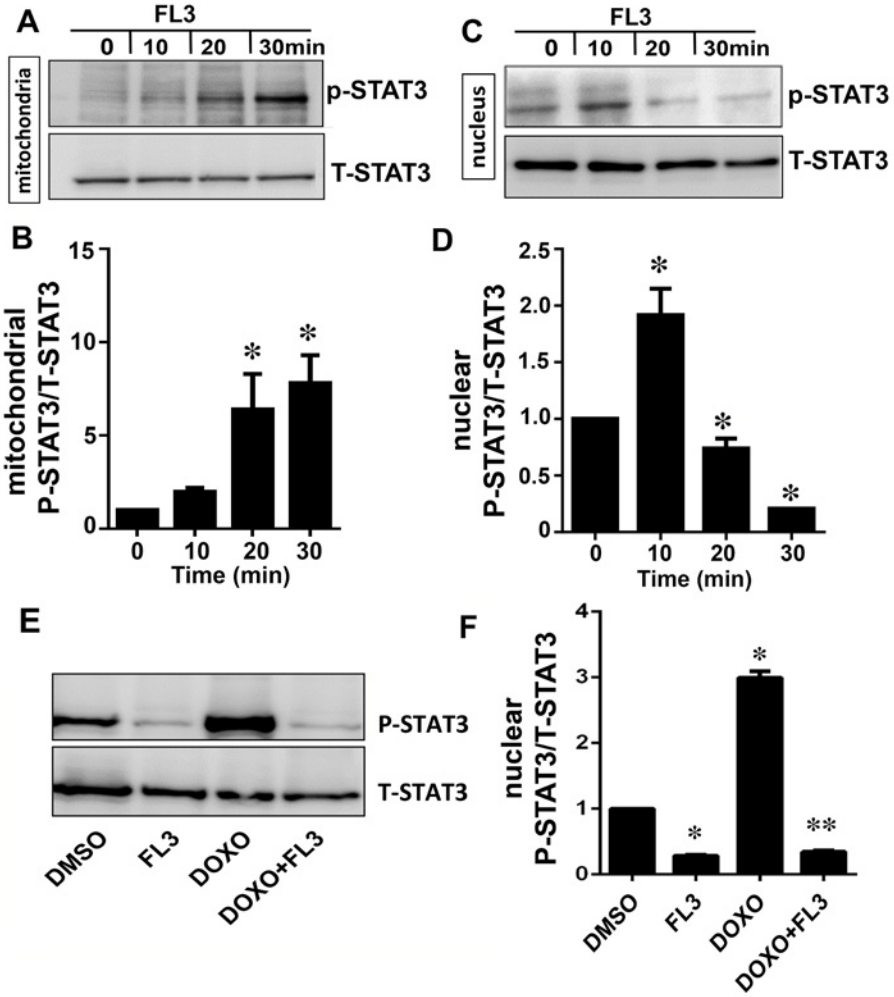

Fig 3. The mitochondrial STAT-3 phosphorylation is correlated with PHB1 translocation to mitochondria by FL3 in cardiomyocytes. A and B. Representative western blot analyses and histogram based quantification of mitochondrial STAT3 activation by phosphorylation. STAT3 was phosphorylated by FL3 in mitochondrial fraction. **C and D.** Representative western blot analyses and **h**istogram based quantification of nuclear STAT3 activation by phosphorylation. STAT3 activation was only detected in nucleus after FL3 treatment. **E and F.** The western blot and histogram show quantitative analyses of nuclear phosphorylated STAT3 levels upon treatment of H9c2 cells with control (DMSO), FL3 (100 nM), doxorubicin (1μM), and FL3 + doxorubicin. Doxorubicin elevated phosphorylated STAT3 levels, which were reduced by FL3 (n = 3; *p < 0.05, compared to vehicle; **p < 0.05, compared to doxorubicin treatment).

doi:10.1371/journal.pone.0141826.g003

interacted with the STAT3 protein, and this interaction induced activation of STAT3 by phosphorylation.

Next, we examined STAT3 activation by phosphorylation in H9c2 cells after FL3 treatment. Using a specific anti-phospho-STAT3 antibody and western blot analysis, we found that FL3 (100 nM) rapidly promoted the phosphorylation of STAT3 in the H9c2 cardiomyocytes: the phosphorylation reached a maximum within 15 min (Figs 4B and 3C). To gain further insight into the activation of STAT3 by PHBs, we tested whether the STAT3 phosphorylation is inhibited by WP1066 [19], an inhibitor of the JAK2 kinase (this reagent is commonly used to block STAT3 activation). WP1066 at 100 nM significantly inhibited the FL3-induced STAT3 activation (Figs 4D and 3E).

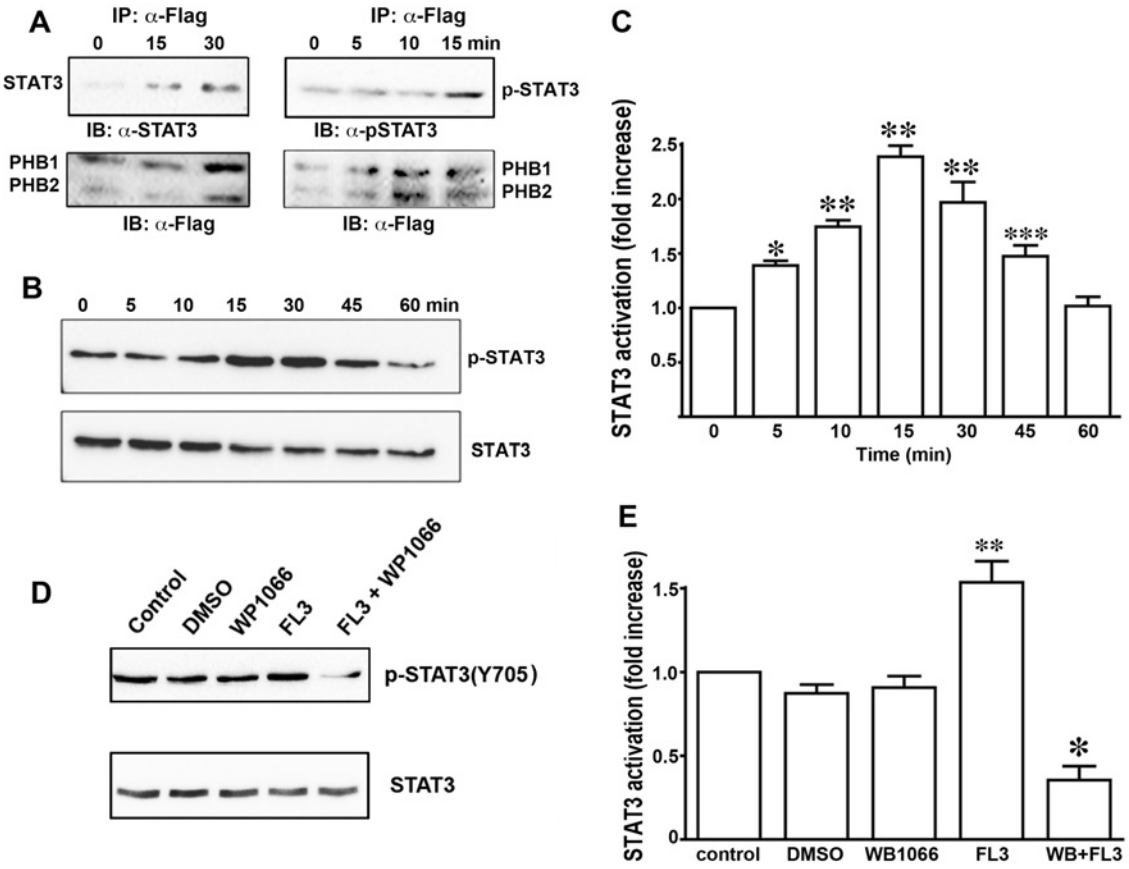

Fig 4. FL3 rapidly induces phosphorylation of STAT3. A. STAT3 coimmunoprecipitates (co-IP) with PHB1. An anti-FLAG antibody was incubated with extracts of the H9c2 cardiomyocytes. Immunoprecipitates were resolved by means of SDS-PAGE and probed for STAT3 and the FLAG tag to detect both PHB1 and PHB2. **B.** Representative western blots of protein lysates of H9c2 cells treated with FL3 (100 nM), by means of antibodies that recognize either phosphorylated (Tyr^{705}) or total STAT3 protein. **C.** Quantitative analysis of the western blots (percentage of phosphorylated STAT3 in total STAT3, $n = 4$; *$p < 0.05$, compared to control; **$p < 0.001$, compared to control; ***$p < 0.01$, compared to control). **D** and **E.** Effects of the Janus kinase 2 (JAK2) inhibitor WP1066 on STAT3 phosphorylation: Representative western blots and quantitative analysis (percentage of phosphorylated STAT3 in total STAT3, $n = 4$; $p < 0.05$, compared to control; **$p < 0.05$, compared to FL3).

doi:10.1371/journal.pone.0141826.g004

FL3 triggers cardioprotective signaling by targeting PHB1 and its signaling

To confirm the involvement of PHBs in the mechanism of action of FL3, we tested whether a knockdown of PHB1 in cardiomyocytes affects the cardioprotective effect of FL3. Accordingly, we transfected the H9c2 cardiomyocytes with siRNAs against PHBs to downregulate PHBs without altering cell survival. Of the two anti-PHB siRNA sequences tested, si-PHB1 at 50 nM or si-PHB1 together with si-PHB2 (10 nM each) downregulated both PHB1 mRNA and protein: by 80% and 70%, respectively. The siRNA-mediated downregulation of PHB1 and PHB2 significantly reduced the cytoprotective effect of FL3 (Fig 5A), whereas transfection with control (nonspecific) siRNA did not. These data indicated that PHB1 and PHB2 were both involved in the mechanism of action of FL3.

To determine whether the STAT3 phosphorylation in cardiomyocytes was indeed involved the cardioprotective mechanism; we compared the apoptosis levels in TUNEL and FACS assays when the H9c2 cardiomyocytes were pretreated with WP1066 or vehicle alone. The TUNEL

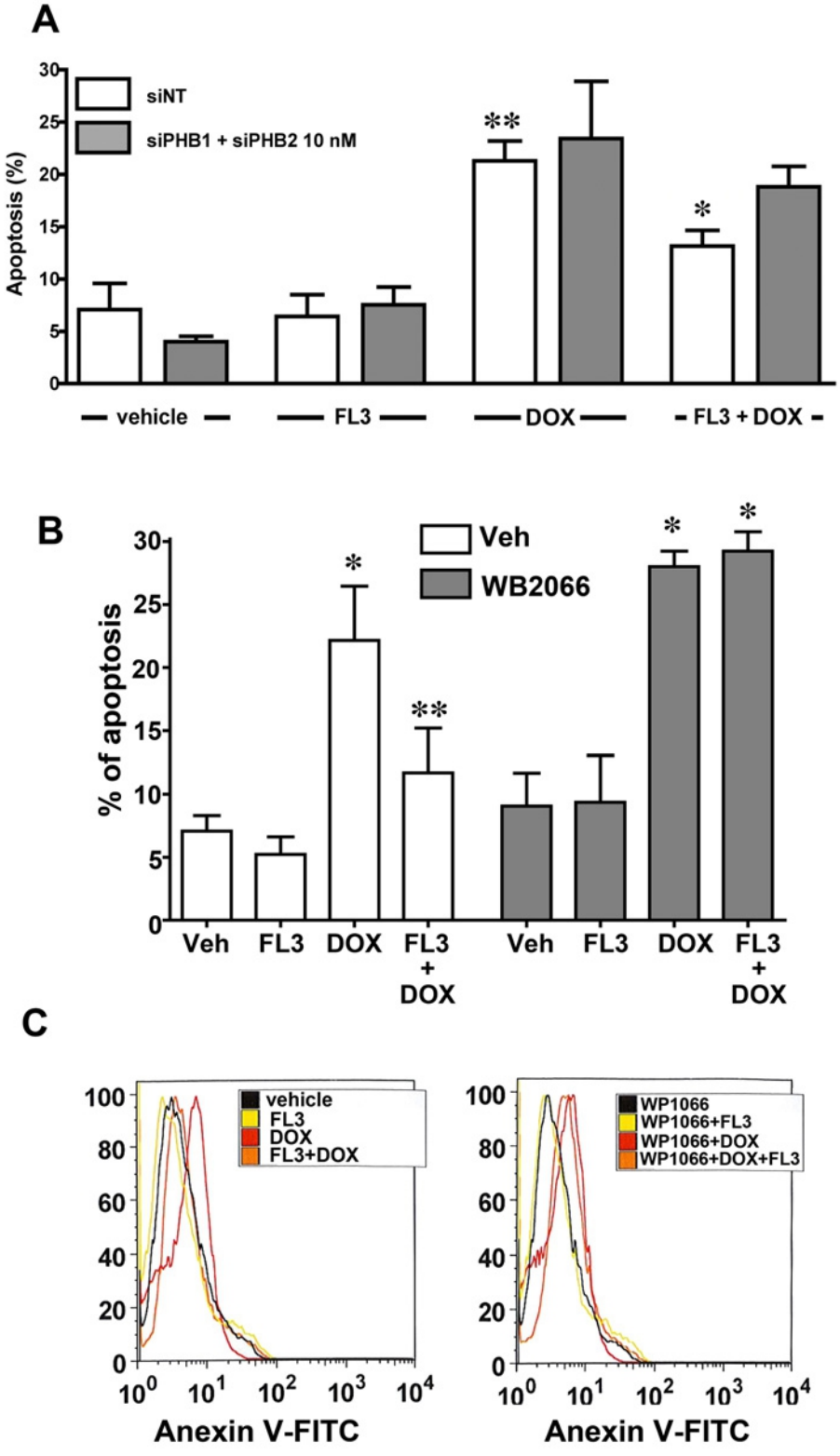

Fig 5. FL3 protects H9c2 cardiomyocytes by acting on PHBs and their signaling target STAT3. A. The histogram shows the percentage of apoptotic cells induced by doxorubicin (1 μM) among H9c2 control cells (transfected with nonspecific small interfering RNA [si-NT]) or the H9c2 cells where PHB1 or PHB2 were

downregulated using specific small interfering RNA (siRNA). Knocking PHB1 or PHB2 down greatly diminished the cardioprotective effect of FL3 (100 nM; $n = 4$ to 5; *p < 0.05, compared to vehicle; **p < 0.05, compared to doxorubicin (doxo). **B.** The TUNEL assay shows the percentage of apoptotic cells in the 4',6-diamidino-2-phenylindole (DAPI)-positive total cell population. **C.** Fluorescence-activated cell sorting (FACS) analysis shows the percentage of the maximum among annexin V-positive cells ($n = 3$; *p < 0.05, compared to vehicle; **p < 0.05, compared to doxorubicin treatment).

doi:10.1371/journal.pone.0141826.g005

(Fig 5B) and FACS data (Fig 5C) revealed that WP1066 strongly attenuated the cardioprotective effect of FL3. Overall, these results supported the notion that phosphorylation of STAT3 is a crucial step in the mechanism of cardioprotective action of FL3.

The PHB1/STAT3 complex is a key participant in the FL3-activated STAT3 pathway

To confirm whether the PHB1/STAT3 complex is involved in the FL3-activated STAT3 pathway, we transiently cotransfected the cells with either anti-PHB1 siRNAs or scrambled RNA as a control, then incubated the cells with FL3, and tested them for STAT3 phosphorylation. The anti-PHB1 siRNA, but not scrambled RNA, strongly attenuated the FL3-induced STAT3 phosphorylation (Fig 6A and 6B). The levels of PHBs in siRNA-nontargeted and siRNA-PHBs

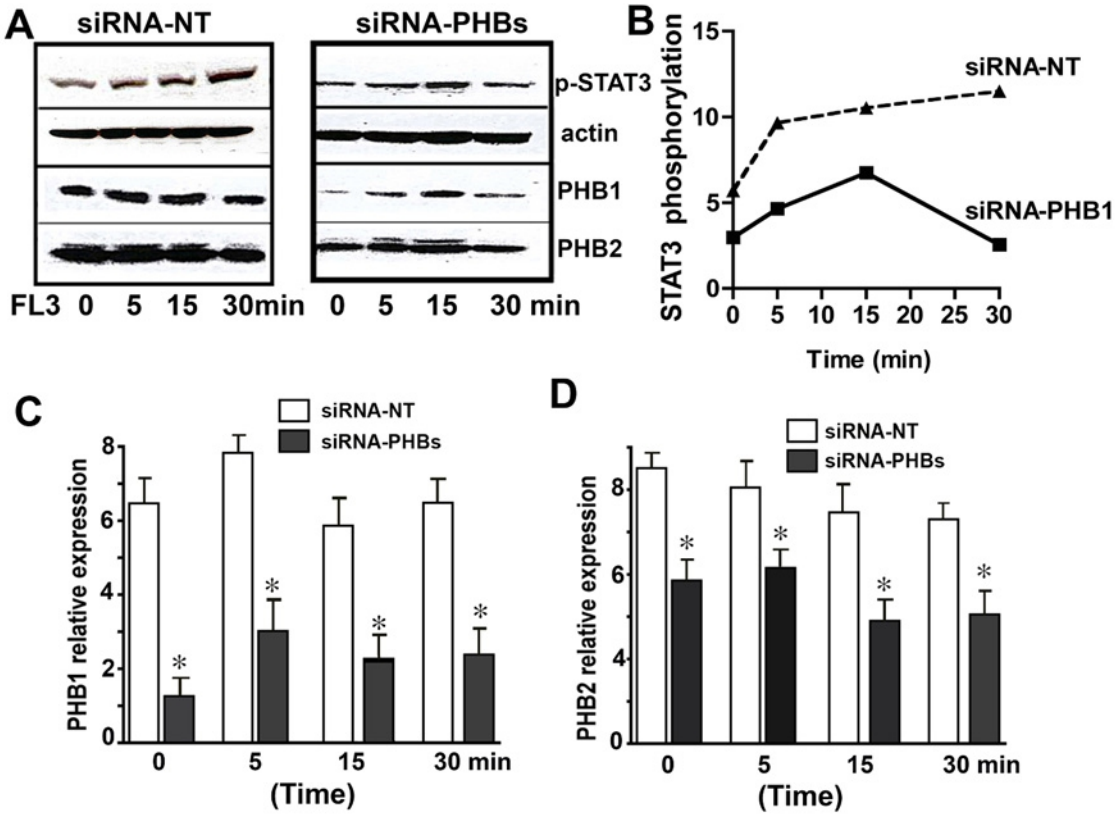

Fig 6. Small-interfering-RNA (siRNA)-mediated downregulation of PHB1 proteins attenuates FL3-induced cardioprotection from doxorubicin toxicity. A. Representative western blots show induction of STAT3 phosphorylation by the synthetic flavagline (FL3) in H9c2 cells transfected with nonspecific siRNA (left) or with anti-PHB1 siRNA (right). **B.** Quantification of phosphorylated STAT3, with normalization to actin ($n = 3$; *p < 0.05, compared to vehicle). FL3-mediated STAT3 activation by phosphorylation was abolished when the expression of PHBs were reduced. **C.** This histogram shows downregulation of PHB1 after transfection of H9c2 cells with anti-PHBs siRNA ($n = 3$; *p < 0.05, compared to vehicle). **D.** This histogram shows downregulation of PHB2 after transfection of H9c2 cells with anti-PHBs siRNA ($n = 3$; *p < 0.05, compared to vehicle).

doi:10.1371/journal.pone.0141826.g006

transfected cells are shown in (Fig 6C and 6D). These results showed that PHB1 was necessary for the STAT3 activation by FL3, and that STAT3 was downstream of PHB1 in the FL3-mediated survival pathway.

Discussion

A study on the cardiac phosphoproteome has already shown PHB1 to be a prime target of doxorubicin [20]. Nonetheless, how the PHB proteins participate in the survival mechanisms against doxorubicin-mediated cardiotoxicity was not known. Here, we show for the first time that FL3 binds to PHBs and translocated PHB1 to mitochondria. Accumulation of PHB1 in mitochondria is associated with STAT3 phosphorylation. It seems that mitochondrial PHB1 accumulation stabilizes mitochondrial membrane, activates mitochondrial STAT3 activation and initiates FL3-mediated cardioprotection. On the opposite, doxorubicin provokes the PHB1 accumulation and STAT3 phosphorylation in nucleus, leading to cardiomyocyte apoptosis (Fig 7).

PHB1 has been reported to promote the survival of many noncancerous cell types, including cardiomyocytes [8,21–26]. Overexpression of PHB1 inhibits the mitochondria-mediated apoptosis pathway in H9c2 cells that is induced by hypoxia. Reduced levels of transcripts and mitochondrial PHB1 proteins were found in the left ventricle of spontaneously hypertensive rats. Heart-specific PHB1-transgenic mice show low levels of apoptosis and mitochondrial fission in the heart, and consequently, a smaller myocardial infarction size after an experimental infarction [20]. Proteomics studies have shown that PHB1 expression increases dramatically in

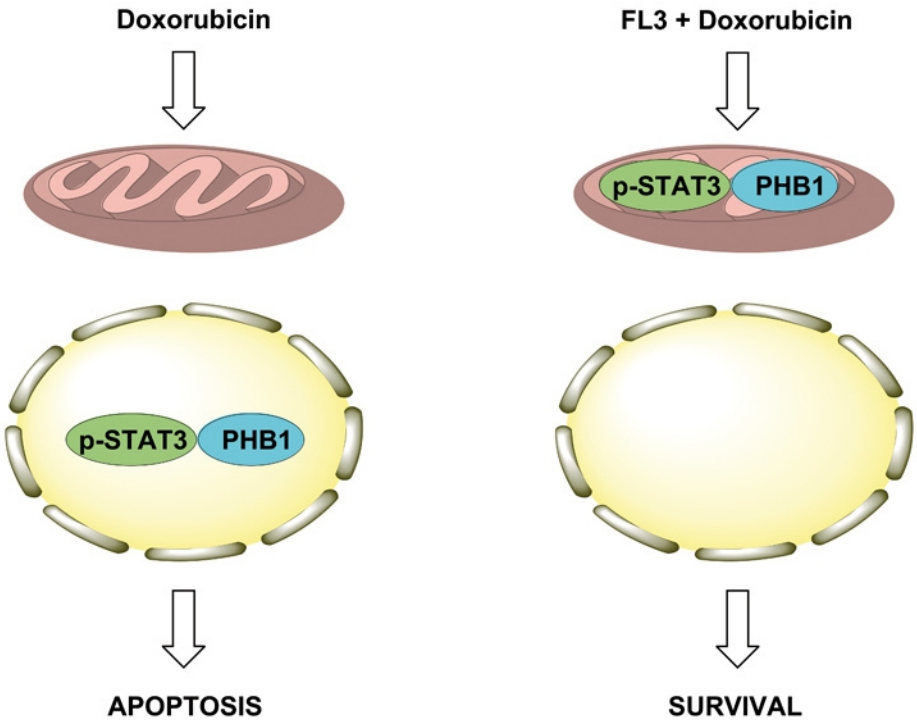

Fig 7. Proposed mechanism of FL3-induced cardioprotection from doxorubicin toxicity. Doxorubicin induces the translocation of PHB1 and phosphorylated STAT3 in the nucleus of cardiomyocytes to induce apoptosis. On the opposite, FL3 induces the translocation of these signaling proteins into mitochondria to protect the cell against the adverse effects of doxorubicin.

doi:10.1371/journal.pone.0141826.g007

cardiomyocytes mitochondria after chronic restraint stress [27]. H_2O_2-induced oxidative stress increases also the mitochondrial content of PHB1 in cardiomyocytes to stabilize mitochondrial membrane potential, inhibit the release of cytochrome c from mitochondria and maintain the mitochondrial function assessed by the preservation of the H^+-ATPase activity [28]. These data indicate that, in mitochondria, PHB1 is a critical factor that protects cardiomyocytes from oxidative stress.

We found here that in cardiomyocytes, FL3 promotes translocation of PHB1 to mitochondria. This observation is in line with other studies showing that translocation of PHB1 from the nucleus to mitochondria is necessary for cytoprotection in ovarian granulosa cells [23,24], pancreatic β-cells [25], and the retinal epithelium [26]. Accumulation of PHB1 in the mitochondrial membrane can stabilize this membrane, blocking the apoptotic machinery.

Several studies indicate that during apoptosis induced by cytotoxic agents PHB1 migrates to the nucleus where it co-localizes with p53 [29, 30]. Interestingly, we found that doxorubicin does not alter total PHB1 levels in H9c2 cells, but promotes accumulation of PHB1 in the nucleus. This effect was abolished by FL3 treatment, which induced the translocation of PHB1 to mitochondria. The total PHB1 levels in H9c2 cells were also significantly induced by FL3 treatment (for 10h) that was reduced by doxorubicin treatment. The increase of PHB1 expression levels could be due to the activation of STAT3 during the preconditioning by FL3. Indeed, STAT3 is known to upregulate PHB1 during oxidative stress [31].

Theiss and collaborators demonstrated that PHB1 induces phosphorylation of STAT3, thereby stimulating its interaction with PHB1 in mitochondria and ensuring consequent protection of intestinal epithelial cells from TNF-α-induced mitochondrial stress and apoptosis [9]. Such a cytoprotective mechanism has not been reported yet in any other cell types. Consistent with the above observations, our results show that in cardiomyocytes, FL3 induces rapid translocation of PHB1 to mitochondria simultaneously with STAT3 phosphorylation.

STAT3 is a transcription factor that drives expression of antiapoptotic and antioxidant genes [32,33]. STAT3 promotes cardiomyocytes survival through 2 types of actions: -in the nucleus it acts as transcription factor to upregulates iNOS and COX-2 and stimulates the adaptation of the heart to ischemic stress [34]. In mitochondria, STAT3 prevents mitochondria-mediated apoptosis, inhibits the opening of mitochondrial permeability transition pores (MPTP) [32] and modulates the electron transport chain [35]. STAT3 phosphorylation [10] and overexpression [11] have been shown to protect cardiomyocytes from apoptosis induced by doxorubicin in heart tissues.

We demonstrated that inhibition of STAT3 activation by WP1066 blocks the cardioprotective effect of FL3, thus confirming that STAT3 activation is essential for prevention of cardiomyocyte death. The mechanistic link between the activation of STAT3 and PHB1 is currently not clear. Both proteins form a complex in cardiomyocytes 15 min after initiation of FL3 treatment—when STAT3 is maximally phosphorylated—suggesting that both events are connected. It is therefore tempting to hypothesize that STAT3 becomes phosphorylated when it interacts with PHB1, especially because FL3 cannot induce STAT3 phosphorylation or protect cardiomyocytes from doxorubicin toxicity in PHB1-deficient cells.

This study seems to provide the first evidence that targeting of PHB1 by small molecules such as FL3 induces cytoprotection via activation of STAT3 signaling in mitochondria. This strategy may turn out to be a valid therapeutic method for protection of the myocardium from anthracycline-induced cardiotoxicity and ischemia/reperfusion-mediated damage. The beneficial effects of mitochondrial STAT3 in the heart have now been demonstrated, but the currently used methods for activation of mitochondrial STAT3 signaling are not very convenient in terms of clinical application, because of lack of specific activator. Indeed, G-CSF, EPO, and IL-11 protect the heart from ischemic injury, doxorubicin cardiotoxicity, or cardiac fibrosis

utilizing mitochondrial STAT3 signaling pathway, however they also activate other signaling pathways that may induce adverse effects [36–38]. Nevertheless, as far as we know, small molecules, such as FL3, have not been reported to activate STAT3 in the heart.

In summary, mitochondrial versus nuclear PHB/STAT3 complex is critical for the cardioprotective effect of FL3 (Fig 7). Because of the importance of STAT3/PHB1 complex in mitochondria as a therapeutic target in heart failure, the effects of flavaglines need to be examined in experimental models of this disease.

Author Contributions

Conceived and designed the experiments: LD CGN. Performed the experiments: RQ OY AG CB QZ JPW. Analyzed the data: RQ OY AG LD JPW CGN. Contributed reagents/materials/analysis tools: CB QZ. Wrote the paper: LD CGN.

References

1. Vejpongsa P, Yeh ET. Prevention of anthracycline-induced cardiotoxicity: challenges and opportunities. J Am Coll Cardiol 2014; 64: 938–945. doi: 10.1016/j.jacc.2014.06.1167 PMID: 25169180
2. Tebbi CK, London WB, Friedman D, Villaluna D, De Alarcon PA, Constine LS, et al. Dexrazoxane-associated risk for acute myeloid leukemia/myelodysplastic syndrome and other secondary malignancies in pediatric Hodgkin's disease. J Clin Oncol 2007; 25: 493–500. doi: 10.1200/JCO.2005.02.3879 PMID: 17290056
3. Basmadjian C, Thuaud F, Ribeiro N, Désaubry L. Flavaglines: potent anticancer drugs that target prohibitins and the helicase eIF4A. Future Med Chem 2013; 5: 2185–2197. doi: 10.4155/fmc.13.177 PMID: 24261894
4. Bernard Y, Ribeiro N, Thuaud F, Turkeri G, Dirr R, Boulberdaa M, et al. Flavaglines alleviate doxorubicin cardiotoxicity: implication of Hsp27. PLoS One 2011; 6: e25302. doi: 10.1371/journal.pone.0025302 PMID: 22065986
5. Ribeiro N, Thuaud F, Bernard Y, Gaiddon C, Cresteil T, Hild A, et al. Flavaglines as potent anticancer and cytoprotective agents. J Med Chem 2012; 55: 10064–10073. doi: 10.1021/jm301201z PMID: 23072299
6. Becker MS, Schmezer P, Breuer R, Haas SF, Essers MA, Krammer PH, et al. The traditional Chinese medical compound Rocaglamide protects nonmalignant primary cells from DNA damage-induced toxicity by inhibition of p53 expression. Cell Death Dis 2014; 5: e1000. doi: 10.1038/cddis.2013.528 PMID: 24434508
7. Polier G, Neumann J, Thuaud F, Ribeiro N, Gelhaus C, Schmidt H, et al. The natural anticancer compounds rocaglamides inhibit the Raf-MEK-ERK pathway by targeting prohibitin 1 and 2. Chem Biol 2012; 19: 1093–1104. doi: 10.1016/j.chembiol.2012.07.012 PMID: 22999878
8. Thuaud F, Ribeiro N, Nebigil CG, Désaubry L. Prohibitin ligands in cell death and survival: mode of action and therapeutic potential. Chem Biol 2013; 20: 316–331. doi: 10.1016/j.chembiol.2013.02.006 PMID: 23521790
9. Han J, Yu C, Souza RF, Theiss AL. Prohibitin 1 modulates mitochondrial function of Stat3. Cell Signal 2014; 26: 2086–2095. doi: 10.1016/j.cellsig.2014.06.006 PMID: 24975845
10. Frias MA, Somers S, Gerber-Wicht C, Opie LH, Lecour S, Lang U. The PGE2-Stat3 interaction in doxorubicin-induced myocardial apoptosis. Cardiovasc Res 2008; 80: 69–77. doi: 10.1093/cvr/cvn171 PMID: 18567640
11. Kunisada K, Negoro S, Tone E, Funamoto M, Osugi T, Yamada S, et al. Signal transducer and activator of transcription 3 in the heart transduces not only a hypertrophic signal but a protective signal against doxorubicin-induced cardiomyopathy. Proc Natl Acad Sci U S A 2000; 97: 315–319. doi: 10.1073/pnas.97.1.315 PMID: 10618415
12. Jacoby JJ, Kalinowski A, Liu MG, Zhang SS, Gao Q, Chai GX, et al. Cardiomyocyte-restricted knockout of STAT3 results in higher sensitivity to inflammation, cardiac fibrosis, and heart failure with advanced age. Proc Natl Acad Sci U S A 2003; 100:12929–34. doi: 10.1073/pnas.2134694100 PMID: 14566054
13. Zhu W, Zhang W, Shou W, Field LJ. P53 inhibition exacerbates late-stage anthracycline cardiotoxicity. Cardiovasc Res 2014; 103: 81–89. doi: 10.1093/cvr/cvu118 PMID: 24812279
14. Yano N, Suzuki D, Endoh M, Tseng A, Stabila JP, McGonnigal BG, et al. Beta-adrenergic receptor mediated protection against doxorubicin-induced apoptosis in cardiomyocytes: the impact of high ambient glucose. Endocrinology 2008; 149: 6449–6461. doi: 10.1210/en.2008-0292 PMID: 18719028

15. Artal-Sanz M, Tavernarakis N. Prohibitin couples diapause signalling to mitochondrial metabolism during ageing in C. elegans. Nature 2009; 461: 793–797. doi: 10.1038/nature08466 PMID: 19812672

16. Destouches D, El Khoury D, Hamma-Kourbali Y, Krust B, Albanese P, Katsoris P, et al. Suppression of tumor growth and angiogenesis by a specific antagonist of the cell-surface expressed nucleolin. PloS one. 2008; 3: e2518. doi: 10.1371/journal.pone.0002518 PMID: 18560571

17. Thuaud F, Bernard Y, Turkeri G, Dirr R, Aubert G, Cresteil T, et al. Synthetic analogue of rocaglaol displays a potent and selective cytotoxicity in cancer cells: involvement of apoptosis inducing factor and caspase-12. J Med Chem 2009; 52: 5176–5187. doi: 10.1021/jm900365v PMID: 19655762

18. Theiss AL, Sitaraman SV. The role and therapeutic potential of prohibitin in disease. Biochim Biophys Acta 2011; 1813: 1137–1143. doi: 10.1016/j.bbamcr.2011.01.033 PMID: 21296110

19. Iwamaru A, Szymanski S, Iwado E, Aoki H, Yokoyama T, Fokt I, et al. A novel inhibitor of the STAT3 pathway induces apoptosis in malignant glioma cells both in vitro and in vivo. Oncogene 2007; 26: 2435–2444. doi: 10.1038/sj.onc.1210031 PMID: 17043651

20. Gratia S, Kay L, Michelland S, Seve M, Schlattner U, Tokarska-Schlattner M. Cardiac phosphoproteome reveals cell signaling events involved in doxorubicin cardiotoxicity. J Proteomics 2012; 75: 4705–4716. doi: 10.1016/j.jprot.2012.02.004 PMID: 22348821

21. Wang K, Liu CY, Zhang XJ, Feng C, Zhou LY, Zhao Y, et al. miR-361-regulated prohibitin inhibits mitochondrial fission and apoptosis and protects heart from ischemia injury. Cell Death Differ. 2015; 22: 1058–1068. doi: 10.1038/cdd.2014.200 PMID: 25501599

22. Chowdhury I, Thompson WE, Thomas K. Prohibitins role in cellular survival through Ras-Raf-MEK-ERK pathway. J Cell Physiol 2014; 229: 998–1004. doi: 10.1002/jcp.24531 PMID: 24347342

23. Chowdhury I, Branch A, Olatinwo M, Thomas K, Matthews R, Thompson WE. Prohibitin (PHB) acts as a potent survival factor against ceramide induced apoptosis in rat granulosa cells. Life Sci 2011; 89: 295–303. doi: 10.1016/j.lfs.2011.06.022 PMID: 21763324

24. Chowdhury I, Thompson WE, Welch C, Thomas K, Matthews R. Prohibitin (PHB) inhibits apoptosis in rat granulosa cells (GCs) through the extracellular signal-regulated kinase 1/2 (ERK1/2) and the Bcl family of proteins. Apoptosis 2013; 18: 1513–1525. doi: 10.1007/s10495-013-0901-z PMID: 24096434

25. Lee JH, Nguyen KH, Mishra S, Nyomba BL. Prohibitin is expressed in pancreatic beta-cells and protects against oxidative and proapoptotic effects of ethanol. FEBS J 2010; 277: 488–500. doi: 10.1111/j.1742-4658.2009.07505.x PMID: 20030709

26. Sripathi SR, He W, Atkinson CL, Smith JJ, Liu Z, Elledge BM, et al. Mitochondrial-nuclear communication by prohibitin shuttling under oxidative stress. Biochemistry 2011; 50: 8342–8351. doi: 10.1021/bi2008933 PMID: 21879722

27. Liu XH, Qian LJ, Gong JB, Shen J, Zhang XM, Qian XH. Proteomic analysis of mitochondrial proteins in cardiomyocytes from chronic stressed rat. Proteomics. 2004; 4: 3167–76. doi: 10.1002/pmic.200300845 PMID: 15378698

28. Liu X, Ren Z, Zhan R, Wang X, Wang X, Zhang Z, et al. Prohibitin protects against oxidative stress-induced cell injury in cultured neonatal cardiomyocyte. Cell stress & chaperones. 2009; 14: 311–9. doi: 10.1007/s12192-008-0086-5 PMID: 18958584

29. Liu YH, Peck K, Lin JY. Involvement of prohibitin upregulation in abrin-triggered apoptosis. Evidence-based complementary and alternative medicine: eCAM. 2012; 2012:605154. doi: 10.1155/2012/605154 PMID: 21961024

30. Song W, Tian L, Li SS, Shen DY, Chen QX. The aberrant expression and localization of prohibitin during apoptosis of human cholangiocarcinoma Mz-ChA-1 cells. FEBS letters. 2014; 588:422–8. doi: 10.1016/j.febslet.2013.12.021 PMID: 24380853.

31. Jia Y, Zhou F, Deng P, Fan Q, Li C, Liu Y, et al. Interleukin 6 protects H_2O_2-induced cardiomyocytes injury through upregulation of prohibitin via STAT3 phosphorylation. Cell Biochem Funct 2012; 30: 426–31. doi: 10.1002/cbf.2820 PMID: 22431190.

32. Boengler K, Hilfiker-Kleiner D, Drexler H, Heusch G, Schulz R. The myocardial JAK/STAT pathway: from protection to failure. Pharmacol Ther 2008; 120: 172–185. doi: 10.1016/j.pharmthera.2008.08.002 PMID: 18786563

33. Hilfiker-Kleiner D, Hilfiker A, Drexler H. Many good reasons to have STAT3 in the heart. Pharmacol Ther 2005; 107: 131–137. doi: 10.1016/j.pharmthera.2005.02.003 PMID: 15963355

34. Bolli R, Dawn B, Xuan YT. Role of the JAK-STAT pathway in protection against myocardial ischemia/reperfusion injury. Trends Cardiovasc Med. 2003; 13: 72–9. PMID: 12586443.

35. Szczepanek K, Chen Q, Larner AC, Lesnefsky EJ. Cytoprotection by the modulation of mitochondrial electron transport chain: the emerging role of mitochondrial STAT3. Mitochondrion 2012; 12: 180–189. doi: 10.1016/j.mito.2011.08.011 PMID: 21930250

36. Harada M, Qin Y, Takano H, Minamino T, Zou Y, Toko H, et al. G-CSF prevents cardiac remodeling after myocardial infarction by activating the Jak-Stat pathway in cardiomyocytes. Nat Med 2005; 11: 305–311. doi: 10.1038/nm1199 PMID: 15723072

37. Hoch M, Fischer P, Stapel B, Missol-Kolka E, Sekkali B, Scherr M, et al. Erythropoietin preserves the endothelial differentiation capacity of cardiac progenitor cells and reduces heart failure during anticancer therapies. Cell Stem Cell 2011; 9: 131–143. doi: 10.1016/j.stem.2011.07.001 PMID: 21816364

38. Obana M, Maeda M, Takeda K, Hayama A, Mohri T, Yamashita T, et al. Therapeutic activation of signal transducer and activator of transcription 3 by interleukin-11 ameliorates cardiac fibrosis after myocardial infarction. Circulation 2010, 121: 684–691. doi: 10.1161/CIRCULATIONAHA.109.893677 PMID: 20100971

Publication N°7

Pro-differentiating effects of a synthetic flavagline on human teratocarcinomal cancer stem-like cells.

Emhemmed, F., Ali Azouaou, S., Zhao, Q., Appert-Collin, A., Bennasroune, A., Schini-Kerth, V. B., Muller, C. D., Désaubry, L., Fuhrmann, G., *Cell Biol Toxicol.*, **2017**, *33*, 295-306.

Cell Biol Toxicol (2017) 33:295–306
DOI 10.1007/s10565-016-9375-4

ORIGINAL ARTICLE

Pro-differentiating effects of a synthetic flavagline on human teratocarcinomal cancer stem-like cells

Fathi Emhemmed · Sarah Ali Azouaou · Qian Zhao · Aline Appert-Collin · Amar Bennasroune · Valérie B. Schini-Kerth · Christian D. Muller · Laurent Désaubry · Guy Fuhrmann

Received: 13 September 2016 / Accepted: 4 December 2016 / Published online: 15 December 2016

Abstract As initiators of the carcinogenic process, cancer stem cells (CSCs) are considered as new targets for anti-cancer therapies. However, these cells are hidden in the cancer bulk and remain relatively insensitive to chemotherapy, which targets their proliferative capacities. Alternatively, growing evidences have pointed out that a differentiation therapy could adversely affect these cells, which consequently should lose their self-renewal properties and become less aggressive. In order to evaluate the differentiation potential of an emerging class of anti-cancer drugs, we used the poorly differentiated teratocarcinomal cell as a model of Oct4-expressing CSC and determined the molecular mechanisms induced by the highly active flavagline FL3. The drug, administrated at sublethal concentration and for long period, was able to downregulate the expression levels of the stemness factors Oct4 and Nanog at both transcriptional and translational levels, concomitantly with a decrease of clonogenicity. The appearance of specific neural markers further demonstrated the differentiation properties of FL3. Interestingly, an expression of active caspase-3 and an upregulation of the expression of the germ cell nuclear factor were observed in treated cells; this suggests that the suppression of Oct4 expression required for the induction of differentiation involves overlapping mechanisms of protein degradation and gene repression. Finally, this study shows that FL3, like all-trans retinoic acid (ATRA), acts as a differentiation inducer of teratocarcinomal cells. Thus, FL3 offers an alternative possibility for cancer treatment since it could target the carcinogenic process by inducing the differentiation of ATRA-resistant and Oct4-expressing CSCs, without toxic side effects on normal cells.

Keywords Cancer stem cells · Differentiation · Flavagline · Oct4 · Teratocarcinoma

Electronic supplementary material The online version of this article (doi:10.1007/s10565-016-9375-4) contains supplementary material, which is available to authorized users.

F. Emhemmed · S. Ali Azouaou · Q. Zhao · C. D. Muller · L. Désaubry
UMR 7200 CNRS, Laboratoire d'Innovation Thérapeutique, Faculté de Pharmacie, Université de Strasbourg, Illkirch, France

A. Appert-Collin · A. Bennasroune
UMR 7369 CNRS, Laboratoire Matrice Extracellulaire et Dynamique Cellulaire, UFR Sciences Exactes et Naturelles, Université de Reims Champagne-Ardenne, Reims, France

V. B. Schini-Kerth · G. Fuhrmann (✉)
UMR 7213 CNRS, Laboratoire de Biophotonique et Pharmacologie, Faculté de Pharmacie, Université de Strasbourg, 74 route du Rhin, B.P. 60024, 67401 Illkirch, France
e-mail: guy.fuhrmann@unistra.fr

L. Désaubry
Sino-French Joint Lab of Food Nutrition/Safety and Medicinal Chemistry, College of Biotechnology, Tianjin University of Science and Technology, Tianjin, China

Introduction

Cancer stem cells (CSCs) are responsible for tumour initiation, invasion and metastasis and are considered to be the main contributors of therapy resistance and cancer recurrence. CSCs might arise from

normal stem cells (NSCs), which are exposed to repetitive mutation-inducing stress injuries. Recent studies suggest that CSCs could also arise from closely related dedifferentiated descendants, which possess, by definition, more restricted lineage-specific competencies (Sharif et al. 2011a).

A growing number of reports show that chemotherapeutic agents are able, to a certain extent, to act on both cancer cells and CSCs, by targeting similar cell processes, including those leading to apoptotic cell death (Ali Azouaou et al. 2015; Emhemmed et al. 2014). This emerging concept of pluralist therapeutic tools has been developed on the basis of accumulating data obtained for several CSC models. Indeed, identification of specific markers has allowed to isolate and characterize CSCs of various types of blood and solid cancers and, as a consequence, has initiated prospective analyses of putative chemotherapeutic drugs, which could efficiently target them (Sharif et al. 2011a). From this point of view, we and others have hypothesized that the malignant counterparts of the embryonic stem cell lines, namely the embryonal carcinoma stem cell lines, could be suitable models of CSCs expressing key stemness factors (Sell, 2004; Sharif et al. 2011b). These cell lines are poorly differentiated pluripotent stem cells with a high degree of malignancy and can be used as surrogate investigational tools for the evaluation of potential anti-cancer agents, as we showed previously (Sharif et al. 2011b).

It has been observed that the degree of aggressiveness of a CSC is proportional to its lineage-specific competencies (Ben-Porath et al. 2008; Sharif et al. 2013). Actually, several studies have reported that the differentiation level of a CSC type is inversely correlated with its resistance capacity to radiotherapy and chemotherapy (Al-Hajj et al. 2004; Sharif et al. 2011a). Disrupting the molecular pathways that control CSC self-renewal and differentiation is therefore an attractive alternative to weaken the aggressiveness and resistance phenotype of the tumour bulk. By targeting these pathways, it is assumed that the CSC can switch from an undifferentiated, highly proliferative and invasive phenotype to a mature and harmless low-growing state ((Sharif et al. 2011a, 2013). The most exhaustively studied differentiation-inducing compounds are retinoids, including vitamin A and its derivatives. As an adjunct to clinical therapy, all-*trans* retinoic acid (ATRA) treatment allows a long-lasting remission of more than 90% of patients with acute promyelocytic leukaemia (Grimwade et al. 2010). Recent studies have also pointed out that ATRA could be an efficient therapeutic tool on other acute myeloid leukaemia subtypes and solid tumours but so far needs to be administrated via specific formulations (Chlapek et al. 2014; Wang et al. 2014). These examples show the strongly positive impact of the differentiation strategy, which is able to block the tumour development and to prevent its recurrence. However, several cancers remain refractory to ATRA, and therefore, new therapeutic strategies have to be developed to cure them (Freemantle et al. 2003).

Flavaglines are a family of natural products with a cyclopenta[*b*]benzofuran skeleton that are extracted from plant of the genus *Aglaia*. Their leader compound, rocaglamide, has been found to exhibit strong anti-leukemic activity (King et al. 1982). Other flavaglines, like rocaglaol or silvestrol, also induce the death of cancer cells, without affecting non-cancerous cells, by acting on two distinct targets, the scaffold proteins prohibitins and the eukaryotic translation initiation factor 4A (Basmadjian et al. 2013). Interestingly, we identified a synthetic flavagline, FL3, which displays enhanced cytotoxicity on both blood and solid cancer cells, when compared to natural flavaglines (Thuaud et al. 2009). Moreover, we recently showed that this compound kills, at submicromolar concentrations, poorly differentiated and highly aggressive cancer stem-like cells but has only little effect on normal stem-like cells. We further demonstrated that this effect was mediated by a p53/p73-independent p38 MAPK-dependent caspase-3-dependent pro-apoptotic mechanism (Emhemmed et al. 2014).

A growing number of in vitro and in vivo studies have shown that several plant-derived compounds are potentially anti-cancer agents since they are able to specifically target the self-renewal properties of CSCs (Pistollato et al. 2015). Moreover, prosurvival and self-renewal signalling pathways share several common molecular components, pointing out the fine-tuned balance which controls CSC growth (Konopleva and Jordan 2011). As a consequence, it is not surprising that some phytochemicals with known anti-survival/anti-proliferative activity could

also target specific nodal points of the self-renewal machinery and its associated differentiation process (Moselhy et al. 2015; Sarkar et al. 2009). In this point of view, it has been observed that the natural anti-cancer compound rocaglamide induces the differentiation of HL-60 promyelocytic cells, in correlation with an arrest of proliferation (Basmadjian et al. 2013; Mata-Greenwood et al. 2001), suggesting that other members of the flavagline family could have a similar dual activity.

The aim of our work was to evaluate the in vitro pro-differentiating properties of the flavagline FL3 on human embryonal teratocarcinoma stem cells NT2/D1 (also known as NTERA-2 cl.D1). This cell line is described as highly pluripotent and undifferentiated, a property associated to a strong expression of the stemness regulator Oct4. Indeed, this transcription factor is essential for self-renewal and maintenance of unrestricted pluripotency (Kuntz et al. 2008). As such, Oct4 binds at the regulatory regions and/or promoters of numerous target genes, which are associated with proliferation, survival and differentiation processes (Jerabek et al. 2014; Sharif et al. 2011a). To gain greater specificity, Oct4 may form protein complexes with two other transcriptional regulators, i.e. the homeobox protein Nanog and the SRY-related HMG-box protein Sox2 (Boyer et al. 2005). It is now accepted that Oct4 is detectable in CSCs from diverse tumour origin (Prud'homme 2012) and its presence, as part of the molecular signature of unrestricted pluripotency, has been observed in poorly differentiated and highly proliferative and invasive cancers (Ben-Porath et al. 2008; Sharif et al. 2011a, 2011b).

Here, we show that FL3 selectively induces differentiation of pluripotent cancer stem-like cells at sublethal nanomolar concentrations. This effect involves a downregulation of the major guardian of a highly pluripotent cell state, namely Oct4, by targeting its degradation and its transcription. As a consequence, cells undergo differentiation in the neural pathway, with the appearance of specific markers, like βIII-tubulin (a microtubule element expressed in neurons) and glial fibrillary acidic protein (GFAP) (an intermediate filament expressed in astrocytes) (Kim et al. 2011). Our study therefore highlights the pro-differentiation properties of flavaglines. Since they act through a mechanism independent of retinoic acid receptor activity, they could be promising alternative chemotherapeutic drugs in ATRA-resistant and Oct4-expressing cancers.

Materials and methods

Cell lines and culture conditions

NT2/D1 (CRL-1973) cell line, purchased from ATCC (LGC Standards, Molsheim, France), was cultivated in DMEM-based media (Sigma-Aldrich, Saint-Quentin-Fallavier, France), supplemented with 10% (*v*/*v*) foetal bovine serum (BioWhittaker, Verviers, Belgium), 50 μg/ml streptomycin, 50 U/ml penicillin and 2 mM glutamine (Sigma-Aldrich). Cells were grown in Petri dishes to 30% confluency prior to treatment. All plates were incubated in humidified atmosphere with 5% CO_2 at 37 °C.

Cell treatment

FL3, synthesized as previously described (Thuaud et al. 2009), and ATRA (Sigma-Aldrich) were diluted at 10 mM in dimethyl sulfoxide (DMSO). For our purpose, the cells were treated with either 10 nM of FL3 or 1 μM ATRA mixed with the cell culture medium. At that concentration, we previously reported that FL3 has no significant toxic effects on cancer cells after 24 h of treatment (Emhemmed et al. 2014). Treatment was carried out till 12 days, and FL3- or ATRA-supplemented medium was changed every 2 days.

Clonogenic assay

Individual spheroids were generated by seeding 200 μl/well of a cell suspension at a density of 1.5×10^4 cells/ml in ultra-low-attachment 96-well plates (Sigma-Aldrich). After 4-day incubation, each spheroid was exposed to either vehicle (DMSO) or FL3 for different times. Image analysis of tumour spheroids and determination of their diameter were carried out by using a Celigo cytometer (Cyntellect Inc., San Diego, CA, USA), as previously described (Vinci et al. 2012).

Immunocytochemistry analysis

Cells at a density of 4×10^4 were seeded in imaging μ-Dishes (Ibidi, Martinsried, Germany) and incubated for 24 h. The cells were then fixed with 4% paraformaldehyde for 15 min, permeabilized with 0.3% Triton X-100 in phosphate-buffered saline (PBS) for 15 min and blocked in 2% normal goat serum for 30 min at room temperature. After rinsing, the cells were incubated with either a rabbit polyclonal anti-Oct4 or anti-Nanog antibody (GeneTex, Irvine, CA, USA), a rabbit polyclonal anti-GFAP antibody (Abgent, San Diego, CA, USA) or a mouse monoclonal anti-βIII-tubulin antibody (Abnova, Taipei City, Taiwan). All the primary antibodies were diluted at 1:200–1:400 in 2% normal goat serum. After 2 h of incubation at room temperature, the cells were washed with PBS and exposed for an additional half hour to either a mouse or a rabbit Alexa Fluor 488-conjugated secondary antibody (Life Technologies, Saint Aubin, France), diluted at 1:2000 in 2% normal goat serum. After rinsing, the cells were stained with Hoechst 33342 (Life Technologies), diluted at 1:10,000 for 5 min. Images were captured using a Leica TCS SP2 laser scanning confocal microscope (Leica Microsystems, Nanterre, France).

Western blot analysis

Exponentially growing cells were treated with the vehicle or FL3 and incubated at different times. The cells were harvested and centrifuged at 200*g* for 10 min at room temperature, and the pellets were resuspended in RIPA buffer (25 mM Tris pH 7.6, 150 mM NaCl, 1% NP-40, 0.1% SDS, 1% sodium deoxycholate) containing protease inhibitors (Sigma-Aldrich). Proteins of cell lysates were then extracted, separated on 8–15% SDS-polyacrylamide gels and transferred to membranes. Immunoblotting was performed as previously described (Sharif et al. 2012), by using either a rabbit polyclonal anti-Oct4, anti-Nanog or anti-Sox2 antibody (GeneTex); a rabbit polyclonal anti-GFAP antibody (Abgent); a mouse monoclonal anti-βIII-tubulin antibody (Abnova); a rabbit monoclonal anti-STAT3 (phospho Y705) antibody (Abcam, Paris, France); a rabbit polyclonal anti-cleaved caspase-3 antibody (Cell Signaling Technology, Danvers, MA, USA); or a rabbit polyclonal germ cell nuclear factor (GCNF) antibody (Abcam). Membranes were subsequently reprobed with a mouse polyclonal anti-beta tubulin antibody (Abcam), a rabbit polyclonal anti-beta actin antibody (Abcam) or a rabbit polyclonal anti-glyceraldehyde-3-phosphate dehydrogenase (GAPDH) antibody (Abcam).

Quantitative RT/PCR analysis

Total RNA from untreated and treated cells was extracted using the EZ-10 DNAaway RNA Mini-prep kit (Bio Basic Inc., Toronto, Canada) following the manufacturer's instructions. PCR reaction was then carried out with 10 ng RNA and 200 nM of specific primers (QuantiTect primers QT00210840, QT01025850, QT00079247 for Oct4, Nanog and GAPDH, respectively; Qiagen, Courtaboeuf, France), using the KAPA SYBR Fast One-Step qRT-PCR kit (Kapa Biosystems Ltd., London, UK), according to the manufacturer's specifications. Amplification was performed on an iCycler MyiQ system (Bio-Rad, Marnes-la-Coquette, France).

Statistical analysis

Data were presented in a bar graph form and expressed as means ± SEM of at least three independent experiments. Statistical evaluation was performed with the one-way ANOVA test, followed by Tukey's post hoc analysis or Student's *t* test using the GraphPad Prism software (GraphPad Software Inc., CA, USA); a *p* value less than 0.05 was considered as significant.

Results

FL3 treatment is able to induce the disappearance of stemness factors and the appearance of neural markers in teratocarcinomal cells

Differentiation involves a steady reduction and, finally, the disappearance of the stemness factors in poorly differentiated CSCs. Accordingly, teratocarcinomal cells treated for 12 days with 10 nM of FL3 showed morphological changes (Supplement Fig. 1), concomitantly with an absence of Oct4 and Nanog, in contrast to untreated cells, which exhibit strong nuclear labelling of both proteins (Fig. 1a). Moreover, FL3-treated teratocarcinomal cells exhibited a strong

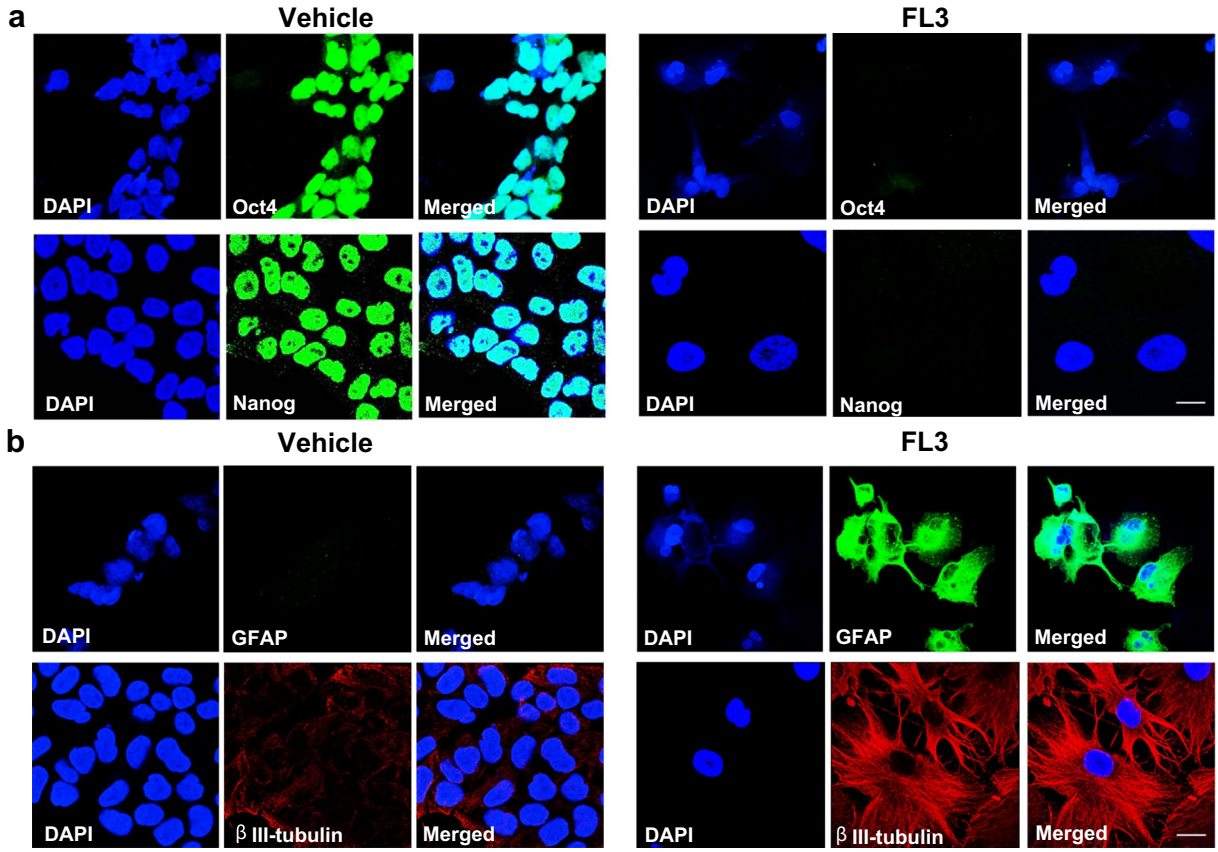

Fig. 1 FL3 treatment induces the disappearance of stemness factors and the appearance of neural markers in NT2/D1 cells. Cells were exposed to either 10 nM of FL3 (*right panels*) or to vehicle (*left panels*). In **a**, the nuclear labelling, in relation with an expression of either Oct4 or Nanog, is not observed in cells treated with FL3 for 12 days, in contrast to untreated cells. In **b**, a high cytoplasmic labelling, in relation with an expression of either GFAP or βIII-tubulin, is observed in cells treated with FL3 for 12 days, in contrast to untreated cells. Nuclei were stained with DAPI. *Scale bar* 10 μm

cytoplasmic labelling of GFAP and βIII-tubulin, which are two main markers of neural differentiation (Kim et al. 2011) (Fig. 1b). These results therefore suggest that FL3 is able to repress the stemness maintenance and to induce a neuro-ectodermic differentiation of embryonal carcinoma cells.

Long-lasting treatment with FL3 at low concentration induces a gradual downregulation of the stemness factors in teratocarcinomal cells

The expression levels of the stemness factor Oct4 and its interactive partners Nanog and Sox2 were monitored during the 12 days of treatment with 10 nM of FL3. As shown in Fig. 2a, b, a progressive, but significant decrease of the expression rates of these transcription factors was observed. At day 8 of treatment, only faint bands were visualized by immunoblotting, suggesting that the embryonal cells have definitively lost their highly pluripotent state. Surprisingly, a detailed analysis of Fig. 2b showed a transitory and reproducible upregulation of Oct4 at day 2 of treatment. It should be noted that such transient upregulation is also observed in mouse P19 teratocarcinomal stem-like cells, when treated with ATRA (Fuhrmann et al. 2001). The molecular mechanisms behind this phenomenon remain to be determined.

The expression patterns of Oct4 are delayed during long-lasting treatment of teratocarcinomal cells with FL3 and ATRA

ATRA is a known differentiation factor of teratocarcinomal cells, which acts as a gene repressor of the stemness factor Oct4. We therefore investigated the behaviour of this transcription factor, by

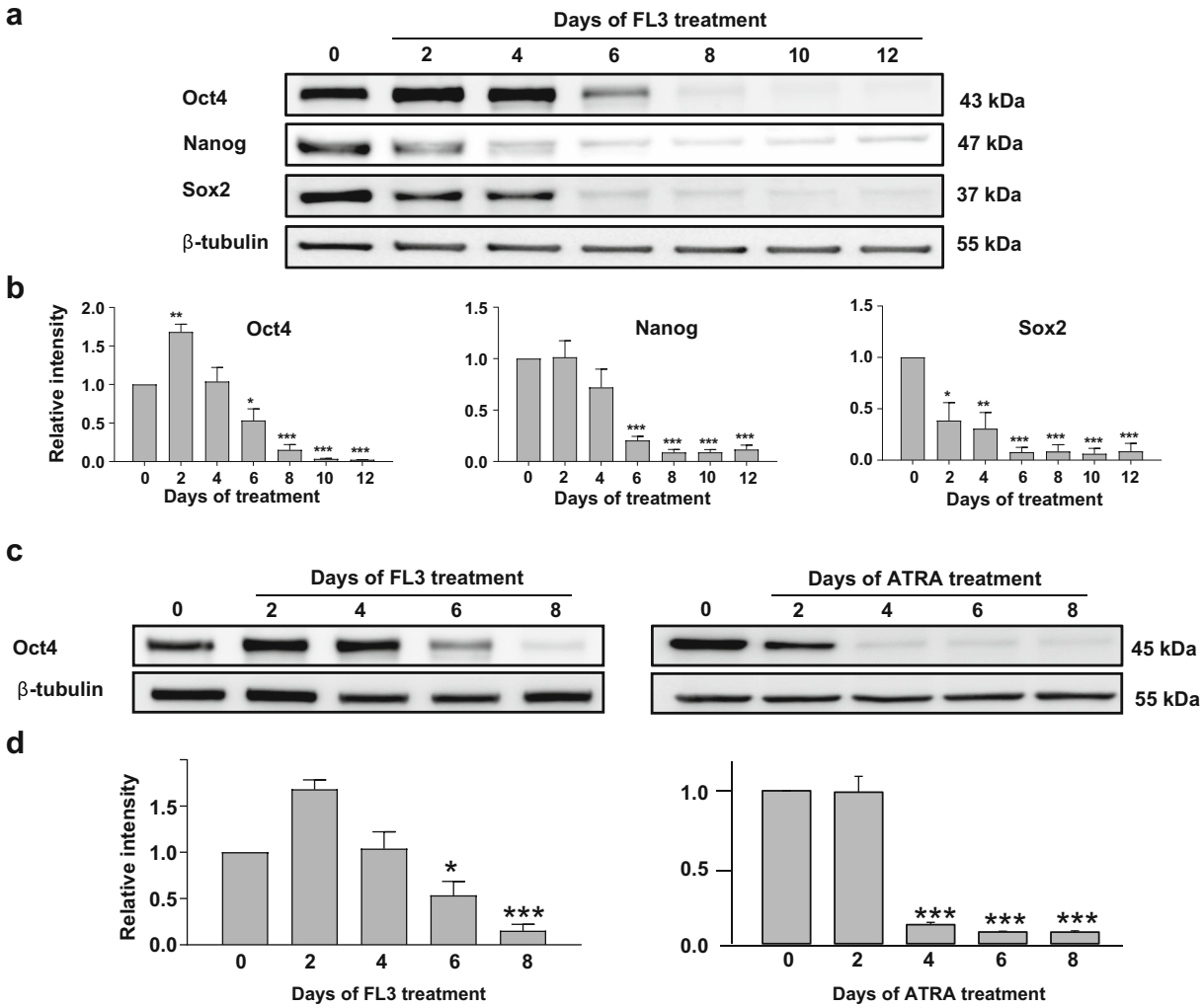

Fig. 2 Time-dependent effects of FL3 or ATRA on the expression levels of stemness factors in NT2/D1 cells. Cells were exposed to 10 nM of FL3 or 1 μM ATRA and incubated at the indicated times. Immunoblotting analyses were performed as described in "Materials and methods" section with the corresponding antibodies. Specific bands were detected with their expected apparent molecular weight. **a**, **c** Representative immunoblotting results. The sequential *panels* in **b**, **d** show densitometry results of the expression of the indicated stemness factors, normalized to β-tubulin expression and given as ratios relative to the value obtained for the untreated sample. Values are means ± SEM of at least three independent experiments; statistically significant: $*p < 0.05$; $**p < 0.01$; $***p < 0.001$ (versus untreated group)

monitoring its expression pattern during a long-lasting treatment with either FL3 (10 nM) or ATRA (1 μM). As shown in Fig. 2c, d, a similar time-dependent decrease of Oct4 expression levels was observed with the two treatments in the cancer stem-like cells. It should be noted, however, that ATRA seemed to act earlier than FL3; indeed, a reduction of Oct4 expression levels of over 50% was detected by day 4 in ATRA-treated cells, whereas, at that time, Oct4 content remained unchanged in FL3-treated cells.

Long-lasting treatment with FL3 at low concentration induces a gradual upregulation of neural markers in teratocarcinomal cells

The expression levels of several neural factors, namely βIII-tubulin (neuronal marker) and GFAP (astrocyte marker) (Kim et al. 2011), were monitored during the 12 days of treatment with FL3 (10 nM). As shown in Fig. 3a, b, a progressive, but significant increase of the expression rates of these neural factors was observed. From day 8 of

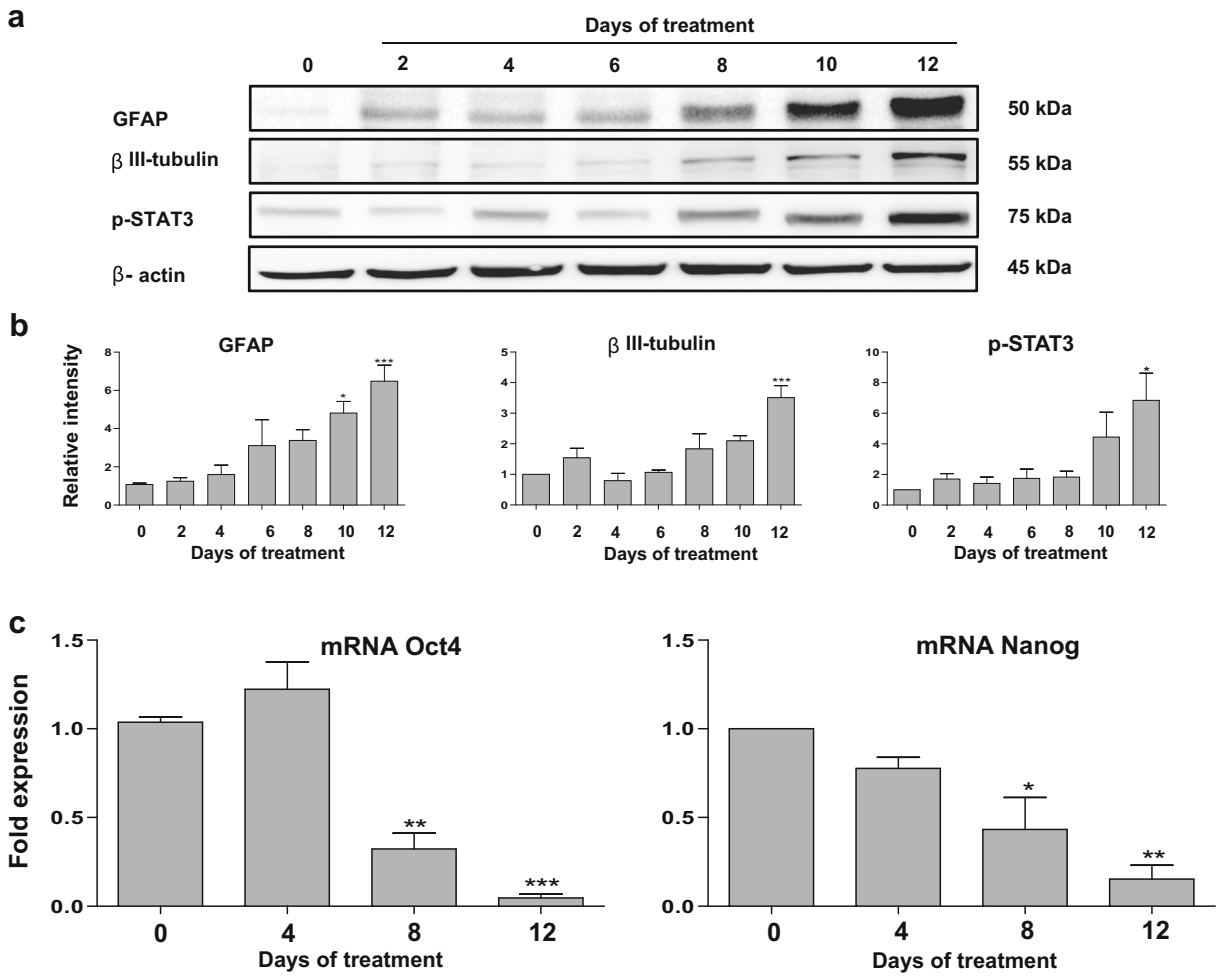

Fig. 3 Time-dependent effects of FL3 on the expression levels of neural markers and mRNA expression levels of stemness factors in NT2/D1 cells. Cells were exposed to 10 nM of FL3 and incubated at the indicated times. Immunoblotting analyses and RT/PCR were performed as described in "Materials and methods" section with the corresponding antibodies or primer pairs, respectively. **a** Representative immunoblotting results with specific bands detected at their expected apparent molecular weight. The three sequential *panels* in **b** show densitometry results of GFAP, βIII-tubulin and phospho-STAT3 expressions normalized to β-actin expression and given as ratios relative to the value obtained for the untreated sample. **c** Results obtained for the expression levels of Oct4 and Nanog transcripts, normalized to the expression levels of GAPDH mRNA and given as ratios relative to the value obtained for the untreated sample. Values are means ± SEM of four independent experiments; statistically significant: $*p < 0.05$; $**p < 0.01$; $***p < 0.001$ (versus untreated group)

treatment, strong bands were visualized by immunoblotting, suggesting that the embryonal cells have definitively switched from a highly undifferentiated state to a neural phenotype. Accordingly, we also observed enhanced levels of phospho-STAT3 Y-705, which are crucial for astrocyte commitment (Cheng et al. 2011; Nagao et al. 2007). These results clearly demonstrated that FL3-treated teratocarcinomal cells have acquired a neural phenotype, with a production of both neurons and astrocytes.

Long-lasting treatment with FL3 at low concentration induces a gradual downregulation of the transcript levels of the stemness factors in teratocarcinomal cells

The expression levels of Oct4 and Nanog mRNAs were monitored during the 12 days of treatment with 10 nM of FL3. As shown in Fig. 3c, a progressive, but significant decrease of the expression rates of both transcripts was observed. These results were in agreement with those obtained at the protein level,

suggesting that the drug could target the regulatory mechanisms involved in both the neosynthesis and the degradation of the two stemness factors.

Long-lasting treatment with FL3 at low concentration inhibits the formation of embryoid bodies from teratocarcinomal cells

The growth of embryonal stem cell-derived spheres was monitored during the 12 days of treatment with 10 nM of FL3. As shown in Fig. 4, the drug significantly repressed the formation of embryoid bodies. At day 12 of the treatment, their diameter was roughly half of that observed for either the vehicle or the control. Thus, these results suggest that FL3 is able to interfere with the self-renewal capacities of the cancer stem-like cells and, as a consequence, to induce differentiation.

Long-lasting treatment with FL3 at low concentration induces a transient expression of cleaved caspase-3 and a gradual upregulation of GCNF in teratocarcinomal cells

The expression levels of active caspase-3 were monitored during the 12 days of treatment with 10 nM of FL3. As shown in Fig. 5a, b, a transient appearance of the main effector of apoptosis could be visualized by immunoblotting, with a peak of expression at days 2 and 4 of the treatment. Furthermore, a gradual, but significant increase of the expression rates of a repressor of Oct4 gene expression, namely GCNF, was observed. These results suggest therefore that the drug targets two different regulatory mechanisms of the Oct4-ome: the first one involves a caspase-3-dependent degradation of Oct4, as we described previously (Emhemmed

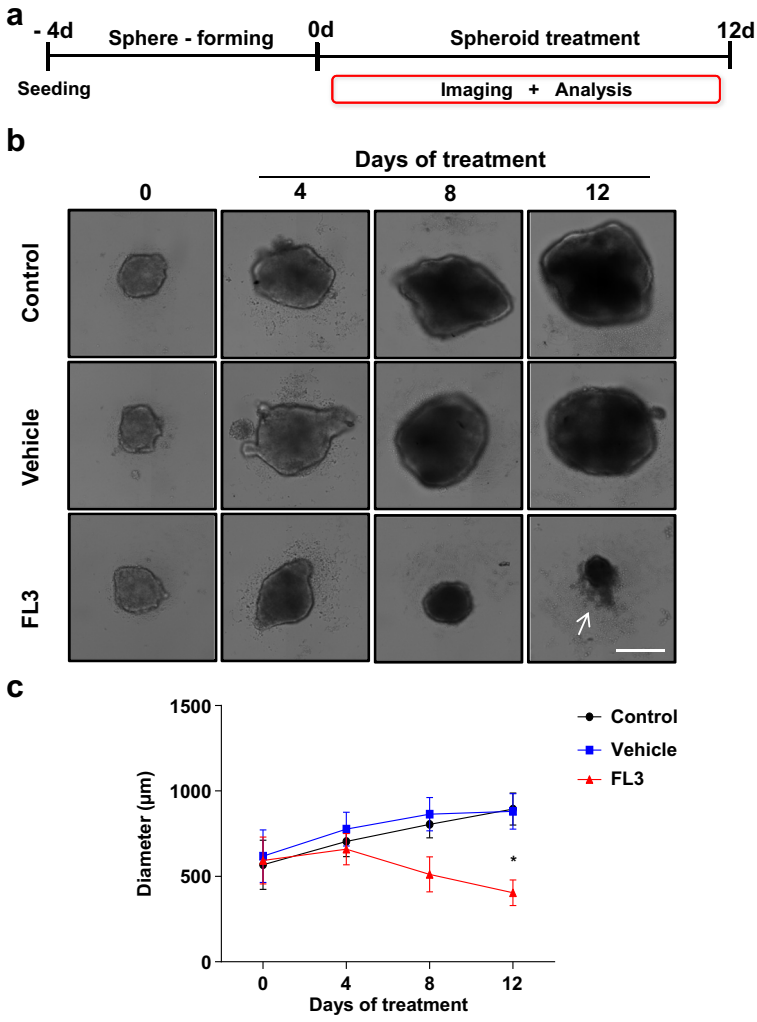

Fig. 4 FL3-dependent inhibition of tumour spheroid growth. **a** Schematic illustration of NT2/D1 spheroid growth kinetics and FL3 treatment procedure. Cells, seeded at day 4, formed spheroids which were treated from day 0 until day 12 with 10 nM of FL3. Imaging and analysis were performed at the indicated times with a Celigo cytometer. **b** Representatives images of spheroids treated or not with either FL3 or vehicle and for the indicated times. Note that FL3-treated spheroids are characterized at day 12 by substantial morphological changes (i.e. cell detachment (see *arrow*)). **c** Curve graph showing the diameter variations of spheroids after treatment with either 10 nm FL3 or vehicle and for the indicated times. Values are means ± SEM of four independent experiments; statistically significant: $*p < 0.05$ (versus untreated group). *Scale bar* 500 µm

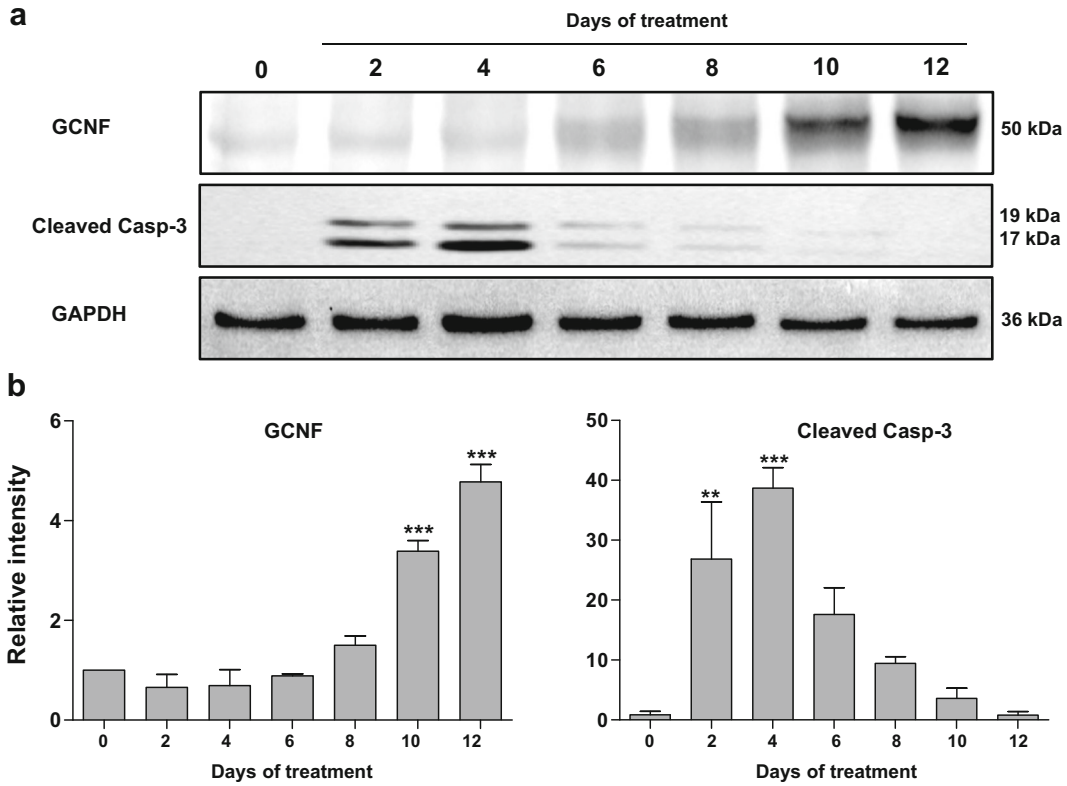

Fig. 5 Time-dependent effects of FL3 on the expression levels of GCNF and cleaved caspase-3 in NT2/D1 cells. Cells were exposed to 10 nM of FL3 and incubated at the indicated times. Immunoblotting analyses were performed as described in "Materials and methods" section with the corresponding antibodies. Specific bands were detected with their expected apparent molecular weight. **a** Representative immunoblotting results. The two sequential *panels* in **b** show densitometry results of GCNF and active caspase-3 expressions normalized to GAPDH expression and given as ratios relative to the value obtained for the untreated sample. Values are means ± SEM of four independent experiments; statistically significant: $^{**}p < 0.01$; $^{***}p < 0.001$ (versus untreated group)

et al. 2014). The second one implicates the transcription factor GCNF that acts as the initial repressor of Oct4 gene activity and which expression is known to be upregulated when teratocarcinomal cells are differentiating, for instance, after ATRA treatment (Fuhrmann et al. 2001).

Discussion

By means of different experimental approaches, we demonstrate that the flavagline FL3 has a strong potential to erase the molecular signature of stemness in embryonal cells and to induce their neural differentiation. In a previous work, we reported that FL3 triggers apoptosis in these cancer stem-like cells, with little effect on normal stem-like cells; this specific effect involves an activation of p38 MAPK and consequently of caspase-3 (Emhemmed et al. 2014). Since flavagline derivatives are acting as multi-target drugs (Basmadjian et al. 2013; Mata-Greenwood et al. 2001), it is expected that they could also modulate the activity of particular components involved in the control of the self-renewal and its associated differentiation process, depending on their concentration and their incubation time. Accordingly, it has been recently demonstrated that anti-cancer drugs, alone or in combination, can recruit different signalling pathways, depending on the order and duration of their delivery (Lee et al. 2012). All this explains why a specific pharmacological agent can lead to a different cellular response, i.e. apoptosis or differentiation.

In the present study, FL3 is administrated at sublethal concentration and for long period; in these conditions, we observed that the drug had no significant effect on the apoptosis rate of both teratocarcinomal cancer stem-like cells and fibroblast normal stem-like cells which, de

facto, do not display an activation of p38 MAPK (data not shown). In contrast, FL3, at that concentration (10 nM), is able to repress in embryonal cancer stem-like cells, the expression of stemness factors at both the transcriptional and translational levels. As a consequence, cells lose their capability to self-renew and to form embryoid bodies. In that point of view, FL3 acts like ATRA, which has been described as a strong repressor of embryonic sphere formation in vitro (Huang et al. 2013). This repression involves an upregulation of p21, which leads to cell cycle arrest in both FL3-treated (data not shown) or ATRA-treated embryonal cells (Malik et al. 2013). Moreover, the subsequent blockage of the self-renewal process has a direct impact on either normal or pathological stem cells, by triggering their differentiation. Accordingly, we observed that long-lasting treated teratocarcinomal cells with FL3 direct their specification towards neural cells, as demonstrated by the appearance of specific markers of either the neuronal or glial specification. Interestingly, similar observations have been reported for ATRA, which preferentially induces a neuroectodermic differentiation of both embryonic and embryonal stem cells (Rohwedel et al. 1999; Xia et al. 2007).

As mentioned previously, cell self-renewal is controlled by specific proteins, which are also expected to be involved in cell survival (Sharif et al. 2011a, b). Indeed, Oct4, as a marker of stemness and unrestricted pluripotency, also plays a central role in the survival of poorly differentiated CSCs (Ben-Porath et al. 2008; Sharif et al. 2011b, 2013). In fact, at the top of the pluripotency regulatory network, Oct4, Nanog and Sox2 work cooperatively to activate or repress numerous target genes devoted to different cell processes like proliferation, survival or differentiation. Downregulation of the expression levels of these transcription factors therefore induces a loss of the self-renewal capacity and promotes either cell death or differentiation (Jerabek et al. 2014; Sharif et al. 2011a).

The molecular determinants of the cell reactivity to a long-lasting treatment of low concentration of FL3 seem to be similar as those described for ATRA. Accordingly, it has been previously observed that a transient/moderate activity of caspase-3 can mediate the differentiation of embryonic stem cells without inducing apoptosis, suggesting that the major component of the programmed cell death pathway could also be involved in the regulation of stem cell development (Abdul-Ghani and Megeney 2008; Fujita et al. 2008). More recently, it has been reported that drug-induced differentiation of embryonal CSCs involves the degradation of stem cell-specific proteins by caspases (Musch et al. 2010). Oct4 and Nanog, as targets of caspase-3 (Emhemmed et al. 2014), are therefore concerned by this degradation-inducing differentiation process. On the other hand, we observed a progressive increase of the expression levels of GCNF in FL3-treated cancer stem-like cells. This orphan nuclear receptor is known to repress Oct4 gene activity by binding specifically within the proximal promoter, and its upregulation in teratocarcinomal cells treated with ATRA initiates Oct4 transcript and protein downregulation during cell differentiation (Fuhrmann et al. 2001). Taken as a whole, long-lasting treatment with low-concentration FL3 activates two different regulatory mechanisms that lead to the loss of pluripotency. The first one involves a caspase-3-dependent degradation of the stemness factors Oct4 and Nanog, and the second one likely involves a GCNF-dependent gene repression of these factors. Further investigations are now necessary in order to validate an attempt to link the two different processes recruited during FL3-associated cell reactivity and Oct4 repression.

Finally, our previous and present findings show that the flavagline FL3 has the potential to induce a downregulation of Oct4 in teratocarcinomal cells, either after a short-term treatment with high concentration (Emhemmed et al. 2014) or a long-lasting treatment with low concentration. However, depending on the treatment conditions, FL3 has either a pro-apoptotic or pro-differentiating effect. In this point of view, the drug could be a novel differentiation factor of other Oct4-expressing CSCs, as FL3 acts on Oct4 network through a mechanism independent of retinoic acid receptor activity, it might become an alternative chemotherapeutic compound in ATRA-resistant blood and solid cancers, which are expressing Oct4.

Acknowledgements This study was supported by grants from the CCIR-GE of the "Ligue contre le Cancer" (Comité du Grand Est, France) to G.F. and the "Association pour la Recherche sur le Cancer" (Grant SFI20111204054, Villejuif, France) to L.D. We are also grateful to AAREC Filia Research and ANRT for fellowships to Q.Z. F.E. was supported by a fellowship from the Higher Education Commission of Libya.

Compliance with ethical standards

Conflict of interest The authors declare that they have no conflict of interest.

References

Abdul-Ghani M, Megeney LA. Rehabilitation of a contract killer: caspase-3 directs stem cell differentiation. Cell Stem Cell. 2008;2:515–6.

Al-Hajj M, Becker MW, Wicha M, Weissman I, Clarke MF. Therapeutic implications of cancer stem cells. Curr Opin Genet Dev. 2004;14:43–7.

Ali Azouaou S, Emhemmed F, Idris-Khodja N, Lobstein A, Schini-Kerth V, Muller CD, et al. Selective ROS-dependent p53-associated anticancer effects of the hypoxoside derivative rooperol on human teratocarcinomal cancer stem-like cells. Investig New Drugs. 2015;33:64–74.

Basmadjian C, Thuaud F, Ribeiro N, Désaubry L. Flavaglines: potent anticancer drugs that target prohibitins and the helicase eIF4A. Future Med Chem. 2013;5:2185–97.

Ben-Porath I, Thomson MW, Carey VJ, Ge R, Bell GW, Regev A, et al. An embryonic stem cell-like gene expression signature in poorly differentiated aggressive human tumors. Nat Genet. 2008;40:499–507.

Boyer LA, Lee TI, Cole MF, Johnstone SE, Levine SS, Zucker JP, et al. Core transcriptional regulatory circuitry in human embryonic stem cells. Cell. 2005;122:947–56.

Cheng PY, Lin YP, Chen YL, Lee YC, Tai CC, Wang YT, et al. Interplay between SIN3A and STAT3 mediates chromatin conformational changes and GFAP expression during cellular differentiation. PLoS One. 2011;6:e22018.

Chlapek P, Neradil J, Redova M, Zitterbart K, Sterba J, Veselska R. The ATRA-induced differentiation of medulloblastoma cells is enhanced with LOX/COX inhibitors: an analysis of gene expression. Cancer Cell Int. 2014;14:51.

Emhemmed F, Ali Azouaou S, Thuaud F, Schini-Kerth V, Désaubry L, Muller CD, et al. Selective anticancer effects of a synthetic flavagline on human Oct4-expressing cancer stem-like cells via a p38 MAPK-dependent caspase-3-dependent pathway. Biochem Pharmacol. 2014;89:185–96.

Freemantle SJ, Spinella MJ, Dmitrovsky E. Retinoids in cancer therapy and chemoprevention: promise meets resistance. Oncogene. 2003;22:7305–15.

Fuhrmann G, Chung AC, Jackson KJ, Hummelke G, Baniahmad A, Sutter J, et al. Mouse germline restriction of Oct4 expression by germ cell nuclear factor. Dev Cell. 2001;1:377–87.

Fujita J, Crane AM, Souza MK, Dejosez M, Kyba M, Flavell RA, et al. Caspase activity mediates the differentiation of embryonic stem cells. Cell Stem Cell. 2008;2:595–601.

Grimwade D, Mistry AR, Solomon E, Guidez F. Acute promyelocytic leukemia: a paradigm for differentiation therapy. Cancer Treat Res. 2010;145:219–35.

Huang FJ, Lan KC, Kang HY, Lin PY, Chan WH, Hsu YC, et al. Retinoic acid influences the embryoid body formation in mouse embryonic stem cells by induction of caspase and p38 MAPK/JNK-mediated apoptosis. Environ Toxicol. 2013;28:190–200.

Jerabek S, Merino F, Schöler HR, Cojocaru V. OCT4: dynamic DNA binding pioneers stem cell pluripotency. Biochim Biophys Acta. 2014;1839:138–54.

Kim ES, Kim GH, Kang ML, Kang YM, Kang KN, Hwang KC, et al. Potential induction of rat muscle-derived stem cells to neural-like cells by retinoic acid. J Tissue Eng Regen Med. 2011;5:410–4.

King ML, Chiang CC, Ling HC, Fujita E, Ochiai M, McPhail AT. X-ray crystal structure of rocaglamide, a novel antileukemic 1H-cyclopenta[*b*]benzofuran from Aglaia elliptifolia. J Chem Soc Chem Commun. 1982;20:1150–1.

Konopleva MY, Jordan CT. Leukemia stem cells and microenvironment: biology and therapeutic targeting. J Clin Oncol. 2011;29:591–9.

Kuntz S, Kieffer E, Bianchetti L, Lamoureux N, Fuhrmann G, Viville S. Tex19, a mammalian-specific protein with a restricted expression in pluripotent stem cells and germ line. Stem Cells. 2008;26:734–44.

Lee MJ, Ye AS, Gardino AK, Heijink AM, Sorger PK, MacBeath G, et al. Sequential application of anticancer drugs enhances cell death by rewiring apoptotic signaling networks. Cell. 2012;149:780–94.

Malik YS, Sheikh MA, Lai M, Cao R, Zhu X. RING finger protein 10 regulates retinoic acid-induced neuronal differentiation and the cell cycle exit of P19 embryonic carcinoma cells. J Cell Biochem. 2013;114:2007–15.

Mata-Greenwood E, Ito A, Westenburg H, Cui B, Mehta RG, Kinghorn AD, et al. Discovery of novel inducers of cellular differentiation using HL-60 promyelocytic cells. Anticancer Res. 2001;21:1763–70.

Moselhy J, Srinivasan S, Ankem MK, Damodaran C. Natural products that target cancer stem cells. Anticancer Res. 2015;35:5773–88.

Musch T, Oz Y, Lyko F, Breiling A. Nucleoside drugs induce cellular differentiation by caspase-dependent degradation of stem cell factors. PLoS One. 2010;5:e10726.

Nagao M, Sugimori M, Nakafuku M. Cross talk between notch and growth factor/cytokine signaling pathways in neural stem cells. Mol Cell Biol. 2007;27:3982–94.

Pistollato F, Giampieri F, Battino M. The use of plant-derived bioactive compounds to target cancer stem cells and modulate tumor microenvironment. Food Chem Toxicol. 2015;75:58–70.

Prud'homme GJ. Cancer stem cells and novel targets for antitumor strategies. Curr Pharm Des. 2012;18:2838–49.

Rohwedel J1, Guan K, Wobus AM. Induction of cellular differentiation by retinoic acid in vitro. Cells Tissues Organs. 1999;165:190–202.

Sarkar FH, Li Y, Wang Z, Kong D. Cellular signaling perturbation by natural products. Cell Signal. 2009;21:1541–7.

Sell S. Stem cell origin of cancer and differentiation therapy. Crit Rev Oncol Hematol. 2004;51:1–28.

Sharif T, Emhemmed F, Fuhrmann G. Towards new anticancer strategies by targeting cancer stem cells with phytochemical compounds. In: Shostak S, editor. Cancer stem cells—the cutting edge. Rijeka: Intech; 2011a. p. 431–56.

Sharif T, Auger C, Bronner C, Alhosin M, Klein T, Etienne-Selloum N, et al. Selective proapoptotic activity of polyphenols from red wine on teratocarcinoma cell, a model of cancer stem-like cell. Investig New Drugs. 2011b;29:239–47.

Sharif T, Alhosin M, Auger C, Minker C, Kim JH, Etienne-Selloum N, et al. *Aronia melanocarpa* juice induces a redox-sensitive p73-related caspase 3-dependent apoptosis in human leukemia cells. PLoS One. 2012;7:e32526.

Sharif T, Stambouli M, Burrus B, Emhemmed F, Dandache I, Auger C, et al. The polyphenolic-rich *Aronia melanocarpa* juice kills teratocarcinomal cancer stem-like cells, but not their differentiated counterparts. J Funct Foods. 2013;5:1244–52.

Thuaud F, Bernard Y, Türkeri G, Dirr R, Aubert G, Cresteil T, et al. Synthetic analogue of rocaglaol displays a potent and selective cytotoxicity in cancer cells: involvement of apoptosis inducing factor and caspase-12. J Med Chem. 2009;52:5176–87.

Vinci M, Gowan S, Boxall F, Patterson L, Zimmermann M, Court W, et al. Advances in establishment and analysis of three-dimensional tumor spheroid-based functional assays for target validation and drug evaluation. BMC Biol. 2012;10:29.

Wang Y, Wang H, Lv X, Liu C, Qi L, Song X, et al. Enhancement of all-trans retinoic acid-induced differentiation by pH-sensitive nanoparticles for solid tumor cells. Macromol Biosci. 2014;14:369–79.

Xia C, Wang C, Zhang K, Qian C, Jing N. Induction of a high population of neural stem cells with anterior neuroectoderm characters from epiblast-like P19 embryonic carcinoma cells. Differentiation. 2007;75:912–27.

Publication N°*8*

Flavaglines ameliorate experimental colitis and protect against intestinal epithelial cell apoptosis and mitochondrial dysfunction.

Han, J., Zhao, Q., Basmadjian, C., Désaubry, L., Theiss, A.L., *Inflamm. Bowel Dis.*, **2016**, *22*, 55-67.

Flavaglines Ameliorate Experimental Colitis and Protect Against Intestinal Epithelial Cell Apoptosis and Mitochondrial Dysfunction

Jie Han, MS, Qian Zhao, MS, Christine Basmadjian, PhD,† Laurent Désaubry, PhD,† and Arianne L. Theiss, PhD**

Background: Flavaglines are a family of natural compounds shown to have anti-inflammatory and cytoprotective effects in neurons and cardiomyocytes. Flavaglines target prohibitins as ligands, which are scaffold proteins that regulate mitochondrial function, cell survival, and transcription. This study tested the therapeutic potential of flavaglines to promote intestinal epithelial cell homeostasis and to protect against a model of experimental colitis in which inflammation is driven by epithelial ulceration.

Methods: Survival and homeostasis of Caco2-BBE and IEC-6 intestinal epithelial cell lines were measured during treatment with the flavaglines FL3 or FL37 alone and in combination with the proinflammatory cytokines tumor necrosis factor (TNF) α and interferon γ. Wild-type mice were intraperitoneally injected with 0.1 mg/kg FL3 or vehicle once daily for 4 days during dextran sodium sulfate–induced colitis to test the in vivo anti-inflammatory effect of FL3.

Results: FL3 and FL37 increased basal Caco2-BBE and IEC-6 cell viability, decreased apoptosis, and decreased epithelial monolayer permeability. FL3 and FL37 inhibited TNFα- and interferon γ–induced nuclear factor kappa B and Cox2 expression, apoptosis, and increased permeability in Caco2-BBE cells. FL3 and FL37 protected against TNFα-induced mitochondrial superoxide generation by preserving respiratory chain complex I activity and prohibitin expression. p38-MAPK activation was essential for the protective effect of FL3 and FL37 on barrier permeability and mitochondrial-derived reactive oxygen species production during TNFα treatment. Mice administered FL3 during dextran sodium sulfate colitis exhibited increased colonic prohibitin expression and p38-MAPK activation, preserved barrier function, and less inflammation.

Conclusions: These results suggest that flavaglines exhibit therapeutic potential against colitis and preserve intestinal epithelial cell survival, mitochondrial function, and barrier integrity.

(Inflamm Bowel Dis 2016;22:55–67)

Key Words: barrier function, prohibitin, intestinal epithelium, TNFα, colitis

Inflammatory bowel diseases (IBD), the most common forms being Crohn's disease and ulcerative colitis, are associated with disturbed intestinal epithelial cell (IEC) homeostasis. IECs structurally provide host defense by forming a single-cell barrier between luminal contents and the underlying intestinal tissue. Epithelial barrier dysfunction is an early event in the pathogenesis of IBD, resulting in increased exposure of intraluminal contents to the mucosal immune system, thereby aggravating the inflammatory condition.[1] Disruption of the epithelial barrier can be manifested by increased epithelial cell apoptosis not equal to epithelial proliferation (ulceration) and/or by alteration of permeability at the tight junctions that establish a semipermeable barrier between epithelial cells, restricting passage of large molecules.[2] Restoring and maintaining the epithelial barrier are critical to limit mucosal inflammation and promote healing.[1] Identification of agents that act to promote epithelial cell homeostasis and barrier integrity in the context of tissue injury or IBD is critical for the development of therapeutic or preventative strategies to promote or maintain mucosal healing.

Flavaglines comprise a family of compounds found in medicinal plants of Southeast Asia that have shown anticancer, anti-inflammatory, and cytoprotective activities.[3] Flavaglines have been reported to reduce neurotoxicity in a mouse model of Parkinson's disease[4] and protect cardiomyocytes from doxorubicin-induced cardiac toxicity.[5] In addition, at nanomolar concentrations, flavaglines inhibit the production of interferon (IFN) γ, TNFα, interleukin 2, and interleukin 4 by T lymphocytes and proinflammatory mediators from microglia and endothelial cells.[4,6] It is well established that flavaglines target prohibitins (PHBs) as their molecular ligands.[3] PHB (B-cell receptor–associated protein 32) and PHB2 (repressor of estrogen receptor activity, B-cell receptor–associated protein 37) are highly conserved proteins

Supplemental digital content is available for this article. Direct URL citations appear in the printed text and are provided in the HTML and PDF versions of this article on the journal's Web site (www.ibdjournal.org).

Received for publication July 29, 2015; Accepted August 4, 2015.

From the *Department of Internal Medicine, Division of Gastroenterology, Baylor Research Institute, Baylor University Medical Center, Dallas, Texas; and †Therapeutic Innovation Laboratory, CNRS/Université de Strasbourg, Illkirch, France.

Supported by National Institutes of Health grants R03-DK098229 (A. L. Theiss) and funds from the Baylor Research Institute. L. Désaubry was supported by the "Association pour la Recherche sur le Cancer." C. Basmadjian and Q. Zhao received fellowships from AAREC Filia Research and ANRT.

The authors have no conflicts of interest to disclose.

Reprints: Arianne L. Theiss, PhD, Department of Internal Medicine, Division of Gastroenterology, 1053 Wadley Tower, 3600 Gaston Avenue, Baylor Research Institute, Baylor University Medical Center, Dallas, TX 75246 (e-mail: arianne.theiss@baylorhealth.edu).

DOI 10.1097/MIB.0000000000000592

Published online 18 September 2015.

with diverse functions, including regulation of cell cycle progression, apoptosis, and transcription, depending on their posttranslational modifications and subcellular localization.[7] The best characterized function of PHB and PHB2 is their role in maintaining the structure and function of mitochondria, including respiration and protein metabolism, while residing in the inner mitochondrial membrane as heterodimers.[8–10] In IECs, PHB is predominantly localized in the mitochondria, where it has been shown to be required for optimal activity of complexes I and IV of the electron transport chain (ETC).[11–14] During IBD, expression of PHB is decreased in uninvolved and inflamed epithelium.[12,14] Epithelial PHB is protective against intestinal inflammation as evidenced by less severe experimental colitis in transgenic mice with IEC-specific PHB overexpression.[15,16] Gene silencing of PHB in cultured IECs induces mitochondrial membrane depolarization and cellular stress pathways, including intracellular reactive oxygen species (ROS) generation and apoptosis.[17] Furthermore, cultured IECs overexpressing PHB exhibit less intracellular ROS and apoptosis,[17] suggesting that relative levels of PHB modulate epithelial cell homeostasis.

In this study, we investigated the anti-inflammatory activity of the flavaglines FL3 and FL37, which are among the most potent of flavaglines tested in a wide variety of pharmacological assays,[18] in cultured IECs and the dextran sodium sulfate (DSS) model of colitis. We also elucidated the mechanism of FL3 and FL37 protection in IECs.

MATERIALS AND METHODS

Cell Culture

Flavaglines FL3 and FL37 were synthesized in our laboratory as previously described.[19,20] The Caco2-BBE human colonic adenocarcinoma epithelial cell line and the nontransformed IEC-6 rat small IEC line were used as in vitro models of polarized intestinal epithelium. Both cell lines were obtained from the American Type Culture Collection (ATCC, Manassas, VA). Cells were grown in Dulbecco's modified Eagle's medium (Caco2-BBE) supplemented with penicillin (40 mg/L), streptomycin (90 mg/L), and 10% fetal bovine serum. Caco2-BBE cells and IEC-6 cells were plated on permeable supports (pore size, 0.4 μm; transwell-clear polyester membranes; Corning, Tewksbury, MA) and cultured for 8 days to allow the cells to polarize. All experiments performed on Caco2-BBE cells were between passages 32 and 45 and IEC-6 cells were between passages 10 and 18. FL3 and FL37 were administered at 1, 10, and 50 nM because previous studies showed that flavaglines exhibit cardioprotective and neuroprotective effects at 1 to 10 nM.[18] Caco2-BBE or IEC-6 cells were treated with 10 ng/mL recombinant human or rat TNFα or 50 ng/mL recombinant human or rat IFNγ, respectively (R&D Systems, Minneapolis, MN).

PHB Knockdown

To achieve PHB knockdown, Caco2-BBE cells were transiently transfected with Stealth RNAi against PHB1 (5′-CAGAAUGUCAACAUCACACUGCGCA-3′) or Stealth RNAi Negative Control Med GC (Life Technologies, Carlsbad, CA) at 20 μm concentration using Amaxa electroporation with Nucleofector kit T (Lonza, Basel, Switzerland).

Induction of Colitis in Mice

Eight-week-old wild-type (C57BL/6) male and female mice were administered orally DSS (molecular weight, 50,000; MP Biomedicals, Solon, OH) at 2.5% (wt/vol) in tap water ad libitum for 6 days. Controls were administered normal tap water throughout the treatment period. Mice were intraperitoneally injected with 0.1 mg/kg FL3 or vehicle (veh) once daily on days 0 to 4. We chose this dose because it proved to be adequate in our previous assays of cardioprotection in mice.[5] Mean DSS water consumption, body weight, and clinical signs of inflammation were assessed daily during the treatment period. All mice were group housed in standard cages under a controlled temperature (25°C) and photoperiod (12-hour light/dark cycle) and were allowed standard chow and tap water ad libitum. All experiments were approved by the Baylor Research Institute Institutional Animal Care and Use Committee.

Sodium Dodecyl Sulfate Polyacrylamide Gel Electrophoresis and Western Immunoblot Analysis

Total protein was isolated from cultured cells or distal colon mucosa from wild-type mice. The samples were separated by sodium dodecyl sulfate polyacrylamide gel electrophoresis using Laemmli's 2× sodium dodecyl sulfate sample buffer and AnyKD gradient polyacrylamide gels (Bio-Rad, Hercules, CA) followed by electrotransfer to nitrocellulose membranes (Bio-Rad). Membranes were incubated with primary antibodies at 4°C overnight and subsequently incubated with corresponding peroxidase-conjugated secondary antibodies. Membranes were washed and immunoreactive proteins were detected using Amersham ECL Plus reagent (GE Healthcare, Piscataway, NJ). PHB antibody was purchased from Thermo Fisher (Waltham, MA); PHB2, Stat3, and ERK1/2 from Santa Cruz Biotechnology (Santa Cruz, CA); phospho-p38-MAPK, p38-MAPK, pERK1/2, pS727-Stat3, pY705-Stat3, pSAPK/JNK, SAPK/JNK, pAKT, AKT, and cleaved caspase 3 from Cell Signaling Technology (Danvers, MA); proliferating cell nuclear antigen (PCNA) from Abcam (Cambridge, MA); p65 from BD Biosciences (San Jose, CA); and Cox2 from Cayman Chemicals (Ann Arbor, MI). Blots were reprobed with β-tubulin or β-actin (Sigma-Aldrich Corp., St. Louis, MO) antibody as a loading control.

Measuring Mitochondrial ROS

Cells were incubated with Hank's balanced salt solution with 5 μM MitoSOX Red Mitochondrial Superioxide Indicator dye (Life Technologies) for 10 minutes at 37°C. Cells were washed twice with warm Hank's balanced salt solution, and fluorescent intensity was measured at 510 nm excitation/580 nm emission. For experiments using complex I or III inhibitors, 15 minutes before collection, cells were treated with 5 μM rotenone

(Sigma-Aldrich), a complex I inhibitor, or 1 μM antimycin A (Sigma-Aldrich), a complex III inhibitor. For experiments using p38-MAPK inhibitor, cells were incubated with 20 μM p38-MAPK inhibitor SB203580 (Sigma-Aldrich) for 1 hour before treatment with FL3, FL37, and TNFα.

Measuring ATP Concentration

The concentration of ATP was determined using the Enlighten ATP Assay Bioluminescence Detection kit (Promega, Madison, WI) according to the manufacturer's protocol.

Detection of Mitochondrial Complex I Activity

The activity of complex I was measured using the Complex I Dipstick Assay kit (Abcam) according to the manufacturer's protocol using 20 μg of protein.

Cytotoxicity Test

Lactate dehydrogenase cytotoxicity detection kit (Clontech, Mountain View, CA) was used to measure cell viability. An aliquot of 100 μL of culture media was added to 100 μL of lactate dehydrogenase reagent, and percent cytotoxicity and percent viable cells were measured according to the manufacturer's protocol.

Measuring Cell Apoptosis

Percentage of apoptotic cells was measured using the Cell Death Detection ELISA Plus kit (Roche, Indianapolis, IN) as described by the manufacturer. As a second measure of apoptosis, cells or colon sections were stained for terminal deoxynucleotidyl transferase–mediated deoxyuridine triphosphate nick-end labeling (TUNEL) as described by the manufacturer's protocol (Roche). The nuclei of cells were stained with 4',6-diamidino-2-phenylindole (Life Technologies). The number of TUNEL-positive cells were quantitated using a fluorescent microscope across 20 fields per treatment for in vitro experiments or across 20 well-oriented crypts per animal for in vivo experiments.

Colonic epithelial cells were isolated from mice as previously described.[21] Total protein was extracted and analyzed by Western blotting for cleaved caspase 3.

Measurement of Transepithelial Electrical Resistance and Macromolecular Permeability In Vitro

Transepithelial electrical resistance was measured with an epithelial voltohmmeter (Millicell-ers; Millipore, Billerica, MA). For permeability assays, cells were incubated in Hank's balanced salt solution. Fluorescein isothiocyanate (FITC)-dextran (10 mg/mL) (molecular weight 4 kDa; Sigma-Aldrich) was added to the apical chamber. The apical and basolateral chambers were sampled at 30 minutes, 1 hour, and 2 hours after the addition of FITC-dextran to the apical chamber. FITC-dextran concentration was quantified through spectrofluorimetry (excitation, 492 nm, emission, 510 nm). Values are shown as rate (nanograms per milliliter per minute) of FITC-dextran translocation to the basolateral reservoir.

Clinical Score Assessment

A clinical activity score was generated using body weight loss, stool consistency, and the presence of occult blood by a guaiac test (Hemoccult Sense; Beckman Coulter, Fullerton, CA) as described previously.[16] The scores for each parameter were added to get a clinical activity score with 12 being the maximal score.

Histological Damage Score

Distal colon was fixed in formalin and stained with hemotoxylin and eosin for histology. Sections were coded for blind microscopic assessment of inflammation. Histological scoring was performed on the basis of 3 parameters: the severity of inflammation, crypt damage, and ulceration as described previously.[16] These values were added to give a maximal histological score of 11.

Myeloperoxidase Activity

Neutrophil infiltration into the distal colon was quantified by measuring myeloperoxidase activity. Briefly, a portion of colon or cecum was homogenized in 1:20 (wt/vol) 50 mmol/L phosphate buffer (pH 6.0) containing 0.5% hexadecyltrimethyl ammonium bromide on ice by using a Polytron homogenizer. The homogenate was sonicated for 10 seconds, freeze thawed 3 times, and centrifuged at 14,000 rpm for 15 minutes. Supernatant was added to 1 mg/mL of *o*-dianisidine hydrochloride and 5×10^{-4}% hydrogen peroxide, and the change in absorbance at 460 nm was measured. One unit of myeloperoxidase activity was defined as the amount that degraded 1 μmol of peroxidase per minute at 25°C.

In Vivo Permeability Assay

Barrier function was assessed using an FITC-labeled dextran method. Briefly, on day 6 of DSS administration, mice were gavaged with permeability tracer (60 mg/100 g body weight of FITC-labeled dextran, FD-4, M_r 4000; Sigma-Aldrich). Serum was collected retro-orbitally 4 hours after FD-4 gavage, and fluorescence intensity of each sample was measured (excitation, 492 nm; emission, 525 nm). FITC-dextran concentrations were determined from standard curves generated by serial dilution of FITC-dextran and normalized to total protein.

Measuring In Vivo Oxidative Damage

Five-micrometer paraffin-embedded sections of colon were analyzed for 4-hydroxynoneal (4-HNE) staining as a marker of lipid peroxidation. Sections were deparaffinized in xylene, rehydrated in ethyl alcohol gradient, incubated in 0.3% H_2O_2 for 30 minutes, and treated with 10 mM sodium citrate buffer (pH 6.0) at 110°C for 20 minutes in a pressure cooker. Sections were blocked with 5% normal goat serum and incubated with 4-HNE antibody (Abcam) overnight at 4°C. After washing with phosphate-buffered saline, sections were incubated with biotinylated secondary antibodies for 30 minutes at room temperature, and color development was performed using the Vectastain ABC kit (Vector Laboratories)

and 3,3'-Diaminobenzidine (Dako, Carpinteria, CA). Sections were counterstained with hematoxylin.

The oxidative damage to proteins was assessed using a protein carbonyl assay kit (Cayman Chemicals) according to the manufacturer's protocol.

Statistical Analyses

Values are expressed as mean ± SEM. Comparisons between FL3 or FL37 treatment versus vehicle control were analyzed by unpaired Student's *t* test. Comparisons between FL3 or FL37 combined with TNFα or IFNγ treatment were analyzed by 2-way analysis of variance, and subsequent pairwise comparisons used Bonferroni post hoc tests to test for significant differences between 2 particular groups. *P* value <0.05 was considered statistically significant in all analyses.

RESULTS

FL3 and FL37 Decrease IEC Apoptosis

An intact intestinal epithelial barrier that prevents the translocation of intraluminal contents and subsequent immune cell activation is an initial event in suppressing inflammation deeper in the bowel wall.[1] Disruption of the epithelial barrier can be manifested by increased epithelial cell apoptosis not balanced with epithelial proliferation. To determine whether very low (nanomolar) doses of FL3 or FL37 affect IEC viability, polarized Caco2-BBE or IEC-6 cell monolayers were treated with increasing concentrations of FL3 or FL37 for 16 hours and markers of cell proliferation or apoptosis were measured. Ten and 50 nanomolar of FL3 or FL37 enhanced cell viability in Caco2-BBE cells as measured by lactate dehydrogenase release (Fig. 1A). IEC-6 nontransformed cells were used as a second in vitro model of IECs. FL3 and FL37 increased viability of IEC-6 cells at the higher doses tested (see Fig. A, Supplemental Digital Content 1, http://links.lww.com/IBD/B116). To determine whether increased cell viability was associated with changes in cell proliferation, PCNA protein expression was measured. FL3 and FL37 did not affect PCNA protein expression in Caco2-BBE cells, suggesting that FL3 and FL37 do not increase cell proliferation (Fig. 1B). FL3 and FL37 decreased Caco2-BBE cell apoptosis measured by enzyme-linked immunosorbent assay (Fig. 1C) and TUNEL staining (Fig. 1D). The number of apoptotic cells was decreased to approximately 5% during treatment with FL3 or FL37 compared with 10% in vehicle-treated cells (Fig. 1D).

FL3 and FL37 Increase Protein Expression of Known Flavagline Targets PHB and PHB2 in IECs

To determine whether FL3 or FL37 alters IEC expression of PHB or PHB2, which are established flavagline targets,[3]

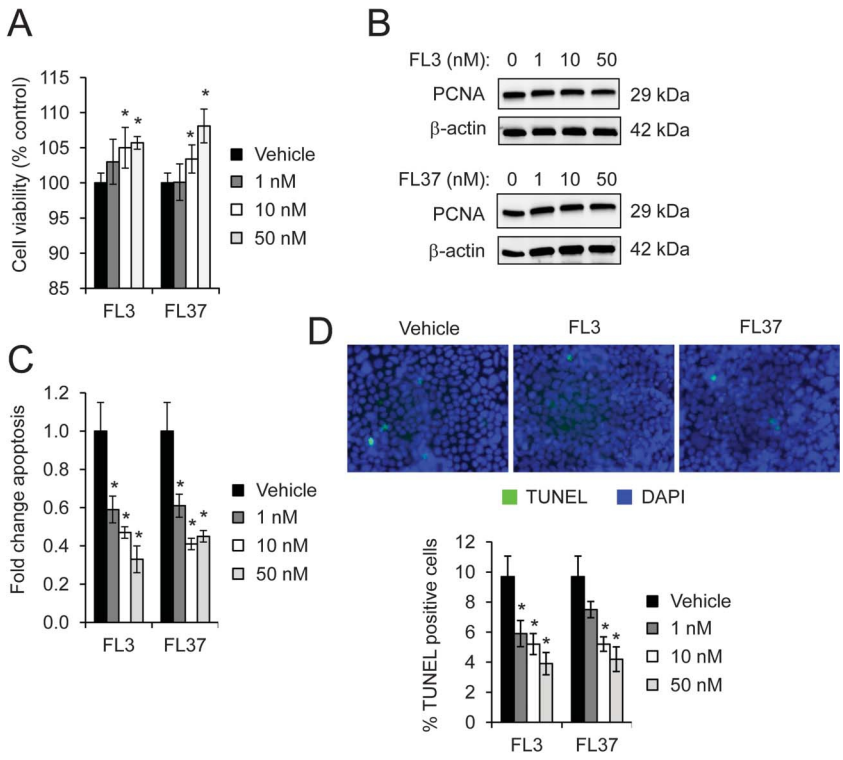

FIGURE 1. FL3 and FL37 decrease apoptosis in Caco2-BBE cells. Cells were treated with increasing concentrations of FL3 or FL37 for 16 hours A, Cell viability using lactate dehydrogenase assay; *$P < 0.05$ versus vehicle; n = 8 per treatment across 2 separate experiments. B, Representative Western blots of PCNA protein expression, a marker of cell proliferation. C, Apoptosis measured by enzyme-linked immunosorbent assay; *$P <$ 0.05 versus vehicle; n = 4 per treatment. D, TUNEL-positive cells were quantified across 20 fields; *$P < 0.05$ versus vehicle.

Caco2-BBE cells were treated with increasing doses of FL3 or FL37. Treatment with FL3 or FL37 at very low (nanomolar) concentrations increased PHB and PHB2 protein levels in Caco2-BBE (Fig. 2A). FL3 and FL37 increased PHB protein expression rapidly, as early as 15 minutes, with peak induction for FL3 between 1 and 2 hours and for FL37 between 15 minutes and 1 hour (Fig. 2B). The induction of PHB2 by FL3 and FL37 showed an identical pattern as PHB. FL3- and FL37-induced PHB and PHB2 protein expression was associated with p38-MAPK activation (Fig. 2B), but not activation of Stat3, SAPK/JNK, ERK, or AKT (see Fig., Supplemental Digital Content 2, http://links.lww.com/IBD/B117). FL3 and FL37 induced PHB and PHB2 protein expression and activation of p38-MAPK in IEC-6 cells in a similar pattern as induction in Caco2-BBE cells (see Fig. B, Supplemental Digital Content 1, http://links.lww.com/IBD/B116).

Pretreatment with FL3 or FL37 Decreases TNFα- or IFNγ-induced Expression of Nuclear Factor Kappa B p65 and Cox2 in IECs

To determine whether flavaglines exhibit anti-inflammatory action in IECs, Caco2-BBE cells were pretreated with increasing concentrations of FL3 or FL37 followed by treatment with tumor necrosis factor (TNF) α or IFNγ, 2 proinflammatory cytokines upregulated during intestinal inflammation. Western blotting revealed that FL3 and FL37 prevented TNFα- or IFNγ-induced nuclear factor kappa B p65 and Cox2 protein expression, which are 2 key proinflammatory pathways in the intestine. This effect of FL3 and FL37 was associated with sustained PHB expression, which is decreased by TNFα or IFNγ (Fig. 3A, B). Similar results were evident in IEC-6 cells, in which 1 and 10 nM FL3 or FL37 pretreatment prevented TNFα-induced nuclear factor kappa B p65

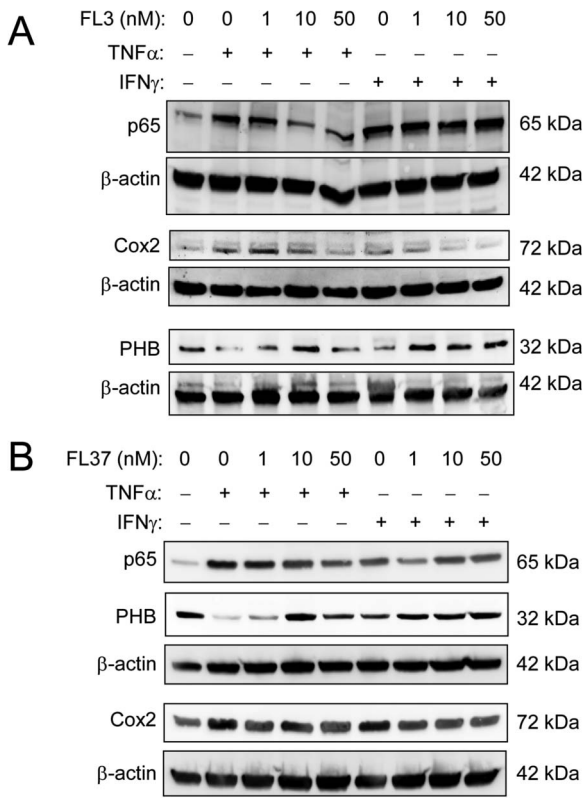

FIGURE 3. Pretreatment with FL3 or FL37 decreases TNFα- or IFNγ-induced expression of nuclear factor kappa B (NFκB) p65 and Cox2 in Caco2-BBE cells. Cells were pretreated with increasing concentrations of FL3 (A) or FL37 (B) for 1 hour, followed by treatment with 10 ng/mL TNFα or 50 ng/mL IFNγ for 16 hours. Total protein was isolated for Western blotting for expression of NFκB p65, Cox2, PHB, and β-actin (loading control).

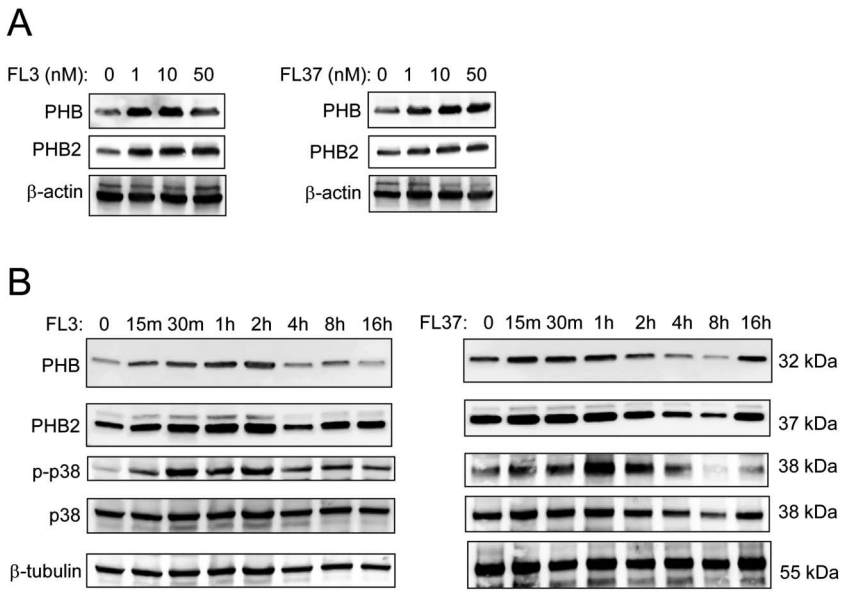

FIGURE 2. FL3 and FL37 increase protein expression of known flavagline targets PHB and PHB2 in IECs. A, Polarized Caco2-BBE cells were treated with increasing concentrations of FL3 or FL37 for 2 hours. Representative Western blots are shown for PHB, PHB2, and β-actin (loading control). B, Caco2-BBE cells were treated with 10 nM FL3 or FL37 for increasing time. Representative Western blots are shown for PHB, PHB2, phospho-p38-MAPK, total p38-MAPK, and β-tubulin (loading control).

and Cox2 induction (see Fig. A, Supplemental Digital Content 3, http://links.lww.com/IBD/B118). All further experiments were performed with FL3 or FL37 at a concentration of 10 nM because this was the lowest most effective dose at preventing TNFα- or IFNγ-induced loss of PHB protein expression.

Pretreatment with FL3 or FL37 Prevented IEC Apoptosis Induced by TNFα or IFNγ

We next determined whether FL3 or FL37 affected cytokine-induced proliferation and/or apoptosis in IECs. TNFα or IFNγ significantly decreased Caco2-BBE cell viability in vehicle-treated cells, with TNFα reducing cell viability by 24% and IFNγ by 11% (Fig. 4A). Pretreatment with 10 nM FL3 or FL37 prevented the reduction in cell viability by TNFα or IFNγ (Fig. 4A). Similar results were evident in IEC-6 cells, in which pretreatment with 10 nM FL3 or FL37 increased cell viability during TNFα or IFNγ treatment (see Fig. B, Supplemental Digital Content 3, http://links.lww.com/IBD/B118). Pretreatment with 10 nM FL3 or FL37 did not affect PCNA protein expression when normalized to β-actin expression during TNFα or IFNγ treatment (Fig. 4B). These results suggest that the protection of cell viability by FL3 and FL37 during TNFα or IFNγ treatment is not associated with increased cell proliferation. TUNEL staining revealed that pretreatment with FL3 or FL37 prevented TNFα- or IFNγ-induced Caco2-BBE apoptosis (Fig. 4C).

Pretreatment with FL3 or FL37 Protects Against Cytokine-induced Barrier Dysfunction in Caco2-BBE Cell Monolayers

Ten nanomolar of FL3 or FL37 increased transepithelial electrical resistance (Fig. 5A) and decreased translocation of FITC-dextran between Caco2-BBE monolayers from the apical chamber to the basolateral chamber (Fig. 5B). Pretreatment with 10 nM FL3 or FL37 prevented TNFα- or IFNγ-induced reduction in transepithelial electrical resistance (Fig. 5A) and increase in FITC-dextran across Caco2-BBE cells (Fig. 5B). These results suggest that FL3 and FL37 enhance intestinal epithelial barrier function basally and protect from barrier dysfunction induced by TNFα and IFNγ.

FL3 and FL37 Preserve Mitochondrial Function During TNFα Treatment

PHB and PHB2, known targets of flavaglines, are predominantly localized to the inner mitochondrial membrane of IECs.[14] Because treatment with FL3 or FL37 decreased basal and

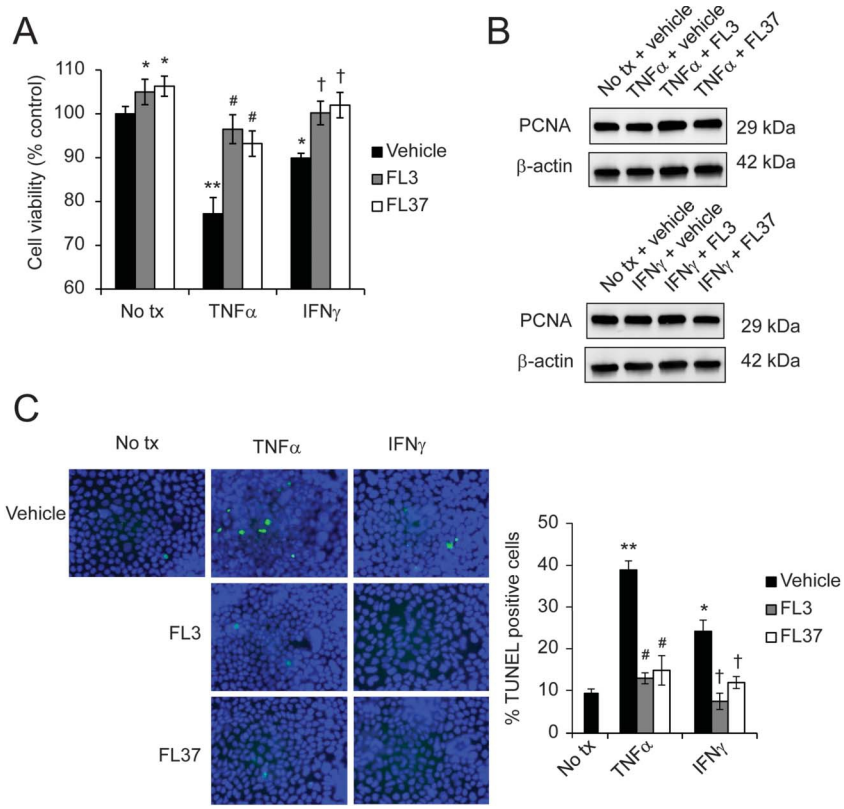

FIGURE 4. Pretreatment with FL3 or FL37 prevented Caco2-BBE apoptosis induced by TNFα or IFNγ. Cells were pretreated with 10 nM FL3 or FL37 for 1 hour, followed by treatment with 10 ng/mL TNFα or 50 ng/mL IFNγ for 16 hours. A, Cell viability using lactate dehydrogenase assay; n = 8 per treatment across 2 separate experiments. B, Representative Western blots of PCNA protein expression, a marker of cell proliferation. C, TUNEL-positive cells were quantified across 20 fields; *$P < 0.05$, **$P < 0.01$ versus no tx + vehicle; #$P < 0.01$ versus TNFα + vehicle; †$P < 0.05$ versus IFNγ + vehicle. No tx, no treatment.

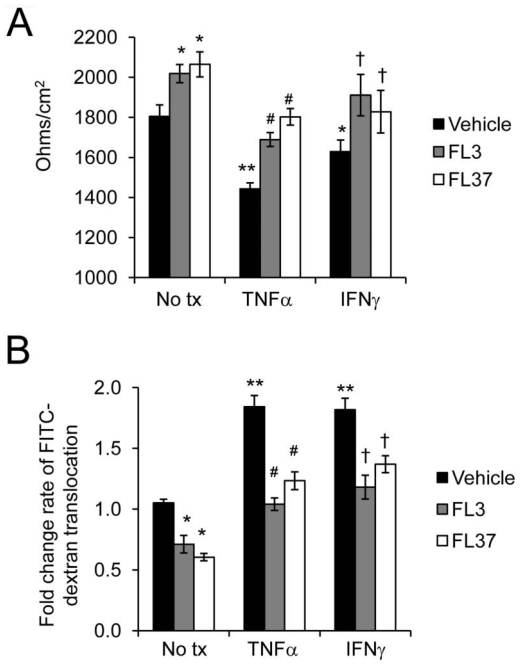

FIGURE 5. Pretreatment with FL3 or FL37 protects against cytokine-induced permeability changes in IECs. Monolayers of polarized Caco2-BBE cells were pretreated with 10 nM FL3 or FL37 for 1 hour, followed by treatment with 10 ng/mL TNFα or 50 ng/mL IFNγ for 16 hours. A, Transepithelial electrical resistance. B, Macromolecular permeability as measured by rate of 4 kDa FITC-dextran translocation from apical to basolateral chamber (nanograms per milliliter per minute); $*P < 0.05$, $**P < 0.01$ versus no tx + vehicle; $\#P < 0.01$ versus TNFα + vehicle; $\dagger P < 0.05$ versus IFNγ + vehicle.

TNFα- or IFNγ-induced apoptosis, we next assessed mitochondrial function, which is known to be dysregulated during IBD and in animal models of colitis[22–28] and plays a central role in cell fate decisions, especially apoptosis.[29] Blockade of forward electron flow through inhibition of ETC complexes leads to electrons accumulating at upstream complexes, ROS generation, and reduced ATP production.[30] Ten nanomolar of FL3 or FL37 increased basal ATP levels, but this did not reach statistical significance (Fig. 6A). TNFα decreased ATP levels in vehicle control cells as shown previously[31–33]; pretreatment with 10 nM FL3 or FL37 prevented TNFα-induced decrease in ATP (Fig. 5A). IFNγ did not affect ATP production and pretreatment with FL3 or FL37 before IFNγ treatment affected ATP levels similar to treatment with the flavaglines alone (Fig. 5A). For this reason, remaining experiments assessed the effect of FL3 or FL37 on changes to mitochondrial function induced by TNFα and not IFNγ.

To determine mitochondrial ROS generation, we used the mitochondrial superoxide detection dye MitoSox Red. Ten nanomolar of FL3 or FL37 did not significantly affect basal mitochondrial ROS production (Fig. 6B). TNFα significantly increased mitoSOX fluorescence in Caco2-BBE cells, as shown previously.[32,33] Pretreatment with 10 nM FL3 or FL37 prevented TNFα-induced mitochondrial ROS production.

Previous studies have shown that TNFα promotes cellular injury predominantly through mitochondrial ROS production resulting from decreased activity of ETC complex I.[34] To determine whether FL3 or FL37 suppresses ROS production induced by complex I, mitoSOX fluorescence was measured in Caco2-BBE cells pretreated with 10 nM FL3 or FL37 followed by TNFα treatment and rotenone (5 μM; complex I inhibitor). The protective effect of FL3 or FL37 on TNFα-induced mitochondrial ROS production was sustained during the addition of rotenone, suggesting that complex I activity is resistant to rotenone inhibition in FL3- or FL37-treated cells (Fig. 6C). FL3 or FL37 did not protect against ROS production induced by the complex III inhibitor antimycin A (1 μM) during TNFα treatment. These results suggest that FL3 and FL37 preserve complex I activity, but not complex III activity, during TNFα treatment. Complex I activity was then measured by the Mitochondrial Dipstick Assay kit. FL3 or FL37 did not alter basal complex I activity in Caco2-BBE cells compared with vehicle control cells (Fig. 6D). TNFα treatment decreased complex I activity in vehicle-treated cells, whereas pretreatment with FL3 or FL37 prevented TNFα inhibition of complex I (Fig. 6D).

Because FL3 or FL37 treatment increases expression of PHB in Caco2-BBE cells (Fig. 2) and because PHB is crucial for complex I assembly and function,[11] we next determined whether PHB was necessary for FL3 or FL37 protection against TNFα-induced mitochondrial ROS production (Fig. 6E). During loss of PHB expression by small interfering RNA transfection, FL3 or FL37 did not protect against mitochondrial ROS production induced by TNFα, suggesting that PHB is necessary for FL3 and FL37 protection against TNFα-induced mitochondrial dysfunction.

p38-MAPK Activation Is Necessary for Protective Effect of FL3 and FL37 on TNFα-induced Mitochondrial-derived ROS and Increased Permeability in Caco2-BBE Cells

Because FL3- and FL37-induced PHB and PHB2 protein expression was associated with p38-MAPK activation (Fig. 2B), but not activation of Stat3, SAPK/JNK, ERK, or AKT (see Fig., Supplemental Digital Content 2, http://links.lww.com/IBD/B117), we next determined whether p38-MAPK activation was essential for FL3 and FL37 protection against TNFα-induced epithelial mitochondrial and barrier dysfunction. SB203580, a p38-MAPK inhibitor, abolished the protective effect of FL3 or FL37 to inhibit TNFα-induced mitochondrial-derived ROS (Fig. 7A) and increased permeability in Caco2-BBE cells (Fig. 7B). SB203580 alone had no effect on mitochondrial ROS production or barrier function.

FL3 Protects Against DSS-induced Colitis

To determine the therapeutic potential of FL3 to reduce acute colitis, wild-type mice were intraperitoneally injected with 0.1 mg/kg FL3 or vehicle once daily on days 0 to 4 and administered DSS on days 0 to 6, which is a well-characterized

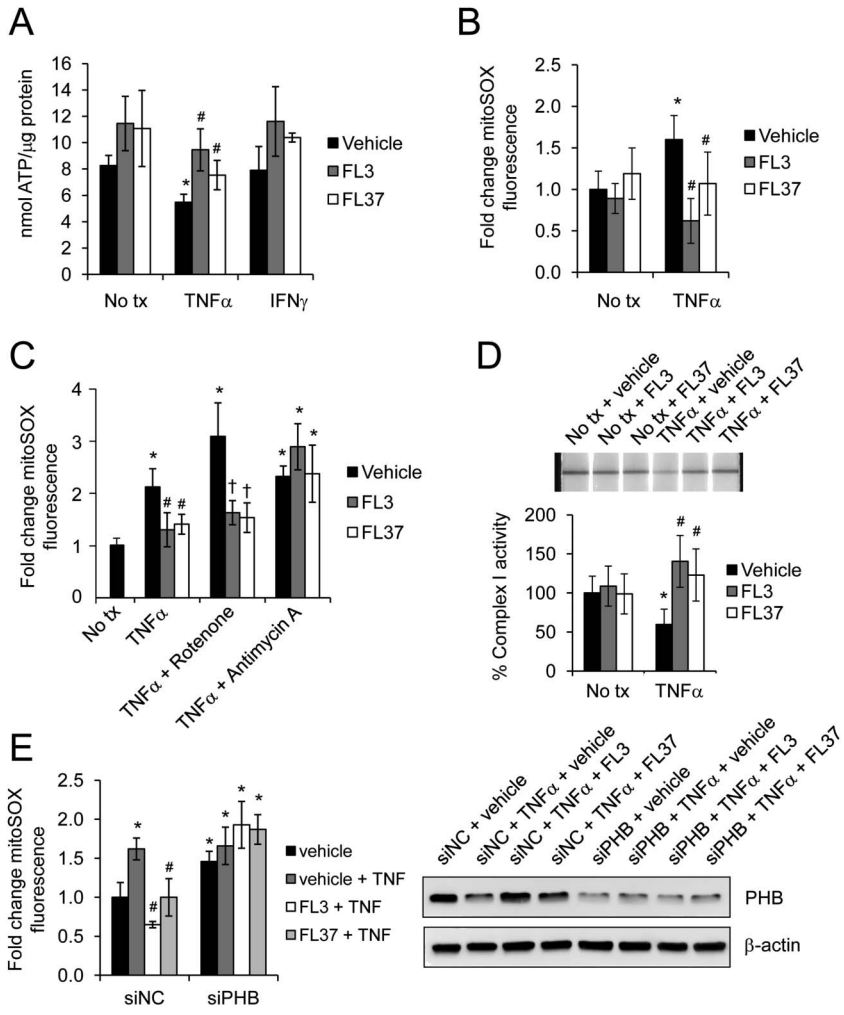

FIGURE 6. FL3 and FL37 preserve mitochondrial function during TNFα treatment. Caco2-BBE cells were pretreated with 10 nM FL3 or FL37 for 1 hour, followed by treatment with 10 ng/mL TNFα or 50 ng/mL IFNγ for 16 hours. A, ATP concentration. B, Mitochondrial ROS levels were measured using mitoSOX dye; n = 8 per treatment across 2 separate experiments. C, 15 minutes before collection, cells were treated with 5 μM rotenone, a complex I inhibitor, or 1 μM antimycin A, a complex III inhibitor. Mitochondrial ROS levels were measured using mitoSOX dye; n = 8 per treatment. D, Mitochondrial complex I activity was determined using the Mitochondrial Dipstick Assay kit. Activity of no tx + vehicle control cells was set to 100%. E, Before pretreatment with FL3 or FL37, cells were transfected with siPHB or siNegative control (siNC) for 72 hours. Mitochondrial ROS levels were measured using mitoSOX dye. Total protein was analyzed by Western blotting to ensure efficiency of PHB knockdown by siPHB; *$P < 0.05$ versus no tx + vehicle; #$P < 0.01$ versus TNFα + vehicle; †$P < 0.05$ versus TNFα + vehicle + rotenone.

model of colonic epithelial ulceration.[35] Mice given vehicle during DSS administration showed significant weight loss starting on day 5 of DSS treatment (Fig. 8A). In contrast, FL3-treated mice maintained their body weight during the course of DSS treatment and exhibited body weights similar to control mice given water. On day 6, the mice treated with DSS were assigned a clinical score consisting of severity of body weight loss, stool consistency, and the presence of gross bleeding or blood in the stool. FL3-treated mice given DSS exhibited a significantly lower clinical score compared with vehicle-treated mice given DSS (Fig. 8B).

DSS-induced colitis is histopathologically characterized by infiltration of inflammatory cells into the mucosa and submucosa, epithelial ulceration, and crypt damage, with the distal colon the most severely affected. Hemotoxylin and eosin–stained sections of distal colon of water control mice treated with FL3 showed similar histology to mice given water and vehicle (Fig. 8C). Distal colon sections of DSS-treated mice given vehicle showed severe inflammatory infiltration, complete crypt loss in focal areas, and increased ulceration. In contrast, mice treated with FL3 during DSS showed moderate inflammatory infiltration, less crypt loss, and less ulceration compared with mice given vehicle (Fig. 8C). Histological scoring of inflammation revealed that FL3-treated mice given DSS exhibited a significantly less damage (severity of inflammatory infiltration, ulceration, and crypt damage) compared with vehicle-treated mice given DSS (Fig. 8B).

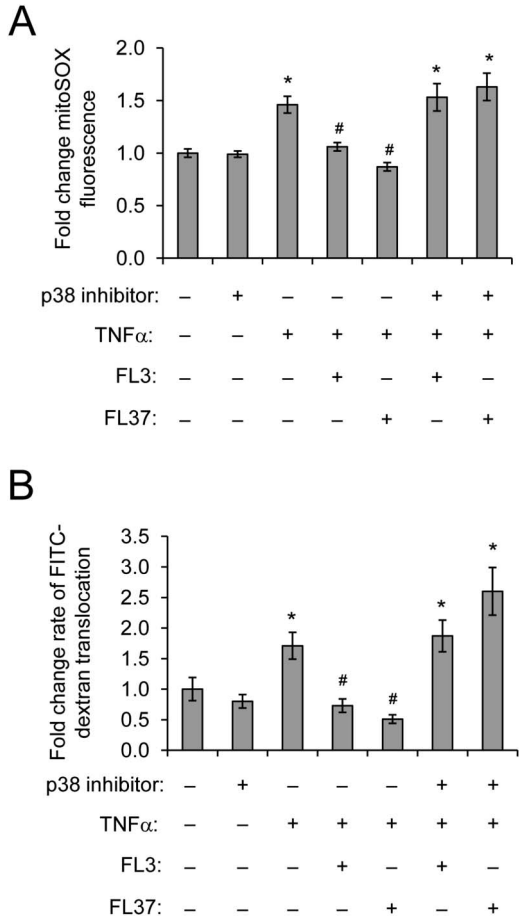

FIGURE 7. p38-MAPK activation is necessary for protective effect of FL3 and FL37 on TNFα-induced mitochondrial-derived ROS and increased permeability. Caco2-BBE monolayers were pretreated with 20 μM p38-MAPK inhibitor SB203580 for 1 hour, then treated with 10 nM FL3 or FL37 for 1 hour, and finally treated with 10 ng/mL TNFα for 16 hours A, Mitochondrial ROS levels were measured using mitoSOX dye; n = 8 per treatment. B, Rate of 4 kDa FITC-dextran translocation from apical to basolateral chamber (nanograms per milliliter per minute); n ≥ 6 per treatment; *$P < 0.05$ versus no tx; #$P < 0.05$ versus TNFα.

A reduction in colon length is a gross indicator of disease severity in the DSS model of colitis. All animals treated with DSS showed reduced colon length compared with water controls; however, shrinkage was less severe in FL3-treated mice compared with vehicle controls (Fig. 8D). In addition, FL3 treatment significantly reduced myeloperoxidase activity, a marker of neutrophil infiltration, in the distal colon during DSS colitis (Fig. 8E). Intestinal permeability was measured using translocation of 4 kDa FITC-dextran into serum in DSS-treated mice. Barrier dysfunction is one of the earliest events in DSS-induced colitis that precedes evident inflammation or mucosal damage. Therefore, we measured intestinal permeability after 3 days of DSS treatment. FL3-treated mice showed decreased FITC-dextran translocation compared with vehicle-treated mice during DSS colitis (Fig. 8F).

To determine whether in vivo effects of FL3 corroborate our in vitro results in cultured IECs, oxidative damage and colonic epithelial apoptosis were measured. FL3 decreased 4-HNE staining (Fig. 9A) and protein carbonyl content (Fig. 9B), markers of lipid peroxidation and oxidative damage to protein, respectively, in the colon of DSS-treated mice compared with vehicle. FL3 did not affect 4-HNE staining or generation of protein carbonyls in water-treated control mice. FL3 treatment abolished cleaved caspase 3 protein expression during DSS colitis in isolated colonic epithelial cells (Fig. 9C), suggesting that FL3 protects against DSS-induced epithelial apoptosis. This was further supported by TUNEL staining of distal colon, which demonstrated that FL3 treatment significantly decreased the number of TUNEL-positive epithelial cells per crypt during DSS colitis (Fig. 9D, E). FL3 did not significantly alter epithelial cleaved caspase 3 expression or the number of TUNEL-positive cells in water-treated control mice.

To determine whether the protective effects of FL3 treatment on DSS-induced colitis were associated with increased expression of PHB or p38-MAPK activation, total protein from distal colon was isolated and assessed by Western blotting. DSS-treated mice given FL3 exhibited increased PHB expression and p38-MAPK activation (Fig. 9F), but not activation of Stat3, SAPK/JNK, ERK, or AKT (see Fig., Supplemental Digital Content 4, http://links.lww.com/IBD/B119).

DISCUSSION

Our study is the first to characterize the therapeutic potential of flavaglines in the intestinal epithelium during inflammation. We show that the flavaglines FL3 and FL37 protect against apoptosis and barrier dysfunction in cultured IECs basally and during proinflammatory cytokine treatment. Protective effects of FL3 were corroborated in vivo, with FL3 administration reducing the severity of DSS-induced colitis and barrier permeability.

Since the first flavagline, rocaglamide, was first isolated in 1992, more than 60 natural flavaglines have been identified.[20,36] Crude extracts from leaves and flowers of different Aglaia (family Meliaceae) plants, from which flavaglines are extracted, are used in several countries of southeast Asia as traditional medicine for the treatment of inflammatory skin diseases and allergic inflammatory disorders, such as asthma.[6] However, these plants contain many classes of pharmacologically active agents, and the above-cited activities may not involve flavaglines but other classes of drugs. Interest in flavaglines as therapeutic compounds stems from their anticancer, anti-inflammatory, and cytoprotective properties. At very low nanomolar concentrations, flavaglines enhance survival of neurons and cardiomyocytes when challenged with numerous stressors.[3] In this study, we assessed the effect of FL3 and FL37 in IECs because both compounds were shown to display in vivo anticancer and cardioprotective effects. As an in vitro model of inflammation, cultured IECs were challenged with TNFα and IFNγ, 2 proinflammatory cytokines involved in IBD pathogenesis.[37,38] Similar to results in neurons and cardiomyocytes, FL3 and FL37 exhibited prosurvival and

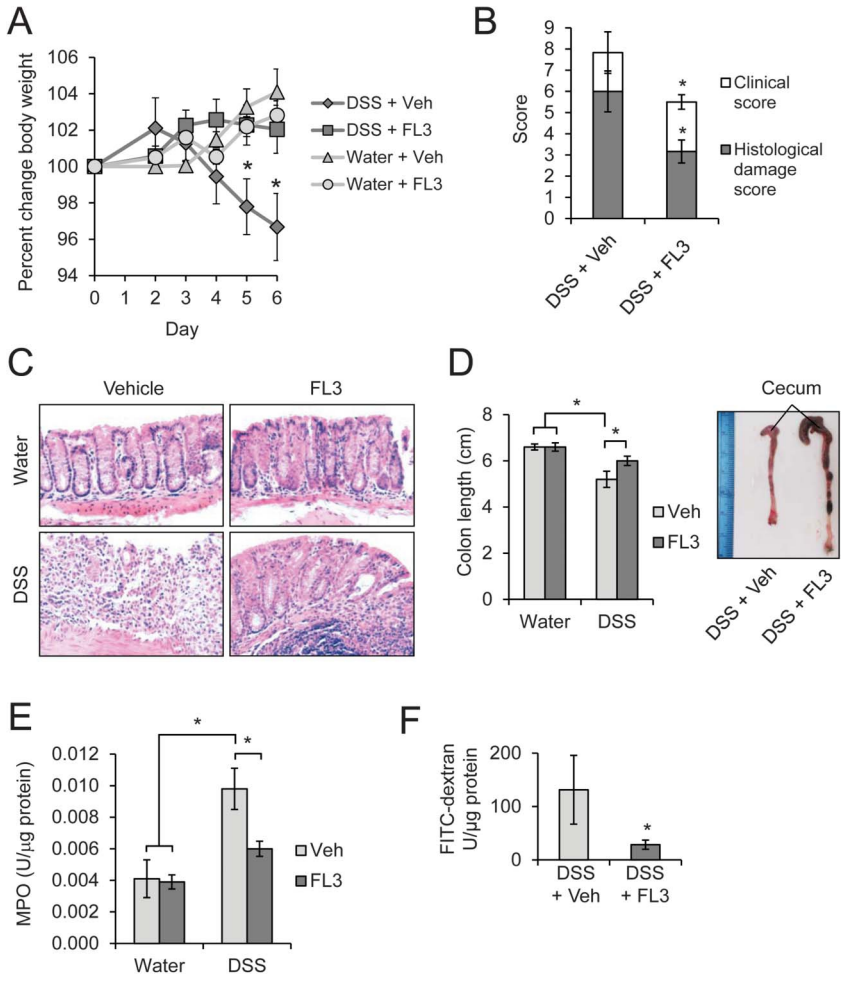

FIGURE 8. FL3 protects against DSS-induced colitis. Mice were given 2.5% DSS for 6 days and intraperitoneally injected with 0.1 mg/kg FL3 or vehicle (veh) once daily on days 0 to 4. Control mice were given regular drinking water throughout the protocol; n = 6 per treatment group across 2 separate experiments with similar results. A, Percent change in body weight; *$P < 0.05$ versus DSS + FL3. B, Clinical and histological damage score; *$P < 0.05$ versus DSS + vehicle. C, Representative photomicrographs of paraffin-embedded hemotoxylin and eosin–stained sections of distal colon. Original magnification, ×20. D, Colon length measured on day 6 of DSS treatment. Photos of representative colons from DSS-treated mice; *$P < 0.05$. E, Neutrophil infiltration into the colon, quantified by measuring myeloperoxidase activity; *$P < 0.05$. F, On day 3 of DSS treatment, mice were gavaged with 4 kDa FITC-dextran. Translocation of fluorescent FITC-dextran across the intestinal epithelium was measured in serum collected 4 hours after gavage; *$P < 0.05$.

anti-inflammatory effects in IECs at nanomolar concentrations during TNFα and IFNγ treatment. FL3 and FL37 inhibited TNFα and IFNγ downstream proinflammatory signaling as evidenced by reduced nuclear factor kappa B and Cox2 expression, maintained cell viability, reduced TNFα- and IFNγ-induced apoptosis, and prevented TNFα- and IFNγ-increased epithelial permeability. We went on to demonstrate that mitochondrial dysfunction, as characterized by increased mitochondrial-derived ROS, reduced activity of ETC complexes and ultimately decreased ATP production, was induced by TNFα[33] but not IFNγ, and was prevented by FL3 or FL37. Importantly, multiple studies have reported mitochondrial dysfunction in the epithelium during IBD and experimental models of colitis.[12,25,27,28,39,40] Recent studies indicate that mitochondria integrate cellular homeostasis signaling and that mitochondrial stress participates in the pathology of IBD.[22,24,41] Our results suggest that FL3 and FL37 protection of mitochondrial function in IECs is associated with decreased apoptosis, enhanced cell viability, and sustained epithelial barrier function during TNFα-induced damage. FL3 and FL37 also protected against IFNγ-induced apoptosis and epithelial barrier dysfunction, but unlike TNFα, these effects of IFNγ were not associated with altered mitochondrial function, suggesting that FL3 and FL37 cytoprotective effects against IFNγ involve signaling pathways beyond those regulating mitochondrial function.

FL3 and FL37 rapidly induced expression of PHB and PHB2 in IECs, which are established flavagline targets.[3] Our study demonstrated that PHB expression was essential for FL3 or FL37 inhibition of TNFα-induced mitochondrial-derived ROS

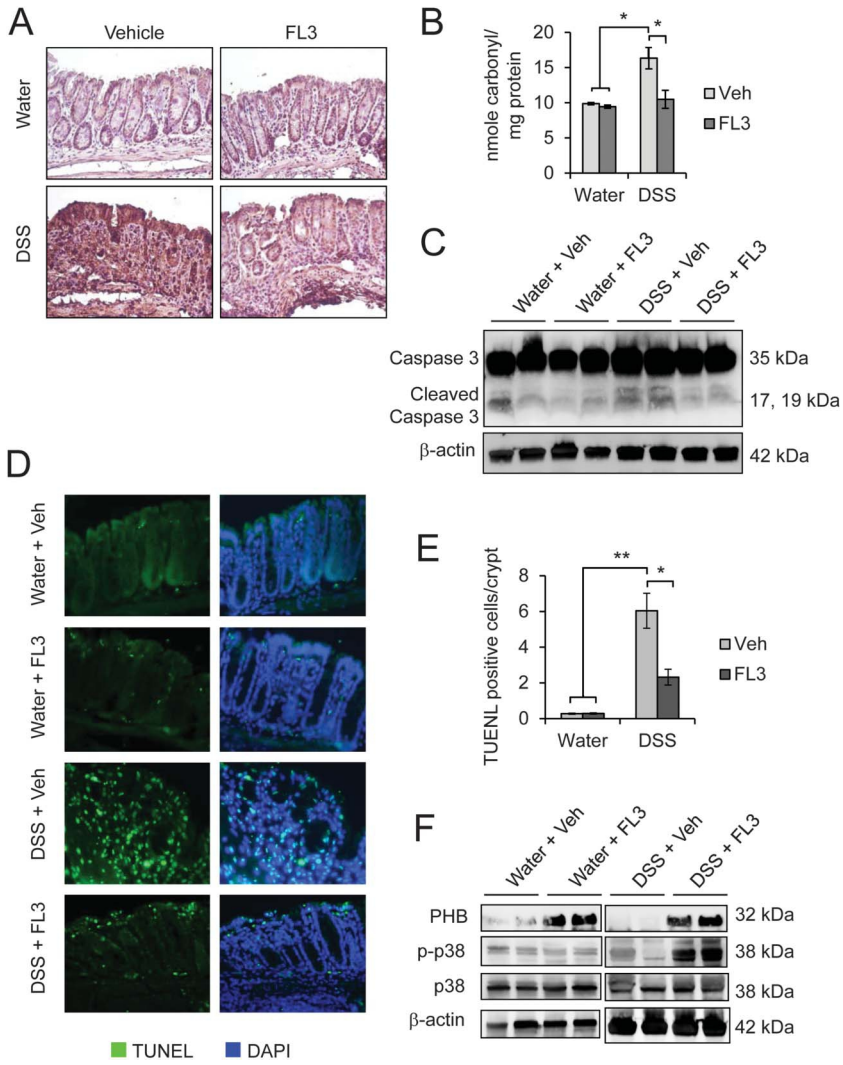

FIGURE 9. FL3 decreased colonic oxidative damage and epithelial apoptosis induced by DSS colitis, and these protective effects were associated with increased PHB and phospho-p38 MAPK expression. A, Immunohistochemistry staining of 4-HNE. B, Protein carbonyl content in the distal colon; *$P < 0.05$, n = 6 per treatment. C, Representative Western blots showing total and cleaved caspase 3 levels in isolated colonic epithelial cells. β-actin is included as a loading control. D, TUNEL staining (green) of colonic sections from mice treated with FL3 or vehicle (veh) during DSS colitis or control (water). Sections were stained with 4′,6-diamidino-2-phenylindole to visualize nuclei (blue). E, Number of TUNEL-positive cells per crypt in well-oriented crypts; *$P < 0.05$, **$P < 0.01$; n = 5 per treatment with a minimum of 20 crypts counted per animal. F, Representative Western blots showing PHB, phospho-p38-MAPK, p38-MAPK, and β-actin in total protein isolated from whole colon.

production in IECs. Furthermore, we show that FL3 and FL37 preserve ETC complex I activity during TNFα treatment. Complex I of the ETC is a predominant site of PHB binding, resulting in optimal activity of complex I and the respiratory chain.[11,13] Previous studies have shown that TNFα reduces PHB expression in IECs,[32,42] which we also confirm in the current study (Fig. 3). Therefore, our results suggest that FL3 and FL37 promote mitochondrial function in IECs during stress induced by TNFα by sustaining PHB expression and ETC complex I activity, which are targets of TNFα-induced damage.[33,42]

FL3 and FL37 rapidly induced activation of p38-MAPK in IECs, but not activation of Stat3, SAPK/JNK, ERK, or AKT. The pattern of p38-MAPK activation during a time course of FL3 or FL37 treatment was similar to that of PHB and PHB2 induction. Activation of p38-MAPK by flavaglines has been demonstrated in lymphocytes, which causes immunosuppression through selective inhibition of the transcription factor nuclear factor of activated T cells (NFAT).[6] NFAT is expressed in the intestinal epithelium where it regulates differentiation, cell cycle, and apoptosis.[43] It is not known whether PHBs mediate activation of p38-MAPK or NFAT by flavaglines.[7] We show that p38-MAPK activation is essential for the protective effects of FL3 and FL37 on IEC barrier permeability and mitochondrial-derived ROS production during TNFα treatment. Future studies will elucidate whether p38-MAPK activation by FL3

or FL37 is downstream of PHBs and whether p38-MAPK activation involves inhibition of NFAT in IECs.

The in vivo therapeutic effect of FL3 was demonstrated using the DSS model of acute colitis in mice. This experimental model of colitis has similarities to human ulcerative colitis, including epithelial cell ulceration and loss of integrity of the mucosal barrier triggering inflammation.[35] Given our results showing that FL3 and FL37 enhance cultured IEC survival and barrier function, the DSS model was optimal to test whether FL3 elicited similar protective effects in vivo. FL3 alone did not alter body weight or induce signs of toxicity in mice, as shown in previous in vivo studies.[5,44] Additionally, colon histology of mice administered FL3 alone was similar to vehicle control mice. Once-daily injection of FL3 concurrent with DSS administration through day 4 prevented weight loss, colon shrinkage, neutrophil activation, histological damage including crypt loss and ulceration, epithelial apoptosis, ROS-induced damage, and epithelial barrier dysfunction. Reduced severity of colitis by FL3 was associated with increased colonic expression of PHB and activation of p38-MAPK, similar to our findings in cultured IECs. Flavaglines are chemical compounds that do not act as antioxidants through a chemical mechanism (as a reductant or radical scavenger) but through their action on PHB signaling. Not surprisingly, there has been considerable interest in developing antioxidant-based therapeutic strategies for the treatment of IBD. Commonly used drugs, in particular sulfasalazine and its active moiety 5-aminosalicylic acid, are potent ROS scavengers. However, targeted antioxidant therapies have not reached clinical efficacy perhaps because of limited cell permeability, short circulating half-life, and/or immunogenicity and the need to be used in large excess compared with the quantity of ROS. In contrast, compounds that promote the resistance and the destruction of ROS by activation of specific signaling pathways may be effective at low concentrations. Our study suggests that flavaglines may provide therapeutic potential against IBD by protecting the intestinal epithelium and reducing oxidative stress. Future studies will determine the bioavailability of flavaglines and their side effects.

Collectively, our in vitro and in vivo data demonstrate that flavaglines exhibit anti-inflammatory effects during colitis and promote IEC survival, mitochondrial function, and barrier integrity. Further preclinical investigations elucidating flavagline mechanism underlying protection against intestinal inflammation and promotion of epithelial cell homeostasis are warranted.

ACKNOWLEDGMENTS

The authors thank the late Dr. Shanthi V. Sitaraman from Emory University, Atlanta, GA, for her scientific guidance. The authors are also grateful to AAREC Filia Research and ANRT for fellowships to C. Basmadjian and Q. Zhao.

Author contributions: *Study concept and design*, L. Désaubry and A. L. Theiss; *acquisition of data*, J. Han, Q. Zhao, C. Basmadjian, and A. L. Theiss; *analysis and interpretation of data*, J. Han and A. L. Theiss; *drafting the manuscript*, J. Han, L. Désaubry, and A. L. Theiss.

REFERENCES

1. Neurath MF, Travis SP. Mucosal healing in inflammatory bowel diseases: a systematic review. *Gut*. 2012;61:1619–1635.
2. Fries W, Belvedere A, Vetrano S. Sealing the broken barrier in IBD: intestinal permeability, epithelial cells and junctions. *Curr Drug Targets*. 2013;14:1460–1470.
3. Thuaud F, Ribeiro N, Nebigil CG, et al. Prohibitin ligands in cell death and survival: mode of action and therapeutic potential. *Chem Biol*. 2013; 20:316–331.
4. Fahrig T, Gerlach I, Horvath E. A synthetic derivative of the natural product rocaglaol is a potent inhibitor of cytokine-mediated signaling and shows neuroprotective activity in vitro and in animal models of Parkinson's disease and traumatic brain injury. *Mol Pharmacol*. 2005;67: 1544–1555.
5. Bernard Y, Ribeiro N, Thuaud F, et al. Flavaglines alleviate doxorubicin cardiotoxicity: implication of Hsp27. *PLoS One*. 2011;6:e25302.
6. Proksch P, Giaisi M, Treiber MK, et al. Rocaglamide derivatives are immunosuppressive phytochemicals that target NF-AT activity in T cells. *J Immunol*. 2005;174:7075–7084.
7. Basmadjian C, Thuaud F, Ribeiro N, et al. Flavaglines: potent anticancer drugs that target prohibitins and the helicase eIF4A. *Future Med Chem*. 2013;5:2185–2197.
8. Nijtmans LG, de Jong L, Artal Sanz M, et al. Prohibitins act as a membrane-bound chaperone for the stabilization of mitochondrial proteins. *EMBO J*. 2000;19:2444–2451.
9. Steglich G, Neupert W, Langer T. Prohibitins regulate membrane protein degradation by the m-AAA protease in mitochondria. *Mol Cell Biol*. 1999; 19:3435–3442.
10. Tatsuta T, Model K, Langer T. Formation of membrane-bound ring complexes by prohibitins in mitochondria. *Mol Biol Cell*. 2005;16:248–259.
11. Bourges I, Ramus C, Mousson de Camaret B, et al. Structural organization of mitochondrial human complex I: role of the ND4 and ND5 mitochondria-encoded subunits and interaction with prohibitin. *Biochem J*. 2004;383:491–499.
12. Hsieh SY, Shih TC, Yeh CY, et al. Comparative proteomic studies on the pathogenesis of human ulcerative colitis. *Proteomics*. 2006;6:5322–5331.
13. Tsutsumi T, Matsuda M, Aizaki H, et al. Proteomics analysis of mitochondrial proteins reveals overexpression of a mitochondrial protein chaperon, prohibitin, in cells expressing hepatitis C virus core protein. *Hepatology*. 2009;50:378–386.
14. Theiss AL, Idell RD, Srinivasan S, et al. Prohibitin protects against oxidative stress in intestinal epithelial cells. *FASEB J*. 2007;21:197–206.
15. Kathiria AS, Butcher MA, Hansen JM, et al. Nrf2 is not required for epithelial prohibitin-dependent attenuation of experimental colitis. *Am J Physiol Gastrointest Liver Physiol*. 2013;304:G885–G896.
16. Theiss AL, Vijay-Kumar M, Obertone TS, et al. Prohibitin is a novel regulator of antioxidant response that attenuates colonic inflammation in mice. *Gastroenterology*. 2009;137:199–208, 208 e1–6.
17. Kathiria AS, Butcher LD, Feagins LA, et al. Prohibitin 1 modulates mitochondrial stress-related autophagy in human colonic epithelial cells. *PLoS One*. 2012;7:e31231.
18. Ribeiro N, Thuaud F, Bernard Y, et al. Flavaglines as potent anticancer and cytoprotective agents. *J Med Chem*. 2012;55:10064–10073.
19. Ebada SS, Lajkiewicz N, Porco JA Jr, et al. Chemistry and biology of rocaglamides (= flavaglines) and related derivatives from aglaia species (meliaceae). *Prog Chem Org Nat Prod*. 2011;94:1–58.
20. Ribeiro N, Thuaud F, Nebigil C, et al. Recent advances in the biology and chemistry of the flavaglines. *Bioorg Med Chem*. 2012;20:1857–1864.
21. Nenci A, Becker C, Wullaert A, et al. Epithelial NEMO links innate immunity to chronic intestinal inflammation. *Nature*. 2007;446:557–561.
22. Bar F, Bochmann W, Widok A, et al. Mitochondrial gene polymorphisms that protect mice from colitis. *Gastroenterology*. 2013;145:1055–1063.e3.
23. O'Morain C, Smethurst P, Levi J, et al. Subcellular fractionation of rectal biopsy homogenates from patients with inflammatory bowel disease. *Scand J Gastroenterol*. 1985;20:209–214.
24. Rath E, Berger E, Messlik A, et al. Induction of dsRNA-activated protein kinase links mitochondrial unfolded protein response to the pathogenesis of intestinal inflammation. *Gut*. 2012;61:1269–1278.
25. Restivo NL, Srivastava MD, Schafer IA, et al. Mitochondrial dysfunction in a patient with crohn disease: possible role in pathogenesis. *J Pediatr Gastroenterol Nutr*. 2004;38:534–538.

26. Santhanam S, Rajamanickam S, Motamarry A, et al. Mitochondrial electron transport chain complex dysfunction in the colonic mucosa in ulcerative colitis. *Inflamm Bowel Dis.* 2012;18:2158–2168.
27. Sifroni KG, Damiani CR, Stoffel C, et al. Mitochondrial respiratory chain in the colonic mucosal of patients with ulcerative colitis. *Mol Cell Biochem.* 2010;342:111–115.
28. Tirosh O, Levy E, Reifen R. High selenium diet protects against TNBS-induced acute inflammation, mitochondrial dysfunction, and secondary necrosis in rat colon. *Nutrition*. 2007;23:878–886.
29. Dorn GW II, Kitsis RN. The mitochondrial dynamism-mitophagy-cell death interactome: multiple roles performed by members of a mitochondrial molecular Ensemble. *Circ Res.* 2015;116:167–182.
30. Szczepanek K, Chen Q, Larner AC, et al. Cytoprotection by the modulation of mitochondrial electron transport chain: the emerging role of mitochondrial STAT3. *Mitochondrion*. 2012;12:180–189.
31. Goossens V, Grooten J, De Vos K, et al. Direct evidence for tumor necrosis factor-induced mitochondrial reactive oxygen intermediates and their involvement in cytotoxicity. *Proc Natl Acad Sci U S A.* 1995;92:8115–8119.
32. Han J, Yu C, Souza RF, et al. Prohibitin 1 modulates mitochondrial function of Stat3. *Cell Signal.* 2014;26:2086–2095.
33. Hansen JM, Zhang H, Jones DP. Mitochondrial thioredoxin-2 has a key role in determining tumor necrosis factor-alpha-induced reactive oxygen species generation, NF-kappaB activation, and apoptosis. *Toxicol Sci.* 2006;91:643–650.
34. Lopez-Armada MJ, Riveiro-Naveira RR, Vaamonde-Garcia C, et al. Mitochondrial dysfunction and the inflammatory response. *Mitochondrion*. 2013;13:106–118.
35. Chassaing B, Aitken JD, Malleshappa M, et al. Dextran sulfate sodium (DSS)-induced colitis in mice. *Curr Protoc Immunol.* 2014;104:Unit 15.25.
36. Ng SC, Lam YT, Tsoi KK, et al. Systematic review: the efficacy of herbal therapy in inflammatory bowel disease. *Aliment Pharmacol Ther.* 2013;38:854–863.
37. Gyires K, Toth EV, Zadori SZ. Gut inflammation: current update on pathophysiology, molecular mechanism and pharmacological treatment modalities. *Curr Pharm Des.* 2014;20:1063–1081.
38. Slebioda TJ, Kmiec Z. Tumour necrosis factor superfamily members in the pathogenesis of inflammatory bowel disease. *Mediators Inflamm.* 2014;2014:325129.
39. Delpre G, Avidor I, Steinherz R, et al. Ultrastructural abnormalities in endoscopically and histologically normal and involved colon in ulcerative colitis. *Am J Gastroenterol.* 1989;84:1038–1046.
40. Vanderborght M, Nassogne MC, Hermans D, et al. Intractable ulcerative colitis of infancy in a child with mitochondrial respiratory chain disorder. *J Pediatr Gastroenterol Nutr.* 2004;38:355–357.
41. Rath E, Haller D. Mitochondria at the interface between danger signaling and metabolism: role of unfolded protein responses in chronic inflammation. *Inflamm Bowel Dis.* 2012;18:1364–1377.
42. Theiss AL, Jenkins AK, Okoro NI, et al. Prohibitin inhibits tumor necrosis factor alpha-induced nuclear factor-kappa B nuclear translocation via the novel mechanism of decreasing importin alpha3 expression. *Mol Biol Cell.* 2009;20:4412–4423.
43. Wang Q, Zhou Y, Jackson LN, et al. Nuclear factor of activated T cells (NFAT) signaling regulates PTEN expression and intestinal cell differentiation. *Mol Biol Cell.* 2011;22:412–420.
44. Thuaud F, Bernard Y, Turkeri G, et al. Synthetic analogue of rocaglaol displays a potent and selective cytotoxicity in cancer cells: involvement of apoptosis inducing factor and caspase-12. *J Med Chem.* 2009;52:5176–5187.

Publication N°*9*

Synergistic effects of eIF4A and MEK inhibitors on proliferation of NRAS-mutant melanoma cell lines.

Malka-Mahieu, H., Girault, I., Rubington, M., Leriche, M., Welsch, C., Kamsu-Kom, N., Zhao, Q., Désaubry, L., Vagner, S., Robert, C., *Cell cycle*, **2016**, *15*, 2405-2409.

Cell Cycle

ISSN: 1538-4101 (Print) 1551-4005 (Online) Journal homepage: http://www.tandfonline.com/loi/kccy20

Synergistic effects of eIF4A and MEK inhibitors on proliferation of NRAS-mutant melanoma cell lines

Hélène Malka-Mahieu, Isabelle Girault, Margot Rubington, Melissa Leriche, Caroline Welsch, Nyam Kamsu-Kom, Qian Zhao, Laurent Desaubry, Stéphan Vagner & Caroline Robert

To cite this article: Hélène Malka-Mahieu, Isabelle Girault, Margot Rubington, Melissa Leriche, Caroline Welsch, Nyam Kamsu-Kom, Qian Zhao, Laurent Desaubry, Stéphan Vagner & Caroline Robert (2016): Synergistic effects of eIF4A and MEK inhibitors on proliferation of NRAS-mutant melanoma cell lines, Cell Cycle, DOI: 10.1080/15384101.2016.1208862

To link to this article: http://dx.doi.org/10.1080/15384101.2016.1208862

Synergistic effects of eIF4A and MEK inhibitors on proliferation of NRAS-mutant melanoma cell lines

Hélène Malka-Mahieu[1,2], Isabelle Girault[1,2], Margot Rubington[1,2], Melissa Leriche[1,2], Caroline Welsch[1,2], Nyam Kamsu-Kom[1,2], Qian Zhao[3], Laurent Desaubry[3], Stéphan Vagner[1,4,5,6,*], Caroline Robert[1,2,7,*]

[1]INSERM U981, Villejuif F-94805, France. [2]Université Paris-Sud, Kremlin-Bicêtre F-94276, France. [3]CNRS-Strasbourg University, UMR7200, Illkirch F-67400, France. [4]Institut Curie, PSL Research University, CNRS UMR3348, F-91405, Orsay, France. [5]Université Paris Sud, Université Paris-Saclay, CNRS UMR3348, F-91405 Orsay, [6]Equipe Labellisée Ligue Contre le Cancer, [7]Gustave Roussy, Dermato-Oncology, Villejuif F-94805, France

*Co-senior authors

Correspondence should be addressed to S.V. (stephan.vagner@curie.fr) and C.R. (caroline.robert@gustaveroussy.fr)

Running title: eIF4A inhibitors in NRAS-mutant melanoma cell lines

Abstract

Activating mutations of the NRAS (neuroblastoma rat sarcoma viral oncogene) protein kinase, present in many cancers, induce a constitutive activation of both the RAS-RAF-MEK-ERK mitogen-activated protein kinase (MAPK) signal transduction pathway and the PI(3)K-AKT-mTOR, pathway. This in turn regulates the formation of the eIF4F eukaryotic translation initiation complex, comprising the eIF4E cap-binding protein, the eIF4G scaffolding protein and the eIF4A RNA helicase, which binds to the 7-methylguanylate cap (m(7)G) at the 5' end of messenger RNAs. Small molecules targeting MEK (MEKi: MEK inhibitors) have demonstrated activity in NRAS-mutant cell lines and tumours, but resistance sets in most cases within months of treatment. Using proximity ligation assays, that allows visualization of the binding of eIF4E to the scaffold protein eIF4G, generating the active eIF4F complex, we have found that resistance to MEKi is associated with the persistent formation of the eIF4F complex in MEKi-treated NRAS-mutant cell lines. Furthermore, inhibiting the eIF4A component of the eIF4F complex, with a small molecule of the flavagline/rocaglate family, synergizes with inhibiting MEK to kill NRAS-mutant cancer cell lines.

Key words: MEK, NRAS, eIF4F, mRNA translation, eIF4A inhibitors

Introduction

Activating mutations of the NRAS (neuroblastoma rat sarcoma viral oncogene) protein kinase inducing a constitutive activation of the MAPK and PI3K/Akt/mTOR pathways[1] are present in 15-20% of melanomas and in a plethora of other cancers types such as leukemia, lung cancers and colorectal cancers.[2,3] The NRAS Q61 mutation, in particular, seems to be associated with an aggressive clinical behaviour and a poor prognosis.[4] NRAS inhibition thus appears as an interesting anticancer strategy, however, until now, no efficient anti-NRAS targeted therapy has been developed. One way to block the MAP-kinase activation cascade in the context of an activated NRAS protein is to inhibit MEK (Mitogen Activated Protein Kinase), downstream from RAS and RAF in the MAPK pathway. MEK inhibitors (MEKi: *e.g.* trametinib, cobimetinib) have demonstrated preclinical activity as well as clinical efficacy in patients with NRAS-mutant tumours.[5] However, as it is the case with most targeted therapies, development of resistance usually occurs within months of treatment.

Beside NRAS mutation which is found in 15% of melanomas, BRAF mutations are present in 40 to 50% of the cases, also leading to a constitutive MAPkinase pathway activation. These two types of mutations are mutually exclusive. In contrast to NRAS, BRAF protein can be specifically targeted by potent BRAF inhibitors (vemurafenib, dabrafenib) which significantly improve the clinical outcome of patients with BRAF mutant advanced melanoma.[6,7]

Combination of BRAF and MEK inhibitors are more effective than BRAF inhibitors to treat patients with BRAF mutant melanoma and are now currently used in the clinic. However, although resistances are delayed when using both drugs as compared to single agents, patients are still confronted to relapses after a median duration of response of about one year. We recently reported that the formation of the eIF4F translation initiation complex was directly involved in the resistance to BRAFi used alone or in combination with MEKi in BRAF-mutant cell lines.[8] Interestingly, all the various and diverse mechanisms underlying anti-BRAF resistance, that were found or known in the BRAF-mutated cell lines that were studied, converged and led to the persistence of the formation of the eIF4F complex. We here extend this study and investigate the potential role of the eIF4F complex in the context of resistance of NRAS-mutant cell lines to MEK inhibitors.

RESULTS AND DISCUSSION

We first investigated the effect of MEKi (trametinib and cobimetinib) on the formation of the eIF4F complex, in various contexts of sensitivity/resistance to MEKi. We thus selected a panel of human NRAS-mutant melanoma cell lines with different sensitivities to these compounds. One of the cell line, denominated IGRMel1, is a new cell line established from a patient seen at Gustave Roussy with a NRAS-mutant metastatic melanoma (see Methods section). All five tested cell lines (SKMel10, SKMel2, M311, M376 and IGRMel1) were verified for their NRAS mutational status and other melanoma's hot spot mutations (see Methods section and Table S1). These cell lines are mutated in NRAS (Q61) and the M376 cell line is also mutated in BRAF

(V600). A short-term proliferation assay showed that the SKMel10 and M311 cell lines were relatively resistant to trametinib and cobimetinib compared to SKMel2, M376 and IGRMel1 cell lines (Fig. 1A). A long-term clonogenic assay confirmed that the SKMel10 cell line was resistant to the two MEKi compared to M376 and IGRMel1 (Fig. 1B). Of note, the SKMel2 cell line was more resistant to both MEKi than the M376 and IGRMel1 cell lines in this assay (Fig. 1B). This experiment could not be performed with the M311 cell lines since it did not form colonies.

To analyze the status of eIF4F complex formation in MEKi resistant/sensitive cell lines, we carried out a proximity ligation assay procedure that we developed previously to evaluate the interaction between eIF4E and eIF4G.[8] We observed that the two MEKi tested induced a significant decrease in eIF4E-eIF4G interactions in the three MEKi-sensitive SKMel2, M376 and IGRMel1 cell lines ($p1$ indicates additive, antagonistic and synergistic effects, respectively.
SKMel10 and M311 cells were treated for 48 h before the WST-1 assay with FL3 (4,1 nM) and variable doses of trametinib and cobimetinib ranging from 64 nM to 5000 nM.
Isobolograms represent the correlation between the observed and the expected effects of the combination of 2 different drugs. The upper left region of the figure represents increasing degrees of synergy.

Clonogenic assays

For clonogenic assays, cells were plated at low density (1-4×10^3 cells per well in a 6-well tissue culture plates) in fresh media. After 24 h, cells were treated with DMSO or drugs at the

indicated concentrations, in duplicates. After 7-14 days cells were stained with 0.5% (w/v) crystal violet in 70% ethanol.

Proximity Ligation Assay

Proximity ligation assays (PLA) were performed on fixed/permeabilized cells. The PLA protocol was followed according to the manufacturers' instructions (Olink Bioscience, Uppsala,Sweden). After blocking, the antibodies were used at the following concentrations : for eIF4E (mouse, clone A-10, SC-271480, Santa Cruz 1:500); for eIF4G (rabbit, 2498; Cell Signaling 1:500). PLA minus and PLA plus probes (containing the secondary antibodies conjugated with oligonucleotides) were added and incubated for 1 h at 37°C. After hybridization, oligonucleotide ligation and a rolling circular amplification were performed. Then, cell nuclei were stained with Olink mounting media containing DAPI. The results were obtained with a scanner (Olympus VS120) and the number of PLA signals per cell was counted (>3 fields) by semi-automated image analysis (ImageJ and oLyvia).

FIGURE LEGENDS

Figure 1. Sensitivity of melanoma cell lines to anti-MEK inhibitors. A. Short-term growth-inhibition assay of the indicated cell lines (SKMel10, M311, SKMel2, M376, IGRMEL1) treated with increasing concentrations of trametinib or cobimetinib. Cell viability was determined using the WST-1 cell proliferation assay. The data are presented as the mean +/- SEM (n=3). B. Long-term colony formation assay of the indicated cell lines. Cells were grown in the absence or presence of trametinib or cobimetinib at the indicated concentrations for 7-14 days. For each cell line, all dishes were fixed at the same time, stained and photographed.

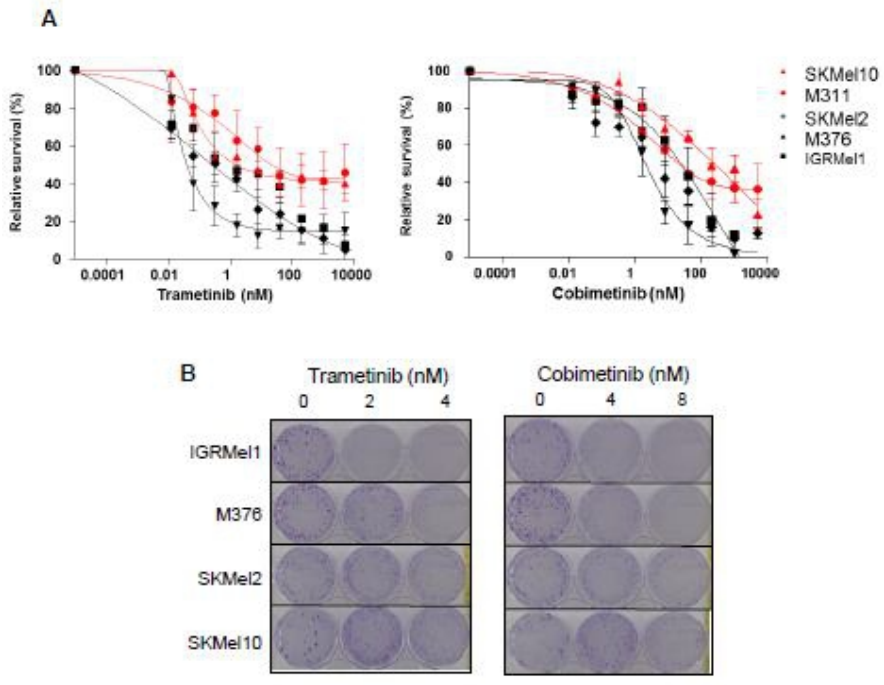

Figure 2. The formation of the eIF4F translation initiation complex is associated with resistance to MEK inhibitors. A. eIF4E–eIF4G interactions detected by proximity ligation assay (PLA) in trametinib/cobimetinib-treated or untreated cell lines. The interactions were visualized as red spots. B. PLA quantification showing the number of eIF4E-eIF4G interactions by cell. The data are presented as the mean s.d (n=4), and differences were assessed with Student's t-test (* $p < 0,05$; ** $p < 0,01$; *** $p < 0,001$)

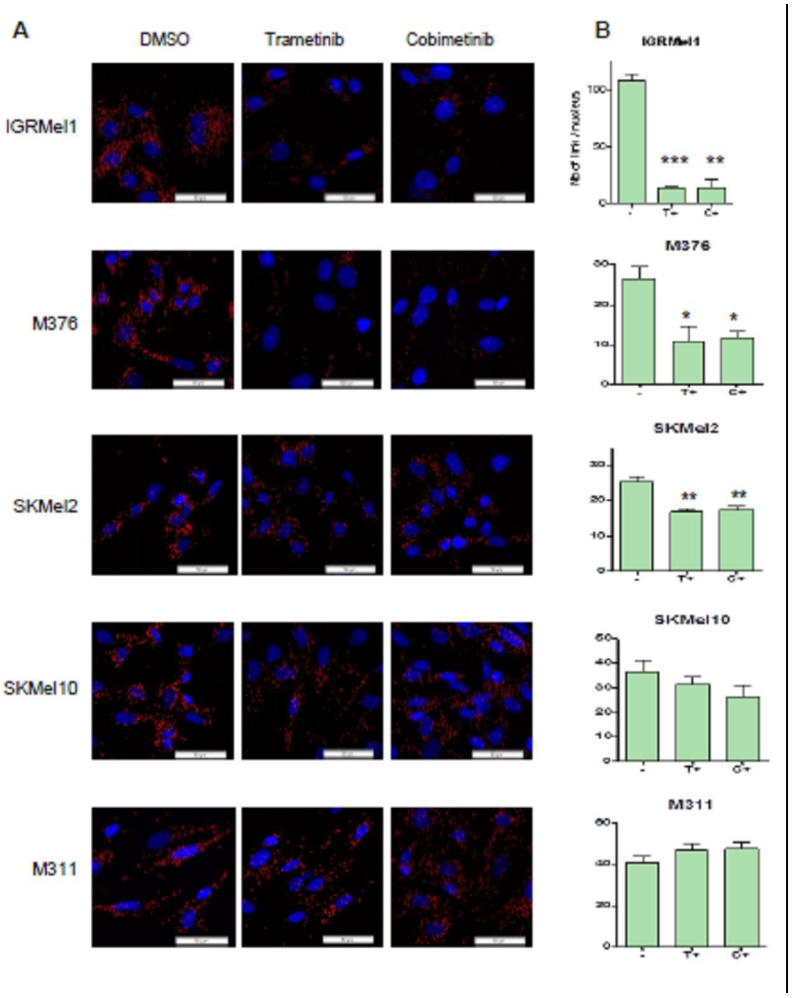

Figure 3. Flavaglines sensitize NRAS-mutated resistant cell lines and synergize with MEK inhibitors. A. Short-term growth-inhibition assay of the indicated cell lines treated with

increasing concentrations of silvestrol or FL3. Cell viability was determined using the WST-1 cell proliferation assay. The data are presented as the mean +/- SEM (n=3). B. Isobologram of the effect of the combination of trametinib or cobimetinib plus FL3 at fixed concentration (4,1 nM) on SKMel10 and M311 cell lines. The Bliss index is shown in square brackets.

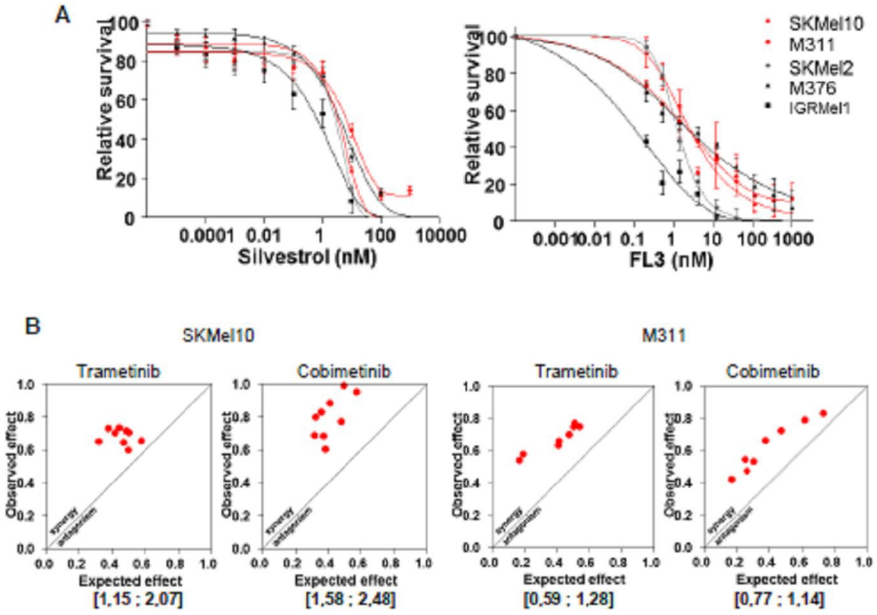

REFERENCES

1. Downward J. Targeting Ras Signalling. *Nat Rev Cancer*. 2003;3:11-22. doi:10.1038/nrc969.

2. Malumbres M, Barbacid M. RAS oncogenes□: the first 30 years. *Nat Rev Cancer*. 2002;3:7-13. doi:10.1038/nrc1097.

3. Schubbert S, Bollag G, Shannon K. Deregulated Ras signaling in developmental disorders□: new tricks for an old dog. *Curr Opin Genet Dev*. 2007;(17):15-22. doi:10.1016/j.gde.2006.12.004.

4. Devitt B, Liu W, Salemi R, et al. Clinical outcome and pathological features associated with NRAS mutation in cutaneous melanoma. *Pigment Cell Melanoma Res*. 2011;(24):666-672. doi:10.1111/j.1755-148X.2011.00873.x.

5. Ascierto P, Schadendorf D, Berking C, et al. MEK162 for patients with advanced melanoma harbouring NRAS or Val600 BRAF mutations: A non-randomised, open-label phase 2 study. *Lancet Oncol*. 2013;14(3):249-256. doi:10.1016/S1470-2045(13)70024-X.

6. Chapman PB, Hauschild A, Robert C, et al. Improved survival with vemurafenib in melanoma with BRAF V600E mutation. *N Engl J Med*. 2011;364(26):2507-2516. doi:10.1056/NEJMoa1103782.

7. Hauschild A, Grob JJ, Demidov L V., et al. Dabrafenib in BRAF-mutated metastatic melanoma: A multicentre, open-label, phase 3 randomised controlled trial. *Lancet*. 2012;380(9839):358-365. doi:10.1016/S0140-6736(12)60868-X.

8. Boussemart L, Malka-Mahieu H, Girault I, et al. eIF4F is a nexus of resistance to anti-BRAF and anti-MEK cancer therapies ´. *Nature*. 2014;513. doi:10.1038/nature13572.

9. Bordeleau ME, Robert F, Gerard B, et al. Therapeutic suppression of translation initiation modulates chemosensitivity in a mouse lymphoma model. *J Clin Invest*. 2008;118(7):2651-2660. doi:10.1172/JC134753.

10. Cencic R, Carrier M, Galicia-Vázquez G, et al. Antitumor activity and mechanism of action of the cyclopenta[b]benzofuran, silvestrol. *PLoS One*. 2009;4(4):e5223.

doi:10.1371/journal.pone.0005223.

11. Gupta S V, Sass EJ, Davis ME, et al. Resistance to the translation initiation inhibitor silvestrol is mediated by ABCB1/P-glycoprotein overexpression in acute lymphoblastic leukemia cells. *AAPS J*. 2011;13(3):357-364. doi:10.1208/s12248-011-9276-7.

12. Thuaud F, Bernard Y, Turkeri G, et al. Synthetic Analogue of Rocaglaol Displays a Potent and Selective Cytotoxicity in Cancer Cells□: Involvement of Apoptosis Inducing Factor and Caspase-12. *J Med Chem*. 2009:5176-5187. doi:10.1021/jm900365v.

Publication N°*10*

Targeting prohibitins with chemical ligands inhibits KRAS-mediated lung tumours.

Yurugi, H., Marini, F., Weber, C., David, K., Zhao, Q., Binder, H., Désaubry, L., Rajalingam, K., *Oncogene*, **2017**, *36*, 1-12.

Oncogene (2017), 1–12

www.nature.com/onc

ORIGINAL ARTICLE

Targeting prohibitins with chemical ligands inhibits KRAS-mediated lung tumours

H Yurugi[1], F Marini[2], C Weber[3], K David[3], Q Zhao[4], H Binder[2], L Désaubry[4,5] and K Rajalingam[1,6]

KRAS is one of the most frequently mutated oncogenes in human non-small cell lung cancers (NSCLCs). RAS proteins trigger multiple effector signalling pathways including the highly conserved RAF-MAPK pathway. CRAF, a direct RAS effector protein, is required for KRAS-mediated tumourigenesis. Thus, the molecular mechanisms driving the activation of CRAF are intensively studied. Prohibitin 1 (PHB1) is an evolutionarily conserved adaptor protein and interaction of CRAF with PHB1 at the plasma membrane is essential for CRAF activation. Here, we demonstrate that PHB1 is highly expressed in NSCLC patients and correlates with poor survival. Targeting of PHB1 with two chemical ligands (rocaglamide and fluorizoline) inhibits epidermal growth factor (EGF)/RAS-induced CRAF activation. Consistently, treatment with rocaglamide inhibited proliferation, migration and anchorage-independent growth of KRAS-mutated lung carcinoma cell lines. Surprisingly, rocaglamide treatment inhibited Ras-GTP loading in KRAS-mutated cells as well as in EGF-stimulated cells. Rocaglamide treatment further prevented the oncogenic growth of KRAS-driven lung cancer allografts and xenografts in mouse models. Our results suggest rocaglamide as a RAS inhibitor and that targeting plasma membrane-associated PHB1 with chemical ligands would be a viable therapeutic strategy to combat KRAS-mediated NSCLCs.

Oncogene advance online publication, 17 April 2017; doi:10.1038/onc.2017.93

INTRODUCTION

RAS GTPases are oncogenes mutated in nearly 30% of human carcinomas. Among the three RAS isoforms (HRAS, NRAS and KRAS), KRAS is the most frequently mutated member of the family.[1,2] Upon activation, RAS triggers multiple signalling pathways. These signalling cascades rely on the activity of kinases that form the major constituent of the 'druggable genome'.[3,4] Many of the RAS effector signalling pathways form highly complex networks that control almost all 'hallmarks of cancer'.[5] Several attempts to target RAS itself have had limited success, though recent studies showed that targeting mutated RAS isoforms in human cancers could still be an effective strategy.[2] RAF kinases are direct RAS effector proteins and they are the founding members of the serine threonine kinase family.[6] Upon activation, RAF kinases phosphorylate and activate MEK1/2, resulting in the activation of ERK1/2, which constitute a three-tier mitogen-activation protein kinase (MAPK) cascade.[7] This pathway controls fundamental cellular processes like proliferation, migration, differentiation and cell survival.[7] Among the three RAF isoforms, BRAF exhibits high basal kinase activity in comparison to CRAF and ARAF.[6,8] RAF kinases like many other kinases function as dimers and interfering with RAF dimerization impairs RAS-mediated MAPK activation.[9] Several small molecule inhibitors targeting the MAPK pathway components have been developed and many of them are pursued in clinics.[10] RAF kinases are also mutationally activated in human cancers, and BRAF is one of the most frequently mutated oncogene in thyroid, skin cutaneous melanoma, colorectal cancers and multiple myelomas.[8,11] Despite BRAF exhibiting high basal kinase activity, CRAF is primarily required for KRAS-mediated lung cancer.[12] Depletion of endogenous CRAF also prevents NRAS-mediated MAPK activation and proliferation in melanomas.[13] *In vitro*, RAS binds with high affinity to the Ras-binding domain (RBD) of CRAF, yet the activation of CRAF by RAS in cells is a multistep process, which involves the interaction of CRAF with prohibitin 1 (PHB1) at the plasma membrane.[14] Previous studies have shown that this interaction is required for the displacement of 14-3-3 from serine 259, thus facilitating the stable association of CRAF to the plasma membrane for full activation.[15] Consistently, augmented expression of PHB1 contributes to increased CRAF activation in cervical carcinoma cells and associated with enhanced migration and metastases in animal models.[16]

PHB1 is the flagship member of the 'PHB domain'-carrying integral membrane proteins and its present in a complex with PHB2.[17] Prohibitins (PHB1/2) are stable as heteromers, and they are responsible for cristae morphogenesis and proper functioning of the mitochondria.[18,19] Since prohibitins have essential functions in mitochondria, a blockade of protein expression through small molecules is limited. However, recent studies revealed that flavaglines, which are natural anti-tumour drugs, directly target the PHB1-CRAF interaction leading to CRAF inactivation, thus opening a novel avenue of targeting CRAF kinase outside the kinase domain.[20] As the structure of the kinase domains is similar, small molecule kinase inhibitors often lead to undesired side effects. Further, cancer patients frequently develop resistances to kinase inhibitors.[21] Thus, targeting oncogenic kinase outside the kinase domain or a protein–protein interaction domain will be an attractive strategy to combat human cancers.

[1]Molecular Signaling Unit-FZI, Institute of Immunology, University Medical Center Mainz, Mainz, Germany; [2]Institute of Medical Biostatistics, Epidemiology and Informatics (IMBEI), University Medical Center Mainz, Mainz, Germany; [3]Indivumed GmbH, Hamburg, Germany; [4]Therapeutic Innovation Laboratory, UMR7200, CNRS/University of Strasbourg, Strasbourg, France; [5]Sino-French Joint Lab of Food Nutrition/Safety and Medicinal Chemistry, College of Biotechnology, Tianjin University of Science and Technology, Tianjin, China and [6]UCT, Mainz, German Cancer Consortium (DKTK), Partner Site Frankfurt/Mainz, DKFZ, Heidelberg, Germany. Correspondence: Professor K Rajalingam, Molecular Signaling Unit-FZI, Institute of Immunology, University Medical Center Mainz, JGU-Mainz, Langebeck street 1, Mainz 55131, Germany.
E-mail: Krishna@uni-mainz.de
Received 16 November 2016; revised 27 February 2017; accepted 28 February 2017

In this study, we demonstrate that PHB1 is highly expressed in human lung cancers, which correlates with poor patient survival. Targeting prohibitins with two different chemical ligands led to inhibition of epidermal growth factor (EGF)/RAS-mediated activation of CRAF kinase. Rocaglamide treatment directly inhibited RAS activation. Furthermore, rocaglamide inhibited the growth of KRAS-mutated lung cancer cells both *in vitro* and *in vivo*. These results suggest that targeting PHB1-CRAF interface could be a possible strategy in treating KRAS-mutated non-small cell lung cancer (NSCLC) cancers.

RESULTS

NSCLC account for $>80\%$ of lung cancers. According to the world cancer report of the World Health Organization, lung cancers contribute to about 20% of total cancer deaths. KRAS is mutated in nearly 17% of lung cancers and most of the KRAS-mutated lung cancers are adenocarcinomas.[2] Previous studies have shown that CRAF, but not BRAF or ARAF, is required for the onset of tumourigenesis in a mouse model of KRAS-driven NSCLCs.[12] Kinase inhibitors that target CRAF-mediated MEK1 activation exhibited pronounced anti-tumour effects in KRAS-mutated tumours.[22] As PHB1 is critically required for the activation of CRAF by RAS, PHB1 expression was investigated in adenocarcinoma and squamous cell carcinoma of the lung. Analysis of The Cancer Genome Atlas (TCGA) data set revealed a high PHB1 RNA expression in human adenocarcinoma and squamous cell carcinoma of the lung (Figures 1a and b). Patients were stratified based on the KRAS and EGFR mutation status. PHB1 was highly expressed in lung cancers regardless of the KRAS or EGFR mutation status (Figures 1c and d, Supplementary Table 1). We also checked the correlation between PHB1 messenger RNA expression and poor prognosis of lung cancer patients. As expected, overexpression of PHB1 was associated with poor patient survival (Figure 1e).

To analyse PHB1 expression in adenocarcinoma and squamous cell carcinoma of human lung as well as in tumour-adjacent normal lung tissue, immunohistochemical analysis of a NSCLC tissue microarray was performed (Figure 2). On the subcellular level, a cytoplasmic as well as membranous staining was observed in tumour cells of both lung cancer subtypes. The staining intensity was mainly weak to moderate for both cytoplasmic and membranous staining within the tumour area, whereby most tumour cells exhibited a cytoplasmic staining. Therewith, *H*-scores between 10 and 190, as well as 5 and 90 were determined for cytoplasmic and membranous anti-PHB1 staining of tumour cells of squamous cell carcinoma. For adenocarcinoma lung tissues, *H*-scores of 40–175 as well as 0–100 were determined for cytoplasmic and membranous staining. If present, the anti-PHB1 staining was only weakly seen within the cytoplasm of non-malignant epithelial cells within tumour-adjacent normal lung tissue. By *H*-score classification, all but three (two squamous cell carcinoma cases and one adenocarcinoma case) cases were classified as PHB1-positive (*H*-score >50), whereby the majority was classified as moderately positive for cytoplasmic PHB1 and weakly positive for membranous PHB1. Tumour-adjacent normal lung tissues were predominantly classified as PHB1-negative (*H*-score $\leqslant 50$).

We then investigated if the PHB1/2 complex could be targeted by chemical ligands such as rocaglamide and fluorizoline, which were previously described among others as PHB1/2 ligands (reviewed in Luan *et al.*[23]). First cell culture experiments using HeLa cells were carried out (Figure 3a). The working concentration of rocaglamide was determined by an MTT assay (Supplementary Figure S1A). We first tested if treatment of cells with rocaglamide or fluorizoline inhibits EGF-mediated CRAF activation as measured by the phosphorylation of MEK1/2. HeLa cells were treated with rocaglamide or fluorizoline for 4 h and then stimulated with EGF for different time points as indicated in the figure. As expected, fluorizoline and rocaglamide treatment prevented the activation of MEK1/2 by EGF (Figure 3b, Supplementary Figure S1B). As localization to the plasma membrane is critical for the activation of CRAF kinase, we performed cell fractionation studies with rocaglamide- or fluorizoline-treated cells after stimulation with EGF. Treatment with rocaglamide reduced plasma membrane-associated fraction of CRAF despite EGF stimulation (Figure 3c). However, fluorizoline treatment failed to prevent this translocation. Consistent with the previous studies, rocaglamide treatment led to disruption of PHB1-CRAF interaction (Figure 3d). As activated RAS induces BRAF-CRAF heteromerization, we tested if treatment with rocaglamide disrupts this interaction. Interestingly, rocaglamide treatment strongly prevented BRAF-CRAF interaction in response to EGF in cells (Figure 3e). As rocaglamide prevented RAF dimerization in response to EGF stimulation, we checked if RAS is indeed activated in rocaglamide- and fluorizoline-treated cells. Rocaglamide but not fluorizoline treatment led to a decrease in active GTP-bound RAS in response to EGF in HeLa cells (Figure 3f, Supplementary Figure S1C). While rocaglamide treatment led to a decrease in active RAS levels, fluorizoline treatment led to disruption of active RAS-CRAF interaction in response to EGF (Supplementary Figure S1C). We then tested if rocaglamide treatment could inhibit KRAS-GTP in cells carrying mutated KRAS. Interestingly, treatment of NCI-H226 cells with rocaglamide led to inhibition of KRAS-GTP loading in these cells in a concentration-dependent manner (Figure 4a). We then checked if rocaglamide treatment directly disrupts the GTP loading of KRAS by employing purified proteins. Presence of rocaglamide in fivefolds excess than the concentrations employed in cells failed to prevent GTP loading of KRAS directly (Figure 4b). These results suggested that rocaglamide is an inhibitor of RAS in cells, and that fluorizoline could disrupt the interaction between CRAF and active RAS in cells.

We then tested if rocaglamide treatment inhibited MEK1/2 activation in immortalized human lung epithelial cells (SALEB). Rocaglamide treatment failed to prevent the basal MEK1/2 activation in this cell type (Figure 4c). We then analysed if rocaglamide inhibits MEK1/2 in SALEB cells transformed with the oncogenic KRAS G12V mutant. Treatment with rocaglamide prevented KRAS-mediated MEK1/2 activation in SALEB-KRAS cells (Figure 4c). Consistent with these observations, rocaglamide treatment strongly inhibited basal MEK1 activation in several cell lines derived from mouse and human lung NSCLC tumours (368T1, 482T1, NCI-H226, Calu-6, Calu-1 and A549) (Figure 4c and Supplementary Figure S2). Consistent with these observations, rocaglamide treatment led to significant inhibition of cell proliferation (Figures 5a and b). In particular, rocaglamide treatment led to a block in neo DNA synthesis, and reduction in the levels of cyclin B1 and D1 (Figure 5c and Supplementary Figure S3A). However, rocaglamide treatment did not lead to cell death in these cell types at least in the time frame of the experiment (Supplementary Figure S3B). As PHB1 is required for cell adhesion and cell migration, we tested if rocaglamide treatment interfered with the adhesion and migration of KRAS-mutated cell lines. Rocaglamide reduced the adhesion of 368T1 and 482T1 cells to extracellular matrix components (Figures 6a and b). Similar results were also obtained in HeLa cells and HCT-116 cells (Supplementary Figure S4A). Depletion of PHB1 was shown to induce intercellular adhesion leading to the formation of cell clumps in *in vitro* cell culture models.[14,23] Rocaglamide treatment led to a similar morphology in the above-mentioned cell lines with reduced actin-rich protrusions (Figure 6c). Consistently, rocaglamide treatment inhibited the migration of both 368T1 and 482T1 cells in two-dimensional matrices (Figures 6d–g). We then tested if rocaglamide prevents KRAS-mediated oncogenesis. Soft agar colony formation assays with KRAS-mutated NSCLC cell lines revealed that rocaglamide treatment almost completely abrogated the anoikis resistance in these cells (Figures 7a–c). Rocaglamide also prevented the soft agar growth of HeLa cells and HCT-116 cells (Supplementary Figure S4B). To finally confirm if the rocaglamide-mediated effects are specific for CRAF but not

BRAF, we conducted experiments in cell lines carrying BRAF V600E. A375, MEL-HO, HT29 and Colo829 cells that endogenously express BRAF V600E were treated with rocaglamide. As expected, rocaglamide treatment did not inhibit MEK1/2 activation in these cell types (Supplementary Figure S5A). Moreover, overexpression of BRAF V600E in HeLa cells reverted MEK1/2 activation and

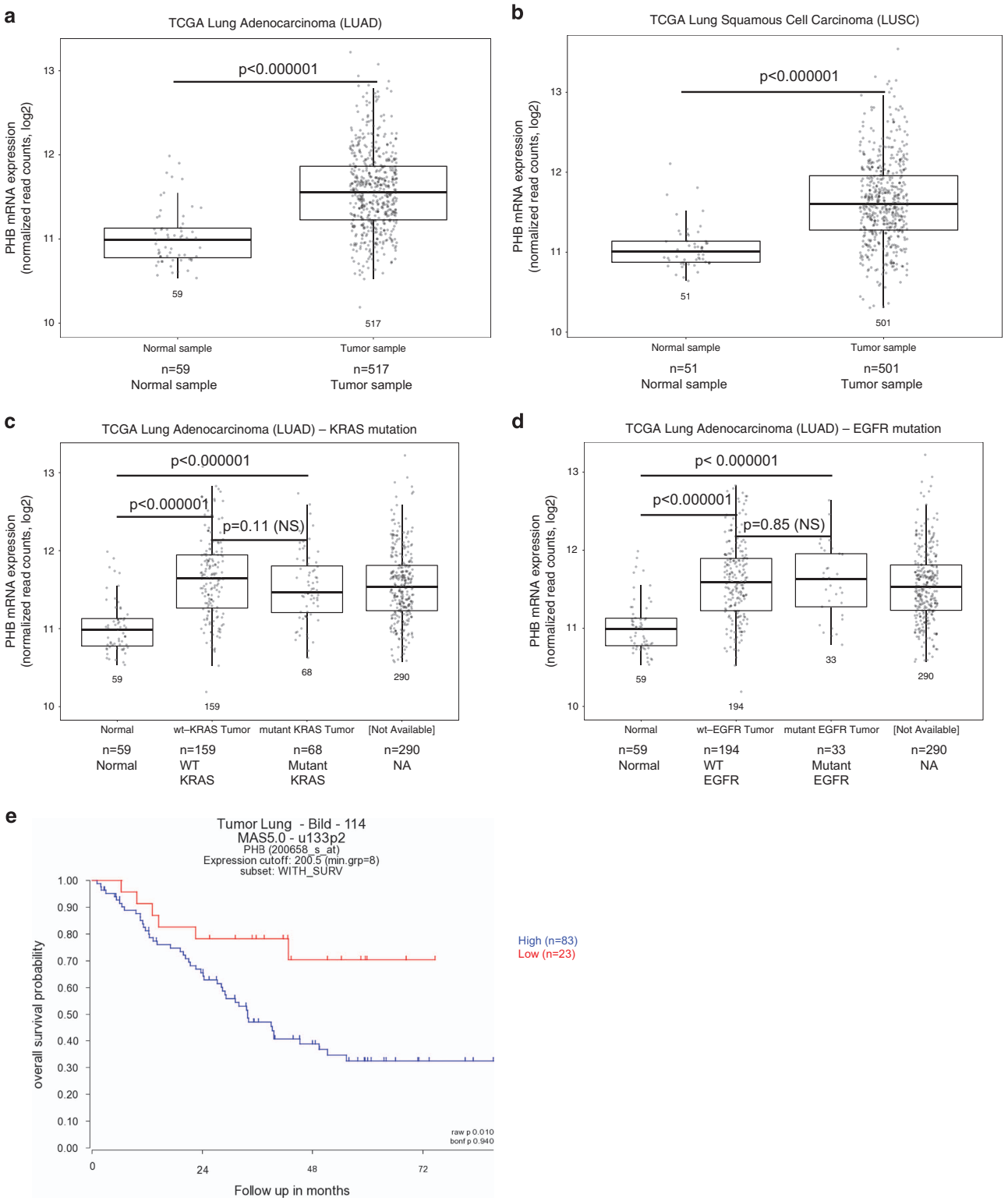

Figure 1. PHB1 is highly expressed in human lung cancers. (**a**–**d**) Expression analyses of PHB1 mRNA in the TCGA lung adenocarcinoma (LUAD) and lung squamous cell carcinoma (LUSC) patient data set, compared to normal samples. Patients were stratified according to the KRAS and EGFR mutation status, as described in Materials and Methods. Box plots represent PHB mRNA expression levels as determined in the RNA-seq experiments. *P*-values were determined by the two-sided Welch's *t*-tests that account for unequal variances in the two populations. The number of patients in each group is indicated by *n*. (**e**) PHB1 expression is correlated with poor prognosis of lung cancer patients. Kaplan–Meier curves were obtained from Genomics analysis and visualization platform (http://r2.amc.nl), and cutoff value was shown in the figure. mRNA, messenger RNA.

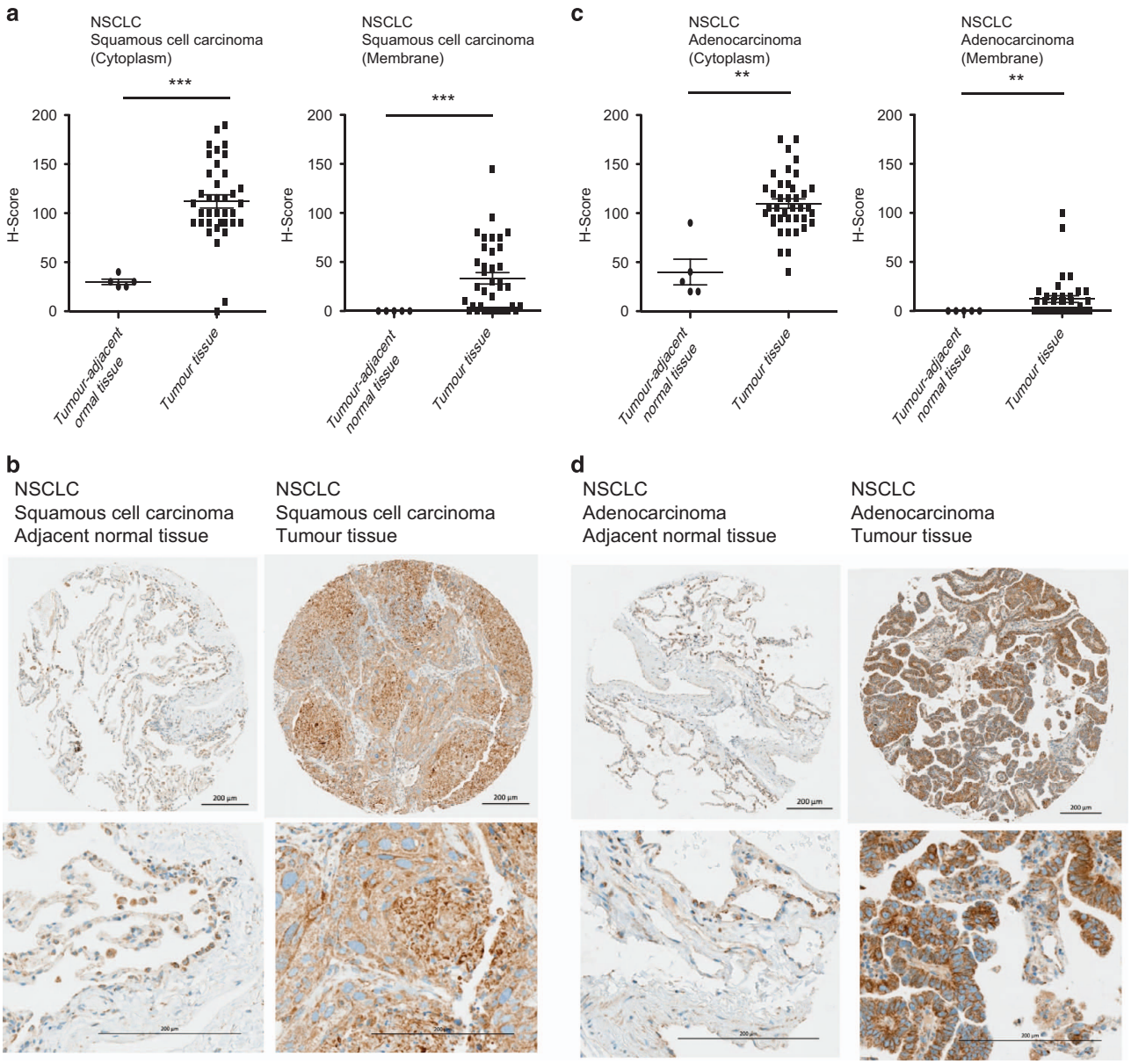

Figure 2. Relatively high PHB1 protein levels are detected in human NSCLC patient tumour tissue. The expression level of PHB1 was pathologically evaluated in the tumour tissue microarray (TMA) as mentioned in the Materials and Methods section. Compared to tumour-adjacent normal lung tissue, anti-PHB1 staining was more intense in the tumour tissue showing a mainly cytoplasmic, but also membranous staining pattern (**a**–**d**). *H*-scores ranged from 10 to 190 and from 40 to 175 for cytoplasmic staining, as well as from 5 to 90 and from 0 to 100 for membranous anti-PHB1 staining in squamous cell carcinoma and adenocarcinoma, respectively (**a**, **c**). All in all, cytoplasmic anti-PHB1 staining was predominant within tumour tissue (**b**, **d**). If present, membranous anti-PHB1 staining was slightly more intense within adenocarcinoma compared to squamous cell carcinoma (**a**, **c**). Welch's *t*-test was employed to test the significance (***$P < 0.001$, **$P < 0.01$).

proliferation in rocaglamide-treated cells (Supplementary Figures S5B and C). Consistently, the migratory, elongated morphology is retained in BRAF V600E cells despite the treatment with rocaglamide (Supplementary Figure S5D and Supplementary Movies 1–4). To further evaluate the effect of rocaglamide on the oncogenic growth of KRAS-mutated NSCLC cell lines, experiments were carried out using animal models. To this end, we established allografts in B6129 SF1/J mice with 482T1 cells and injected rocaglamide (2.5 mg/kg) into the allografted mice as mentioned in the Materials and Methods section. Over time, we detected that rocaglamide significantly inhibited the growth of 482T1 allografts in this immunocompetent mouse model (Figures 7d and e). We also checked the phosphorylation of CRAF and MEK1/2 within the tumour tissue. The tumour tissues isolated from rocaglamide-treated mice contained less phosphorylated CRAF and MEK1/2 compared to DMSO-treated tumour tissues (Supplementary Figure S6). Further xenograft experiments of nonobese diabetic/severe combined immune deficiency (NOD/SCID) mice were performed. Consistent with the soft agar assays, rocaglamide injections prevented the growth of NCI-H226 xenografts as shown in Figures 7f–h. Taken together, these results confirmed that targeting of PHB-CRAF with rocaglamide inhibited oncogenicity in KRAS-mutated NSCLC cancers.

DISCUSSION

The high frequency of RAS mutations in human cancers aroused an enormous interest to target RAS directly. Therefore, several

farnesyl transferase inhibitors have been developed.[1] However, farnesyl transferase inhibitors exhibited severe side effects and thus the focus was turned to the downstream RAS effectors, especially kinases. Given the clinical success of tyrosine kinase inhibitors, several potent inhibitors were developed to target the downstream serine threonine kinases like RAF. Soon after the discovery that CRAF, the first known serine threonine kinase, binds to RAS-GTP, MEK1 was identified as a substrate of CRAF.[24] This led to the identification of the mitogen-activated protein kinase cascade CRAF-MEK1/2-ERK1/2 and established the paradigm of MAPK signalling with RAS functioning as a molecular switch to relay signals from the extracellular milieu to the nucleus through the kinase cascades, which promote oncogenesis. Several RAS effectors were identified subsequently, which together contribute to various aspects of tumourigenesis, metastases and drug resistance.[25] Among the three RAF isoforms, BRAF has gained special attention, as the BRAF V600E mutation is frequent in melanomas. Vemurafenib (a kinase inhibitor that targets the BRAF V600E mutated form) is a potent BRAF inhibitor and showed enormous clinical success even so patients rapidly develop resistance[26] through CRAF overexpression or by gaining RAS mutations. Furthermore, in patients with RAS mutations, RAF inhibitors induced activation of MAPK paradoxically by promoting the dimerization of RAF isoforms.[10] Activated RAS triggered the

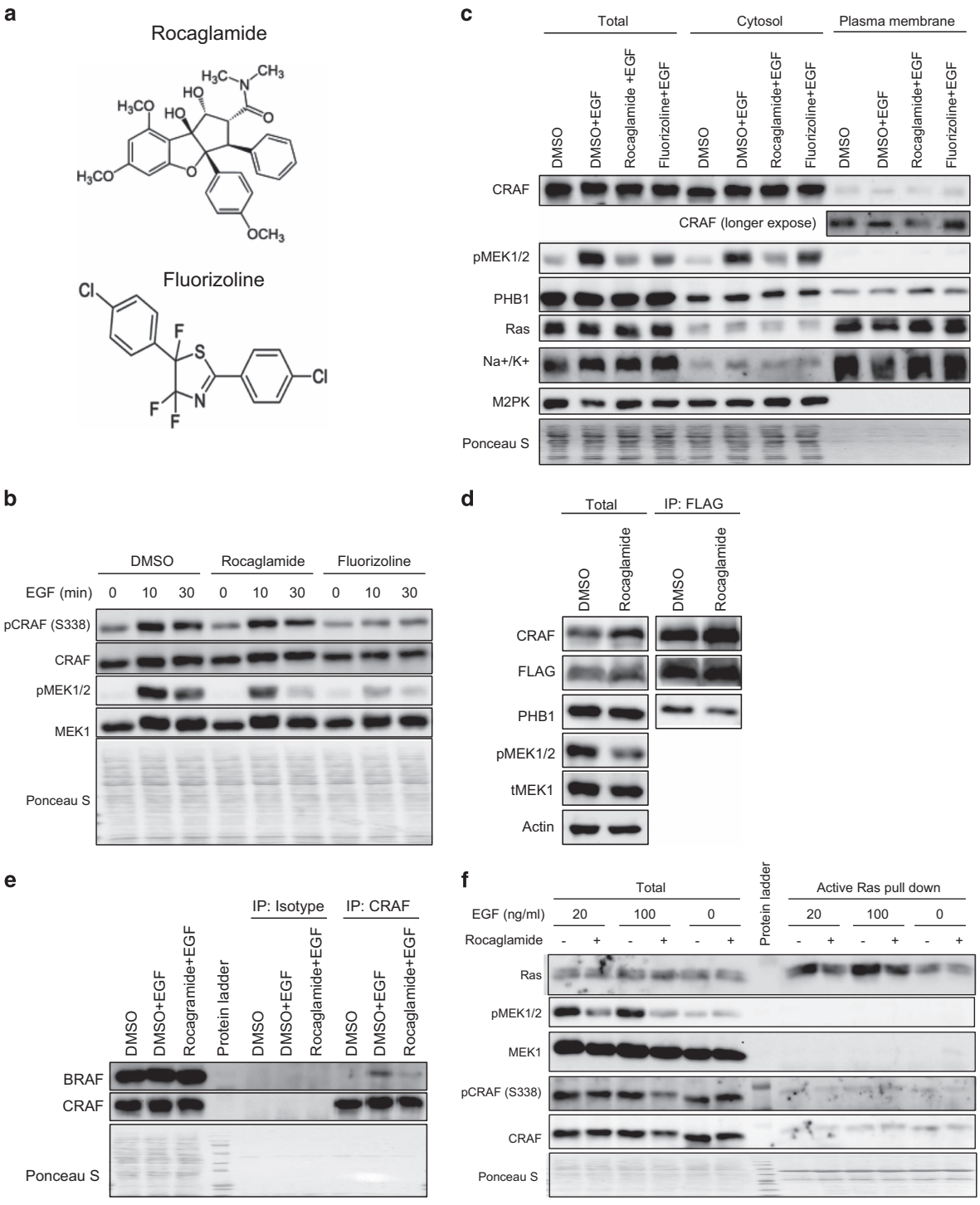

formation of BRAF-CRAF heterodimers, which exhibit high kinase activity.[27,28] In many RAS-mutated cancer cases, CRAF serves as a MAPK cascade driver. Therefore, intense efforts are made to understand the biochemistry of CRAF activation. While active RAS binds to CRAF with high affinity, stable association of CRAF in the plasma membrane is required for the full activation of the kinase.[29] Plasma membrane-associated PHB1 functions as a membrane anchor as loss of PHB1 or disruption of PHB1-CRAF complex prevents CRAF activation. Previous studies have shown that PHB1 can be phosphorylated in the lipid raft fractions contributing to CRAF activation and cervical cancer metastases.[17] Multiple agents leading to inactivation of CRAF kinase and the MAPK cascade can target the CRAF-PHB1 interface. For instance, bacterial and viral pathogens target surface-expressed PHB1 to their benefit and the Vi polysaccharide of *Salmonella typhi* interacts with the PHB1/2 complex leading to a block in ERK1/2 activation.[30] Prohibitins were also found to be surface exposed in T cells and recent studies identified Siglec-9 as a ligand of PHB1/2 complex.[31] Interaction of Siglec-9 with the PHB1/2 complex prevented RAF-MAPK activation in T cells leading to reduced IL-2 production.[32] While PHB1 is shown to be possibly associated with the plasma membrane through palmitoylation at C69, the mechanisms driving the surface expression of PHB1 are unclear.[33] PHB1 was also shown to be localized in mitochondria as well as nuclei, and is thought to contribute to a variety of functions such as cell cycle, metabolism and growth control. The discovery that plasma membrane-associated prohibitin can be targeted by rocaglamide opens a novel therapeutic avenue and the results are already exploited in the treatment of tumours.[23,34] In this study, we demonstrated that PHB1 is highly expressed in human lung cancer, which is one of the most common cancer types and the leading cause of cancer-related morbidity irrespective of sex or population. We demonstrated that targeting the PHB1/2 complex with chemical ligands such as rocaglamide prevents KRAS-mediated tumourigenesis both *in vitro* and *in vivo*. A second PHB1 ligand, fluorizoline, prevented the RAS-CRAF interaction in cells (Supplementary Figure S1C) and prevented MEK1/2 activation in response to EGF (Figures 3b and c).

Treatment with rocaglamide also inhibited RAS activation in response to EGF and reduced GTP-loaded RAS in KRAS-mutated cell lines. Though the mechanisms behind the rocaglamide-mediated inhibition of RAS are unclear, it is possible that targeting prohibitins could impair the plasma membrane microdomains in which active RAS is located. Rocaglamide binding might immobilize PHB1/2 complex in the plasma membrane, which may have an effect on the stability of RAS-GTP in cells. One cannot rule out the possibility that rocaglamide has yet another target(s) that could impair RAS activation. As RAS has long been thought to be undruggable, recent studies shed some light into this dogma. Since rocaglamide treatment prevented RAS activation and rocaglamide-mediated effects seem to be tumour cell-specific and seem to protect non-malignant cells,[35] further studies are important. Taken together, these results open a novel avenue of targeting CRAF kinase with PHB1 ligands and further unveil a RAS inhibitor that could be further explored to combat RAS-mediated tumours.

MATERIALS AND METHODS

Cell culture

368T1 and 482T1 cells were a kind gift from Tyler Jacks lab and cultured in DMEM (10% heat inactivated foetal bovine serum (FBS)). NCI-H226 (CRL-5826, ATCC, Manassas, VA, USA) and A549 cells (a kind gift from Susan Horwitz) were authenticated by Eurofin genomics (Ebersberg, Germany, http://www.eurofinsgenomics.com/en/home.aspx). These cells were cultured in RPMI-1640 (10% heat inactivated FBS). Calu-1 cell was obtained from Sigma-Aldrich (St Louis, MO, USA) and cultured in MCcoy's 5A medium (10% heat inactivated FBS). SALEB and SAKRAS (a kind gift from Scott Randell) were cultured in serum-free CnT-BM1 medium with CnT-17.S supplement pack (CELLnTEC, Bern, Switzerland). Calu-6 was purchased from ATCC. HeLa (DSMZ) and HCT-116 (a gift from Ulf Rapp) were authenticated by Eurofin genomics. Calu-6 and HeLa cells were cultured in DMEM (10% heat inactivated FBS). A375, MEL-HO, HT29 and Colo829 cells were used as BRAF V600E carrying cell lines, and RPMI-1650 (A375 and MEL-HO), MCcoy's 5A medium (HT29) and DMEM (Colo829) with 10% FCS were used as a growth medium. For stimulation with EGF, HeLa cells were cultured in a 12-well plate or a 10 cm dish. Once the cells reach near confluence (70–80%), medium was exchanged to serum-free medium, and rocaglamide (200 nM, Active Biochem, Kowloon, Hong Kong) and fluorizoline (10 μM) were added to the medium. After 4 h of starvation in the presence of PHB ligands, the cells were stimulated by EGF (40-217, NatuTec, Frankfurt am Main, Germany) at 20 or 100 ng/ml of final concentration for 5–30 min. Fluorizoline was synthesized as described in Perez-Perarnau *et al.*[36] For live/dead staining, 482T1 cell was treated in a 12-well plate and cultured with rocaglamide (50 and 200 nM) for 24 h, and then treated with 5 μM Cell tracker CMFDA and 5 μg/ml of propidium iodide (PI) for 30 min. The cells were observed under a fluorescent microscope (DMi8, Leica, Wetzlar, Germany).

Antibodies

Anti-phospho CRAF antibody S338 (#9427), anti-phospho MEK1/2 (#9154), anti-MEK1 antibody (#2352) and anti-PARP antibody (#9542) were purchased from Cell Signalling Technology (Danvers, MA, USA). Anti-BRAF antibody (sc-5284) and anti-CRAF antibody (sc-133) were purchased from Santa Cruz (Dallas, TX, USA). Mouse anti-PHB1 antibody (MA5-12858) and anti-sodium/potassium ATPase alpha antibody (MA3-928) were

Figure 3. Targeting PHB1 with two different ligands led to the inhibition of RAS-CRAF-MEK pathway. (**a**) The chemical structures of PHB1 ligands (rocaglamide and fluorizoline). (**b**) The effect of rocaglamide and fluorizoline treatment on RAS-MAPK activation. HeLa cells were cultured in a serum-free medium with rocaglamide (200 nM) and fluorizoline (10 μM) for 4 h. After incubation, EGF (final concentration 20 ng/ml) was added and the cells were collected after 0, 10, 30 min of stimulation. Immunoblot analyses were performed with the cell lysates to detect the activation of CRAF and MEK1/2. The total levels of CRAF and MEK1 were monitored (described in Materials and Methods section). Ponceau S staining of the entire membrane serves as a loading control. (**c**) HeLa cells were treated as mentioned earlier and stimulated with EGF for 30 min. The cells were lysed, and the cytosol and plasma membrane fractions were prepared as mentioned in the Materials and Methods section. The purity of the individual fractions was monitored by the presence of specific subcellular markers. Sodium potassium ATPase (Na^+/K^+) was employed as a plasma membrane marker and M2PK was employed as a cytosolic marker. Ponceau S staining was performed as a loading control. (**d**) Rocaglamide treatment inhibits CRAF-PHB1 interaction. HeLa cells were transiently transfected with FLAG-tagged CRAF with polyethylenimine transfection reagent. After 48 h of transfection, the cells were lysed and the FLAG-tagged CRAF was immunoprecipitated by employing FLAG beads. The co-precipitation of endogenous PHB1 was tested by immunoblots. The levels of CRAF, pMEK1/2, MEK1 and PHB was monitored in the total cell lysates. Actin was used as a loading control. (**e**) Rocaglamide treatment disrupts CRAF-BRAF heterodimer formation. HeLa cells were treated with rocaglamide (200 nM) as mentioned in **b** and stimulated with 100 ng/ml of EGF for 5 min. The cells were lysed and the endogenous CRAF protein was immunoprecipitated as mentioned in the Materials and Methods section. The complex formation between BRAF and CRAF was tested by immunoblots. (**f**) Rocaglamide treatment (200 nM) inhibits Ras activation. After 30 min of stimulation with EGF (20, 100 ng/ml), HeLa cells were collected for active Ras pull-down assay as mentioned in the Materials and Methods section. Total cell lysates and the precipitated proteins from a crypt pull-down assay employing GST-RAF-RBD were used for immunoblot analysis.

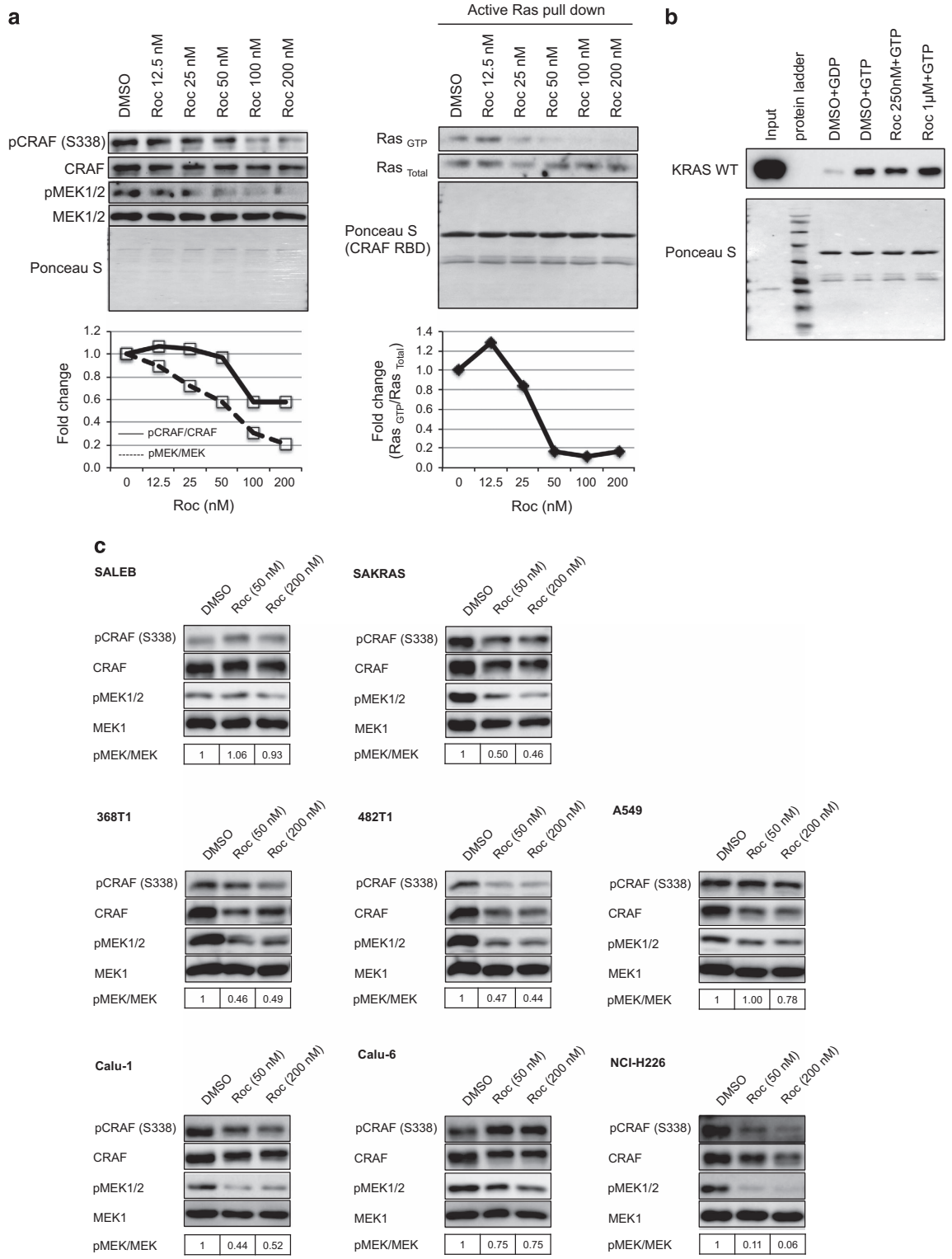

Figure 4. Treatment with rocaglamide prevents RAS activation. (**a**) NCI-H226 cells were incubated with indicated concentrations of rocaglamide and the activation of RAS was monitored as mentioned in the Materials and Methods section. In the total cell lysates, the phosphorylation status of MEK1 and CRAF were tested. The quantification of the blots is presented below. (**b**) Rocaglamide did not inhibit direct GTP loading of KRAS *in vitro*. Recombinant KRAS was incubated with GTP/GDP in the presence of rocaglamide and the loading of GTP-KRAS was monitored by a crypt pull-down assay employing RAF-RBD. (**c**) Rocaglamide treatment inhibits phosphorylation of MEK1/2 in several cell types. Cells were treated with rocaglamide (Roc, 50 nM, 200 nM) for 24 h in complete cell culture medium. The cells were subsequently lysed directly in SDS–PAGE sample buffer, and the activation status of MEK and CRAF was monitored by immunoblot analysis. The control samples were treated with DMSO. The band intensity was calculated by Image J and the mean of relative intensity from at least two independent experiments was shown below the blot. The result from DMSO-treated cells was taken as 1. The representative image was shown in the figure.

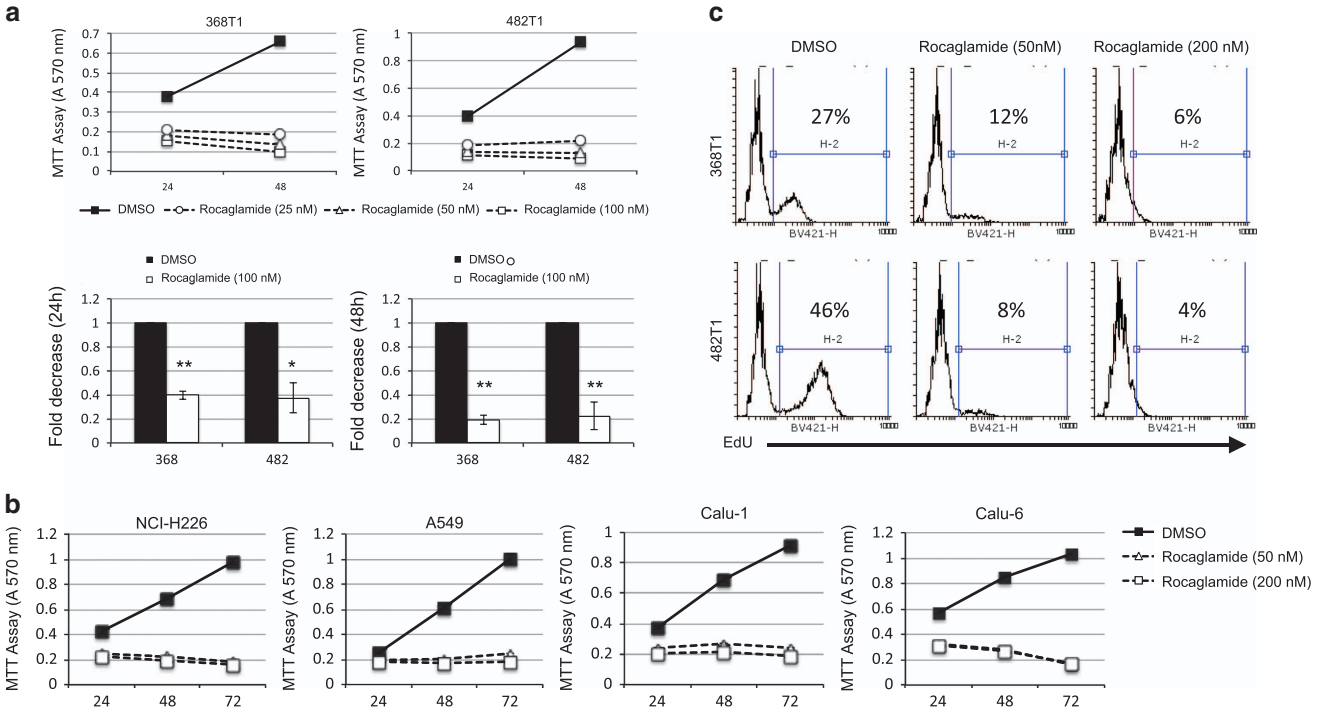

Figure 5. The effect of rocaglamide treatment on tumour cell proliferation. (**a**) Rocaglamide treatment inhibits the proliferation of KRAS-mutated NSCLC tumour cell lines. 368T1 and 482T1 cells were cultured in a 96-well plate with DMSO or rocaglamide (25–200 nM) for 24 h and 48 h (upper panel). MTT assay was used to measure the rate of proliferation. The histograms show the quantification of the data presented in the upper panel ($n = 3$). The relative decrease in the proliferation of rocaglamide-treated cells compared to DMSO-treated controls is illustrated. Data represent mean ± s.d. of three independent experiments (**$P < 0.01$, *$P < 0.05$). (**b**) Rocaglamide treatment inhibits cell proliferation in several lung cancer cell lines. All cell lines unless otherwise mentioned were cultured for 24, 48, and 72 h (*x* axis) in the presence of DMSO or rocaglamide (50, 200 nM). MTT assay was performed as mentioned in **a**. Shown are data from a single representative experiment. (**c**) Rocaglamide treatment inhibits DNA synthesis. After treatment with rocaglamide for 24 h, EdU assay was performed to evaluate the amount of newly synthesized DNA by flow cytometry analysis following the manufacturer's instructions. The population of cells with neo DNA was gated in every condition.

purchased from Thermo Fisher Scientific (Boston, MA, USA). Rabbit anti-PHB1 antibody (GTX101105) and anti-cyclin B1 antibody (GTX100911) were purchased from GENETEX (Hsinchu City, Taiwan). Anti-cyclin D1 antibody (1677–1) was purchased from Epitomics (Burlingame, CA, USA). Anti-M2PK antibody (S-1) was purchased from Schebo Biotech (Gießen, Germany). Horseradish peroxidase (HRP)-conjugated antibodies for mouse and rabbit IgG were obtained from Novex (Boston, MA, USA, A16066 and A16096, respectively). HRP-conjugated anti-FLAG M2 antibody was purchased from Sigma-Aldrich.

Immunohistochemistry

The staining and analysis of NSCLC tumour tissue were performed by Indivumed GmbH using tissue microarrays of adenocarcinoma ($N = 39$ spots) and squamous cell carcinoma ($N = 37$ spots), as well as matching tumour-adjacent normal lung tissues ($N = 5$ spots each). Indivumed GmbH (Hamburg, Germany) duly obtained all ethical permissions for performing these studies.

Immunohistochemistry was implemented on the Discovery XT staining platform (Roche Diagnostics, Mannheim, Germany/Ventana Medical Systems, Tucson, AZ, USA), using the monoclonal anti-PHB1 antibody clone MA5-12858 (Thermo Fisher Scientific). Formalin-fixed paraffin embedded tissue microarrays were sliced into 3–5 µm sections and mounted on SuperFrost Plus glass slides (Roth, Karlsruhe, Germany). Haematoxylin and eosin-stained sections were prepared according to Indivumed's standard operating procedure. For immunohistochemistry, slides were deparaffinized within the staining instrument and immunostained using the Discovery ChromoMap DAB Kit (Roche Diagnostics) as well as OmniMap anti-Mouse HRP secondary antibody. All samples were blocked with 2% normal goat serum for 8 min prior to primary antibody incubation, which was performed for 20 min at room temperature.

Semi-quantitative evaluation of the anti-PHB1 immunohistochemistry staining was carried out by Indivumed's pathologist. Therefore, membranous as well as cytoplasmic anti-PHB1 staining of tumour cells within the tumour area and non-malignant epithelial cells within the tumour-adjacent normal lung tissue were analysed using the *H*-score classification.[37] The percentages of weakly, moderately and strongly stained tumour/epithelial cells were estimated, and the *H*-score was calculated as follows: *H*-score = (weak)%+(moderate)% × 2(strong)% × 3. The table below shows the H-score classification based on the resulting score ranges from 0 to 300.

Table *H*-score classification

H-*score*	*Classification*
0–50	Negative
51–100	Weakly positive
101–200	Moderately positive
201–300	Strongly positive

Phalloidin staining

482T1 cells were seeded in six-well plates on coverslips. After 1 day, rocaglamide was added to the well (200 nM) and cultured for 24 h. After rocaglamide treatment, staining of cells with phalloidin was performed using Oregon Green 488 Phalloidin (O7466, Molecular Probes, Boston, MA, USA) following the manufacturer's instructions.

Immunoblot analysis

All cells were cultured in 12-well plates for immunoblotting analysis. At 50–80% confluence, rocaglamide (50 or 200 nM) was added and the cells were cultured for 24 h. After washing with cold phosphate buffered saline (−), SDS–PAGE sample buffer (70 mM Tris–HCl pH 6.8, 40% glycerol, 0.3% SDS, 100 mM DTT and BPB) was added to the well. HeLa cells seeded in 10 cm dishes were stimulated with EGF and the cells were collected. Plasma membrane isolation was performed using plasma membrane

protein extraction kit (ab65400, Abcam, Cambridge, UK) following the manufacturer's instructions. The sample was subjected to 10% SDS–PAGE followed by immunoblotting analysis on nitrocellulose membrane (GE Healthcare, Chalfont St Giles, UK). After transfer, membrane was blocked with 3% BSA/TBST (20 mM Tris–HCl pH 7.5, 150 mM NaCl, 0.05% Tween-20) at room temperature for nearly 1 h. After blocking, membrane

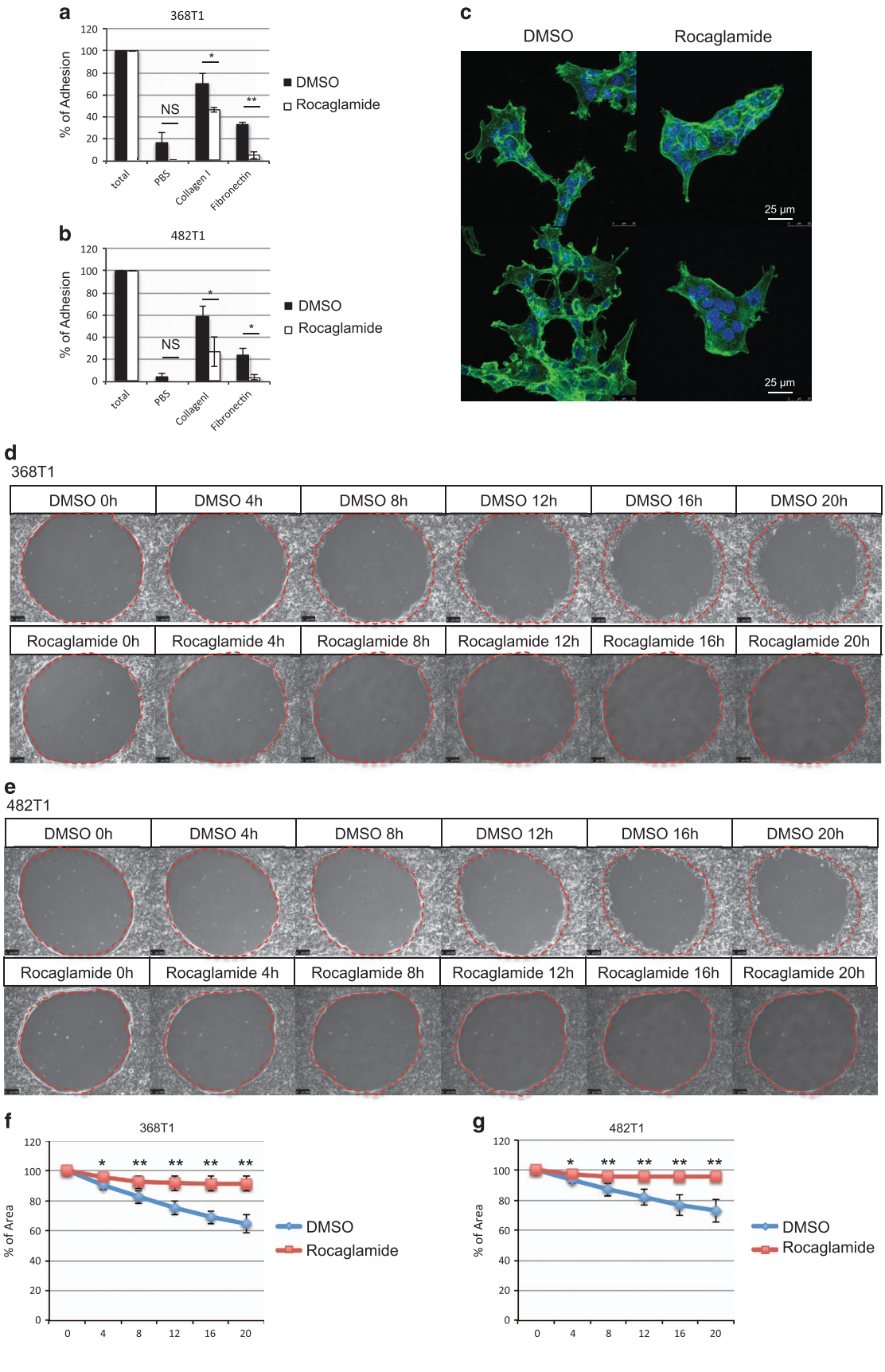

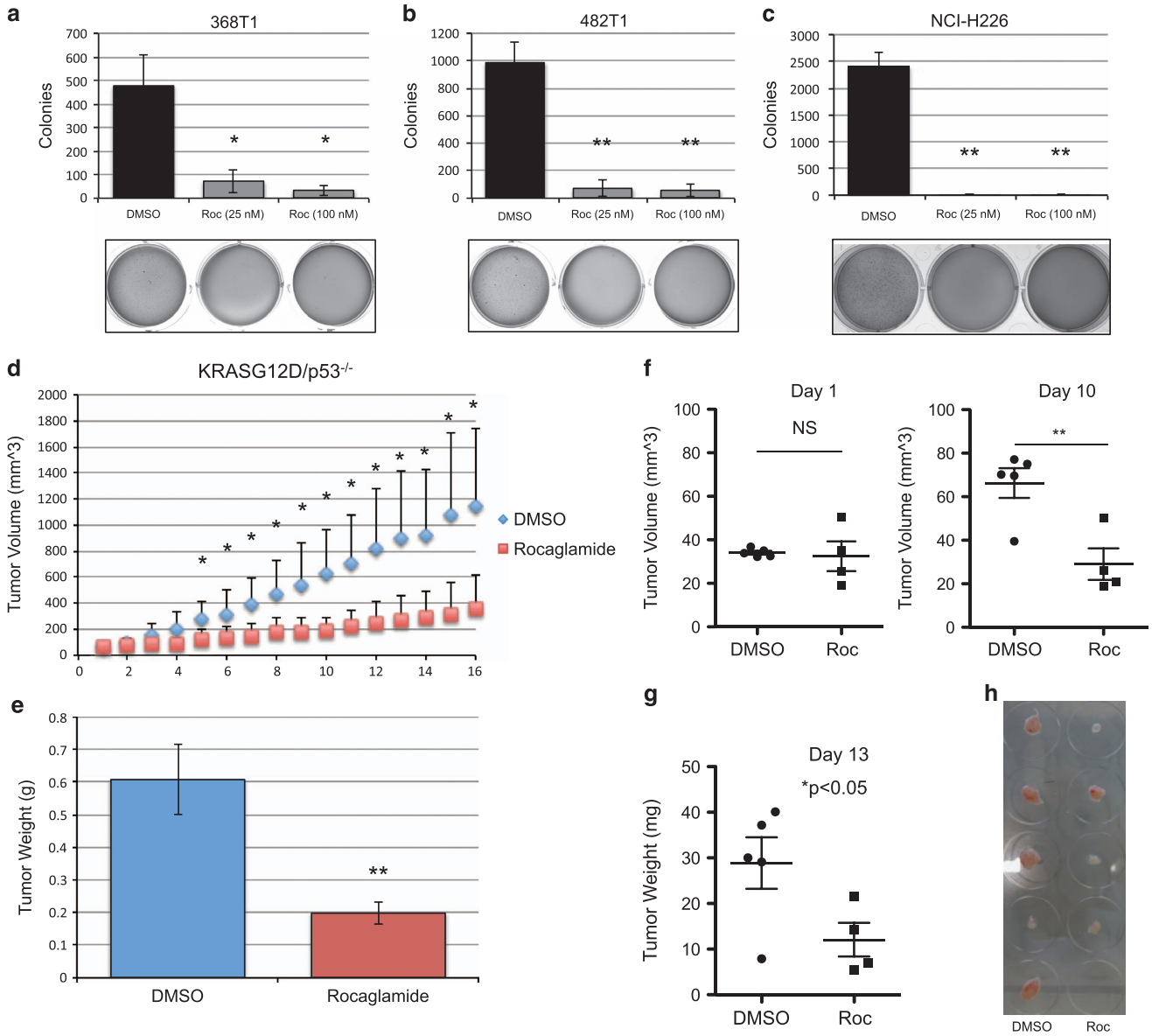

Figure 7. Rocaglamide treatment prevents NSCLC tumour growth both *in vitro* and *in vivo*. (**a**–**c**) Rocaglamide treatment inhibits colony formation of NSCLC cancer cell lines. Soft agar colony formation assay was performed with DMSO or rocaglamide (Roc)-treated tumour cells for 2 weeks and the number of colonies formed was quantified by Image J as mentioned in the Materials and Methods section. Data represent mean ± s.d. of three independent experiments and representative images were shown. $^{**}P < 0.01$, $^{*}P < 0.05$. (**d**–**h**) Rocaglamide treatment inhibits tumour growth *in vivo*. 482T1 cells were subcutaneously injected to the immune competent mice and treated with rocaglamide (Roc, 2.5 mg/kg) after 10 days for 16 days. During the course of treatment, the tumour volume was measured with calipers and plotted. Data indicate mean ± s.d. ($n = 7$), $^{*}P < 0.05$ (**d**). After 16 days, mice were killed and the net wet weight of tumours was measured. Data indicate mean ± s.d. ($n = 7$), $^{**}P < 0.01$ (**e**). NCI-H226 cells were subcutaneously injected to the nonobese diabetic/severe combined immune deficiency mice and treatment was started after 12 days of tumour incidence. Tumour volume was calculated as mentioned earlier. Data indicate mean ± s.e.m. ($n = 5$ mice for DMSO-treated condition and $n = 4$ mice from rocaglamide-treated condition), $^{**}P < 0.01$ (**f**). After 13 days, mice were killed, and the wet weight of tumours was measured and the image was taken by a digital camera. Data indicate mean ± s.e.m. ($n = 5$ mice for DMSO-treated condition and $n = 4$ mice from rocaglamide-treated condition). $^{*}P < 0.05$ (**g**, **h**).

Figure 6. Treatment with rocaglamide prevents cell adhesion and migration. (**a**, **b**) Treatment with rocaglamide inhibits tumour cell adhesion to several components of extracellular matrix (ECM). Tumour cells were treated either with DMSO or rocaglamide (100 nM) for 24 h and were detached from the cell culture plates using 2 mM EDTA/PBS. The cells were counted with a hemocytometer, and equal numbers of cells were seeded onto 96-well plates coated with various ECM components. The floating cells were washed away with PBS, and the viable, attached cells were measured with an MTT assay. One set of samples was used as a control where the cells were not washed away and the values obtained with MTT assay was calculated as 100%. Data represent mean ± s.d. of three independent experiments ($^{**}P < 0.01$, $P < 0.05$). (**d**–**g**) A rocaglamide treatment inhibits cell migration. Two-dimensional migration of tumour cells was monitored in DMSO or rocaglamide (200 nM)-treated tumour cells for 20 h as mentioned in the Materials and Methods section. The quantification of the area covered was presented. Shown are data representing mean ± s.d. of three independent experiments ($^{**}P < 0.01$, $^{*}P < 0.05$). NS, not significant.

was incubated with primary antibody diluted in 1% BSA/TBST at 4 °C overnight. After washing with TBST, membrane was incubated with HRP-conjugated secondary antibody for an hour followed by enhanced chemiluminescence (ECL)-based detection (WBKLS0500, Millipore, Billerica, MA, USA).

Active Ras pull-down assay

Active Ras pull-down and detection kit (16117, Thermo Fisher Scientific) or purified GST-tagged CRAF Ras-binding domain (CRAF-RBD) was employed to detect GTP-bound Ras following the instructions of the manufacturer. For the GST-CRAF pull-down assay, GST-CRAF RBD1-149 construct was obtained from Prof. Channing Der (#13338, Addgene, Cambridge, MA, USA) and the GST-tagged protein was purified following the standard procedures. Rosette (DE) competent cell was used for the protein expression and the protein expression was induced at around O.D. 0.6, 16 °C with 0.1 mM IPTG for overnight. The bacteria were washed with phosphate buffered saline (PBS) once and lysed in 1% NP-40, 20 mM Tris–HCl pH 8.0, 200 mM NaCl. Sonicated lysate was used for the GST purification. After incubation, the beads were washed with 20 mM Tris–HCl pH 8.0, 200 mM NaCl and used for the active Ras pull-down assay. After incubation, the RAS bound to RBD-GST was washed, and the precipitated sample was subjected to SDS–PAGE and immunoblotting analysis.

KRAS WT protein was used for the *in vitro* active KRAS pull-down assay. The recombinant KRAS protein (1 μg protein) was incubated with GDP or GTPγS in the presence of rocaglamide (250 nM, 1 μM) or DMSO. The active RAS pull downs were performed by employing the RAS-GTP detection kit following the manufacturer's instructions.

Immunoprecipitation assays

HeLa cells were transfected with N-terminal FLAG CRAF plasmid for 48 h with polyethylenimine solution. One microgram of plasmid and 5.4 μl of 10 mM polyethylenimine was mixed in 100 μl of PBS and incubated for 10 min at room temperature. After incubation, transfection reagent was added dropwise to HeLa cells cultured in 12-well plates. After treatment with rocaglamide (200 nM) or EGF stimulation (described above), cells were lysed in the lysis buffer (25 mM Tris–HCl pH 7.2, 150 mM NaCl, 1% NP-40, 5% glycerol, 5 mM $MgCl_2$, with EDTA-free proteinase inhibitor cocktail (4693159001, Sigma-Aldrich)), and centrifuged at 4 °C and at 13 000 r.p.m. for 15 min. Anti-FLAG M2 magnetic beads (M8823, Sigma-Aldrich) were added to the supernatant and the sample was rotated at 4 °C for at least 2 h, The beads were washed with the lysis buffer and the precipitated proteins were detected using the immunoblot analyses.

For detecting CRAF-BRAF heteromerization, HeLa cells were serum starved and stimulated with EGF as mentioned above, and the cells were lysed in lysis buffer (20 mM Tris–HCl pH 8.0, 137 mM NaCl, 1% NP-40, 10% glycerol, with EDTA-free proteinase inhibitor cocktail (4693159001, Sigma-Aldrich)) after washing once with ice-cold PBS. The samples were incubated on ice for 30 min. The lysate was centrifuged at 13 000 r.p.m. and 4 °C for 20 min. After centrifugation, 2 μg of anti-CRAF antibody (sc-133, Santa Cruz) and 5 μl of protein A/G magnetic beads (B23201, http://www.biotool.com) were added to the supernatant and rotated at 4 °C for 5 h. The beads were washed with the lysis buffer twice and SDS-sample buffer (70 mM Tris–HCl pH 6.8, 40% glycerol, 0.3% SDS, 100 mM DTT and BPB) was added to the beads. Total lysate and beads-bound protein were loaded onto an SDS–PAGE gel and subjected to immunoblotting analyses.

Cell proliferation assay

Cell proliferation assay was performed by employing the Cell Proliferation Kit I (Roche, Basel, Switzerland). Cells were seeded in a 96-well cell culture plate with or without rocaglamide in 100 μl of complete growth medium. After 24–48 h, 10 μl of MTT solution was added and incubated in CO_2 incubator for 2–4 h. After incubation, 100 μl of solubilization buffer was added to each well and incubated overnight in CO_2 incubator. Absorbance of the solubilized MTT was measured by absorbance plate reader (O.D. 570).

EdU assay

368T1 and 482T1 cells were treated with rocaglamide (200 nM) in a 12-well cell culture plate for 24 h. After the treatment, EdU DNA synthesis assay was performed using Click-iT EdU pacific blue Imaging Kit (Thermo Fisher Scientific). The cells were incubated EdU for 1 h and incorporated EdU was stained with pacific blue ligand. All staining protocol was performed as described in the manufacture's instructions. After staining, the histogram of pacific blue-positive cells was measured by flow cytometer.

Two-dimensional migration assay

One microlitre of 1.5% agarose was placed as a drop on a six-well plate, and 368T1, 482T1 and NCI-H226 cells were seeded onto these plates. Reaching confluence, rocaglamide was added to the plate (200 nM) and cultured for 6 h. After 6 h, the agarose spot was removed by aspirator and the cell migration was monitored by placing the entire plate under a DMi8 wide-field microscope system (Leica).

Soft agar colony formation assay

Agarose solution of 1.5% was mixed with 2× growth medium (20% FBS, with or without 200 nM rocaglamide) and placed with 1.5 ml of 0.75% agarose/1× growth medium in a six-well plate, and incubated at room temperature for at least 10 min to solidify agarose. 368T1, 482T1 and NCI-H226 cells were diluted in a 2× growth medium (20% FBS, with or without 200 nM rocaglamide) and mixed with 0.9% agarose solution. Cell suspension of 1.5 ml in 0.45% agarose in 1× growth medium was added to the bottom agarose layer. The cells seeded in soft agar were cultured for 2–4 weeks followed by the staining with crystal violet solution. The images were taken under a ChemiDoc Touch (Bio-Rad, Hercules, CA, USA) equipment and the number of colonies was counted by the Image J software (NIH, Bethesda, MA, USA).

Adhesion assay

Rat tail collagen I of 10 μg/ml (BD, San Diego, CA, USA) and 20 μg/ml of human plasma fibronectin (FC010, Millipore) in 50 μl of PBS was added to a 96-well plate and incubated at 4 °C overnight. 368T1 and 482T1 cells were cultured with or without 100 nM rocaglamide for 24 h and collected by 2 mM EDTA in PBS. Cell suspension (1×10^6 cells per ml, 100 μl in each well) was added to the plate and incubated at 37 °C for 30 min. After incubation, unattached cells were washed out with PBS and the amount of attached cells was measured using the MTT assay (Cell Proliferation Kit I, Roche).

Tumour growth assay *in vivo*

B6129 SF1/J mice were purchased from Jackson (stock No.101043, Bar Harbor, ME, USA). Nonobese diabetic/severe combined immune deficiency (NOD/SCID) mice were obtained from our own breeding unit at the Translational Animal Research Center at the University of Mainz. A total of 5×10^4 cells (482T1) were subcutaneously injected to B6/129 F1 mouse and 1×10^6 cells (NCI-H226) were subcutaneously injected to nonobese diabetic/severe combined immune deficiency mice into the back. After 10 days (482T1) and 12 days (NCI-H226), rocaglamide (2.5 mg/kg, 1.25 mg/ml in 1% DMSO/olive oil) was injected into the mice (intraperitoneal administration) for 16 days (482T1) and 13 days (NCI-H226). Tumour volume ($L \times W^2/2$) and the weight were measured every day. All animals were handled according to the ethical guidelines of the state of Rheinland Pfalz.

TCGA analysis

Gene expression data were downloaded from the TCGA GDAC Firehose portal (Broad Institute TCGA Genome Data Analysis Center (2016): Firehose stddata__2016_01_28 run. Broad Institute of MIT and Harvard, doi:10.7908/C11G0KM9). For analysing PHB expression, the normalized RSEM counts were used after log-2 transformation. Clinical information on the KRAS and EGFR mutation status were retrieved from the UCSC Cancer Genomics Browser (https://genome-cancer.ucsc.edu/). For computing statistical significance of the differences in the mean expression values, two-sided Welch *t*-tests were used, to account for unequal variances in the two populations, with the R statistical software (version 3.3.0, Vienna, Austria, https://www.r-project.org/).

Statistic analysis

P-values were obtained by Welch's *t*-test in Excel and $P < 0.05$ was considered as a significant difference.

Significance

Lung cancers are a major causative of cancer deaths. Seventeen per cent of lung cancers carry mutations in the KRAS oncogene. Targeting of PHB1 blocks CRAF kinase activation and KRAS-mediated tumourigenesis. PHB1 is highly expressed in NSCLC patients and correlates with poor patient

survival. These results open a novel avenue of targeting PHB1-CRAF interface in treating lung cancers.

CONFLICT OF INTEREST

The authors declare no conflict of interest.

ACKNOWLEDGEMENTS

We thank Alexandra Dimitrijevic for the excellent technical assistance, and Dr Melzer for her help and advice with the animal experiments. We thank Professors Tyler Jacks, Susan Horwitz, Scott Randell, Channing Der and Ulf Rapp for contributing several constructs and cell lines that are employed in this study. We thank Professor Hartmut Juhl and Dr Bernd Gromoll (Indivumed GmbH) for assistance with the analyses of the NSCLC tissue microarrays. This work is supported through a BIS–PLUS3 fellowship of the Boehringer Ingelheim Stiftuing to KR. KR is a Heisenberg Professor of the DFG (RA1739/4-1) and a GFK fellow. A generous financial support for this work was provided by the 'Association pour la Recherche sur le Cancer' to LD. We are also grateful to AAREC Filia Research and the 'Association Nationale de la Recherche et de la Technologie' (ANRT) for fellowships to QZ.

AUTHOR CONTRIBUTIONS

HY conceived, designed and performed most of the experiments, analysed, interpreted the data and wrote the manuscript. FM and HB contributed to bioinformatics analyses. CW contributed to the staining and analyses of NSCLC tissue microarray. KD contributed to the design and analysis. QZ and LD contributed to the synthesis of fluorizoline. KR contributed to the conception, design, analysis, interpretation of the data, and wrote the manuscript with input from all the authors and supervised the project.

REFERENCES

1 Downward J. Targeting RAS signalling pathways in cancer therapy. *Nat Rev Cancer* 2003; **3**: 11–22.
2 Vasan N, Boyer JL, Herbst RS. A RAS renaissance: emerging targeted therapies for KRAS-mutated non-small cell lung cancer. *Clin Cancer Res* 2014; **20**: 3921–3930.
3 Hopkins AL, Groom CR. The druggable genome. *Nat Rev Drug Discov* 2002; **1**: 727–730.
4 Mitin N, Rossman KL, Der CJ. Signaling interplay in Ras superfamily function. *Curr Biol* 2005; **15**: R563–R574.
5 Dhillon AS, Hagan S, Rath O, Kolch W. MAP kinase signalling pathways in cancer. *Oncogene* 2007; **26**: 3279–3290.
6 Wellbrock C, Karasarides M, Marais R. The RAF proteins take centre stage. *Nat Rev Mol Cell Biol* 2004; **5**: 875–885.
7 Raman M, Chen W, Cobb MH. Differential regulation and properties of MAPKs. *Oncogene* 2007; **26**: 3100–3112.
8 Davies H, Bignell GR, Cox C, Stephens P, Edkins S, Clegg S *et al.* Mutations of the BRAF gene in human cancer. *Nature* 2002; **417**: 949–954.
9 Rajakulendran T, Sahmi M, Lefrancois M, Sicheri F, Therrien M. A dimerization-dependent mechanism drives RAF catalytic activation. *Nature* 2009; **461**: 542–545.
10 Downward J. Targeting RAF: trials and tribulations. *Nat Med* 2011; **17**: 286–288.
11 Fleuren ED, Zhang L, Wu J, Daly RJ. The kinome 'at large' in cancer. *Nat Rev Cancer* 2016; **16**: 83–98.
12 Blasco RB, Francoz S, Santamaria D, Canamero M, Dubus P, Charron J *et al.* c-Raf, but not B-Raf, is essential for development of K-Ras oncogene-driven non-small cell lung carcinoma. *Cancer Cell* 2011; **19**: 652–663.
13 Dumaz N, Hayward R, Martin J, Ogilvie L, Hedley D, Curtin JA *et al.* In melanoma, RAS mutations are accompanied by switching signaling from BRAF to CRAF and disrupted cyclic AMP signaling. *Cancer Res* 2006; **66**: 9483–9491.
14 Rajalingam K, Wunder C, Brinkmann V, Churin Y, Hekman M, Sievers C *et al.* Prohibitin is required for Ras-induced Raf-MEK-ERK activation and epithelial cell migration. *Nat Cell Biol* 2005; **7**: 837–843.
15 Fischer A, Baljuls A, Reinders J, Nekhoroshkova E, Sibilski C, Metz R *et al.* Regulation of RAF activity by 14-3-3 proteins: RAF kinases associate functionally with both homo- and heterodimeric forms of 14-3-3 proteins. *J Biol Chem* 2009; **284**: 3183–3194.
16 Chiu CF, Ho MY, Peng JM, Hung SW, Lee WH, Liang CM *et al.* Raf activation by Ras and promotion of cellular metastasis require phosphorylation of prohibitin in the raft domain of the plasma membrane. *Oncogene* 2013; **32**: 777–787.
17 Mishra S, Ande SR, Nyomba BL. The role of prohibitin in cell signaling. *FEBS J* 2010; **277**: 3937–3946.
18 Merkwirth C, Dargazanli S, Tatsuta T, Geimer S, Lower B, Wunderlich FT *et al.* Prohibitins control cell proliferation and apoptosis by regulating OPA1-dependent cristae morphogenesis in mitochondria. *Genes Dev* 2008; **22**: 476–488.
19 Merkwirth C, Langer T. Prohibitin function within mitochondria: essential roles for cell proliferation and cristae morphogenesis. *Biochim Biophys Acta* 2009; **1793**: 27–32.
20 Polier G, Neumann J, Thuaud F, Ribeiro N, Gelhaus C, Schmidt H *et al.* The natural anticancer compounds rocaglamides inhibit the Raf-MEK-ERK pathway by targeting prohibitin 1 and 2. *Chem Biol* 2012; **19**: 1093–1104.
21 Lovly CM, Shaw AT. Molecular pathways: resistance to kinase inhibitors and implications for therapeutic strategies. *Clin Cancer Res* 2014; **20**: 2249–2256.
22 Lito P, Saborowski A, Yue J, Solomon M, Joseph E, Gadal S *et al.* Disruption of CRAF-mediated MEK activation is required for effective MEK inhibition in KRAS mutant tumors. *Cancer Cell* 2014; **25**: 697–710.
23 Luan Z, He Y, Alattar M, Chen Z, He F. Targeting the prohibitin scaffold-CRAF kinase interaction in RAS-ERK-driven pancreatic ductal adenocarcinoma. *Mol Cancer* 2014; **13**: 38.
24 Rajalingam K, Schreck R, Rapp UR, Albert S. Ras oncogenes and their downstream targets. *Biochim Biophys Acta* 2007; **1773**: 1177–1195.
25 Niault T, Baccarini M. Targets of Raf in tumorigenesis. *Carcinogenesis* 2010; **31**: 1165–1174.
26 Manzano JL, Layos L, Buges C, de Los Llanos Gil M, Vila L, Martinez-Balibrea E *et al.* Resistant mechanisms to BRAF inhibitors in melanoma. *Ann Transl Med* 2016; **4**: 237.
27 Freeman AK, Ritt DA, Morrison DK. Effects of Raf dimerization and its inhibition on normal and disease-associated Raf signaling. *Mol Cell* 2013; **49**: 751–758.
28 Weber CK, Slupsky JR, Kalmes HA, Rapp UR. Active Ras induces heterodimerization of cRaf and BRaf. *Cancer Res* 2001; **61**: 3595–3598.
29 Leevers SJ, Paterson HF, Marshall CJ. Requirement for Ras in Raf activation is overcome by targeting Raf to the plasma membrane. *Nature* 1994; **369**: 411–414.
30 Sharma A, Qadri A. Vi polysaccharide of Salmonella typhi targets the prohibitin family of molecules in intestinal epithelial cells and suppresses early inflammatory responses. *Proc Natl Acad Sci USA* 2004; **101**: 17492–17497.
31 Yurugi H, Tanida S, Ishida A, Akita K, Toda M, Inoue M *et al.* Expression of prohibitins on the surface of activated T cells. *Biochem Biophys Res Commun* 2012; **420**: 275–280.
32 Yurugi H, Tanida S, Akita K, Ishida A, Toda M, Nakada H. Prohibitins function as endogenous ligands for Siglec-9 and negatively regulate TCR signaling upon ligation. *Biochem Biophys Res Commun* 2013; **434**: 376–381.
33 Ande SR, Mishra S. Palmitoylation of prohibitin at cysteine 69 facilitates its membrane translocation and interaction with Eps 15 homology domain protein 2 (EHD2). *Biochem Cell Biol* 2010; **88**: 553–558.
34 Doudican NA, Orlow SJ. Inhibition of the CRAF/prohibitin interaction reverses CRAF-dependent resistance to vemurafenib. *Oncogene* 2016; **36**: 423–428.
35 Becker MS, Schmezer P, Breuer R, Haas SF, Essers MA, Krammer PH *et al.* The traditional Chinese medical compound Rocaglamide protects nonmalignant primary cells from DNA damage-induced toxicity by inhibition of p53 expression. *Cell Death Dis* 2014; **5**: e1000.
36 Perez-Perarnau A, Preciado S, Palmeri CM, Moncunill-Massaguer C, Iglesias-Serret D, Gonzalez-Girones DM *et al.* A trifluorinated thiazoline scaffold leading to pro-apoptotic agents targeting prohibitins. *Angew Chem Int Ed Engl* 2014; **53**: 10150–10154.
37 McCarty Jr KS, Miller LS, Cox EB, Konrath J, McCarty KS Sr. Estrogen receptor analyses. Correlation of biochemical and immunohistochemical methods using monoclonal antireceptor antibodies. *Arch Pathol Lab Med* 1985; **109**: 716–721.

Supplementary Information accompanies this paper on the Oncogene website (http://www.nature.com/onc)

Qian ZHAO

Approche synthétique de produits naturels anticancéreux, les flavaglines

Résumé

Nous avons développé trois accès synthétiques performants à des cyclopentènones fonctionnalisées en exploitant des réactivités inattendues que nous avons découvertes.

Nous avons aussi effectué la première synthèse d'isostères des flavaglines substitués par un groupement formylamino ou mésylamino en position 1b et ainsi démontré l'importance de l'hydroxyl en cette position pour la cytotoxicité de ces composés.

De plus, nous avons aussi contribué à l'exploration du potentiel thérapeutique des flavaglines et d'un autre ligand des prohibitines, la fluorizoline, dans le traitement des cancers et de l'inflammation chronique des intestins, ainsi que dans la prévention des effets adverses des chimiothérapies au niveau cardiaque.

Mots-clés : flavaglines, cyclopentènones, cyclisation catalysée à l'or, réaction de Nazarov, eIF4A, prohibitines, cancer, chimiorésistance.

Synthetic approaches of anticancer natural products, the flavaglines

Abstract

We have developed three novel synthetizes of functionalized cyclopentenones based on unexpected reactivities that we discovered.

We also developed the first synthesis of flavaglines isostere substituted by a formylamino or mesylamino group on the position of 1b, and demonstrated the importance of a hydroxyl group on this position for cytotoxicity.

Moreover, we contributed to the exploration of the therapeutic potential of flavaglines and another ligand of prohibitins, fluorizoline, in the treatment of cancers and intestinal chronic inflammation, and also in the prevention of the cardiac adverse effects in anticancer treatments.

Key words: flavaglines, cyclopentenones, gold-catalyzed cyclization, Nazarov reaction, eIF4A, prohibitins, cancer, chemoresistance.